

# **DESIGN AND EVALUATION OF HOT MELT EXTRUDED TRANSDERMAL PATCHES**

---



**ESRA'A KHALEEL AHMAD ALBARAHMIEH**

**Thesis submitted for degree of Doctor of Philosophy**

**University of East Anglia  
School of Pharmacy**

**July 2013**

© This copy of the thesis has been supplied on condition that anyone who consults it is understood to recognise that its copyright rests with the author and that use of any information derived there from must be in accordance with current UK Copyright Law. In addition, any quotation or extract must include full attribution

## Abstract

In recent years, there has been a growing interest towards the use of transdermal drug delivery systems (TDDS). However, a great challenge in this arena is the formidable barrier posed by the skin that can limit permeation of therapeutic agents. Therefore, there is a need for novel strategies or enhancement techniques to deliver the drug across the skin. The use of hot melt extrusion technology (HME) to prepare these TDDS is also generating considerable interest in the pharmaceutical field. This work combines these interests through preparation of several hot melt extruded formulations screened for their potential for transdermal development. A substantial database has been generated on physicochemical characteristics of these formulations with a prime focus on their *in vitro* drug release and permeation properties.

Processing parameters (temperature, heating duration and mixing speed) for preparing hot melt extruded compositions comprising ibuprofen (model drug) and various carrier excipients were established with minimal thermal degradation. Ibuprofen displayed a plasticizing effect enough to perform extrusion. HME processing facilitated the formation of solid solutions and dispersions. The feasibility of delivering ibuprofen from Eudragit RS PO-based extruded patches was investigated. The formation of solid solutions with high drug loading (35% w/w) was achieved in relatively stable extruded Eudragit RS PO matrices under dry conditions. However, these systems were associated with limited drug release. This has given the way to explore the effect of addition of release modifiers (sucrose, methylcellulose, Xantural®75, Pluronic® F127, Gelucire 44/14) and hydration influence. Gelucire 44/14 containing formulations emerged as the most satisfactory systems which improved *in vitro* drug permeation profiles significantly by means of hydration. Intriguing structural changes upon hydration are believed to facilitate drug release as observed from the medicated and non-medicated formulations. These include consistency changes, softening of the extruded films and surface imperfections. Similar changes were detected *in vivo* using non-medicated Eudragit RS PO/Gelucire 44/14 carrier extruded systems after human skin occlusion. This employed strategy holds the promise for potential of a novel transdermal drug delivery activated by hydration.



## **Acknowledgments**

It has been an honour and privilege working under the supervision of Professor Duncan Craig and Dr Sheng Qi. Without their encouragement, motivation and vast knowledge this project would not have been materialized. I would also like to express my gratitude to German Jordanian University for their financial support.

I would like to express my deepest appreciation to Professor Duncan Craig, Dr Sheng Qi, and Professor Peter Belton for their technical support, patience and advices. A special gratitude must also go to Dr Jonathan Moffat and Dr Sarah Otun for their assistance and training. Also, I like to thank the participants in the clinical study and all the members of staff of University of East Anglia whom provided continuous support throughout my PhD. Special thanks to Mr. Bertrand Leze, Mr. Roy Carter and Mr. Peter.

My sincere thanks go to all the past and present members of the research group. I will be grateful forever for your love. A special mention must be made to Dr Sue, Dr Kate, Dr Min, Germeen, Joanne, Sam, Fatima and Ziyi.

Foremost, i would like to thank Alah whom blessed me with my precious mother 'Yusra', she is the heart pumping love and inspiration in my soul, and my beloved brothers 'Mutaz' and 'Muthaffer, whom are the blood flowing in my veins. Without their love, understanding and support this work was not possible.

بسم الله الرحمن الرحيم  
{قَالَ رَبِّ اشْرَحْ لِي صَدْرِي ۝ وَيَسِّرْ لِي أَمْرِي ۝ وَاحْلُلْ عُقْدَةً مِنْ لِسَانِي ۝ يَفْقَهُوا قَوْلِي}  
صدق الله العظيم

FOR MUM (YUSRA), MUTAZ & MUTHAFFER

# Table of Contents

<b>ABSTRACT.....</b>	<b>2</b>
<b>ACKNOWLEDGMENTS.....</b>	<b>3</b>
<b>TABLE OF CONTENTS .....</b>	<b>5</b>
<b>LIST OF FIGURES .....</b>	<b>11</b>
<b>LIST OF TABLES .....</b>	<b>32</b>
<b>LIST OF SYMBOLS .....</b>	<b>37</b>
<b>LIST OF ABBREVIATIONS .....</b>	<b>38</b>
<b>CHAPTER 1: INTRODUCTION.....</b>	<b>40</b>
1.1 GENERAL INTRODUCTION .....	41
1.2 HOT MELT EXTRUSION (HME) FOR PHARMACEUTICAL SYSTEMS.....	41
1.2.1 Extrusion processing.....	42
1.2.2 Extruder types .....	45
1.2.3 HME formulation development .....	46
1.2.3.1 Active ingredients .....	47
1.2.3.2 Carrier systems.....	47
1.2.3.3 Processing aids.....	48
1.2.4 Characterisation of the hot melt extrudate .....	51
1.2.5 HME for transdermal drug delivery .....	54
1.3 TRANSDERMAL DRUG DELIVERY SYSTEMS (TDDS) .....	55
1.3.1 Skin drug delivery: topical versus transdermal drug delivery systems .....	57
1.3.2 Skin structure and anatomy .....	57
1.3.2.1 Epidermis .....	58
1.3.2.2 Dermis.....	60
1.3.3 Absorption pathways.....	60
1.3.4 Transdermal drug delivery system design.....	61
1.3.4.1 Permeation through the stratum corneum and its enhancement.....	64
1.4 RESEARCH OBJECTIVES .....	66
<b>CHAPTER 2: MATERIALS AND GENERAL METHODS.....</b>	<b>67</b>
2.1 MATERIALS .....	68
2.1.1 Model drug.....	68
2.1.1.1 Description .....	68
2.1.1.2 Medical rationale.....	69
2.1.1.3 Selection of ibuprofen .....	69

2.1.2 Carrier excipients .....	71
2.1.2.1 Eudragit RS PO.....	71
2.1.2.2 Sucrose .....	73
2.1.2.3 Methyl cellulose.....	73
2.1.2.4 Xantural®75.....	74
2.1.2.5 Pluronic® F127 .....	75
2.1.2.6 Gelucire 44/14.....	76
2.1.3 Sourcing of the used materials .....	77
2.2 METHODS .....	78
2.2.1 Preparation of hot melt extruded transdermal patches .....	78
2.2.2 Characterisation methods used for the evaluation of hot melt extruded formulations for transdermal delivery.....	79
2.2.2.1 Thermoanalytical techniques .....	79
2.2.2.1.1 Differential scanning calorimetry (DSC).....	80
2.2.2.1.2 Modulated temperature DSC (MTDSC) .....	83
2.2.2.1.3 Thermogravimetric analysis (TGA).....	87
2.2.2.1.4 Hot stage microscopy (HSM).....	90
2.2.2.2 Dynamic vapor sorption (DVS) analysis .....	91
2.2.2.3 Attenuated total reflection-Fourier transform infrared spectroscopy (ATR-FTIR) .....	92
2.2.2.4 Powder X-ray diffraction (PXRD).....	95
2.2.2.5 Scanning electron microscopy (SEM) .....	97
2.2.2.6 Texture analysis (TA) .....	98

### **CHAPTER 3: CHARACTERISATION OF IBUPROFEN AND THE CARRIER**

<b>EXCIPIENTS INTENDED FOR HOT MELT EXTRUSION .....</b>	<b>101</b>
3.1 INTRODUCTION .....	102
3.2 METHODOLOGY.....	102
3.3 RESULTS AND DISCUSSION .....	104
3.3.1 Model drug.....	104
3.3.1.1 Thermoanalytical investigations .....	104
3.3.1.2 Morphological and spectroscopic properties.....	110
3.3.2 Carrier excipients .....	111
3.3.2.1 Eudragit RS PO.....	111
3.3.2.1.1 Thermoanalytical investigations .....	111
3.3.2.1.2 Morphological and spectroscopic properties.....	116
3.3.2.2 Sucrose .....	117
3.3.2.2.1 Thermoanalytical investigations .....	117
3.3.2.2.2 Morphological and spectroscopic properties.....	119

3.3.2.3 Methyl cellulose.....	120
3.3.2.3.1 Thermoanalytical investigations .....	120
3.3.2.3.2 Morphological and spectroscopic properties.....	122
3.3.2.4 Xantural®75.....	124
3.3.2.4.1 Thermoanalytical investigations .....	124
3.3.2.4.2 Morphological and spectroscopic properties.....	126
3.3.2.5 Pluronic® F127.....	127
3.3.2.5.1 Thermoanalytical investigations .....	127
3.3.2.5.2 Morphological and spectroscopic properties.....	129
3.3.2.6 Gelucire 44/14.....	131
3.3.2.6.1 Thermoanalytical investigations .....	131
3.3.2.6.2 Spectroscopic properties .....	133
3.4 CONCLUSIONS .....	134

#### **CHAPTER 4: FORMULATION DEVELOPMENT AND PHYSICOCHEMICAL CHARACTERISATION OF HOT MELT EXTRUDED IBUPROFEN-EUDRAGIT RS PO FILMS FOR TRANSDERMAL DELIVERY..... 136**

4.1 INTRODUCTION.....	137
4.2 METHODOLOGY.....	138
4.2.1 Preparation of physical mixtures.....	138
4.2.2 Preparation of hot melt extruded ibuprofen in Eudragit RS PO .....	138
4.2.3 General methods .....	139
4.3 RESULTS AND DISCUSSION .....	141
4.3.1 Investigation into thermal stability of the ibuprofen-Eudragit RS PO physical mixes for processing <i>via</i> hot melt extrusion .....	141
4.3.2 Assessment of the miscibility and compatibility of ibuprofen-Eudragit RS PO hot melt extruded systems.....	143
4.3.3 Influence of the relative humidity on the saturation solubility of ibuprofen in Eudragit RS PO extrudates .....	163
4.3.3.1 Investigations into the saturation solubility of hot melt extruded ibuprofen in Eudragit RS PO after storage study at 0% relative humidity.....	163
4.3.3.2 Investigations into the saturation solubility of hot melt extruded ibuprofen in Eudragit RS PO after storage study at 60% relative humidity.....	168
4.3.4 Fragility assessment of ibuprofen-Eudragit RS PO extruded systems.....	173
4.4 CONCLUSIONS .....	176

#### **CHAPTER 5: *IN VITRO* IBUPROFEN RELEASE AND PERMEATION STUDIES FROM HOT MELT EXTRUDED EUDRAGIT RS PO FILMS..... 178**

5.1 INTRODUCTION.....	179
-----------------------	-----

5.2 EXPERIMENTAL METHODOLOGIES .....	180
5.2.1 <i>In vitro</i> drug release studies .....	180
5.2.1.1 Preparation of phosphate buffer solution (pH =7.2) .....	182
5.2.1.2 Equilibrium saturation solubility.....	182
5.2.1.3 Evaluation of drug release.....	182
5.2.2 <i>In vitro</i> permeation (diffusion) studies.....	186
5.2.3 Modelling of <i>in vitro</i> permeation profiles.....	189
5.3 RESULTS AND DISCUSSION .....	192
5.3.1 <i>In vitro</i> release studies.....	193
5.3.2 <i>In vitro</i> permeation (diffusion) studies.....	196
5.3.3 <i>In vitro</i> permeation studies model fitting .....	199
5.4 CONCLUSIONS .....	201
<b>CHAPTER 6: THE EFFECT OF VARIATION OF DESIGN PARAMETERS ON THE RELEASE AND PERMEATION PROPERTIES OF IBUPROFEN FROM HOT MELT EXTRUDED CARRIERS.....</b>	<b>202</b>
6.1 INTRODUCTION.....	203
6.2 EFFECTS OF VEHICLE FORMULATIONS .....	203
6.2.1 Methodology .....	203
6.2.2 Results and discussion .....	204
6.2.2.1 Fabrication and development of hot melt extruded Eudragit RS PO-based films loaded with ibuprofen and intended for transdermal drug delivery .....	204
6.2.2.2 <i>In vitro</i> release of ibuprofen from the viable hot melt extruded formulations .....	225
6.2.2.3 <i>In vitro</i> permeation studies of the selected formulations .....	234
6.3 EFFECTS OF HYDRATION .....	244
6.3.1 Methodology .....	245
6.3.2 Results and discussion .....	246
6.3.2.1 Hydration dependence of the <i>in vitro</i> permeation of ibuprofen from hot melt extruded films .....	246
6.4 CONCLUSIONS .....	260
<b>CHAPTER 7: INVESTIGATION INTO EUDRAGIT RS PO/GELUCIRE 44/14 HOT MELT EXTRUDED FILMS AS PROMISING CARRIER SYSTEMS FOR IBUPROFEN TRANSDERMAL DELIVERY .....</b>	<b>263</b>
7.1 INTRODUCTION.....	264
7.2 CHARACTERISATION OF THE EUDRAGIT RS PO/GELUCIRE 44/14 HOT MELT EXTRUDED FILMS .....	264
7.2.1 Methodology .....	265

7.2.2 Results and discussion .....	266
7.2.2.1 Investigation into thermal properties using conventional DSC (cDSC) and modulated temperature DSC (MTDSC).....	266
7.2.2.2 Characterisation by X-ray powder diffraction (PXRD) and scanning electron microscopy (SEM) .....	277
7.2.2.3 A note on the decomposition of Gelucire 44/14 and Eudragit RS PO using the selected temperature of the extrusion.....	279
7.3 ATR-FTIR ASSESSMENT OF THE EUDRAGIT RS PO/GELUCIRE 44/14 HOT MELT EXTRUDED FILMS .....	281
7.3.1 Methodology .....	281
7.3.2 Results and discussion .....	282
7.3.3 A note on the observed behaviour of Eudragit RS PO/Gelucire 44/14 physical mixtures under thermal treatment by hot stage microscopy (HSM) .....	296
7.4 HYDRATION BEHAVIOUR OF EUDRAGIT RS PO/GELUCIRE 44/14 HOT MELT EXTRUDED FILMS .....	298
7.4.1 Investigation into water sorption properties of Eudragit RS PO/Gelucire 44/14 hot melt extruded systems .....	298
7.4.1.1 Methodology .....	299
7.4.1.2 Results and discussion .....	299
7.4.2 Investigation into the influence of hydration on the properties of Eudragit RS PO/Gelucire 44/14 hot melt extruded systems.....	306
7.4.2.1 Methodology .....	306
7.4.2.2 Results and discussion .....	308
7.5 THE BEHAVIOUR OF AGED EUDRAGIT RS PO/GELUCIRE 44/14 HOT MELT EXTRUDED FILMS WITH AND WITHOUT IBUPROFEN.....	329
7.5.1 Methodology .....	329
7.5.2 Results and discussion .....	331
7.5.2.1 Characterisation of the aged carrier systems of Eudragit RS PO/Gelucire 44/14 hot melt extruded films .....	331
7.5.2.2 Characterisation of the aged hot melt extruded films of Eudragit RS PO/Gelucire 44/14 loaded with ibuprofen .....	343
7.5.2.3 <i>In vitro</i> permeation studies of ibuprofen from Eudragit RS PO/Gelucire 44/14-based extruded films: Effect of ageing .....	356
7.6 CONCLUSIONS .....	364
<b>CHAPTER 8: INFLUENCE OF OCCLUSION-INDUCED HYDRATION ON THE PROPERTIES OF EUDRAGIT RS PO/GELUCIRE 44/14 HOT MELT EXTRUDED SYSTEMS: <i>IN VIVO</i> BEHAVIOUR.....</b>	<b>367</b>
8.1 INTRODUCTION .....	368

8.2 METHODOLOGY.....	369
8.3 RESULTS AND DISCUSSION .....	370
8.4 CONCLUSIONS .....	385
<b>CHAPTER 9: CONCLUSIONS AND FUTURE WORK .....</b>	<b>386</b>
9.1 CONCLUSIONS .....	387
9.2 FUTURE WORK.....	393
<b>REFERENCES.....</b>	<b>396</b>
<b>APPENDIX.....</b>	<b>426</b>



## List of Figures

<b>Figure 1.1:</b> Schematic side view of a twin-screw extruder set-up comprising a feed hopper, barrel heaters, twin screws connected to a drive unit and an outlet representing a die system. The solids are conveyed, melted and pumped into the die. Reproduced from <a href="http://www.polymerprocessing.com">www.polymerprocessing.com</a> .....	43
<b>Figure 1.2:</b> A schematic diagram illustrating HME influence on achieving dispersive and distributive mixing .....	44
<b>Figure 1.3:</b> Schematic of the cross section view of the different screws' rotations in twin-screw extruder. Reproduced from <a href="http://www.iscrewbarrel.com">www.iscrewbarrel.com</a> .....	46
<b>Figure 1.4:</b> Schematic presentation of incorporating modes of the drug in an amorphous carrier matrix (commonly polymeric material) using HME technology. (A) Refers to solid crystalline dispersion of crystalline drug particles with a polymeric carrier; (B) to solid glassy suspension of amorphous drug domains (clusters) with a polymeric carrier and (C) represents solid solution of amorphous drug molecularly dispersed between amorphous polymeric chains.....	52
<b>Figure 1.5:</b> Cross section of the skin, highlighting the epidermis, dermis, hypodermis and stratum corneum. Reproduced from <a href="http://www.omnimedicalsearch.com">www.omnimedicalsearch.com</a> .....	58
<b>Figure 1.6:</b> Illustration of the possible pathways of molecules' permeation throughout the skin (transverse section view). Reproduced from <a href="http://www.cdc.gov">www.cdc.gov</a> .....	61
<b>Figure 1.7:</b> Common structural elements of simple transdermal drug delivery system (Scheindlin, 2004).....	62
<b>Figure 2.1:</b> Chemical structure of ibuprofen.....	69
<b>Figure 2.2:</b> Eudragit RS PO chemical structure ( <a href="http://eudragit.evonik.com">eudragit.evonik.com</a> ).....	72
<b>Figure 2.3:</b> Structural formula of sucrose (Rowe et al., 2009).....	73
<b>Figure 2.4:</b> Structural formula of methylcellulose. R=CH <sub>3</sub> or H (Kazuto et al., 1999) .....	74
<b>Figure 2.5:</b> Structural formula of xanthan gum (Rowe et al., 2009).....	75
<b>Figure 2.6:</b> Structural formula of Pluronic® F127, a=101, b=56 (Rowe et al., 2009) .....	76
<b>Figure 2.7:</b> Thermo Scientific Haake Minilab II Micro Compounder. Insert showing magnification of the melting zone with twin screw assembly. Reproduced from <a href="http://www.thermo.com">www.thermo.com</a> .....	79
<b>Figure 2.8:</b> Schematic diagram of heat flux DSC .....	81
<b>Figure 2.9:</b> Schematic of typical DSC curve includes commonly observed transitions .....	83
<b>Figure 2.10:</b> Temperature regimen as a function of time for conventional and modulated temperature DSC (Craig and Reading, 2007) .....	84

<b>Figure 2.11:</b> Thermoanalytical curve of quench-cooled PET showing the simple deconvolution (separation) of the MTDSC heat flow signals (Thomas, 2005) .....	86
<b>Figure 2.12:</b> Schematic diagram of common TG apparatus .....	89
<b>Figure 2.13:</b> TA Instruments TGA Q5000 IR. Reproduced from <a href="http://www.tainstruments.com">www.tainstruments.com</a> .....	89
<b>Figure 2.14:</b> TA Instruments Q5000 SA Dynamic Vapor Sorption Analyzer. Reproduced from <a href="http://www.tainstruments.com">www.tainstruments.com</a> .....	92
<b>Figure 2.15:</b> Schematic of a single reflection ATR system .....	94
<b>Figure 2.16:</b> Bruker IFS 66/S, Burkert optics spectrometer (left side) equipped with a Golden Gate ATR accessory from Specac Limited (right side).....	94
<b>Figure 2.17:</b> Diagram of powder X-ray diffractometer (Morris et al, 2011) .....	96
<b>Figure 2.18:</b> Diagram illustrating Bragg's law reflection .....	96
<b>Figure 2.19:</b> Schematic diagram of the main parts of a scanning electron microscope .....	97
<b>Figure 2.20:</b> TA-XT2 Texture Analyzer Stable Microsystems, Ltd. (Surrey, UK) equipped with a 5 kg load cell and fitted with a Perspex cylindrical probe.....	98
<b>Figure 2.21:</b> A typical force-time curve obtained from two cycles texture profile analysis test, with the peak (A) resulting from first compression cycle and peak (C) from the second compression cycle .....	99
<b>Figure 3.1:</b> TGA weight loss profile of crystalline ibuprofen heated at $10^{\circ}\text{C min}^{-1}$ to $300^{\circ}\text{C}$ .....	105
<b>Figure 3.2:</b> Heat flow signal of ibuprofen heated at $10^{\circ}\text{C min}^{-1}$ in standard aluminium pans.....	106
<b>Figure 3.3:</b> Heat flow signal of ibuprofen cycled at $10^{\circ}\text{C min}^{-1}$ (see text). Highlighted cycle after re-heating from $-70^{\circ}\text{C}$ is showing a magnified insert of the observed glass transition event .....	106
<b>Figure 3.4:</b> MTDSC heating scan of ibuprofen in standard aluminium pans. Underlying scan rate of $1^{\circ}\text{C min}^{-1}$ with a modulation amplitude of $\pm 0.265^{\circ}\text{C}$ and a period of 100 seconds. The signals have been offset for clarity .....	108
<b>Figure 3.5:</b> MTDSC reversing heat flow signal (A) and non-reversing heat flow signal (B) of ibuprofen in standard aluminium pans. Underlying scan rate of $1^{\circ}\text{C min}^{-1}$ with a modulation amplitude of $\pm 0.265^{\circ}\text{C}$ and a period of 100 seconds. Insert showing magnification of associated glass transition temperature (A).....	109
<b>Figure 3.6:</b> SEM image of crystalline ibuprofen.....	110
<b>Figure 3.7:</b> PXRD diffractogram of crystalline ibuprofen.....	110
<b>Figure 3.8:</b> ATR-FTIR spectrum of crystalline ibuprofen.....	111
<b>Figure 3.9:</b> TGA weight loss profile of Eudragit RS PO heated at $10^{\circ}\text{C min}^{-1}$ to $300^{\circ}\text{C}$ .....	112

<b>Figure 3.10:</b> Heat flow signal of Eudragit RS PO heated at $10^{\circ}\text{C min}^{-1}$ in standard aluminium pans .....	113
<b>Figure 3.11:</b> Modulation heat flow signal over the reversing heat flow signal passing through Eudragit RS PO glass transition temperature. Underlying scan rate of $2^{\circ}\text{C min}^{-1}$ with a modulation amplitude of $\pm 0.212^{\circ}\text{C}$ and a period of 40 seconds .....	114
<b>Figure 3.12:</b> MTDSC heating scan of Eudragit RS PO in standard aluminium pans. Underlying scan rate of $2^{\circ}\text{C min}^{-1}$ with a modulation amplitude of $\pm 0.212^{\circ}\text{C}$ and a period of 40 seconds. The signals have been offset for clarity .....	115
<b>Figure 3.13:</b> MTDSC reversing heat flow signal of Eudragit RS PO in standard aluminium pans. Underlying scan rate of $1^{\circ}\text{C min}^{-1}$ with a modulation amplitude of $\pm 0.265^{\circ}\text{C}$ and a period of 100 seconds .....	115
<b>Figure 3.14:</b> SEM image of amorphous Eudragit RS PO polymer .....	116
<b>Figure 3.15:</b> PXRD diffractogram of Eudragit RS PO .....	116
<b>Figure 3.16:</b> ATR-FTIR spectrum of Eudragit RS PO .....	117
<b>Figure 3.17:</b> TGA weight loss profile of sucrose heated at $10^{\circ}\text{C min}^{-1}$ to $300^{\circ}\text{C}$ ...	118
<b>Figure 3.18:</b> MTDSC heating scan of sucrose in standard aluminium pans. Underlying scan rate of $1^{\circ}\text{C min}^{-1}$ with a modulation amplitude of $\pm 0.265^{\circ}\text{C}$ and a period of 100 seconds. The signals have been offset for clarity .....	118
<b>Figure 3.19:</b> SEM image of crystalline sucrose .....	119
<b>Figure 3.20:</b> PXRD diffractogram of crystalline sucrose .....	119
<b>Figure 3.21:</b> ATR-FTIR spectrum of crystalline sucrose .....	120
<b>Figure 3.22:</b> TGA weight loss profile of methylcellulose heated at $10^{\circ}\text{C min}^{-1}$ to $300^{\circ}\text{C}$ .....	121
<b>Figure 3.23:</b> MTDSC heating scan of methylcellulose in standard aluminium pans. Underlying scan rate of $1^{\circ}\text{C min}^{-1}$ with a modulation amplitude of $\pm 0.265^{\circ}\text{C}$ and a period of 100 seconds. The signals have been offset for clarity .....	122
<b>Figure 3.24:</b> SEM image of methylcellulose .....	123
<b>Figure 3.25:</b> PXRD diffractogram of methylcellulose .....	123
<b>Figure 3.26:</b> ATR-FTIR spectrum of methylcellulose .....	124
<b>Figure 3.27:</b> TGA weight loss profile of Xantural®75 heated at $10^{\circ}\text{C min}^{-1}$ to $300^{\circ}\text{C}$ .....	125
<b>Figure 3.28:</b> MTDSC heating scan of Xantural®75 in standard aluminium pans. Underlying scan rate of $1^{\circ}\text{C min}^{-1}$ with a modulation amplitude of $\pm 0.265^{\circ}\text{C}$ and a period of 100 seconds. The signals have been offset for clarity .....	125
<b>Figure 3.29:</b> SEM image of Xantural®75 .....	126
<b>Figure 3.30:</b> PXRD diffractogram of Xantural®75 .....	126
<b>Figure 3.31:</b> ATR-FTIR spectrum of Xantural® 75 .....	127
<b>Figure 3.32:</b> TGA weight loss profile of Pluronic® F127 heated at $10^{\circ}\text{C min}^{-1}$ to $300^{\circ}\text{C}$ .....	128

<b>Figure 3.33:</b> MTDSC heating scan of Pluronic® F127 in standard aluminium pans. Underlying scan rate of $1^{\circ}\text{C min}^{-1}$ with a modulation amplitude of $\pm 0.265^{\circ}\text{C}$ and a period of 100 seconds. Inset showing magnification of predicted glass transition temperature. The signals have been offset for clarity .....	129
<b>Figure 3.34:</b> SEM image of Pluronic® F127 .....	130
<b>Figure 3.35:</b> PXRD diffractogram of Pluronic® F127 .....	130
<b>Figure 3.36:</b> ATR-FTIR spectrum of Pluronic® F127 .....	131
<b>Figure 3.37:</b> TGA weight loss profile of Gelucire 44/14 heated at $10^{\circ}\text{C min}^{-1}$ to $300^{\circ}\text{C}$ .....	132
<b>Figure 3.38:</b> MTDSC heating scan of Gelucire 44/14 in standard aluminium pans. Underlying scan rate of $1^{\circ}\text{C min}^{-1}$ with a modulation amplitude of $\pm 0.265^{\circ}\text{C}$ and a period of 100 seconds. The signals have been offset for clarity .....	132
<b>Figure 3.39:</b> PXRD diffractogram of Gelucire 44/14 .....	133
<b>Figure 3.40:</b> ATR-FTIR spectrum of Gelucire 44/14 .....	134
<b>Figure 4.1:</b> TGA weight loss profiles of ibuprofen-Eudragit RS PO physical mixes at different drug loadings (w/w %) .....	142
<b>Figure 4.2:</b> Total weight loss percentages of ibuprofen-Eudragit RS PO physical mixes with different drug loadings (w/w %) measured at $100^{\circ}\text{C}$ for four minutes using TGA.....	142
<b>Figure 4.3:</b> Exemplary DSC thermograms (heating rate of $1^{\circ}\text{C min}^{-1}$ ) of ibuprofen-Eudragit RS PO physical mixtures compared to the pure ibuprofen (A). Extrapolated onset of melting of ibuprofen as a function of volume fraction of Eudragit RS PO (Each data point represents the mean $\pm$ S.D. of three measurements), measured at a scan rate of $1^{\circ}\text{C min}^{-1}$ (B).....	146
<b>Figure 4.4:</b> Estimation of Flory-Huggins interaction parameter between ibuprofen and Eudragit RS PO based on Eq. (4.5). Each data point represents the mean $\pm$ S.D. of three measurements.....	147
<b>Figure 4.5:</b> Photographs of freshly prepared hot melt extruded ibuprofen in Eudragit RS PO produced at different drug loadings between 1-40 % (w/w).....	149
<b>Figure 4.6:</b> Variation of the observed torque values during hot melt extrusion as a function of changing ibuprofen loadings (w/w %) in Eudragit RS PO. Each data point represents the mean $\pm$ S.D. of three observations .....	149
<b>Figure 4.7:</b> MTDSC reversing heat flow signals of ibuprofen-Eudragit RS PO extrudates with different drug loadings (w/w %) in standard aluminium pans. Underlying scan rate of $1^{\circ}\text{C min}^{-1}$ with a modulation amplitude of $\pm 0.265^{\circ}\text{C}$ and a period of 100 seconds. Arrows indicate the assigned Mid-point glass transition temperatures .....	150

<b>Figure 4.8:</b> MTDSC heating scan of hot melt extruded 40% (w/w) ibuprofen in Eudragit RS PO in standard aluminium pans. Underlying scan rate of $1^{\circ}\text{C min}^{-1}$ with a modulation amplitude of $\pm 0.265^{\circ}\text{C}$ and a period of 100 seconds.....	151
<b>Figure 4.9:</b> Theoretical glass transition temperature values predicted by G-T equation of the ibuprofen-Eudragit RS PO mixes in comparison to the experimental values obtained from reversing heat flow signals of the MTDSC measurements ( $1^{\circ}\text{C min}^{-1}$ ) of their equivalent hot melt extruded systems (Figure 4.7 and 4.8). ....	152
<b>Figure 4.10:</b> Analysis of the ibuprofen-Eudragit RS PO system according to the G-T Equation (4.9). Theoretical glass transition temperatures of these systems ( $T_{g_{\text{mix}}}$ ) were predicted according to G-T model whereas the observed $T_{g_{\text{mix}}}$ were obtained from reversing heat flow signals of the MTDSC measurements at $1^{\circ}\text{C/min}$ of their equivalent hot melt extruded systems (Figure 4.7 and 4.8 ) .....	154
<b>Figure 4.11:</b> PXRD diffractograms of ibuprofen, Eudragit RS PO, physical mixtures of ibuprofen-Eudragit RS PO systems at different drug loadings (w/w%) (A) and fresh hot melt extruded systems equivalent to the studied physical mixes (B).....	155
<b>Figure 4.12:</b> SEM micrographs illustrating the surface morphologies of fresh hot melt extruded ibuprofen in Eudragit RS PO (I) at different drug loadings (A-F), whereby A = 1%(w/w), B = 5%(w/w), C = 10%(w/w), D = 15% (w/w), E = 20%(w/w), F = 25 % (w/w), G = 30 %(w/w), H =35 %(w/w) and I = 40 %(w/w)	156
<b>Figure 4.12 (Contd.):</b> SEM micrographs illustrating the cross sections of fresh hot melt extruded ibuprofen in Eudragit RS PO (II) at different drug loadings (A-F), whereby A = 1%(w/w), B = 5%(w/w), C = 10%(w/w), D = 15% (w/w), E = 20%(w/w), F = 25 % (w/w), G = 30 %(w/w), H =35 %(w/w) and I = 40 %(w/w)	157
<b>Figure 4.13:</b> Amorphous ibuprofen production using cDSC method. Highlighted green cycle represents: (I) first cycle of the heating at $10^{\circ}\text{C/min}$ , (II) second cycle of rapid cooling (quenching) at $20^{\circ}\text{C/min}$ and (III) third cycle of reheating at $10^{\circ}\text{C/min}$ .....	159
<b>Figure 4.14:</b> Reference ATR-FTIR spectra of the crystalline, amorphous ibuprofen (A) and Eudragit RS PO (B) .....	160
<b>Figure 4.15:</b> ATR-FTIR spectra of ibuprofen-Eudragit RS PO physical mixtures at different drug loadings (w/w %) (A) and their corresponding fresh hot melt extruded systems (B). Absorption intensities of these spectra vary. Used “marker” region for crystalline ibuprofen is enclosed in orange rectangle .....	162
<b>Figure 4.16:</b> MTDSC reversing heat flow signals of ibuprofen-Eudragit RS PO extrudates with different drug loadings (w/w%) after ageing for one month at 0%RH/ $25^{\circ}\text{C}$ . Underlying scan rate of $1^{\circ}\text{C min}^{-1}$ with a modulation amplitude of $\pm 0.265^{\circ}\text{C}$ and a period of 100 seconds. Arrows indicate the assigned Mid-point glass transition temperatures.....	164

<b>Figure 4.17:</b> Representative MTDSC heat flow signals (total and reversing) of ibuprofen-Eudragit RS PO extrudate at 40% (w/w) drug loading measured for fresh samples and after ageing for one month at 0%RH/25°C. Underlying scan rate of 1°C min <sup>-1</sup> with a modulation amplitude of ±0.265°C and a period of 100 seconds .....	164
<b>Figure 4.18:</b> Comparison between glass transition temperatures (Mid-point T <sub>g</sub> ) of the fresh samples and samples stored for one month at 0%RH/25°C of the hot melt extruded ibuprofen in Eudragit RS PO systems at different drug loadings (w/w%). T <sub>g</sub> values were obtained from reversing heat flow signals of the MTDSC measurements at 1°C/min. Each data point represents the mean±S.D. of three measurements.....	165
<b>Figure 4.19:</b> PXRD diffractograms of hot melt extruded ibuprofen-Eudragit RS PO systems at different drug loadings (w/w%) after storage for one month at 0% RH/25°C.....	166
<b>Figure 4.20:</b> SEM images of the surface (left side) and cross section (right side) of hot melt extruded ibuprofen in Eudragit RS PO at 35% (w/w) drug loading after ageing for one month at 0%RH/25°C.....	167
<b>Figure 4.21:</b> ATR-FTIR spectra of surface and cross section of ibuprofen-Eudragit RS PO extrudate at 35% (w/w) drug loading aged for one month at 0%RH/25°C. Used “marker” region for crystalline ibuprofen is enclosed in orange rectangle ....	167
<b>Figure 4.22:</b> MTDSC reversing heat flow signals of hot melt extruded ibuprofen-Eudragit RS PO systems at 10% (w/w) drug loading (A) and 20% (w/w) drug loading (B), examined on 0 day (fresh) and after 10, 20, 30 days of storage at 60% RH/ 25°C, measured at 1°C/min underlying heating rate with a modulation amplitude of ±0.265°C and a period of 100 seconds .....	169
<b>Figure 4.22 (Contd.):</b> MTDSC reversing heat flow signals of hot melt extruded ibuprofen-Eudragit RS PO systems at 30% (w/w) drug loading (C), examined on 0 day (fresh) and after 10, 20, 30 days of storage at 60% RH/ 25°C, measured at 1°C/min underlying heating rate with a modulation amplitude of ±0.265°C and a period of 100 seconds .....	170
<b>Figure 4.23:</b> TGA weight loss profiles of hot melt extruded ibuprofen-Eudragit RS PO systems at different drug loadings (w/w %) after ageing for one month at 60%RH/25°C.....	170
<b>Figure 4.24:</b> PXRD diffractograms of hot melt extruded ibuprofen-Eudragit RS PO systems at different drug loadings of: (A) 10% (w/w), (B) 20% (w/w) and (C) 30% (w/w), examined on 0 day (Fresh) and after 10, 20, 30 days of storage at 60% RH/ 25°C.....	172
<b>Figure 4.25:</b> SEM images of the surfaces (left side) and cross sections (right side) of hot melt extruded ibuprofen in Eudragit RS PO at different drug loadings (w/w %) after ageing for one month at 60%RH/25°C .....	173

<b>Figure 4.26:</b> Fragility plots of fresh hot melt extruded ibuprofen-Eudragit RS PO films at drug loading of: (A) 10 % (w/w), (B) 20 % (w/w) and (C) 30% (w/w) .....	175
<b>Figure 5.1:</b> Modified dissolution apparatus for characterising <i>in vitro</i> release of the hot melt extruded films .....	180
<b>Figure 5.2:</b> Copley dissolution bath .....	181
<b>Figure 5.3:</b> Chromatogram of ibuprofen in acetonitrile: deionized water: phosphoric acid (50:50:1, (v/v)) mobile phase at flow rate of 1ml/min detected at 225 nm .....	184
<b>Figure 5.4:</b> Calibration curve of ibuprofen in phosphate buffer solution (pH 7.2) measured at 223 nm .....	185
<b>Figure 5.5:</b> Calibration curve of ibuprofen by HPLC measured at 225 nm, flow rate of 1ml/min and using acetonitrile: deionized water: phosphoric acid (50:50:1, (v/v)) mobile phase .....	185
<b>Figure 5.6:</b> A 6-station PermeGear Franz Cell diffusion system with a V-Series magnetic stirrer .....	187
<b>Figure 5.7:</b> Compartments of a 9mm jacketed vertical Franz Cell (PermeGear) with a 5ml receptor volume.....	187
<b>Figure 5.8:</b> Calibration curve of ibuprofen in diethyl ether measured at 222 nm...	189
<b>Figure 5.9:</b> Comparative release profiles of ibuprofen from hot melt extruded films at different drug loadings in phosphate buffer solution (pH 7.2) at 37.0±0.1°C. Each data point represents the mean±S.D. of three measurements.....	194
<b>Figure 5.10:</b> Comparative dissolution profiles of ibuprofen from crystalline drug, physical mixture and Eudragit RS PO-based extrudate at 10% w/w drug load in phosphate buffer solution (pH 7.2) at 37.0±0.1°C. Each data point represents the mean±S.D. of three measurements.....	195
<b>Figure 5.11:</b> Comparative release profiles of ibuprofen from Eudragit RS PO extruded films at 30% w/w drug load tested on freshly basis (Fresh) and after ageing for one month at 0%RH/25°C (Aged) in phosphate buffer solution (pH 7.2) at 37.0±0.1°C. Each data point represents the mean±S.D. of three measurements.....	196
<b>Figure 5.12:</b> Diffusion profile of ibuprofen from saturated solutions in phosphate buffer solution (pH=7.2) tested approximately at 32°C and permeated across silicone membrane into phosphate buffer solution (pH=7.2) at 37°C. Each data point represents the mean±S.D. of three measurements.....	197
<b>Figure 5.13:</b> Comparative diffusion profiles of ibuprofen from hot melt extruded films with Eudragit RS PO tested approximately at 32°C and permeated across silicone membrane into phosphate buffer solution (pH=7.2) at 37°C. Each data point represents the mean±S.D. of no less than three measurements.....	198
<b>Figure 5.14:</b> Comparative diffusion profiles of ibuprofen from Eudragit RS PO-based extrudates at 30% (w/w) drug loading (fresh vs. aged samples stored for one	

month at 0%RH/25°C), tested approximately at 32°C and permeated across silicone membrane into phosphate buffer solution (pH=7.2) at 37°C. ....	199
<b>Figure 6.1:</b> MTDSC heating scans of different hot melt extruded films (see Table 6.3) in standard aluminium pans. Underlying scan rate of 1°C min <sup>-1</sup> with a modulation amplitude of ±0.265°C and a period of 100 seconds. The traces have been offset for clarity .....	210
<b>Figure 6.2:</b> MTDSC heating scans of different hot melt extruded films containing methylcellulose, Eudragit RS PO and ibuprofen (see Table 6.3) in standard aluminium pans. Underlying scan rate of 1°C min <sup>-1</sup> with a modulation amplitude of ±0.265°C and a period of 100 seconds. The traces have been offset for clarity .....	212
<b>Figure 6.3:</b> MTDSC heating scans of different hot melt extruded films containing Xantural® 75, Eudragit RS PO and ibuprofen (see Table 6.3) in standard aluminium pans. Underlying scan rate of 1°C min <sup>-1</sup> with a modulation amplitude of ±0.265°C and a period of 100 seconds. The traces have been offset for clarity.....	213
<b>Figure 6.4:</b> MTDSC heating scan of FM7 hot melt extruded film containing Pluronic® F127 Eudragit RS PO ibuprofen ratio of (1:6:3) in standard aluminium pans. Underlying scan rate of 1°C min <sup>-1</sup> with a modulation amplitude of ±0.265°C and a period of 100 seconds. The traces have been offset for clarity.....	214
<b>Figure 6.5:</b> MTDSC total heat flow signal of the FM7 physical mix Pluronic® F127 Eudragit RS PO ibuprofen ratio of (1:6:3) in standard aluminium pans. Underlying scan rate of 1°C min <sup>-1</sup> with a modulation amplitude of ±0.265°C and a period of 100 seconds.....	215
<b>Figure 6.6:</b> MTDSC heating scans of different hot melt extruded films containing Gelucire 44/14, Eudragit RS PO and ibuprofen (see Table 6.3) in standard aluminium pans. Underlying scan rate of 1°C min <sup>-1</sup> with a modulation amplitude of ±0.265°C and a period of 100 seconds. The traces have been offset for clarity.....	216
<b>Figure 6.7:</b> X-ray powder diffraction profiles of raw materials, physical mixture (sucrose, Eudragit RS PO and ibuprofen) and the corresponding hot melt extruded films of FM1 composition.....	218
<b>Figure 6.8:</b> X-ray powder diffraction profiles of raw materials, physical mixtures (methylcellulose, Eudragit RS PO and ibuprofen) and the corresponding hot melt extruded films of FM3 (low level of methylcellulose) and FM4 (high level of methylcellulose) compositions.....	219
<b>Figure 6.9:</b> X-ray powder diffraction profiles of raw materials, physical mixtures (Xantural® 75, Eudragit RS PO and ibuprofen) and the corresponding hot melt extruded films of FM5 and FM6 compositions.....	219
<b>Figure 6.10:</b> X-ray powder diffraction profiles of raw materials, physical mixture (Pluronic® F127, Eudragit RS PO and ibuprofen) and the corresponding hot melt extruded films of FM7 composition.....	220



<b>Figure 6.11:</b> X-ray powder diffraction profiles of raw materials, physical mixtures (Gelucire 44/14, Eudragit RS PO and ibuprofen) and the corresponding hot melt extruded films of FM9 (low level of Gelucire 44/14) and FM10 (high level of Gelucire 44/14) compositions .....	221
<b>Figure 6.12:</b> SEM morphological features of the surfaces (column A) and cross sections (column B) obtained for different fresh extruded films loaded with ibuprofen (see text or Table 6.3 for their compositions) .....	223
<b>Figure 6.13:</b> SEM images of the surfaces (column A) and cross sections (column B) for fresh FM9 and FM10 extruded films. Column C: photographs illustrating the deformations of the tested films post SEM scanning .....	224
<b>Figure 6.14:</b> Ibuprofen release profiles from hot melt extruded films of FM0 (Eudragit RS PO as a carrier) and FM1 (Eudragit RS PO and sucrose as carriers) formulations in phosphate buffer solution (pH=7.2) at $37.0\pm0.1^{\circ}\text{C}$ . Each data point represents the mean $\pm$ S.D. of three measurements.....	226
<b>Figure 6.15:</b> Ibuprofen release profiles from hot melt extruded films of FM0 (Eudragit RS PO as a carrier), FM3 (10% (w/w) methylcellulose and 60% (w/w) Eudragit RS PO as carriers) and FM4 (60% (w/w) methylcellulose and 10% (w/w) Eudragit RS PO as carriers) formulations in phosphate buffer solution (pH=7.2) at $37.0\pm0.1^{\circ}\text{C}$ . Each data point represents the mean $\pm$ S.D. of three measurements.....	227
<b>Figure 6.16:</b> Ibuprofen release profiles from hot melt extruded films of FM0 (Eudragit RS PO as a carrier), FM5 (10% (w/w) xanthan gum and 60% (w/w) Eudragit RS PO as carriers) and FM6 (60% (w/w) xanthan gum and 10% (w/w) Eudragit RS PO as carriers) formulations in phosphate buffer solution (pH=7.2) at $37.0\pm0.1^{\circ}\text{C}$ . Each data point represents the mean $\pm$ S.D. of three measurements.....	228
<b>Figure 6.17:</b> Ibuprofen release profiles from hot melt extruded films of FM0 (Eudragit RS PO as a carrier), FM-I (2.5% (w/w) xanthan gum and 67.5% (w/w) Eudragit RS PO), FM-II (5% (w/w) xanthan gum and 65% (w/w) Eudragit RS PO) and FM5 (10% (w/w) xanthan gum and 60% (w/w) Eudragit RS PO) formulations in phosphate buffer solution (pH=7.2) at $37.0\pm0.1^{\circ}\text{C}$ . Each data point represents the mean $\pm$ S.D. of three measurements.....	229
<b>Figure 6.18:</b> Photographs of hot melt extruded films of ibuprofen with Eudragit RS PO and different proportions of xanthan gum after 24 hours of dissolution in phosphate buffer solution (pH=7.2) at $37\pm0.1^{\circ}\text{C}$ .....	230
<b>Figure 6.19:</b> Ibuprofen release profiles from hot melt extruded films of FM0 (Eudragit RS PO as a carrier) and FM7 (Eudragit RS PO and Pluronic® F127 as carriers) formulations in phosphate buffer solution (pH=7.2) at $37.0\pm0.1^{\circ}\text{C}$ . Each data point represents the mean $\pm$ S.D. of three measurements.....	230
<b>Figure 6.20:</b> Ibuprofen release profiles from hot melt extruded films of FM0 (Eudragit RS PO as a carrier), FM9 (10% (w/w) Gelucire 44/14 and 60% (w/w)	

Eudragit RS PO as carriers) and FM10 (20% (w/w) Gelucire 44/14 and 50% (w/w) Eudragit RS PO as carriers) formulations in phosphate buffer solution (pH=7.2) at  $37.0 \pm 0.1^\circ\text{C}$ . Each data point represents the mean  $\pm$  S.D. of three measurements..... 231

**Figure 6.21:** Comparative diffusion profiles of ibuprofen from (A) FM0 (Eudragit RS PO as a carrier) and FM5 (10% (w/w) xanthan gum and 60% (w/w) Eudragit RS PO as carriers) extruded films and (B) from FM-I (2.5% xanthan gum), FM-II (5% xanthan gum) and FM5 films, tested approximately at  $32^\circ\text{C}$  and permeated across silicone membrane into phosphate buffer solution (pH=7.2) at  $37^\circ\text{C}$ . Each data point represents the mean  $\pm$  S.D. of no less than three measurements..... 235

**Figure 6.22:** Ibuprofen diffusion profiles from hot melt extruded films of FM0, FM7, FM9 and FM10 formulations tested approximately at  $32^\circ\text{C}$  and permeated across silicone membranes into phosphate buffer solution (pH=7.2) at  $37^\circ\text{C}$ . Each data point represents the mean  $\pm$  S.D. of no less than three measurements..... 236

**Figure 6.23:** Observed melting endotherm in the MTDSC total heat flow signals of FM5 (10% (w/w) xanthan gum and 60% (w/w) Eudragit RS PO as carriers) extruded film examined before (fresh) and after the permeation experiment. Underlying scan rate of  $1^\circ\text{C min}^{-1}$  with a modulation amplitude of  $\pm 0.265^\circ\text{C}$  and a period of 100 seconds..... 239

**Figure 6.24:** Observed melting endotherms in the MTDSC total heat flow signals of FM7 (10% (w/w) Pluronic® F127 and 60% (w/w) Eudragit RS PO as carriers) extruded film before (fresh) and after the permeation experiment in comparison to its equivalent physical mixture. ‘A’ and ‘B’ symbols denoted for peaks related to ibuprofen and Pluronic® F127, respectively. Underlying scan rate of  $1^\circ\text{C min}^{-1}$  with a modulation amplitude of  $\pm 0.265^\circ\text{C}$  and a period of 100 seconds..... 240

**Figure 6.25:** Observed melting endotherms in the MTDSC total heat flow signals of FM9 (10% (w/w) Gelucire 44/14 and 60 % (w/w) Eudragit RS PO as carriers) extruded film examined before (fresh) and after the permeation experiment in comparison to its equivalent physical mixture. ‘A’ and ‘B’ symbols denoted for peaks related to ibuprofen and Gelucire 44/14, respectively. Underlying scan rate of  $1^\circ\text{C min}^{-1}$  with a modulation amplitude of  $\pm 0.265^\circ\text{C}$  and a period of 100 seconds . 241

**Figure 6.26:** Observed melting endotherms in the MTDSC total heat flow signals of FM10 (20% (w/w) Gelucire 44/14 and 50% (w/w) Eudragit RS PO as carriers) extruded film before (fresh) and after the permeation experiment in comparison to its equivalent physical mixture. ‘A’ symbol denoted for peak related to ibuprofen whereas ‘B-I’ and ‘B-II’ symbols denoted for peaks related to Gelucire 44/14. Underlying scan rate of  $1^\circ\text{C min}^{-1}$  with a modulation amplitude of  $\pm 0.265^\circ\text{C}$  and a period of 100 seconds ..... 242

**Figure 6.27:** Observed melting endotherm in the MTDSC total heat flow signals of the control extruded FM0 film (Eudragit RS PO as a carrier) examined before (fresh)

and after the permeation experiment. Underlying scan rate of  $1^{\circ}\text{C min}^{-1}$  with a modulation amplitude of  $\pm 0.265^{\circ}\text{C}$  and a period of 100 seconds ..... 243

**Figure 6.28:** PermeGear Franz Cell diffusion system includes six jacketed Franz cells; securely located to a stirrer. The receptor chambers were filled with phosphate buffer solution (pH=7.2) maintained at  $37^{\circ}\text{C}$  and covered with silicone membranes. Humidity indicator cards were mounted on the top of each donor chamber and all openings were sealed with double layers of Parafilm® ..... 246

**Figure 6.29:** Ibuprofen diffusion profiles from hot melt extruded films of (A) FM5 (60% (w/w) Eudragit RS PO and 10% (w/w) xanthan gum as carriers) tested approximately at  $32^{\circ}\text{C}$  and permeated across silicone membrane into phosphate buffer solution (pH=7.2) at  $37^{\circ}\text{C}$ . Control: samples without hydration. Test 1: each sample was placed in 0.3 ml of PBS (pH=7.2) in the donor chamber of the Franz cells. Test 2: samples were moistened at 95%RH/ $25^{\circ}\text{C}$  for three hours prior testing in the Franz cells. Each data point represents the mean $\pm$ S.D. of no less than three measurements ..... 247

**Figure 6.29 (Contd.):** Ibuprofen diffusion profiles from hot melt extruded films of (B) FM9 (60% (w/w) Eudragit RS PO and 10% (w/w) Gelucire 44/14 as carriers) and (C) FM10 (50% (w/w) Eudragit RS PO and 20% (w/w) Gelucire 44/14 as carriers) tested approximately at  $32^{\circ}\text{C}$  and permeated across silicone membrane into phosphate buffer solution (pH=7.2) at  $37^{\circ}\text{C}$ . Control: samples without hydration. Test 1: each sample was placed in 0.3 ml of PBS (pH=7.2) in the donor chamber of the Franz cells. Test 2: samples were moistened at 95%RH/ $25^{\circ}\text{C}$  for three hours prior testing in the Franz cells. Each data point represents the mean $\pm$ S.D. of no less than three measurements ..... 248

**Figure 6.30:** Summary of the measured percentage water contents of different hot melt extruded films (see text for their compositions) determined by TGA on freshly basis immediately after extrusion (before treatment) and after incubation at 95%RH/ $25^{\circ}\text{C}$  for three hours in the DVS (after treatment) ..... 249

**Figure 6.31:** The time corresponding to 80% or higher of the cumulative percentage permeation of the ibuprofen from hot melt extruded films of Eudragit RS PO-based films containing Xantural® 75 (FM5 composition), Gelucire 44/14 (FM9 and FM10 compositions) tested approximately at  $32^{\circ}\text{C}$  and permeated across silicone membrane into phosphate buffer solution (pH=7.2) at  $37^{\circ}\text{C}$ . Test 1: each sample was placed in 0.3 ml of PBS (pH=7.2) in the donor chamber of the Franz cells. Test 2: samples were moistened at 95%RH/ $25^{\circ}\text{C}$  for three hours prior testing in the Franz cells .... 249

**Figure 6.32:** Representative photographs of shape and consistency changes of hot melt extruded films removed from Franz cells post testing (top row) and exposed to 0.3 ml PBS (pH=7.2) at  $32^{\circ}\text{C}$  to imitate Test 1 condition over three hours and under glass slides (bottom row). (I) FM5 films (10% (w/w) xanthan gum) after Test 1 and

Test 2. (II) FM9 films after Test 1 and Test 2 or FM10 after Test 2. (III) FM9 films (10% (w/w) Gelucire 44/14). (IV) liquid-like emulsion of hydrated FM10 films (20% (w/w) Gelucire 44/14). Images of these films before the tests were captured in Table 6.2.....	253
<b>Figure 6.33:</b> Variation of the percent relative humidity (%RH) over 120 hours inside the donor chambers of Franz Cell diffusion system encompasses receptor chambers covered with silicone membranes and filled with phosphate buffer solution (pH=7.2) maintained at 37°C. Each measurement recorded from humidity indicator card represents the mean±S.D. of six measurements.....	254
<b>Figure 6.34:</b> Relative humidity values as recorded from Franz cells (from Figure 6.33) at the time point corresponding to the maximum total permeation from formulations of FM5 (10% (w/w) xanthan gum), FM9 (10% (w/w) Gelucire 44/14) and FM10 (20% (w/w) Gelucire 44/14), tested at different hydration levels .....	255
<b>Figure 6.35:</b> Ibuprofen diffusion profiles from hot melt extruded Eudragit RS PO-based films which contain 10% (w/w) and 20% (w/w) Gelucire 44/14 in FM9 and FM10 systems, respectively, tested at approximately 32°C and permeated across silicone membrane into phosphate buffer solution (pH=7.2) at 37°C. Each sample was hydrated with 0.14 ml of PBS (pH=7.2) in the donor chamber of the Franz cells. Each data point represents the mean±S.D. of no less than three measurements .....	257
<b>Figure 6.36:</b> MTDSC reversing heat flow signals for fresh hot melt extruded FM9 (10% (w/w) Gelucire 44/14) removed at different times from the permeation experiment in the Franz-type diffusion cells. The tested samples were hydrated with 0.14 ml of PBS (pH=7.2) in the donor chambers of the Franz cells at approximately 32°C. Underlying scan rate of 1°C min <sup>-1</sup> with a modulation amplitude of ±0.265°C and a period of 100 seconds .....	259
<b>Figure 6.37:</b> MTDSC reversing heat flow signals for fresh hot melt extruded FM10 (20% (w/w) Gelucire 44/14) films removed at different times from the permeation experiment in the Franz-type diffusion cells. The tested samples were hydrated with 0.14 ml of PBS (pH=7.2) in the donor chambers of the Franz cells at approximately 32°C. Underlying scan rate of 1°C min <sup>-1</sup> with a modulation amplitude of ±0.265°C and a period of 100 seconds .....	260
<b>Figure 7.1:</b> Heat flow signal for Gelucire 44/14 and FM-A physical mixture heated at 10°C min <sup>-1</sup> in standard aluminium pans. See Table 7.1 for composition .....	267
<b>Figure 7.2:</b> Heat flow signal for Gelucire 44/14 and FM-B physical mixture heated at 10°C min <sup>-1</sup> in standard aluminium pans. See Table 7.1 for composition .....	268
<b>Figure 7.3:</b> MTDSC heating scans (total and reversing heat flow signals) of Gelucire 44/14 (closed circles) and FM-A physical mixture (open squares) in standard aluminium pans. Underlying scan rate of 1°C min <sup>-1</sup> with a modulation amplitude of ±0.265°C and a period of 100 seconds.....	268

<b>Figure 7.4:</b> MTDSC heating scans (total and reversing heat flow signals) of Gelucire 44/14 (closed circles) and FM-B physical mixture (open squares) in standard aluminium pans. Underlying scan rate of $1^{\circ}\text{C min}^{-1}$ with a modulation amplitude of $\pm 0.265^{\circ}\text{C}$ and a period of 100 seconds.....	269
<b>Figure 7.5:</b> Heat flow signal for FM-A hot melt extruded film (Gelucire 44/14 Eudragit RS PO ratio of 1:6) heated at $10^{\circ}\text{C min}^{-1}$ in standard aluminium pans .....	272
<b>Figure 7.6:</b> Heat flow signal for FM-A hot melt extruded film (Gelucire 44/14 Eudragit RS PO ratio of 1:6) heated at $1^{\circ}\text{C min}^{-1}$ in standard aluminium pan.....	273
<b>Figure 7.7:</b> MTDSC heating scans of FM-A hot melt extruded film (Gelucire 44/14 Eudragit RS PO ratio of 1:6) in standard aluminium pans. Underlying scan rate of $1^{\circ}\text{C min}^{-1}$ with a modulation amplitude of $\pm 0.265^{\circ}\text{C}$ and a period of 100 seconds .	274
<b>Figure 7.8:</b> Heat flow signal for FM-B hot melt extruded film (Gelucire 44/14 Eudragit RS PO ratio of 2:5) heated at $10^{\circ}\text{C min}^{-1}$ in standard aluminium pans .....	275
<b>Figure 7.9:</b> Heat flow signal for FM-B hot melt extruded film (Gelucire 44/14 Eudragit RS PO ratio of 2:5) heated at $1^{\circ}\text{C min}^{-1}$ in standard aluminium pans .....	275
<b>Figure 7.10:</b> MTDSC heating scans of FM-B hot melt extruded film (Gelucire 44/14 Eudragit RS PO ratio of 2:5) in standard aluminium pans. Underlying scan rate of $1^{\circ}\text{C min}^{-1}$ with a modulation amplitude of $\pm 0.265^{\circ}\text{C}$ and a period of 100 seconds .	276
<b>Figure 7.11:</b> X-ray powder diffraction profiles of the raw materials, physical mixtures and their corresponding hot melt extruded films of Gelucire 44/14 and Eudragit RS PO of FM-A (Gelucire 44/14 Eudragit RS PO ratio of 1:6) and FM-B (Gelucire 44/14 Eudragit RS PO ratio of 2:5) systems .....	277
<b>Figure 7.12:</b> Morphological features of the surface (A-I) and cross section (A-II) of the fresh extrudate of FM-A system (Gelucire 44/14 Eudragit RS PO ratio of 1:6)	278
<b>Figure 7.13:</b> Morphological features of the surface (B-I) and cross section (B-II) of the fresh extrudate of FM-B system (Gelucire 44/14 Eudragit RS PO ratio of 2:5)	279
<b>Figure 7.14:</b> MTDSC heating scans of Gelucire 44/14 in standard aluminium pans (A). Underlying scan rate of $1^{\circ}\text{C min}^{-1}$ with a modulation amplitude of $\pm 0.265^{\circ}\text{C}$ and a period of 100 seconds.....	280
<b>Figure 7.14 (Contd.):</b> MTDSC heating scans of Eudragit RS PO in standard aluminium pans (A). Underlying scan rate of $1^{\circ}\text{C min}^{-1}$ with a modulation amplitude of $\pm 0.265^{\circ}\text{C}$ and a period of 100 seconds .....	281
<b>Figure 7.15:</b> Overlay of superimposable ATR-FTIR spectra of the surface and cross section of hot melt extruded films of system FM-A (A) and system FM-B (B). See text for their compositions .....	283
<b>Figure 7.16:</b> Overlay of the ATR-FTIR spectra of the physical mixtures and corresponding hot melt extruded films of FM-A (Gelucire 44/14 Eudragit RS PO ratio of 1:6) system (A) and FM-B (Gelucire 44/14 Eudragit RS PO ratio of 2:5) system (B). See text for composition .....	285

**Figure 7.17:** Histograms of the integrated relative percentage areas of Eudragit RS PO (a) and Gelucire 44/14 (b), of the alkyl C-H group stretching ( $3172\text{--}2702\text{ cm}^{-1}$ ), C=O stretching of the ester groups ( $1857\text{--}1605\text{ cm}^{-1}$ ) and C-O stretch of alcohols (primary or secondary) of Gelucire 44/14 and C-CO-C stretching in Eudragit RS PO ( $1547\text{--}885\text{ cm}^{-1}$ ). Samples were examined as the following sets: Control (no thermal treatment). At the temperature of extrusion ( $120^{\circ}\text{C}$ ). The cooled samples to the room temperature after thermal treatment (solidified samples). Average values of three spectra of each set were calculated and S.D. error bars were estimated accordingly ..... 287

**Figure 7.18:** Histograms of the integrated relative percentage areas of FM-A system (1: 6 ratio of Gelucire 44/14: Eudragit RS PO), for both physical mixture (PM) and equivalent fresh extruded film. The alkyl C-H group stretching related to the region between  $3172$  and  $2702\text{ cm}^{-1}$ , C=O stretching of the ester groups ( $1857\text{--}1605\text{ cm}^{-1}$ ) and C-O stretch of alcohols (primary or secondary) of Gelucire 44/14 and C-CO-C stretching in Eudragit RS PO ( $1547\text{--}885\text{ cm}^{-1}$ ). Samples were examined as the following sets: Control (no thermal treatment). At the temperature of extrusion ( $120^{\circ}\text{C}$ ). The cooled samples after thermal treatment at the room temperature (solidified samples). Average values of three spectra of each set were calculated and S.D. error bars were estimated accordingly ..... 289

**Figure 7.19:** Histograms of the integrated relative percentage areas of FM-B system (2: 5 ratio of Gelucire 44/14: Eudragit RS PO), for both physical mixture (PM) and equivalent fresh extruded film. The alkyl C-H group stretching related to the region between  $3172\text{--}2702\text{ cm}^{-1}$ , C=O stretching of the ester groups ( $1857\text{--}1605\text{ cm}^{-1}$ ) and C-O stretch of alcohols (primary or secondary) of Gelucire 44/14 and C-CO-C stretching in Eudragit RS PO ( $1547\text{--}885\text{ cm}^{-1}$ ). Samples were examined as the following sets: Control (no thermal treatment). At the temperature of extrusion ( $120^{\circ}\text{C}$ ). The cooled samples after thermal treatment at the room temperature (solidified samples). Average values of three spectra of each set were calculated and S.D. error bars were estimated accordingly ..... 290

**Figure 7.20:** ATR-FTIR spectra of hot melt extruded films of (A) FM-A (Gelucire 44/14 Eudragit RS PO ratio of 1:6) system and (B) FM-B (Gelucire 44/14 Eudragit RS PO ratio of 2:5) system (absorption intensities of these spectra vary) ..... 292

**Figure 7.21:** ATR-FTIR spectra of (1) Eudragit RS PO-subtracted spectrum of physical mixture containing Eudragit RS PO Gelucire 44/14 in a ratio of 6:1, without thermal treatment (control), (2) molten Gelucire 44/14 at the extrusion temperature ( $120^{\circ}\text{C}$ ), (3) solidified Gelucire 44/14 after thermal treatment at extrusion temperature and (4) Eudragit RS PO-subtracted spectrum of extruded film containing Eudragit RS PO Gelucire 44/14 in a ratio of 6:1 (FM-A system) ..... 293

<b>Figure 7.22:</b> ATR-FTIR spectra of (1) Eudragit RS PO-subtracted spectrum of physical mixture containing Eudragit RS PO Gelucire 44/14 in a ratio of 5:2, without thermal treatment (control), (2) molten Gelucire 44/14 at the extrusion temperature (120°C), (3) solidified Gelucire 44/14 after thermal treatment at extrusion temperature and (4) Eudragit RS PO-subtracted spectrum of extruded film containing Eudragit RS PO Gelucire 44/14 in a ratio of 5:2 (FM-B system) .....	295
<b>Figure 7.23:</b> ATR-FTIR Eudragit RS PO-subtracted spectra of extruded films containing Eudragit RS PO Gelucire 44/14 in the ratios of 6:1 (FM-A system) and 5:2 (FM-B system) .....	296
<b>Figure 7.24:</b> Hot stage microscope images captured at specific temperatures for physical mixture of FM-A composition (Gelucire 44/14 Eudragit RS PO ratio of 1:6) while being heated at 5°C per minute .....	297
<b>Figure 7.25:</b> Hot stage microscope images captured at specific temperatures for physical mixture of FM-B composition (Gelucire 44/14 Eudragit RS PO ratio of 2:5) while being heated at 5°C per minute .....	298
<b>Figure 7.26:</b> Weight percent versus time signal for Gelucire 44/14 at 25°C with an RH ramp from 0 to 95% (A) .....	300
<b>Figure 7.26 (Contd.):</b> Weight percent versus time signal for Eudragit RS PO at 25°C with an RH ramp from 0 to 95% (B).....	301
<b>Figure 7.27:</b> Overlay of the moisture content of Gelucire 44/14 (open squares) and Eudragit RS PO (filled circles) according to the relative humidity at 25°C.....	301
<b>Figure 7.28:</b> Moisture uptake of Eudragit RS PO (A) and Gelucire 44/14 (B) expressed as percentage of weight change versus time, both tested at 95%RH/25°C. Samples were examined as the following sets: untreated (no thermal treatment), at the temperature of extrusion (120°C) followed by solidification at room temperature (treated) .....	303
<b>Figure 7.29:</b> Moisture uptake for the samples of FM-A (Gelucire 44/14 Eudragit RS PO ratio of 1:6) system (A) expressed as percentage of weight change versus time tested at 95%RH/25°C. Samples were examined as the following sets: untreated physical mixtures (filled circles), treated physical mixtures at the temperature of extrusion (120°C) followed by solidification at room temperature (open squares) and samples prepared <i>via</i> hot melt extrusion (filled stars).....	304
<b>Figure 7.29 (Contd.):</b> Moisture uptake for the samples of FM-B system (Gelucire 44/14 Eudragit RS PO ratio of 2:5) system (B) expressed as percentage of weight change versus time tested at 95%RH/25°C. Samples were examined as the following sets: untreated physical mixtures (filled circles), treated physical mixtures at the temperature of extrusion (120°C) followed by solidification at room temperature (open squares) and samples prepared <i>via</i> hot melt extrusion (filled stars) .....	305

<b>Figure 7.30:</b> Representative TGA weight loss profiles of (A) control extruded film while (B) for tested extruded films in dissolution bath and (C) for tested extruded films in Franz-type diffusion cells. All heated at $10^{\circ}\text{C min}^{-1}$ to $150^{\circ}\text{C}$ .....	309
<b>Figure 7.31:</b> Representative MTDSC profiles of tested FM-A (left) and FM-B (right) films in the dissolution experiment showing the dehydration (water-desorption) event in the non reversing and total heat flow signals. Underlying scan rate of $1^{\circ}\text{C min}^{-1}$ with a modulation amplitude of $\pm 0.265^{\circ}\text{C}$ and a period of 100 seconds.....	311
<b>Figure 7.32:</b> MTDSC reversing heat flow signals of fresh hot melt extruded (A) FM-A (Gelucire 44/14 Eudragit RS PO ratio of 1:6) and (B) FM-B (Gelucire 44/14 Eudragit RS PO ratio of 2:5) films examined after testing in the dissolution bath for 24 hours ( $t=24$ hrs), followed by drying at 0% relative humidity/ $25^{\circ}\text{C}$ for one week (0%RH/ $25^{\circ}\text{C}/1\text{wk}$ ) and compared to the controls of: fresh films ( $t=0$ hr) and after ageing for one week at the same storage conditions (0%RH/ $25^{\circ}\text{C}/1\text{wk}$ ). Underlying scan rate of $1^{\circ}\text{C min}^{-1}$ with a modulation amplitude of $\pm 0.265^{\circ}\text{C}$ and a period of 100 seconds.....	313
<b>Figure 7.33:</b> X-ray powder diffraction profiles of the raw materials, physical mixtures and their corresponding hot melt extruded films of Gelucire 44/14 Eudragit RS PO 1:6 ratio (FM-A composition, A) and 2:5 ratio (FM-B composition, B). The films were examined after testing in the dissolution bath for 24 hours ( $t=24$ hrs), followed by storage under dry conditions for one week at 0% relative humidity, $25^{\circ}\text{C}$ to allow drying (0%RH/ $25^{\circ}\text{C}/1\text{wk}$ ) and compared to the controls of fresh extruded films ( $t=0$ hr).....	315
<b>Figure 7.34:</b> SEM images of the surfaces (S) and cross sections (Cs) of FM-A extruded films after the dissolution testing ( $t=24$ hrs) represented by A series, followed by drying at 0%RH/ $25^{\circ}\text{C}$ for one week and shown in B series. Examples on the micro-cracks are enclosed by orange rectangles. See text for composition.....	317
<b>Figure 7.35:</b> SEM images of the surfaces (S) and cross sections (Cs) of FM-B extruded films after the dissolution testing ( $t=24$ hrs) represented by A series, followed by drying at 0%RH/ $25^{\circ}\text{C}$ for one week and shown in B series. (B-S-1) is an insert showing magnification of granules (dashed orange square) detected on the surface of FM-B extruded films after drying. Examples on the micro-cracks are enclosed by orange rectangles. See text for composition.....	319
<b>Figure 7.36:</b> MTDSC reversing heat flow signals of hot melt extruded FM-A (A) and FM-B (B) films after testing in the Franz-type diffusion cells at different times and compared to their respective controls ( $t=0$ hour). Underlying scan rate of $1^{\circ}\text{C min}^{-1}$ with a modulation amplitude of $\pm 0.265^{\circ}\text{C}$ and a period of 100 seconds. See text for composition.....	322



<b>Figure 7.37:</b> SEM images of the surfaces and cross sections of FM-A extruded films at different testing times using Franz-type diffusion cells. PLM images represent pattern of the tested surfaces with polarized light microscopy .....	324
<b>Figure 7.38:</b> SEM images of the surfaces and cross sections of FM-B extruded films at different testing times using Franz-type diffusion cells. PLM images represent pattern of the tested surfaces with polarized light microscopy .....	327
<b>Figure 7.39:</b> MTDSC reversing heat flow signals (A) for aged hot melt extruded FM-A films at different storage conditions for one month whereby (B) is showing representative MTDSC profile of samples stored at 75%RH/25°C with enlarged insert of the relaxation endotherm occurring simultaneously after the glass transition temperature and detected in the non-reversing heat flow signal. Underlying scan rate of 1°C min <sup>-1</sup> with a modulation amplitude of ±0.265°C and a period of 100 seconds .....	332
<b>Figure 7.40:</b> MTDSC reversing heat flow signals for aged hot melt extruded FM-B films at different storage conditions for one month. Underlying scan rate of 1°C min <sup>-1</sup> with a modulation amplitude of ±0.265°C and a period of 100 seconds.....	333
<b>Figure 7.41:</b> Weight change percent profiles at 75%RH humidity level versus temperature for the aged FM-A (Gelucire 44/14 Eudragit RS PO ratio of 1:6) and FM-B (Gelucire 44/14 Eudragit RS PO ratio of 2:5) systems under 0%RH/25°C for one month.....	335
<b>Figure 7.42:</b> Overlay of X-ray powder diffraction profiles of FM-A and FM-B extruded system aged for one month at 0%RH/25°C, 75%RH/25°C and 75%RH/40°C .....	336
<b>Figure 7.43:</b> SEM images of the surfaces and cross sections of FM-A extruded films at different storage conditions for one month. (B-I) is an insert showing magnification of granules (dashed orange square) detected on the surface of FM-A extruded films aged under 75%RH/25°C. Examples on the observed micro-cracks and granules (crystals) are enclosed by orange squares and blue circles, respectively .....	337
<b>Figure 7.44:</b> SEM images of the surfaces and cross sections of FM-B extruded films at different storage conditions for one month. (B-I) and (C-I) are inserts showing magnifications of granules (dashed orange square) detected on the surface of FM-B extruded films aged under 75%RH/25°C and 75%RH/40°C, respectively. Examples on the observed micro-cracks and granules (crystals) are enclosed by orange squares and blue circles, respectively .....	339
<b>Figure 7.45:</b> MTDSC reversing heat flow signals of aged hot melt extruded FM9 films (Gelucire 44/14; Eudragit RS PO: ibuprofen ratio of 1:6:3) at different storage conditions for one month in comparison to the fresh tested film.....	344

<b>Figure 7.46:</b> Overlay of X-ray powder diffraction profiles of FM9 extruded systems aged for one month at 0%RH/25°C, 75%RH/25°C and 75%RH/40°C in comparison to their corresponding fresh sample, physical mixture and pure crystalline components i.e. ibuprofen and Gelucire 44/14 .....	345
<b>Figure 7.47:</b> Polarized light images of the (A) ibuprofen crystals and (B) Gelucire 44/14 .....	346
<b>Figure 7.48:</b> Hot stage microscope images capturing the melting of the crystals after ageing for one month of the FM9 samples (I) under 0%RH/25°C and (II) under 75%RH/25°C. Samples were heated at 1°C min <sup>-1</sup> . Arrows indicate the area associated with the onset of melting (in black), the Gelucire 44/14 spherulites (in thick yellow) and ibuprofen crystals (in red). Orange cross marks the movement of the sample as a result of its expansion. Circular bubbles are due to nitrogen gas entrapped during manufacturing of these loaded samples .....	347
<b>Figure 7.48 (Contd.):</b> Hot stage microscope images of the FM9 samples stored at 75%RH/40°C for month. These samples showed only signs of liquefaction or glass disappearance as displayed in (III) set. Samples were heated at 1°C min <sup>-1</sup> . Arrows indicate the area associated with the onset of softening (in black) .....	348
<b>Figure 7.49:</b> MTDSC reversing heat flow signals for aged hot melt extruded FM10 films (Gelucire 44/14: Eudragit RS PO: ibuprofen ratio of 2:5:3) at different storage conditions for one month in comparison with the fresh tested film.....	350
<b>Figure 7.50:</b> Overlay of X-ray powder diffraction profiles of FM10 extruded systems aged for one month at 0%RH/25°C, 75%RH/25°C and 75%RH/40°C in comparison to their corresponding fresh sample, physical mixture and pure crystalline components i.e. ibuprofen and Gelucire 44/14 .....	352
<b>Figure 7.51:</b> Hot stage microscope images capturing the melting of the crystals after ageing for one month of the FM10 samples (I) under 0%RH/25°C and (II) under 75%RH/25°C. Samples were heated at 1°C min <sup>-1</sup> . Arrows indicate the area associated with the onset of melting (in black), the Gelucire 44/14 spherulites (in thick yellow) and ibuprofen crystals (in red). Orange cross marks the movement of the sample as a result of its expansion. Circular bubbles are due to nitrogen gas entrapped during manufacturing of these loaded samples .....	353
<b>Figure 7.51 (Contd.):</b> Hot stage microscope images capturing the melting of the crystals after ageing for one month of the FM10 samples stored at 75%RH/40°C which showed mainly signs of liquefaction or glass disappearance as displayed in (III) set. Samples were heated at 1°C min <sup>-1</sup> . Arrows indicate the area associated with the onset of melting or softening (in black) and ibuprofen crystals (in red) .....	354
<b>Figure 7.52:</b> Ibuprofen diffusion (permeation) profiles from hot melt extruded films of aged FM9 system (1:6:3 ratio of Gelucire 44/14:Eudragit RS PO:ibuprofen) for one month at different conditions and compared to the fresh samples, tested	

approximately at 32°C and permeated across silicone membrane into phosphate buffer solution (pH=7.2) at 37±0.1°C. Aliquot 0.3 ml of this solution was applied into each film to achieve hydration. Each data point represents the mean±S.D. of no less than three measurements.....357

**Figure 7.53:** Ibuprofen diffusion (permeation) profiles from hot melt extruded films of aged FM10 system (2:5:3 ratio of Gelucire 44/14:Eudragit RS PO:ibuprofen) for one month at different conditions and compared to the fresh samples, tested approximately at 32°C and permeated across silicone membrane into phosphate buffer solution (pH=7.2) at 37±0.1°C. Aliquot 0.3 ml of this solution was applied into each film to achieve hydration. Each data point represents the mean±S.D. of no less than three measurements.....358

**Figure 7.54:** The time corresponding to 80% or higher of the cumulative percentage permeation of ibuprofen from the hot melt extruded films of aged FM9 (lower content of Gelucire 44/14) and FM10 (higher content of Gelucire 44/14) systems for one month at different conditions and compared to their respective fresh samples, tested approximately at 32°C and permeated across silicone membrane into phosphate buffer solution (pH=7.2) at 37±0.1°C. Aliquot 0.3 ml of this solution was applied into each film to achieve hydration .....359

**Figure 7.55:** Representative photographs of the aged FM10 films demonstrating shape change appearance seen before (A) and after (B) the permeation study using Franz-type diffusion cells with the applied hydration volume of 0.3 ml PBS (pH=7.2) .....360

**Figure 8.1:** The percent water absorption capacity of the hot melt extruded films of (A) FM-A and (B) FM-B systems at different time intervals of hydration. Control samples: samples incubated under 75%RH/25°C. Test (a) samples: samples applied to the skin under occlusion. Test (b) samples: samples removed from Franz diffusion cells after being hydrated using PBS solution (detailed in Chapter 7). Error bars represent ±S.D. of not less than three measurements.....371

**Figure 8.2:** The percent swelling ratio of the hot melt extruded films of (A) FM-A and (B) FM-B systems at different time intervals of hydration. Control samples: samples incubated under 75%RH/25°C. Test (a) samples: samples applied to the skin under occlusion. Test (b) samples: samples removed from Franz diffusion cells after being hydrated using PBS solution (detailed in Chapter 7). Error bars represent ±S.D. of not less than three measurements.....372

**Figure 8.3:** Glass transition temperatures detected from MTDSC reversing heat flow signals scans of (A) FM-A and (B) FM-B system at different time intervals of hydration. Underlying scan rate of 1°C min<sup>-1</sup> with a modulation amplitude of ±0.265°C and a period of 100 seconds. Control samples: encompass fresh sample (t=0hours) and samples incubated under 75%RH/25°C, tested at different times. Test

(a) samples: samples applied to the skin under occlusion. Test (b) samples: samples removed from Franz diffusion cells after being hydrated using PBS solution (detailed in Chapter 7). Error bars represent  $\pm$ S.D. of not less than three measurements..... 374

**Figure 8.4:** Melting enthalpies detected from MTDSC total heat flow signals scans of FM-B system at different time intervals of hydration. Underlying scan rate of  $1^{\circ}\text{C min}^{-1}$  with a modulation amplitude of  $\pm 0.265^{\circ}\text{C}$  and a period of 100 seconds. Control samples: encompass fresh sample ( $t=0$ hours) and samples incubated under 75%RH/ $25^{\circ}\text{C}$ , tested at different times. Test (a) samples: samples applied to the skin under occlusion. Test (b) samples: samples removed from Franz diffusion cells after being hydrated using PBS solution (detailed in Chapter 7). Error bars represent  $\pm$ S.D. of not less than three measurements..... 375

**Figure 8.5:** Overlay plot of representative ATR-FTIR spectra of Gelucire 44/14 inside FM-A extruded films (Gelucire 44/14 Eudragit RS PO ratio of 1:6) at different occlusion times arranged in ascending order (3-24 hours) and compared to the Gelucire 44/14 spectrum in the equivalent control extruded film incubated at 75%RH/ $25^{\circ}\text{C}$ . (I) and (II) represent shoulders around  $1107\text{ cm}^{-1}$  and  $1096\text{ cm}^{-1}$ , respectively. These spectra were obtained through subtraction of Eudragit RS PO spectra ..... 380

**Figure 8.6:** Overlay plot of representative ATR-FTIR spectra of Gelucire 44/14 inside control extruded samples of FM-B composition (Gelucire 44/14 Eudragit RS PO ratio of 2:5) at different times of storage at 75%RH/ $25^{\circ}\text{C}$  arranged in ascending order (3-24 hours). (I) and (II) represent shoulders around  $1107\text{ cm}^{-1}$  and  $1096\text{ cm}^{-1}$ , respectively. These spectra were obtained through subtraction of Eudragit RS PO spectra ..... 381

**Figure 8.7:** Overlay plot of representative ATR-FTIR spectra of Gelucire 44/14 inside FM-B extruded films (Gelucire 44/14 Eudragit RS PO ratio of 2:5) at different occlusion times arranged in ascending order (3-24 hours). (I) and (II) represent shoulders around  $1107\text{ cm}^{-1}$  and  $1096\text{ cm}^{-1}$ , respectively. These spectra were obtained through subtraction of Eudragit RS PO spectra ..... 381

**Figure 8.8:** Representative plots of ATR-FTIR spectra of Gelucire 44/14 around  $1347\text{ cm}^{-1}$  peak, inside FM-B extruded films at different occlusion times (left side plot) and compared to the Gelucire 44/14 spectra in the equivalent control extruded film incubated at 75%RH/ $25^{\circ}\text{C}$  (right side plot), overlaid in ascending order of sampling times (3-24 hours). These spectra were obtained through subtraction of Eudragit RS PO spectra..... 382

**Figure 8.9:** Effect of hydration time on the measured peak hardness forces of the extruded films of (A) FM-A and (B) FM-B compositions applied to the skin under occlusion, referred as test samples and compared to their corresponding control

extruded samples stored at 75%RH/25°C. Error bars represent ±S.D. of no less than three measurements..... 383

**Figure 8.10:** Effect of the Gelucire 44/14 concentration on the measured peak hardness forces of the extruded films of (A) FM-A and (B) FM-B compositions applied to the skin under occlusion, referred as test samples and compared to their corresponding control extruded samples. Controls encompass fresh sample (t=0hours) and samples incubated under 75%RH/25°C, tested at different times. Error bars represent ±S.D. of no less than three measurements..... 384

## List of Tables

<b>Table 1.1:</b> Plasticizers used in pharmaceutical dosage forms (approved by FDA) and listed according to their chemical structures (Crowley et al., 2007) .....	50
<b>Table 1.2:</b> Common physical and analytical techniques used for the characterisation of hot melt extruded formulations (Kolter et al., 2010; Li et al., 2013) .....	53
<b>Table 1.3:</b> Main advantages of utilizing HME process (continuous with laminating and coating unit) for the manufacture of transdermal drug delivery systems (Wolff, 2000) .....	55
<b>Table 2.1:</b> Physicochemical properties of the ideal drug candidate for transdermal administration in comparison to the ibuprofen properties. <sup>a</sup> (Ghosh and Jasti, 2005), <sup>b</sup> (British Pharmacopoeia Commission, 2011), <sup>c</sup> (Hadgraft et al., 2000) .....	70
<b>Table 2.2:</b> Fatty acid distribution in Gelucire 44/14 (Chambin et al., 2004) .....	77
<b>Table 2.3:</b> Materials' sourcing .....	77
<b>Table 3.1:</b> Summary of the thermal properties of the raw materials (as received) intended for processing <i>via</i> HME, as estimated from the used TGA and MTDSC techniques. *: corresponds to the onset of the leading endothermic peak (see section 3.3.2.6.1) .....	135
<b>Table 4.1:</b> Example of the solubility parameter calculation ( $\delta t$ ) using component group contributions of ibuprofen (A) (Krevelen and Hoftyzer, 1976) according to Equations 4.1 to 4.2 (B) .....	144
<b>Table 4.2:</b> Summary of the cDSC results of the fresh hot melt extruded ibuprofen-Eudragit RS PO films at different drug loadings .....	175
<b>Table 5.1:</b> Expected release rate kinetics according to the power model (Korsmeyer et al., 1983) .....	192
<b>Table 5.2:</b> Calculated (actual) percent drug loadings of hot melt extruded samples of Eudragit RS PO at different ibuprofen loadings and loading efficiencies using hot melt extrusion technique. *Average $\pm$ S.D. of three determinations has been reported .....	193
<b>Table 5.3:</b> Quantification of the drug recovered in the silicone membranes after the end of the permeation experiments (over seven days) for examined Eudragit RS PO extruded films formulated with different ibuprofen loadings. *Average $\pm$ S.D. of three determinations has been reported .....	198
<b>Table 5.4:</b> (A) Fit correlation coefficients ( $R^2$ ) of different applied kinetic models and (B) possible interpretation of the measured release exponents from the power law model and their correlation coefficients ( $R^2$ ), both for the permeation profiles of ibuprofen formulated with different levels (loads) in hot melt extruded Eudragit	

RS PO films. Aged samples under 0%RH/25°C for one month with 30%(w/w) drug loading were also evaluated.....	200
<b>Table 6.1:</b> Formulation and extrusion temperatures for hot melt extruded films of ibuprofen with different carriers .....	205
<b>Table 6.2:</b> Eudragit RS PO-based hot melt extruded films loaded with ibuprofen: composition and their visual appearance .....	207
<b>Table 6.3:</b> Overview of the descriptions of the Eudragit RS PO-based hot melt extruded films loaded with ibuprofen .....	208
<b>Table 6.4:</b> Description of Eudragit RS PO-based hot melt extruded films loaded with ibuprofen and different amounts of Xantural® 75 polymer .....	228
<b>Table 6.5:</b> Ibuprofen extruded formulations, extent of phase separation (number of observed phases) and physical appearance along with drug crystalline state and <i>in vitro</i> release (see text or Table 6.3 for their compositions).....	232
<b>Table 6.6:</b> Estimated relative percentage crystallinity of ibuprofen from different hot melt extruded formulations before and after the end of the permeation experiments (see text or Table 6.3 for their compositions).....	239
<b>Table 6.7:</b> Fit correlation coefficients ( $R^2$ ) of different applied kinetics models for the permeation profiles of the FM5 (10% (w/w) xanthan gum), FM9 (10% (w/w) Gelucire 44/14) and FM10 (20% (w/w) Gelucire 44/14) films tested under different hydration conditions. Control: samples without hydration. Test 1: each sample was placed in 0.3 ml of PBS (pH=7.2) in the donor chamber of the Franz cells. Test 2: samples were moistened at 95%RH/25°C for three hours prior testing in the Franz cells .....	251
<b>Table 6.8:</b> Interpretation of the measured release exponents from the power law model and their correlation coefficients ( $R^2$ ) for the permeation profiles of the FM5 (10% (w/w) xanthan gum), FM9 (10% (w/w) Gelucire 44/14) and FM10 (20% (w/w) Gelucire 44/14) films tested under different hydration conditions. Control: samples without hydration. Test 1: each sample was placed in 0.3 ml of PBS (pH=7.2) in the donor chamber of the Franz cells. Test 2: samples were moistened at 95%RH/25°C for three hours prior testing in the Franz cells .....	252
<b>Table 6.9:</b> (A) Fit correlation coefficients ( $R^2$ ) of different applied kinetics models and (B) possible interpretation of the measured release exponents from the power law model and their correlation coefficients ( $R^2$ ), both for the permeation profiles of the FM9 and FM10 films under the condition of hydration with 0.14 ml of PBS (pH=7.2) in the donor chambers of the Franz cells.....	258
<b>Table 7.1:</b> Formulation and description of the placebo Eudragit RS PO/Gelucire 44/14 hot melt extruded films .....	266

<b>Table 7.2:</b> Summary of the MTDSC experiment with the underlying heating rate $1^{\circ}\text{C min}^{-1}$ , modulation amplitude of $\pm 0.265^{\circ}\text{C}$ and period of 100 seconds. Values were measured as mean $\pm$ S.D (n=3). (See Table 7.1 for composition).....	269
<b>Table 7.3:</b> Summary of the calculated percent crystallinity of Gelucire 44/14 in the physical mixtures of FM-A (Gelucire 44/14 Eudragit RS PO ratio of 1:6) and FM-B (Gelucire 44/14 Eudragit RS PO ratio of 2:5) from cDSC and MTDSC experiments.....	270
<b>Table 7.4:</b> Summary of the water content (w/w%) of different samples determined at the apparent moisture equilibrium level of 95%RH/25°C (method B) and measured by DVS (n=2, mean $\pm$ SD) .....	305
<b>Table 7.5:</b> The water uptake properties and weight loss measurements of the hot melt extruded films of FM-A (Gelucire 44/14 Eudragit RS PO ratio of 1:6) and FM-B (Gelucire 44/14 Eudragit RS PO ratio of 2:5) systems after dissolution testing in phosphate buffer solution (pH=7.2) at $37\pm 0.1^{\circ}\text{C}$ . Wc represents the water content measured <i>via</i> TGA immediately after the test ( $W_{c1}$ ) and after drying under 0%RH/RT for one week ( $W_{c2}$ ). Values represent mean $\pm$ S.D (n=2).....	310
<b>Table 7.6:</b> Summary of the MTDSC results derived from the reversing heat flow signals of the hot melt extruded FM-B films examined as shown in Figure 7.32 (B). Values represent mean $\pm$ S.D (n=2).....	314
<b>Table 7.7:</b> Photographs illustrating the colour changes of the hot melt extruded films of the FM-A and FM-B systems pre and post the dissolution experiment .	316
<b>Table 7.8:</b> Water uptake properties of the hot melt extruded films of FM-A system as analysed at each sampling time in Franz-type diffusion cells .....	320
<b>Table 7.9:</b> Water uptake properties of the hot melt extruded films of FM-B system as analysed at each sampling time in Franz-type diffusion cells .....	320
<b>Table 7.10:</b> Summary of the assignments of the proposed crystalline peaks of Gelucire 44/14 from Eudragit RS PO-subtracted extruded films ATR-FTIR spectra of FM-A (Gelucire 44/14 Eudragit RS PO ratio of 1:6) system tested at different times using Franz-type diffusion cells .....	325
<b>Table 7.11:</b> Summary of the assignments of the proposed crystalline peaks of Gelucire 44/14 from Eudragit RS PO-subtracted extruded films ATR-FTIR spectra of FM-B (Gelucire 44/14 Eudragit RS PO ratio of 2:5) system tested at different times using Franz-type diffusion cells .....	328
<b>Table 7.12:</b> Summary of the assignments of the proposed crystalline peaks of Gelucire 44/14 from Eudragit RS PO-subtracted extruded films ATR-FTIR spectra of FM-A (Gelucire 44/14 Eudragit RS PO ratio of 1:6) system examined after storage for one month at different conditions .....	341
<b>Table 7.13:</b> Summary of the assignments of the proposed crystalline peaks of Gelucire 44/14 from Eudragit RS PO-subtracted extruded films ATR-FTIR spectra	



of FM-B (Gelucire 44/14 Eudragit RS PO ratio of 2:5) system examined after storage for one month at different conditions. The spectrum of the raw Gelucire 44/14 extracted from the equivalent physical mixture spectrum (no thermal treatment) was displayed along other spectra at peak (A) region to show similarity ..... 342

**Table 7.14:** A summary of the correlation between the temperatures associated with disappearance of the spherulites (\*) and rod-shape crystals (\*\*) as obtained from hot stage microscopy and the melting temperature at the peak ( $T_{m(p)}$ ) and at the baseline ( $T_{m(b)}$ ) of the last peak recorded from MTDSC reversing heat flow signals (aged FM9 films) ..... 349

**Table 7.15:** A summary of the correlation between the temperatures associated with disappearance of the spherulites (\*) and rod-shape crystals (\*\*) as obtained from hot stage microscopy and the melting temperature at the peak ( $T_{m(p)}$ ) and at the baseline ( $T_{m(b)}$ ) of the last peak recorded from MTDSC reversing heat flow signals (aged FM10 films) ..... 355

**Table 7.16:** Fit correlation coefficients ( $R^2$ ) of different applied kinetic models for the permeation profiles of the FM9 and FM10 films tested after ageing at different conditions for one month and compared to the fresh films..... 361

**Table 7.17:** Interpretation of the measured release exponents from the power law model and their correlation coefficients ( $R^2$ ) for the permeation profiles of the FM9 and FM10 films tested after ageing at different conditions for one month and compared to the fresh films..... 362

**Table 7.18:** Fit correlation coefficients ( $R^2$ ) of the zero order model describing the first phase of the permeation profiles of the FM9 and FM10 films tested after ageing at different conditions for one month and compared to the fresh films.... 363

**Table 8.1:** Representative polarized light microscope images capturing the surface appearance of the FM-A and FM-B extruded films, occluded on the skin at various time points in comparison to their corresponding control samples incubated at 75%RH/25°C. Examples on the observed oil-like streaks are enclosed by orange squares, and fine crystallites by blue circles. ( — ) Represents a scale bar that corresponds to 300  $\mu$ m..... 376

**Table 8.2:** Representative SEM images showing surfaces and cross-sections of the FM-A extruded films (circa 15 % w/w Gelucire 44/14), occluded on the skin at various time points and compared to the control samples incubated at 75%RH/25°C. Examples on the observed micro-cracks are enclosed by orange squares..... 377

**Table 8.3:** Representative SEM images showing surfaces and cross-sections of the FM-B extruded films (circa 30% w/w Gelucire 44/14), occluded on the skin at various time points and compared to the control samples incubated at

75%RH/25°C. Examples on the observed micro-cracks and small crystallites are enclosed by orange squares and blue circles, respectively .....378

## List of Symbols

$\Delta\beta$ : difference of the expansion coefficient below and above glass transition temperature  
b: heating rate  
CD: concentration of the drug in the bulk medium  
Cp: heat capacity  
 $C_{s,m}$ : solubility of the drug in the membrane  
Cs: saturated solubility of the drug in the dissolution medium  
 $C_V$ : concentration of the drug dissolved in the vehicle  
D, d: Dalton, dry  
 $D_m$ : diffusion coefficient of the drug in the membrane  
Ehi: group contribution to the hydrogen bonding energy  
Fdi: group contribution to the dispersion forces  
Fpi: group contribution to the polar forces  
h: hour  
i: structural group within a molecule  
J: flux  
K: sample specific parameter  
 $K^0$ : zero order constant  
 $K_1$ : first order constant  
 $K_H$ : Higuchi release constant  
L: diffusion path length  
log D: octanol-water distribution coefficient  
log P (n-octanol/water): partitioning coefficient  
m: ratio of the volume of the polymer to that of the lattice site, milli  
Mid-point Tg: glass transition temperature measured at the midpoint of the transition  
 $m_{\Delta h}$ : fragility parameter  
n: release exponent, number  
N: Newton  
Q: heat  
R: thermal resistance, universal gas constant  
 $R^2$ : linear correlation coefficient  
 $t \geq 80\%$ : the time necessary to the release of higher than or equal to 80% of the drug  
t: time  
 $t^{1/2}$ : square root of time  
 $T_{f,ref}$ : reference fictive temperature  
 $T_f$ : fictive temperature  
Tg: glass transition temperature

$T_{g_{mix}}$ : glass transition temperature of multi-component system  
 $T_{m(b)}$ : melting temperature at the baseline  
 $T_{m(onset)}$ : extrapolated onset as melting temperature  
 $T_{m(p)}$ : melting temperature at the peak  
 $T_m$ : melting temperature  
 $T_M^{mix}$ : melting temperature of the drug in the presence of the polymer  
 $T_M^{pure}$ : melting temperature of the drug in the absence of the polymer  
 $V$ : dissolution medium volume, molar volume, volt  
 $w$ : weight, weight fraction  
 $W_0$ : initial weight  
 $Wc$ : water content  
 $w_t$ : total weight  
 $x$ : drug solubility mole fraction  
 $\beta_c$ : cooling rate  
 $\gamma_{(drug)}$ : activity coefficient of the drug in the polymer at solubility limit  
 $\delta_d$ : the dispersion Hansen solubility parameter  
 $\Delta H$ : enthalpy  
 $\delta_h$ : the hydrogen-bonding Hansen parameter solubility parameter  
 $\Delta H_{fus}$ : heat of fusion  
 $\Delta H_{melt}$ : melt enthalpy  
 $\delta_p$ : polar Hansen solubility parameter  
 $\Delta T$ : temperature difference  
 $\delta t$ : total solubility parameter  
 $\lambda$ : wavelength  
 $\rho$ : density  
 $\Phi_{drug}$ : volume fraction of the drug  
 $\Phi_{polymer}$ : volume fraction of the polymer  
 $\chi$ : Flory-Huggins interaction parameter  
 $\omega$ : angular frequency

## List of Abbreviations

$^{\circ}C\ min^{-1}$ : Degree Celsius per minute  
 ATR: Attenuated total reflection  
 ATR-FTIR: Attenuated total reflection-Fourier transform infrared spectroscopy  
 BCS: Biopharmaceutics classification system  
 cDSC: Conventional or standard DSC  
 DSC: Differential scanning calorimetry

DVS: Dynamic vapor sorption

Eq.: Equation

FDA: Food and drug administration

G44/14: Gelucire 44/14

GIT: Gastrointestinal tract

GMPs: Good manufacturing practices

GRAS: Generally recognized as safe

grp.: group

G-T: Gordon-Taylor

HLB: Hydrophilic-Lipophilic Balance

HME: Hot melt extrusion

HPLC: High pressure liquid chromatography

HSM: Hot stage microscopy

IR: Infrared

Jg<sup>-1</sup>: Joule per gram

MC: Methyl cellulose

MFCs: Mass flow controllers

MTDSC: Modulated temperature DSC

NIR: Near infrared

NSAIDs: Non-steroidal anti-inflammatory drugs

ODS: octadecyl-silica stationary phase

PAT: Process analytical technology

PBS: Phosphate buffer solution (system)

PEO: Polyoxyethylene

PHF: Peak hardness force

PLC: Poly-ε-caprolactone

PLM: Polarized light microscope

PM: Physical mixture

PPO: Polyoxypropylene

PXRD: Powder X-ray diffraction

RCDR %: relative cumulative percent drug released

RCS: Refrigerated cooling system

RH: Relative humidity

Rpm: Rotation per minute

ssNMR: Solid state nuclear magnetic resonance

TA: Texture analysis

TDDS: Transdermal drug delivery systems

TG: Thermogravimetry

TGA: Thermogravimetric analysis

## **Chapter 1: Introduction**

## 1.1 General introduction

In pharmaceutical drug delivery research around 40% of drug delivery candidate products are under clinical evaluation for transdermal applications (Barry, 2001; Dhamecha et al., 2009) with approximately 500 trials listed on ClinicalTrials.gov in June 2012 (Watkinson, 2013). This illustrates the strong trend towards the use of the skin as one of the main routes of administration for the next decade. Similarly, the growing interest in the use of hot melt extrusion (HME) technology presents a range of opportunities to design responsive drug delivery systems that can combine the benefits of transdermal delivery and HME processing technology. Therefore, the work in this thesis details the development of various hot melt extruded formulations in attempt to design simple matrix-type patches for transdermal drug delivery, evaluated on the basis of solid state characteristics, *in vitro* drug release and permeation performance. Before a more detailed introduction of the research objectives is given, a review of hot melt extrusion and transdermal drug delivery is provided.

## 1.2 Hot melt extrusion (HME) for pharmaceutical systems

Hot melt extrusion (HME) technology is emerging as one of the most widely used techniques for pharmaceutical applications. This technique was originally established in the plastic and food industry during the mid 1930s (Crowley et al., 2007). There is ample literature on the dosage forms and drug delivery systems prepared *via* melt extrusion such as granules (Gryczke et al., 2011), pellets (Young et al., 2003), tablets (Bruce et al., 2005), suppositories (Byrne and Aylott, 1981), implants (Gosau and Müller, 2010), stents (Healy and Dorfman, 1997), topical and transdermal systems (Aitken-Nichol et al., 1996; Breitenbach et al., 2009; Repka et al., 1999).

Hot melt extrusion can be defined as a process whereby a raw material is extruded through a die system under conditions of elevated temperature, mixing and pressure. As an effectively continuous process, high throughput rates are possible (Breitenbach, 2002). The extrusion system or the extruder consists of two main parts: a conveying system, where the material is massed, mixed and transported, and a die system which transform the material into the desired shape.

A review by Crowley et al. (2007) showed that hot melt extrusion compares favourably with traditional pharmaceutical processing techniques due to it being associated with fewer unit operations and greater product content uniformity, as well as offering a solvent-free process that is capable of solid-dispersion formation of poorly soluble drugs with improved bioavailability.

### 1.2.1 Extrusion processing

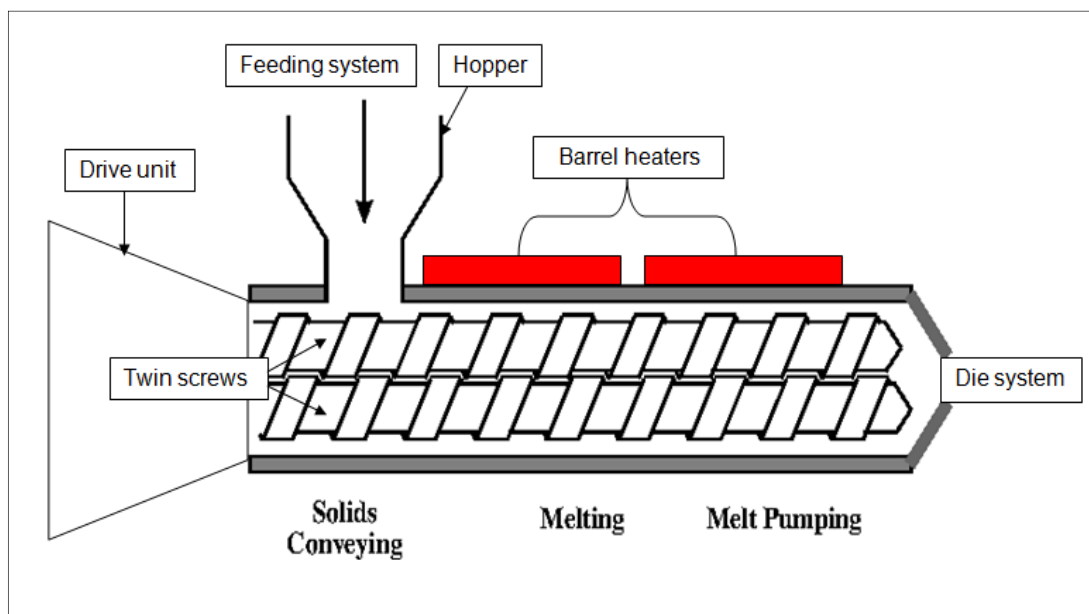
Generally, the HME technique is suitable for thermostable drugs and polymers which have appropriate thermoplastic behaviour. This technology usually comprises the following steps: (a) the drug and the polymer(s) are blended for content uniformity; (b) this mix is fed into the extruder, whereby parameters are adjusted according to the formulation prepared; and (c) the resultant extruded product (usually strands or films) need to be cooled by passing over a chilled roll, for example. In order to understand the melt extrusion itself, we can divide the process into the following steps in sequential order (Breitenbach, 2002):

- 1-Feeding stage;
  - 2-Conveying of the mass (dispersive and distributive mixing);
  - 3-Flow through the die;
  - 4-Pumping outside into downstream processing (cooling, cutting or collecting the extrudate).
- These will be discussed in the context of the development of an HME process.

Ever since HME first found its place in the pharmaceutical manufacturing operations, attention towards design issues, includes polymer type and amount, drug selection, processing conditions and parameters employed has become of immense importance for successful product development. Process parameters are divided up into monitoring and controlling parameters. Barrel temperature, feed rate and screw speed are controlling parameters; whereas motor load and melt pressure are monitoring parameters (Chokshi and Zia, 2004). To understand these processing parameters, it would be useful to have initially a brief overview of the extruder parts. Hot melt extrusion system or the extruder is typically composed of a feeding hopper, barrel(s), single or twin screws, and the die as exemplified in Figure 1.1. These parts are controlled and operated *via* connection to a central drive electronic control unit and a motor. Therefore, process control can be applied on the zone temperature, screw speed with optional monitoring devices of the pressure and extrusion torque.



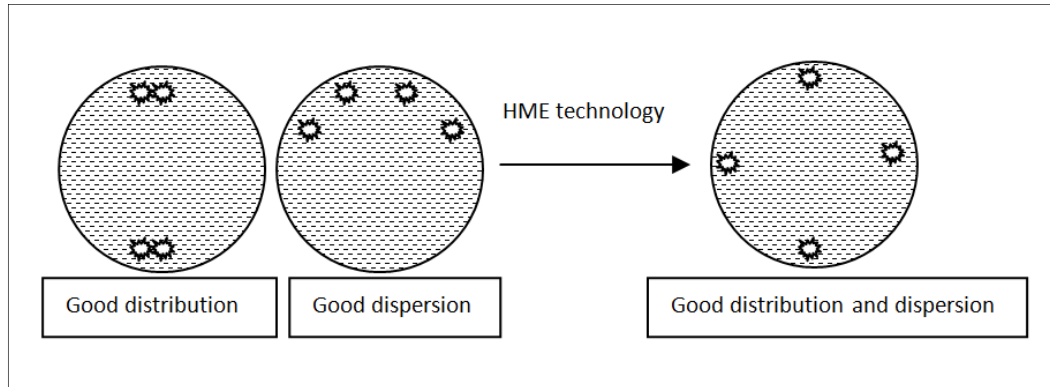
Downstream equipment for the extruder is used for collection and cooling, such as a conveyor belt and cutting. Additional or auxiliary equipment for the extruder consist of on-line or in-line process analytical technology (PAT) that is used for real time product quality evaluation. Examples include near infrared (NIR), Raman, ultrasound and laser systems (Maniruzzaman et al., 2012).



**Figure 1.1: Schematic side view of a twin-screw extruder set-up comprising a feed hopper, barrel heaters, twin screws connected to a drive unit and an outlet representing a die system. The solids are conveyed, melted and pumped into the die. Reproduced from [www.polymerprocessing.com](http://www.polymerprocessing.com)**

In hot melt extrusion, heat is applied to the material to enable its flow, hence a prerequisite of this material to be used in hot melt extrusion is thermal stability at the selected processing temperature. However, even thermally sensitive drugs can be processed using HME, if the process design is manipulated. For example, short processing times at low temperatures can solve the problem. During the extrusion, the barrel is heated at temperatures that allow melting or liquefaction of the conveyed solids. These temperatures are usually determined based on the glass transition ( $T_g$ ) or melting temperature ( $T_m$ ) of the polymer(s) and drug. The segmental mobility of the material is very high when the glass transition temperature ( $T_g$ ) is below the set temperature. Therefore, a solid crystalline or a glassy system at temperature higher than its melting or glass transition temperature, respectively, is assumed to have better mixing ability due to high molecular mobility and lack of rigidity.

Another integral parameter in extrusion is a combination of the screw speed and feeding rate. The level of extruder filling is determined by this parameter. Constant feed rate and screw speed will mean a constant amount of material in the extruder. As a consequence, the applied mixing and residence time will remain constant. This means an efficient dispersive and distributive mixing as depicted in Figure 1.2. Dispersive mixing de-aggregates suspended particles in the molten mass, while distributive mixing, ideally, divides and recombines the material to ensure content uniformity (Chokshi and Zia, 2004). Alternatively, the main monitoring parameters which encompass motor load and melt pressure depend on the feed rate and screw speed, which depend on the viscosity and molecular weight of polymer and drug as well as polymer miscibility in binary mixtures (Breitenbach, 2002). For example, at constant temperature, as the viscosity and molecular weight of the material increase, lower feeding rate and faster rotation of the screw might be required to aid in the conveying, mixing and transportation of this material, resulting in a high motor amperage and barrel pressure. However, in some cases the melt viscosity is very high that the screw(s) will not be able to rotate. In this case, other avenues are used to improve processing conditions. Higher temperatures and/or incorporating plasticizers in the formulation can lower melt viscosities (Karl et al., 2011).



**Figure 1.2: A schematic diagram illustrating HME influence on achieving dispersive and distributive mixing**

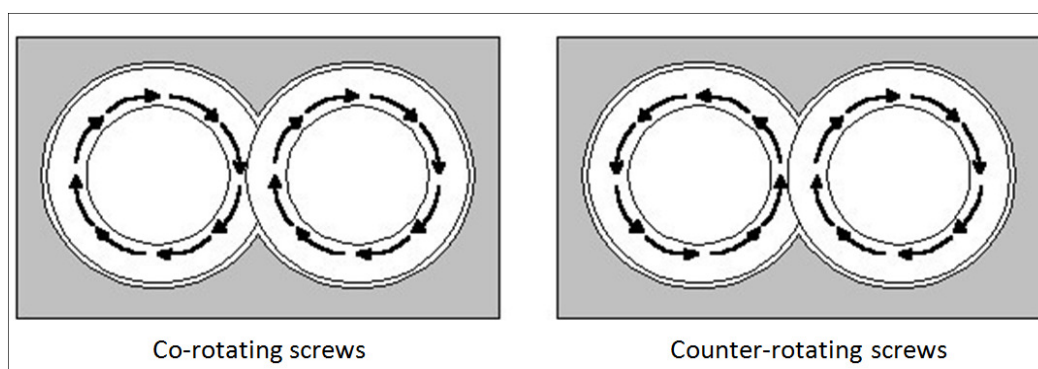
### 1.2.2 Extruder types

Various types of extruders which are used for pharmaceutical purposes must meet regulatory requirements. Thus the contact parts must not be reactive, additive or absorptive with the product. Usually the processing units are made of stainless steel to resist abrasion, corrosion and adhesion (Ghebre-Selassie and Martin, 2003). In addition, the equipment is configured for cleaning and validation for pharmaceutical extrusion in accordance with Good Manufacturing Practices (cGMPs).

These pharmaceutical grade extruders can be either ram extruders or screw extruders. Screw extruders operate with (a) rotating screw(s) inside a heated barrel. On the other hand, the ram extruders or piston-fed extruder works under the principle of high pressure ram displacement to push materials through the die. However, lack of temperature uniformity and limited melting capacity in this type usually generate products with lower homogeneity in comparison to the extrudate produced by screw extruders (Crowley et al., 2007; Ghebre-Selassie and Martin, 2003). Therefore, screw extruders are more useful for pharmaceutical needs.

Screw extruders can be classified as single-screw extruder and twin-screw extruders. The twin-screw extruder is the most widely used and preferred for pharmaceutical applications. Single-screw extruders consist of one screw, while twin-extruders utilize two screws that are usually arranged side by side. The use of two screws allows different configurations to be obtained. For example, as illustrated in Figure 1.3, a co-rotating design allows the rotation of the screws in the same directions, whereas in a counter-rotating configuration screws rotate in the opposite direction. In most cases, co-rotating design is primarily used in pharmaceutical manufacturing. This design allows high rotation speeds associated with high outputs while good mixing and conveying properties are maintained (Kolter et al., 2010). This type is associated with lower screw and barrel wear than counter-rotating extruders. However, counter-rotating design is useful when very high shear regions are needed, as the material can be squeezed through the gap between the two screws when they come together.

Overall, twin-screw extruders are commonly the extruders of choice in the pharmaceutical industry. These extruders have many advantages over single screw extruders such as versatility of the designs which allow convenient material feeding, better mixing, high capability of heat and mass transfer, shorter residence time with less tendency to overheat, which accounts for a decrease in the material degradation. In addition to the “self-cleaning” property that is related to the self-wiping of the intermeshing design, presenting a clean environment required by GMP regulations for pharmaceutical extrusion (Hudson, 1995).



**Figure 1.3: Schematic of the cross section view of the different screws' rotations in twin-screw extruder. Reproduced from [www.iscrewbarrel.com](http://www.iscrewbarrel.com)**

### 1.2.3 HME formulation development

Mixtures of active drug and functional excipients are commonly employed in HME applications to formulate various dosage forms and delivery system. Major ingredients of these excipients used in HME process may be generally classified as matrix carriers comprising polymeric carriers, release-modifying agents, plasticizers, and various additives such as antioxidants or thickening agents. The availability of materials of pharmaceutical grade that are eligible for extrusion is increasing steadily, with most of the materials used currently having been used previously for production of traditional dosage forms (Singhal et al., 2011). As mentioned previously, thermal stability is essential for any extrusion process, in addition to acceptable chemical and physical stability, low toxicity and, for the carrier systems it is usually required that they be pharmacologically inert.

### 1.2.3.1 Active ingredients

The major drawback of the HME technology is relatively high shear forces and temperatures that restrict application to thermo-stable drug substances. However, thermolabile drugs can still be extruded if the processing time is short or the required processing temperature is reduced by incorporation of plasticizers. For example, thermosensitive p-amino salicylic acid (Verreck et al., 2006) and hydrocortisone (Repka et al., 1999) have been extruded successfully using plasticizers. In some cases, the drug itself may function as a plasticizer such as ibuprofen (Kidokoro et al., 2001; Siepmann et al., 2006), chlorpheniramine maleate (Wu and McGinity, 1999) and itraconazole (Rambali et al., 2003).

Depending on the unique properties of the extruded drug and excipients formulated therein, the drug substance may be completely dissolved as a solid solution or dispersed as a solid dispersion or a combination. Performance as well as processability and stability can be influenced by the drug state in the extruded final dosage form. For example, solid dispersions may be more stable and easily processed in comparison to solid solution systems (Crowley et al., 2007).

### 1.2.3.2 Carrier systems

Hot melt extrudate production involves blending of the drug into carrier system comprised of one or more meltable substances. The selection of appropriate carrier(s) is critical factor in the design and development of HME formulation to impart the required properties to the final extruded product, such as obtaining the desired release profile of the drug substance or limiting the burst effect by incorporation of viscosity inducing agent.

Investigation of the processing conditions and attributes of the raw materials is typically performed on the basis of the thermal properties, such as thermal stability, and the rheological properties, such as acceptable melt viscosity for processing. While thermal properties can be characterised using various thermoanalytical techniques, like differential scanning calorimetry and thermogravimetric analysis, melt viscosity can be measured indirectly from torque, melt pressure and motor amperage associated with the HME process.

The resistance of the viscous material to the shearing action of the melting process is measured by the torque, which is defined as the mechanical work needed to move material through an extruder. The energy consumed by the motor to transfer this material is measured by the drive motor amperage, and the pressure initiated from material compaction within the extruder, melting and pumping towards the die system is known as the melt pressure. These measures are proportional to the material viscosity and can be useful to reflect the processing environment. For instance, it may be used for comparative analysis of the torque between studied systems, thus their resistance for processing *via* the HME technique.

However, the most important information to know is that all extruders have a limited operating window of a maximum operating temperature and rotational speed. Therefore, proper intervention is warranted in some cases, for example, plasticizer can improve the processing conditions by decreasing the melt viscosity and avoid improper conditions. Otherwise, the machine will be susceptible to physical damage and the used drug, excipient or additives to degradation (Coppens et al., 2005).

Examples on the main categories of the commonly used carriers in the HME to prepare various dosage forms comprise polymeric carriers of polymethacrylates like Eudragit RS/RL (Zheng et al., 2004), Eudragit E (Qi et al., 2008a) and Eudragit S (Bruce et al., 2005), cellulosic derivatives such as ethylcellulose and hydroxypropylcellulose, polyethylene glycol, polyethylene oxide and their copolymers (Hall and Read, 2012). In addition to the non-polymeric carriers which include wide range of waxes like carnauba wax, microcrystalline wax (De Brabandera et al., 2000) and lipid carriers (Mehuys et al., 2004) such as polyglycolised glycerides lipids (Gelucires®).

#### 1.2.3.3 Processing aids

Processing aids are group of materials that offer remedies for the problems that might be encountered during the manufacturing of the extruded systems, thus enhancing HME processing condition. As for any pharmaceutical preparation, these additives should be of pharmaceutical grade and have good compatibility with other components of the formulation intended for extrusion.

#### 1.2.3.3.1 Plasticizers

Polymeric carriers employed in HME may require plasticizers to facilitate their extrusion and enhance processing conditions. Plasticizers are compounds that can decrease the glass transition temperature and melt viscosity of a polymer (Verreck, 2012). This could be attributed to increase free volume between polymer chains. Rigid and hard polymers have low free volume and the molecules cannot move past each other easily. Addition of small molecules such as plasticizers can separate the polymer molecules, increasing the free volume. Thus applying relatively lower temperature after incorporation of the plasticizers could supply the polymer molecules with enough energy to vibrate and move past each other rapidly, making the system more flexible. Other interventions which could increase free volume include modification of the backbone of the polymeric material by addition of side chains or end groups (Wilkes et al., 2005).

Typically, plasticizers would reduce the need of excessive temperature to process hard polymers. In doing so, localized overheating, depolymerisation or oxidation of the polymers and thermal degradation can be avoided for both the drug and the polymer, thus a better quality of the product can be attained (Verhoeven et al., 2008). It has been also demonstrated that improving the conditions of HME processing by reducing required temperature, energy and torque for the material to melt and flow, can be reflected positively on the homogeneity of the mixing/dispersion of the drug in the polymeric matrix and content uniformity of the extruded product (Thumma et al., 2008). Plasticizers may also alter the drug release rate, so a judicious choice of the plasticizer type (hydrophobic vs. hydrophilic) and a balance between enough amount of plasticizer to facilitate extrusion, while maintaining the desired drug release profile are required (Coppens et al., 2005).

Plasticizers are often low molecular weight compounds. Heinamaki and coworkers (1994) found that elongation percentage or ductility was mainly ascribed to the molecular weight of the plasticizer (polyethylene glycol), so the lower molecular weight and thus the size it has, the system will be more elastic. Table 1.1 lists plasticizers approved by the Food and Drug Administration (FDA) for use in pharmaceutical dosage forms. Moreover, the potential of pressurized carbon dioxide as a “temporary” plasticizer has been investigated. Efficient reduction of processing temperature was demonstrated (Verreck et al., 2006a) with its ability to work as a foaming agent, thereby increasing the porosity of the extruded formulations, resulting in their enhanced dissolution (Verreck et al., 2006b).

In some formulations, the active moiety (drug) can act as a plasticizer during processing (section 1.2.3.1). Polymers themselves such as polyethylene oxide (PEO 100K) and poly ( $\epsilon$ -caprolactone) (PLC) have shown plasticizing effect (Lyon et al., 2008; Crowley et al., 2002). Additionally, some surfactants, such as Tween 80 and sodium lauryl sulphate, have been also reported to act as both plasticizers and solubilizers (Ghebremeskel et al., 2007). The existence of all-in-one ingredient or combining more than one property needed for efficient formulation preparation is an integral factor in formulation design. Fewer ingredients in the formulation means less ingredient variability, better economic efficiency and less probability of adverse reactions or the need of elaborative compatibility testing.

Type	Examples
Citrate esters	Triethyl citrate, tributyl citrate, acetyl triethyl citrate, acetyl tributyl citrate
Fatty acid esters	Butyl stearate, glycerol monostearate, stearyl alcohol
Sebacate esters	Dibutyl sebacate
Phthalate esters	Diethyl phthalate, Dibutyl phthalate, dioctyl phosphate
Glycol derivatives	Polyethylene glycol, Propylene glycol
Others	Triacetin, mineral oil, castor oil
Vitamin E TPGS	D- $\alpha$ -tocopheryl polyethylene glycol 1000 succinate

**Table 1.1: Plasticizers used in pharmaceutical dosage forms (approved by FDA) and listed according to their chemical structures (Crowley et al., 2007)**

#### 1.2.3.3.2 Other additives

For systems prone to oxidation or light degradation, various materials can be added to improve their stability during storage or prevent their degradation during processing. Examples include light absorbers such as benzotriazole ultraviolet light absorber, preventive antioxidant like ascorbic acid, which undergoes oxidation preferentially, protecting by that other components from attack by oxygen (Singhal et al., 2011).

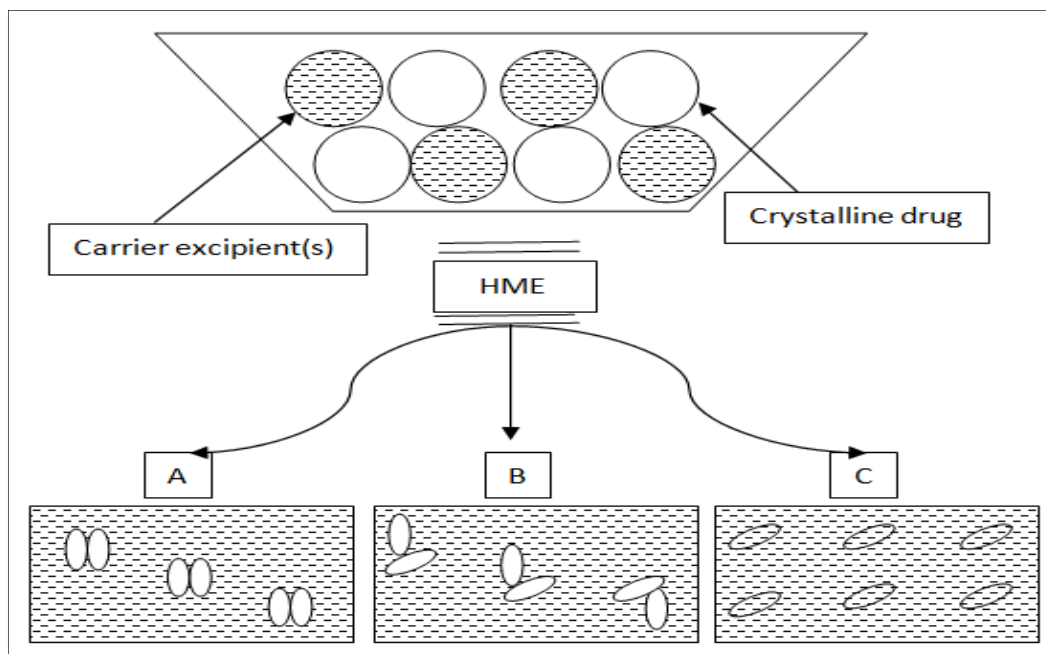


Other materials have been used in HME processing comprise, but not limited to, lubricants and pH modifying agents. Citric acid monohydrate, for instance, was found to act as a plasticizer and pH-modifying agent, facilitating HME processing and adjusting the system micro-environmental pH, which modulate drug release (Bruce et al., 2005). Thermal lubricants, like waxy glyceryl monostearate and triethyl citrate were found to lower melt viscosity and decrease both the glass transition temperature and the melt viscosity, respectively, thereby improving thermal processing during hot melt extrusion (Zhu et al., 2004).

#### **1.2.4 Characterisation of the hot melt extrudate**

HME technology has been utilized for several applications in pharmaceutical field; however, a key application is the ability to produce solid molecular solution/dispersion of the active pharmaceutical ingredients in a matrix (Andrews and Jones, 2010) without being restricted by solvent concerns. The strategy for characterising extruded product containing an active pharmaceutical ingredient is usually dependent on the physical state of the drug in the extruded mix to differentiate between solid solution and solid dispersion systems. The formation of these systems is one of the important interventions in pharmaceutical applications to improve solubility and dissolution rate. Therefore, their characterisation is important for some impacts that they could have. For example, while dissolution rate can be improved by enhanced wetting behaviour of hydrophobic drugs with hydrophilic polymers in solid dispersion, solid solution systems can improve dissolution rate due to the amorphous nature of the product (Chokshi and Zia, 2004).

Materials can be combined using HME to form broadly called “solid dispersions”. Solid dispersion systems refer to a group of solid products consisting at least two different components, e.g. drug and polymer (Patidari et al., 2011). While a number of classifications have been described in the literature of these systems, the most commonly used distinguishable feature is based on the molecular state of the drug in the carrier matrix. In pharmaceutical applications, the most encountered types are solid crystalline suspension, solid glassy suspension and solid glassy solution as presented in Figure 1.4.



**Figure 1.4: Schematic presentation of incorporating modes of the drug in an amorphous carrier matrix (commonly polymeric material) using HME technology. (A) Refers to solid crystalline dispersion of crystalline drug particles with a polymeric carrier; (B) to solid glassy suspension of amorphous drug domains (clusters) with a polymeric carrier and (C) represents solid solution of amorphous drug molecularly dispersed between amorphous polymeric chains**

By definition, if the drug is dissolved at molecular level, thus the drug forms one phase system with polymer, it is referred to as a solid solution; whereas, if the drug is in a two phase system with polymer, it is referred to as a solid dispersion (Chokshi et al., 2007). The drug in this case is partly molecularly dispersed and exists as amorphous domains (clusters), giving rise to glassy solid suspension or found as crystalline particles and referred to as a solid crystalline dispersion (Kolter et al., 2010). The biggest challenge that might be encountered during characterisation of these systems is to ascertain how the drug is actually dispersed within the carrier at the molecular level (Craig, 2002). In recent years there has been growing interest in advancing research towards new approaches to meet these challenges. Qi and co-workers have conducted appreciable research on the use of micro- and nano-characterisation methods to identify the physical state of the drug in the HME formulations, such as microthermal analysis (Qi et al., 2008a) and localized nanothermal analysis using atomic force microscope with a thermal probe, photothermal Fourier-Transform infrared microspectroscopy (Qi et al., 2011) and solid state proton nuclear magnetic resonance (NMR) relaxometry (Qi et al., 2010).

However, it is customary to rely on the absence of crystallinity to indicate that the drug is molecularly dispersed. Analytical methods that have been used to characterise hot melt extrudates are summarized in Table 1.2. The characterisation of hot melt extrudate using these techniques reveals many important aspects like their solid state structure, thermodynamic properties and changes such as phase separation, crystallization and structural relaxation.

Thermoanalytical and gravimetric methods	Differential scanning calorimetry Hot stage microscopy Microthermal analysis Thermogravimetric analysis Dynamic vapour sorption
Dissolution testing	<i>In vitro</i> and <i>in vivo</i>
X-ray diffraction	Powder X-ray diffraction Small angle X-ray scattering
Spectroscopic Methods	Infrared, Near infrared and Raman spectroscopy Solid-state nuclear magnetic resonance
Microscopic Methods	Polarized light microscopy Scanning electron microscopy Transmission electron microscopy Atomic force microscopy

**Table 1.2: Common physical and analytical techniques used for the characterisation of hot melt extruded formulations (Kolter et al., 2010; Li et al., 2013)**

### 1.2.5 HME for transdermal drug delivery

Hot melt extrusion is a versatile technique that has proven useful in the design and reformulation of different pharmaceutical preparations for various purposes that include enhanced dissolution rate, improved bioavailability, modification or controlling of the drug release and taste masking of the bitter taste active drugs (Madana and Madanb, 2012; Williams et al., 2010). Whilst the main focus is placed on the production of solid solution/dispersion systems to enhance drug delivery for oral route, the utility of HME has also been extended as an attractive technique to produce different drug delivery systems for topical, transdermal and parenteral applications.

The majority of the transdermal drug patches are prepared by the solvent cast method, whereby the adhesive polymer solution is coated over a backing membrane, and is dried to remove the solvent. Afterwards, a release liner is laid on the top of the adhesive and is laminated (Delgado-Charro and Guy, 2001). However, HME technology is currently being explored and used in the pharmaceutical field to produce transungual (Mididoddi et al., 2006; Trey et al., 2007), transmucosal (Munjal et al., 2006; Palem et al., 2013) and transdermal films (Breitenbach et al. 2009; Crowley et al., 2004; Crowley et al., 2009; Repka et al., 1999) because it offers several advantages over traditional processing methods (Prodduturi et al., 2007). In particular, it avoids the usage of organic or aqueous solvents, offers a short processing time with continuous processing of products, and eliminates environmental concerns (Aitken-Nichol et al., 1996). In addition, preparation of transdermal films in a single processing step makes it economic wise technique. HME has also been shown to overcome decreased elongation or elasticity and increased film tensile strength after physical aging of the films produced by solvent casting approach (Gutierrez-Rocca and McGinity, 1993; Repka et al., 1999).

In the hot melt procedure the molten polymers are mixed with the active ingredient without the use of any solvents, that could be hazardous, and the melts are spread over a backing layer. These materials should be “benign”, such as generally recognized as safe substances to decrease the risk of possible skin irritation and/or sensitization (Barry, 2001). Generally, substances used with proven safety in oral route can be used for investigations for potential transdermal delivery (Hadgraft et al., 2000).

Table 1.3 lists some advantages of using continuous HME as reviewed by Wolff (2000) in production of transdermal drug delivery systems, wherein coating and laminating unit is attached to the die system to combine the melt extrusion films with substrate for transdermal applications to provide single continuous manufacturing process.

Characteristics	Positive impact on
Solvent and water-free method	Manufacturing costs (less) Physicochemical long-term stability Biocompatibility Environmental Compatibility
Continuous process	Processing time (shortened) Scale-up Manufacturing costs (less)
Compact, small-sized equipment	Floor space requirements (less) Capital costs (less)
Automated process, electronically controlled and continuously monitored on-line	Batch control Manufacturing costs (less)
Capability of die coating	Product yield

**Table 1.3: Main advantages of utilizing HME process (continuous with laminating and coating unit) for the manufacture of transdermal drug delivery systems (Wolff, 2000)**

### 1.3 Transdermal drug delivery systems (TDDS)

Being the most expansive organ of the human body, the skin has been used as an administration site for pharmaceuticals. The drugs can be introduced for local and systemic action through dermal and transdermal route, respectively. However, the concept of delivering drugs through the skin for systemic treatment has been challenged over the past few years. This is because the skin and more specifically, the skin's outermost layer - the stratum corneum - forms the main barrier to diffusion of the permeants through the skin. On the one hand this provides a protective shield against the entry of foreign material and possible invasion of pathogens, and on the other hand, it limits the transport of drugs.

However, the skin offers a tempting criteria of a large (1-2 m<sup>2</sup>) and potential accessible surface for drug delivery. Moreover, transdermal applications, relative to other routes, provide a variety of advantages inherent in the transdermal route, including: elimination of gastrointestinal absorption problems and the hepatic first pass effect, reduction of the frequent dosing, predictable and extended duration of activity, improved patient compliance, quick termination by simple removal of the system from the skin surface, and possible self-administration (Delgado-Charro and Guy, 2001). So drug delivery across the skin can achieve the main objectives of (Cevec and Vierl, 2010):

- minimal invasiveness, or non invasiveness of an application;
- improved drug pharmacokinetics;
- targeted drug delivery.

On the other hand, limitations of transdermal drug delivery are posed by the skin's barrier function. The factors which limit the success of transdermal drug delivery systems (TDDS) can be summarized in the following points (Barichello et al., 2006):

- Local skin irritation related to certain drugs and formulation.
- Limitation of the dose of the drug that could be delivered transdermally.
- The lag time associated with delivery of the drug across the skin; resulting in a delay in the onset of action.
- Variation of absorption rate, based on the site of application, skin type and patient age.

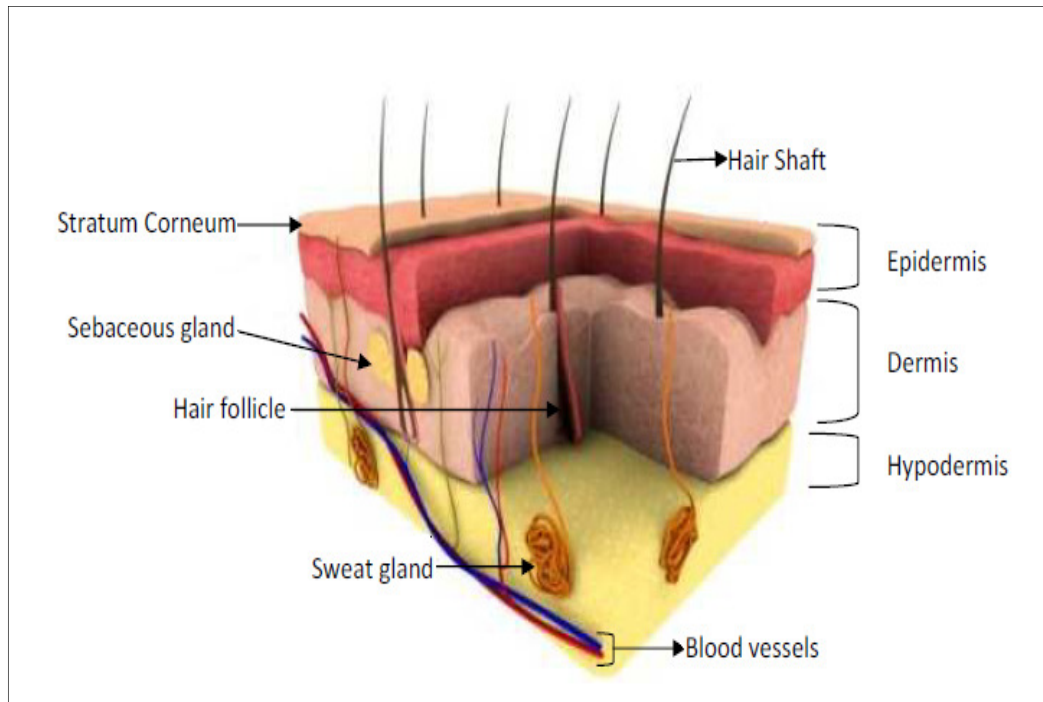
Ideally, potent drug molecules with low molecular weights (<600 Dalton), low melting points, which is usually correlated with good ideal solubility, high but balanced partition coefficient as too large value could inhibit clearance by viable tissues, and a good solubility in both mineral oil and water (greater than 1mg/ml) can satisfy the requirements of efficient transdermal delivery, through effective penetration across the stratum corneum (Barry, 2001; Kusum et al., 2003). Today, there is a wide spectrum of conditions where the treatment is achieved by the use of transdermal drug delivery. Motion sickness, nicotine drug patches for smokers, Parkinson's disease, angina pectoris, and contraception are a few examples of these conditions.

### 1.3.1 Skin drug delivery: topical versus transdermal drug delivery systems

Topical delivery is the term used for localized treatment of the dermatological condition where the medication is not targeted for systemic delivery; examples include treatment of dermatological conditions like eczema or psoriasis by topical application. Examples of drugs delivered topically include corticosteroids, antifungals, antivirals, antibiotics, antiseptics, local anesthetics, and antineoplastics. Whereas, the terms for topical formulations containing drugs showing systemic action are transdermal delivery systems or transdermal therapeutic systems. Transdermal delivery may be defined as the delivery of a drug across intact skin, in which a direct access into the blood stream is achieved with a sufficient therapeutic amount (Sugibayashi and Morimoto, 1994). Transdermal delivery systems are also termed 'patches'. These are defined as a self-discrete dosage, loaded with a certain amount of the medicine (drug) and when applied onto the skin surface, a specific dose will be delivered to the systemic circulation over a period of time (Wokovich et al., 2006). Scopolamine, nitroglycerin, clonidine, estradiol, fentanyl, nicotine and testosterone are examples of active agents delivered transdermally.

### 1.3.2 Skin structure and anatomy

In order to understand the mode of transdermal drug delivery action it is important to address some physiological aspects of the skin that are related to drug delivery. The skin is the largest organ of our body and macroscopically consists of two distinct layers: the dermis which forms the bulk of skin, and overlying it avascular epidermis. The dermis is a layer with a high vascular structure that is made up of connective tissue elements, and includes the pilosebaceous units, sweat glands, dermal adipose cells, mast cells, and infiltrating leucocytes. The epidermis composed primarily of keratinocytes (Menon, 2002). The dermal-epidermal junction is highly convoluted ensuring a maximal contact area (Delgado-Charro and Guy, 2001). The structure of human skin is portrayed in Figure 1.5.



**Figure 1.5: Cross section of the skin, highlighting the epidermis, dermis, hypodermis and stratum corneum. Reproduced from [www.omnimedicalsearch.com](http://www.omnimedicalsearch.com)**

#### 1.3.2.1 Epidermis

The epidermis is the uppermost layer of the skin. Epidermis is stratified and about 100-150  $\mu\text{m}$  thick. It comprises four distinct layers, namely the stratum basale, stratum spinosum, stratum granulosum and stratum corneum (Kulkarni, 2010). As it is a non-vascularised tissue, it receives its nutrition by diffusion from the capillary system of the dermis. The keratinocytes comprise the major cellular component and are responsible for the evolution of the barrier function.



The stratum basale, or basal layer, is responsible for progressive renewal of the epidermis. The cells that result from the mitotic activity of these epidermal stem cells, the keratinocytes, migrate in the direction of the stratum corneum. The next layer of the epidermis is the stratum spinosum, where the high number of desmosomes that connect adjacent cells accounts for the spiny appearance of these cells. In this layer an increased synthesis of proteins and lipids takes place in the cells. The layer above the stratum spinosum, the stratum granulosum, contains flattened cells with keratohyalin granules. Lamellar bodies which contain stacks of lipid vesicles are concentrated in the upper part of the granular cells (Menon, 2002). Epidermal cells undergo extensive differentiation, starting from the highly proliferative basal layer, until they form the stratum corneum.

#### 1.3.2.1.1 Stratum corneum

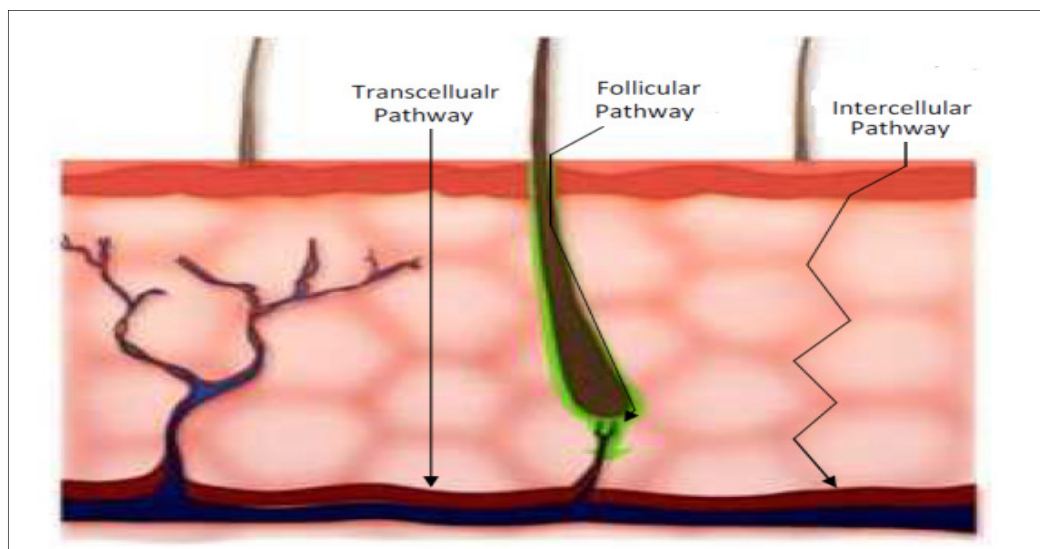
The stratum corneum, with its unique architecture, is often compared to a wall made of bricks and mortar as described by Peter Elias (1983). With the fully differentiated corneocytes comprising the bricks, embedded in the intercellular lipids, which represents the mortar. This outermost layer of the skin, where it plays a critical role in barrier function, is a heterogeneous non-living structure, formed by keratinized cells, protein-rich cells, and intercellular lipid layers. The phospholipids are absent in the stratum corneum, wherein they are the usual components of the membrane of living cells. The lipids form bi-layers and their acyl chains can exist as gel and as liquid crystalline states. The transition between these two states occurs at certain temperatures, without loss of the bilayer structure (Curatolo, 1987). The principal lipids of the stratum corneum are ceramide, free fatty acids and cholesterol (Elias, 1991). The non-polar lipids are saturated, and the membrane structures formed by these lipids are less permeable than a typical plasma membrane, thus providing a formidable barrier to the diffusion of drug molecules (Ghosh and Jasti, 2005). Thus, the barrier function of stratum is usually linked directly to its structure and composition, which is highly organized and predominantly lipophilic (Delgado-Charro and Guy, 2001). Stratum corneum is covered by a thin film called “acid-mantle”, due to its acidic pH in the range between 4.2-5.6, which is believed to result from lactic acid and carboxylic amino acids in sebaceous and eccrine sweat glands secretions (Washington et al., 2003). Therefore, the surface of the skin pH is around 5 (Hadgraft et al., 2000).

### 1.3.2.2 Dermis

The dermis, the thickest skin layer, is mainly comprised of connective tissues that provide support for the epidermis and other appendageal structures, specifically the hair follicles and sweat glands (Menon, 2002). This layer incorporates blood and lymphatic vessels, where the resorption of the drugs that passed across the epidermis can take place. It therefore represents the access point for molecules transdermally absorbed to the systemic circulation (Flynn and Stewart, 1988). The hypodermis is the innermost layer of the skin and provides its thermal insulation. It consists of the subcutaneous tissue filled with fat cells, fibroblasts and macrophages (Kulkarni, 2010).

### 1.3.3 Absorption pathways

A drug can penetrate through the skin, before it reaches the systemic circulation, by transcellular route (across the cells), intercellular route (between the cells), or through “shunt” pathways across the skin provided by appendageal structures, such as hair follicles and sebaceous glands (Barry, 2001). However, these skin appendages occupy only ~0.1% of the total human skin surface, thus the contribution of this pathway is usually considered to be small, though it is important for transportation of polar molecules and peptides. In contrast, the transcellular pathway represents the major route for drug transport (Aulton, 2007). Consequently, the lipid solubility of a molecule is vital for its transdermal delivery, since the extracellular space is concentrated with lipids. The different pathways of drug transport through the skin are shown in Figure 1.6.



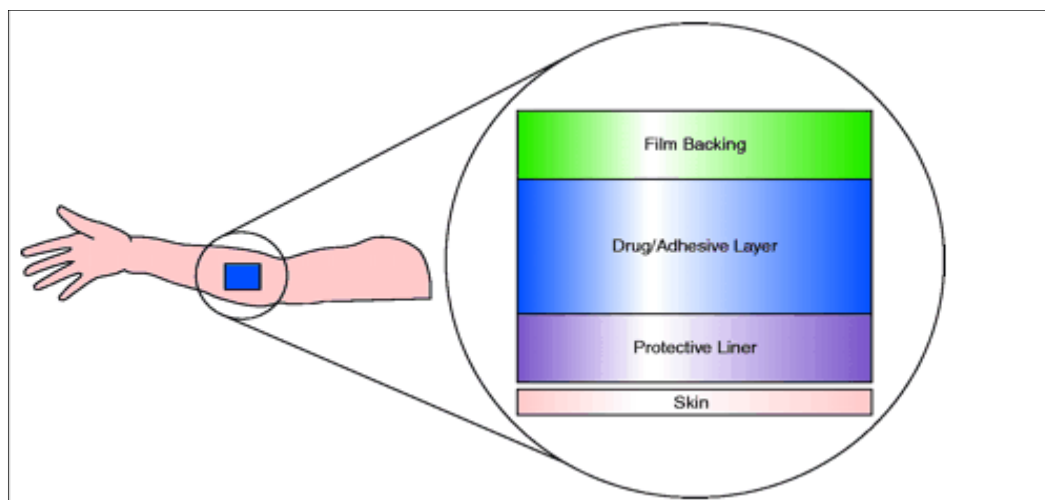
**Figure 1.6: Illustration of the possible pathways of molecules' permeation throughout the skin (transverse section view). Reproduced from [www.cdc.gov](http://www.cdc.gov)**

### 1.3.4 Transdermal drug delivery system design

Simple passive transdermal systems are often known as 'patches' which are diversely referred to as a matrix system, a reservoir system, or a drug-in-adhesive system. The classification is usually based on the components and fabrication of the systems. In general, reservoir systems composed of the medicine in a liquid, high volatile solvent that facilitates drug permeation after applying to the skin. Whereas the drug-in-adhesive or matrix systems do not employ these volatile solvents. Instead, they use absorption enhancers that do not volatilize during the preparation process and would be solubilised with the components in the matrix (Grawe et al., 2005). Reservoir systems are multi-layered systems and usually not cost effective to produce due to its complicated architecture (Stricker, 1983). The matrix systems are simplest in concept, consisting only of a layer of the drug that may be embedded in the adhesive matrix (monolithic). Owing to its simplicity, it is the most commonly form of transdermal/transmucosal systems (Prodduturi et al., 2007). However, the main structural elements of transdermal patches are common to all transdermal system designs, and these elements as shown in Figure 1.7 are (Buskirk et al., 1997):

- Backing material: the layer that provides integrity to the system.
- Drug layer or reservoir: the layer or layers which contain the drug substance.
- Protective liner (release liner): a removable film that protects the adhesive layer while the system is in the package.

- Adhesive system: materials (adhesives) that adheres the system to the skin or various layers in the transdermal system to each other.



**Figure 1.7: Common structural elements of simple transdermal drug delivery system (Scheindlin, 2004)**

In order to design a transdermal drug delivery system (TDDS), an understanding of the manufacturing attributes, as well as variables present in the formulation components of the product is important, because these factors may affect the reproducibility of release of the active drug substance to the stratum corneum and epidermis. This includes changes in the formulation composition involving adhesives, solvents, viscosity modifying agents that may have a significant effect on drug release. Therefore, adjustment in the levels of the patches' components may be made in order to maintain proper drug release and/or product adhesion/wear characteristics while minimizing irritation. Adhesion in TDDS is of prime importance to the safety, efficacy and quality of these systems. For example, poor or lack adhesion can result in improper dosing of patients while fallen patches can be picked up by children with a risk of accidental dosing (Wokovich et al., 2006).

Proper design of the delivery system can also influence positively the control of the plasma profile of administered drugs, especially those which have a short half-life or a high elimination rate constant. In general, the main measures that control active substance permeation across the skin from a transdermal patch are (Grawe et al., 2005):

- Particle size of the active substance-polymer.
- Active substance concentration and thermodynamic activity.
- Release surface area of the transdermal system.
- Solubility of the active substance in the polymer.
- Interaction of the active substance-polymer with the adsorbate water from the skin.
- Crystallinity of the active substance in the polymer.

Several techniques and tools have been developed to enhance the transdermal absorption of drugs. In general, they can be classified into two types. The first type is formulation-oriented. In this approach, efficient permeation across the skin can be attained through proper selection of the drug and optimization of the type and/or amount of the carrier system. The second type is skin barrier function-oriented. There are two approaches of this type. The first one modifies the barrier properties of the skin using chemical enhancers or physical stimuli such as an electric pulse or ultrasound. Significant skin toxicity or irritancy sometimes limits the use of these techniques for clinical applications. The second approach utilizes the modification of the thermodynamic activity of drug molecules in the vehicle used to deliver the drug. This does not require physicochemical alteration of the skin barrier, and therefore will be safer than the former one. A method using supersaturation may be categorized in the second type. In a supersaturated system, the drug molecules are dispersed in a vehicle at a level greater than its solubility inside this matrix or vehicle, resulting in temporarily high thermodynamic activity thereby leading to high skin permeability (Inoue et al., 2005).

#### 1.3.4.1 Permeation through the stratum corneum and its enhancement

Drug molecules released from a transdermal delivery system first partition into the stratum corneum, then diffuse into the lower layer of the skin and are finally transported into the blood stream. The drug concentration in the plasma after transdermal delivery is determined by the balance between the permeation rate across the skin (input) and the elimination/distribution rate in the body (Tojo, 1988). The thickness of the human stratum corneum, and the distance from the skin surface to the microcirculation, are 10-20  $\mu\text{m}$  and 150-200  $\mu\text{m}$ , respectively. Most drugs will penetrate the skin approximately proportionally to the concentration gradient between the upper and the lower side of the skin (Schaefer et al., 1982).

The basis for diffusion through membranes, such as the skin, is best described by Fick's diffusion law. According to this law, permeation through membranes is determined by the concentration gradient of the diffusing substance along the cross section of the membrane. Thus, the flux 'J' of a drug through the stratum corneum is given in the following equation:

$$J = (D_m C_{s,m} / L) \cdot (C_v / C_{s,v}) \quad (\text{Eq.1.1})$$

where  $D_m$  represents the diffusion coefficient of the drug in the membrane,  $C_{s,m}$  its solubility in the membrane,  $L$  the diffusion path length across the membrane,  $C_v$  the concentration of the drug dissolved in the vehicle and  $C_{s,v}$  the solubility of the drug in the vehicle (Moser et al., 2001). One of the strategies which may be postulated to improve permeation, based on this law, is *via* increasing the ratio  $C_v / C_{s,v}$ , i.e. the degree of saturation of the drug in the vehicle (the supersaturation approach). Supersaturated systems enhance the diffusive driving force for the drug delivery due to high thermodynamic activity or chemical potential of these systems. However, drug recrystallization from these metastable formulations makes this relationship short-lived.

A permeation enhancer can also be used with the general recognition that an ideal permeation enhancer will be pharmacologically inert and devoid of any toxicity or irritancy to the skin with reversible action (Escobar-Chávez, 2010). But it is unlikely that any enhancer will be found that has all of these properties, and compromises will have to be made. Water is perhaps the ideal enhancer. Hydrated skin is generally more permeable, due to the decreasing cohesive strength of the stratum corneum (Hadgraft, 1999). Common enhancers are usually lipophilic, low-volatile liquids such as fatty esters, medium or long-chain alcohols, emulsifiers, and terpenes. These additives generally improve skin resorption

properties (Horstmann et al., 1998), and their actions are mainly based on disturbing the lipid double-layers of the stratum corneum and weaken its diffusion-resistance structures.

Ethanol, for example, is frequently used in many transdermal systems as a permeation enhancer. The most common mechanisms proposed for its penetration enhancing activity involve increase of the drug solubility in the used vehicle (Pershing et al., 1990), in the stratum corneum (Megrab et al., 1995b) and may also (at high concentrations or prolong exposure) disrupt stratum corneum through extraction of its lipids (Morrow et al., 2007; Williams and Barry, 2004). Another example is fatty acids, such as oleic acid and lauric acid, which have been used to enhance the permeation of hydrophilic and lipophilic molecules by inducing defects and disordering the lipid structure of the stratum corneum (Benson, 2005).

#### 1.3.4.1.1 Hydration as a skin absorption accelerator

Normally the stratum corneum has a water content of approximately 20%, which lies primarily in the keratin layers between the horny cells (Repka and McGinity, 2001). The water content of the stratum corneum may attain equilibrium with the underlying tissues when the skin is soaked in water, exposed to higher humidity, or occluded without maceration. It is commonly believed that increased tissue hydration improves skin penetration of both hydrophilic and lipophilic drugs (Williams and Barry, 2004).

The mechanism by which water enhances transdermal permeation is not yet fully understood. One proposed mechanism stated that the high water content due to occlusion might hydrate the polar head groups of the bilayer, causing them to swell and disrupt the lipid domains. Therefore, the stratum corneum becomes disorganized and less cohesive, and hence more permeable (Warner et al., 1999). In another embodiment, lacunar domains embedded in the stratum corneum might expand laterally, interconnect and form continuous pore pathway at sites of desmosomal dissolution (Elias et al., 2002). This might enhance transdermal drug delivery. Finally, water within the tissue that could exist under excessive hydration as a result of prolonged occlusion, for instance, would alter the solubility of the permeants in the stratum corneum and modify their skin partitioning (Benson, 2005).

## 1.4 Research objectives

In pharmaceutical research there is a strong interest towards finding a novel formulation strategy that can synergize the concept of simplicity, safety and enhanced release program for transdermal applications. Therefore the aim of this thesis was to explore the concept of using hydration from the skin as a trigger for drug release from transdermal patches produced using hot melt extrusion. In this context, this work attempts to develop approaches to comprehensively characterise, understand and evaluate the formulated extruded transdermal patches, wherein described design issues such as carrier/drug optimization and understanding of the hydration influence as a modifying technique were discussed. Different methods and tools were employed for these investigations and ibuprofen was used as the model pharmaceutical drug throughout this work. General objectives were:

- Prediction of drug-carrier miscibility and determination of processing parameters for hot melt extrusion. The aim was to realize adequate HME processing to form solid solutions or dispersions where the drug remains miscible to boost the efficiency of these systems for longer. This work was mainly described in Chapter 4 and Chapter 6.
- To characterise and understand the physicochemical properties, *in vitro* drug release and *in vitro* permeation behaviour associated with the developed melt embeddings' patches in this study. The aim was to screen their potential for transdermal development. This work was detailed throughout the thesis.
- To modify the carrier system for improved drug release through variation of the type and amount of the materials incorporated in the assessed formulations. This work was described in Chapter 6.
- To examine the relationship between modified hot melt extruded products and hydration. The aim was to assess the hydration influence as a favourable approach to enhance permeation profiles *in vitro*. This work was outlined in Chapter 6, and led to the assessment of the most promising platform formulations.
- To evaluate the potential of the carrier systems of the promising platform extruded formulations to become a novel approach of transdermal drug delivery under the influence of hydration *in vitro* and *in vivo*. This work was described in Chapter 7 and Chapter 8.



## **Chapter 2: Materials and General methods**

## 2.1 Materials

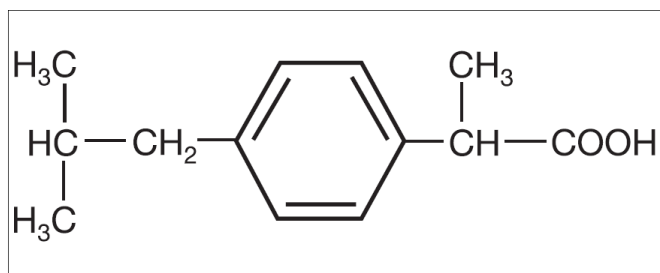
In order to explain the selection of the materials used to formulate extruded films in this work, a theoretical background is provided in this section, which in turn is subdivided into three parts that deal with the used model drug (section 2.1.1), carrier excipients (section 2.1.2) and then the source of these materials (section 2.1.3).

### 2.1.1 Model drug

Ibuprofen is one of the most commonly used non-steroidal anti-inflammatory agents (NSAIDs). Due to its many interesting physicochemical and biochemical properties, ibuprofen is used regularly as a model drug (Cano et al., 2001). In this work, ibuprofen was also selected as a model drug. The following sections will attempt to review its main properties and the factors which led to its choice.

#### 2.1.1.1 Description

Ibuprofen [2-(4-isobutyl-phenyl) propionic acid] molecule with an empirical formula  $C_{13}H_{18}O_2$  and a structural formula presented in Figure 2.1 has a molecular weight of 206.28 and it is hydrophobic in nature. Its octanol-water distribution coefficient gave log D values of 3.7, 3.6, 2.1 and 1.2 at pH values of 1, 4, 6 and 7, respectively (Higgins et al., 2001). A partition coefficient (log P (n-octanol/water)) value was reported in the range between 3.51 - 3.72 (Hadgraft et al., 2000). Ibuprofen is a Biopharmaceutics Classification System (BCS) Class II drug, which has high permeability and pH-dependent solubility (Potthast et al., 2005). Ibuprofen is a relatively weak organic acid with a pKa of 4.55 (Fini et al., 1995). This drug exists in the form of white or almost white, crystalline powder or colourless crystals. Ibuprofen has a melting point between 75-78°C and it is practically insoluble in water, freely soluble in acetone, methanol and in methylene chloride (British Pharmacopoeia Commission, 2011).



**Figure 2.1: Chemical structure of ibuprofen**

#### 2.1.1.2 Medical rationale

Ibuprofen has two enantiomers S (+) and R (-). The pharmacodynamic activity resides mostly in the dextrorotatory isomer, with (S) configuration (Shen, 1972). Nevertheless, R (-) ibuprofen has been found to undergo extensive inversion into active S (+) upon metabolism (Oliary et al., 2005). However, the racemic mixture of the two enantiomers is usually used. Having analgesic, anti-inflammatory and antipyretic activity (Sheth et al., 1980), ibuprofen has been used widely as analgesic and antirheumatic drug. Moreover, its proven efficacy and tolerability make it “the drug of choice” for treatment of many mild to moderate painful conditions, such as pain associated with headache, migraine and dysmenorrhoea, as well as, management and treatment of osteoarthritis and rheumatoid arthritis and other musculoskeletal disorders (Rasenack and Müller, 2002; Valle-Jones et al., 1984).

#### 2.1.1.3 Selection of ibuprofen

Despite being categorized as one of the safest NSAIDs available (Potthast et al., 2005), ibuprofen may produce gastrointestinal tract (GIT) adverse effects if administered orally. In addition to that, the short plasma half-life of almost  $2.0 \pm 0.5$  hours (Mäkelä et al., 1981; Davis, 1998) following the oral dosing requires frequent administration to maintain the desired steady state levels. With such frequent dosing regimens, patient compliance was found to be fairly poor (Sarkar et al., 1988). Therefore introduction of new NSAIDs or changing the route of administration to approaches such as the transdermal route would overcome these problems, through avoiding GIT pathway and to decrease the dose frequency using retard transdermal dosage form, thus a sustained and constant drug levels can be attained. Moreover, hepatic first-pass metabolism would be avoided using this route. However, the high doses (200-800 mg every 4-6 hours) needed to deliver therapeutic amounts of this drug is considered one of the main challenges to deliver it across skin.

Hence, a novel strategy is required to improve its transport *via* transdermal route in enough amounts.

As detailed in Chapter 1, for a drug to be successfully delivered into the blood stream transdermally, many requirements have to be fulfilled. As shown in Table 2.1, ibuprofen has many of the favourable properties that can be utilized to capture the benefits of its use in transdermal dosage forms, such as transdermal patches. In addition to that, Castelli et al. (2003) proposed ibuprofen ability to work as a lipid “fluidiser”, which is attributed to ibuprofen surface active properties (Fini et al, 1995), leading to its “self-permeation” and even permeation enhancement of other drugs across the skin as found by Al-Saidan (2004).

Molecular property	<sup>a</sup> Ideal drug	Ibuprofen
Molecular weight (D)	<400	206.28
Melting point (°C)	<200	<sup>b</sup> 75-78
Partition coefficient (logP <sub>(o/w)</sub> )	Between-1.0 and 4	<sup>c</sup> 3.51-3.72
Permeability coefficient (cm/h)	>0.5x10 <sup>-3</sup>	<sup>c</sup> 4.36x10 <sup>-2</sup>

**Table 2.1: Physicochemical properties of the ideal drug candidate for transdermal administration in comparison to the ibuprofen properties.** <sup>a</sup> (Ghosh and Jasti, 2005), <sup>b</sup> (British Pharmacopoeia Commission, 2011), <sup>c</sup> (Hadgraft et al., 2000)

It is worth to mention that since ibuprofen contains carboxylic acid, it can dissociate depending on the pH of the site of action and its pKa. Though unionized entities are suggested to be the main species that can pass readily across the lipid membrane (Aulton, 2007), it has been found that ionized molecules of ibuprofen and other NSAIDs can also permeate effectively due to enhanced solubility which is directly related to the maximum flux into the skin (Hadgraft et al., 2000). Thus, it can be concluded that ibuprofen with all aforementioned features can be chosen for a potential delivery using transdermal route that can circumvent problems associated with its oral delivery.

Several commercially available topical formulations contain ibuprofen, such as Ibuspray, Deep Relief Gel. However, the preparation of transdermal formulations containing ibuprofen is still growing. More recently, Strategic Science & Technologies, LLC (SST) has developed a method to successfully deliver ibuprofen transdermally. This product had the New Drug Application approval and it is in Phase III trials (<http://www.ebdgroup.com>, 2012).

Patches as transdermal drug delivery system are commonly prepared using the solvent casting method. Because of the low aqueous solubility of ibuprofen, the mode of preparation using this method necessitates the use of organic solvents. This is associated with environmental concerns, increased expenses and residual solvents that could elicit skin irritation. Therefore, it would be useful to develop these transdermal systems using another approach, such as hot melt extrusion (HME). As detailed in Chapter 1, HME is a solvent free method and, alongside other advantages, it has been used extensively in the recent years to disperse poorly water soluble drugs in polymers for enhanced delivery. The selection of ibuprofen in this study for processing *via* HME is also of particular interest. This drug can act as a plasticizer during processing (Kidokoro et al., 2001; Siepmann et al., 2006). Thus, association of plasticizing effect which can improve the processability, flexibility and elasticity of polymers and the active moiety in one agent i.e. ibuprofen, will limit possible side effects that could result otherwise from usage of many excipients for formulations intended for transdermal delivery. Therefore, ibuprofen is an ideal drug for evaluating the efficiency of extruded formulations for transdermal drug delivery designed as patches.

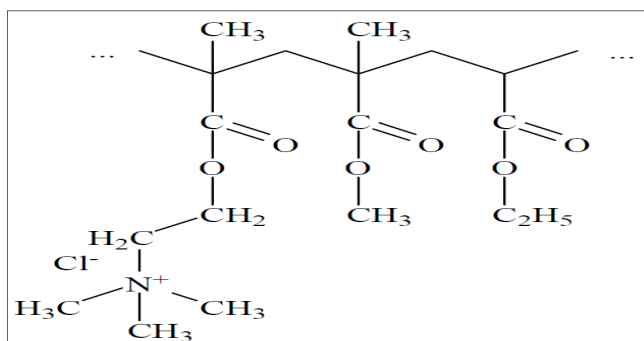
### 2.1.2 Carrier excipients

Several excipients in this section are described, wherein Eudragit RS PO was used as a basic component in the extruded formulations. Other excipients were chosen to tailor the release of ibuprofen from Eudragit RS PO extruded matrices as will be detailed in Chapter 6, with the aim to obtain delivery systems well accepted by the skin. Thermal stability for extrusion and physical characteristics of these materials will be evaluated in Chapter 3.

#### 2.1.2.1 Eudragit RS PO

Eudragit RS is one type of the well known biocompatible polymethacrylate polymers (Josephine et al., 2011). Eudragit RS is a copolymer synthesized from acrylic acid and methacrylic acid esters with 5% of functional quaternary ammonium groups (Rowe et al., 2009). The structural formula of this polymer is depicted in Figure 2.2. This cationic acrylic copolymer (Type B) is water insoluble (Perumal et al., 1999), yet able to swell and become permeable to solutes, due to the presence of the ionized hydrophilic ammonium groups (Pignatello et al., 2004). However, the presence of the ammonium groups as salts makes it permeable in a pH-independent manner (Rowe et al., 2009). Eudragit RS PO is the powder form of this polymer, which occurs as a fine white powder with amine-like odor. Eudragit RS PO is a glassy polymer with glass transition temperature of about 50-55°C (Fujimori et al. 2005; Kidokoro et al., 2001). The main feature of a glassy polymer is the transition from

largely brittle glassy behaviour at low temperature to a rubbery or viscoelastic state at high temperature. This polymer has been widely used in pharmaceutical delivery systems for sustained drug delivery (Oth and Moës, 1989), hot melt extrusion (Wu and McGinity, 2003), micro-encapsulation (Perumal, 2001), nanoparticles (Adibkia et al., 2011; Lopodota et al., 2009), antiretroviral drug delivery (Khan et al., 2008), colon delivery (Kaur and Kim, 2009). It has also been used in transdermal drug delivery (Cilurzo et al., 2006; Gohel and Nagori, 2009; Kusum et al., 2003), thanks to its biocompatibility and biological safety (Fujimori et al. 2005).

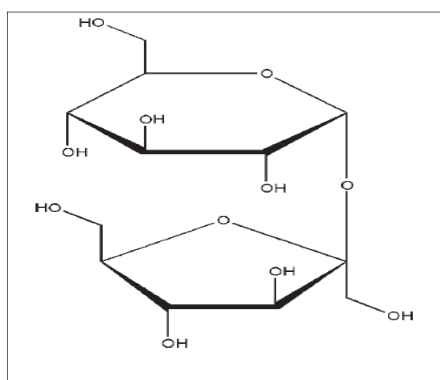


**Figure 2.2: Eudragit RS PO chemical structure (eudragit.evonik.com)**

As Eudragits are approved pharmaceutical materials for hot melt extrusion (Andrews et al., 2009) and being described in the context of skin application with no known toxicity, Eudragit RS PO represents a good choice for preparation of the transdermal systems using hot melt extrusion. Moreover, its ability to provide sustained release depending on the applied concentration (Rapolu et al., 2012), Eudragit RS can provide appropriate dosing input for short-lived drugs as ibuprofen. However, it is worth mentioning that for ibuprofen, the design of formulation depends on the indication. For example, rapid release is required for acute onset pain, but rheumatoid arthritis treatment might require slow sustained release pattern to drive patient compliance of less frequent dosing. The relatively high viscosity of Eudragit RS (Kim et al., 2002) might contribute to enhance dispersive mixing during the extrusion as suggested by Kolter et al. (2010), especially when combined with a plasticizer such as ibuprofen to enhance processability during extrusion. Therefore, all these features might explain why Eudragit RS PO could be adequate parent polymer, used basically in this work as a vehicle or carrier for potential transdermal delivery of ibuprofen formulated by HME technology.

### 2.1.2.2 Sucrose

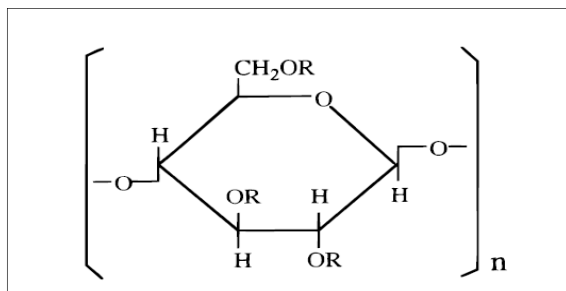
Beet sugar or sucrose is  $\beta$ -D-fructofuranosyl- $\alpha$ -D-glucopyranoside with a chemical structure shown in Figure 2.3. It is one of the most widely used pharmaceutical excipients for oral formulations and generally considered as a safe material (Rowe et al., 2009). In skin preparations, this sugar has been used in both topical formulations (Repka et al., 2002) and wound dressings (Knutson et al., 1981). Utilizing the known ability of carbohydrate sugar carriers to enhance wettability of the drugs due to their polar heads (Das et al., 2011; Saharan et al., 2009), and because of its general safety in addition to availability and low cost (Polat and Linhardt, 2001), crystalline sucrose has been used in this work.



**Figure 2.3: Structural formula of sucrose (Rowe et al., 2009)**

### 2.1.2.3 Methyl cellulose

Methyl cellulose (MC) is derived from cellulose in which the hydroxyl groups are substituted with methyl ether with different degrees (Kazuto et al., 1999). The grade used in this study (Methocel A4C Premium MC) has approximately 27.5 to 31.5 % methoxyl, yielding good water solubility (Colorcon, 2009), which occurs as white to off-white color powder. The structure of this polymer is presented in Figure 2.4. This water-soluble polymer is generally regarded as non-toxic, non-allergenic and non-irritant material that is widely used in oral, topical formulations (Rowe et al., 2009) and transdermal systems (Edwards, 1998; Grawe et al., 2005). Due to the hydrophilicity of this polymer and its tolerable immunological properties, this polymer was investigated as an adjuvant that is capable of modulating release properties of the studied patches for potential transdermal application.



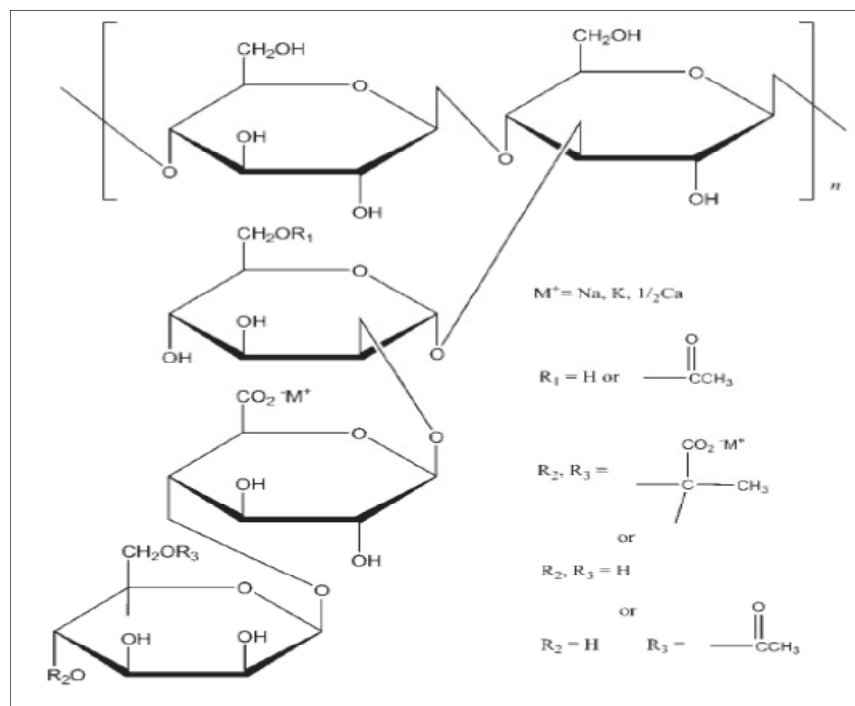
**Figure 2.4: Structural formula of methylcellulose. R=CH<sub>3</sub> or H (Kazuto et al., 1999)**

#### 2.1.2.4 Xantural®75

Xantural®75 is a cream colored free flowing fine powder with particle size of approximately 75µm of xanthan gum (CPKelco, 2003). Xanthan gum is a natural gum obtained by microbial fermentation with *Xanthomonas campestris*. The term “gum” usually refers to a group of industrially useful polysaccharides (glycans) or their derivatives. Xanthan gum is a polysaccharide consisting D-glucose and D-mannose as the dominant hexose units, along with D-glucuronic acid which gives this polymer a negative charge (anionic material), and is prepared as sodium, potassium, or calcium salt (Zohuriaan and Shokrolahi, 2004). The structural formula is illustrated in Figure 2.5.

As a hydrophilic polymer, xanthan gum can be used to tailor the drug release profile. This polymer can display a high degree of swelling due water uptake, polymer relaxation and possibility of pore formation which could contribute to the drug release (Mundargi et al., 2007; Munday and Cox, 2000; Verhoeven et al., 2006). Xanthan gum is a non-toxic, biocompatible material which does not show any skin irritating or allergenic effect in rabbits or guinea pigs, respectively, following skin exposure (Rowe et al., 2009). It has been described in transdermal applications (Dezfuli et al., 2012; Masiz et al., 1998) and hot melt extruded formulations (Fukuda et al., 2006; Verhoeven et al., 2006).

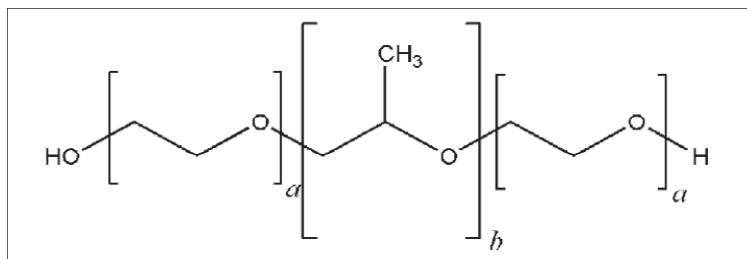




**Figure 2.5: Structural formula of xanthan gum (Rowe et al., 2009)**

#### 2.1.2.5 Pluronic® F127

Pluronic® F127 or poloxamer 407 is a non-ionic tri-block copolymer of polyoxyethylene (PEO)-polyoxypropylene (PPO)-polyoxyethylene (PEO) (Moore et al., 2000). It occurs as white, waxy, free-flowing flakes with a structural formula presented in Figure 2.6. It is the least toxic grade of the commercially available poloxamers (Hatefi and Amsden, 2002). This semi-crystalline polymer is believed to have crystalline domains of PEO and amorphous segments of PPO (Smithey et al., 2007; Yin et al., 2005). While the polyoxyethylene segments are hydrophilic, the polyoxypropylene segments are hydrophobic, giving rise to its amphiphilic character with HLB value of 22 (Cunha-Filho et al., 2012). Poloxamers are used as solubilising agents and vehicles for drug delivery systems and has been described in topical and transdermal systems, owing to their non-irritating and non-sensitising properties (Chi et al., 1996, Escobar- Chávez et al., 2006).



**Figure 2.6: Structural formula of Pluronic® F127, a=101, b=56 (Rowe et al., 2009)**

#### 2.1.2.6 Gelucire 44/14

Gelucire 44/14 is a GRAS material that has been used for many years in oral delivery systems which belongs to the Lauroyl polyoxylglycerides (macroglycerides) family. It consists of a mixture of monoesters, diesters and triesters of glycerol, and monoesters and diesters of polyethylene glycols (Rowe et al., 2009). Gelucire 44/14 is manufactured by *Gattefossé SA, Saint Priest, France*, from the reaction of hydrogenated palm kernel oil with polyethylene glycol (PEG) 1500 or PEG 33. Its composition, thereof, is approximately: 20% mono-, di-, and triglycerides, 72% mono- and di-fatty acid esters of PEG 1500 and 8% free PEG 1500 (Gattefossé, 2000). The fatty acid distribution of this amphiphilic excipient is shown in Table 2.2. Gelucire 44/14 is inert semi-solid which occurs as a white to pale-yellow waxy material. Gelucire 44/14 is mainly crystalline with less than 17% amorphous regions and some liquid glycerol (Svensson et al, 2004). It is identified by two values: a nominal melting point of approximately 44°C and the HLB (Hydrophilic-Lipophilic Balance) value of 14. It is surface active excipient (Kawakami et al. 2004), water-soluble (Ahuja et al., 2007), which does not absorb moisture or show limited water uptake at humidity levels below 80%RH, at room temperature (Gattefossé, 2000). This is thought to be brought about by assuming that each component of Gelucire 44/14 absorbs water independently. Thus, at low relative humidity levels up to 70%RH, a small amount will be absorbed corresponding to the low amount of liquid glycerol, followed by surge water uptake by PEG33 and PEG esters at RH values above 70% and 80%, respectively (Svensson et al., 2004).

Because of its useful properties such as solubilising ability (Karatas et al., 2005; Kawakami et al., 2004), self-emulsifying properties (Chambin et al., 2004; Kale and Patravale, 2008; Kallakunta et al., 2013; Rowe et al., 2009), Gelucire 44/14 had a numerous pharmaceutical applications, such as improved drug release (Antunes et al., 2013) and bioavailability enhancement (Barker et al., 2003; Kale and Patravale, 2008; Yüksel et al., 2003). It has been

used to a limited extent for topical delivery (Li, et al., 2008; Mandawgade and Patravale, 2008; Nicholas, and John, 2003) and there are no reports that we are aware of regarding any irritation or toxicity associated with application to the skin.

Fatty acid distribution	Percentage in Gelucire 44/14
Caprylic acid (C8)	4-10
Capric acid(C10)	3-9
Lauric acid(C12)	40-50
Myristic acid(C14)	14-24
Palmitic acid(C16)	4-14
Stearic acid(C18)	5-15

**Table 2.2: Fatty acid distribution in Gelucire 44/14 (Chambin et al., 2004)**

### 2.1.3 Sourcing of the used materials

Model drug	Ibuprofen	Ibuprofen 25 US Quality Lot No.: IB1T0513 BASF company
Carrier excipients	Eudragit RS PO	Lot No.: G091038159 Evonik Röhm Pharma polymers
	Sucrose	Lot No.: 0001434877 SIGMA Life Science Sigma-Aldrich.com
	Methylcellulose	METHOCEL A4C PREMIUM Lot No.: DT319838 Colorcon company
	Xantural®75	Lot No.: 6g2349K CPKelco (A Huber Company)
	Pluronic® F127	Lot No.:027K0033 Sigma-Aldrich, BASF
	Gelucire 44/14	Lot No.: 105656 Gattefossé SA, Saint Priest, France

**Table 2.3: Materials' sourcing**

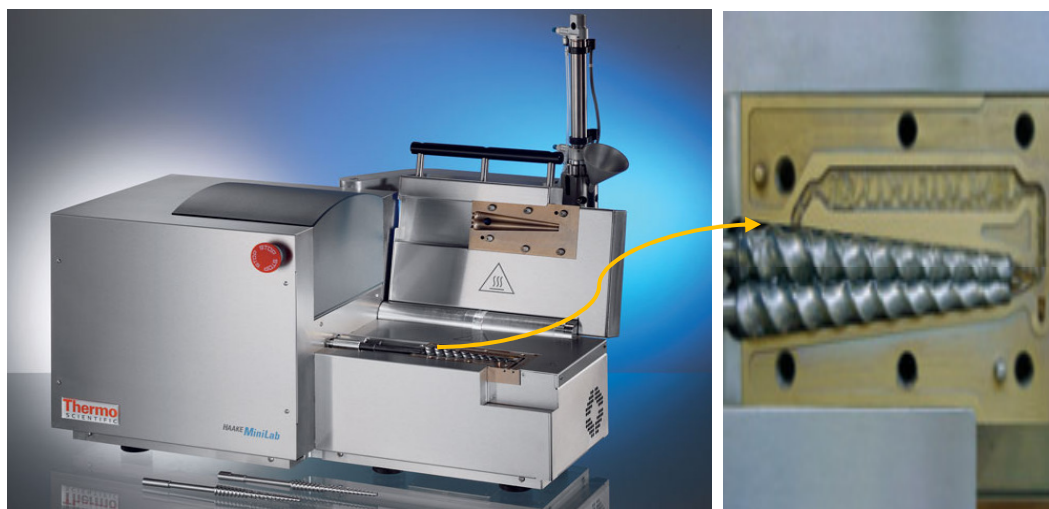
## 2.2 Methods

An overview of the various experimental techniques used throughout this study is covered in this section. However, the methods used to assess *in vitro* release and *in vitro* permeation of the drug from the extruded formulations were detailed and described during corresponding chapter.

### 2.2.1 Preparation of hot melt extruded transdermal patches

Transdermal drug delivery systems as patches can be prepared by either solvent casting method or by hot melt extrusion technology. As detailed in Chapter 1, though solvent casting is widely used to produce these systems, doubts arise over its high costs, long processing times, environmental concerns and residual solvent that may cause some skin irritation (Aitken-Nichol et al., 1996). Hot melt extrusion method appears to overcome these problems and has found its place in pharmaceutical field for numerous applications such as production of topical and transdermal films (Breitenbach et al. 2009; Crowley et al., 2004; Crowley et al., 2009; Mididoddi et al., 2006; Repka et al., 1999 ;Trey et al., 2007).

The hot melt extrusion method chosen in this work depends on the drug and the carrier excipients involved, hence the employed parameters might vary and will be discussed in Chapter 4 and 6. However, in a generic and basic sense this process involved the following steps: (a) Mixing of the drug and carrier excipients to form a powder blend. (b) Heating the barrel at the set temperature and determine the speed for screws' rotation. (c) Feeding the extruder by the powder blend through a hopper. (d) Flushing the melt through a die after being cycled for appropriate time (residence time inside the extruder) to ensure good mixing. (e) Collecting the product (extrudate) from the outlet along customized conveyor belt, spread over a backing layer, such as aluminium foil, and to allow for cooling at room temperature. (f) Cutting the extrudate into the desired dimensions. In this work, the extrusion was performed using a co-rotating twin-screw extruder (Haake Minilab II Micro Compounder, Thermo Scientific), shown in Figure 2.7. This type of extruders is considered the most important type in industry, due to its ability to perform at high rotation speeds, allowing high outputs yet keeping good mixing and conveying properties (Kolter et al., 2010). For purging purposes before the production of each individual batch, a cleaning polymer (Asaclean U, Evonik industrial, Lot No. 07813) was fed into the extruder at 180°C and circulated for ten minutes as recommended by the manufacturer.



**Figure 2.7: Thermo Scientific Haake Minilab II Micro Compounder. Insert showing magnification of the melting zone with twin screw assembly. Reproduced from [www.thermo.com](http://www.thermo.com)**

## **2.2.2 Characterisation methods used for the evaluation of hot melt extruded formulations for transdermal delivery**

### **2.2.2.1 Thermoanalytical techniques**

Thermoanalytical techniques are used to explore a range of chemical and physical properties. From pharmaceutical perspective, these techniques have been used extensively to characterise pharmaceutical materials from phase transitions to drug-excipient compatibility, in addition to the prediction of long-term behaviour such as physical stability (Craig and Reading, 2007). The findings of each technique are a valuable source of information; however, it is often more useful to have more than one technique to complete or confirm the characterisation of the material. In this work, differential scanning calorimetry (DSC) was used in its conventional and modulated modes, in addition to thermogravimetric analysis (TGA) and hot stage microscopy (HSM) techniques.

### 2.2.2.1.1 Differential scanning calorimetry (DSC)

#### 2.2.2.1.1.1 Basic principle and instrumentation

Differential scanning calorimetry is a technique that measures the change of the difference in the heat flow to the sample and to a reference sample, as a function of time and temperature, while they are subjected to a controlled program in a specified temperature, time and atmosphere (Höhne et al., 1996), providing detailed information about both physical and energetic properties of a substance (Clas et al., 1999). There are two commercially available types of DSC operating systems: heat flux and power compensation. In brief, heat flux DSC performs using a single furnace, heat flows into two identical platforms, one contains the sample pan and the second for an empty reference pan. Thermocouples are positioned beneath the platforms in a back-to-back arrangement to measure the temperature difference between the sample and the reference as a function of the voltage developed from the thermocouples, allowing measurements of the heat flow. On the other hand, power compensation DSC has two individual furnaces, one for the sample pan and the second for an empty reference pan. The temperature difference between the sample and the reference is compensated for by varying the electrical power supplied to the two furnaces. Therefore, in this case heat flow is derived from direct measurements of electrical power required to sustain the heating of the two pans at a constant temperature.

The TA Instruments DSC used during this thesis operated by heat flux and a basic schematic is shown in Figure 2.8. During DSC experiment the measurement of the differential heat flow can be explained by Ohm's Law as follows:

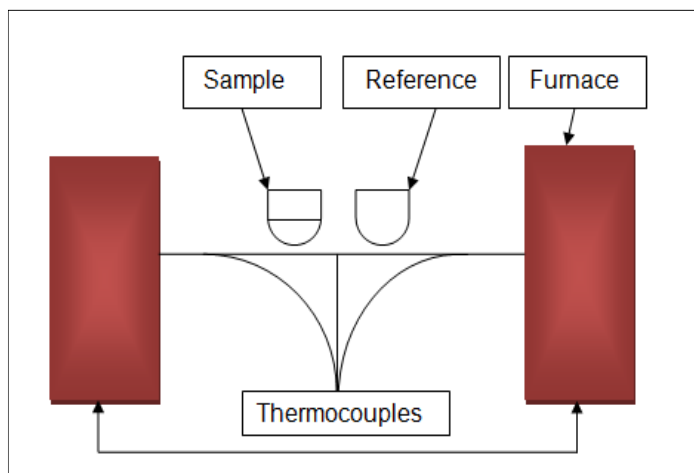
$$\frac{dQ}{dt} = \frac{\Delta T}{R} \quad (\text{Eq.2.1})$$

where  $Q$  = heat,  $t$  = time,  $(dQ/dt)$  represents the heat flow,  $\Delta T$  = temperature difference between sample and reference and  $R$  is the thermal resistance in the heat flow path between the furnace and the pan (Craig and Reading, 2007). The reference pan is essential to eliminate influences that might affect the differential heat flow, such as the heat adsorption by the pan, allowing better measurements of the material properties. Furthermore, the  $\Delta T$  signal requires calibration using high purity calibration standards to ensure that heat flow is a function of temperature as will be discussed in the following section.

Heat capacity of the studied material ( $C_p$ ) determines the heat flow signal during the experiment, thus a DSC signal can be expressed as:

$$\frac{dQ}{dt} = C_p \frac{dT}{dt} \quad (\text{Eq.2.2})$$

where  $dQ/dt$  represents the heat flow,  $dT/dt$  represents the heating rate and  $C_p$  is the heat capacity defined as the amount of heat required to raise the temperature of one gram of the material by one degree Celsius (Craig and Reading, 2007).



**Figure 2.8: Schematic diagram of heat flux DSC**

#### 2.2.2.1.1.2 Instrument calibration and sample preparation

The reliability of the results obtained by DSC depends on proper instrument calibration. Defined calibration procedures are usually performed which involve the use of highly pure materials known as calibration standards with known enthalpies of melting and materials with known heat capacities.

DSC calibration typically takes three steps. The first step is called baseline calibration, which records the instrument performance with an empty DSC cell over a temperature range, followed by using aluminium oxide (sapphire) disks to verify cell resistance and capacitance. The second step is used for cell constant/heat flow calibration. In this procedure indium is usually used, because it can be useful for both enthalpy and temperature calibrations. In this step the literature melting temperature is compared to the observed experimental value, from which cell constant is calculated and fed into the software of the

machine to correct the heat flow. Third step is usually recommended to ensure accurate measurements as close as possible to the studied transition temperatures. Therefore, temperature calibration is performed over the temperature range of interest, using standards with known transition temperatures, where their peak temperatures and peak areas are then determined and programmed into the instrument. In this work, these steps were conducted prior experimentation to achieve calibration of the conventional or standard DSC (cDSC) mode. Indium standard ( $T_m$  156.6°C, Heat of fusion  $28.6 \pm 0.2$  J/g) was used to calibrate the DSC temperature and enthalpy scale. Other calibrants used were N-Octadecane ( $T_m$  28.2°C), Benzoic acid ( $T_m$  122.4°C) and Tin ( $T_m$  231.9°C) for temperature calibration over the temperature range used and experiment conditions.

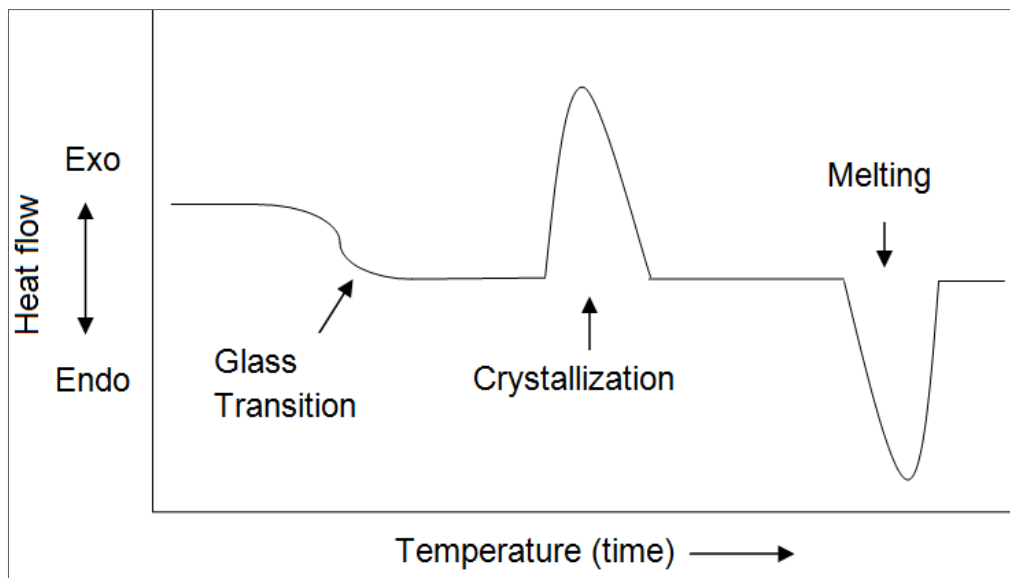
All experiments were carried out under inert atmosphere, using nitrogen to create reproducible atmosphere around sample and reference during the experiment, purged at a rate of 50 ml/min. The mass of each empty sample pan was matched to the mass of the empty reference pan within  $\pm 0.05$  mg. Throughout this thesis, consistency of sample size and repeatability ( $n=3$ ) were taken into consideration in attempt to provide reproducible results. Samples were loaded and crimped into TA standard aluminium pans. The flatness of the bottoms of the pans was checked before loading into the DSC cell to ensure good heat transfer between the DSC and the pan as recommended by Craig and Reading (2007). DSC of Q series (1000) equipped with a refrigerated cooling system (TA Instruments, United Kingdom) was used to obtain data. Further details about the methods developed and used are outlined in the relevant sections. Analyses were performed using TA Universal Analysis 2000 software.

#### 2.2.2.1.1.3 Information derived from differential scanning calorimetry (DSC)

DSC measures the total energy associated with a thermal event at any particular temperature or time interval and the data is usually presented as a plot of heat flow against temperature as illustrated in Figure 2.9. Ideally, the empty pans of sample and reference will result in the heat flow signal as a horizontal line known as the baseline. Changes of the heat capacity between the sample and the reference indicate the occurrence of thermal transition(s) accompanied by displacement of this baseline, such as the jump observed when the material goes through its glass transition region or the peaks during melting or crystallization events, etc., as shown in the DSC curve in Figure 2.9. Endothermic and exothermic thermal events are usually expressed as downward and upward peaks, respectively. The area under the curve is proportional to the total enthalpic change.



DSC is widely used in the pharmaceutical field to assess various materials through providing qualitative and quantitative information about the physicochemical properties of these materials. Examples include compatibility studies of drug with excipients (Mura et al, 1995; Mura et al., 1998; Pignatello et al., 2004), effect of moisture on glass transition and stability (Jain et al., 1998; Steendam et al., 2001), kinetic investigations (Macêdo and Nascimento, 2002) and polymorphic transition (Marthi et al., 1992).



**Figure 2.9: Schematic of typical DSC curve includes commonly observed transitions**

#### 2.2.2.1.2 Modulated temperature DSC (MTDSC)

In thermal analysis techniques, conventional DSC is an integral tool to measure different samples' response that is associated with temperature and energy change after application of a linear heating signal. An extent to this technique is the modulated temperature DSC (MTDSC). This method involves more complex temperature profile; however, represents a great potential in physical characterisations and general use in pharmaceutical sciences that yet to be further explored.

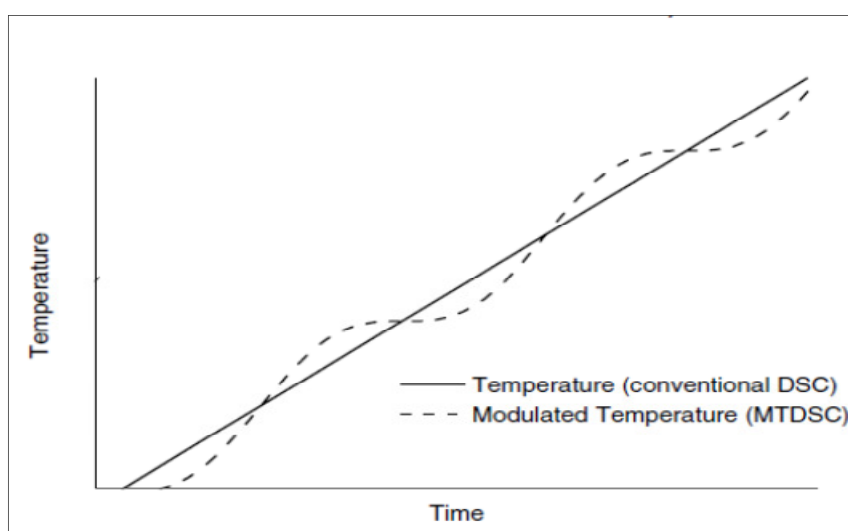
##### 2.2.2.1.2 .1 Principle of operation

Modulated temperature DSC (MTDSC) is a technique which measures the difference in heat flow between a sample and an inert reference in the same heat flux cell design as the conventional DSC. However, this technique lies in a software modification whereby a different heating profile is applied to allow the superimposition of a modulation (oscillation)

on the underlying conventional linear signal as illustrated in Figure 2.10. This perturbation (a sinusoidal wave in most cases) of the temperature regimen is combined with mathematical procedures to yield a profile that allows the deconvolution of different sample behaviours. The resulting MTDSC heat flow can be expressed as:

$$\frac{dQ}{dt} = Cp \frac{dT}{dt} + f(t, T) \quad (\text{Eq.2.3})$$

where  $Q$  is the (heat) energy,  $Cp$  is the heat capacity,  $T$ = the absolute temperature,  $t$  = time, and  $f(t, T)$  is some function of time and temperature that governs the response associated with the physical or chemical transformation (Coleman and Craig 1996).



**Figure 2.10: Temperature regimen as a function of time for conventional and modulated temperature DSC (Craig and Reading, 2007)**

In the MTDSC measurements, the heating rate is modulated as a result of modulating temperature. This allows separation of the reversing (heat flow associated with heat capacity) and non-reversing (heat flow associated with kinetically controlled chemical or physical process), because the sample's response to the modulation is different from its response to the linear component of the heating program (Craig and Reading 2007).

Proceeding with the deconvolution or separation of these components, the following equations of the MTDSC temperature program is applied:

$$T = T_0 + bt + B\sin(\omega t) \quad (\text{Eq.2.4})$$

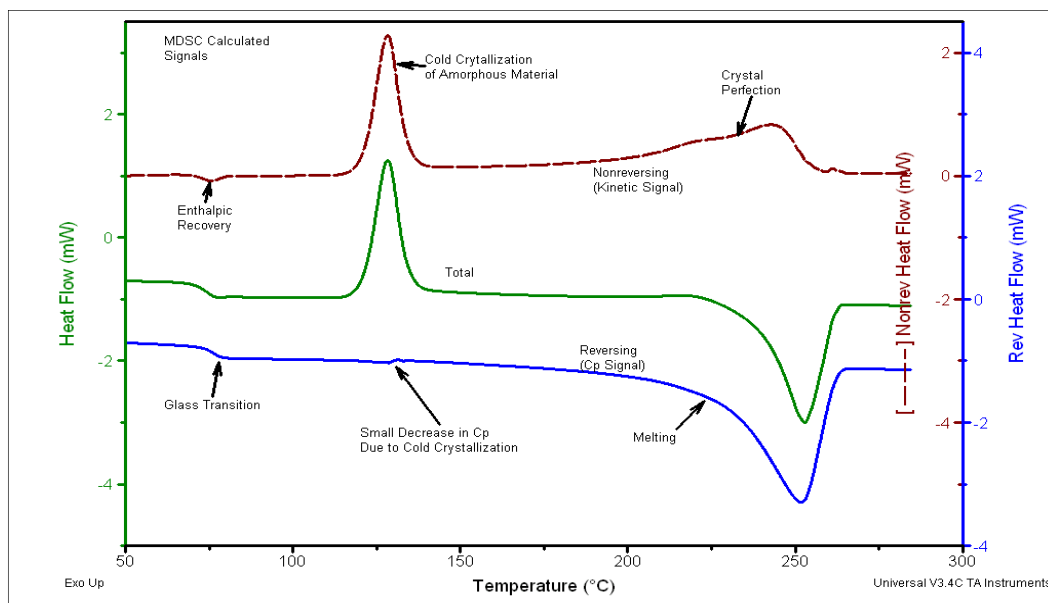
Where  $T_0$  is the starting temperature,  $b$ = the heating rate,  $B$ = the amplitude of the modulated temperature and  $\omega$  is the frequency. Therefore the equation (2.3) can be rewritten as:

$$\frac{dQ}{dt} = Cp(b + B\omega \cdot \cos(\omega t)) + f'(t, T) + C \sin(\omega t) \quad (\text{Eq.2.5})$$

Where  $f'(t, T)$  is the average underlying kinetic response,  $C$  = the amplitude of the kinetic response to the sine wave modulation, and the sinusoidal heating rate corresponds to  $(b + B\omega \cdot \cos(\omega t))$  and equivalent to  $dT/dt$  (Coleman and Craig 1996).

Therefore the reversing heat flow is obtained from the heat capacity component of the total heat flow ( $Cp \cdot dT/dt$ ). The reversing heat capacity can be derived by dividing the amplitude of the modulated heating flow by the amplitude of the modulated heating rate. This value can be multiplied by the linear component of the heating rate ( $b$ ) to obtain reversing heat flow. This is associated with reversing transitions such as glass transition and most melting. The non-reversing heat flow is obtained by subtracting the reversing heat flow from the total heat flow. It is typically associated with the transitions that are non-instantaneous or reversible over the course of the time and temperature of their detection. It is associated with the kinetic components ( $f'(t, T)$ ) and involves transitions such as crystallization, enthalpy recovery, decomposition and loss of a volatile such as water.

By way of example, Figure 2.11 shows the results of simple deconvolution for MTDSC heat flow signals of quench-cooled polyethylene terephthalate (PET). However, true sample modulation might not be achieved during a melting process. This is because uniform temperature within the sample during melting event, which is associated with large amount of enthalpy, is often difficult. Thus, reversing heat capacity would be frequency dependent during this event. Therefore, unless isothermal measurements are ensured, only qualitative assessment of melting is useful using MTDSC (Craig and Reading, 2007).



**Figure 2.11: Thermoanalytical curve of quench-cooled PET showing the simple deconvolution (separation) of the MTDSC heat flow signals (Thomas, 2005)**

#### 2.2.2.1.2.2 Instrumentation

In order to maximize the quality of the results obtained by MTDSC measurements, there are three key experimental conditions that can be optimized, namely, the modulation period, the modulation amplitude and the underlying heating rate. A proper selection of these parameters has a profound influence on the measurements undertaken. In other words, the period of modulation must be sufficiently long to allow enough time for heat to flow between the sensor and the sample. Whereas the modulation amplitude should be chosen to provide a good sensitivity (large enough) to reveal the event with a sufficiently slow underlying heating rate to provide a number of modulation cycles over transitions of interest (at least six modulated cycles), thus better resolution. Normally, periods of 30 to 100 seconds are used, the modulation temperature amplitude in the range of  $\pm 0.1^{\circ}\text{C}$  to  $\pm 1.0^{\circ}\text{C}$  and underlying heating rates between 1 to  $5^{\circ}\text{C}/\text{min}$  (Craig and Reading, 2007).

MTDSC experiments were performed using the same DSC machine (TA Instrument DSC Q1000) and the sample preparation, DSC calibration (three steps) detailed for conventional DSC experiments are the same herein. However, MTDSC mode experiment necessitates a fourth set of calibration to calibrate heat capacity signals (heat capacity calibration). This calibration is required for more accurate quantification of the deconvoluted results, through reversing heat capacity calibration. For that purpose, clear disk of aluminium oxide was used

as a calibration standard, whereby the heat capacity constant determined by simply dividing the literature heat capacity of that standard by the measured heat capacity, both at the mid-point of the studied temperature range. Further details regarding the parameters set for the MTDSC experiments are described within the relevant experimental section in Chapter 3.

#### 2.2.2.1.2 .3 Pharmaceutical applications

MTDSC has lend itself as a well-established technique to characterise pharmaceutical systems, such as detection of phase separation (Six et al., 2003) and as a complementary technique to understand and investigate drug delivery systems, especially those based on polymeric materials (Wang et al., 2005).

This technique is the method of choice to study glassy systems or amorphous materials, where an excellent detection of glass transitions can be made (Hill et al, 1998). It can enhance the resolution, through slow underlying heating rate, without affecting sensitivity. In fact it increases the sensitivity, through high rate of temperature change. This would result in generation of high heat capacity signal (and hence the reversing signal), where a signal to noise ratio is enhanced and subtle (weak) glass transitions are apparent. In addition to that, the measurements will not be effected by the shifting in the instrumental baseline, because the heat capacity will be calculated from the modulated amplitude. On the other hand, conventional DSC is better than MTDSC for melting measurements. As mentioned in earlier discussion, the melting event is a complex process to be truly modulated. The melting is a linear function of heating rate and in MTDSC technique this linear response may be lost. Hence, there is a limited applicability of MTDSC to study this event quantitatively.

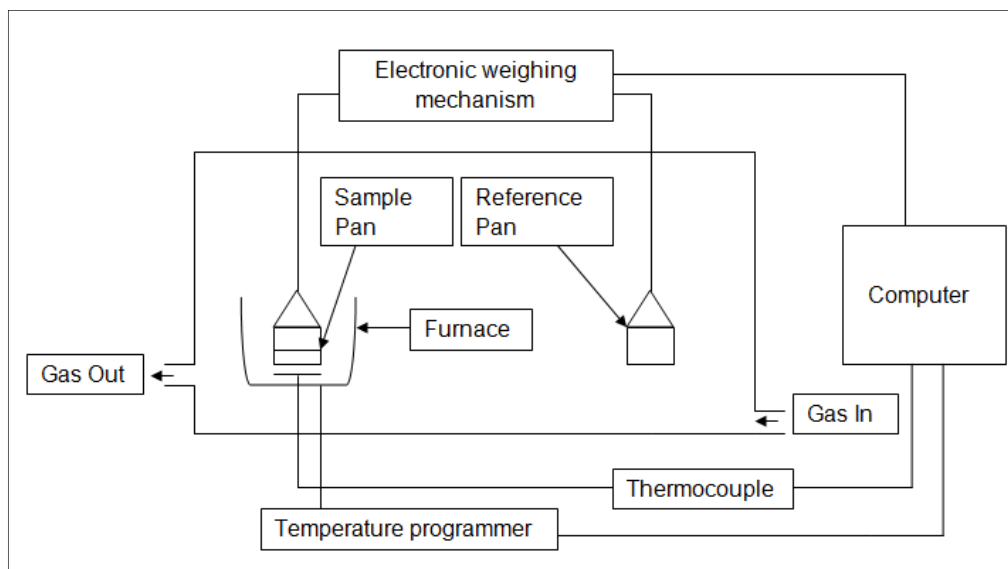
#### 2.2.2.1.3 Thermogravimetric analysis (TGA)

Thermogravimetric analysis (TGA) is one of the simplest and oldest thermal analysis techniques. This technique involves measurement of weight loss as a function of temperature in a controlled atmosphere or weight gain also as a function of time at a single temperature (Hunt and James, 1993). Thermogravimetric analysis (TGA) describes any experimental method whereby changes in mass are used to study physical or chemical process. In this work, TGA was used to investigate the thermal decomposition to assess thermal stabilities and to study water content of the samples. It is noteworthy to mention that mass loss measurements do not detect melting or other phase changes.

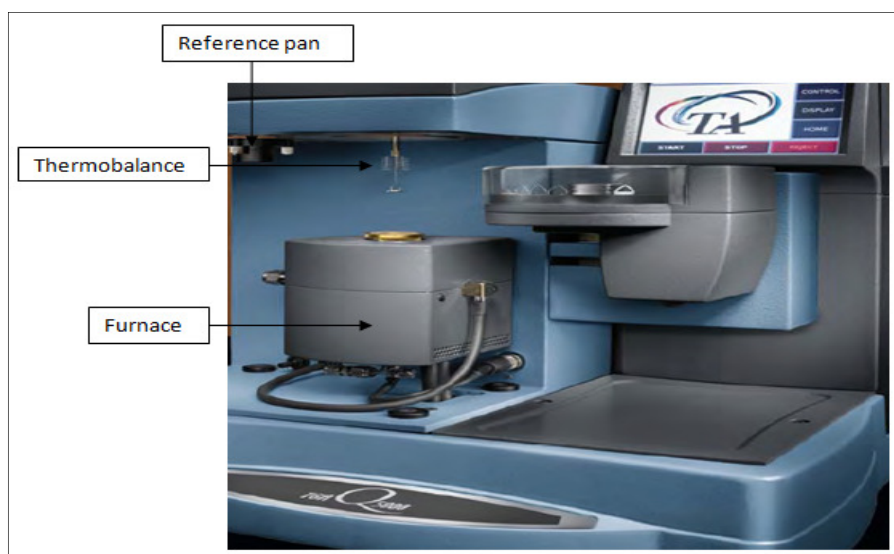
#### 2.2.2.1.3.1 Instrumentation

Common apparatus of thermogravimetry (TG) are depicted in Figure 2.12. Thermobalance is the main part of TG, it encompasses furnace equipped with a temperature control system, and thus the heat transferred to the sample is adjusted to a constant or programmed temperature. A thermocouple is placed close to the sample holder to measure and record sample temperature. Samples, which are usually contained in open light aluminium or platinum pans, are incubated in reaction container, which should be thermally stable and inert, under controlled atmosphere, usually inert gas. Taring of the empty sample pan is performed before the sample is loaded to ensure that the balance giving the accurate reading, therefore reference empty pan of the same size and type is used on the tare side for proper operation. The balance operates on a null position, which is usually restored using a magnetic force generated by an electric current acting on a magnetic material. Sample size should be small enough to avoid uncertainties associated with temperature variations within the sample yet representative of the bulk material and performing repeated identical experiments can verify the results.

The modes of operation can be isothermal, wherein the sample temperature is held constant throughout the experiment or variation mode, thus the temperature is changed with time according to a specified program. A constant rate of temperature increase has been widely used (incremental variation mode). To optimize performance it may be necessary to perform calibration, which is usually for temperature and mass. Mass calibration is usually performed using standard weights. The temperature calibration is often obtained using the Curie point magnetic method with SRM Nickel described in American Society for Testing and Materials (E1582-93). In this work, TGA was operated in standard variation mode and isothermal mode using TA Instrument TGA Q5000 IR shown in Figure 2.13. Samples were placed in tared open aluminium pans on the sample holder. Experimental methods employed are detailed in the relevant sections. All TGA experiments were performed with a dry nitrogen gas purged at flow rates of  $25 \text{ ml min}^{-1}$  and  $10 \text{ ml min}^{-1}$  through the furnace and TGA head, respectively. Data were treated mathematically using TA Universal Analysis 2000 software.



**Figure 2.12: Schematic diagram of common TG apparatus**



**Figure 2.13: TA Instruments TGA Q5000 IR. Reproduced from [www.tainstruments.com](http://www.tainstruments.com)**

#### 2.2.2.1.3.2 Pharmaceutical applications

As aforementioned, thermogravimetry (TG) is an attractive experimental technique for investigations of processes that may cause a weight loss in a material. In pharmaceutical sciences, TGA has been used to characterise various drugs and excipients. Most studies using this method to measure the temperature range in which dehydration occurs and the quantity of water lost and determination of the material stability at high temperatures. The potential of using TGA in conjunction with complementary techniques such as X-ray diffraction (XRD) and differential scanning calorimetry (DSC) has been investigated in many works (Bettinetti et al., 1999; Dash and Tyle, 1996; Grisedale et al., 2012) to obtain more detailed analysis. During assessment of the glassy material, for example, water content determination by TGA appears as integral tool to supplement DSC analysis, whereby measured levels of water as a plasticizer can be correlated to the glass transition temperature changes.

#### 2.2.2.1.4 Hot stage microscopy (HSM)

Hot stage microscopy is a unique analytical technique that combines the microscopy and thermal analysis to characterise the physical properties of the materials while being exposed to a controlled temperature program. This technique serves as a complementary tool to other pharmaceutical techniques such as DSC and TGA (Vitez et al., 1998), providing a balanced picture of the solid physical properties under investigation. The introduction of photographic equipment to this technique expanded its utility to capture on video or as digital images visualized thermal events.

HSM used in this project was to allow visualisation of the dissolution of one component into another component melt, in attempt to predict compatibility of these materials (Forster et al., 2001). HSM was also used as a conjunction tool to evaluate thermal transitions observed using MTDSC technique. The apparatus consists of a camera mounted above polarized light microscope (PLM), into which the sample is mounted on a glass slide and enclosed in the hot stage. PLM was also used without heating accessory (hot stage) as a supplementary technique to the SEM studies, due to its good ability of crystalline structure recognition.

HSM studies were carried out using a Leica DML S2 polarized microscope (Wetzlar GmbH, Germany), connected to a Mettler Toledo FP82HT hot stage microscope and a FP90 central processor, equipped with a video capture system (JVC digital colour video camera) connected to a PC. Studio86Design Capture software (Version 4.1) was used to analyse



results. Full experimental details are given in the relevant sections of corresponding chapters.

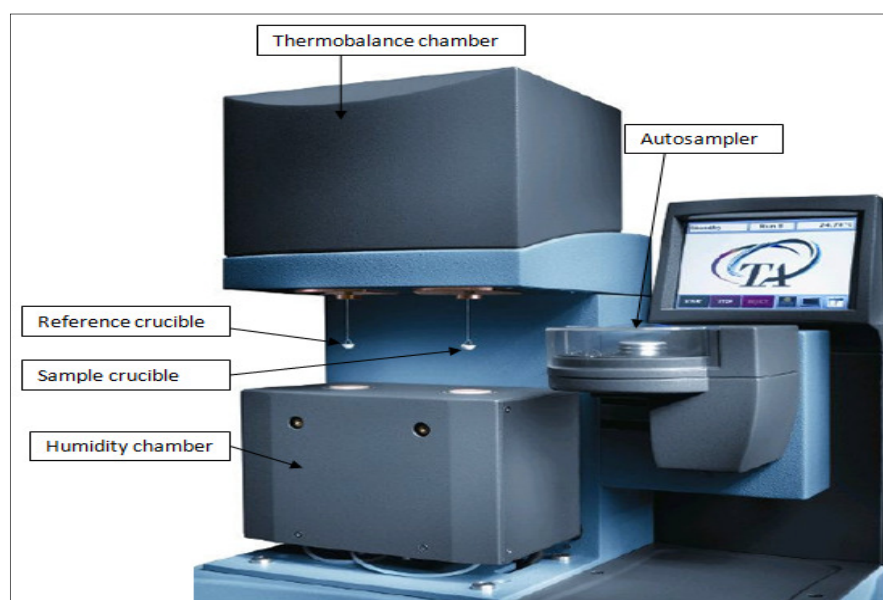
#### **2.2.2.2 Dynamic vapor sorption (DVS) analysis**

Dynamic vapor sorption analysis (DVS) is a technique, whereby the effect of exposure to a controlled conditions of temperature and humidity on the materials is measured gravimetrically using a sensitive microbalance that detect weight changes of a sample and a reference. DVS has several applications that are used to investigate the moisture sorption behaviour of the materials, providing better understanding of the affinity and or interactions of water within these materials. This is of particular importance in pharmaceutical fields as the stability, performance and properties of the pharmaceutical material may be influenced by their moisture sorption.

The DVS studies in this project were undertaken using TA Q5000 SA analyzer, consists of a vertical nulling microbalance in which the sample and reference hang-down wires and pans are enclosed in a humidity- and temperature-controlled chamber. A dry nitrogen gas is purged at a rate of  $10 \text{ ml min}^{-1}$  to assure the dryness of the balance housing. TA Instrument DVS used here and shown in Figure 2.14 has pair of mass flow controllers (MFCs), which are placed to purge the nitrogen gas to the humidity chamber, which contains the humidifier, sample and reference measurements chamber. Thereby these MFCs allow adjustment of the amount of wet and dry gas to obtain desired humidities. Temperature is also controlled to achieve consistent atmosphere for precise measurements. Sensors are located adjacent to the sample and reference holders to enable humidity and temperature regulation. The loss or uptake of moisture is therefore recorded gravimetrically in comparison to an empty reference using sensitive microbalance. This balance (thermobalance) is enclosed in well-insulated chamber, gas-purged and operates on a null position, allowing high sensitivity and accuracy of detection of weight changes, free from any interference such as vapour condensation or electrostatic forces, which could otherwise affect the accuracy and precision of the measurements.

In this work, DVS experiments were performed in three different modes, namely, isotherm and isohume modes and as a function of time. In isotherm mode, the samples are exposed to a series of humidity step changes at a constant temperature. However, isohume mode operates in a series of temperature step changes at a constant humidity level. These modes are useful to give indication about physicochemical changes that can occur as a function of these variables (humidity or temperature at a given humidity level), such as the hydration

state changes of the tested sample. The third mode was maintaining the sample at a given humidity level and constant temperature for three hours. This experiment was used for preparatory purposes of the samples, thus a humidification is achieved under controlled conditions. Samples were placed in standard aluminium open pans (surface area of approximately  $38.48 \text{ mm}^2$ ) to unify the exposed surface area to the moisture and loaded into hemi-sphere quartz sample crucibles ( $180 \text{ }\mu\text{L}$ ). This assembly was tared prior each experimentation with matched empty reference hemi-sphere quartz crucible containing empty standard aluminium pan. However, in the preparatory experiment, the samples were placed directly into tared DVS crucibles. Experimental methods are detailed in the relevant sections. Analyses were performed using TA Universal Analysis 2000 software.



**Figure 2.14: TA Instruments Q5000 SA Dynamic Vapor Sorption Analyzer. Reproduced from [www.tainstruments.com](http://www.tainstruments.com)**

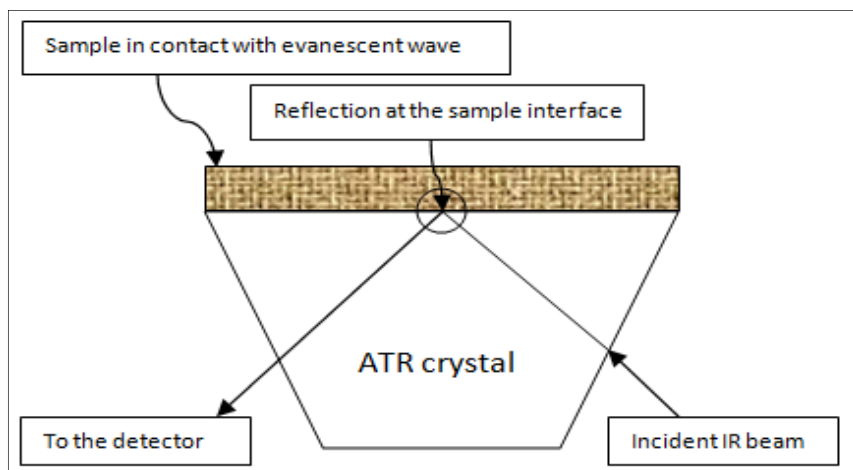
### **2.2.2.3 Attenuated total reflection-Fourier transform infrared spectroscopy (ATR-FTIR)**

Infrared (IR) spectroscopy is a well-established technique and routine procedure in pharmaceutical field that can be used to acquire data quickly for characterising the composition and geometry of molecules and crystals. An electromagnetic wave in the infrared region (wavenumber between  $4000 \text{ cm}^{-1}$  and  $400 \text{ cm}^{-1}$ ) is passed through the sample and is absorbed by the bonds of the molecules in the sample causing them to stretch or bend. The wavelength of the radiation absorbed is characteristic of the bond absorbing it and the greater change in dipole moment during a vibration; the higher the intensity of absorption. In

a spectrometer, any remaining IR, not absorbed by the molecule is transmitted through the sample to a detector. The fraction of transmitted light allows determination of the frequencies at which the absorption of energy occurs in the infrared region of the electromagnetic spectrum. Because the frequencies and intensities of the modes are sensitive to physical and chemical structure, the observation of bands in well-defined ranges can indicate the presence of particular groups (fingerprinting) by applying the principle of group frequency correlations. This enabled many applications in pharmaceutical field, such as drug-polymer interaction studies and crystallinity investigations. The latter is usually monitored if the crystalline or amorphous materials give distinct vibration band(s). Therefore, changes can be correlated with the peak intensity, shape or position (Khanna and Khun, 1997). Moreover this technique can be used for quantification based on the principle of linear proportionality between IR absorbance and the number density of vibrating species (Hunt and James, 1993), thus the intensities of bands are related to the functional groups concentration producing them (Socrates, 2001).

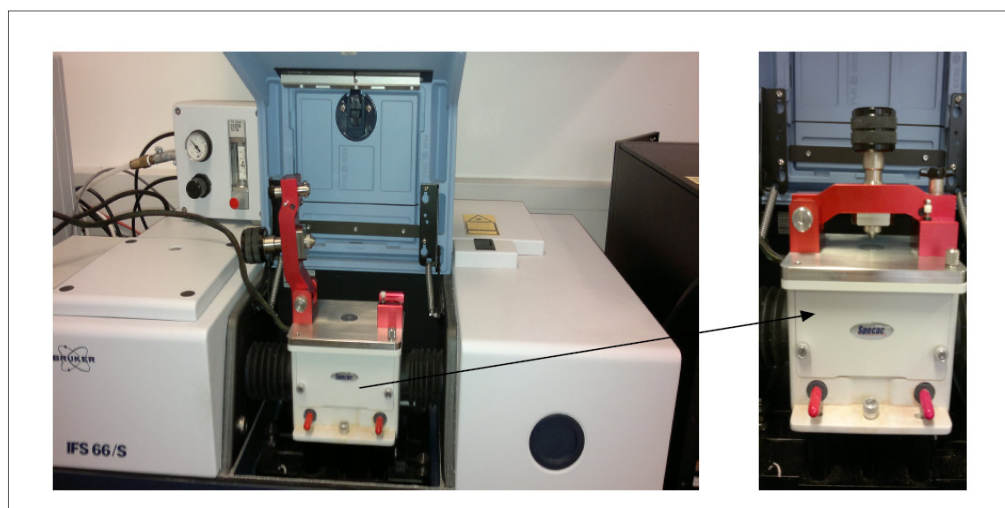
#### 2.2.2.3.1 Instrumentation

Fourier transform instruments are the most widely used instruments, wherein the IR signal is produced as an interferogram which can be treated mathematically using equation called 'Fourier transform' in order to extract the spectrum from a series of overlapping frequencies. The introduction of the attenuated total reflection (ATR) mode enabled FTIR to become valuable tool to characterise various polymeric matrices, drugs found in them and elucidate their interaction (Watson, 2005). ATR requires no special sample preparation and provides a non-destructive mean for evaluating solid or liquid samples. The sample is simply placed on the surface of the ATR crystal which is usually made of diamond or germanium. Infrared beam enters at an angle greater than the critical and is totally and internally reflected by the crystal, but attenuated by absorption from the sample contact layer as shown in Figure 2.15. The fraction of the light reaching into the sample is known as evanescent wave. At each reflection point the wave extends within the penetration depth (typically few microns) and existing beam will be analyzed to provide ATR-FTIR spectra of the studied material within this range. The most important consideration needed when testing a certain sample is to achieve high contact with the surface of refractive index and clean IR-transparent prism, to have better characterisation of the material under study (Hunt and James, 1993).



**Figure 2.15: Schematic of a single reflection ATR system**

The ATR-FTIR studies were carried out using a Bruker optics IFS 66/S spectrometer (Coventry, UK) equipped with a Golden Gate ATR accessory from Specac Limited (Orpington, UK), shown in Figure 2.16, over a range of  $4000\text{--}550\text{ cm}^{-1}$  with 32 scans at a resolution of  $4\text{ cm}^{-1}$ . Using the same parameters, ATR-FTIR spectra were also collected for heated samples utilising a Golden Gate heated diamond attenuated reflection top-plate with a 3000 series high stability temperature controller with RS232 control from Specac Ltd. (Kent, UK). Analyses were performed using Omnic software (version 6.1a).

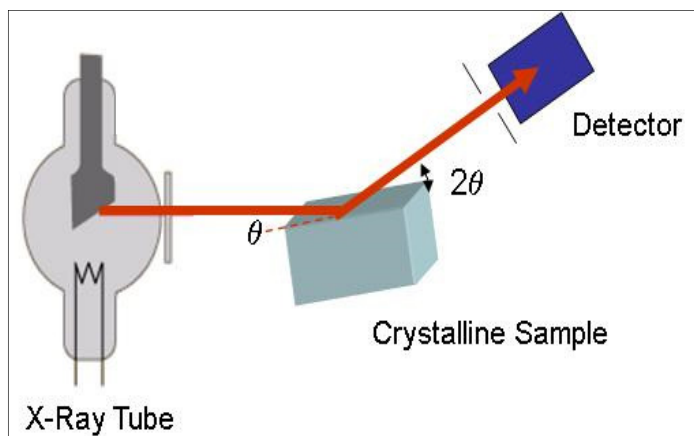


**Figure 2.16: Bruker IFS 66/S, Bruker optics spectrometer (left side) equipped with a Golden Gate ATR accessory from Specac Limited (right side)**

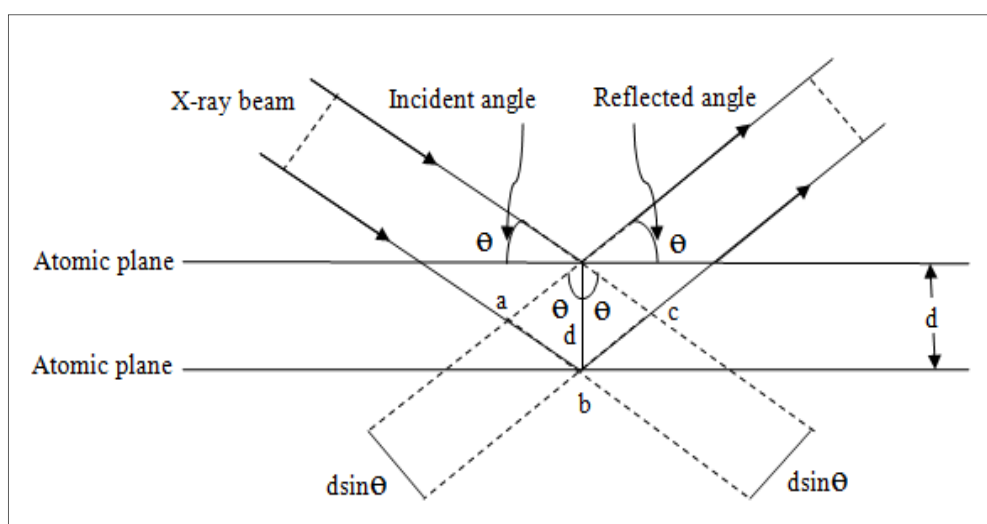
#### 2.2.2.4 Powder X-ray diffraction (PXRD)

PXRD is one of the primary techniques used in pharmaceutical solid state characterisation. Simplicity and non-destructive sample preparation led to the extensive use of this technique to trace crystallinity, to confirm the identity of mixed crystal phases and to detect amorphous regions in various materials. PXRD operates on the principle that the diffraction pattern for every crystalline phase is a unique as a fingerprint and determined by their individual uniform crystal structure. This fingerprint, when properly interpreted, allows for identification of the studied material.

A typical X-ray diffractometer consists of three basic elements; X-ray tube (generator) in which copper is the most commonly used, sample holder and X-ray detector as shown in Figure 2.17. The X-ray beam emitted from the tube and passed through the sample. When X-ray beam hits an atom in the molecule, the electrons around the atom oscillate with the same frequency as the incident beam. The atoms in the crystal have long range order and the leaving beam consists of large number of scattered rays. The intensity and position of these rays are recorded by a detector. The diffraction of X-ray by the crystal can be explained by Bragg's diffraction (1918). In this model, crystal has a definite separation distance between its atomic or lattice planes called d-space. For a monochromatic X-ray beam with a wavelength  $\lambda$ , scattered from a crystal lattice, peaks of scattered intensity are observed only when the distance traveled by the ray reflected from successive atomic planes differs by a complete number (n) of wavelengths (Cullity, 1978). In Figure 2.18, this path length is (abc). The diffraction will occur when the path length difference is equal to an integer number of wavelengths ( $n\lambda$ ). Geometrically, (ab) equals (bc) and both are equal to the distance (d) times the sine of the reflected angle  $\Theta$  ( $d\sin \Theta$ ). So Bragg's law is usually expressed as  $n\lambda = 2 d\sin \Theta$ . The diffractogram, therefore, will be the intensity of the diffracted beam plotted against the angle of the leaving beam. The peaks in the diffractogram will correspond to the characteristic d-spacing sets of the atoms' arrangements in the molecules within the sample.



**Figure 2.17: Diagram of powder X-ray diffractometer (Morris et al, 2011)**

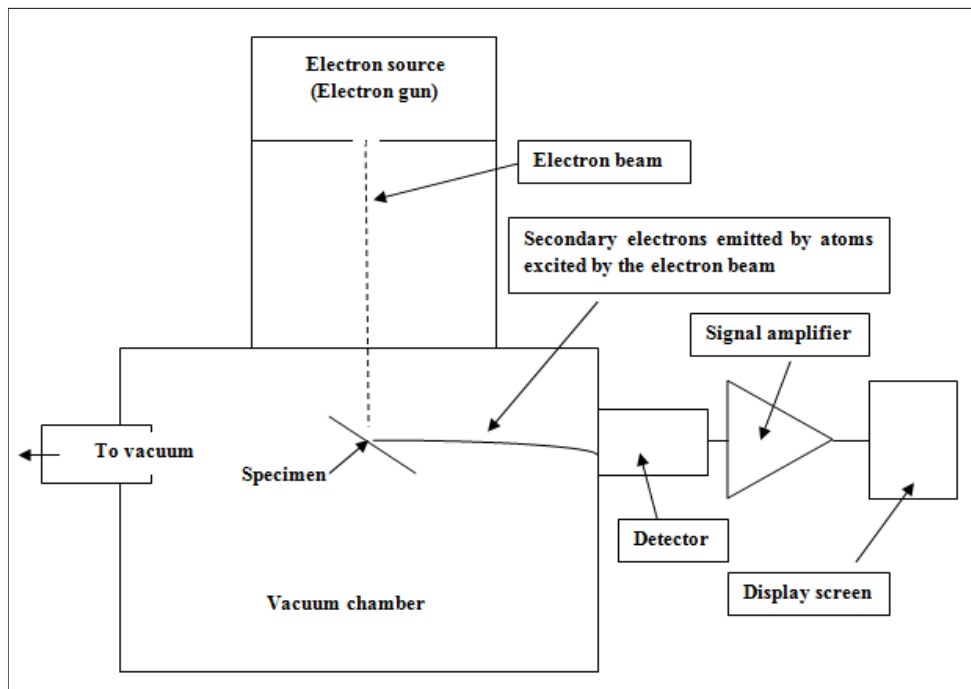


**Figure 2.18: Diagram illustrating Bragg's law reflection**

PXRD studies were carried out using X-ray powder diffractometer (ARL Xtra, manufactured by Thermo Fisher Scientific) equipped with X-ray tube (Copper, wavelength of 1.540562 Angstrom). Scanning speed of 1.2 °/min over the  $2\theta$  range from 2 to 60 degrees was used with a step size of 0.01 degree and 0.5 second per step, using a 40 kV generator and a 20 mA stream. Smooth plane surfaces were ensured for the tested samples when packed or pressed into the sample holders.

### 2.2.2.5 Scanning electron microscopy (SEM)

SEM is a type of electron microscopy that uses focused beam of high energy electrons to magnify the surface of the sample. Therefore information about surface topography, external morphology is produced with high magnification yet a good resolution, due to the great depth of the applied field. As seen in Figure 2.19, SEM operates using a fine beam of electrons which is scanned across the sample surface. The beam interacts with sample and a detector monitors the signals that result from the electron beam-sample interaction. The electrons emitted from the sample surface amplified to build up the SEM image from the detector signal. During SEM functioning, the beam current of the electrons penetrating the sample can generate heat. Therefore, heat damage can take place for susceptible sensitive samples.



**Figure 2.19: Schematic diagram of the main parts of a scanning electron microscope**

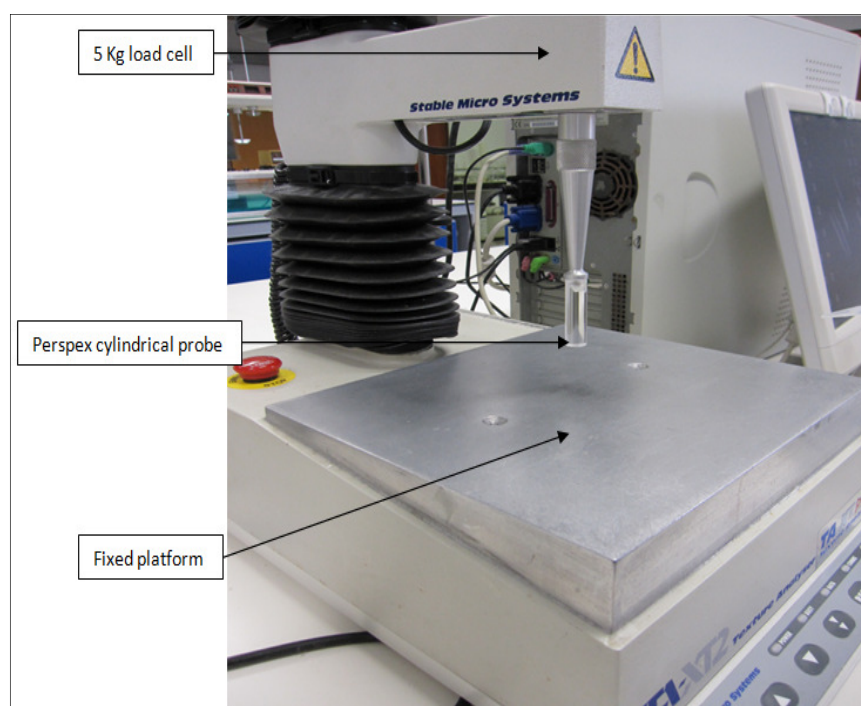
To increase the stability of the produced images and increase sample resolution, coating of the samples under vacuum sputter is essential. Therefore the surface become more conductive and static electric charges are dislodged from the specimen. A thin layer of conductive material is usually used to coat the samples, such as gold and silver. In this study, SEM studies were carried out using scanning electron microscope (JSM 5900LV, manufactured by JEOL, Japan), which was fitted with a tungsten (W) filament and an acceleration voltage of 20 kV with a 10 mm working distance, was used to obtain SEM



images. The samples were mounted onto stubs using double-sided tape and were gold coated by a Polaron SC7640 sputter gold coater manufactured by Quorum Technologies (UK), using Plasma current of 20 mA, Voltage: 2.1 kV for 30 seconds.

#### 2.2.2.6 Texture analysis (TA)

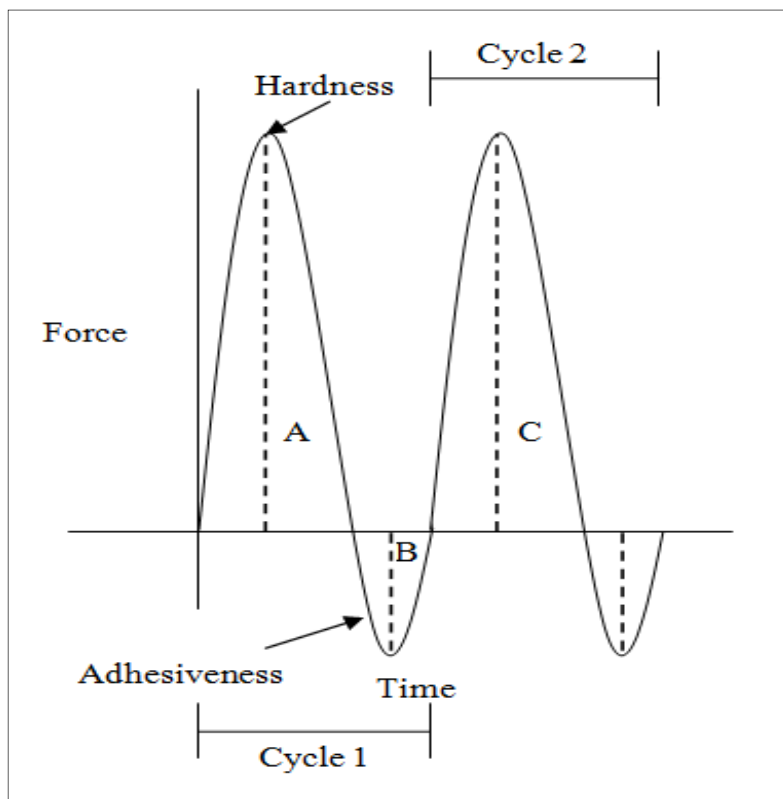
Texture analysis is a penetrometry technique that is usually used to provide information about mechanical properties of the studied material through measurements of the material response to tension, compression, penetration and bending. Therefore, texture analyzers operate by applying controlled forces to the material and recording its response. Texture analyzer instrument consists typically of a probe, load cell and sample stage or platform, as shown in Figure 2.20. The sample is placed over the platform of the instrument. The probe is positioned above the sample and held by a load cell connected to a movable arm. The probe is usually placed close to the sample and is pushed into the sample and withdrawn away from it according to a control program. When the test starts, the probe is programmed to travel at a defined and constant speed to contact the sample and penetrates the sample up to a chosen depth. Then the probe detaches from the sample to its original position prior the test.



**Figure 2.20: TA-XT2 Texture Analyzer Stable Microsystems, Ltd. (Surrey, UK) equipped with a 5 kg load cell and fitted with a Perspex cylindrical probe**



Many textural parameters can be analyzed in only one test using this technique. Therefore, texture analysis has been applied as a useful method to investigate mechanical properties of transdermal films such as hardness and adhesiveness (Abdul Rasool et al., 2011; Cilurzo et al., 2008; Repka et al., 2003; Yener et al., 2010). Generally, the texture profile analysis curve measures force as a function of time as shown in Figure 2.21. This curve provides several textural parameters as hardness, adhesiveness and cohesiveness. Hardness parameter can be defined as the peak force needed to reach a given deformation (Szczesniak, 1963) during the first compression cycle (here peak A). Adhesiveness is related to surface properties of the tested material and represents the work necessary to pull the probe away from the sample (negative force area, here area B). Cohesiveness represents the strength of the internal bonds making up the body of the material (Szczesniak, 1963) and can be defined as the ratio of the positive force area during the second compression portion to that during the first compression (here area C/ area A).



**Figure 2.21:** A typical force-time curve obtained from two cycles texture profile analysis test, with the peak (A) resulting from first compression cycle and peak (C) from the second compression cycle

In this work, the hardness values as measured by the force of load (in grams and equals to 9.8 mN) using TA technique was used to indicate flexibility of hot melt extruded Gelucire 44/14/Eudragit RS PO films for transdermal delivery. Films were obtained after their application to the skin of healthy volunteers after occlusion. The hydration of these films was achieved by skin occlusion. The changes in hardness as a result of hydration, the relationship of these changes to the hydration times, as well as the correlation between the Gelucire 44/14 concentration and the hardness (with and without hydration) were investigated and detailed in Chapter 8.

TA studies on the extruded films (in both dry and wet states) were carried out using TA-XT2 Texture Analyzer (Stable Micro system, UK), shown in Figure 2.20, with a 5 kg load cell, a force measurement accuracy of 0.0025% and a distance resolution of 0.0025 mm. The penetration profiles of the probe were used to obtain the force of load required to compress the films (in grams), indicating their hardness. The probe used (Perspex cylindrical) with 11.6 mm diameter was calibrated for height measurements, held above the sample by 4 mm of its original height. The pre-test speed was set up at 1 mm/second, the test speed at 0.5 mm/second and the penetration depth of 60% of the film's height. The study was carried out with two repeats obtained for each sample at room temperature. Texture Expert Exponent software was used to perform analyses.

### **Chapter 3: Characterisation of ibuprofen and the carrier excipients intended for hot melt extrusion**

### 3.1 Introduction

For a compound that is intended to be used in hot melt extrusion for a design of a pharmaceutical product, an understanding of its characteristics is essential for at least two reasons. Firstly, to establish processing conditions (such as extrusion temperature and screw speed). Secondly, to provide understanding of the relationship between the raw material properties and the final product i.e. extrudate which can affect its performance and/or quality attributes. This chapter is provided to gain insight into the properties of the raw materials selected for performing hot melt extrusion in this work as detailed in Chapter 2 with the ultimate aim to formulate a drug delivery system for transdermal application. Extrudability of the raw materials appears to be influenced by two key features, which are thermal properties of the used drug or polymer and include thermal stability and their T<sub>g</sub> or T<sub>m</sub>, in addition to the melt viscosity (Chokshi et al., 2005). A characterisation program was provided in section 3.3 which is divided into two parts for the major constituents, namely, the drug and carrier excipients. Each part is further subdivided into two parts for each material. The first part is thermoanalytical investigations which describe thermal properties as probed using DSC and TGA techniques. The second part details some of the solid state characteristics of these materials, which are believed to be the most relevant for understanding the physical properties of the real extruded samples containing mixtures of the drug and carrier excipient(s).

### 3.2 Methodology

The basic research techniques and materials selection were explained in Chapter 2. In this section analytical methods which employed these techniques will be presented to characterise the selected materials. Methods included TGA and DSC in its conventional and modulated modes, which were used and developed to establish thermal properties of the main components. Standard DSC or conventional DSC (cDSC) was used at a heating rate of 10°C min<sup>-1</sup> to study both ibuprofen as a model drug and Eudragit RS PO as the parent main polymeric carrier. Samples (9.00-10.00 mg) of ibuprofen were initially subjected to two steps. Step1: equilibration at -70°C, isothermal heating for 5 minutes, step2: heating to 100°C at 10°C min<sup>-1</sup> (Figure 3.2). The glass transition temperature and crystallization of ibuprofen were investigated using a second method of three steps or cycles. The first cycle: heating to 100°C at 10°C min<sup>-1</sup>, cooling to -70°C (10°C/min) in the second cycle followed by a reheating step (cycle 3) to 100°C (10°C/min) as presented in Figure 3.3. Eudragit RS PO

(9.00-10.00 mg) samples were subjected to two steps; include equilibration at 30°C, isothermal heating for 5 minutes and then heating to 100°C at 10°C min<sup>-1</sup> (Figure 3.10).

In the MTDSC experiments, the first method was applied to deconvolute the glass transition event of Eudragit RS PO with an underlying heating rate of 2°C/min, a modulation period of 40 seconds and amplitude of 0.212°C and included two steps. Step 1: equilibration at 30°C and modulation  $\pm 0.212^\circ\text{C}$  with a period of 40 seconds, isothermal heating for 5 minutes, step 2: heating to 100°C (2°C/min), as shown in Figures 3.11 and 3.12. The second method was developed with the objective to enhance sensitivity of the measurements, using higher amplitude of 0.265°C and a period of 100 seconds, where the heating rate was 1°C/min. The parameters of this MTDSC method were employed to characterise Eudragit RS PO, ibuprofen and the rest of tested materials in this work to provide finer analysis of their thermal transitions. Samples (9.00-10.00 mg) were subjected to two steps. Step1: equilibration at -70°C and modulation  $\pm 0.265^\circ\text{C}$  with a period of 100 seconds, isothermal heating for 5 minutes, step 2: heating to a final temperature (1°C/min). The final temperature varies according to the tested material and in this chapter it was between 100-250°C. Conventional DSC and MTDSC measurements were carried out using TA Instrument DSC Q1000, equipped with a refrigerated cooling system (RCS) and calibration was performed prior each analysis as detailed in Chapter 2. Data were treated mathematically using TA Universal Analysis 2000 software and nitrogen was used as the purge gas through the DSC cell at a flow rate of 50 ml/min. TA instruments standard pans were used for all calorimetric studies; the mass of each empty sample pan was matched to the mass of the empty reference pan within  $\pm 0.05$  mg and all the measurements were performed in triplicate.

Thermal stability of the materials was studied using thermogravimetric analysis, which was performed using TGA Q5000 IR (TA Instruments, U.K). Samples (10.00-12.00 mg) were subjected to a single step of heating from 30°C to 300°C at a heating rate of 10°C min<sup>-1</sup>. All TGA runs were performed in open aluminium pans with a dry nitrogen gas purged at flow rates of 25 ml min<sup>-1</sup> and 10 ml min<sup>-1</sup> through the furnace and TGA head, respectively. Data were treated mathematically using TA Universal Analysis 2000 software to illustrate weight loss percentage and weight derivative loss signals. The latter is usually more sensitive for detection of the closely occurring multiple weight losses.

Other analytical techniques used to investigate physicochemical properties of the used materials were SEM, PXRD and ATR-FTIR. Scanning electron microscopy (SEM) was used to observe the morphological features of these materials. The samples were mounted onto stubs using double-sided tape and were gold coated, in order to increase conductivity of the electron beam, by a Polaron SC7640 sputter gold coater manufactured by Quorum Technologies (UK), using Plasma current of 20 mA, Voltage: 2.1 kV for 30 seconds. The photographs taken were obtained using scanning electron microscope (JSM 5900LV, manufactured by JEOL, Japan) fitted with a tungsten (W) filament, acceleration voltage of 20 kV and 10 mm working distance.

To investigate crystallinity of the ibuprofen and carrier excipients, qualitative PXRD analysis was performed using X-ray powder diffractometer (ARL Xtra, manufactured by Thermo Fisher Scientific) equipped with X-ray tube (Copper, wavelength of 1.540562 Angstrom) over the  $2\theta$  range from 2 to 60 degrees, scanning speed of  $1.2^\circ/\text{min}$  (step: 0.01 degree, 0.5 sec/step) using a 40 kV generator and a 20 mA stream. In addition, attenuated total reflectance-Fourier-transform infrared (ATR-FTIR) spectrometry (Bruker IFS 66/S, Bruker optics equipped with a Golden Gate ATR accessory from Specac Limited) was used to investigate the most characteristic functional groups of the used materials which can aid in interpretation of molecular interactions, if any, in the mixtures of these materials. Spectra of these components were collected over a range of  $4000\text{--}550\text{ cm}^{-1}$ , 32 scans at a resolution of  $4\text{ cm}^{-1}$ . Omnic software (version 6.1a) was used to analyze results. All weighing in this work was performed using XS205, Dual range analytical balance (Mettler Toledo).

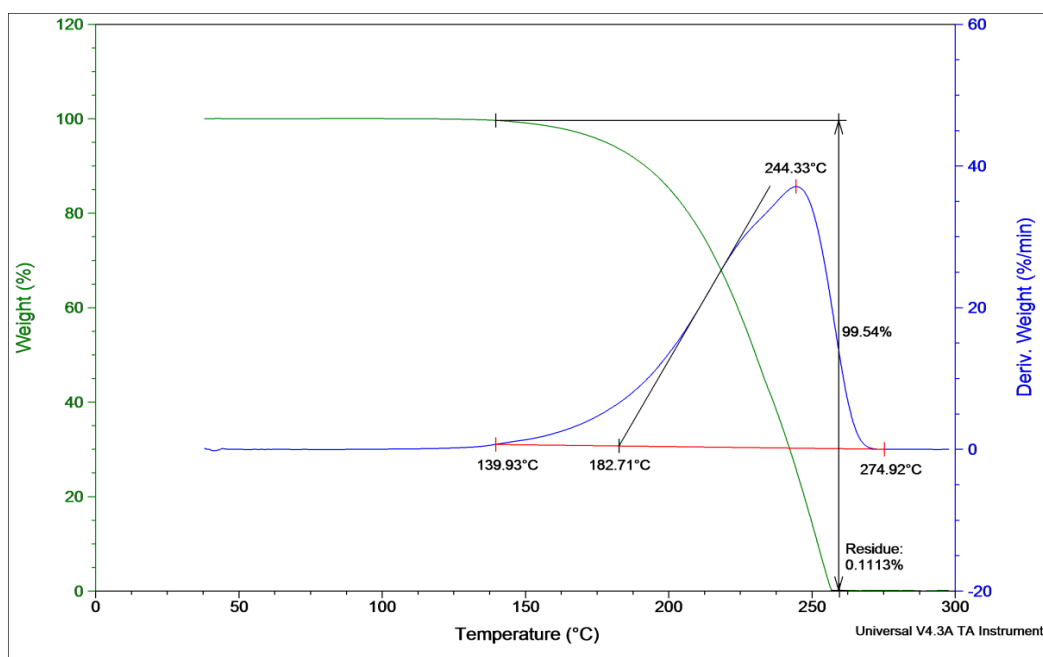
### 3.3 Results and discussion

#### 3.3.1 Model drug

##### 3.3.1.1 Thermoanalytical investigations

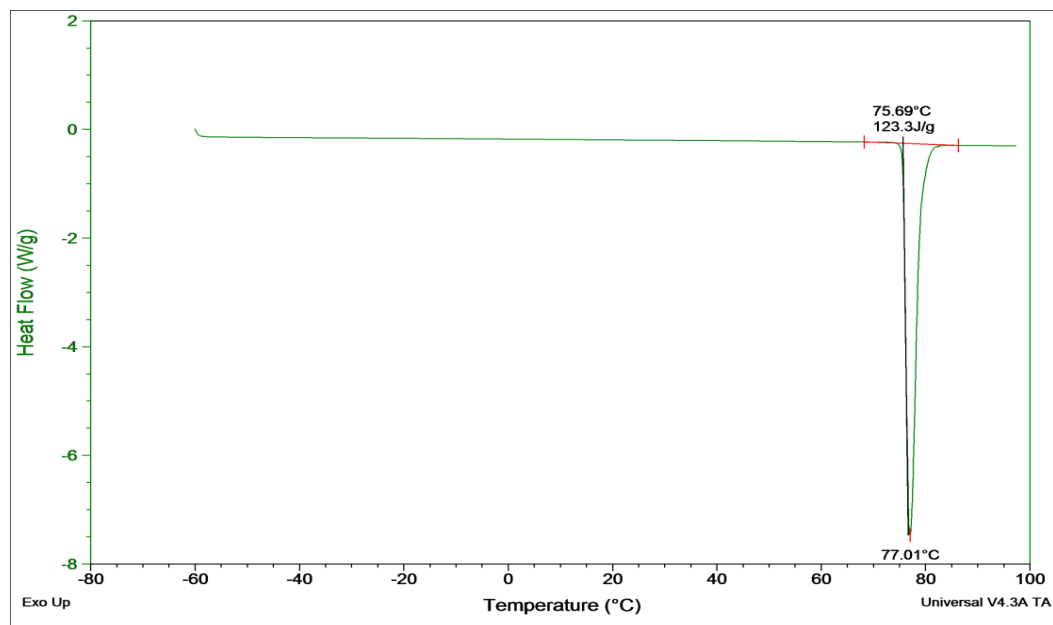
Ibuprofen was chosen as a model drug for the reasons detailed in Chapter 2. TGA was used to estimate the onset of decomposition of this drug as a function of weight loss, thereby approximating its thermal stability. Figure 3.1 shows the percentage and derivative weight loss signals of ibuprofen heated at a rate of  $10^\circ\text{C min}^{-1}$ . It can be seen from this figure that the decomposition starts approximately around  $140^\circ\text{C}$  and the sample disappeared after the finish of the run with a final temperature of  $300^\circ\text{C}$ , indicating complete decomposition. Thus, it could be inferred that extrusion temperature that can be employed should be less

than 140°C. However, it is expected to have extra heat generated from screw friction during the mixing process inside the extruder (Crowley et al., 2007). Therefore, it is believed that extrusion temperatures equal or below 120°C might be favourably selected to avoid or at least minimize this drug degradation while processing. At this temperature (120°C), less than 0.1% of the ibuprofen weight loss was detected.

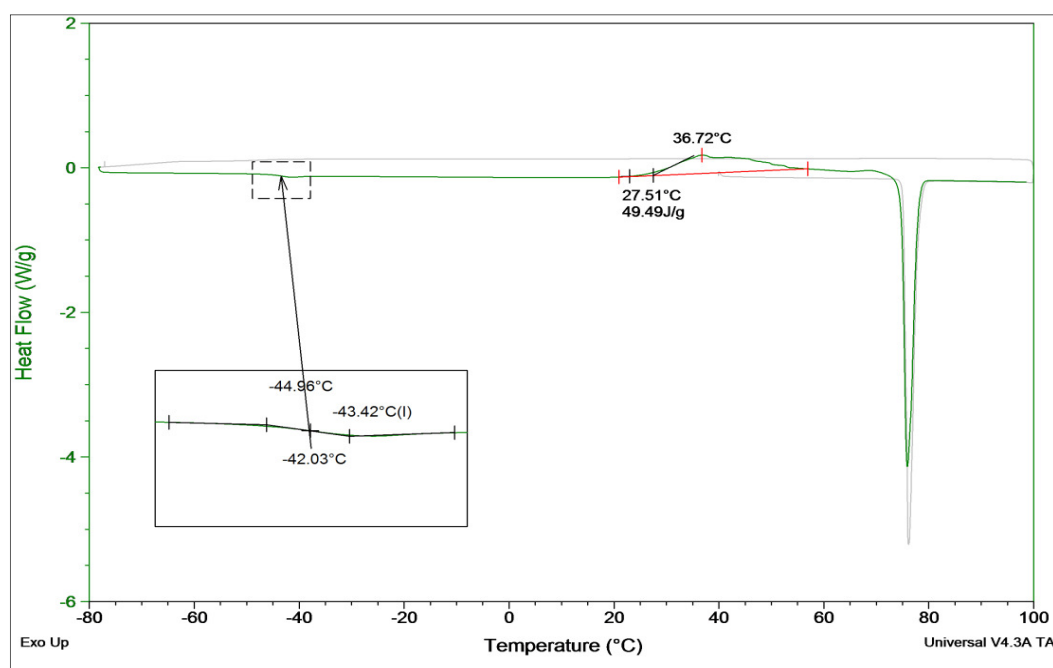


**Figure 3.1: TGA weight loss profile of crystalline ibuprofen heated at 10°C min<sup>-1</sup> to 300°C**

DSC experiments were performed in both its conventional and modulated modes to determine major thermal events of ibuprofen. Conventional or standard DSC (cDSC) measures heat flow of a sample providing information about its physicochemical properties qualitatively and quantitatively as detailed in Chapter 2. The initial cDSC experiments using a standard heating rate of 10°C min<sup>-1</sup> and standard aluminium pans are demonstrated in Figure 3.2 to Figure 3.3.



**Figure 3.2:** Heat flow signal of ibuprofen heated at 10°C min<sup>-1</sup> in standard aluminium pans



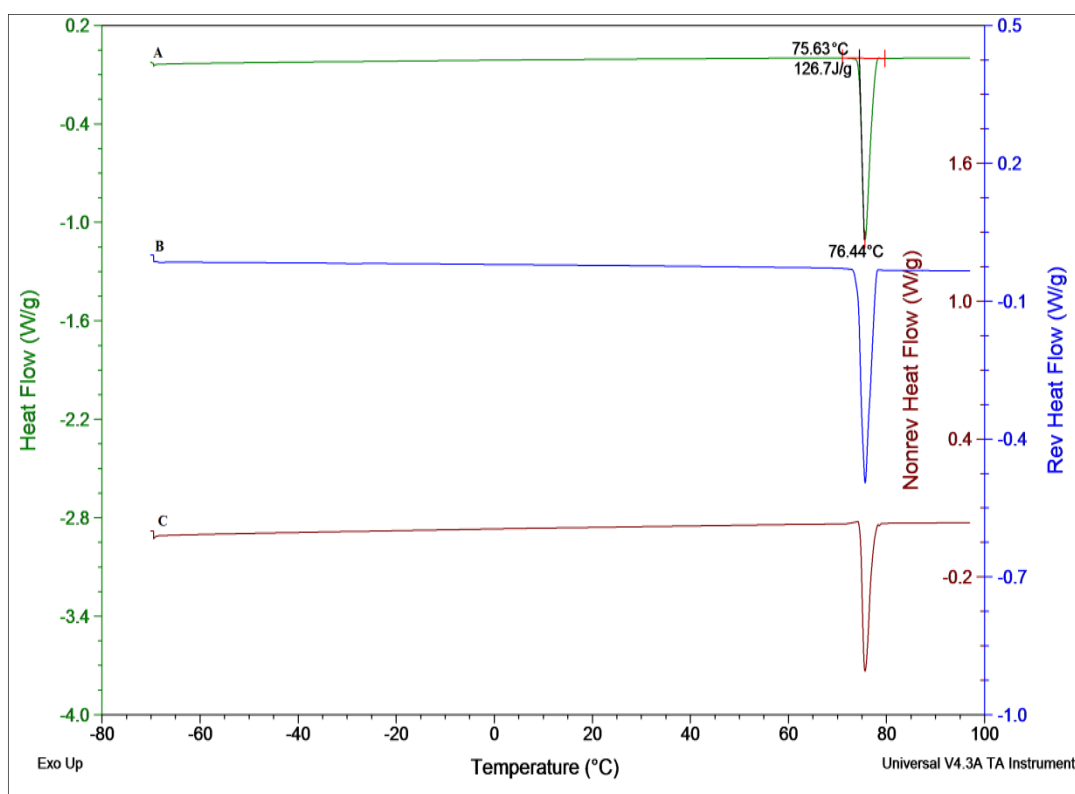
**Figure 3.3:** Heat flow signal of ibuprofen cycled at 10°C min<sup>-1</sup> (see text). Highlighted cycle after re-heating from -70°C is showing a magnified insert of the observed glass transition event



This crystalline drug give rises to an endothermic melting peak at  $76.8 \pm 0.3^\circ\text{C}$  measured as the peak temperature and at  $75.5 \pm 0.3^\circ\text{C}$  as the extrapolated onset value ( $T_{m(\text{onset})}$ ) as presented in Figure 3.2. In order to study the amorphous form and subsequent recrystallization of this drug, supercooled ibuprofen was made inside DSC. Quench or rapid cooling of the melt is a well known approach to produce amorphous material or small crystallites. Therefore, the drug was heated till  $100^\circ\text{C}$  to ensure melting and then cooled to  $-70^\circ\text{C}$  at  $10^\circ\text{C min}^{-1}$ , followed by reheating till  $100^\circ\text{C}$  as highlighted in Figure 3.3. In this highlighted third cycle of this protocol an inclination in the DSC graph was observed between  $-45^\circ\text{C}$  and  $-42^\circ\text{C}$ , which is characteristic of an amorphous material passing through its glass transition temperature. A Mid-point temperature of this transition was found at  $-43.4 \pm 0.2^\circ\text{C}$  ( $n=3$ ), which agrees well with the reported value for amorphous ibuprofen of approximately  $-45^\circ\text{C}$  (Dudognon et al., 2008). The next thermal event seen in this cycle was an exothermic peak with a maximum at  $36.7 \pm 0.1^\circ\text{C}$ , indicating rearrangement of molecules or recrystallization of the amorphous phase into the stable crystalline phase. Subsequent to this recrystallization exotherm, melting endotherm of crystalline ibuprofen was observed.

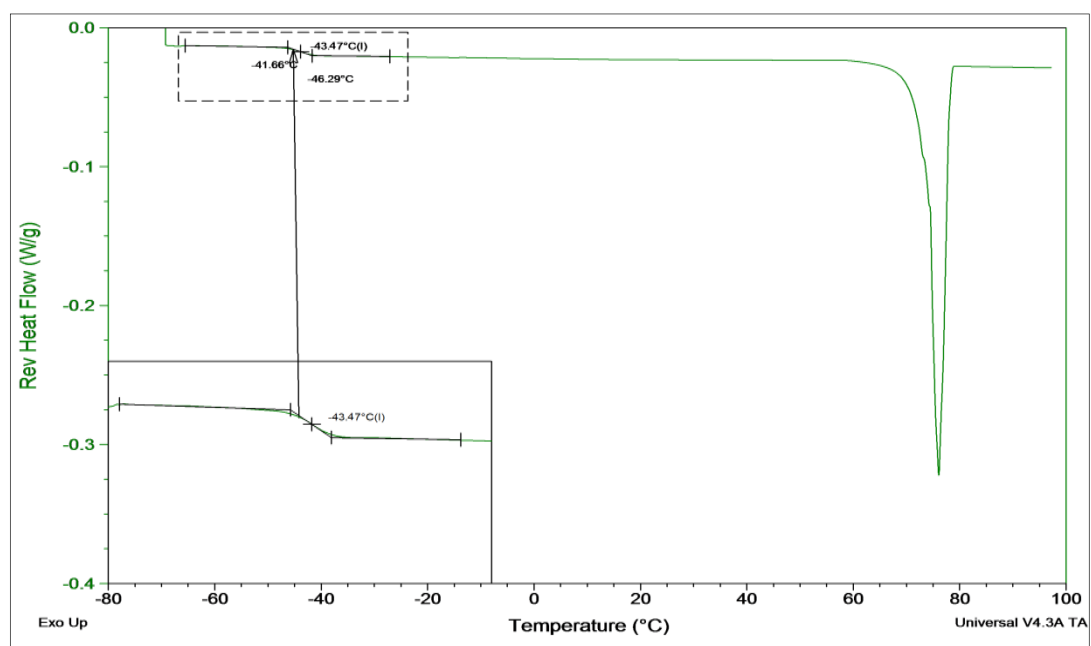
MTDSC as explained in Chapter 2 is performed through application of temperature modulation over the underlying heating rate of standard DSC. This results in enhancement of both resolution and sensitivity. Therefore, weak or overlapped events can be distinguished effectively, wherein reversing heat flow signal shows heat capacity components while kinetic heat flow is detected in the non-reversing signal. The experimental procedure used for MTDSC in this characterisation was based on parameters developed for determination of the glass transition temperature of Eudragit RS PO as will be discussed in section 3.3.2. Though MTDSC is a useful technique, it is relatively complicated in comparison to the cDSC and it may also have limitations with respect to the melting characterisation (Chapter 2), but since ibuprofen will be mixed primarily with Eudragit RS PO, their characterisation will be achieved using this method. Therefore, it would be useful to examine ibuprofen individually, to relate its fingerprints (thermal events) detected from the used parameters in this MTDSC method when examined as a mixture with this polymer.

Figure 3.4 shows the MTDSC profile of crystalline ibuprofen. A melting endotherm was observed in all the signals and determined from total heat flow signal at  $75.7\pm0.2^\circ\text{C}$  measured as the extrapolated onset value ( $T_{m(\text{onset})}$ ) and at  $76.4\pm0.1^\circ\text{C}$  as the peak temperature. Following the same aforementioned protocol of cooling the ibuprofen melt at  $10^\circ\text{C min}^{-1}$ , the third cycle was obtained using the applied MTDSC method with an underlying heating ramp rate at  $1^\circ\text{C min}^{-1}$ , a period of 100 seconds and amplitude of  $\pm0.265^\circ\text{C}$  to  $100^\circ\text{C}$ . This cycle is displayed in Figure 3.5 which shows reversing and non-reversing heat flow signals for partially amorphized ibuprofen. A glass transition temperature was detected from the reversing heat flow signal at  $-43.4\pm0.2^\circ\text{C}$  while non-reversing signal revealed broad recrystallization exotherm at approximately  $35.7\pm0.3^\circ\text{C}$  (peak temperature).

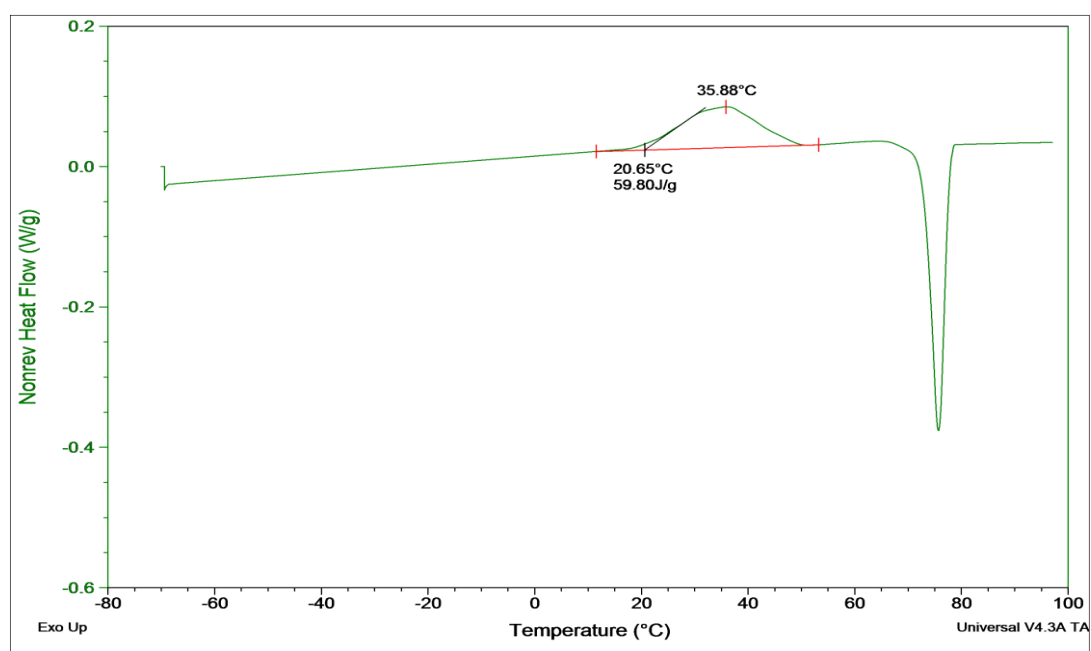


**Figure 3.4:** MTDSC heating scan of ibuprofen in standard aluminium pans. Underlying scan rate of  $1^\circ\text{C min}^{-1}$  with a modulation amplitude of  $\pm0.265^\circ\text{C}$  and a period of 100 seconds. The signals have been offset for clarity

(A)



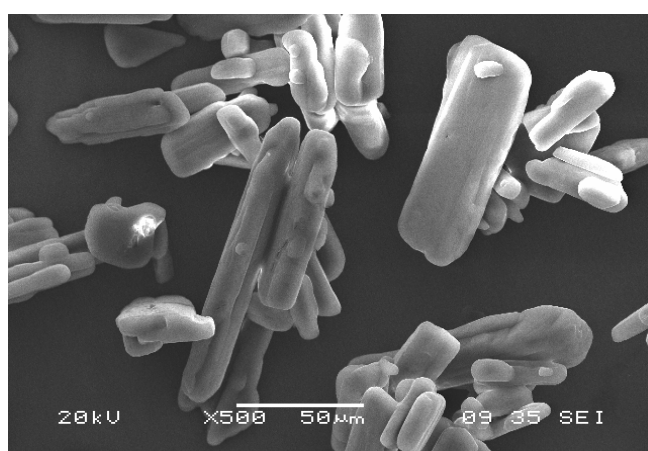
(B)



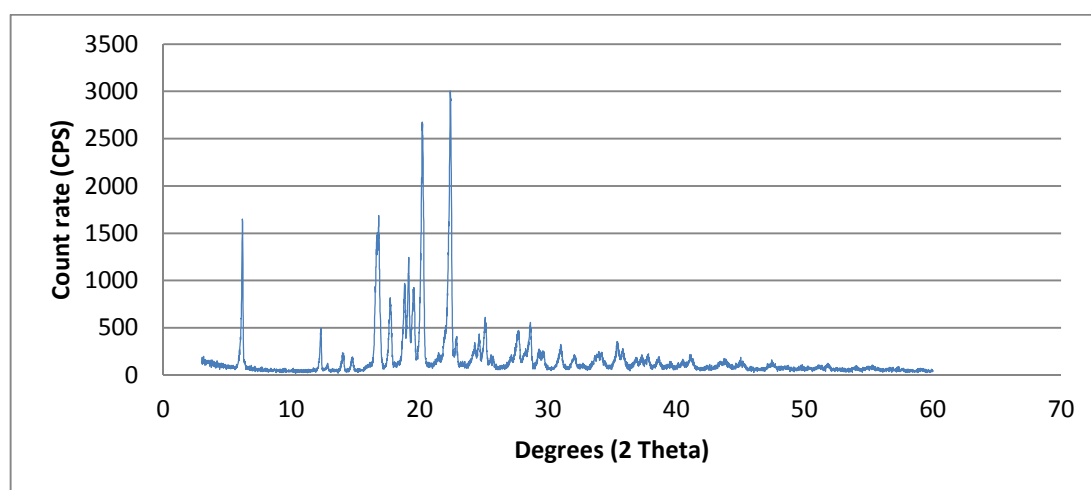
**Figure 3.5:** MTDSC reversing heat flow signal (A) and non-reversing heat flow signal (B) of ibuprofen in standard aluminium pans. Underlying scan rate of  $1^{\circ}\text{C min}^{-1}$  with a modulation amplitude of  $\pm 0.265^{\circ}\text{C}$  and a period of 100 seconds. Insert showing magnification of associated glass transition temperature (A)

### 3.3.1.2 Morphological and spectroscopic properties

Ibuprofen occurs as a white crystalline material with a common crystal form of needle-shape habit with rough surface (Rasenack and Müller, 2002) as shown in the SEM micrograph in Figure 3.6. Using PXRD technique, each crystalline solid has a unique X-ray pattern. A diffractogram would result from X-ray interactions with electrons of the constituent molecules. For crystalline material, this diffractogram or PXRD profile is usually characterised with clearly defined peaks with varying intensities associated with uniform lattice spacing as seen in Figure 3.7 for crystalline ibuprofen.

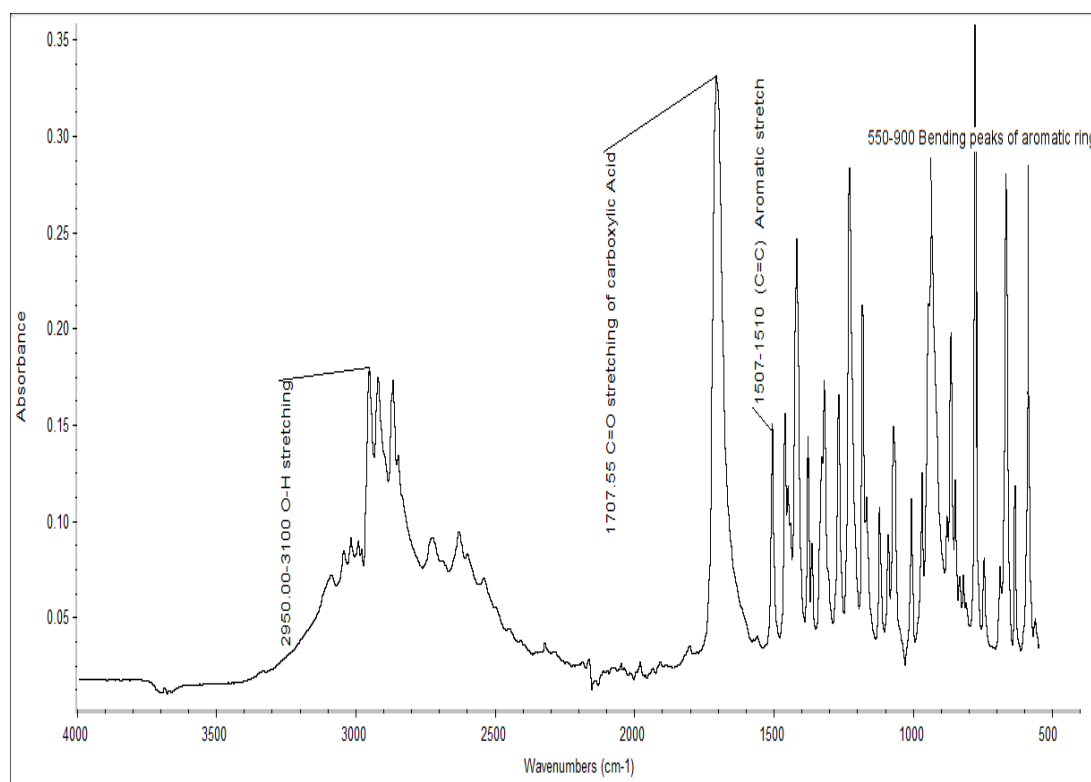


**Figure 3.6: SEM image of crystalline ibuprofen**



**Figure 3.7: PXRD diffractogram of crystalline ibuprofen**

ATR-FTIR is also a valuable tool to derive information characteristic for studied sample through analyzing its molecular vibrations. The studied sample is usually described by treating it as a collection of individual functional groups, each of which corresponds to absorbance band assigned from group frequency correlation. This is illustrated in the ATR-FTIR spectrum of ibuprofen in Figure 3.8, wherein major functional groups are assigned. It is worth to mention that hydroxyl O-H stretching broadness observed in this spectrum is a result of superimposition of the alkyl C-H stretching.



**Figure 3.8:** ATR-FTIR spectrum of crystalline ibuprofen

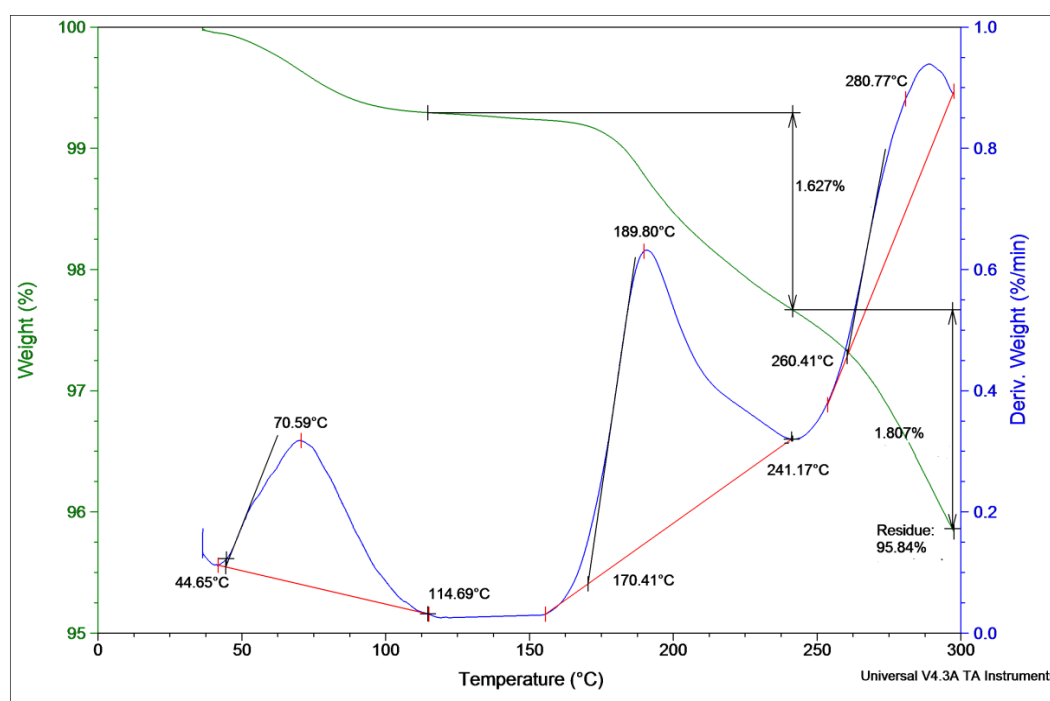
### 3.3.2 Carrier excipients

#### 3.3.2.1 Eudragit RS PO

##### 3.3.2.1.1 Thermoanalytical investigations

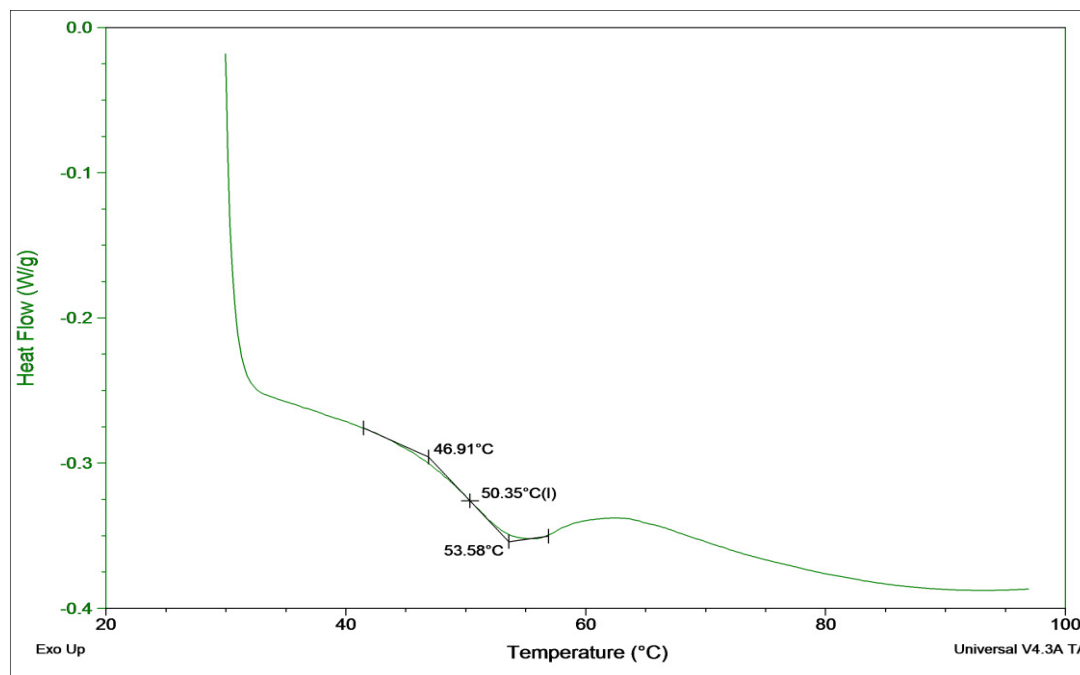
The work in this study was made using the parent polymer Eudragit RS PO, which was selected to be a major constituent of the blend composition with ibuprofen (see Chapter 2). Therefore, characterisation of its properties can aid in understanding of its behaviour when blended with the drug and fabricated using HME technology.

TGA demonstrated three weight losses as detected from weight loss derivative curve in Figure 3.9. An initial weight loss was observed in the region between 45-115°C, indicating water loss. This polymer showed a thermal stability over the investigated temperature frame below 170°C with no signs of degradation. This agrees with Lin and Yu (2000) findings, whom employed DSC, TGA and ATR-FTIR/DSC microscopy techniques to investigate thermal stability of this polymeric grade. However after ~170°C, further two weight losses occurred, indicating decomposition. In comparison to ibuprofen, Eudragit RS PO is more stable thermally and thus extrusion temperature should be selected carefully with regard to the drug, wherein relatively low temperatures should be applied, preferably less than 120°C as aforeindicated.



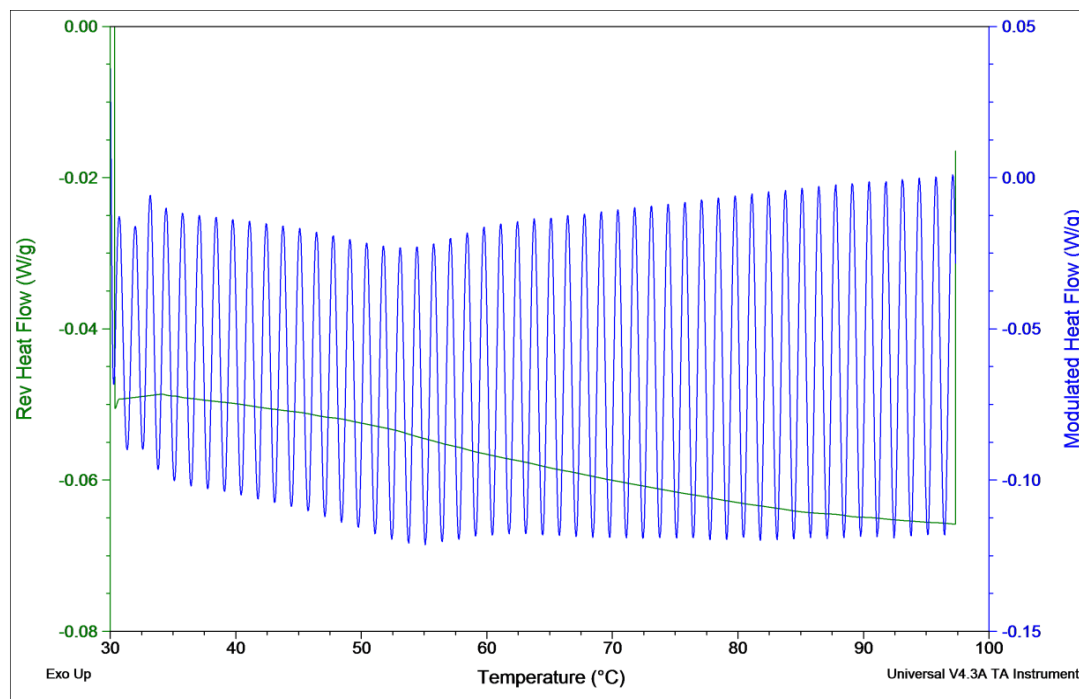
**Figure 3.9:** TGA weight loss profile of Eudragit RS PO heated at 10°C min<sup>-1</sup> to 300°C

As for ibuprofen, cDSC at 10°C min<sup>-1</sup> was used to address thermal behaviour of Eudragit RS PO as shown in Figure 3.10. Being amorphous, no fusion peaks were detected for this polymer; however, a glass transition event was observed and complicated with a broad endotherm due to possible partial water loss around 55-60°C, supported by TGA findings.



**Figure 3.10: Heat flow signal of Eudragit RS PO heated at  $10^{\circ}\text{C min}^{-1}$  in standard aluminium pans**

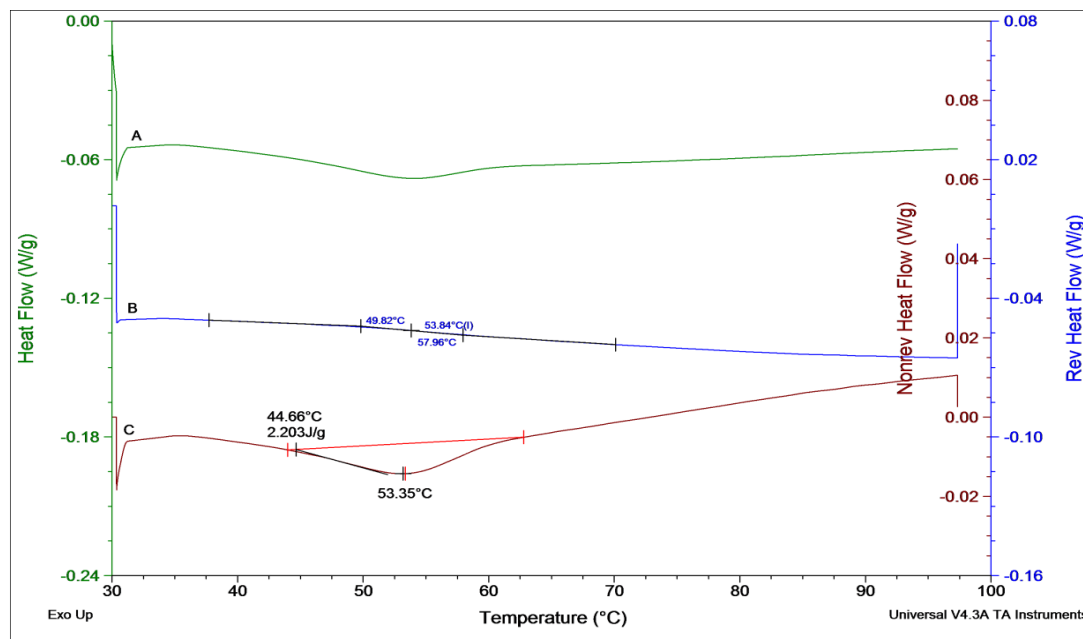
As previously stated, MTDSC is the technique of choice to separate out the kinetic components from those related to heat capacity components in non-reversing and reversing heat flow signals, respectively. Therefore, MTDSC was used to detect glass transition temperature of the Eudragit RS PO. The most commonly used MTDSC parameters of a modulation with an underlying heat rate of  $2^{\circ}\text{C min}^{-1}$ , a period of 40 seconds and  $\pm 0.212^{\circ}\text{C}$  amplitude were employed. Figure 3.11 shows that these parameters were able to produce more than six modulated cycles (approximately 10) through glass transition temperature of Eudragit RS PO as recommended by Craig and Reading (2007) to allow better distinction of thermal events using MTDSC. The full MTDSC profile of Eudragit RS PO is shown in Figure 3.12.



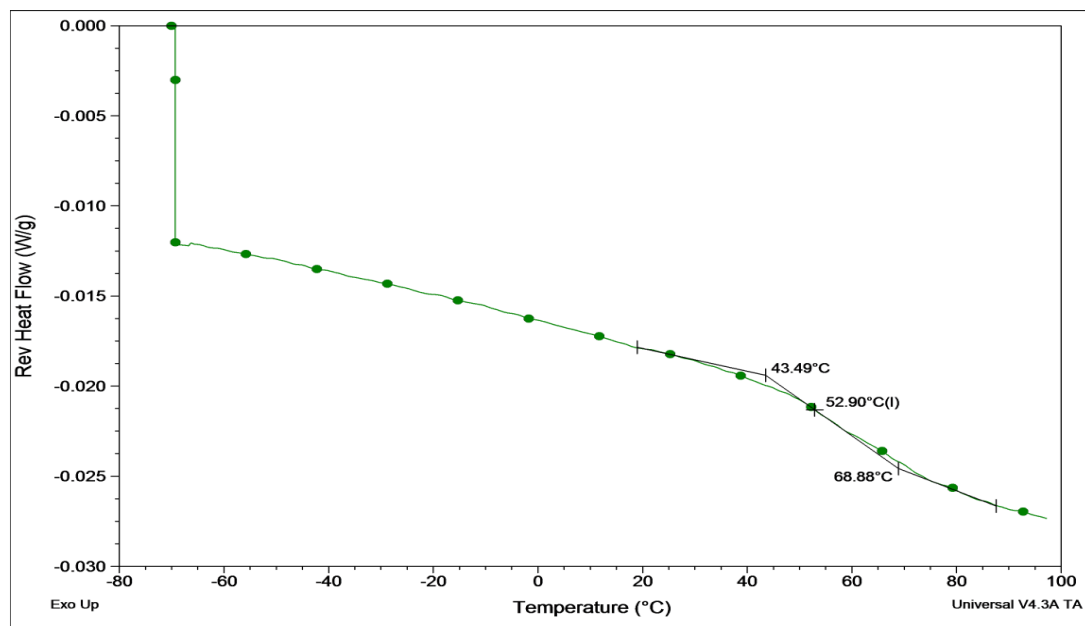
**Figure 3.11: Modulation heat flow signal over the reversing heat flow signal passing through Eudragit RS PO glass transition temperature. Underlying scan rate of  $2^{\circ}\text{C min}^{-1}$  with a modulation amplitude of  $\pm 0.212^{\circ}\text{C}$  and a period of 40 seconds**

As seen in Figure 3.12, MTDSC traces of the reversing signal showed glass transition of Eudragit RS PO separated from water desorption endotherm, which appeared otherwise in the non-reversing heat flow signal as a broad peak. The glass transition temperature was determined as the Mid-point and equals approximately  $53.5^{\circ}\text{C}$ . Though deconvolution was achieved successfully in this method, the glass transition appeared as a weak signal. Consequently, this experimental method was amended with the objective to enhance sensitivity. Through application of relatively higher amplitude of  $\pm 0.265^{\circ}\text{C}$ , a longer period of 100 seconds with an underlying heating rate of  $1^{\circ}\text{C min}^{-1}$ , the glass transition temperature was more distinct and clearly seen around  $53.3 \pm 0.5^{\circ}\text{C}$  (Mid-point  $T_g$ ,  $n=3$ ) from the reversing heat flow signal as shown in Figure 3.13. The results of this method indicated its appropriateness for better distinguishing of Eudragit RS PO glass transition.





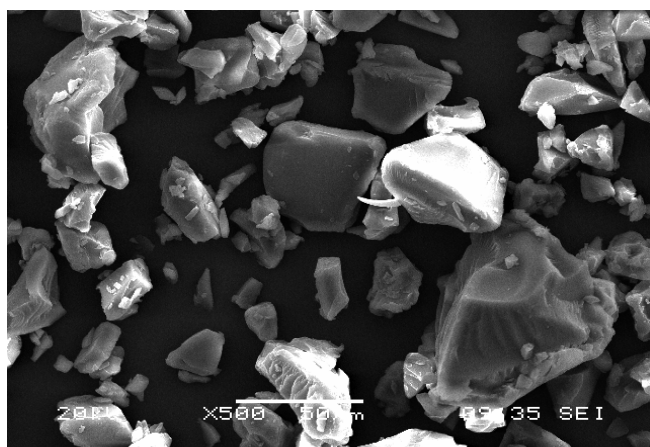
**Figure 3.12:** MTDSC heating scan of Eudragit RS PO in standard aluminium pans. Underlying scan rate of  $2^{\circ}\text{C min}^{-1}$  with a modulation amplitude of  $\pm 0.212^{\circ}\text{C}$  and a period of 40 seconds. The signals have been offset for clarity



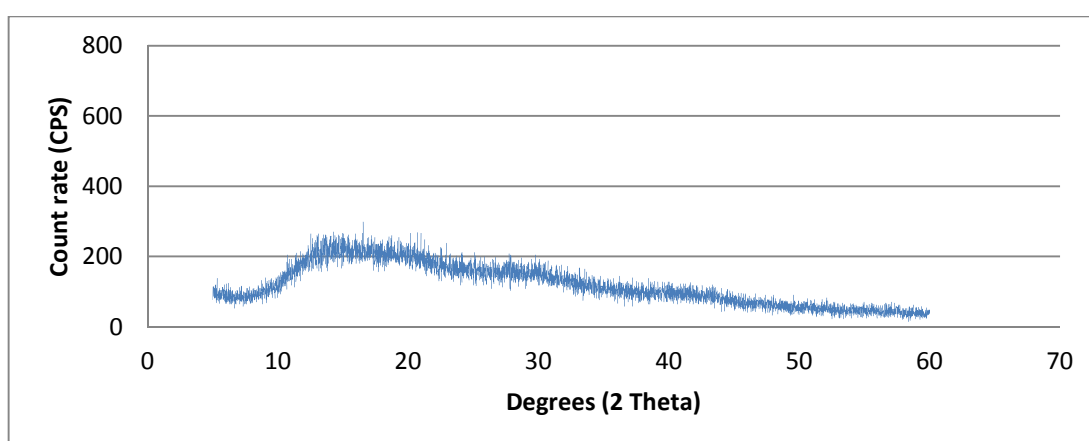
**Figure 3.13:** MTDSC reversing heat flow signal of Eudragit RS PO in standard aluminium pans. Underlying scan rate of  $1^{\circ}\text{C min}^{-1}$  with a modulation amplitude of  $\pm 0.265^{\circ}\text{C}$  and a period of 100 seconds

## 3.3.2.1.2 Morphological and spectroscopic properties

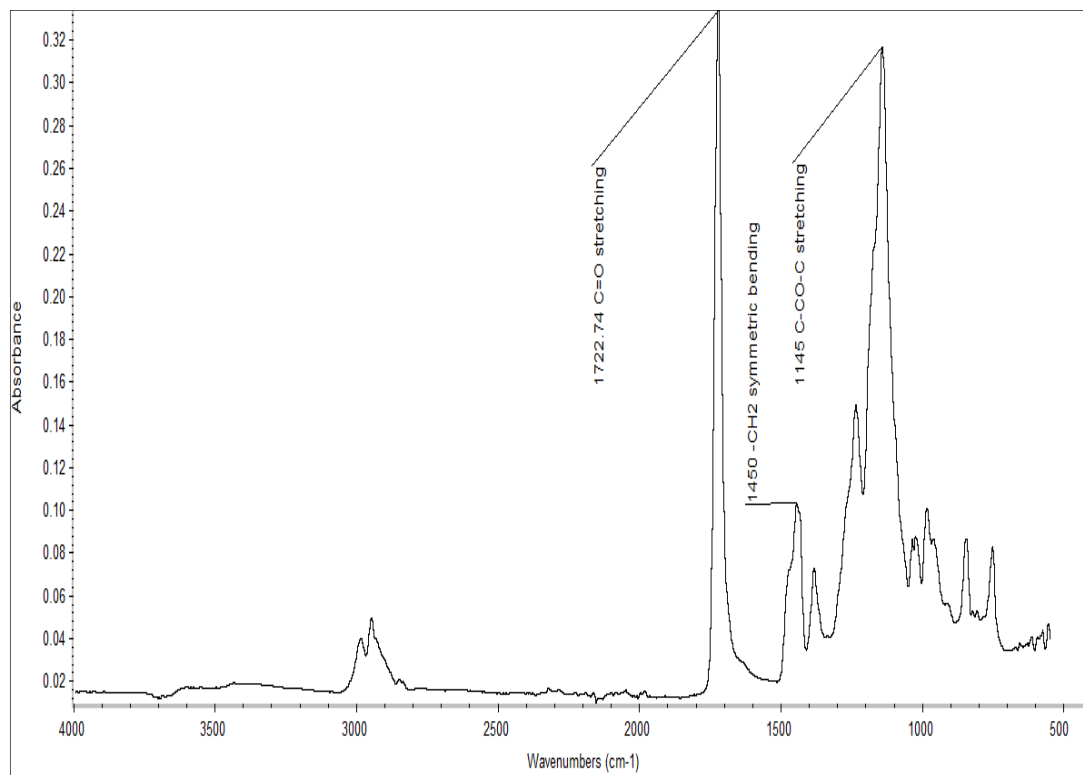
Eudragit RS PO occurs as a fine white powder and Figure 3.14 shows the shape of its particles under SEM. This amorphous polymer produced broad background signal with no defined peaks upon examination using PXRD (Figure 3.15). This is a result of the relative randomness of the molecular arrangements in the amorphous material; thereby a halo-pattern is usually manifested in the PXRD diffractogram. The absorption information derived from the ATR-FTIR spectrum of Eudragit RS PO in Figure 3.16 shows characteristic peaks at  $1723\text{ cm}^{-1}$  due to carbonyl stretching and at  $1145\text{ cm}^{-1}$  which is related to (C-CO-C) stretching in the ester group, in addition to  $(\text{CH}_2\text{-})$  symmetric bending at  $1450\text{ cm}^{-1}$ .



**Figure 3.14:** SEM image of amorphous Eudragit RS PO polymer



**Figure 3.15:** PXRD diffractogram of Eudragit RS PO



**Figure 3.16: ATR-FTIR spectrum of Eudragit RS PO**

### 3.3.2.2 Sucrose

#### 3.3.2.2.1 Thermoanalytical investigations

As a function of temperature, TGA experiment indicated that a sign of sucrose weight loss started around 188-190°C as shown in Figure 3.17. This could be referred as the approximate onset of degradation, indicating thermal stability of sucrose below this temperature. In Figure 3.18, the MTDSC traces of this sugar showed an endothermic peak detected from total heat flow signal related to sucrose melting at  $175.2 \pm 1.8^\circ\text{C}$  ( $T_{m(\text{onset})}$ ). Slightly above this melting peak, a decomposition exotherm was detected from the non-reversing heat flow signal with a maximum approximately at 187°C. This is expected because of sucrose sensitivity for decomposition near its melting point (Feuge et al., 1973). Therefore, it would be recommended to perform hot melt extrusion of sucrose at temperatures below its melting temperature. This necessitates incorporation of plasticizer to lower required processing temperature and in this case it is the active moiety i.e. ibuprofen.

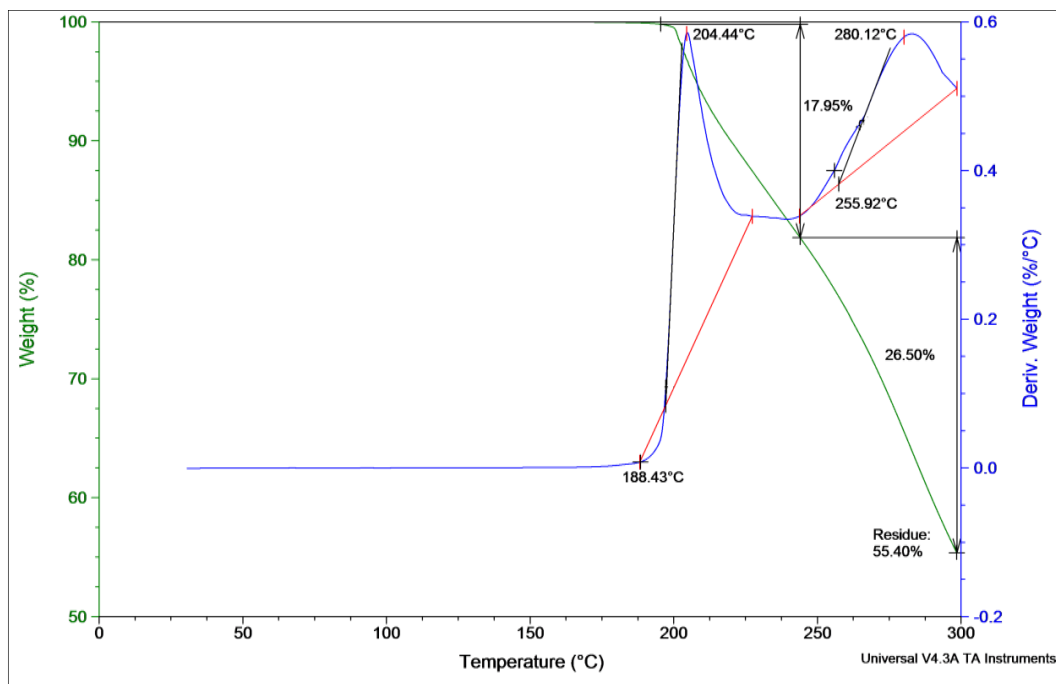


Figure 3.17: TGA weight loss profile of sucrose heated at  $10^{\circ}\text{C min}^{-1}$  to  $300^{\circ}\text{C}$

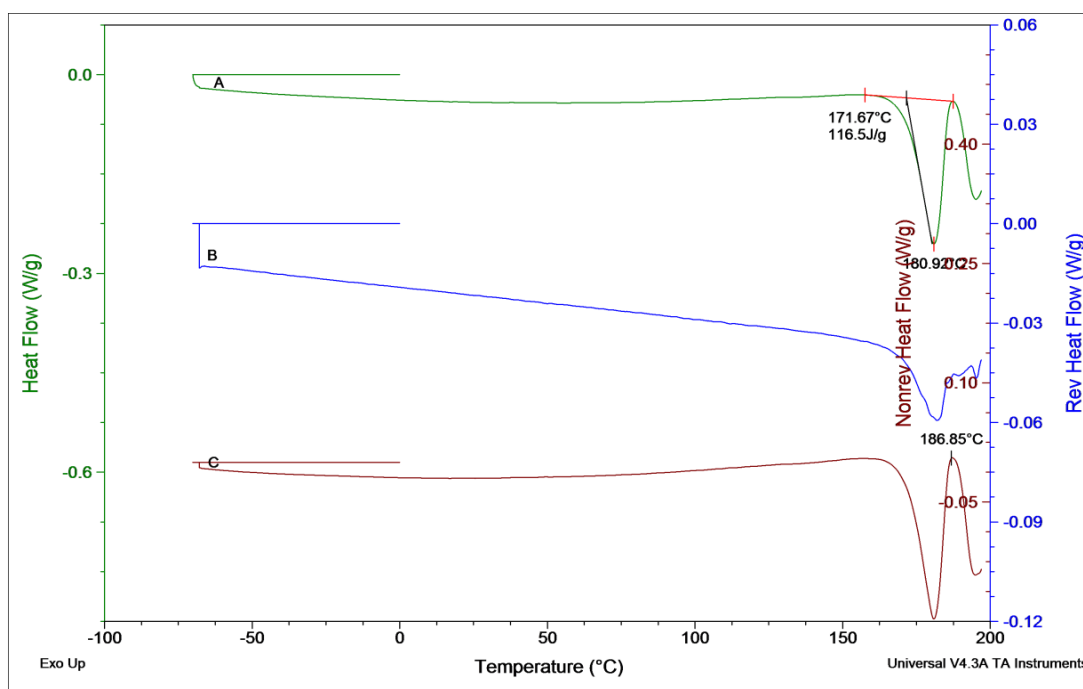
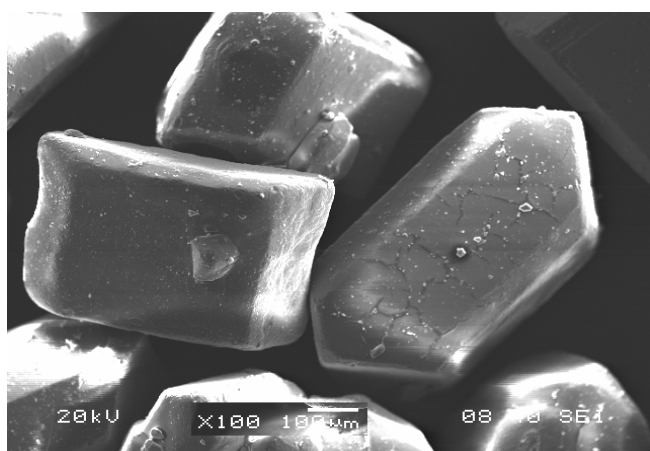


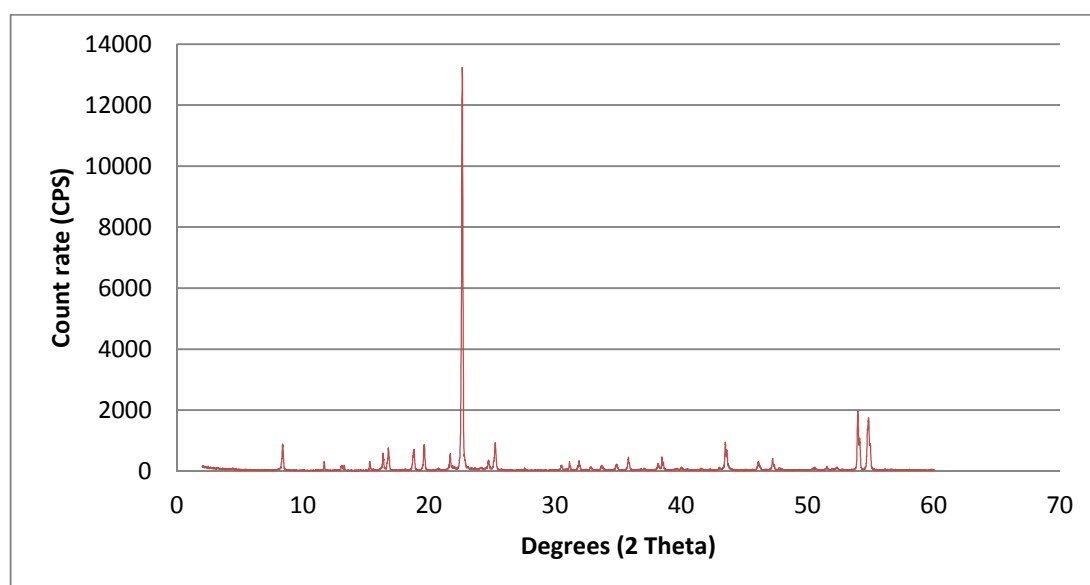
Figure 3.18: MTDSC heating scan of sucrose in standard aluminium pans. Underlying scan rate of  $1^{\circ}\text{C min}^{-1}$  with a modulation amplitude of  $\pm 0.265^{\circ}\text{C}$  and a period of 100 seconds. The signals have been offset for clarity

## 3.3.2.2.2 Morphological and spectroscopic properties

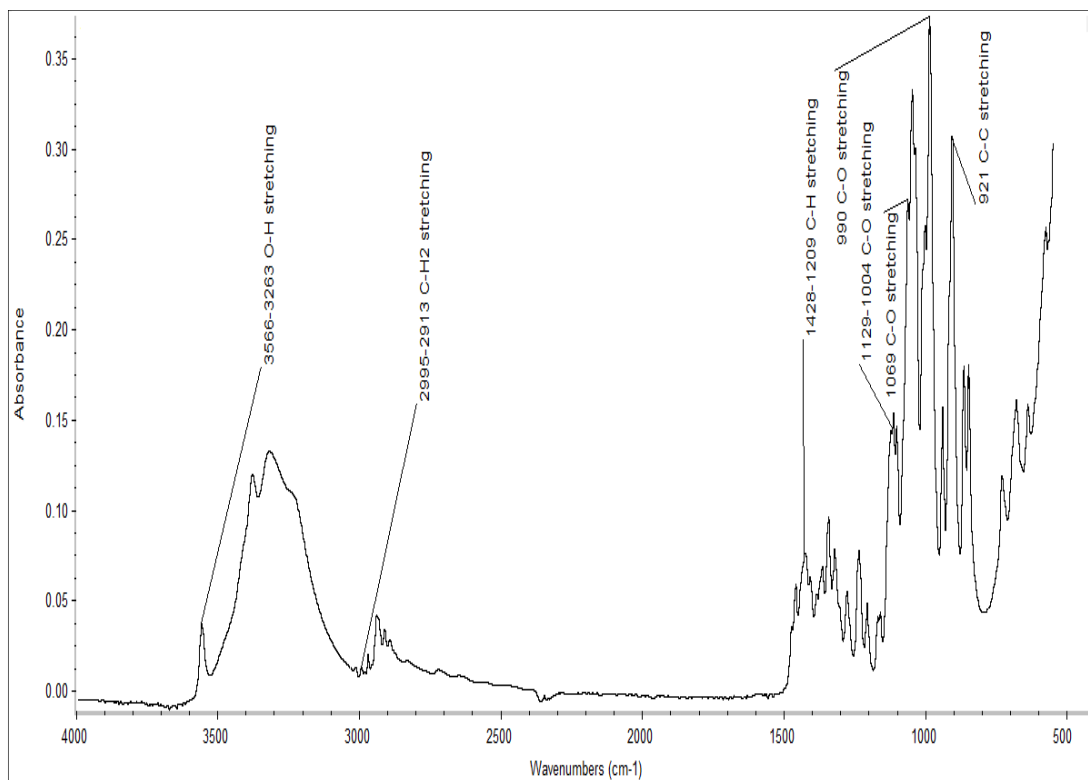
Sucrose is crystalline material which appeared as crystalline blocks with oblong shape and slanted edges under SEM as depicted in Figure 3.19. This sugar exhibited sharp, intense and well-defined peaks in its PXRD profile displayed in Figure 3.20, implying highly ordered crystalline nature. In addition, Figure 3.21 shows major functional groups of sucrose assigned in its ATR-FTIR spectrum as suggested by Brizuela et al. (2012), whom combined theoretical and experimental approaches to characterise this complex sugar using IR spectroscopy.



**Figure 3.19: SEM image of crystalline sucrose**



**Figure 3.20: PXRD diffractogram of crystalline sucrose**



**Figure 3.21: ATR-FTIR spectrum of crystalline sucrose**

### 3.3.2.3 Methyl cellulose

#### 3.3.2.3.1 Thermoanalytical investigations

Thermal stability of methylcellulose, as for previous materials, was studied using TGA and the obtained weight loss pattern is shown in Figure 3.22 after heating to 300°C at 10°C min<sup>-1</sup>. One stage decomposition was detected, which started around 200°C. Before that, an early minor weight loss was detected between approximately 34-84°C. This event could be attributed to moisture desorption from the surface of this hydrophilic polymer. Further MTDSC examination of this polymer supported this observation as illustrated in Figure 3.23. In this figure, traces of MTDSC signals permitted separation of three main thermal events. The first event was small endothermic peak, detected from total heat flow signal with an extrapolated onset at approximately -21.6°C. This endotherm was followed by broad endothermic peak, detected from non-reversing heat flow signal with extrapolated onset around 56°C. The first event could be related to the melting of frozen water. Usually loosely bound water on the surface of hydrophilic polymer freezes at temperature lower than that of bulk water and melt before 0°C (Hatakeyama and Hatakeyama, 1998). The frozen form of this water melts at about -15° to -35°C (Joshi and Wilson, 1995). Therefore, water present in

methycellulose is likely to be surface moisture. The second event is also believed to correspond to water desorption from this polymer and correlates well with TGA results. The third event is the glass transition temperature as determined from reversing heat flow signal at  $103.0 \pm 0.1^\circ\text{C}$  (Mid-point  $T_g$ ,  $n=3$ ) for this polymer grade (Methocel A4C Premium), indicating its amorphous structure.

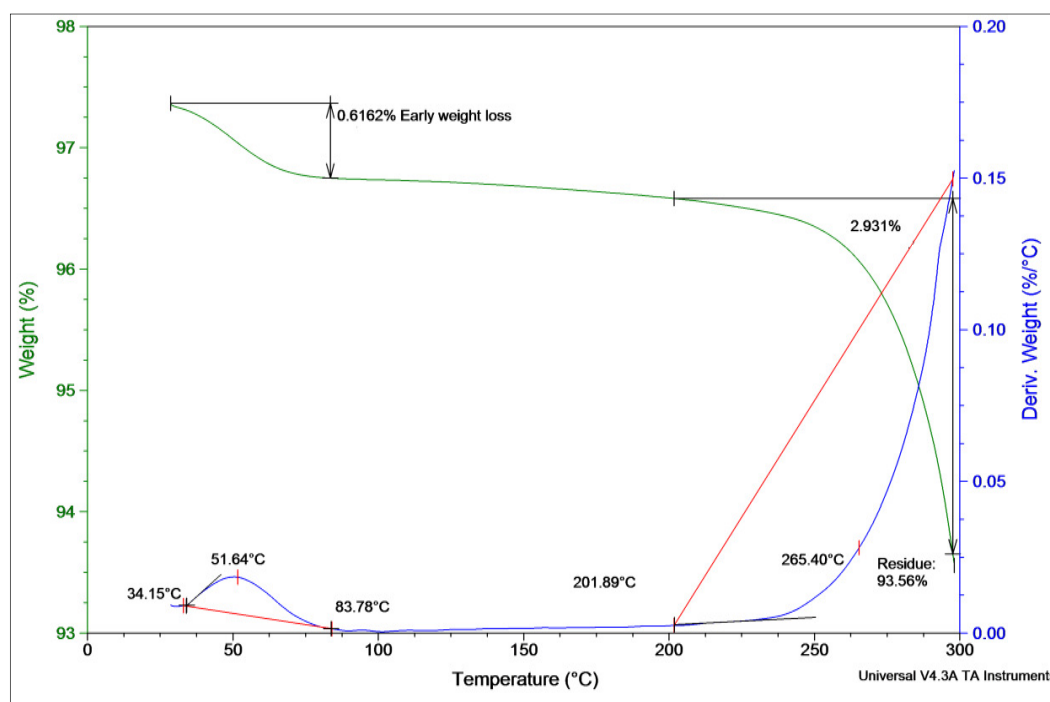
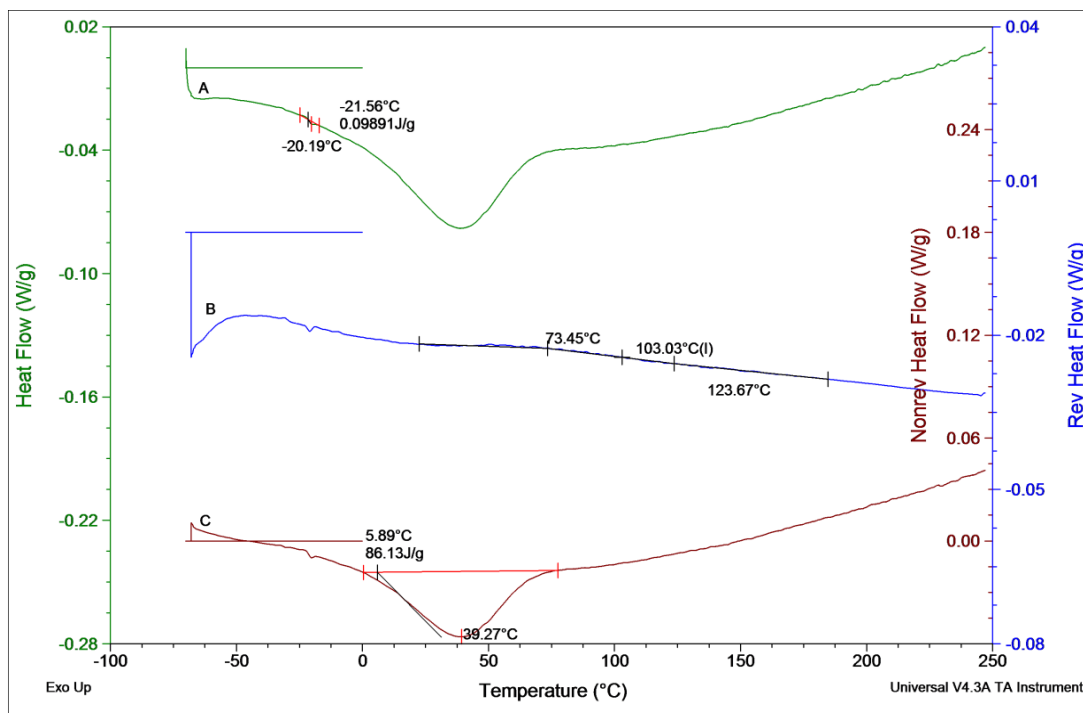


Figure 3.22: TGA weight loss profile of methylcellulose heated at  $10^\circ\text{C min}^{-1}$  to  $300^\circ\text{C}$



**Figure 3.23: MTDSC heating scan of methylcellulose in standard aluminium pans. Underlying scan rate of 1°C min<sup>-1</sup> with a modulation amplitude of ±0.265°C and a period of 100 seconds. The signals have been offset for clarity**

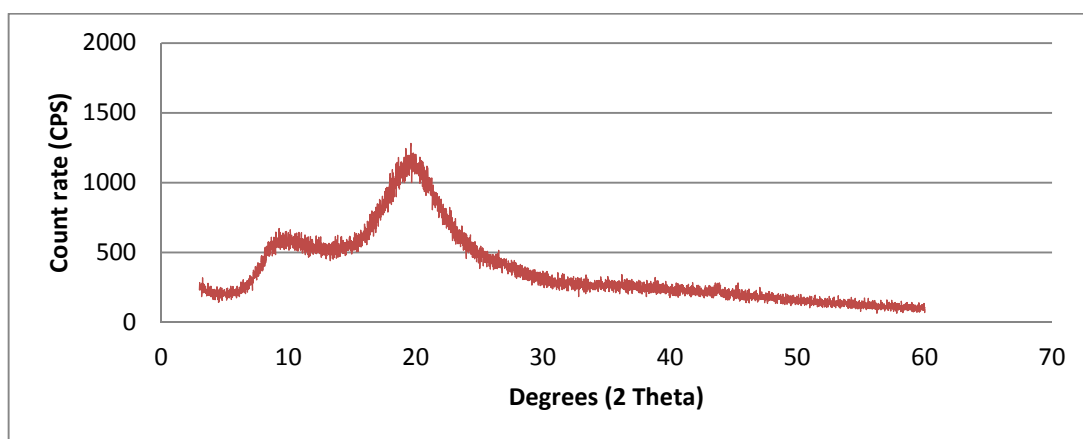
### 3.3.2.3.2 Morphological and spectroscopic properties

As detailed in Chapter 2, methylcellulose is substituted from cellulose. In this substitution, hydroxyl groups of cellulose are replaced with methoxyl groups. The grade used in this study (Methocel A4C Premium) showed a fibrous-like shape of its particles under SEM (Figure 3.24) and exhibited a halo diffraction pattern in its PXRD diffractogram as seen in Figure 3.25, which is pertinent pattern to the amorphous material. Therefore, it could be inferred that the used grade of methylcellulose in this study is more likely to have amorphous nature as indicated by the absence of melting peaks and diffraction peaks in MTDSC and PXRD results, respectively. ATR-FTIR spectrum of this polymer showed three main characteristic bands. As seen in Figure 3.26, a typical hydroxyl stretching appeared at 3500 cm<sup>-1</sup>, whereas alkyl stretching appeared at 2826 cm<sup>-1</sup>, which presents in the methyl ether groups (Babu et al., 2007). The C-O stretching vibration is assigned in the 1250-950 cm<sup>-1</sup> region (Buslov et al., 2008).

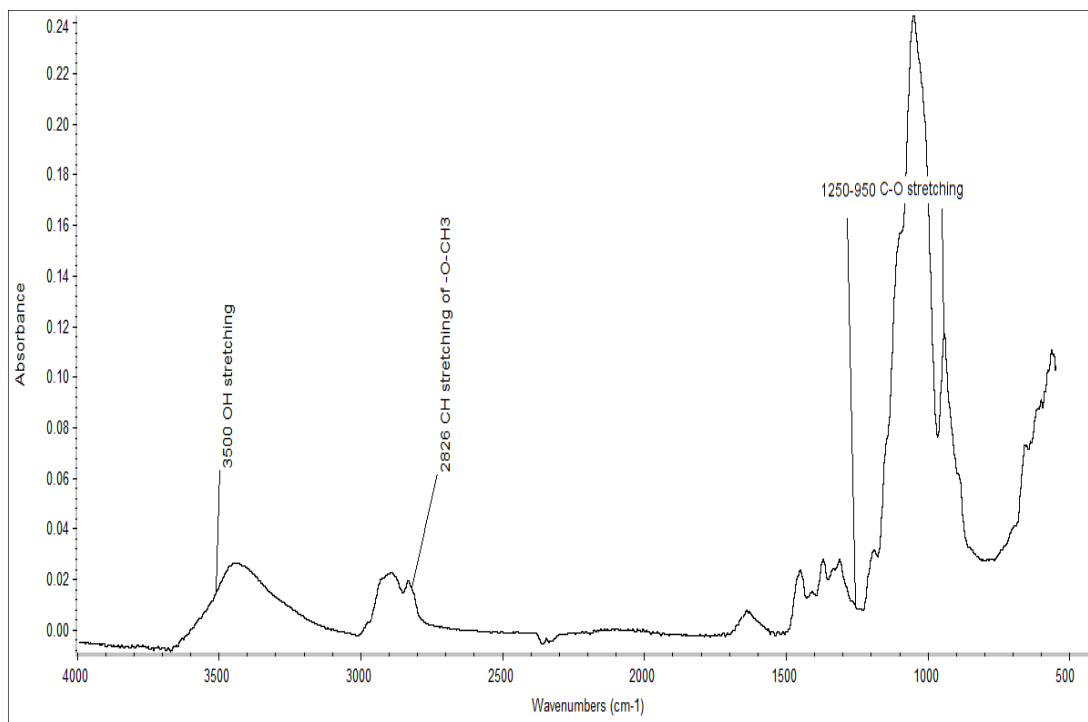




**Figure 3.24: SEM image of methylcellulose**



**Figure 3.25: PXRD diffractogram of methylcellulose**



**Figure 3.26: ATR-FTIR spectrum of methylcellulose**

### 3.3.2.4 Xantural®75

#### 3.3.2.4.1 Thermoanalytical investigations

The TGA profile of Xantural®75 or xanthan gum shows an initial weight loss between approximately 34 and 125°C corresponds to the evaporation of the moisture content as seen from weight loss derivative curve (blue curve) in Figure 3.27. The extrapolated onset of the degradation for this polymer is almost at 235.2°C, where 14.6% (w/w) of decomposition took place. MTDSC scanning revealed broad endothermic peak between 39.9 and 150°C, which is likely related to the desorption of the moisture as indicated in the TGA results, and appeared in the total and non-reversing heat flow signals in Figure 3.28. In this figure, a single glass transition was detected around  $37.7 \pm 2.6^\circ\text{C}$  (Mid-point  $T_g$ ,  $n=3$ ), as determined from the reversing heat flow signals. Because of its natural origin, xanthan gum characterisation, such as glass transition temperature ( $T_g$ ), might vary depending on the source of this material. For example, while Argin-Soysal et al. (2009) reported its  $T_g$  value at 143°C, Kocherbitov et al. (2010) estimated this value at 60°C.

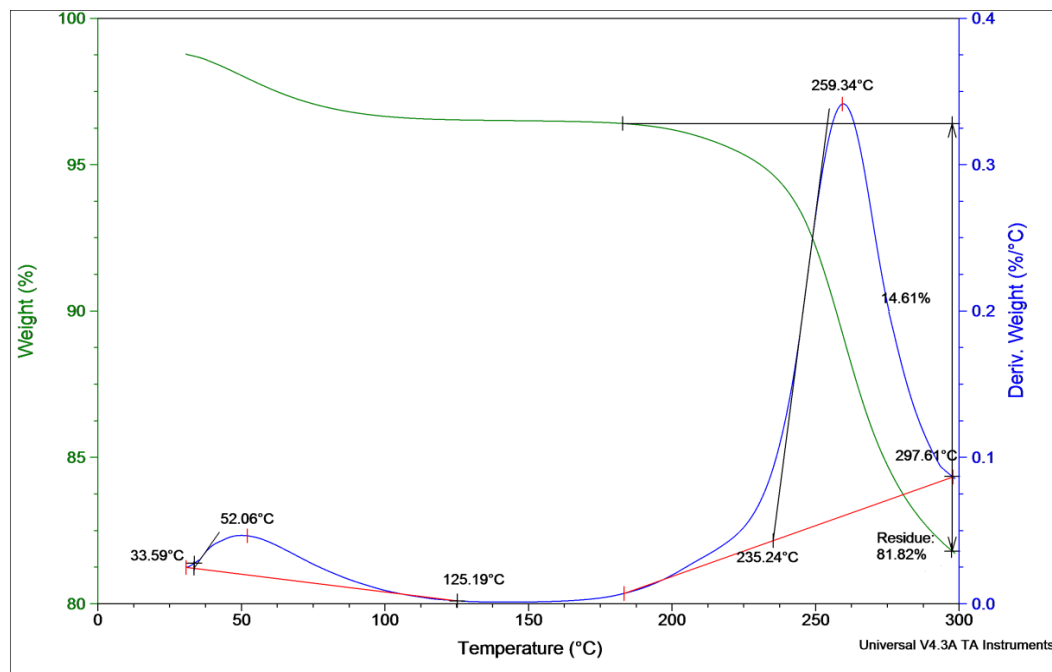


Figure 3.27: TGA weight loss profile of Xantural®75 heated at  $10^{\circ}\text{C min}^{-1}$  to  $300^{\circ}\text{C}$

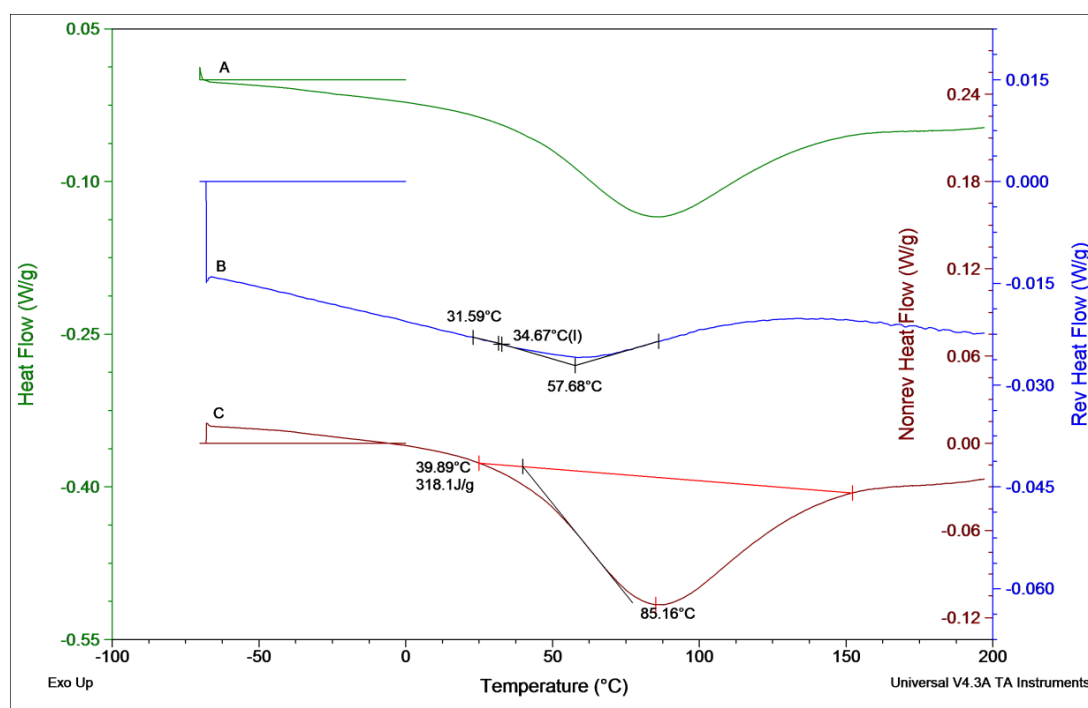


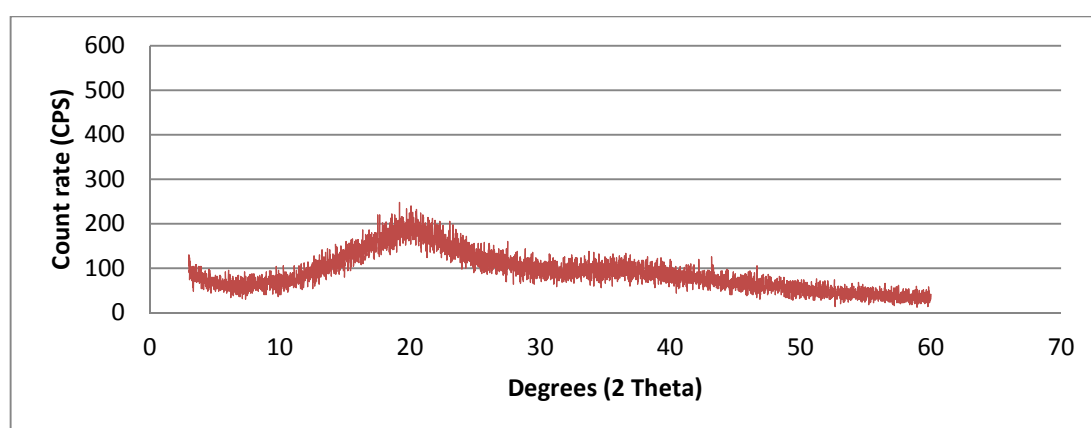
Figure 3.28: MTDSC heating scan of Xantural®75 in standard aluminium pans. Underlying scan rate of  $1^{\circ}\text{C min}^{-1}$  with a modulation amplitude of  $\pm 0.265^{\circ}\text{C}$  and a period of 100 seconds. The signals have been offset for clarity

## 3.3.2.4.2 Morphological and spectroscopic properties

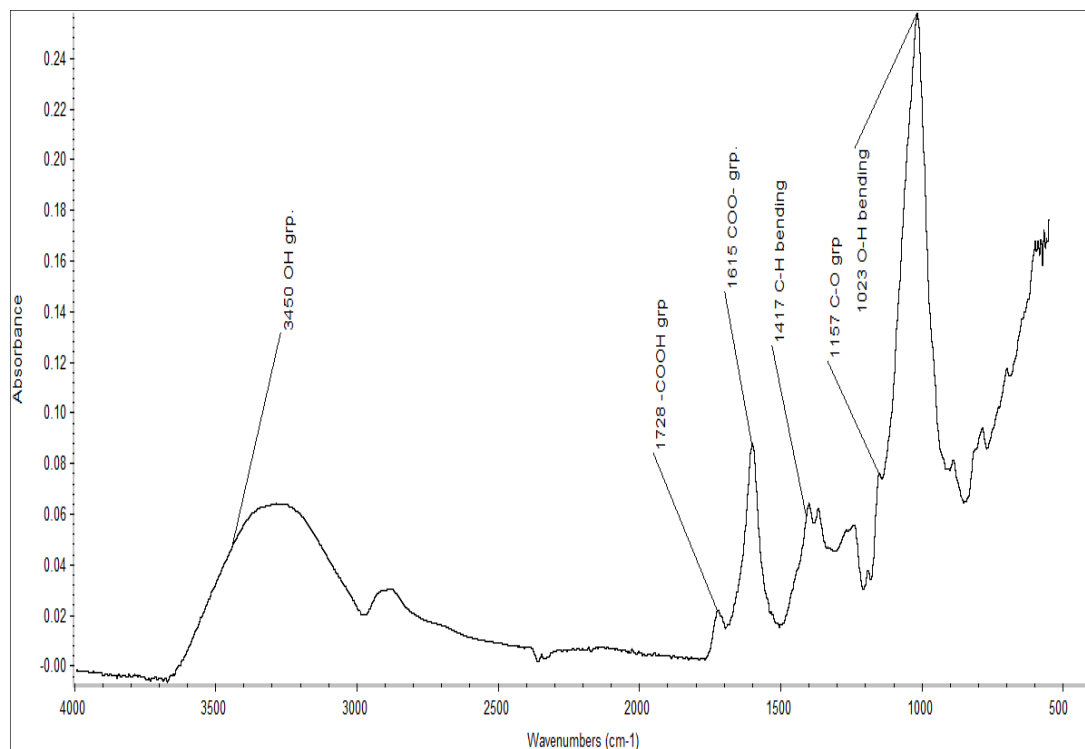
SEM image depicted in Figure 3.29 shows that Xantural®75 powder exhibited irregular granular shape. PXRD profile of this polymer in Figure 3.30 did not show diffraction peaks, clearly indicating amorphous structure. This amorphicity is supported by MTDSC findings. The chemical structure of this polymer as studied using ATR-FTIR is displayed in Figure 3.31. Hydroxyl stretching was detected at  $3450\text{ cm}^{-1}$ , carboxylic acid and C-O group at  $1728\text{ cm}^{-1}$  and  $1157\text{ cm}^{-1}$ , respectively (Lii et al.,2003). Other absorbance bands were  $1615\text{ cm}^{-1}$  related to carboxylate group,  $1417\text{ cm}^{-1}$  due to C-H bending and  $1023\text{ cm}^{-1}$  correlated with hydroxyl bending (Mundargi and Patil, 2007).



**Figure 3.29: SEM image of Xantural®75**



**Figure 3.30: PXRD diffractogram of Xantural®75**



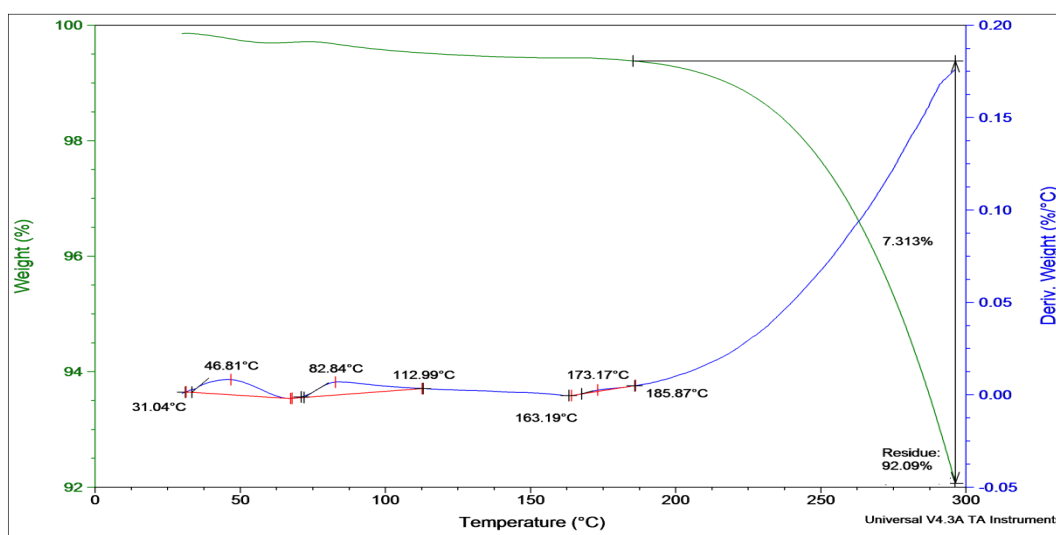
**Figure 3.31: ATR-FTIR spectrum of Xantural® 75**

### 3.3.2.5 Pluronic® F127

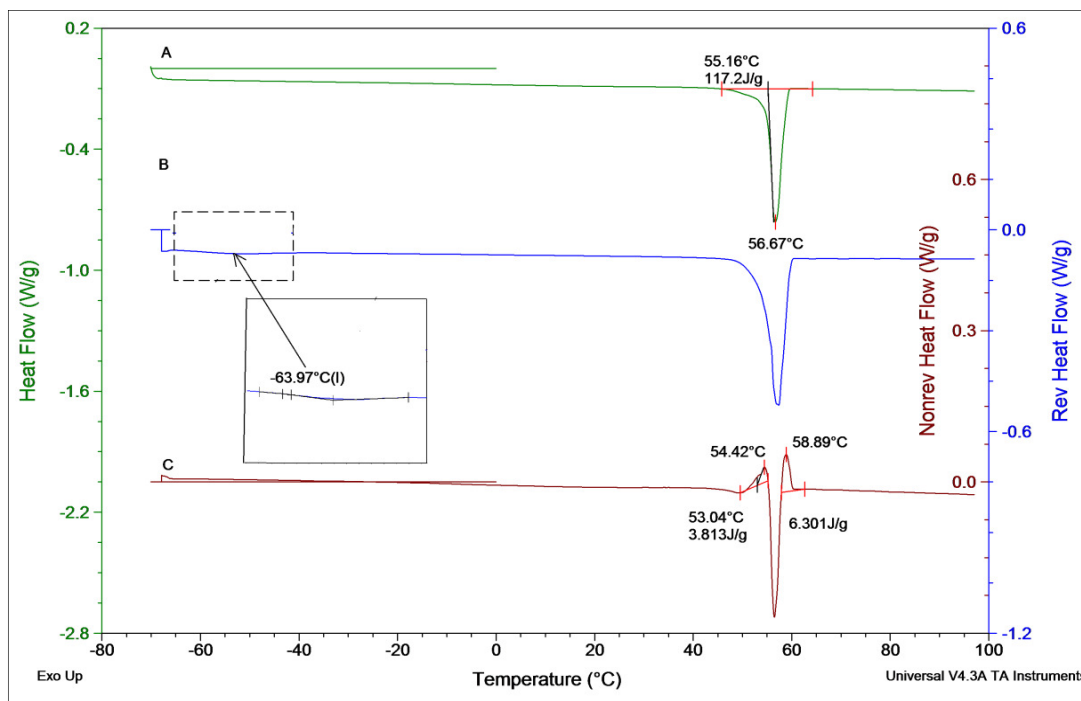
#### 3.3.2.5.1 Thermoanalytical investigations

Pluronic® F127 or poloxamer 407 is a semi-crystalline polymer which exhibits its hydrophilicity due to the presence of polyoxyethylene segments as documented in Chapter 2. The moisture in this polymer liberated over a temperature range between approximately 31-113°C in a step-wise fashion as seen clearly from the weight loss derivative curve in its TGA profile displayed in Figure 3.32. In this figure, decomposition started insignificantly around 163.2°C with less than 0.1% (w/w) weight loss; however, the main degradation occurred after 185.9°C.

MTDSC profile of this polymer is illustrated in Figure 3.33. This profile showed a broad melting peak with a peak temperature at  $56.7 \pm 0.3^\circ\text{C}$  and  $T_{m(\text{onset})}$  at  $54.2 \pm 1.2^\circ\text{C}$ , as measured from the total heat flow signals. Since semicrystalline polymers constitute a distribution of crystallites, it would be expected to have this relatively broad melting peak (Craig and Reading, 2007). Exothermic shoulders associated with the melting peak were detected in both total and non-reversing heat flow signals. This could be related to recrystallization of the amorphous fractions which undergo different degree of perfection. A small glass transition temperature was detected from the reversing heat flow signal at  $-63.5 \pm 0.7^\circ\text{C}$  (Mid-point  $T_g$ ,  $n=2$ ). This temperature was found to be close to the reported glass transition temperature of amorphous polyoxypropylene (PPO) segments of poloxamer polymer, occurring approximately at  $-65^\circ\text{C}$  (Smithey et al., 2007).



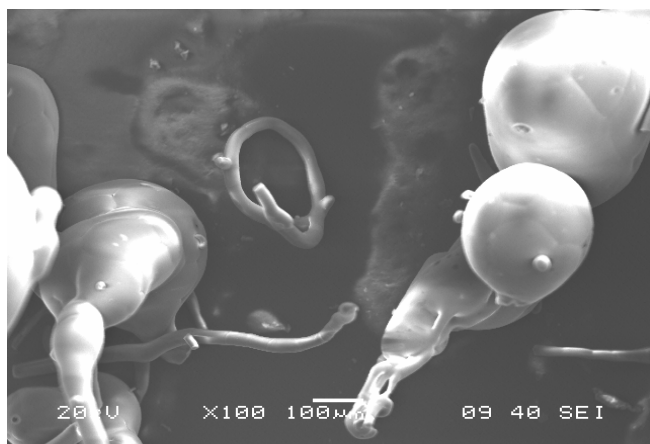
**Figure 3.32: TGA weight loss profile of Pluronic® F127 heated at  $10^\circ\text{C min}^{-1}$  to  $300^\circ\text{C}$**



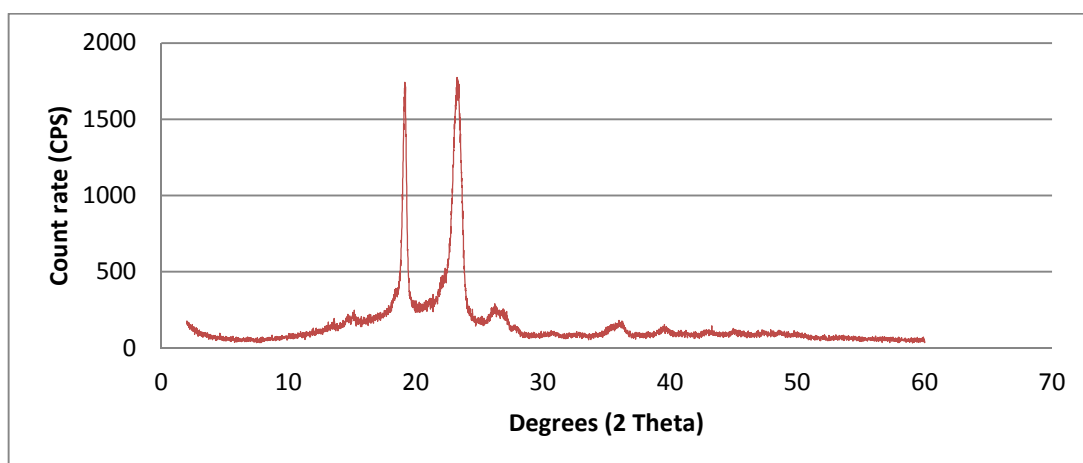
**Figure 3.33: MTDSC heating scan of Pluronic® F127 in standard aluminium pans. Underlying scan rate of  $1^{\circ}\text{C min}^{-1}$  with a modulation amplitude of  $\pm 0.265^{\circ}\text{C}$  and a period of 100 seconds. Inset showing magnification of predicted glass transition temperature. The signals have been offset for clarity**

#### 3.3.2.5.2 Morphological and spectroscopic properties

SEM image of the white flaky Pluronic® F127 in Figure 3.34 shows particles with different shapes, mostly as spheres and rods. PXRD diffractogram in Figure 3.35 distinguished two diffraction peaks of this polymer, indicating crystalline material presence. This PXRD profile matches polyoxyethylene (PEO) diffraction pattern for this polymer as reported by Yin et al. (2005), thereby supporting possible presence of the other main component of this polymer i.e. PPO as amorphous material. Three characteristic bands of this poloxamer were indicated in the ATR-FTIR spectrum, as presented in Figure 3.36. Hydroxyl stretching at  $3505\text{ cm}^{-1}$ , alkyl C-H stretching at  $2975\text{ cm}^{-1}$  and an intense band at  $1103\text{ cm}^{-1}$ , which is related to C-O-C ether stretching (Zhang and Lam, 2005).

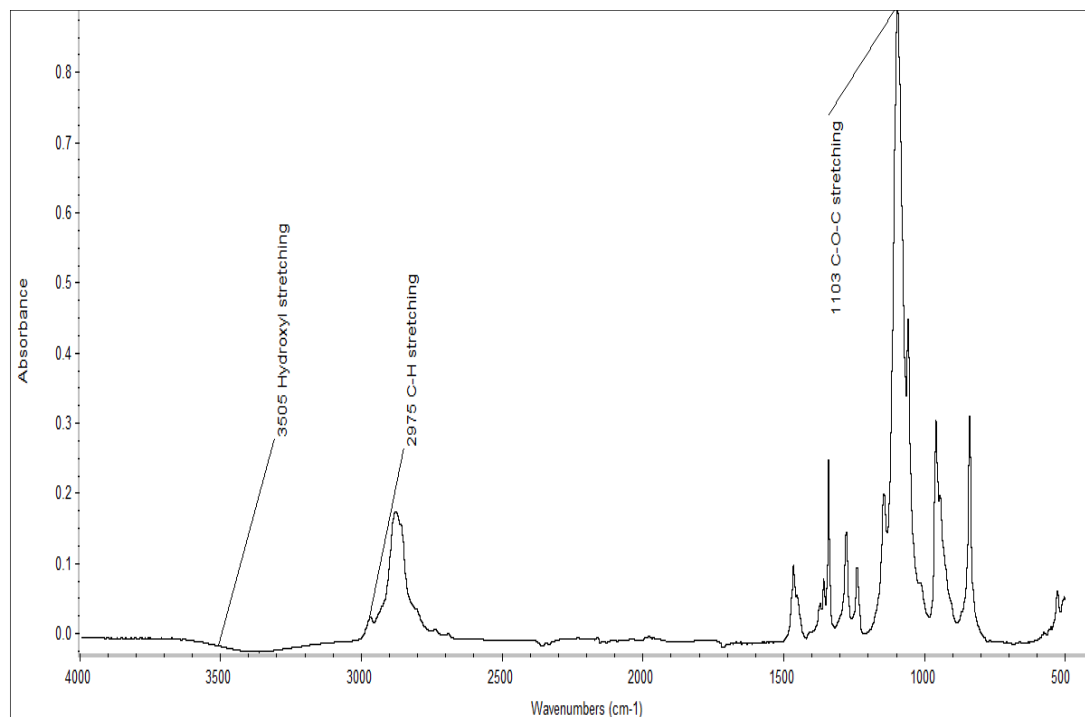


**Figure 3.34: SEM image of Pluronic® F127**



**Figure 3.35: PXRD diffractogram of Pluronic® F127**





**Figure 3.36: ATR-FTIR spectrum of Pluronic® F127**

### 3.3.2.6 Gelucire 44/14

#### 3.3.2.6.1 Thermoanalytical investigations

Gelucire 44/14 is amphiphilic multi-component excipient with a lipidic nature and polymeric constituents as detailed in Chapter 2. TGA examination of this lipid gave two stages of decomposition preceded by initial weight loss ascribed to moisture desorption as shown in Figure 3.37. The first stage of decomposition starts around 152.4°C followed by the second major decomposition stage that starts around 170.6°C. Therefore, thermal stability of this material can be maintained below 150°C. As previously mentioned in Chapter 2, part of this lipid denotes the melting point, which is 44°C. However, the melting of Gelucire 44/14 occurs at a range of temperatures, which despite being relatively narrow range (Gattefossé, 2007) is reasonably expected due to many components in this excipient which exhibit different melting points. This broad melting peak was detected from MTDSC traces in Figure 3.38. As determined from the total heat flow signal, this peak seems to have two fractions. The one which has higher melt  $\Delta H$  (larger peak) will be called primary melting endotherm which occurs at  $39.5 \pm 0.8^\circ\text{C}$  ( $T_{m(\text{onset})}$ ) while the secondary melting fraction corresponds to the small leading shoulder-like endotherm at  $32.1 \pm 1.4^\circ\text{C}$  ( $T_{m(\text{onset})}$ ).

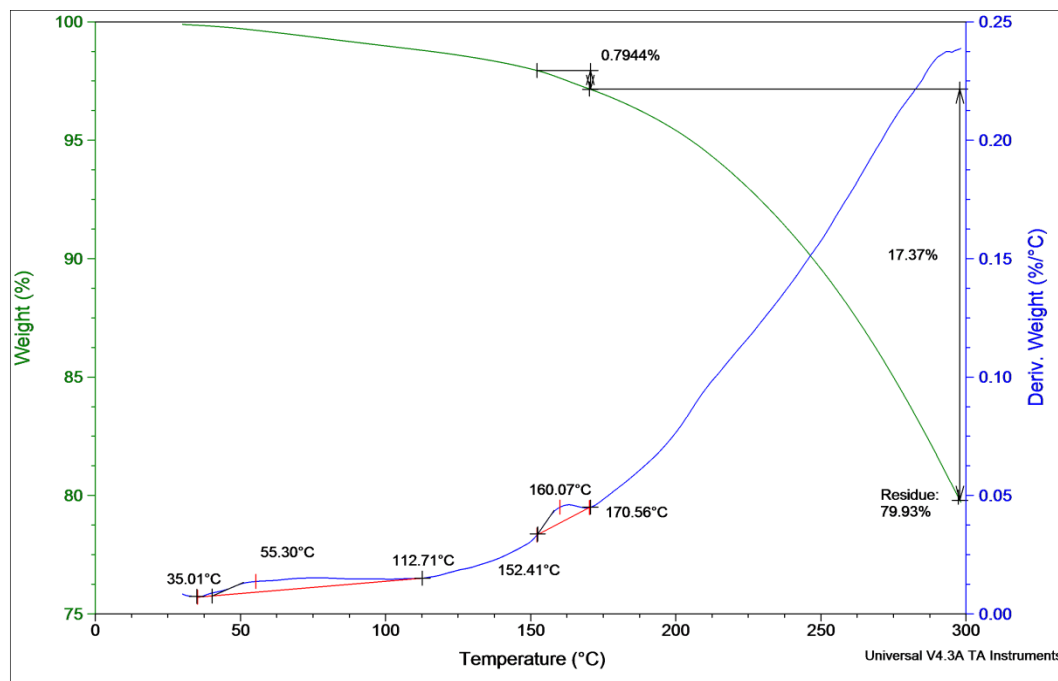


Figure 3.37: TGA weight loss profile of Gelucire 44/14 heated at 10°C min<sup>-1</sup> to 300°C

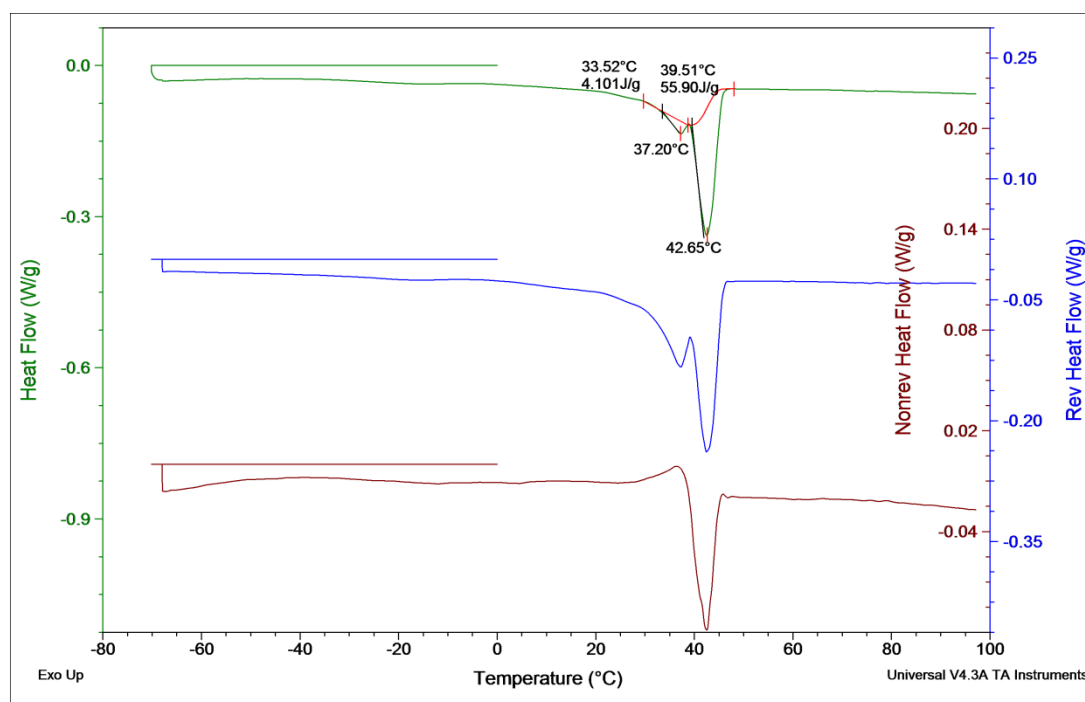
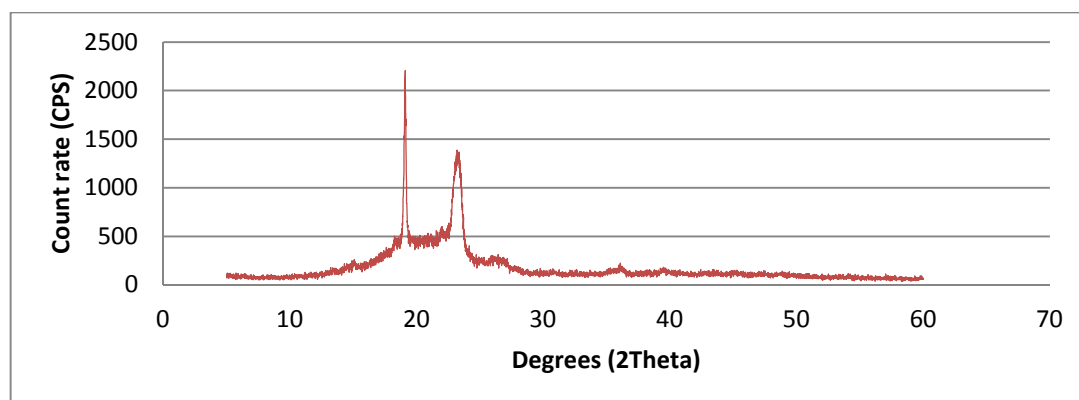


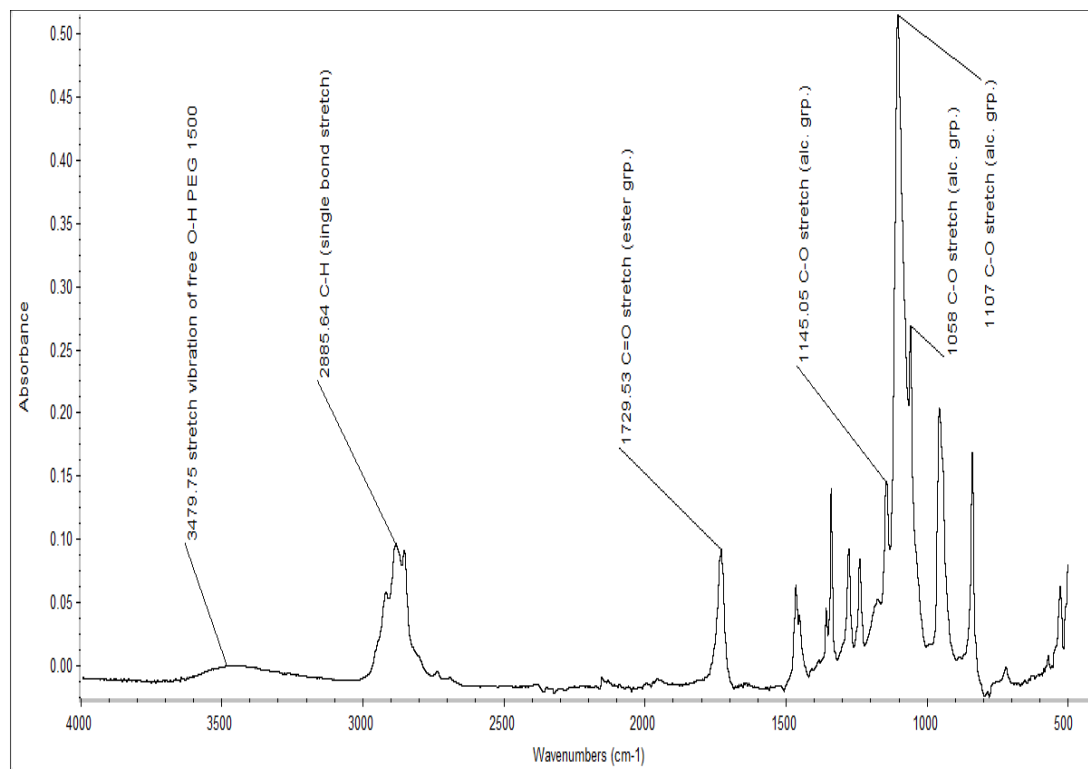
Figure 3.38: MTDSC heating scan of Gelucire 44/14 in standard aluminium pans. Underlying scan rate of 1°C min<sup>-1</sup> with a modulation amplitude of  $\pm 0.265^\circ\text{C}$  and a period of 100 seconds. The signals have been offset for clarity

## 3.3.2.6.2 Spectroscopic properties

Using SEM technique documented in Chapter 2, the beam current of electrons flow will hit the sample and a heat can build up on the sample. For low-melting point materials as Gelucire 44/14, the tested samples can melt under examination which will affect the results through contamination of the secondary electrons emitted from the surface of these samples after being dislodged by a focused electron beam moving across their surfaces. Therefore, SEM was not used to characterise Gelucire 44/14. PXRD profile illustrated in Figure 3.39 for Gelucire 44/14 showed two main diffraction peaks, indicating the presence of crystalline material. Figure 3.40 shows ATR-FTIR spectrum of Gelucire 44/14, wherein recognizable peaks were assigned as: hydroxyl stretching around  $3479\text{ cm}^{-1}$  from free PEG 1500 found in its structure,  $2885\text{ cm}^{-1}$  due to alkyl group C-H stretching, carbonyl stretching around  $1729\text{ cm}^{-1}$  from ester groups and peaks around  $1145$ ,  $1107$  and  $1058\text{ cm}^{-1}$  from C-O stretching, which are related to either primary or secondary alcohol groups as suggested by Siripuram et al. (2010).



**Figure 3.39: PXRD diffractogram of Gelucire 44/14**



**Figure 3.40: ATR-FTIR spectrum of Gelucire 44/14**

### 3.4 Conclusions

The aim of the work described in this chapter was to characterise the behaviour of the materials prior actual processing *via* HME. This could explain two objectives, one for optimisation the temperature of extrusion as main experimental condition through understanding of the thermal properties of these materials. The second objective represents an attempt to construct a small library of the main physical features of these materials that could be used as fingerprints to separate superimposed data obtained in the future, from characterisation of their blends of more than one component. This objective was covered under sections of morphological and spectroscopic properties for the model drug i.e. ibuprofen and carrier excipients. SEM, PXRD and ATR-FTIR appeared as suitable techniques to supplement the characteristics of these materials with one exception for Gelucire 44/14. This lipid with its waxy nature, low melting point was not suitable for examination under SEM due to sample damage from generated heat during the test.

On the other hand, TGA and DSC techniques were essential to understand decomposition and major thermal transition(s), respectively, of the studied samples. This was detailed under sections of thermoanalytical investigations. With regard to the DSC experiments, MTDSC permits the separation of overlapping phenomena and allowed greater detection of thermal events using developed method of  $\pm 0.265^{\circ}\text{C}$  amplitude with a period of 100 seconds and underlying heating rate of  $1^{\circ}\text{C min}^{-1}$ . As shown in Table 3.1, the temperatures below which these materials were thermally stable are high enough to perform extrusion above characterised Tg or Tm of these materials. It was recommended therefore that temperature of extrusion for these mixes to be selected far below the decomposition temperature of the component with the lowest thermal stability. This temperature could be suggested between 10-20 $^{\circ}\text{C}$  below the degradation onset. In this range of extrusion temperature, it would be still higher than glass transition temperature (Tg) or melting temperature (Tm) of the used constituents, ensuring proper mixing of the liquefied or melted components, respectively. Moreover, unpredicted thermal degradation due to rise of the set extruder temperature due to generated heat from the extruder screws' friction would be minimized. In addition, less energy would be wasted. For mixes contain ibuprofen, the required processing temperature could be set lower than decomposition temperature of the suggested range and a bit lower than glass transition temperature or melting point of the used components, because of ibuprofen ability to act as a plasticizer (Kidokoro et al., 2001; Siepmann et al., 2006).

Tested material	Estimated thermal stability range ( $^{\circ}\text{C}$ )	Estimated melting point temperature ( $T_{m(\text{onset})}$ , $^{\circ}\text{C}$ )	Estimated glass transition temperature (Mid-point Tg, $^{\circ}\text{C}$ )
Ibuprofen	<140	75.7 $\pm$ 0.2	-43.4 $\pm$ 0.2
Eudragit RS PO	<170	-	53.3 $\pm$ 0.5
Sucrose	<187	175.2 $\pm$ 1.8	-
Methyl cellulose	<200	-	103.0 $\pm$ 0.1
Xantural®75	<235	-	37.7 $\pm$ 2.6
Pluronic® F127	<163	54.2 $\pm$ 1.2	-63.5 $\pm$ 0.7
Gelucire 44/14	<150	32.1 $\pm$ 1.4*	-

**Table 3.1: Summary of the thermal properties of the raw materials (as received) intended for processing *via* HME, as estimated from the used TGA and MTDSC techniques. \*: corresponds to the onset of the leading endothermic peak (see section 3.3.2.6.1)**

**Chapter 4: Formulation development and physicochemical characterisation of hot melt extruded ibuprofen-Eudragit RS PO films for transdermal delivery**

## 4.1 Introduction

The previous chapter detailed characterisation of the constituent materials that were used throughout this study in the hot melt extrusion. This is of immense practical importance as the way in which pharmaceutical formulations act depends mainly upon the physicochemical properties of the components used. However, in order to have a better understanding of the formulation performance, it is essential to characterise the formulation as a whole. In this context attention was placed on providing comprehensive characterisation of hot melt extruded formulation of ibuprofen in Eudragit RS PO using a multi-disciplinary approach combining DSC, PXRD, SEM and ATR-FTIR techniques.

This chapter is divided into four sections dealing with three objectives. The first objective is subdivided into finding suitable parameters to embed ibuprofen in Eudragit RS PO using HME and then examination of the drug solubility in this polymer. HME was selected as being an attractive approach for production of films intended for transdermal delivery, mainly due to avoidance of the use of organic solvents as detailed in Chapter 1. Thus, in a first step section 4.3.1 examines suitability of the selected extrusion temperature on thermal stability of ibuprofen-Eudragit RS PO blends. This is followed by section 4.3.2 which discusses theoretical and experimental approaches to predict miscibility between Eudragit RS PO and ibuprofen and how they correlate with the hot melt extrusion process. This is essential, as characterisation of drug solubility within a transdermal drug delivery system (TDDS) is one of the key parameters to understand and predict its performance, since flux is a function of solubility equilibrium (Ahmad et al., 2004). The second objective is to approximate equilibrium saturation solubility of the drug in the Eudragit RS PO extruded formulations *via* monitoring the phase separation in real time at high and low relative humidities as will be detailed in section 4.3.3. While assessment of the saturation concentration is non-trivial, there is uncertainty regarding how the solubility in a matrix alters on exposure to moisture. Indeed, while care may be taken to prevent product exposure to moisture during storage, this will not preclude sorption when that product is applied to the skin. Therefore, it is of interest to assess the saturation solubility of the TDDS in the dry state and in presence of moisture, thereby providing a better prediction of performance *in situ*. The third objective is to elucidate the tendency of ibuprofen-Eudragit RS PO extruded formulations for physical ageing through fragility assessment as will be discussed in section 4.3.4. This can be taken into account when stabilization strategies are designed for the final product to ensure consistency of the mechanical properties and/or performance which could be affected by drug recrystallization.

## **4.2 Methodology**

### **4.2.1 Preparation of physical mixtures**

Physical mixes of ibuprofen and Eudragit RS PO were prepared for at least two major purposes. One of the purposes is to compare with the respective hot melt extruded systems, where known amounts of crystalline ibuprofen were physically mixed with Eudragit RS PO using pestle and mortar. This method was also used to prepare these blends for hot melt extrusion. A second purpose was estimation of the miscibility between ibuprofen and Eudragit RS PO using melting point depression approach. In this study, the physical mixtures of Eudragit RS PO containing 1%-90% by weight of ibuprofen were prepared and weighed (10 mg) in aluminium standard DSC pans. These pans were placed in desiccators containing phosphorous pentoxide at room temperature (~25°C) for one day to dry them and then taken out and crimped with aluminium lids for analysis.

### **4.2.2 Preparation of hot melt extruded ibuprofen in Eudragit RS PO**

Hot melt extrusion process has a number of parameters to be optimized to allow proper melt embedding of the drug in polymeric carrier(s) as described in Chapter 1. The method used ultimately in this work was based mainly on selecting extrusion temperature which allows rotation of the screws with acceptable torque values. Torque values were considered acceptable when a homogenous extrudate is obtained with the minimal possible residence time of extrusion at the selected mixing speed. More importantly, the temperature was chosen below degradation temperatures of ibuprofen and Eudragit RS PO, which were determined using TGA in Chapter 2. The temperature was also selected from the recommended temperature range of performing extrusion as reviewed by Crowley et al. (2007), wherein a temperature of 15-60°C above the melting or the glass transition temperature is usually set to achieve proper mixing. Therefore, physical mixes of ibuprofen-Eudragit RS PO were compounded in a co-rotating twin screw extruder (Haake Minilab II Micro Compounder) using a temperature of 100°C from the feed to the die end and a screw speed of 100 rpm for four minutes. The resulted extrudates were prepared at different drug loadings until opaque extrudate was produced. Therefore, a concentration range of 1-40% (w/w) of ibuprofen was used. These extrudates were collected and cooled along a customised conveyer belt and kept in polyethylene bags for further evaluation.



### 4.2.3 General methods

A wide variety of techniques were used in this chapter to perform characterisation of the physical mixes with corresponding extruded systems of ibuprofen in Eudragit RS PO. TGA was used to estimate thermal stability as a function of weight loss of ibuprofen-Eudragit RS PO physical mixes. For this purpose, isothermal heating mode of a TA Instruments TGA Q5000 IR was employed to obtain the thermogravimetric analysis curves. Samples (10-12 mg) were held at 100°C for four minutes and the percentage weight loss was recorded. The samples were heated at a rate of 100°C/min to reach the desired isothermal temperature. This technique was also used to determine water content of the extruded samples during the storage study (60%RH/25°C). The stored samples (~10 mg) were taken out from humidity chambers and were heated at 10°C/min from 30°C to 250°C. All TGA runs were performed in open aluminium pans with a dry nitrogen gas purged at flow rates of 25 ml min<sup>-1</sup> and 10 ml min<sup>-1</sup> through the furnace and TGA head, respectively.

Conventional DSC and MTDSC measurements were carried out using TA Instrument DSC Q1000, equipped with a refrigerated cooling system (RCS) and calibration was performed prior each analysis as detailed in Chapter 2. Data were treated mathematically using TA Universal Analysis 2000 software and nitrogen was used as the purge gas through the DSC cell at a flow rate of 50 ml/min. TA instruments standard pans were used for all calorimetric studies and the mass of each empty sample pan was matched to the mass of the empty reference pan within ±0.05 mg and all measurements were performed in triplicate. In the MTDSC experiments, the method developed in Chapter 3 was employed. Using amplitude of ±0.265 °C, period of 100 seconds and underlying heating rate of 1°C/min, samples were subjected to two steps in this method. The first step was equilibration at -70°C, isothermal heating for 5 minutes followed by a second step of heating to 100°C. The standard mode of this method (without modulation) was applied to estimate miscibility between Eudragit RS PO and ibuprofen using melting point depression approach. Thus, samples of their physical mixtures of approximately 10 mg at different ibuprofen loadings were prepared as described in section 4.2.1 and examined accordingly. The slow heating rate in this method (1°C min<sup>-1</sup>) is believed to provide enough time for mixing through the timescale of the experiment, therefore to provide good approximation to the efficient mixing provided in hot melt extrusion technology. However, the MTDSC of this method was used to study thermal transition of the extruded samples throughout this study and the detected glass transition temperatures were in all cases taken at the midpoint of the transitions from the reversing heat flow signals. All measurements were performed in triplicate.

Standard (conventional) DSC was also used to estimate fragility of the fresh extruded samples using a protocol of cooling at various rates, followed by heating at a constant rate through the glass transition region of these samples. Therefore, fresh extruded samples (4.00-6.00 mg) of Eudragit RS PO loaded with ibuprofen 10-30% (w/w) were subjected to three steps using 10°C/min as the reheating rate and on the range which covers glass transition temperature region for the tested extrudates, determined previously using MTDSC. The first step was equilibration at 70°C, isothermal heating for 5 minutes and then a second step of cooling to -20°C at different rates for each cycle: 2, 5, 10 and 20 °C/min. In each individual cooling rate experiment, isothermal condition was maintained for 5 minutes at -20°C. The third step involved reheating to 70°C (10°C/min). cDSC was also used to amorphize crystalline ibuprofen by a quench from its melt, as one of the most widely used strategy to produce amorphous material. Therefore, crystalline ibuprofen in open standard aluminium pan was heated at 10°C/min to 100°C, then cycled rapidly to -70°C at 20°C/min followed by heating at 10°C/min to 100°C.

Attenuated total reflectance-Fourier-transform infrared (ATR-FTIR) spectrometry (Bruker IFS 66/S, Bruker optics equipped with a Golden Gate ATR accessory from Specac Limited) was used to investigate the molecular interactions between ibuprofen in Eudragit RS PO in the extruded formulations. Therefore spectra of the physical mixes of these components were compared to the corresponding extruded systems over a range of 4000-550 cm<sup>-1</sup>, 32 scans at a resolution of 4 cm<sup>-1</sup>. Furthermore, this method was utilized to confirm recrystallization of ibuprofen in the extruded samples, qualitatively. Omnic software (version 6.1a) was used to analyze results and perform comparison.

Using methods documented in Chapter 3, qualitative PXRD was used to detect crystalline ibuprofen in the extruded samples as compared to the respective physical mixes, whereas SEM was used to visualise crystalline ibuprofen of the extruded samples and thus detecting any sign of phase separation on that basis. For that purpose, morphological features of the surface and cross sections of the extruded formulations were examined. Storage studies of extruded ibuprofen-Eudragit RS PO films with drug loadings of 1-40% (w/w) were performed under different humidity levels for one month. The extruded films were stored at 0%RH and 60%RH, both at room temperature (24±1°C). Airtight jars were used as humidity chambers with phosphorus pentoxide to achieve dryness (0%RH), and saturated salt solutions of sodium bromide in distilled water to control relative humidity to a level of ~60%RH at room temperature (O'Brien, 1948). These chambers were prepared two days before sample storage to enable equilibrium to be achieved. Humidity strips were incubated

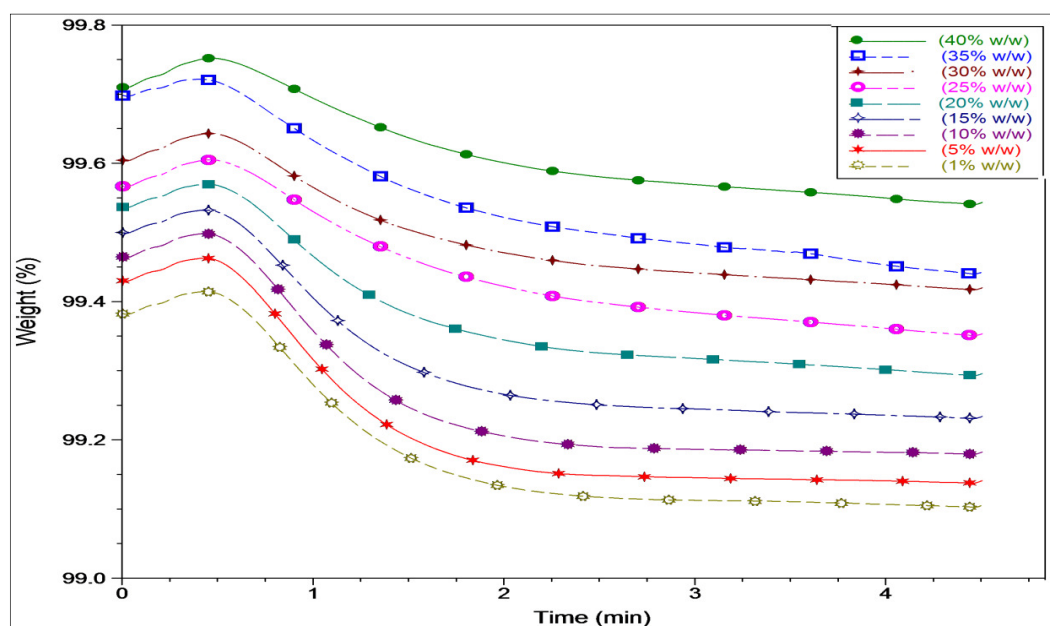
in these chambers to check the relative humidity values. All weighing in this work was performed using XS205, Dual range analytical balance (Mettler Toledo).

### **4.3 Results and discussion**

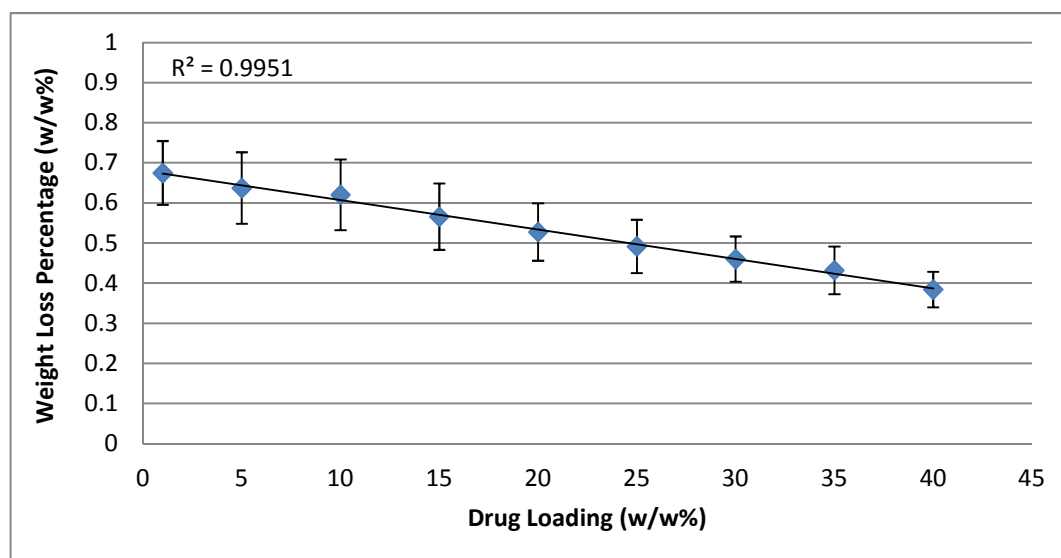
#### **4.3.1 Investigation into thermal stability of the ibuprofen-Eudragit RS PO physical mixes for processing *via* hot melt extrusion**

Temperature used for hot melt extrusion is important processing parameter, which is selected and optimized on the basis of uniform extrudate formation and avoiding thermal decomposition. The first condition was met using 100°C during extrusion of ibuprofen-Eudragit RS PO blends with acceptable torque values, which will be discussed in the following section. The second condition; however, can be evaluated through addressing of the thermal degradation of these materials. Thermal degradation of the ibuprofen and Eudragit RS PO was detailed in Chapter 3 using TGA and showed that these materials would be stable at relatively high temperature as 100°C. However, in this study the isothermal mode of thermogravimetric analysis was used to gain insight into thermal stability of the used ibuprofen-Eudragit RS PO blends with respect to HME processing temperature and time. Therefore, these blends were held at 100°C for the selected dwelling time inside the extruder (4 minutes), with the objective of mimicking the used hot melt extrusion conditions.

Figure 4.1 and Figure 4.2 show the comparative TGA results as a function of drug loading of the examined ibuprofen-Eudragit RS PO physical mixes. It was noted that weight loss is increased with increasing Eudragit RS PO content in these mixes. This is likely to be due to moisture desorption from this polymer as shown previously in Chapter 3. However, the relative thermal stability after four minutes of heating at 100°C for all these mixes can be considered acceptable, due to insignificant observed weight losses (less than 1% (w/w)) at all the studied drug loadings. This supports the use of these parameters during extrusion of ibuprofen and Eudragit RS PO with minimal concerns of thermal instability.



**Figure 4.1:** TGA weight loss profiles of ibuprofen-Eudragit RS PO physical mixes at different drug loadings (w/w %)



**Figure 4.2:** Total weight loss percentages of ibuprofen-Eudragit RS PO physical mixes with different drug loadings (w/w %) measured at 100°C for four minutes using TGA

### 4.3.2 Assessment of the miscibility and compatibility of ibuprofen-Eudragit RS PO hot melt extruded systems

Miscibility behaviour of the drug with the polymer and possible solubility in solid dispersions can be estimated using solubility parameters, which are directly related to the cohesive energy density of a molecule (Greenhalgh et al., 1999). The solubility parameters of the ibuprofen and Eudragit RS PO were correlated with the Hansen (partial) solubility parameter model. This model was proposed to approximate total cohesive energy density (Savova et al., 2007) and can be utilized to predict the compatibility of pharmaceutical materials (Mohammad et al., 2011). In this model, the total energy is divided into individual components, namely, dispersion, polar and hydrogen bonding. On the basis that “like dissolves like”, the similarity of the relative strengths of these forces that present in the studied materials relates to possible good solubility (Stefanis and Panayiotou, 2008). This can be estimated through calculation of the total solubility parameter ( $\delta_t$ ) as follows (Hansen, 1967):

$$\delta_t = (\delta_d^2 + \delta_p^2 + \delta_h^2)^{0.5} \quad (\text{Eq.4.1})$$

where  $\delta_d$  is the dispersion Hansen solubility parameter,  $\delta_p$  is the polar Hansen solubility parameter and  $\delta_h$  is the hydrogen-bonding Hansen parameter solubility parameter. Using group contributions of the structural groups of the studied materials as complied with Krevelen and Hoftyzer (1976), these solubility parameters can be predicted as follows:

$$\delta_d = \frac{\sum F_{di}}{V} \quad (\text{Eq.4.2})$$

$$\delta_p = \frac{\sqrt{\sum F_{pi}^2}}{V} \quad (\text{Eq.4.3})$$

$$\delta_h = \sqrt{\frac{\sum E_{hi}}{V}} \quad (\text{Eq.4.4})$$

where (i) is the structural group within the molecule, ( $F_{di}$ ) is the group contribution to the dispersion forces, ( $F_{pi}$ ) is the group contribution to the polar forces, ( $E_{hi}$ ) is the group contribution to the hydrogen bonding energy, and (V) is the molar volume.

Accordingly the overall value of solubility parameters ( $\delta_t$ ) for ibuprofen and Eudragit RS PO were calculated based on the group contributions of their structural components, which were depicted in Chapter 2. These values were found equal to 19.26 and 17.45 ( $\text{J}/\text{cm}^3$ )<sup>1/2</sup> for ibuprofen and Eudragit RS PO polymer, respectively. Therefore a good miscibility between these two components is predicted as difference less than  $\pm 6.3$  ( $\text{J}/\text{cm}^3$ )<sup>1/2</sup> indicates good miscibility (Sears and Touchette, 1982). An example of the solubility parameter calculation is provided in Table 4.1.

(A)			
Structural group	Fdi ( $\text{J}^{1/2}.\text{cm}^{3/2}.\text{mol}^{-1}$ )	Fpi ( $\text{J}^{1/2}.\text{cm}^{3/2}.\text{mol}^{-1}$ )	Ehi ( $\text{J}/\text{mol}$ )
3(CH <sub>3</sub> )	1260	0	0
1(CH <sub>2</sub> )	270	0	0
2(CH)	160	0	0
1(COOH)	530	420	10000
1Phenylene	1270	110	0

(B)			
Equation (4.2)	$\delta_d$ ( $\text{J}^{1/2}.\text{cm}^{3/2}$ )	$\delta_p$ ( $\text{J}^{1/2}.\text{cm}^{3/2}$ )	$\delta_h$ ( $\text{J}^{1/2}.\text{cm}^{3/2}$ )
	17.76	2.21	7.13
Equation (4.1) $\delta_t = 19.26 \text{ J}^{1/2}.\text{cm}^{3/2}$			

**Table 4.1: Example of the solubility parameter calculation ( $\delta_t$ ) using component group contributions of ibuprofen (A) (Krevelen and Hoftyzer, 1976) according to Equations 4.1 to 4.2 (B)**

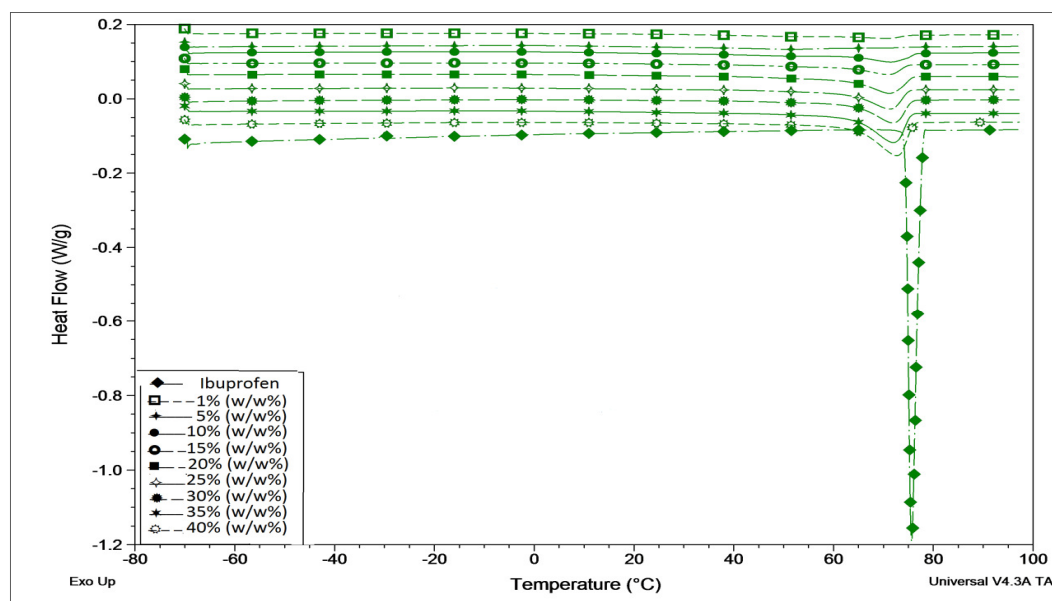
In recent years, a melting point depression thermodynamic model has also been demonstrated as a feasible approach to predict miscibility of pharmaceutical materials (Djuris et al., 2013; Marsac et al., 2006; Papageorgiou et al., 2011; Yang et al., 2013). Marsac et al., (2006) suggested application of the Flory-Huggins theory to estimate drug-polymer miscibility through determination of the interaction parameter “ $\chi$ ”. In this work, “ $\chi$ ” was determined experimentally from melting point depression data using DSC and the following equation:

$$(1/T_M^{\text{mix}}) - (1/T_M^{\text{pure}}) = (-R/\Delta H_{\text{fus}}) [\ln \Phi_{\text{drug}} + (1 - 1/m) \Phi_{\text{polymer}} + \chi \Phi_{\text{polymer}}^2] \quad (\text{Eq.4.5})$$

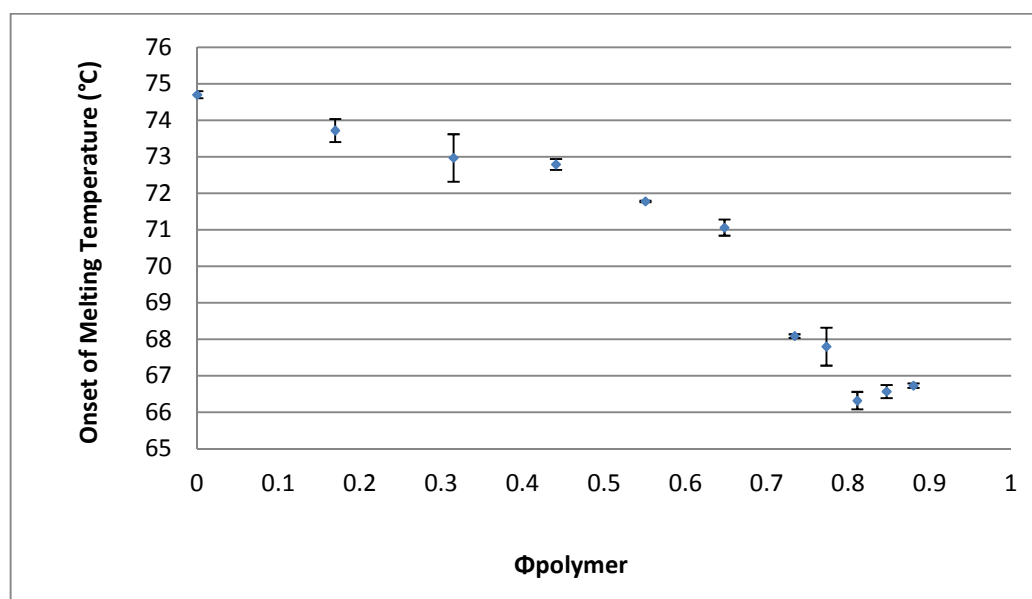
where  $T_M^{\text{mix}}$  is the melting temperature of the drug in the presence of the polymer,  $T_M^{\text{pure}}$  is the melting temperature of the drug in the absence of the polymer,  $\Delta H_{\text{fus}}$  is the heat of fusion of the pure drug, and  $m$  is the ratio of the volume of the polymer to that of the lattice site (defined here by the volume of the drug),  $\Phi_{\text{drug}}$  is the volume fraction of the drug,  $\Phi_{\text{polymer}}$  is the volume fraction of the polymer,  $\chi$  is the Flory-Huggins interaction parameter and  $R$  is the universal gas constant. This equation provides an estimate of the interaction parameter at temperatures close to the melting point of the drug and requires that there is enough physical interaction between the drug and the polymer for melting point depression to be manifested, in addition to thermal stability over the temperature range of interest.

The melting point depression of crystalline ibuprofen blended with amorphous Eudragit RS PO was observed with increasing the volume fraction of this polymer as shown in Figure 4.3 (A) and (B). The temperature reduction is predicted to be caused by the decrease of the chemical potential of the drug by the addition of a miscible diluent (Papageorgiou et al., 2011). The occurrence of the melting point depression of the ibuprofen can be explained by the ease of possible interaction or mixing between the molten drug and the polymer at the used temperature (100°C). This temperature is higher than the melting point of ibuprofen (74.7°C as the extrapolated onset value and 76.4°C “offset value”, Chapter 3) and glass transition temperature of Eudragit RS PO (53.3±0.5°C, Mid-point T<sub>g</sub>, Chapter 3), thus molten drug is believed to equilibrate with the “liquid-like” polymer, wherein the melting point depression is kinetically favourable to be manifested.

(A)



(B)



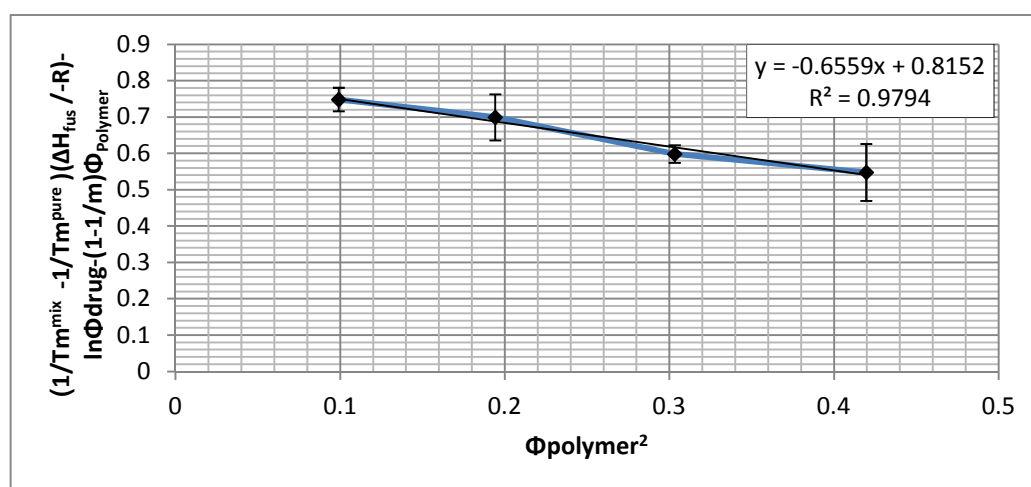
**Figure 4.3:** Exemplary DSC thermograms (heating rate of  $1^{\circ}\text{C min}^{-1}$ ) of ibuprofen-Eudragit RS PO physical mixtures compared to the pure ibuprofen (A). Extrapolated onset of melting of ibuprofen as a function of volume fraction of Eudragit RS PO (Each data point represents the mean $\pm$ S.D. of three measurements), measured at a scan rate of  $1^{\circ}\text{C min}^{-1}$  (B)



The resultant equilibrium melting temperatures can be then analyzed using Equation (4.5) and plotted as shown in Figure 4.4 to estimate Flory-Huggins interaction parameter “ $\chi$ ”. The value of this parameter can be derived from the slope of this plot and was (-0.6559). This negative value predicts miscibility (Marsac et al., 2006) based on the data from the volume fraction of the polymer that yielded linear relationship ( $R^2$  value of 0.9794 was obtained). Furthermore, this interaction parameter was used to estimate the drug miscibility limit based on the following equation:

$$\ln \gamma_{\text{drug}} = \ln (\Phi_{\text{drug}}/x_{\text{drug}}) + (1-(1/m)) \Phi_{\text{Polymer}} + \chi \Phi_{\text{Polymer}}^2 \quad (\text{Eq.4.6})$$

where  $\gamma_{\text{(drug)}}$  is the activity coefficient of the drug in the polymer at solubility limits,  $m$  is the ratio of the volume of the material to the lattice site,  $x$  is the drug solubility mole fraction,  $\chi$  is the Flory-Huggins interaction parameter and  $\Phi$  is the volume fraction of the material as modelled by Marsac et al. (2006). With the assumption that the activity coefficient is the same at the solubility limit of the drug in the polymer (Marsac et al., 2009), the solubility limit of ibuprofen in Eudragit RS PO was calculated and was found to be around 47% (w/w).



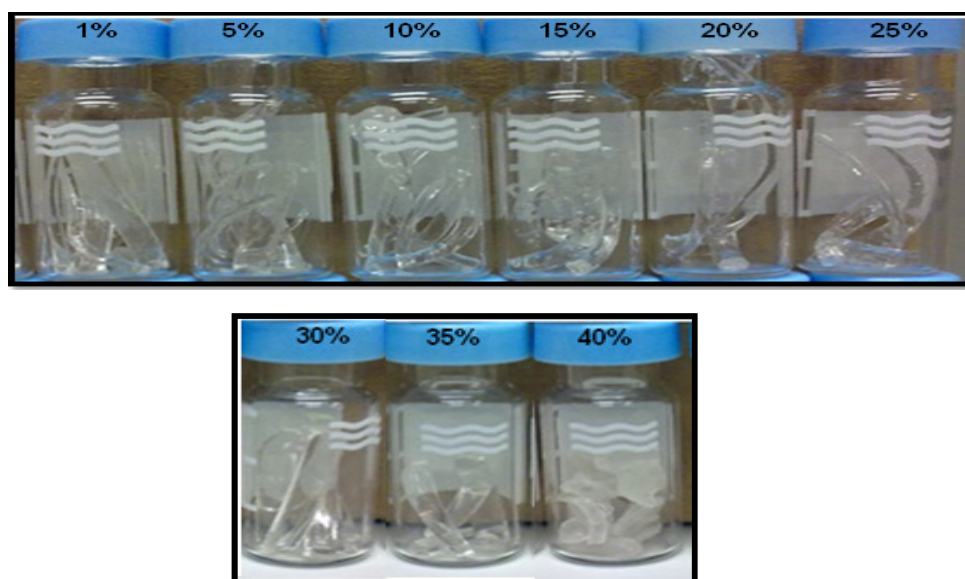
**Figure 4.4: Estimation of Flory-Huggins interaction parameter between ibuprofen and Eudragit RS PO based on Eq. (4.5). Each data point represents the mean $\pm$ S.D. of three measurements**

The aforementioned calculations involved using the density of the ibuprofen, which equals 1.05g/cm<sup>3</sup> (Marsac et al., 2009; Sun, 2004), the mean density of the Eudragit RS PO, which was estimated experimentally and found to be approximately equal to 0.57 g/cm<sup>3</sup> (determination of bulk density was carried out in compliance with ICH Guidelines Q4B,

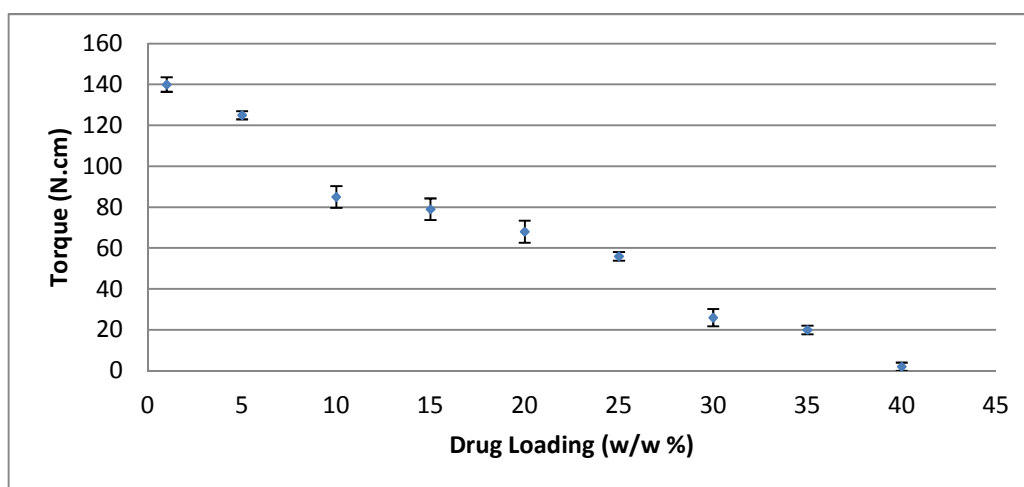
Annex 13, EMA/CHMP/ICH/405290/2010), the molecular weight of ibuprofen, which equals 206.28 g/mol and molecular weight of Eudragit RS PO (assuming 100 repeat units in the polymer; Evonik, n.d.), which equals 35000 g/mol.

At this point, solubility parameter calculations (theoretical approach) and interaction parameter (experimental approach) indicated good miscibility between ibuprofen and Eudragit RS PO. The latter approach predicted ibuprofen miscibility up to a certain limit in Eudragit RS PO (~47% w/w). The question therefore arises as to how does this agree with the solubility or dispersibility of the hot melt extruded ibuprofen in Eudragit RS PO, and what types of molecular interactions, if any, exist between these two components.

To address these issues, the hot melt extruded systems of ibuprofen in Eudragit RS PO were prepared and characterised using MTDSC, PXRD, SEM and ATR-FTIR techniques. For the hot melt extrusion process, the aforementioned parameters in section 4.2 were suitable to produce translucent hot melt extrudates of Eudragit RS PO containing 1-35% by weight of ibuprofen. However at 40% (w/w) drug loading the opacity was higher compared to other extrudates as shown in Figure 4.5. It was also observed that torque values inside the extruder were decreased gradually as a function of increased drug loading as illustrated in Figure 4.6. This parameter is directly proportional to the viscosity of the molten material. This implies that ibuprofen decreased the melt viscosity and could be explained by the ability of this drug to work as a plasticizer (Kidokoro et al., 2001; Siepmann et al., 2006), facilitating the movement of the mixture inside the extruder towards the die system.



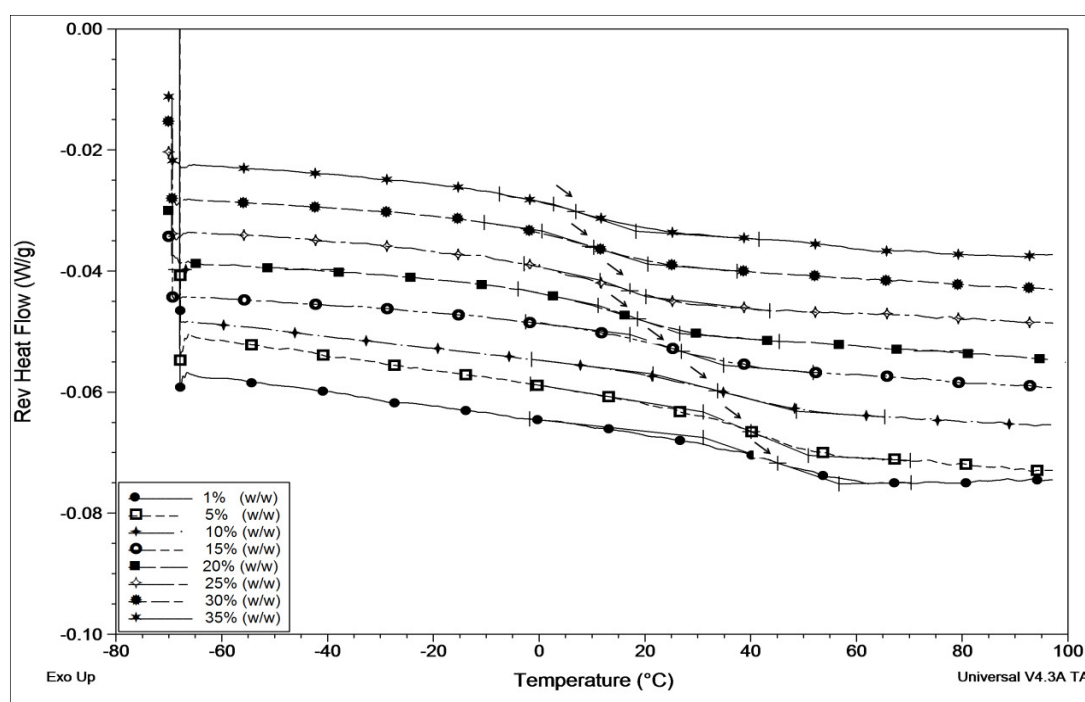
**Figure 4.5:** Photographs of freshly prepared hot melt extruded ibuprofen in Eudragit RS PO produced at different drug loadings between 1-40 % (w/w)



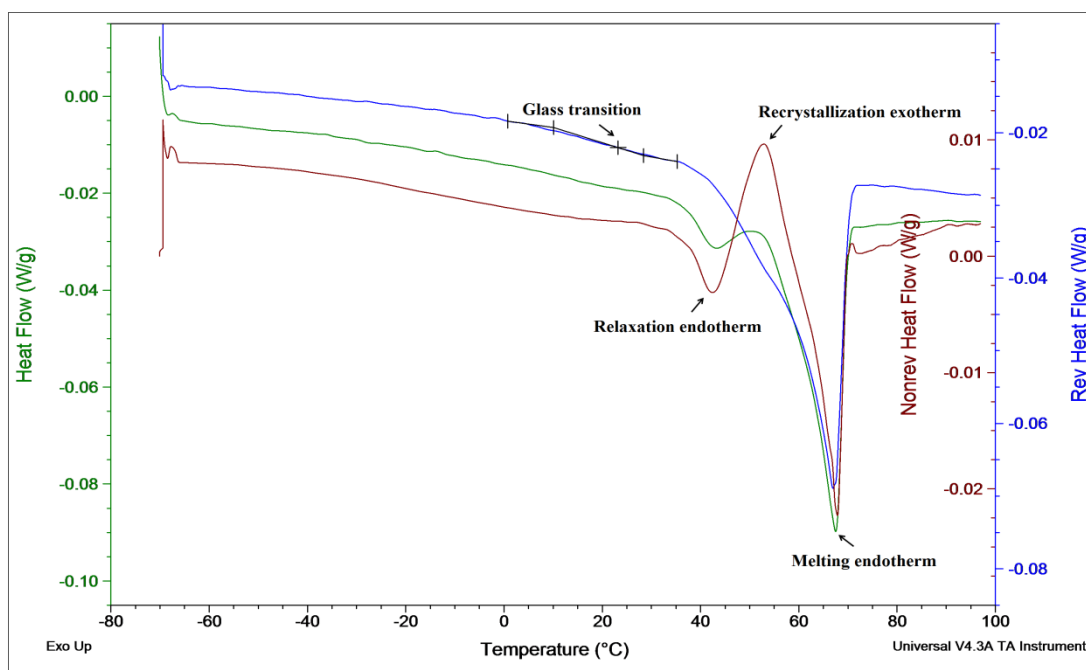
**Figure 4.6:** Variation of the observed torque values during hot melt extrusion as a function of changing ibuprofen loadings (w/w %) in Eudragit RS PO. Each data point represents the mean $\pm$ S.D. of three observations

These extrudates were characterised by single glass transition temperatures over a concentration range of 1-35 % (w/w) drug loading as indicated in the MTDSC measurements shown in Figure 4.7. In this figure, the reversing heat flow signals were used to help in the correct assignment of the glass transitions of these extrudates, as detailed in Chapter 2. The presence of single glass transition temperature implies single phase system,

which refers as to solid solution system with the drug molecularly dispersed in the interstitial spaces between the amorphous polymer chains (Crowley et al., 2007). Moreover, the glass transition temperature of these extruded systems decreased with increasing drug loading as indicated in the shift of the arrows in Figure 4.7. This clearly shows that the ibuprofen is acting as efficient plasticizer for Eudragit RS PO. In contrast to these systems, hot melt extruded systems at 40 % (w/w) drug loading showed a broad melting endotherm in the MTDSC measurements (Figure 4.8), thereby a binary-phase system was formed or solid dispersion. This system is characterised with a glass transition temperature at  $23.2 \pm 1.9^\circ\text{C}$  ( $n=3$ , Mid-point  $T_g$ ), representing the amorphous phase. In addition, this system showed an endothermic peak related to the melting of the surplus ibuprofen with a depressed extrapolated onset melting temperature of  $57.4 \pm 0.5^\circ\text{C}$  ( $n=3$ ), which represents the crystalline phase.



**Figure 4.7:** MTDSC reversing heat flow signals of ibuprofen-Eudragit RS PO extrudates with different drug loadings (w/w%) in standard aluminium pans. Underlying scan rate of  $1^\circ\text{C min}^{-1}$  with a modulation amplitude of  $\pm 0.265^\circ\text{C}$  and a period of 100 seconds. Arrows indicate the assigned Mid-point glass transition temperatures



**Figure 4.8: MTDSC heating scan of hot melt extruded 40% (w/w) ibuprofen in Eudragit RS PO in standard aluminium pans. Underlying scan rate of  $1^{\circ}\text{C min}^{-1}$  with a modulation amplitude of  $\pm 0.265^{\circ}\text{C}$  and a period of 100 seconds**

The compositional variation of the glass transition temperature of the previously described extruded systems of ibuprofen and Eudragit RS PO was further studied using Gordon-Taylor (G-T) equation. This equation is used most often in the amorphous pharmaceutical materials due to its simplicity and reliability (Zografis and Hancock, 1997). Assuming ideal behaviour of no specific interactions and perfect volume additivity during mixing of the studied mixtures, this equation can be used to predict glass transition temperature of these mixes with small positive or negative deviations. These deviations might indicate drug-polymer interaction as reviewed by Qian et al. (2010).

To start with the first implication of this equation, it can be represented as follows (Gordon and Taylor, 1952):

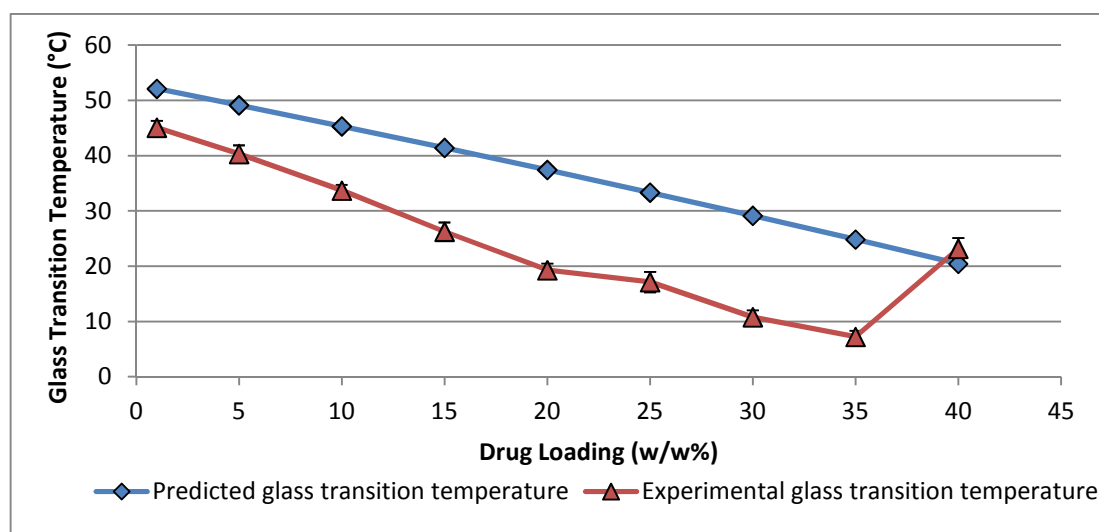
$$T_{g_{\text{mix}}} = (T_{g_1}w_1 + T_{g_2}w_2K) / (w_1 + Kw_2) \quad (\text{Eq.4.7})$$

where  $T_{g_1}$  and  $T_{g_2}$  are the glass transition temperatures of components 1 and 2, respectively, whereby  $T_{g_{\text{mix}}}$  is the predicted glass transition temperature of their mixture,  $w_1$  and  $w_2$  are

the weight fractions of component 1 and 2 in the mixture.  $K$  is a sample-specific parameter which can be estimated using the popular Simha-Boyer rule (Simha and Boyer, 1962):

$$K \cong \rho_1 T_{g1} / \rho_2 T_{g2} \quad (\text{Eq.4.8})$$

where  $\rho_1$  is the density of component 1 and  $\rho_2$  is the density of component 2. Using Equations 4.7 and 4.8, the predicted theoretical values of glass transition temperatures of the binary extruded systems of ibuprofen (component 1) and Eudragit RS PO (component 2) with varying compositions is shown in Figure 4.9. As can be seen from this Figure, the experimental data deviate negatively from the theoretical values obtained from the G-T equation up to 35% (w/w) drug concentration. This could be ascribed to the aforementioned plasticizing effect of the ibuprofen, wherein the glass transition temperature of these blends was lowered with increasing drug load. However, at 40% (w/w) ibuprofen loading, excess drug recrystallized which may limit the sliding motion of the materials in the mix and results in the observed increase of the glass transition temperature that almost meets with the predicted or theoretical value derived from G-T model.

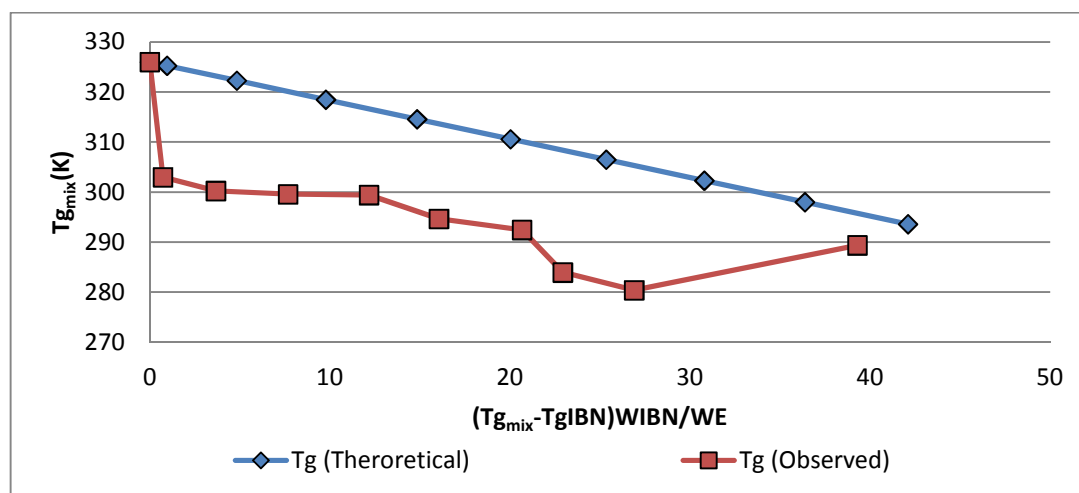


**Figure 4.9:** Theoretical glass transition temperature values predicted by G-T equation of the ibuprofen-Eudragit RS PO mixes in comparison to the experimental values obtained from reversing heat flow signals of the MTDSC measurements ( $1^\circ\text{C min}^{-1}$ ) of their equivalent hot melt extruded systems (Figure 4.7 and 4.8)

The Gordon-Taylor equation can also be used to evaluate random miscibility of the pharmaceutical binary glass systems at a segmental level (Fukuoka et al., 1989), or as a conjunction tool to the ATR-FTIR measurements to investigate possible interaction between the studied components (Fujimori et al., 2005) through the following rearrangements:

$$T_{g_{mix}} = -k [(T_{g_{mix}} - T_2) w_2 / w_1] + T_1 \quad (\text{Eq.4.9})$$

where subscripts 1 and 2 denote components 1 and 2, respectively,  $w_1$  and  $w_2$  are the weight fractions of component 1 and 2.  $T_1$  and  $T_2$  are the  $T_g$  values of components 1 and 2, and  $k$  is a coefficient defined by  $k = \Delta\beta_1 / \Delta\beta_2$ , where  $\Delta\beta$  expresses the difference of the expansion coefficient below and above  $T_g$ . Considering component 1 as Eudragit RS PO (E) and component 2 as ibuprofen (IBU), the resulted plot of the glass transition temperatures of the ibuprofen-Eudragit RS PO systems according to Equation 4.9 is depicted in Figure 4.10. It can be observed that a linear relationship was established using the theoretical glass transition temperatures of the binary mixtures of ibuprofen and Eudragit RS PO. This complies with the assumption of the G-T equation of the “ideal” behaviour of no orienting interaction and volume additivity (Moustafine et al., 2006). However, using the experimental or observed glass transition of these mixes, a large negative deviation was observed from the “ideal” behaviour and the linearity was lost. This indicates that the randomness of the mixing between these components is less likely to occur, with a possibility to have specific interaction(s). The latter could be further explored in the coming discussion using ATR-FTIR measurements.

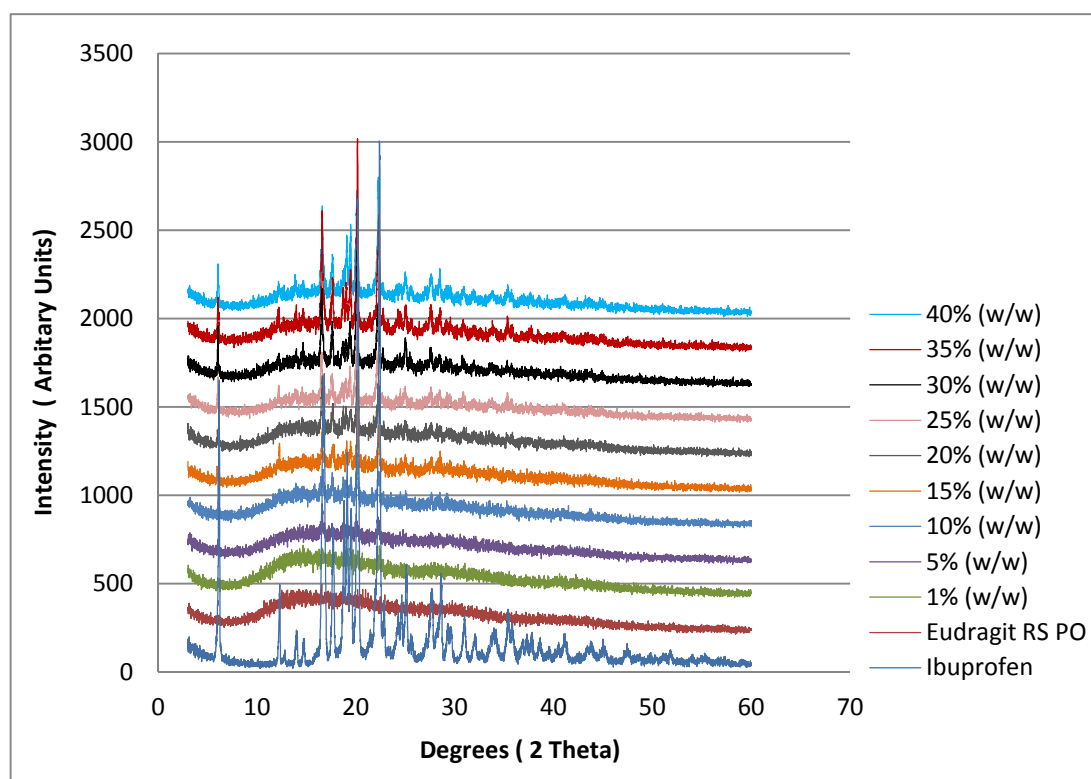


**Figure 4.10: Analysis of the ibuprofen-Eudragit RS PO system according to the G-T Equation (4.9). Theoretical glass transition temperatures of these systems ( $T_{g_{mix}}$ ) were predicted according to G-T model whereas the observed  $T_{g_{mix}}$  were obtained from reversing heat flow signals of the MTDSC measurements at 1°C/min of their equivalent hot melt extruded systems (Figure 4.7 and 4.8 )**

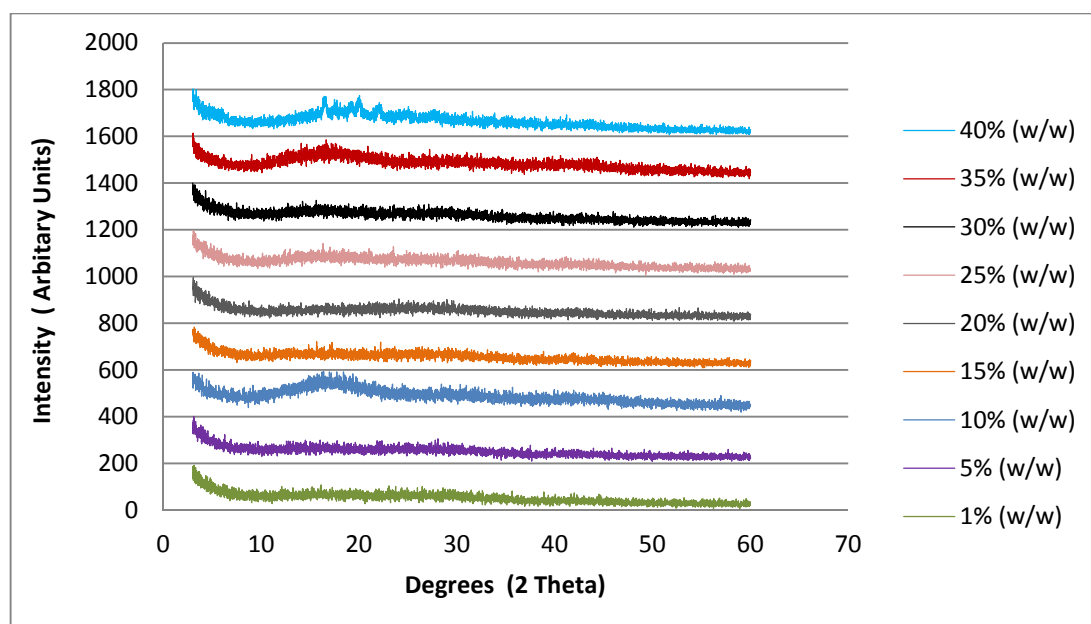
Overall, the miscibility of the hot melt extruded systems of ibuprofen in Eudragit RS PO exhibiting single glass transition temperatures up to 35% (w/w) drug loading might not be infallible indicator of the miscibility of the drug as molecular dispersion within these matrices. Thus, further characterisation using techniques like PXRD, SEM and ATR-FTIR can add more details to assess the possible one-phase solid solution formation, as will be demonstrated in this discussion. Figure 4.11 shows an overlay of the X-ray powder diffraction profiles (diffractograms) of the hot melt extruded systems of ibuprofen in Eudragit RS PO at different drug loadings in comparison to their equivalent physical mixes. The diffraction peaks appeared in the physical mixtures over the concentration range 1-35 % (w/w) of ibuprofen were absent in all diffractograms of the equivalent extrudates, which showed alternatively broad halos, indicating amorphicity of the extruded systems. However, at higher ibuprofen content of 40% (w/w), extruded system showed clear diffraction peaks related to the crystalline ibuprofen. Nevertheless, in comparison to the corresponding physical mixture, the diffractogram shows a visible decrease in the resolution of the ibuprofen characteristic peaks, suggesting a decrease in the structural uniformity and an increase in the presence of the amorphous drug in the extruded system.



(A)



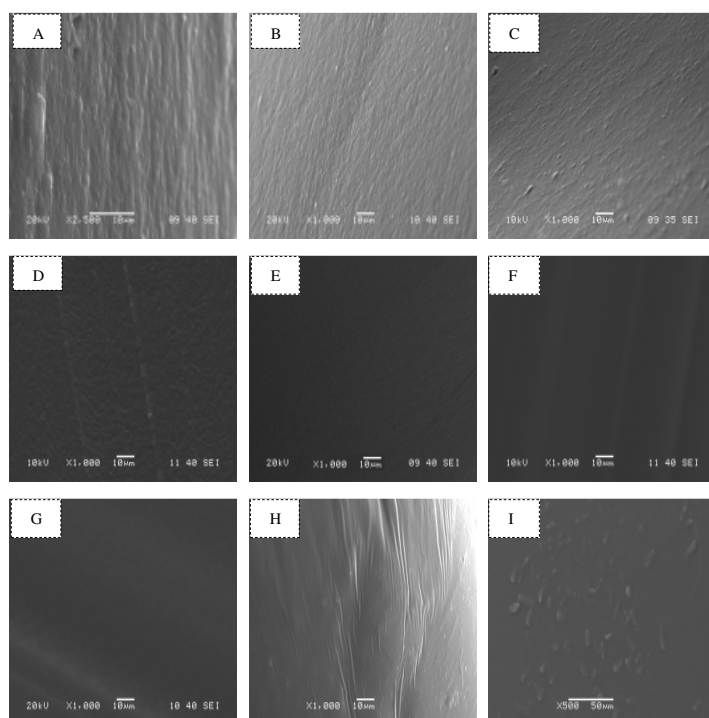
(B)



**Figure 4.11: PXRD diffractograms of ibuprofen, Eudragit RS PO, physical mixtures of ibuprofen-Eudragit RS PO systems at different drug loadings (w/w %) (A) and fresh hot melt extruded systems equivalent to the studied physical mixes (B)**

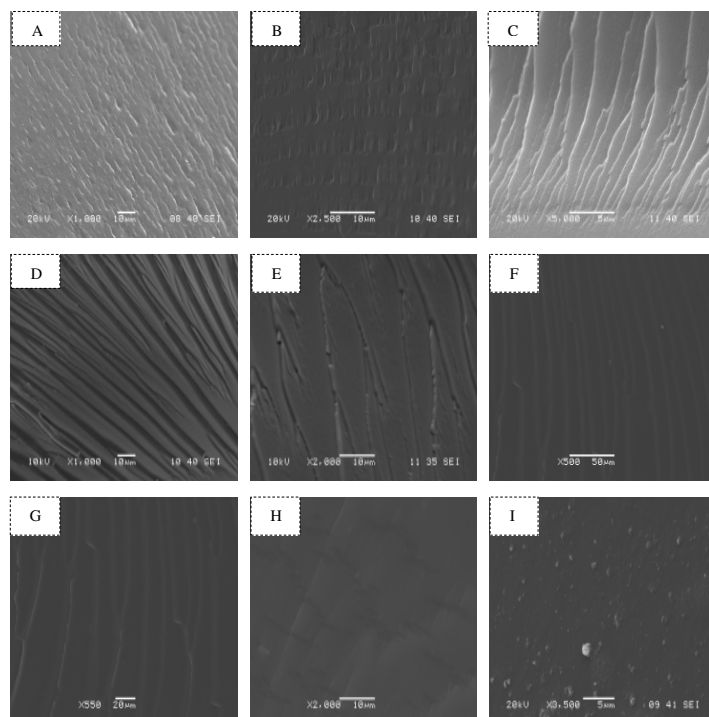
Microscopic examination using SEM of the fresh hot melt extruded systems of ibuprofen and Eudragit RS PO is shown in Figure 4.12 (I) and (II). The surfaces and cross sections of these extruded systems up to 35% (w/w) drug loading were observed with no visible drug crystals, supporting drug miscibility within the Eudragit RS PO matrices. However, ibuprofen crystals were visible on both the surface and the cross section of the extruded system at 40 % (w/w) drug loading, suggesting that ibuprofen content exceeded the drug solubility in the polymer (i.e. supersaturation). Less importantly, the effect of increasing drug loading was shown to enhance the smoothness of the examined surfaces and observed elasticity during the cut of the extruded systems for SEM examination up to 35% (w/w) drug loading, which could be ascribed to ibuprofen plasticizing effect.

(I) Surfaces



**Figure 4.12: SEM micrographs illustrating the surface morphologies of fresh hot melt extruded ibuprofen in Eudragit RS PO (I) at different drug loadings (A-F), whereby A = 1%(w/w), B = 5%(w/w), C = 10%(w/w), D = 15% (w/w), E = 20%(w/w), F = 25 % (w/w), G = 30 % (w/w), H = 35 % (w/w) and I = 40 % (w/w)**

(II) Cross sections



**Figure 4.12 (Contd.): SEM micrographs illustrating the cross sections of fresh hot melt extruded ibuprofen in Eudragit RS PO (II) at different drug loadings (A-F), whereby A = 1%(w/w), B = 5%(w/w), C = 10%(w/w), D = 15% (w/w), E = 20%(w/w), F = 25 % (w/w), G = 30 %(w/w), H =35 %(w/w) and I = 40 %(w/w)**

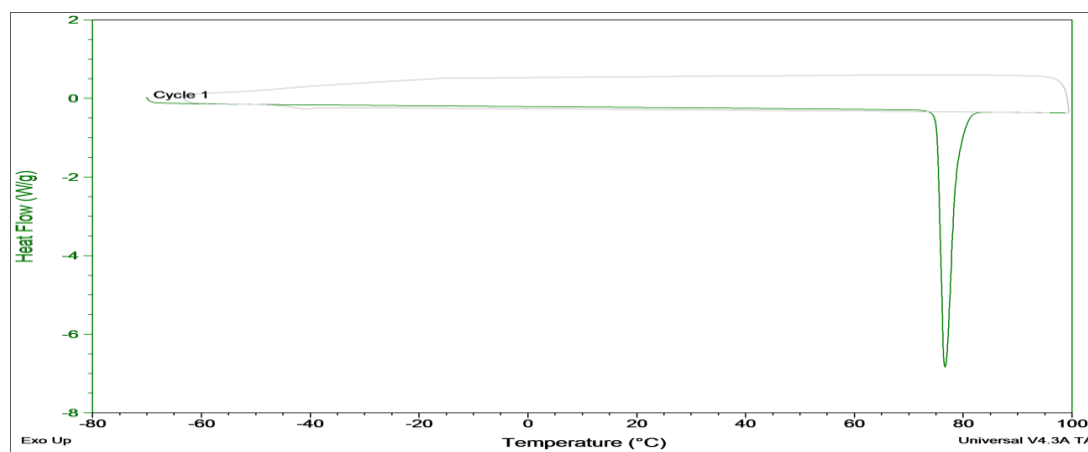
In summary, MTDSC analysis, PXRD results and SEM images revealed that a molecular dispersion as solid solution is formed in the studied hot melt extruded systems when the content of ibuprofen does not exceed 35% (w/w) in the Eudragit RS PO. These extrudates were translucent, characterised by a single glass transition temperature (which decreased with drug loading from 53.3°C to 7.2°C for 0 to 35% loaded systems) and the absence of crystalline diffraction pattern observed using PXRD, supported by SEM images which revealed clarity from visible ibuprofen crystals. On the other hand, higher content of ibuprofen at 40%(w/w) drug loaded extrudate represents the supersaturation level, characterised by a broad endothermic peak in MTDSC measurements, diffraction peaks in PXRD results related to surplus crystalline ibuprofen. Drug recrystallization was visible in the SEM images of these extrudates. In the light of these results, it could be also inferred that performed solubility parameter calculations together with the used thermodynamic model of melting point depression approach elucidated good correlation with the experimental findings of the solubility of ibuprofen in Eudragit RS PO hot melt extrudates, which might suggest their usefulness for prediction of drug-polymer miscibility prior setting-up HME

process. However, it is worth pointing out that observed overestimation of the solubility from melting point depression predictive model is likely due to estimation at higher temperatures close to the melting of the drug.

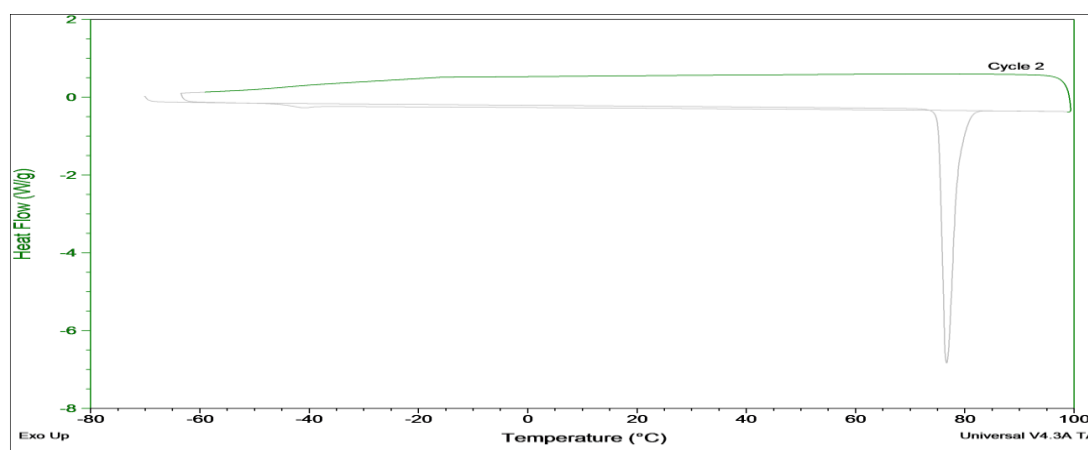
The preliminary investigation of the possible interactions between ibuprofen and Eudragit RS PO using G-T model is now evaluated using ATR-FTIR spectroscopy. Thus the nature and the extent of possible interaction(s) between ibuprofen and Eudragit RS PO at different drug loadings can be investigated. Therefore spectra of Eudragit RS PO, crystalline ibuprofen, amorphous ibuprofen, physical mixtures of them at different drug loadings in comparison to their equivalent extruded systems are shown in Figure 4.14 and Figure 4.15.

As described in the methodology (section 4.2), amorphous ibuprofen was prepared in DSC pans by quenching of its melt. As illustrated in Figure 4.13 the crystalline ibuprofen underwent melting in the first heating cycle. In the second cycle, the melt was rapidly cooled (quenched) and crystallization was avoided (absence of exothermic peak in the DSC thermogram). On subsequent heating the glass transition of ibuprofen was clearly seen in the third cycle with no melting endotherm. Thus it was concluded that ibuprofen was amorphized and tested immediately using ATR-FTIR. Amorphous material can be differentiated from crystalline material using ATR-FTIR technique. While crystalline material is usually characterised by sharp absorbance bands, the amorphous state can result in band broadening or disappearance in a definite broadening case. This is attributed to the non-specific intermolecular bonding in comparison to the crystalline material.

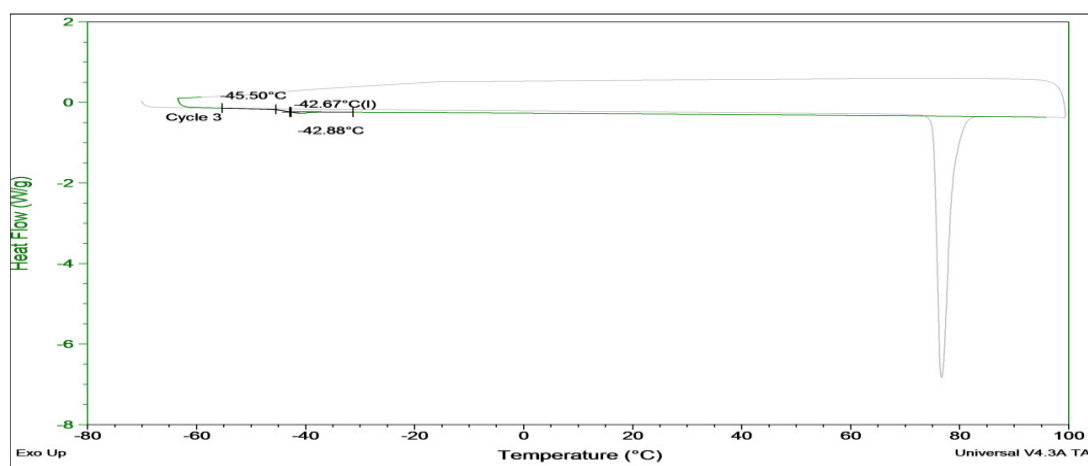
(I)



(II)



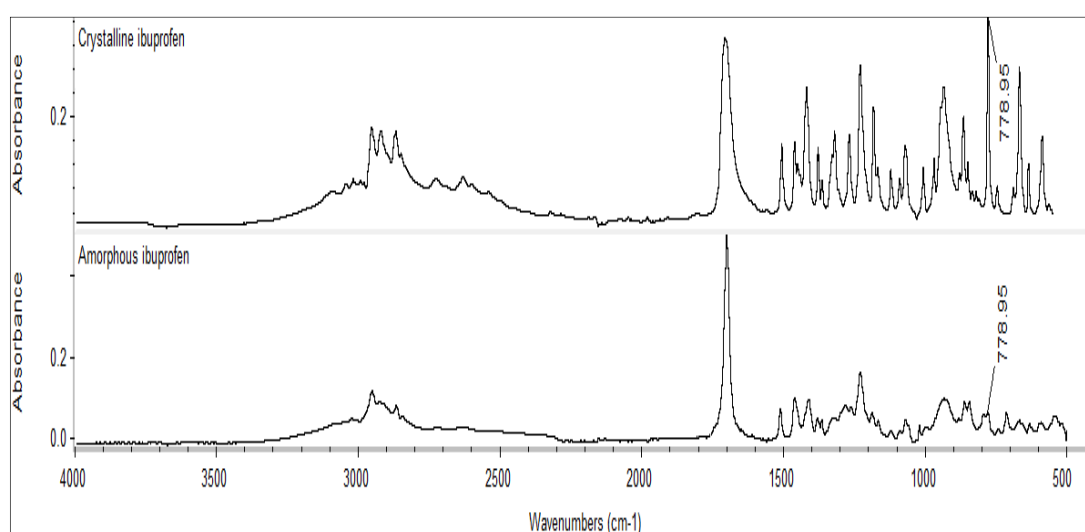
(III)



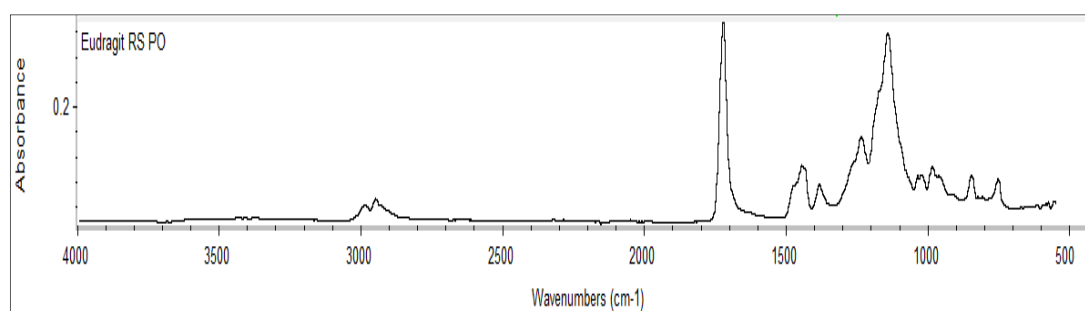
**Figure 4.13: Amorphous ibuprofen production using cDSC method. Highlighted green cycle represents: (I) first cycle of the heating at 10°C/min, (II) second cycle of rapid cooling (quenching) at 20°C/min and (III) third cycle of reheating at 10°C/min**

The reference spectra of the ibuprofen in Figure 4.14 (A) showed that peaks in the region of  $900\text{--}550\text{ cm}^{-1}$ , due to the bending vibrations of aromatic ring, can be used to mark the differences between the amorphous and crystalline state of this drug. In particular absorbance band around  $779\text{ cm}^{-1}$ , due to the ( $=\text{C-O}$ -bending) of carboxylic acid (Bhende and Jadhav, 2012). As seen in Figure 4.14 (A) this band can be used as a characteristic peak corresponding to the crystalline ibuprofen due to its marked sharpness compared to the amorphous ibuprofen. In addition, it does not overlap with the Eudragit RS PO bands observed in Figure 4.14 (B).

(A)



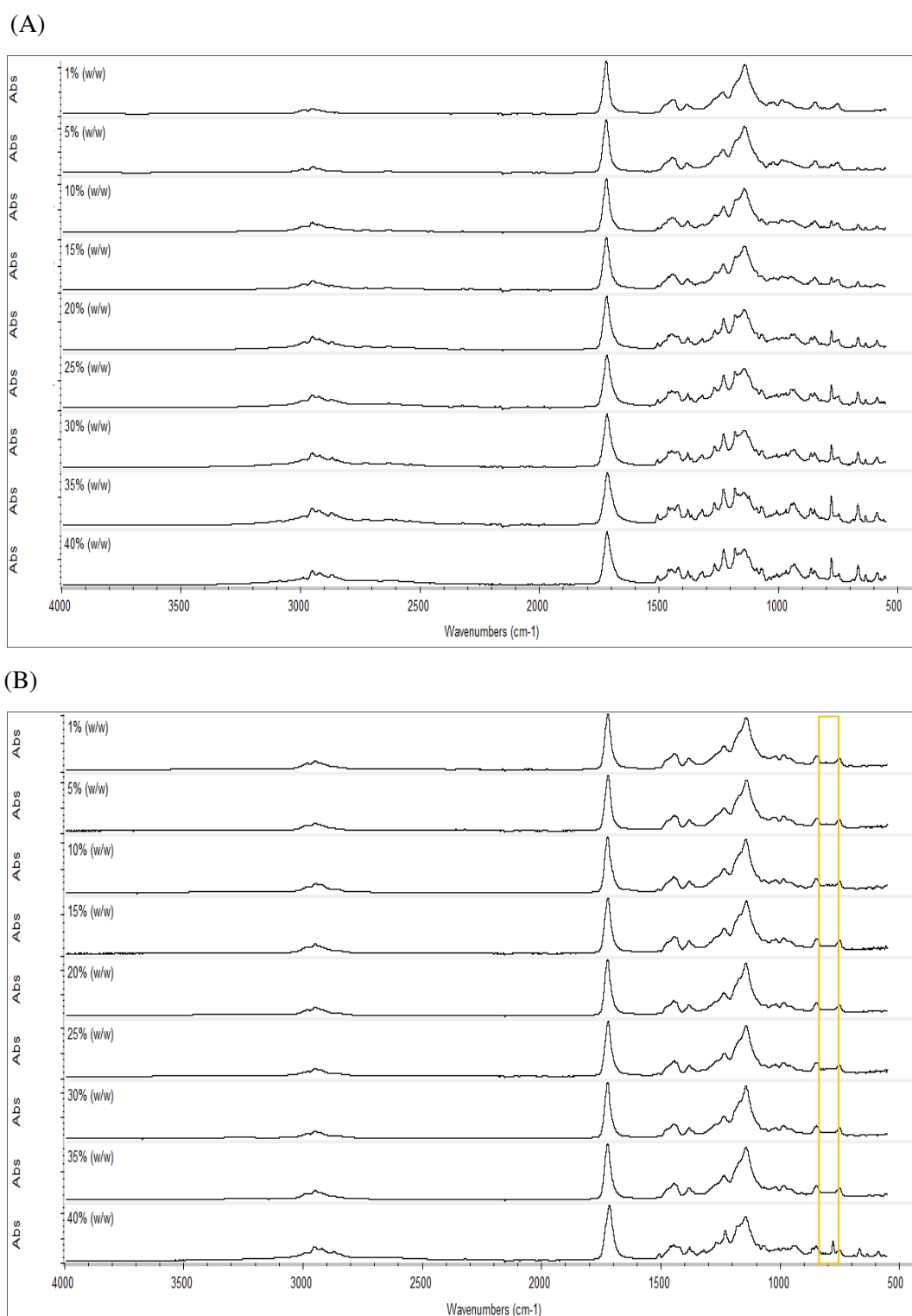
(B)



**Figure 4.14: Reference ATR-FTIR spectra of the crystalline, amorphous ibuprofen (A) and Eudragit RS PO (B)**

In the ATR-FTIR spectrum of crystalline ibuprofen carboxylic acid appears around  $1708\text{ cm}^{-1}$ , hydroxyl stretching vibration in the  $3100\text{-}2950\text{ cm}^{-1}$  region, aromatic stretch ( $\text{C}=\text{C}$ ) in the  $1507\text{-}1510\text{ cm}^{-1}$  region and bending peaks of aromatic ring in the  $900\text{-}550\text{ cm}^{-1}$  region (Figure 4.14(A)). On the other hand Eudragit RS PO spectrum shows characteristic peaks around  $1723\text{ cm}^{-1}$  (carbonyl stretching), at  $1145\text{ cm}^{-1}$  due to ( $\text{C}-\text{CO}-\text{C}$ ) stretching in the ester group and ( $\text{CH}_2$ -) symmetric bending at  $1450\text{ cm}^{-1}$  (Figure 4.14 (B)). The ATR-FTIR spectra of the physical mixtures of crystalline ibuprofen in Eudragit RS PO and their equivalent extrudates are presented in Figure 4.15. It is noteworthy that spectra of the surfaces of the extruded systems are effectively identical to their cross sections (data not shown here) at all drug loadings, indicating possible homogeneity of the extruded formulations (Qi et al., 2008a).

The carbonyl stretch modes appear around  $1722\text{-}1717\text{ cm}^{-1}$  in all the physical mixtures, which associate the stretching of the carboxyl group of the drug and the ester group of the polymer (Figure 4.15 (A)). These modes did not change in the corresponding extrudates (Figure 4.15 (B)). Notably, the Eudragit RS PO bands hid most of the peaks of ibuprofen in the extruded systems in comparison to their physical mixes in the  $1450\text{-}550\text{ cm}^{-1}$  region. However, the breadth (bandwidth) of these bands was slightly more relative to the Eudragit RS PO, suggesting the presence of diffused (broadened) amorphous ibuprofen bands. This hypothesis is supported by the appearance of characteristic crystalline peak of ibuprofen at 40 % (w/w) drug loading in these extrudates as highlighted in Figure 4.15 (B). Thus, when the concentration of the drug exceeded the miscibility in the polymer, the ibuprofen recrystallized and its bands become more distinguished (sharpened) and appeared in this region ( $1450\text{-}550\text{ cm}^{-1}$ ) similar to the physical mix, which otherwise contains crystalline ibuprofen. Overall, these observations ruled out the possibility of chemical interaction between ibuprofen and Eudragit RS PO after being extruded but supported previous results obtained by MTDSC, PXRD and SEM findings that maximum drug load for the production of glassy solid solution of the extruded ibuprofen-Eudragit RS PO systems is 35% (w/w).



**Figure 4.15: ATR-FTIR spectra of ibuprofen-Eudragit RS PO physical mixtures at different drug loadings (w/w %) (A) and their corresponding fresh hot melt extruded systems (B). Absorption intensities of these spectra vary. Used “marker” region for crystalline ibuprofen is enclosed in orange rectangle**

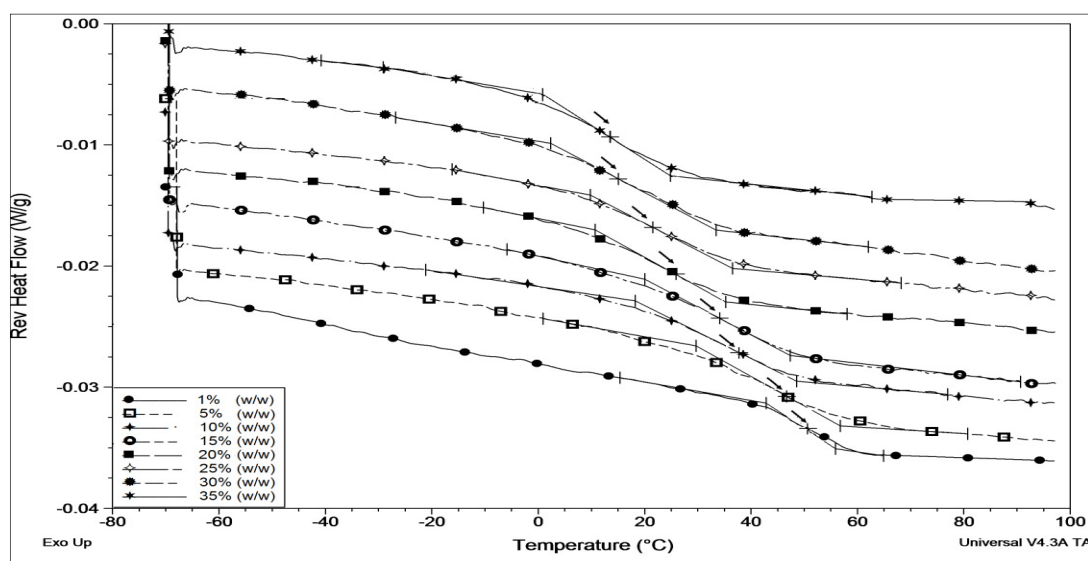


### **4.3.3 Influence of the relative humidity on the saturation solubility of ibuprofen in Eudragit RS PO extrudates**

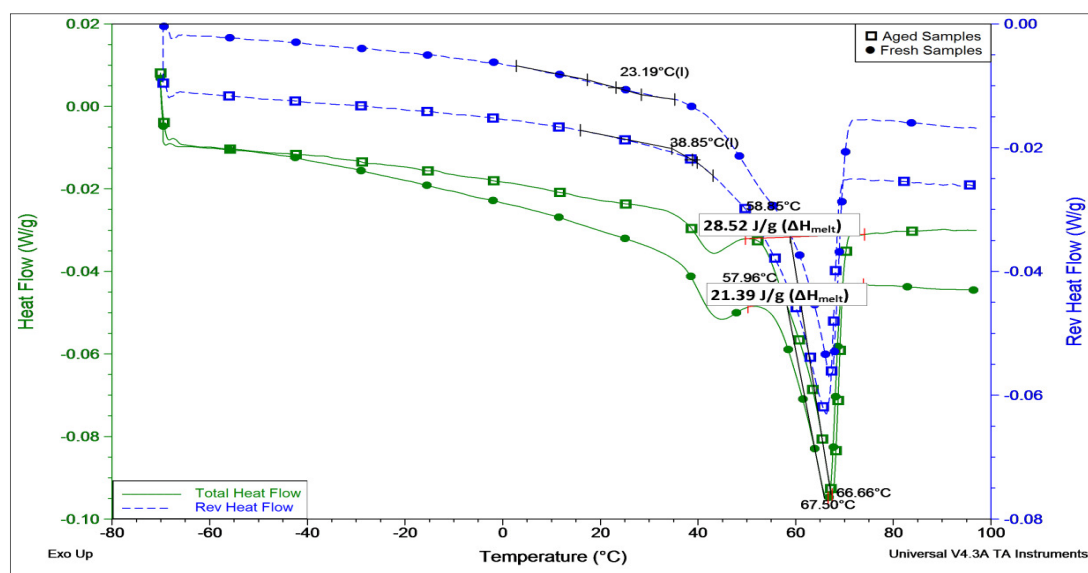
The previous section revealed what can be considered as the “apparent” solubility of the ibuprofen in Eudragit RS PO extrudates on freshly basis. This is because the complexities associated with the estimation of the actual degree of the solid solubility of these extruded systems. For example, this parameter is expected to be influenced by the phase behaviour of the extruded systems with time, after removal of the experienced intense mixing and subsequent stress during the HME process. In addition, the meta-stability of the amorphous material and tendency towards recrystallization as a function of time and other perturbation factors such as elevated temperatures or exposure to moisture. Thus, the following discussion will focus on defining the approximate equilibrium saturation solubility of the drug in the Eudragit RS PO extruded systems in terms of their physical stability. In other words, the solid saturation solubility value will represent the drug loading in the extruded system before any inclination to phase separation or drug recrystallization after storage at the chosen condition.

#### **4.3.3.1 Investigations into the saturation solubility of hot melt extruded ibuprofen in Eudragit RS PO after storage study at 0% relative humidity**

After storage under dry conditions (a relative humidity of 0% at ~25°C) for one month, the aged samples of ibuprofen-Eudragit RS PO extrudates up to 35% (w/w) drug loading were transparent. Furthermore, they were characterised by only single glass transition temperatures as assigned from the MTDSC reversing heat flow signals in Figure 4.16. These observations were similar to the fresh samples (previous section), suggesting that aged samples remained as solid solutions. However, opaque extrudate at 40% (w/w) ibuprofen loading converted into white colour. In addition, the drug melt enthalpy ( $\Delta H_{\text{melt}}$ ) was relatively higher than fresh samples as illustrated in the MTDSC total heat flow signals in Figure 4.17. These observations indicate increased crystallinity at this drug loading after ageing, which is reasonably expected in the light of known meta-stability associated with supersaturated systems.

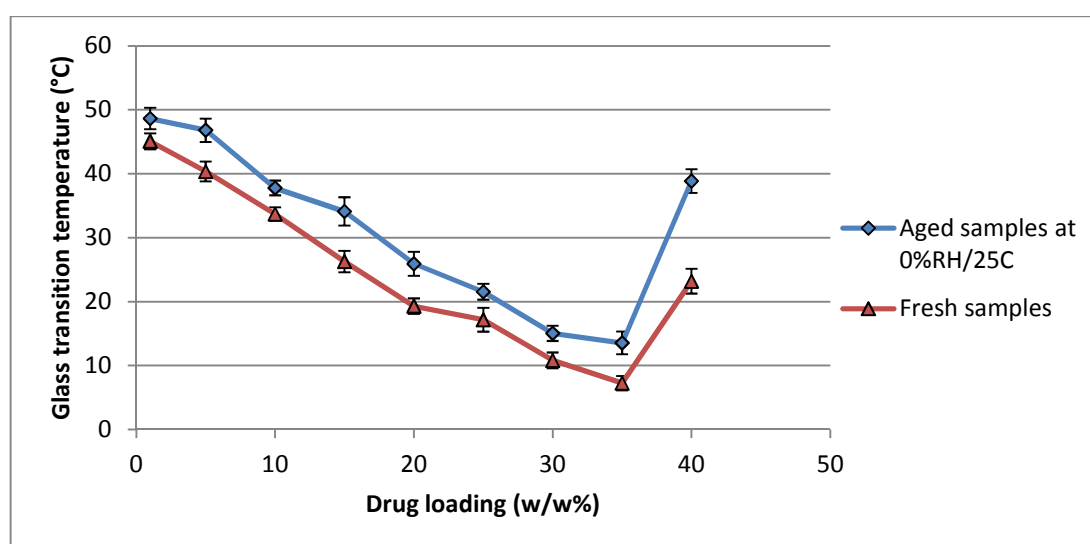


**Figure 4.16:** MTDSC reversing heat flow signals of ibuprofen-Eudragit RS PO extrudates with different drug loadings (w/w%) after ageing for one month at 0%RH/25°C. Underlying scan rate of  $1^{\circ}\text{C min}^{-1}$  with a modulation amplitude of  $\pm 0.265^{\circ}\text{C}$  and a period of 100 seconds. Arrows indicate the assigned Mid-point glass transition temperatures



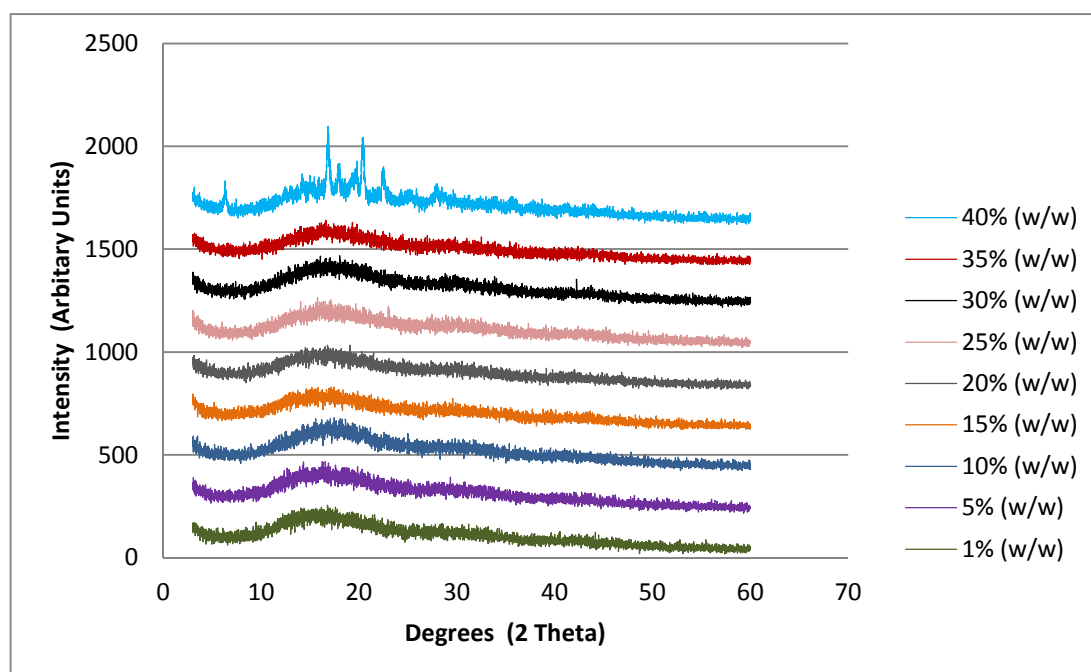
**Figure 4.17:** Representative MTDSC heat flow signals (total and reversing) of ibuprofen-Eudragit RS PO extrudate at 40% (w/w) drug loading measured for fresh samples and after ageing for one month at 0%RH/25°C. Underlying scan rate of  $1^{\circ}\text{C min}^{-1}$  with a modulation amplitude of  $\pm 0.265^{\circ}\text{C}$  and a period of 100 seconds

Figure 4.18 compares the measured glass transition temperatures of the studied aged extrudates with those observed just after extrusion (fresh extrudates). This figure illustrates a slight increase of the glass transition temperature after ageing under dry conditions over the concentration range of 1-35% (w/w) ibuprofen loading. Conversely, a clear increase was observed at 40% (w/w) drug loading. This reflects the dynamic of these systems while they are trying to equilibrate after the stress experienced during the extrusion process. On the other hand, increased ibuprofen recrystallization at 40% (w/w) concentration after ageing was associated with higher T<sub>g</sub> value than fresh extruded system. This could be explained by possible limited plasticizing effect contributed by ibuprofen on the glass transition temperature of Eudragit RS PO after its separation as a crystalline phase.



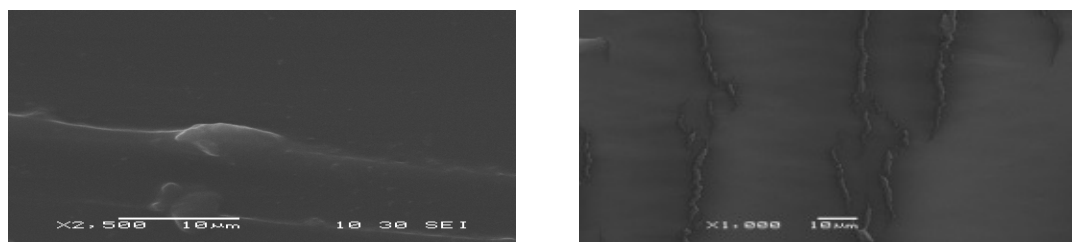
**Figure 4.18:** Comparison between glass transition temperatures (Mid-point T<sub>g</sub>) of the fresh samples and samples stored for one month at 0%RH/25°C of the hot melt extruded ibuprofen in Eudragit RS PO systems at different drug loadings (w/w%). T<sub>g</sub> values were obtained from reversing heat flow signals of the MTDSC measurements at 1°C/min. Each data point represents the mean±S.D. of three measurements

The PXRD results supported MTDSC results. Figure 4.19 shows an overlay of PXRD diffractograms (profiles) of the aged extruded samples at different ibuprofen loadings. Compared to the fresh samples studied in the previous section (Figure 4.11), the PXRD patterns over the concentration range of 1-35% (w/w) drug loading gave a similar characteristic amorphous halo, thus no indication of crystallinity. However, extruded samples at 40% (w/w) ibuprofen loading showed a visible increase in the resolution of the characteristic ibuprofen peaks, indicating an increase in the structural uniformity and crystalline material.

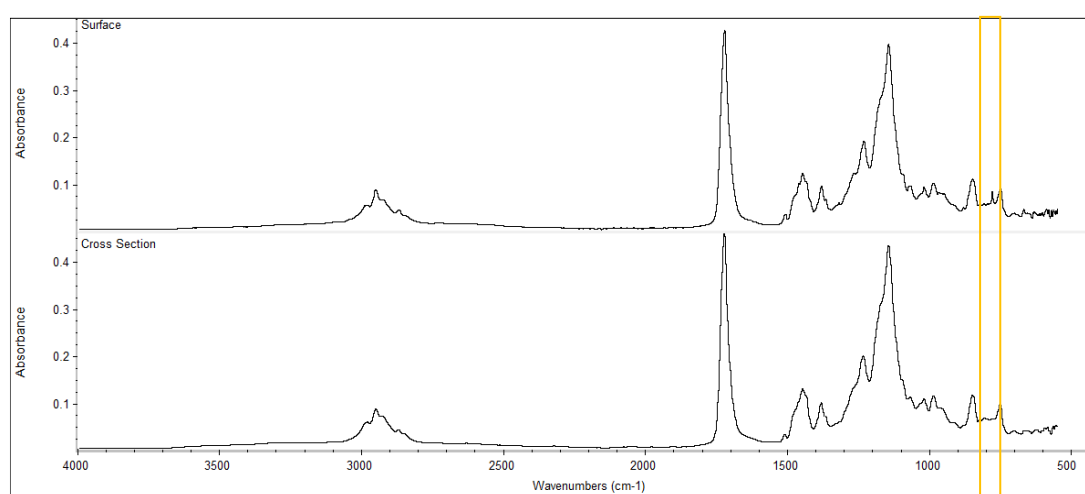


**Figure 4.19: PXRD diffractograms of hot melt extruded ibuprofen-Eudragit RS PO systems at different drug loadings (w/w %) after storage for one month at 0% RH/25°C**

Furthermore, the aged samples were examined under SEM. Interestingly, there were no visible crystalline ibuprofen in these samples similar to the fresh samples (see Fig.4.12) only up to 30% (w/w) drug loading. Conversely, at 35% (w/w) drug loading, micro-crystallites were detected on the surface of these aged extrudates as shown in Figure 4.20. ATR-FTIR was also used to investigate this observation as shown in Figure 4.21. This figure indicates the presence of crystalline ibuprofen mainly on the surface of these samples as visualized from sharpening of the characteristic (marker) absorbance band of crystalline ibuprofen around  $779\text{ cm}^{-1}$ . Therefore, ATR-FTIR confirmed SEM observation, clearly implying that ibuprofen had been recrystallized in the aged extruded system at 35% (w/w) drug loading.



**Figure 4.20: SEM images of the surface (left side) and cross section (right side) of hot melt extruded ibuprofen in Eudragit RS PO at 35% (w/w) drug loading after ageing for one month at 0%RH/25°C**



**Figure 4.21: ATR-FTIR spectra of surface and cross section of ibuprofen-Eudragit RS PO extrudate at 35% (w/w) drug loading aged for one month at 0%RH/25°C. Used “marker” region for crystalline ibuprofen is enclosed in orange rectangle**

Overall, the findings in this section gave insight into how hot melt extruded systems of ibuprofen in Eudragit RS PO equilibrate, in terms of their physical stability, in a low humidity environment after one month. A combined analytical approach was used to ascertain the drug dispersion in a solid solution in these extrudates after ageing. Ibuprofen appeared to remain molecularly dispersed up to 35% (w/w) drug loading, similar to the fresh samples, as indicated from MTDSC and PXRD studies. However, SEM investigations showed a presence of crystalline ibuprofen on the surface of 35% (w/w) drug loading extrudate, which was also detected by ATR-FTIR measurements. Therefore, it is reasonably to consider that solid saturation solubility of the extruded ibuprofen-Eudragit RS PO after one month of storage at 0%RH/25°C corresponds to 30 % (w/w) ibuprofen loading. This is surprising given the low values of  $T_g$  observed (Figure 4.18). Therefore, it is suggested that

the reported high viscosity of Eudragit RS (Kim et al., 2002) is responsible for limiting the collision of ibuprofen molecules and subsequent crystallization. Additionally, the polymer viscosity increases with the decrease in the temperature during the cooling of the extrudate (Crowley et al., 2007).

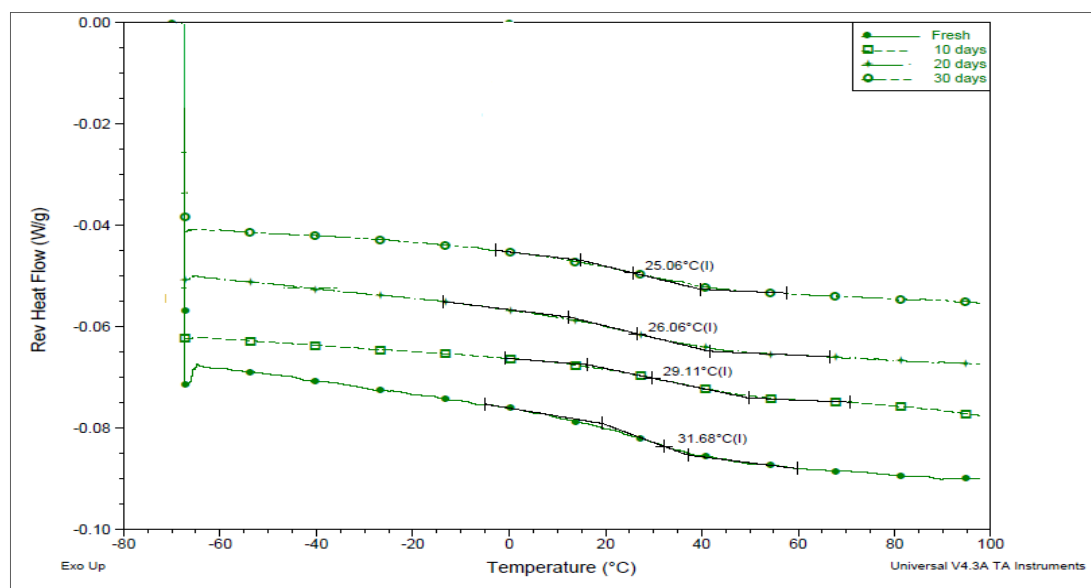
#### **4.3.3.2 Investigations into the saturation solubility of hot melt extruded ibuprofen in Eudragit RS PO after storage study at 60% relative humidity**

The objective of this study was to understand how water will affect the extent of solid state miscibility of ibuprofen-Eudragit RS PO extruded systems. These extrudates were allowed to equilibrate with a surrounding humidity level of 60% RH at room temperature for one month.

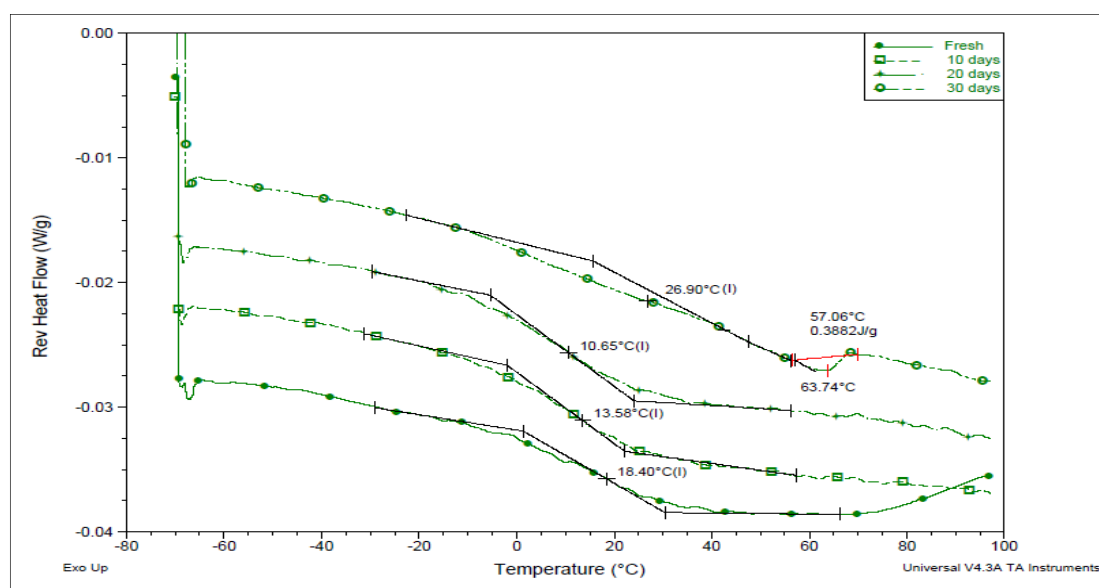
Representative reversing heat flow signals of MTDSC data of these aged samples are given in Figure 4.22 (A), (B) and (C). The glass transition temperature was assigned accordingly from these signals and notably it was lowered to values from  $31.7 \pm 0.1^\circ\text{C}$  and  $9.6 \pm 0.2^\circ\text{C}$  of 10-30% ibuprofen loaded systems to  $25.1 \pm 0.4^\circ\text{C}$  and  $3.2 \pm 0.2^\circ\text{C}$  before any recrystallization was detected. The water content of these samples was measured using TGA, where broad single step weight loss of the tested samples was observed from  $30^\circ\text{C}$  to  $120^\circ\text{C}$ , indicating water loss (Figure 4.23). Water contents of approximately 1.14 wt. % and 0.84 wt. % for the 10% and 30% loaded systems, respectively, were measured after one month of storage at 60% RH/ $25^\circ\text{C}$ . This would imply the powerful role of water as a plasticizer for these extruded samples, because even small amounts of water were enough to depress the glass transition temperatures of these glassy systems.

Furthermore, it was observed that melting endotherm of ibuprofen, indicating recrystallization, appeared at drug loadings higher than 10% (w/w) after ageing for 20 days and 30 days of 30% (w/w) and 20%(w/w) drug loaded extrudates, respectively. This could be explained by further reduction of the glass transition temperatures of these extruded systems due to moisture uptake. Consequently, as the Tg of the extruded system becomes sufficiently lower than the storage temperature due to plasticization by water, enhanced molecular mobility of ibuprofen molecules would be expected with subsequent recrystallization.

(A)

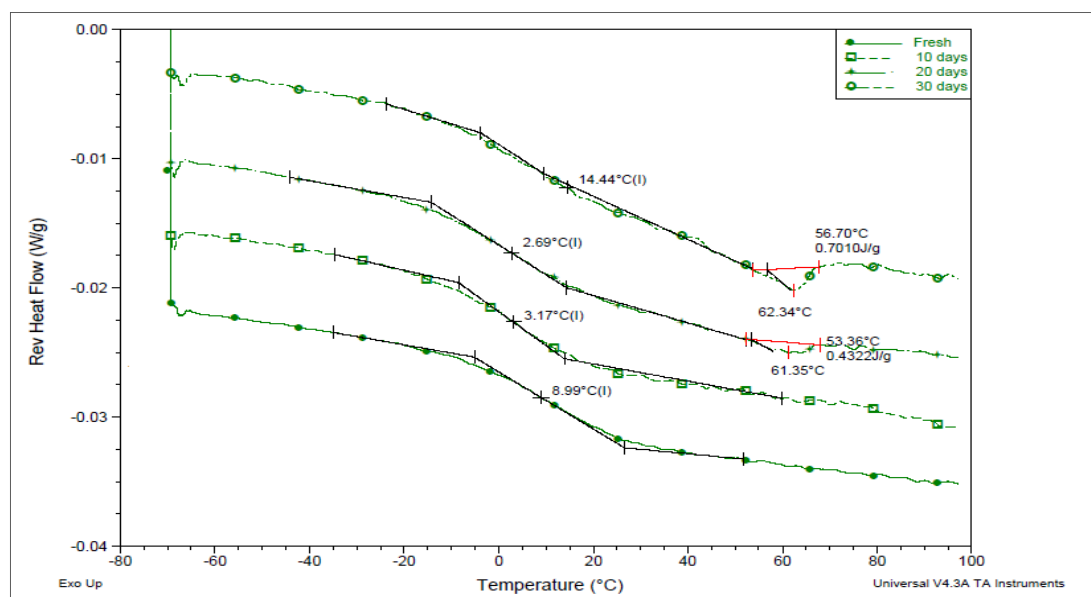


(B)

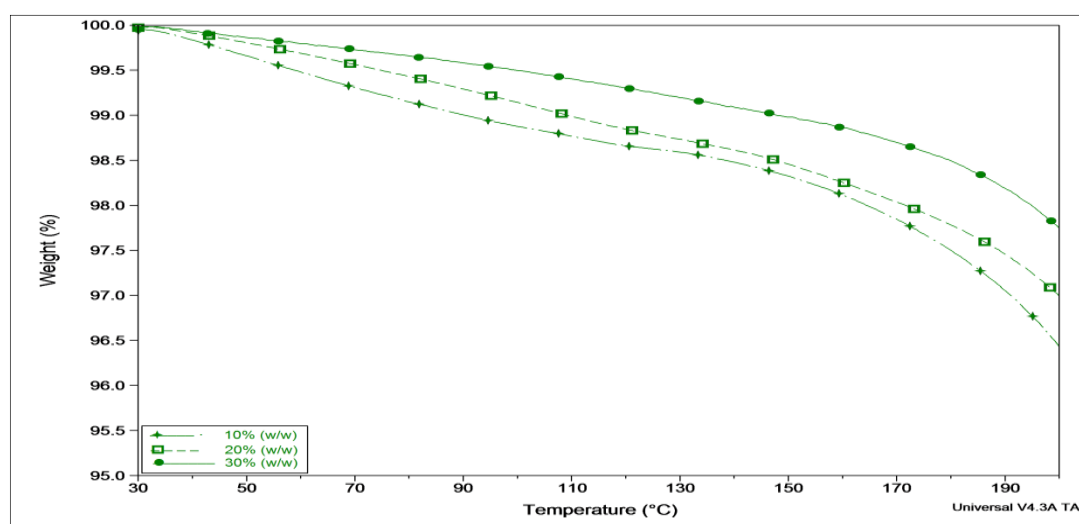


**Figure 4.22:** MTDSC reversing heat flow signals of hot melt extruded ibuprofen-Eudragit RS PO systems at 10% (w/w) drug loading (A) and 20% (w/w) drug loading (B), examined on 0 day (fresh) and after 10, 20, 30 days of storage at 60% RH/ 25°C, measured at 1°C/min underlying heating rate with a modulation amplitude of  $\pm 0.265^\circ\text{C}$  and a period of 100 seconds

(C)



**Figure 4.22 (Contd.): MTDSC reversing heat flow signals of hot melt extruded ibuprofen-Eudragit RS PO systems at 30% (w/w) drug loading (C), examined on 0 day (fresh) and after 10, 20, 30 days of storage at 60% RH/ 25°C, measured at 1°C/min underlying heating rate with a modulation amplitude of  $\pm 0.265^\circ\text{C}$  and a period of 100 seconds**



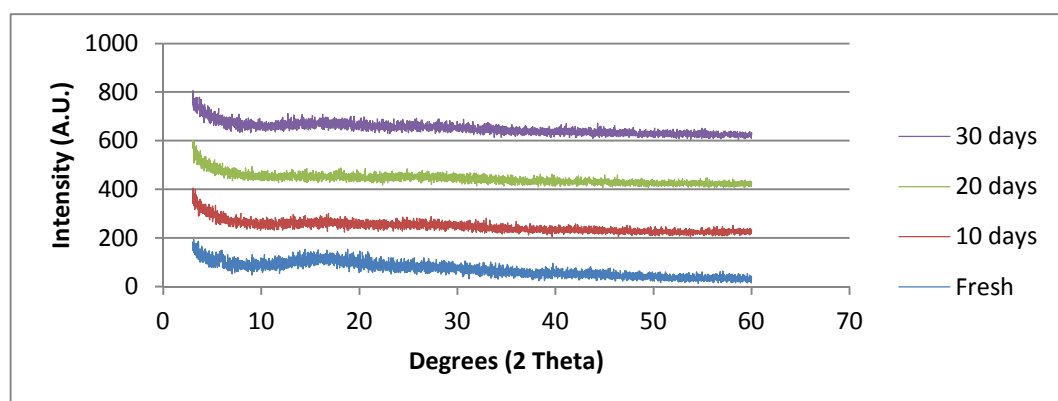
**Figure 4.23: TGA weight loss profiles of hot melt extruded ibuprofen-Eudragit RS PO systems at different drug loadings (w/w %) after ageing for one month at 60%RH/25°C**



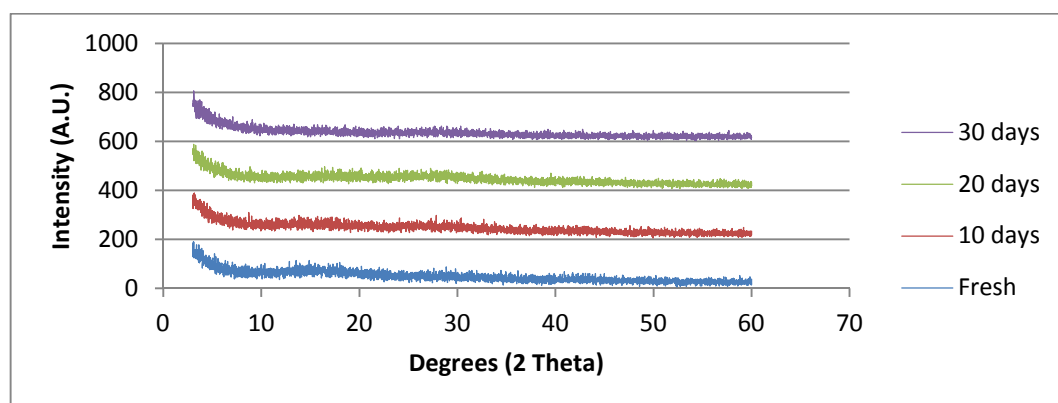
PXRD was also used to monitor ageing of these extruded systems and excepting extrudates at 40% (w/w) drug loading (data not shown here), there was no indication of crystallinity with the PXRD patterns remained halo as shown in Figure 4.24. This could be attributed to low levels of crystallinity in these aged extrudates below detection limits of this technique.

However, in agreement with the MTDSC experiments, ibuprofen crystals were visible under the SEM of the aged extruded systems with drug loading higher than 10% (w/w) as illustrated in Figure 4.25. In this figure, few drug crystals appeared mainly on the surfaces of these extrudates and increased with increasing drug loading. Overall, this section indicates that the solubility of ibuprofen in Eudragit RS PO extrudate had been reduced to circa 10% (w/w) after one month. While crystallization on water uptake is well known, it is surprising that the effect was so marked with such a small decrease in  $T_g$  and may reflect equilibrium solubility changes.

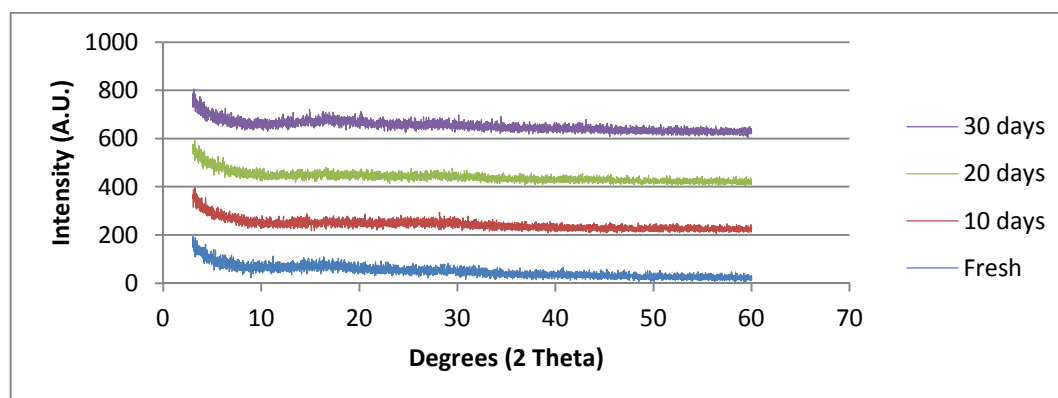
(A)



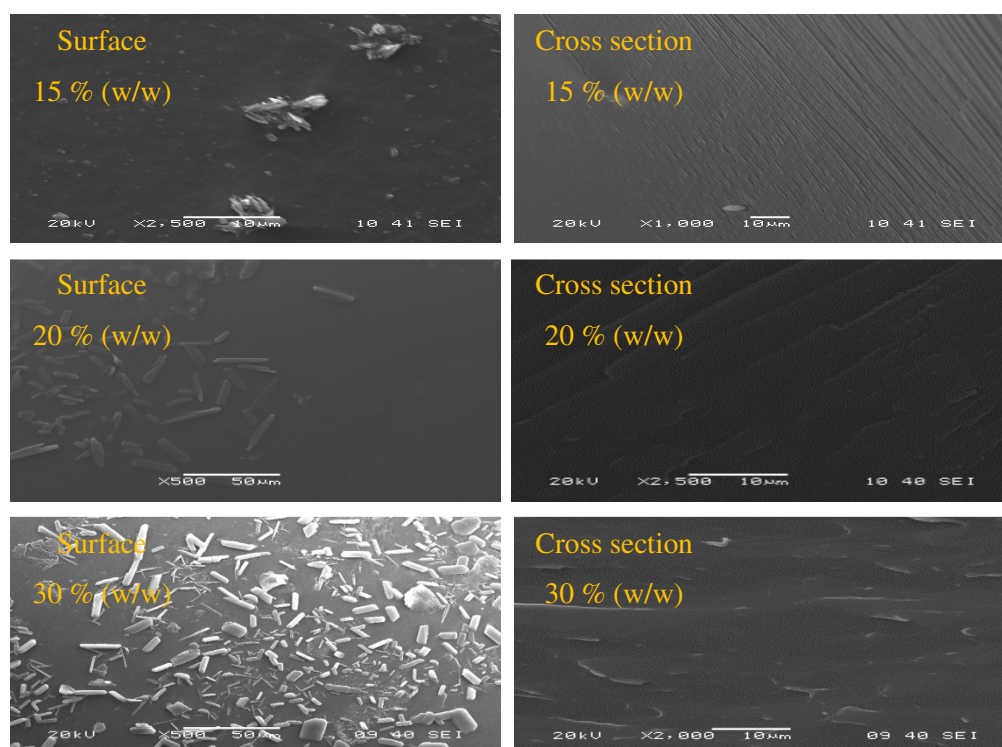
(B)



(C)



**Figure 4.24: PXRD diffractograms of hot melt extruded ibuprofen-Eudragit RS PO systems at different drug loadings of: (A) 10% (w/w), (B) 20% (w/w) and (C) 30% (w/w), examined on 0 day (Fresh) and after 10, 20, 30 days of storage at 60% RH/ 25°C**



**Figure 4.25:** SEM images of the surfaces (left side) and cross sections (right side) of hot melt extruded ibuprofen in Eudragit RS PO at different drug loadings (w/w %) after ageing for one month at 60% RH/25°C

#### 4.3.4 Fragility assessment of ibuprofen-Eudragit RS PO extruded systems

In the previous section the equilibrium saturation solubility of the extruded mixtures of ibuprofen in Eudragit RS PO was characterised and approximated for specified storage conditions at room temperature with two relative humidity levels (0%RH and 60% RH). These systems showed good stability and maintained high solid solubility after ageing at dry conditions (up to 30% (w/w) drug loading), though storage temperature was around or higher than their glass transition temperature. With the knowledge that some glassy systems may show good kinetic stability around  $T_g$  but may have the potential to collapse into crystals below their glass transition temperature due to structural relaxation (Qi et al., 2008b), it was useful to examine fragility parameter of the binary extruded systems of ibuprofen in Eudragit RS PO in this study. This parameter can be correlated to the molecular mobility behaviour of the studied glassy (amorphous) system, giving a complementary indirect measure to understand its physical stability.

This work was performed on the extruded Eudragit RS PO systems loaded with 10-30% (w/w) ibuprofen to estimate their fragility parameters, with a goal to identify qualitatively the propensity of their physical ageing. This ageing measured by fragility usually refers to the tendency of the system to decrease its glass transition temperature at lower temperatures, which enhances molecules mobility and increases the chance for crystallization to occur. Using fictive temperature approach, conventional DSC (cDSC) can be used to determine fragility parameter depending on the scanning rate as suggested by Robertson et al., (2000). Fictive temperature concept was first proposed by Tool (1953), who described it as the temperature at which the liquid structure is frozen in. The fictive temperature is defined as the extrapolated intersection of the pre-transition and post-transition DSC heat flow baselines transposed to enthalpy units that is related to the contribution of the structural relaxation process to the properties of the glass (Cassel, 2002). This temperature depends only on the previous cooling rate through the glass transition temperature (thermal history), regardless the heating rate used for its measurement (Yue et al., 2004). Therefore, Equation 4.10 can be used to correlate the fragility parameter with the fictive temperature (Robertson et al., 2000) as follows:

$$m_{\Delta h} = - (d \log \beta_c) / (d(T_{f,ref}/T_f)) \quad (\text{Eq.4.10})$$

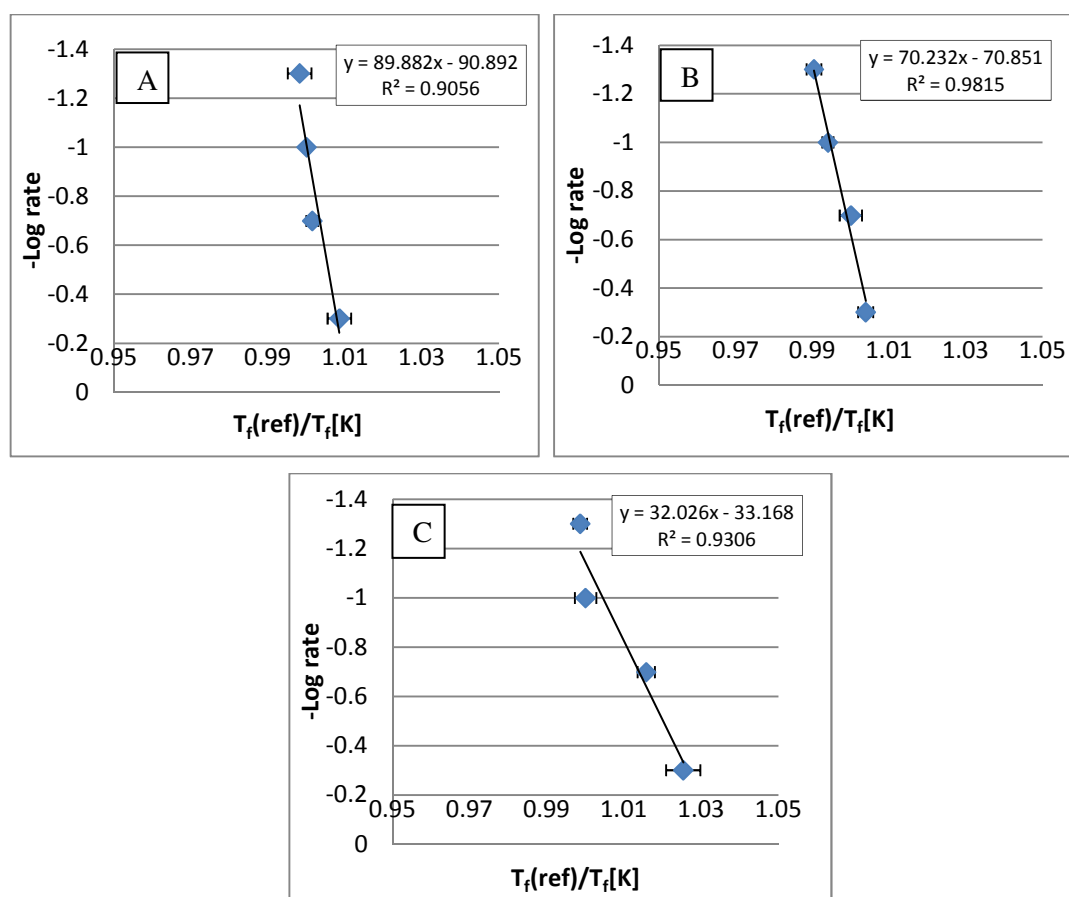
where  $\beta_c$  is the prior cooling rate,  $T_f$  is the fictive temperature measured in the heating cycle,  $T_{f,ref}$  is the reference fictive temperature and  $m_{\Delta h}$  is the fragility parameter. Wherein the value of  $T_{f,ref}$  should be obtained from the fictive temperature of the cooling rate equivalent to reheating rate used, because the value of the fictive temperature would be very close to the glass transition temperature and thus called limiting fictive temperature (Yue et al., 2004).

By cooling at various rates: 2, 5, 10 and 20°C/min, followed by heating at a constant (arbitrary) rate of 10°C/min through the glass transition region of the studied extruded systems, the variation of the  $T_f$  with the cooling rate was used to define an enthalpic fragility parameter,  $m_{\Delta h}$  (Hodge, 1994). The fictive temperatures measured for these extrudates using cDSC are summarized in Table 4.2. Values in this table were used in Eq.4.10 to obtain plots shown in Figure 4.26, whereby the fragility parameters can be estimated from the slopes of the resulted lines, determined using a least squares best fit, from these fragility plots (Cassel, 2002). As clear from this figure, the estimated fragility parameters fall below 100 (around 89.9, 70.2 and 32.0 for 10%, 20% and 30% (w/w) drug loaded extrudates, respectively), resembling behaviour of strong, non-fragile systems (Borde et al, 2002). Therefore, it is less likely for the studied extruded systems to show physical relaxation of their glassy state and

ultimately crystallization of the drug, if they stored at temperatures below their glass transition temperatures.

Drug Loading (w/w %)	10% (w/w)	20% (w/w)	30% (w/w)
cooling rate	$T_f \pm \text{s.d.}/^{\circ}\text{C}$	$T_f \pm \text{s.d.}/^{\circ}\text{C}$	$T_f \pm \text{s.d.}/^{\circ}\text{C}$
2°C/min	19.6±0.5	16.7±0.5	9.3±1.1
5°C/min	21.7±0.2	17.8±0.3	12.0±0.2
10°C/min	22.1±0.1	19.5±0.2	16.5±0.6
20°C/min	22.6±0.4	20.3±0.7	16.9±0.2

**Table 4.2: Summary of the cDSC results of the fresh hot melt extruded ibuprofen-Eudragit RS PO films at different drug loadings**



**Figure 4.26: Fragility plots of fresh hot melt extruded ibuprofen-Eudragit RS PO films at drug loading of: (A) 10 % (w/w), (B) 20 % (w/w) and (C) 30 % (w/w)**

#### 4.4 Conclusions

The aim of the work described in this chapter was to continue characterising the ibuprofen and Eudragit RS PO for miscibility and interactions as a whole formula produced by hot melt extrusion. Hot melt extrusion technology was utilized successfully for the development of solid solutions of ibuprofen at high loading (up to 35% w/w) incorporated in Eudragit RS PO. The theoretical approaches of miscibility estimation using solubility parameters and melting point depression provided relatively good prediction of the practical solubility found for the studied extruded systems. Ibuprofen and Eudragit RS PO did not exhibit significant interactions but appeared to form compatible blends, supported by the one phase system existence of these systems i.e. solid solutions.

Section 4.3.1 detailed the initial characterisation of the physical mixes of ibuprofen and Eudragit RS PO for thermal stability before extrusion. TGA results demonstrated minimal weight losses after thermal treatment of these mixes at the extrusion temperature for the intended mixing time, indicating low degradation and thermal stability at these conditions.

Section 4.3.2 elucidated the potential use of solubility parameter and melting point depression thermodynamic model as tools to predict compatibility and miscibility of ibuprofen in Eudragit RS PO and correlated this with the solubility of this drug in Eudragit RS PO hot melt extrudate. This included the use of various techniques such as DSC, PXRD, SEM and ATR-FTIR for characterisation of the dispersibility of ibuprofen-Eudragit RS PO extruded systems. The glass transition temperatures of these systems were decreased with increasing drug loading due to the presence of the plasticizer i.e. ibuprofen, which aided in the extrudability of ibuprofen-Eudragit RS PO blends. Composition range within which the drug-polymer miscibility may be regarded as the solubility of the drug in the polymer was 35% (w/w) as confirmed by aforementioned techniques.

Section 4.3.3 detailed the use of DSC, PXRD, ATR-FTIR, and SEM techniques for approximation of the extent of solid state miscibility or equilibrium saturation solubility under two relative humidity levels for one month. This achieved through monitoring of the phase behaviour of the selected solid solutions of ibuprofen-Eudragit RS PO extrudates. It was noted that the equilibrium solubility composition of the extruded mixture without phase separation or drug recrystallization slightly dropped under dry conditions (0%RH/25°C) to 30% (w/w) drug loading. However, a significant decrease in the miscibility was noted on storage at 60% RH/25°C despite the water uptake being relatively low, indicating extra molecular mobility resulting from the strong plasticizing effect of water, wherein the drug is also poorly soluble. This part also provides insight into the physical stability of these drug-polymer mixtures under selected storage conditions and recommended storage under dry conditions to maintain high solubility of ibuprofen in Eudragit RS PO extrudate. The results of MTDSC and PXRD showed some agreement with each other, especially in 0%RH/25°C storage study for detection of ibuprofen crystals, thus indicating phase separation. However, ATR-FTIR and SEM appeared as viable techniques for detection and visualization, respectively, of low amounts or small crystallites of ibuprofen undetected by PXRD or MTDSC techniques.

Section 4.3.4 provides prediction of the tendency of miscible extruded ibuprofen-Eudragit RS PO systems towards physical relaxation (ageing) using the fragility parameter. The results revealed strong glassy systems, from which we can infer that storage of the studied solid solutions under temperatures less than their glass transition temperatures might not affect their stability in terms of drug recrystallization.

**Chapter 5: *In vitro* ibuprofen release and permeation studies from hot melt extruded Eudragit RS PO films**



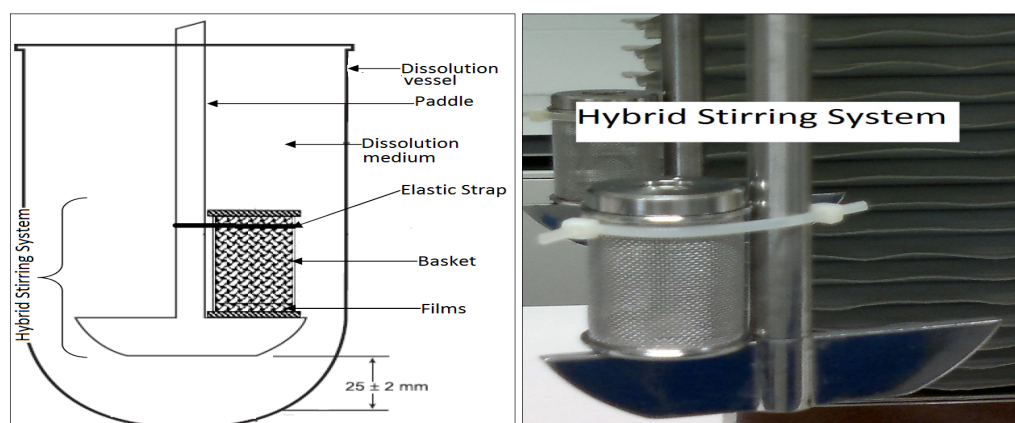
## 5.1 Introduction

*In vitro* performance testing of transdermal films with respect to drug release and skin permeation can be achieved using dissolution apparatus and Franz-type diffusion cells, respectively. *In vitro* dissolution test for transdermal delivery systems is referred to drug release or *in vitro* release study (Siewert et al., 2003), which concerns the evaluation of the release of the drug in a dissolution medium, wherein the drug is generally dissolved. However, in the case of transdermal pharmaceutical systems, it is also important to understand to which degree the tested formulation or the used product design may affect the drug permeation through the skin by *in vitro* permeation testing. Therefore the ultimate goal of the *in vitro* permeation studies is analogous to that of *in vitro* release studies, as a valuable measure of product quality, reflecting the thermodynamic activity of the drug substance in the pharmaceutical product. Consequently, the data derived from both experiments can be utilized together to evaluate the drug release behaviour of delivery systems and define biopharmaceutical characteristics to ensure that the developed formulations can be used or otherwise optimised to achieve the delivery of the therapeutic levels of drug to the site of action. Therefore, the aim of the present chapter is to assess relative suitability of Eudragit RS PO-based hot melt extruded films to deliver ibuprofen transdermally in terms of their contribution to the *in vitro* drug release and *in vitro* permeation profiles. Section 5.2 comprehensively outlines the theory and set up of the *in vitro* dissolution/release and Franz diffusion cells system techniques and describes the kinetic modelling that can be used to assess mechanism(s) of drug release and permeation. Section 5.3 subsequently details the results obtained from these two experiments with the kinetic modelling of the obtained permeation profiles to explain the release kinetics of ibuprofen from the tested films.

## 5.2 Experimental methodologies

### 5.2.1 *In vitro* drug release studies

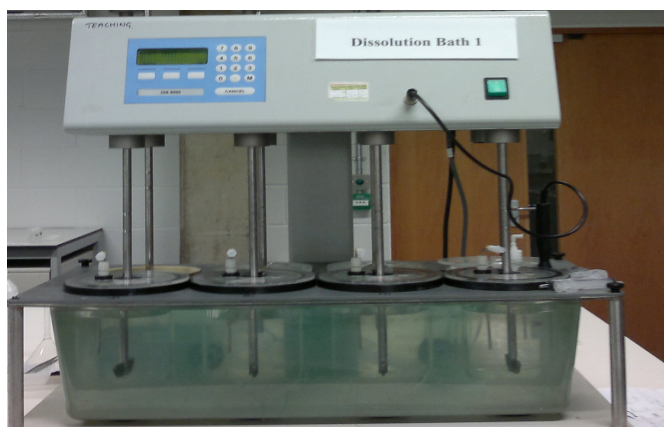
For transdermal drug delivery systems, drug release studies are usually performed using different compendia apparatus (PhEur, 2005; USP31, 2008) and generally they are paddle over disk method (USP apparatus 5/PhEur 2.9.4.1), rotating cylinder method (USP apparatus 6/PhEur 2.9.4.3), reciprocating disk method (Apparatus 7) and paddle over extraction cell method (PhEur 2.9.4.2). However, several different and appropriate apparatuses can be used for the drug release testing and in our case the best approach proposed was the use of the paddle and vessel assembly with the addition of a stainless steel basket. The design of this hybrid basket-paddle system, as illustrated in Figure 5.1, was adapted from Grundy et al. (1997), thereby the advantage of high agitation from the paddle apparatus can be combined to the benefit of sample floating prevention using the basket apparatus.



**Figure 5.1: Modified dissolution apparatus for characterising *in vitro* release of the hot melt extruded films**

*In vitro* dissolution/release testing in this study was utilized to estimate drug release from the formulations prepared by hot melt extrusion using a Copley Scientific DIS8000 dissolution bath attached to a Copley Scientific FH16-D heating unit (Figure 5.2). This experiment can indirectly reflect the amount of the drug that can be available for absorption to systemic circulation, thus aiding selection of the appropriate formulation candidate for *in vitro* permeation testing or correlation. Concerning the dissolution medium, many studies employ a phosphate buffer system with pH = 7.2 to 7.4, due to similarity with the blood or plasma compartment (Mitu et al., 2011). Consequently, a phosphate buffer system (PBS) was

prepared with a pH = 7.2 (section 5.2.1.1) to account for physiological relevance of the systemic pool wherein the drug will be delivered (Gavali et al., 2010; Itoh et al., 1990). In addition, it has been reported that saturation solubility of ibuprofen in this medium (PBS, pH = 7.2) is almost  $3.74 \pm 0.14$  mg/ml (Dabbagh and Taghipour, 2007). Consequently it may be expected that dissolution will not be limited by the ibuprofen solubility in this medium, allowing reasonable dissolution time windows which in turn provide a convenient test framework.



**Figure 5.2: Copley dissolution bath**

The term sink condition usually refers to situations whereby the volume of the medium is three times or more (five or even ten) times the volume required to form saturated solution of a drug substance in this medium (Rohrs, 2001). However, these conditions can be acceptable if the drug concentration in the dissolution medium does not exceed 10 to 20% of the saturation concentration or solubility of the solute, as suggested by Hoa and Kinget (1996). Therefore, it was important to ensure that saturation solubility of the ibuprofen is determined experimentally in our dissolution medium rather than simply to use the reported value (section 5.2.1.2). In this work, a volume of 900 ml of the dissolution medium was used as usually specified in the pharmacopoeias and the samples' weights were determined accordingly, using the following equation (Gowthamarajan and Singh, 2010):

$$\text{The maximum dissolvable dose of the drug} = (V \times C_s) / (C_s/CD) \quad (\text{Eq.5.1})$$

Where V is the dissolution medium volume,  $C_s$  is the saturated solubility of the drug in the medium and CD is the concentration of the drug in the bulk medium.  $(C_s/CD)$  should be greater than or equals 3 to achieve sink condition.

#### 5.2.1.1 Preparation of phosphate buffer solution (pH =7.2)

The dissolution media were prepared by weighing individual buffer components into tared weighing boats. 34.02 g of potassium dihydrogen orthophosphate was transferred into a clean 5 L volumetric flask and a quantity of deionized water was added (~2 L), then the mixture was stirred until all the solids were dissolved. Then 0.2M sodium hydroxide was prepared by dissolving 7.99 g of sodium hydroxide into 1 L volumetric flask through addition of sufficient deionized water to produce 1000 ml and then stirred for enough time (~20 minutes) to ensure that they are fully dissolved. Afterwards 875 ml of 0.2M sodium hydroxide was mixed into the 5 L volumetric flask mixture and a further amount of water was added to produce a final volume of 5 L. The pH of the solution was checked using a pH meter, and when necessary adjusted using small quantities of NaOH or HCl as needed.

#### 5.2.1.2 Equilibrium saturation solubility

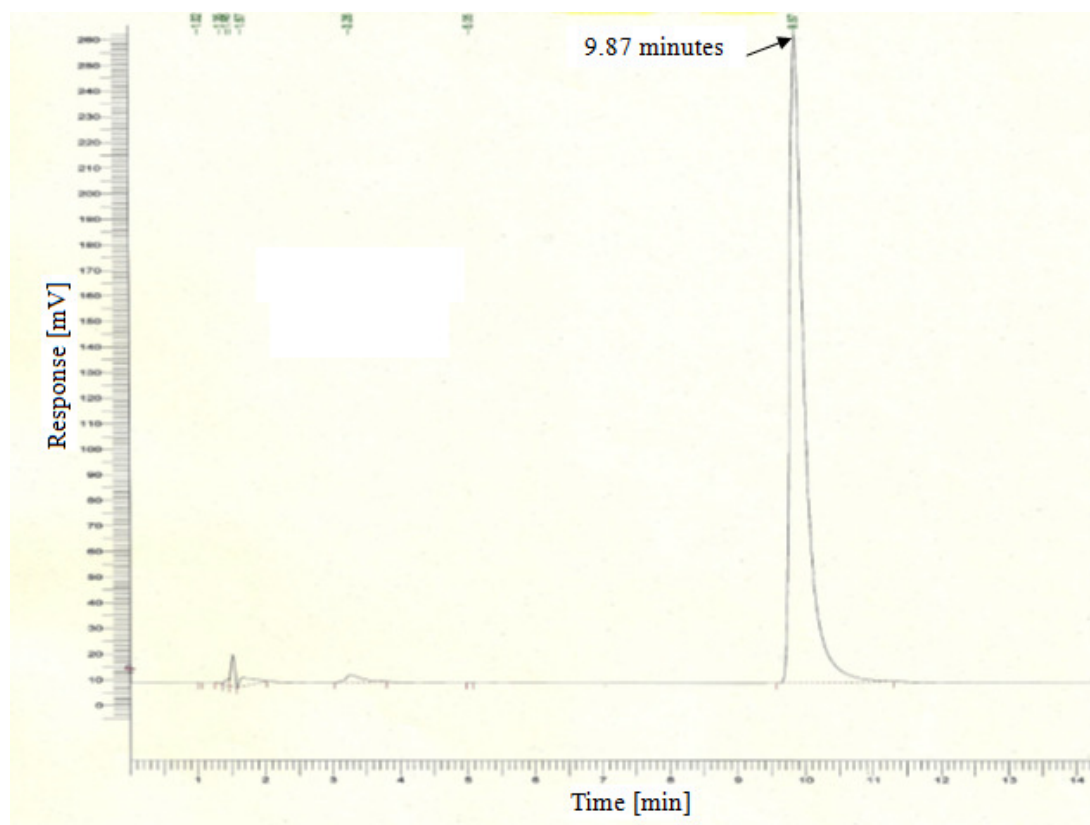
Saturation solubility of ibuprofen in phosphate buffer solution (pH = 7.2) was estimated through weighing excess amounts of crystalline powdered ibuprofen. Each sample of 0.50 g was introduced separately into 10 ml conical flask containing 5 ml of phosphate buffer solution (pH 7.2). The sealed flasks were stirred on a magnetic stirrer for 72 hours at 37°C and equilibrated for 2 hours. Then the solutions (supernatant) were filtered through 0.20 µm membrane filters (Sartorius stedim biotech Minisart®), and the filtrates were suitably diluted and analyzed using UV spectrophotometer at 223 nm (PerkinElmer, Lambda XLS). Determinations were carried out in triplicate.

#### 5.2.1.3 Evaluation of drug release

Hot melt extruded films based on Eudragit RS PO and formulated with different ibuprofen loadings (10-40%w/w) were prepared as described in Chapter 4. The films were cut manually and the dimensions were measured with an electronic digital caliper (MS092 Toolzone Vernier Caliper, UK). The tested films had similar dimensions of approximately 6mmx4mmx1mm (length, diameter, thickness) and of a total weight of not less than 2500 mg. The weighing was performed using a XS205 dual range analytical balance (Mettler Toledo). The prepared hot melt extruded films with 10% (w/w) ibuprofen loading corresponds to the saturation solubility of ibuprofen in Eudragit RS PO extruded matrices after equilibration or ageing at 60%RH/25°C for one month as detailed in Chapter 4. Therefore, the inclusion of water at this storage conditions did not compromise the physical

stability of these films at this drug loading, because the solid solution of ibuprofen in Eudragit RS PO matrix was maintained. Consequently, these aged films were evaluated to elucidate the possible role of conserved water molecules in their structure on the *in vitro* release behaviour. Ground hot melt extruded samples were obtained at this drug loading and compared to their equivalent physical mixtures and crystalline ibuprofen. On the other hand, equilibration at 0%RH/25°C for one month indicated that higher drug loading (30% w/w) were physically stable (Chapter 4) as the ibuprofen was molecularly dispersed in Eudragit RS PO. To further assess the impact of ageing on these films at 30% (w/w) ibuprofen loading, aged samples under these conditions were compared to the fresh fabricated samples.

In all the experiments, the dissolution medium consisted of 900 ml phosphate buffer (pH 7.2) was maintained at  $37.0 \pm 0.1^\circ\text{C}$  using a dissolution bath (Copley Apparatus, UK), and the stirring rate was set at 100 rpm. A volume of 5 ml of sample was withdrawn at specified time intervals and replaced immediately with the same volume of fresh dissolution medium, which was maintained at  $37.0 \pm 0.1^\circ\text{C}$ . The samples then filtered using a  $0.20\ \mu\text{m}$  filter (Sartorius stedim biotech Minisart<sup>®</sup>) and analyzed using an appropriate method, either by UV spectrophotometer (PerkinElmer, Lambda XLS) at  $\lambda_{\text{max}}$  determined for ibuprofen (223 nm) or by high performance liquid chromatography (reversed phase) using HPLC (Perkin-Elmer) instrument equipped with an ODS-Hypersil C18 column ( $5\ \mu\text{m}$ ,  $150 \times 4.6\ \text{mm}$  I.D.) and a degasser unit. The mobile phase (HPLC grades) consisted of a 50:50:1 (v/v) mixture of acetonitrile: deionized water: phosphoric acid and the flow rate was set at 1ml/min. The UV detector was set at 225 nm, at which ibuprofen showed maximum absorbance using this mobile phase. Chromatography was performed at  $25^\circ\text{C}$ ; the injection volume was  $100\ \mu\text{l}$ . Under these conditions, the retention time for ibuprofen was approximately 9.87 min as shown in Figure 5.3.

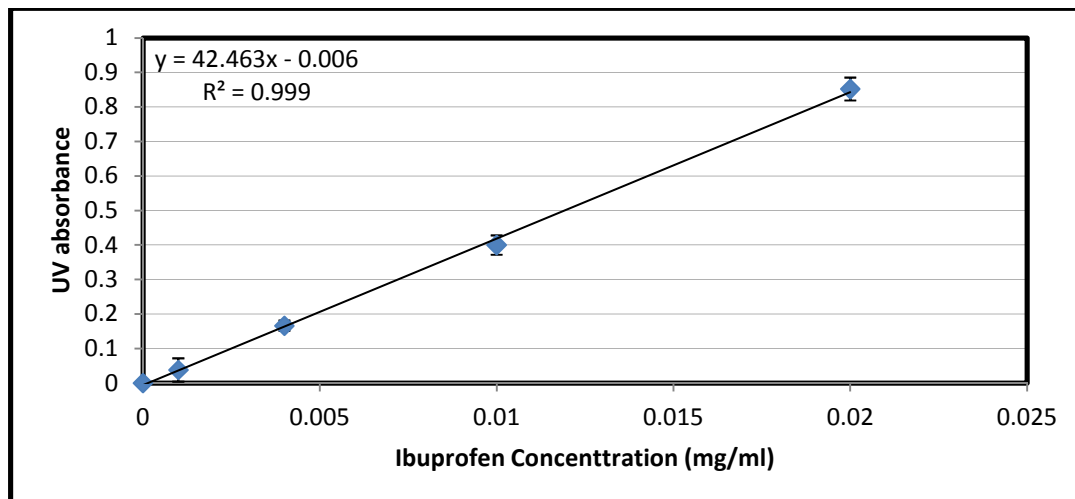


**Figure 5.3: Chromatogram of ibuprofen in acetonitrile: deionized water: phosphoric acid (50:50:1, (v/v)) mobile phase at flow rate of 1ml/min detected at 225 nm**

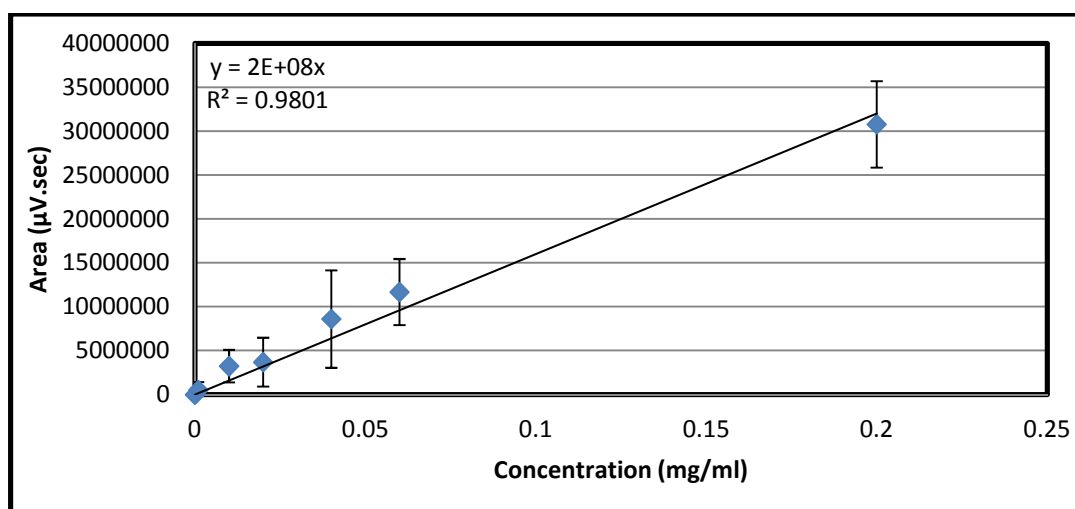
#### 5.2.1.3.1 Preparation of calibration standard

Calibration standard serves as an indication of the linear correlation between absorbance and drug concentration over the required range, in which the wavelength of maximum absorbance can be determined. Hence, a series of drug solutions were prepared with suitable concentrations using phosphate buffer (pH 7.2) and scanned from 200 to 400 nm using UV spectrophotometer (PerkinElmer, Lambda XLS) to detect  $\lambda_{\text{max}}$ , at which ibuprofen showed the maximum absorbance and it was 223 nm. Phosphate buffer solution (pH 7.2) was used as analytical blank to zero the spectrophotometer prior each measurement. Consequently a calibration curve was constructed, as shown in Figure 5.4, to perform necessary calculations of the drug amount released or dissolved in different samples. In addition to that, a calibration curve by HPLC was constructed through preparation of series of drug solutions with suitable concentrations using the mobile phase that was set to flow at a rate of 1ml/min wherein the elution was monitored at 225 nm (Figure 5.5). As indicated by the regression equations in Figure 5.4 and 5.5, these calibration standards had good correlations between the studied drug concentrations and responses (UV absorbance or area under the retention

peak of ibuprofen) as detected by the used method in UV spectrophotometer or HPLC, respectively.



**Figure 5.4:** Calibration curve of ibuprofen in phosphate buffer solution (pH 7.2) measured at 223 nm



**Figure 5.5:** Calibration curve of ibuprofen by HPLC measured at 225 nm, flow rate of 1ml/min and using acetonitrile: deionized water: phosphoric acid (50:50:1, (v/v)) mobile phase



#### 5.2.1.3.2 Measurements of drug content

Each tested batch of the different formulations was assayed for the ibuprofen content prior to each *in vitro* release and permeation study. Approximately 450 mg sample of the films were dissolved with 50 ml of methanol with 0.4 ml phenolphthalein solution. The resultant solution was titrated with 0.1M sodium hydroxide until a faint pink colour obtained (end-point). The volume of the titre (0.1M NaOH) used to produce this colour change was corrected by means of a blank titration, which alternatively was performed each time and consumed 0.1-0.2 ml of the titre volume. The calculations of the content of each sample was conducted on the basis that each ml of 0.1M sodium hydroxide is equivalent to 20.63 mg of  $C_{13}H_{18}O_2$  (British Pharmacopoeia Commission, 2010) and the titration was repeated three times.

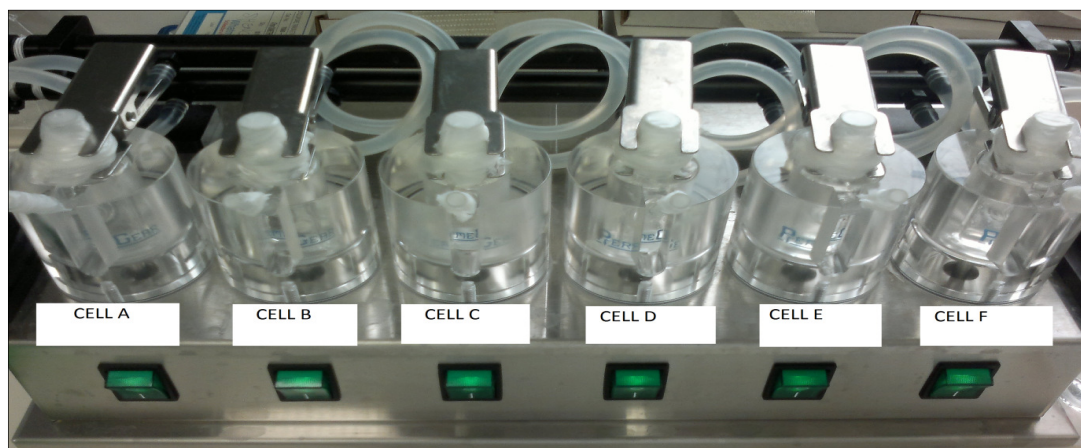
#### 5.2.2 *In vitro* permeation (diffusion) studies

*In vitro* drug permeation testing is an important tool for the characterisation of transdermal systems and has been shown, in some cases, to provide a good correlation with biological response. Thus, it can be used as a surrogate option for *in vivo* studies which are often expensive to perform and obtaining ethical approval can be limiting for their progress (Pellet et al., 1997a). In order to empower this correlation (*in vitro/in vivo*), it is recommended to design the experiment with *in vitro* conditions that mimic or simulate anatomical site and physiological conditions at the site of application, such as the skin for topical and transdermal drug delivery systems (TDDS), and site of drug release, such as systemic circulation for TDDS, and in other words, to model *in vivo* performance i.e. bioavailability.

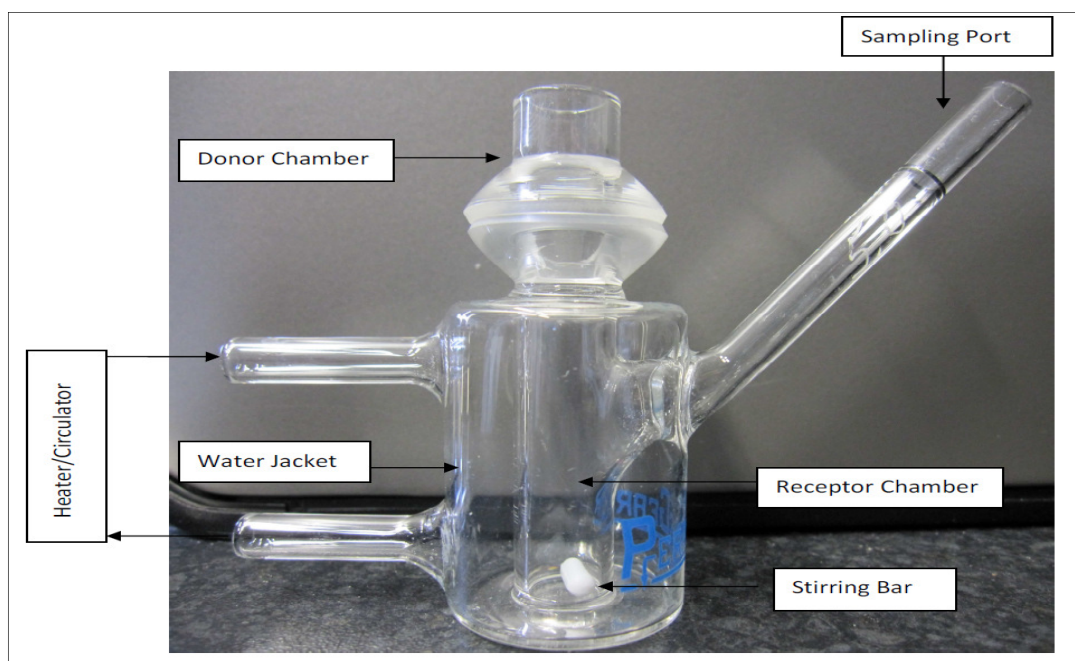
A Franz Cell diffusion system composed of six diffusion cells with identical characteristics were used to measure the release of ibuprofen from different formulae through silicone membranes (Figure 5.6). Jacketed Franz cells were connected to a water bath maintained at 37°C as depicted in Figure 5.7. However, the measured temperature in the donor chambers was approximately 32±1°C, mimicking normal skin temperature (Green et al., 1979). The receptor chambers were filled with 5ml phosphate buffer (pH 7.2). The silicone membranes (SSP®, 102 µm thickness) were cut into suitable sizes to cover the diffusion areas of the diffusion cells (0.7854 cm<sup>2</sup>), and were placed between donor and receptor chambers. Silicone membranes were selected because of their rate limiting characteristics akin to those of skin (Pellett et al., 1997b). These membranes were soaked previously in isopropyl myristate (IPM) for 1 hour, because the latter has bipolar properties that tend to mimic the



biochemical composition of the skin (Megrab et al., 1995a; Raghavan et al., 2000). Therefore, they can be used as skin model membranes.



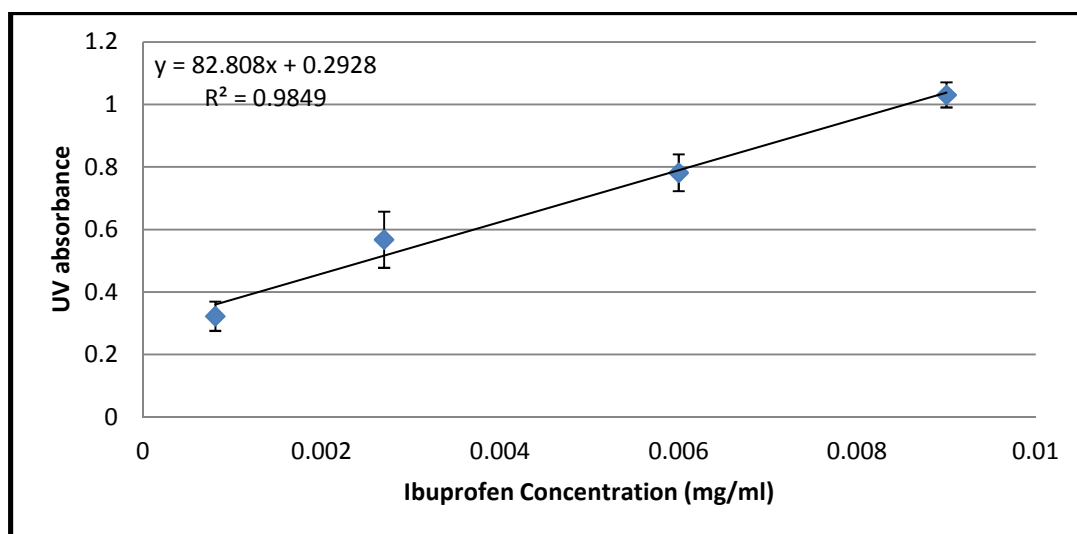
**Figure 5.6:** A 6-station PermeGear Franz Cell diffusion system with a V-Series magnetic stirrer



**Figure 5.7:** Compartments of a 9mm jacketed vertical Franz Cell (PermeGear) with a 5ml receptor volume

Eudragit RS PO hot melt extruded films loaded with ibuprofen at different levels (10-40% w/w) were tested. Each sample had approximate dimensions of 6mmx4mmx1mm (length, diameter, thickness) and weighed out individually before loading using a XS205 dual range analytical balance (Mettler Toledo). Details of the preparation process have been given in previous chapter and each batch was assayed prior testing (see section 5. 2.1.3.2). The donor chambers of the Franz system were secured by the clamps and the tested samples were placed on the top of the silicone membranes. The sampling ports and the donor chambers were covered with double layers of Parafilm® to minimise evaporation from the openings. The receptor solution was maintained in sink conditions with respect to the drug and stirred at a fixed speed of 500 revolutions per minute. Aliquots of 0.2 ml were taken of the receptor phase, at specified time intervals, and evaluated spectrophotometrically at a wavelength of 223 nm that was unaffected by other components that might be released together with the drug (section 5.2.1.3.1). To best characterise the permeation properties of ibuprofen in the used experiment design without vehicle influence i.e. Eudragit RS PO, a saturated solution of ibuprofen in PBS medium (pH 7.2) was run in a similar procedure to the extruded films using a volume of 0.3 ml to fill the donor chamber.

Extruded samples with the highest drug loading and showed best physical stability after storage at 0%RH/25°C for one month were around 30%w/w drug loading (see Chapter 4). These samples can be considered the prototype to deliver high doses of ibuprofen and thus, in like manner to the *in vitro* release studies, the permeation studies were used as a quality control tool to indicate if any deviation of the permeation profiles of these aged samples from those obtained immediately after fabrication. Cumulative percentage drug permeated was established for each test set of not less than three tested samples. At the end of each permeation experiment, the silicone membranes were immersed for 36 hours in 10 ml diethyl ether under constant stirring (200 rpm) at room temperature to extract the drug in case it was deposited or retained in these membranes. The extraction solutions were filtered through 0.45 µm membrane filters (HT Tuffryn® membranes, Acrodisc® syringe filters), and the filtrates were suitably diluted and analyzed using UV spectrophotometer at 222 nm (PerkinElmer, Lambda XLS) wherein a calibration standard was constructed in the same manner as detailed in section 5.2.1.3.1, using series of ibuprofen solutions prepared with suitable concentrations in diethyl ether (Figure 5.8).



**Figure 5.8: Calibration curve of ibuprofen in diethyl ether measured at 222 nm**

### 5.2.3 Modelling of *in vitro* permeation profiles

One important element for the scientific development of any new solid dosage is to recognize the manner by which the drug is dissolved or released from that pharmaceutical delivery system, hence its applicability for the intended use. This is usually described by kinetic models in which the dissolved /released amount of the drug is a function of the test time. The drug release from a polymeric matrix-type transdermal film can be defined as the process of the exposure of drug solutes from the polymeric system to the release medium. This might be a simple definition of a more complex process, in which many factors can contribute to the drug release kinetics. For example, drug crystallinity, particle size and solubility, the structural properties of the polymeric system, and the release environment (Grassi and Grassi, 2005).

In this work, the principal mechanism of ibuprofen release will be elucidated as a function of the *in vitro* kinetics of release and permeation of ibuprofen, chosen as model drug, from Eudragit RS PO hot melt extruded transdermal films (patches). The choice of the mathematical models was evaluated considering the most relevant and commonly used mathematical models to describe the TDDS. The curve fitting and thus the applicability of the kinetic models employed was judged using the linear correlation coefficient,  $R^2$ . The following models were employed to study the permeation (diffusion) profiles:

1. Zero order kinetics:

This model can be represented by the following equation:

$$\frac{W_t}{W_\infty} = K^\circ t \quad (\text{Eq.5.2})$$

In this relation, the plotted fraction of the dissolved/released drug ( $\frac{W_t}{W_\infty}$ ) against time (t) will be linear as the same amount of the drug is released within a unit of time.  $K^\circ$  is the zero order release constant. This pattern of release is, in theory, the method of choice to achieve a steady-state release for a prolonged pharmacological action (Costa and Lobo, 2001).

2. First order kinetics:

This model can be expressed by the following relation:

$$\frac{W_t}{W_\infty} = 1 - e^{-K_1 t} \quad (\text{Eq.5.3})$$

The drug released amount is assumed to follow exponential decline over time, manifesting a decrease in rate with time. Hence, a graphic of natural logarithm of the fraction of the drug to be released ( $1 - (\frac{W_t}{W_\infty})$ ) versus time (t) will be linear.  $K_1$  is the first order release constant.

### 3. Higuchi model (Square Root Law):

This model in its simplified form can be described in the following manner:

$$\frac{W_t}{W_\infty} = K_H t^{1/2} \quad (\text{Eq.5.4})$$

where the fraction of dissolved/released drug ( $\frac{W_t}{W_\infty}$ ) is a linear function of square root of time ( $t^{1/2}$ ), if the release process is diffusion dependent.  $K_H$  is the Higuchi release constant. This equation is valid with the assumptions that the diffusivity of the drug is constant during the release and the polymer system(s) should not dissolve or swell when exposed to the release medium (Perrie and Rades, 2010).

### 4. Korsmeyer-Peppas model (Power Law):

This model is commonly used for pharmaceutical polymeric dosage forms to have insight into a multi or even unknown release mechanism(s). Korsmeyer et al. (1983) derive the following equation:

$$\frac{W_t}{W_\infty} = a t^n \quad (\text{Eq.5.5})$$

This equation describes systems with Fickian (diffusion controlled) and Non-Fickian (anomalous) behaviour, where (a) is a constant incorporating the properties of the macromolecular polymeric systems and the drug (Reza et al., 2003) and (n), known as the release exponent, is used to characterise different kinetics and release mechanisms as follows:

1. If the diffusion is the main drug release mechanism,  $n=0.5$ .
2. Anomalous transport will be followed for system of n values between 0.5 and 1.0, as well as for low values of n ( $n < 0.5$ ) as reported by Gao (2011). This case is usually associated with the drug release that is governed by both diffusion and swelling (Perrie and Rades, 2010).
3. Case-II transport, which is assumed to be mainly swelling controlled release, will have a value of  $n=1.0$ .
4. Values of n higher than 1.0 will describe a super case-II transport, which is controlled by the swelling and relaxation of the polymer(s).

However,  $n$  value will depend on the geometry of the studied system. The above proposed mechanisms will fit with slab or plane sheets, whereas in case of cylinder-shape system  $n = 0.45$  instead of 0.5 and 0.89 instead of 1. For spheres,  $n$  will be 0.43 instead of 0.5 and 0.85 instead of 1. In addition to that, this value can be used to express the kinetics of the release mechanisms as shown in Table 5.1. It is important to mention that determination of the exponent  $n$  should be based on the first 60% of the fractional release (Ritger and Peppas 1987), although Rinaki et al. (2003) suggested the applicability of this model to the whole drug release profile. This model can be useful as well to validate the applicability of Higuchi models, which holds only for system controlled by pure diffusion mechanism. These models can aid understanding the release mechanism of the embedded drug and will potentially allow the operator to identify if that mechanism will vary from different systems according to the composition or the conditions of the application. If the kinetics of these systems vary, they still can be compared in a non-model approach, such as the time necessary to the release of higher than or equal to 80% of the drug, ( $t \geq 80\%$ ).

Release Exponent ( $n$ )	Rate as a function of time
0.5	$t^{-0.5}$
$0.5 < n < 1.0$	$t^{n-1}$
1.0	Zero order release
Higher than 1.0	$t^{n-1}$

**Table 5.1: Expected release rate kinetics according to the power model (Korsmeyer et al., 1983)**

### 5.3 Results and discussion

The saturated solubility of ibuprofen in the phosphate buffer solution (pH 7.2) at 37°C was determined as  $4.49 \pm 0.29$  mg/ml. This value correlated relatively well with the reported value of  $3.74 \pm 0.14$  mg/ml obtained by Dabbagh and Taghipour (2007). Accordingly the weight of drug used in the *in vitro* release/dissolution experiments and for permeation studies could be considered to represent sink conditions. Table 5.2 lists the assayed drug loadings of different formulations, which reflected a good loading efficiency. The percent loading efficiency is defined as the experimental drug loading over the theoretical value expressed as a percentage. Therefore, it could be inferred that possible drug loss during preparation of the formulation was minimal and therefore will not be expected to account for less than 100% *in vitro* release or permeation profiles of the tested films.

Drug loading (Theoretical)	Drug loading (Actual)	Drug loading efficiency
(w/w %)	±SD* (w/w %)	± SD* (%)
10	9.93±0.26	99.33±2.65
20	19.87±0.26	99.33±1.32
30	29.80±0.46	99.33±1.53
40	39.27±0.26	98.18±0.66

**Table 5.2: Calculated (actual) percent drug loadings of hot melt extruded samples of Eudragit RS PO at different ibuprofen loadings and loading efficiencies using hot melt extrusion technique. \*Average ± S.D. of three determinations has been reported**

### 5.3.1 *In vitro* release studies

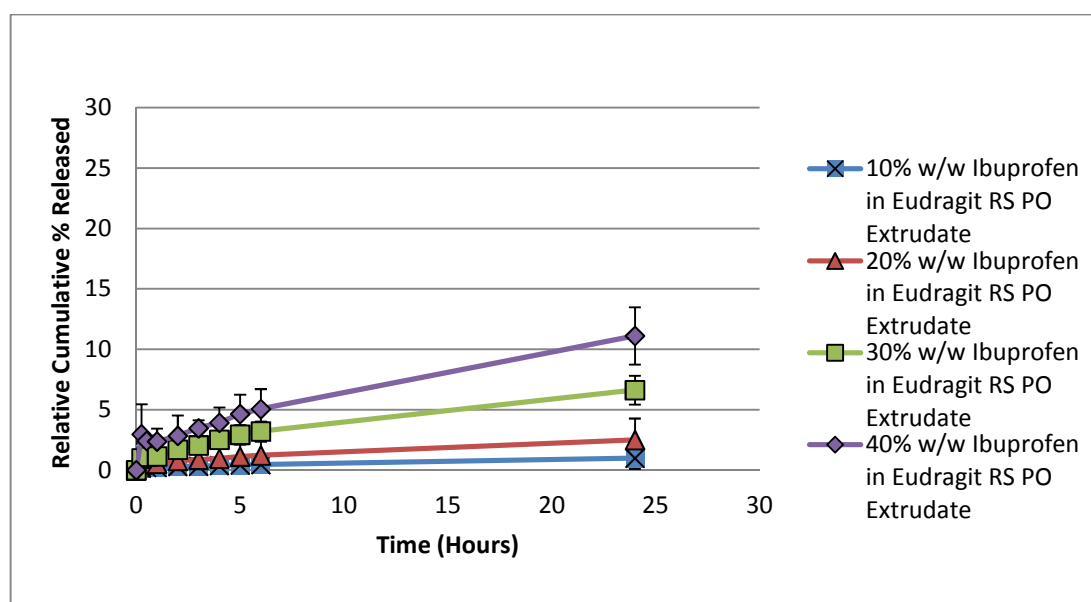
Hot melt extruded films of ibuprofen at different loadings in Eudragit RS PO were evaluated for their release behaviour over 24 hours. The release studies were performed for freshly prepared films up to 40%w/w drug loading, which represents the supersaturation level of ibuprofen in Eudragit RS PO extrudates (Chapter 4). The drug release quantification was performed using HPLC, to ensure that only ibuprofen is considered in the measurements and that no degradation products are interfering with the detection signal. These values were then compared to the UV absorbance values obtained spectrophotometrically, which showed no significant difference (data not shown) and thus UV data were adapted for the remainder of the study.

*In vitro* cumulative percent ibuprofen released from the extruded films increased as a function of increased drug loading as shown in Figure 5.9. The following formula was used to calculate the relative cumulative percent drug released (RCDR %) of the extruded formulations for each drug loading:

$$\text{RCDR \% at time (n)} = \frac{\text{Cumulative percent drug released at time (n)}}{\text{Drug loading percentage}} \times 100 \quad (\text{Eq.5.6})$$



The amount of ibuprofen released (expressed as cumulative percentage drug release) from these extruded films increased with the increase of drug loading. However, all the tested formulations with different drug loadings were associated with slow rate and poor release (Figure 5.9). This low percentage of drug release can be ascribed to the thermal treatment of the water-swellable Eudragit RS PO during extrusion. Azmari et al. (2005) and Hasanzadeh et al. (2009) found that drug release can be retarded from Eudragit RS matrix when it is thermally treated to temperatures above its glass transition temperature ( $53.3 \pm 0.5^\circ\text{C}$ , Chapter 3) possibly due to rearrangement of its network into more coalesced structure as indicated from less porous matrix. Hence, this is believed to create extra physiological stress needed to be broken prior drug release.

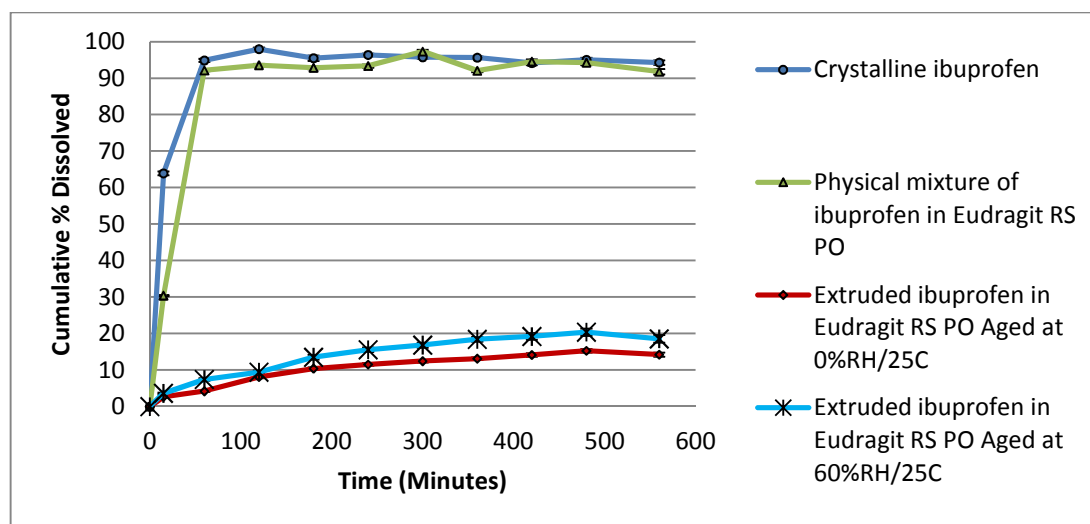


**Figure 5.9: Comparative release profiles of ibuprofen from hot melt extruded films at different drug loadings in phosphate buffer solution (pH 7.2) at  $37.0 \pm 0.1^\circ\text{C}$ . Each data point represents the mean  $\pm$  S.D. of three measurements**

Extrudate with a drug load of 10% w/w represents the equilibrium saturation solubility of ibuprofen in Eudragit RS PO after one month of incubation under ambient conditions of 60%RH/25°C (Chapter 4). Therefore, water coexists in its structure under these conditions without affecting the physical stability. As seen in Figure 5.10, these extruded films with only 1.14% (w/w) water content showed higher amount of dissolved ibuprofen in the dissolution medium compared to those aged for the same duration but at dry conditions (0%RH/25°C). This might indicate a possible role of water in this release enhancement, though not significant (~5% increase in the cumulative amount of the dissolved drug). This

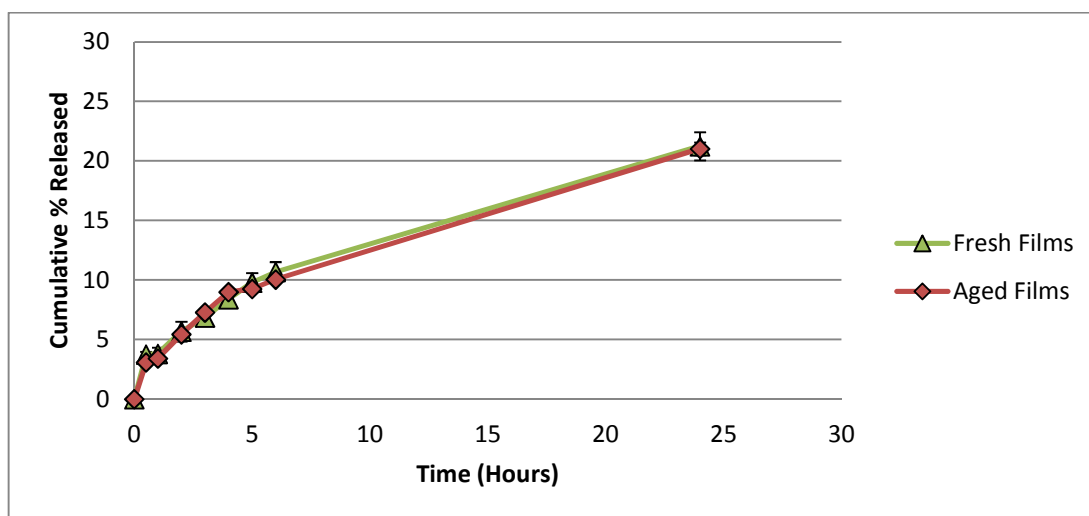


may suggest that the drug remained entrapped in extruded films can be liberated using advents that improve its partitioning into the elution medium to achieve a reasonable rate and extent of release. It was also noticed that these formulations provided retarded release pattern compared to the fast immediate dissolution profiles of crystalline ibuprofen and equivalent physical mixture.



**Figure 5.10: Comparative dissolution profiles of ibuprofen from crystalline drug, physical mixture and Eudragit RS PO-based extrudate at 10% w/w drug load in phosphate buffer solution (pH 7.2) at  $37.0\pm0.1^{\circ}\text{C}$ . Each data point represents the  $\text{mean}\pm\text{S.D.}$  of three measurements**

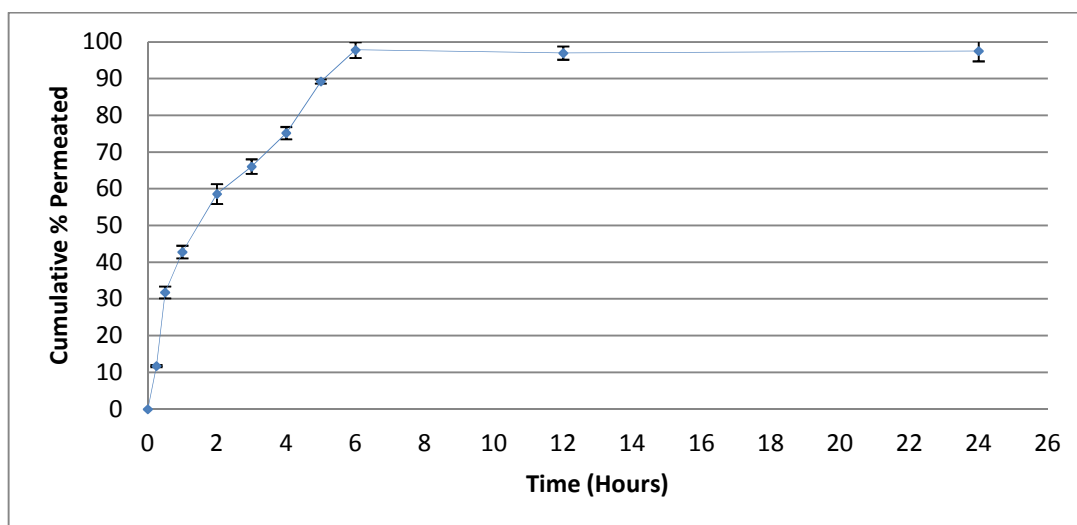
As the ibuprofen release was found to be a function of drug loading for these extruded films, it is recommended to continue the development stages of these systems with the films at high drug content that lie within solubility limits of the ibuprofen in the Eudragit RS PO matrices. Therefore, films at 30% w/w drug loading were selected and investigated for their proposed physical stability (Chapter 4) in terms of any potential change in their *in vitro* release profiles. As depicted in Figure 5.11, the films aged for one month at 0%RH/25°C showed superimposable release profiles to the ones tested on freshly basis, supporting their physical stability.



**Figure 5.11: Comparative release profiles of ibuprofen from Eudragit RS PO extruded films at 30% w/w drug load tested on freshly basis (Fresh) and after ageing for one month at 0%RH/25°C (Aged) in phosphate buffer solution (pH 7.2) at 37.0±0.1°C. Each data point represents the mean±S.D. of three measurements**

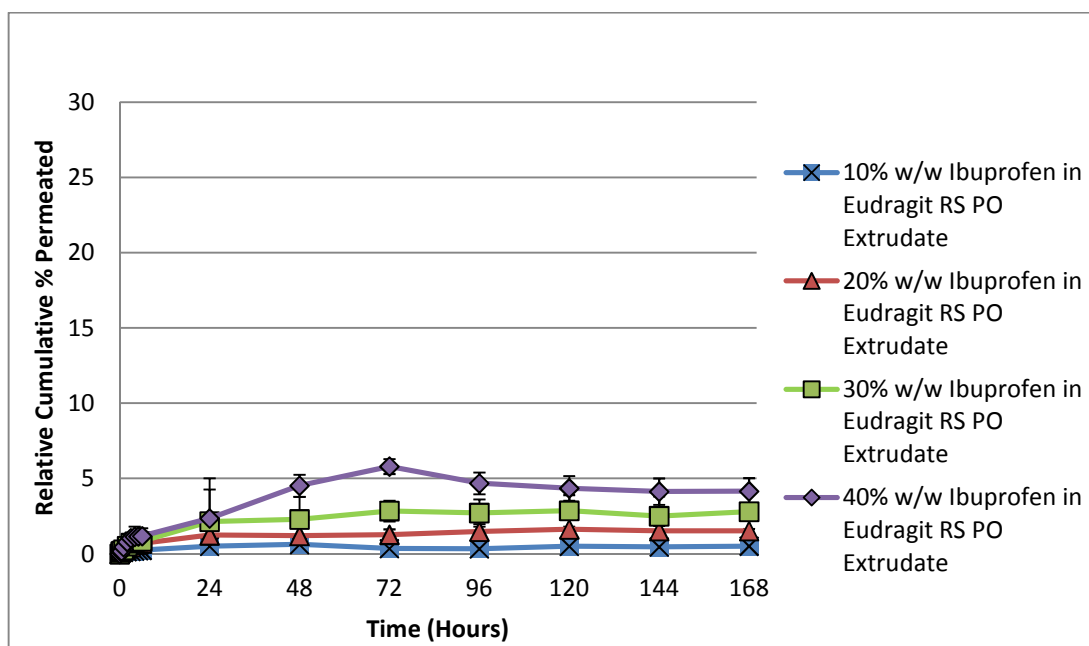
### 5.3.2 *In vitro* permeation (diffusion) studies

For skin-mimicking membranes such as the silicone-based membranes used here, it is appropriate to ask to what extent these membranes control the drug permeation. This is important as unnecessary proliferation of method design or formulation fabrication can be avoided if the drug physicochemical properties limited or prevented its diffusion across these membranes. Therefore, saturated solutions of ibuprofen in PBS (pH 7.2) were examined and, as shown in Figure 5.12, the permeation of the total amount of the ibuprofen was almost completed after 6 hours with circa 97.8% cumulative percent permeation. This indicates that ibuprofen diffusion *per se* across the silicone membrane does not necessitate permeation enhancement.



**Figure 5.12: Diffusion profile of ibuprofen from saturated solutions in phosphate buffer solution (pH=7.2) tested approximately at 32°C and permeated across silicone membrane into phosphate buffer solution (pH=7.2) at 37°C. Each data point represents the mean $\pm$ S.D. of three measurements**

For the extruded films tested in the permeation experiments we have two interfaces, the extrudate-membrane interface and the membrane-receptor solution interface. Therefore, the ibuprofen molecules have to get out from the extruded films into the silicone membrane. Thereafter the molecules will be available to partition into the second interface and dissolve in the receptor phase. In Figure 5.13, the hot melt extruded films of ibuprofen in Eudragit RS PO showed poor penetration into the receptor phase. This was predicted as the release was limited by the extrudates themselves as indicated earlier in the *in vitro* release studies. Again, data here came to confirm that the drug release with subsequent measured permeation is a function of drug loading. Relative percent of drug permeated was calculated using Formula (5.6). Drug recovered from retention in the silicone membranes after the diffusion experiment was less than 0.5 mg for all tested films at different ibuprofen loading as indicated in Table 5.3. This implies that certain amount of the drug was needed to equilibrate with the membranes, and such disposition could impart, though not mainly, in the observed low percent of ibuprofen permeation.



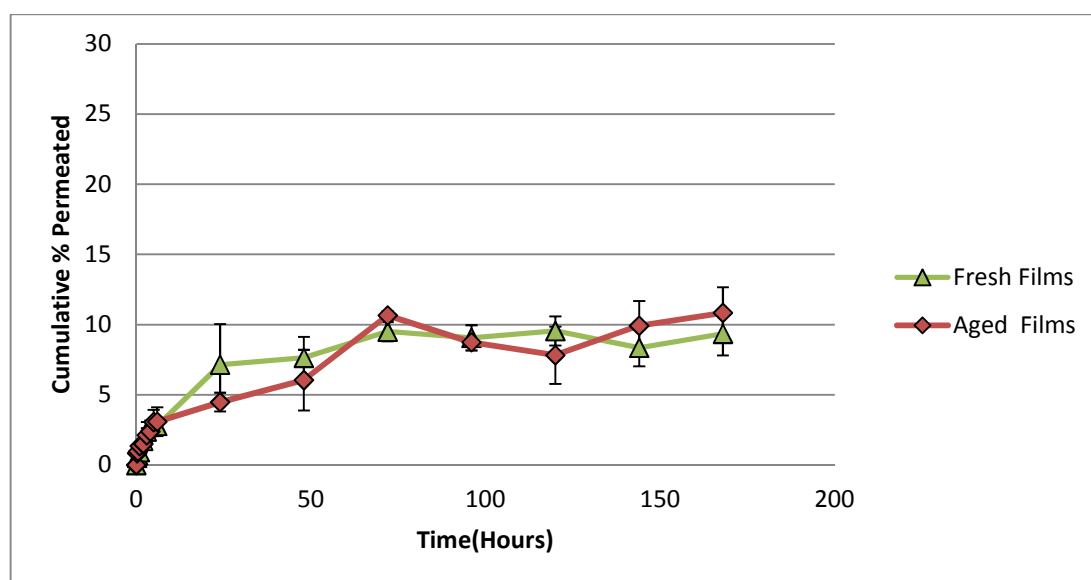
**Figure 5.13: Comparative diffusion profiles of ibuprofen from hot melt extruded films with Eudragit RS PO tested approximately at 32°C and permeated across silicone membrane into phosphate buffer solution (pH=7.2) at 37°C. Each data point represents the mean±S.D. of no less than three measurements**

Drug loading (w/w%)	Amount recovered (mg)*	Percentage of the drug recovered in relative to the loaded dose (%)*
10	0.27±0.01	12.44±0.31
20	0.30±0.13	6.93±0.67
30	0.36±0.04	5.54±0.38
40	0.38±0.34	4.43±0.45

**Table 5.3: Quantification of the drug recovered in the silicone membranes after the end of the permeation experiments (over seven days) for examined Eudragit RS PO extruded films formulated with different ibuprofen loadings. \*Average ± S.D. of three determinations has been reported**

In a diffusion experiment, the test duration is usually set to achieve 85% of the drug permeation or until the plateau is reached. Therefore, the experiments were extended over seven days until a plateau was reached. However, overall drug released and permeated were low. Therefore, these films can be used but with modulation appropriate to deliver ibuprofen, which is used in high doses (200-800 mg every 4-6 hours). Thus, modifications

can be applied to enhance drug release in reasonable amounts. In order to achieve that, a prototype is needed. As shown in the *in vitro* release assessment section, 30% w/w drug loaded formulation appears to be the most suitable choice as a prototype at this stage. A further permeation experiment of the aged films at this drug loading was conducted to check if the performance of these films will keep up as the fresh samples, in terms of the *in vitro* permeation behaviour. The diffusion profiles of the aged samples were approximately the same as fresh samples after seven days, with mean deviations less than 2% between the two observed profiles (Figure 5.14), indicating good physical stability under the used ageing conditions which supported previous findings of the same in the previous chapter and section herein.



**Figure 5.14: Comparative diffusion profiles of ibuprofen from Eudragit RS PO-based extrudates at 30% (w/w) drug loading (fresh vs. aged samples stored for one month at 0%RH/25°C), tested approximately at 32°C and permeated across silicone membrane into phosphate buffer solution (pH=7.2) at 37°C**

### 5.3.3 *In vitro* permeation studies model fitting

Through interpretation of the kinetics of drug release from the studied systems, the release mechanism can be explained. Data of the *in vitro* permeation was fitted to the zero-order equation, the first-order equation and the Higuchi and Korsemeyer-Peppas (power) models. The correlation coefficients of different applied mathematical models are included in Table 5.4. On the basis that the higher the correlation coefficient the better the model, the first

order equation was most suitable to explain the observed profiles. The power model also fitted these profiles well, predicting anomalous transport of the ibuprofen from the matrices. This indicates that a combination of diffusion and swelling are the possible dominant mechanisms to control the drug release from these systems.

(A)

Used Kinetic model	First order model	Zero order model	Higuchi square-root of time model
Drug loading of the tested samples (w/w%)	$R^2$	$R^2$	$R^2$
10	0.9870	0.6277	0.8200
20	0.9653	0.7373	0.9004
30	0.9805	0.7382	0.8997
30 (Aged)	0.9426	0.8638	0.9466
40	0.9695	0.7707	0.9501

(B)

Kinetic model		Korsmeyer-Peppas model (Power law)	
Drug loading of the tested samples (w/w%)	$R^2$	Release exponent (n)	Expected release mechanism
10	0.9457	0.36	Anomalous transport
20	0.9498	0.39	Anomalous transport
30	0.9591	0.46	Anomalous transport
30 (Aged)	0.9816	0.41	Anomalous transport
40	0.9548	0.55	Anomalous transport

**Table 5.4: (A) Fit correlation coefficients ( $R^2$ ) of different applied kinetic models and (B) possible interpretation of the measured release exponents from the power law model and their correlation coefficients ( $R^2$ ), both for the permeation profiles of ibuprofen formulated with different levels (loads) in hot melt extruded Eudragit RS PO films. Aged samples under 0%RH/25°C for one month with 30 % (w/w) drug loading were also evaluated**

## 5.4 Conclusions

The potential of Eudragit RS PO based hot melt extruded films to deliver ibuprofen at a reasonable rate and extent is yet to be achieved. Characterisation of the *in vitro* release properties of these films showed a low release from these films due to possible coalescence of the used Eudragit RS PO matrices after thermal treatment using hot melt extrusion technology. The release found to be dependent on the drug load and water inclusion in these films might facilitate drug liberation. Thus, adjustments of these formulations to achieve desired release may involve judicious choice of hydrophilic components, enabling fluid access into these extruded films. With respect to the *in vitro* permeation behaviour, the controlling (retarding) role of the Eudragit RS PO matrices on the drug permeation was evident in comparison to the diffusion of the ibuprofen from its saturated solution across the silicone membranes. Films at 30% w/w drug loading were chosen as a prototype to introduce further advents to optimise and establish usefulness of these formulations. Good physical stability of these films addressed in Chapter 4 was shown here as comparable *in vitro* release and *in vitro* permeation profiles between aged samples under dry conditions for one month and fresh samples. By fitting the *in vitro* permeation data of all the tested films into zero order, first order, Higuchi and power model, it was concluded that the ibuprofen release from Eudragit RS PO films followed first order kinetics and was diffusion and swelling mediated. Both *in vitro* release/dissolution and *in vitro* permeation studies aided in better understanding of the release of the ibuprofen from the tested films and directed the need of modification.

**Chapter 6: The effect of variation of design parameters on the release and permeation properties of ibuprofen from hot melt extruded carriers**



## 6.1 Introduction

In the previous chapter the performance of the developed Eudragit RS PO extruded matrices with ibuprofen was discussed. In spite of their promising properties in terms of solubility and stability, problems related to retarded release and concomitantly poor permeation profiles were encountered. These ‘poor’ profiles can limit the efficiency to deliver non-potent active substances such as ibuprofen, whereby higher doses are needed to achieve therapeutic levels. However, these systems present a viable option to deliver drug transdermally if the challenge of delivering sufficient amounts of the ibuprofen can be met. Therefore, this chapter aims to realize the potential of using these systems through investigation of some enhancement techniques through variation of design parameters. Section 6.2 details the first design parameter based on drug/carrier optimisation through introduction of various classes of hydrophilic polymers, in particular considering processability, solid state characteristics, *in vitro* release and permeation profiles. Section 6.3 explores hydration as another design parameter and the use of this enhancement strategy for selected vehicles to attain optimal drug permeability.

## 6.2 Effects of vehicle formulations

The previous chapter indicated that Eudragit RS PO matrices, when extruded with ibuprofen, provide a controlling role that influences the rate and amount of ibuprofen release, although optimisation is needed to achieve the desired release of the drug. Therefore, this section is devoted to discuss the formulation influence on the *in vitro* ibuprofen release and permeation from modified hot melt extruded films (matrix-type patches).

### 6.2.1 Methodology

Physical mixtures of the drug and the carrier blend of Eudragit and other hydrophilic excipients were prepared by simple mixing in a pestle and mortar. The mixes were fed into a co-rotating twin screw extruder (Haake Minilab II Micro Compounder) equipped with a sheet-shaped die. Determination of the minimum ratio between these components was based on 30% w/w ibuprofen loading, which represents the solubility limit of this drug in the parent polymer i.e. Eudragit RS PO. Each batch size was formulated with total weight of 10 grams. Temperatures of 90-100°C from the feed to the die end were used according to the formulation prepared and a screw speed was set at 100 rpm for four minutes, which was

found to be suitable for the extrusion of these mixtures. The resultant extruded films were cooled along a customised conveyer belt to room temperature, where the melts spread out over aluminium foil. These films were separated into unit doses of roughly equal size (approximately 24 mm<sup>3</sup>). The films were measured for thickness using a Vernier caliper. The films were stored between aluminium sheets, except for the ones containing Gelucire® 44/14, which were stored between silicone sheets due to their high stickiness. The films were labelled and stored in desiccators at room temperature until further evaluations.

The extrudable mixtures obtained as described above were characterised using techniques of MTDSC, PXRD and SEM and compared when appropriate with the equivalent physical mixes. These experiments were the same as detailed in Chapter 3. The *in vitro* drug release experiment (dissolution test) and *in vitro* permeation studies were also carried out for the selected optimised formulations in the same procedure described in Chapter 5. Ibuprofen retained in the silicone membranes in permeation studies was extracted with diethylether as detailed in Chapter 5. Each membrane was placed in 10 ml diethylether, stirred at 200 rpm for 36 hours. The extraction solutions were filtered through 0.45µm membrane filters (Acrodisc® syringe filters), and the filtrates were suitably diluted and analyzed using UV spectrophotometer at 222 nm (PerkinElmer, Lambda XLS). All the reported values were measured as mean±S.D (n=3) unless otherwise mentioned in the relevant section.

## 6.2.2 Results and discussion

### 6.2.2.1 Fabrication and development of hot melt extruded Eudragit RS PO-based films loaded with ibuprofen and intended for transdermal drug delivery

In the initial part of this investigation, the key consideration was the addition of a third excipient, with hydrophilic properties to modify drug release, to the Eudragit RS PO and ibuprofen, which could be extruded effectively. Therefore, it is reasonable at this stage to aim for the necessary adjustments on the ratios of these excipients (modifiers) that will permit processing with acceptable yield characteristics, these being flexibility without high fluidity and suitable robustness of the cooled product. The scope of the specifications for the use of these excipients for transdermal drug delivery system and their thermal stability for extrusion process were covered in Chapter 2 and Chapter 3, respectively.



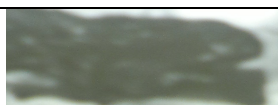


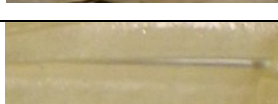

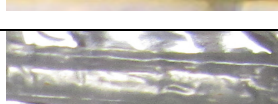



Among the key factors that were considered relating to the processing, the extrusion temperature was of principal interest with its subsequent influence on acceptable torque values that permits efficient material transfer towards the outlet of the extruder. During the extrusion process, the system needs to be at the minimum temperature that is required to allow rotation of the screws; inclusion of a plasticizer can further improve processing conditions *via* reducing the torque needed. Because ibuprofen can be an efficient plasticizer (Kidokoro et al., 2001), it is expected to enhance the processability and film flexibility. As illustrated in Table 6.1, temperatures of 90-100°C were found to be suitable to perform extrusion of the combinations studied with average torque values range between 5-26 Ncm, except for formula with the code of FM4 (high level of methylcellulose), whereby a torque value of  $150 \pm 5$  (n=2) Ncm was required, indicating high viscosity. It is noteworthy that both Pluronic® F127 and Gelucire 44/14 melt at comparatively low temperatures (see Chapter 3) and showed low viscosities which collectively permitted their extrusion at 90°C.

Carrier system(s) with drug loading of 30% w/w	Carrier blend(s) (% w/w)	Extrusion temperature (°C)	Formula code
Eudragit RS PO	70	100	FM0 (Control)
Eudragit RS PO/ Sucrose ratios	60:10	100	FM1
	50:20	100	FM2
Eudragit RS PO/ Methyl cellulose ratios	60:10	100	FM3
	10:60	100	FM4
Eudragit RS PO/ Xantural® 75 ratios	60:10	100	FM5
	10:60	100	FM6
Eudragit RS PO/ Pluronic® F127 ratios	60:10	90	FM7
	50:20	90	FM8
Eudragit RS PO/ Gelucire 44/14 ratios	60:10	90	FM9
	50:20	90	FM10

**Table 6.1: Formulation and extrusion temperatures for hot melt extruded films of ibuprofen with different carriers**

The amount of modifier added to the parent polymer i.e. Eudragit RS PO to make the carrier blend for ibuprofen was selected at two levels for each system. The first level involved the addition of a relatively small amount of this excipient, in attempt not to affect established high miscibility of ibuprofen in Eudragit RS PO at the used drug loading (30%w/w). Therefore the carrier blend was formulated with the ibuprofen in a ratio of 1:6:3 (new material: Eudragit RS PO: ibuprofen). The second level, which is the higher amount of the excipient, is almost a complete step into exchange the Eudragit RS PO carrier system with the newly introduced material in a ratio of 6:1:3 (new material: Eudragit RS PO: ibuprofen). This strategy worked well only for methyl cellulose and Xantural® 75. The second level was not achievable in sucrose, Pluronic® F127 and Gelucire 44/14 as the extruded material was liquid and could not stream into the outlet. Thus the higher level possible was for a ratio of 2:5 of the new material (hydrophilic excipient): Eudragit RS PO and was only feasible with Gelucire 44/14 (FM10). Extrudates produced using sucrose (FM2) and Pluronic® F127 (FM8) at this high ratio lacked a definite shape and were difficult to collect and spread over the aluminium foil for a uniform film production as depicted in Table 6.2. Apart from these formulations (FM2, FM8), films listed in this table were considered as successful to move into the following stages of this study.

As shown in Table 6.2, films produced with Pluronic® F127 (FM7) and Gelucire 44/14 (FM9-FM10) were translucent clear strands similar to the control films, which contain only Eudragit RS PO and ibuprofen, coded as FM0. However, the films extruded with methyl cellulose were either golden clear extrudates (FM3) or like flat breads cream-coloured films (FM4). Yellowish extrudates were also produced with the formulations containing Xantural® 75, which appear to be translucent at FM5 composition and opaque in FM6 formula. These discolorations are believed to be related to the colour of the raw material of methylcellulose or Xantural® 75 which occur as yellowish-white powders. Their onset temperatures for decomposition as detailed in TGA measurements in Chapter 3 were far higher than the used extrusion temperature; therefore, they are not expected to degrade. The extruded films with sucrose, coded as FM1, exhibited an almost white colour as the melting of sucrose was not completed at the selected extrusion temperature, which was not increased in order to avoid ibuprofen degradation.

Carrier system(s) with drug loading of 30% w/w	Carrier blend(s) (% w/w)	Photos (macroscopic appearance)	Formula code
Eudragit RS PO	70		FM0 (Control)
Eudragit RS PO/ Sucrose ratios	60:10		FM1
	50:20		FM2
Eudragit RS PO/ Methyl cellulose ratios	60:10		FM3
	10:60		FM4
Eudragit RS PO/ Xantural® 75 ratios	60:10		FM5
	10:60		FM6
Eudragit RS PO/ Pluronic® F127 ratios	60:10		FM7
	50:20		FM8
Eudragit RS PO/ Gelucire 44/14 ratios	60:10		FM9
	50:20		FM10

**Table 6.2: Eudragit RS PO-based hot melt extruded films loaded with ibuprofen: composition and their visual appearance**

The visual examination and measured thickness of the successfully extruded films are described in Table 6.3. The level of stickiness or tackiness was assessed qualitatively by holding these films between thumb and index finger. Extruded films which contained Gelucire 44/14 were found to have the highest observed stickiness, whereas films containing Pluronic® F127, sucrose or low level of Xantural® 75 (FM5) showed medium stickiness profiles. This is an important feature to address, especially at the last steps of final product development, as “stickiness” would allow the film to adhere to the skin. Good adhesion of the patch to skin is a prime element for safety and efficiency of TDDS as detailed in Chapter 1.

Carrier system(s) with drug loading of 30% w/w	Carrier blend(s) (% w/w)	Formula code	Appearance	Thickness (±0.02mm)
Eudragit RS PO	70	FM0 (Control)	Smooth, no cracks, low stickiness.	1
Eudragit RS PO/ Sucrose ratio	60:10	FM1	Smooth, no cracks, medium stickiness.	1
Eudragit RS PO/ Methyl cellulose ratios	60:10	FM3	Rough, no cracks, low stickiness.	1
	10:60	FM4	Rough, cracked, no stickiness.	2
Eudragit RS PO/ Xantural® 75 ratios	60:10	FM5	Smooth, no cracks, medium stickiness.	1
	10:60	FM6	Smooth, sporadic cracks, low stickiness.	2
Eudragit RS PO/ Pluronic® F127 ratio	60:10	FM7	Smooth, no cracks, medium stickiness.	1
Eudragit RS PO/ Gelucire 44/14 ratios	60:10	FM9	Smooth, no cracks, high stickiness.	1
	50:20	FM10	Smooth, no cracks, high stickiness.	2

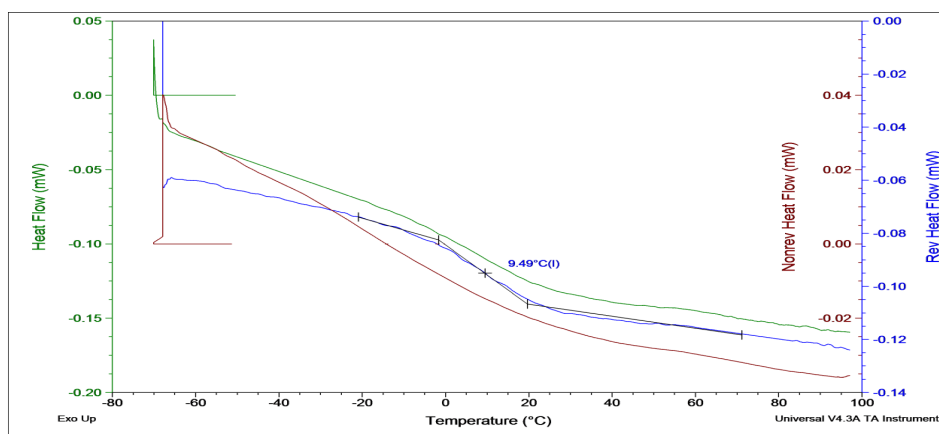
**Table 6.3: Overview of the descriptions of the Eudragit RS PO-based hot melt extruded films loaded with ibuprofen**

Furthermore, the film thicknesses with compositions of FM4 (high level of methylcellulose), FM6 (high level of Xantural® 75) and FM10 (high level of Gelucire 44/14) were higher than predicted as the extruded materials leaves the equipment through an orifice or die with an approximate opening of 1 mm, hence there is an expected film thickness of almost 1 mm. This could be explained by the die-swelling phenomenon sometimes encountered with the extrusion process (Zhang and McGinity, 1999). The material inside the extruder will be exposed to mechanical stress induced by rotating screws. Once it moves out the equipment, and depending on its viscoelastic properties, it may recover or swell with resultant increase in its thickness. Though this high thickness did not exceed 2 mm, an intervention was made to unify its value with other extrudates. Thus a roller was used to spread these films to approximate thickness of 1 mm. This was feasible only for FM6 and FM10 compositions as their extruded melt remained semisolid for appreciable time and were relatively easy to control, whereas FM4 films containing high level of methylcellulose were stiff (non elastic) and brittle, thereby limiting their adjustments.

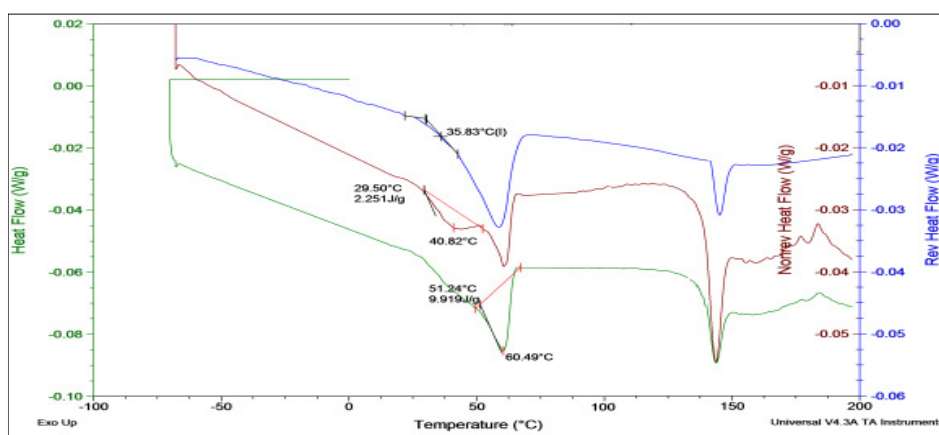
As part of the design, the second stage of this work focused on the ability of the acceptable extruded samples (i.e. extrudable from the first stage; see Table 6.3) to form soluble mixes, so the drug is dissolved in the solid state without phase separation. Therefore the phase behaviour of these extruded films was investigated through solid state characterisation using MTDSC and PXRD while the morphological features of these extrudates were assessed using SEM. Dealing with multi-component systems such as these extruded films necessitated the application of MTDSC, thereby enabling the deconvolution of complex and overlapping thermal events. In particular, the thermal events were complicated by water interactions, as observed in Chapter 3 for the raw materials owing to their hydrophilicity.

The MTDSC profiles of representative samples are shown from Figure 6.1 through to Figure 6.6. The reversing heat flow signals were used to assign the glass transition temperature (Midpoint-T<sub>g</sub>), whereas the melting endotherm was identified from the total heat flow signals. Crystallization and water dehydration were drawn from the non-reversing signals. The dehydration led to broad endothermic peaks over an approximate temperature range of 30 to 90°C, while crystallization was manifested as exothermic peak described in the relevant discussion. As shown in Figure 6.1, FM0 formula (Eudragit RS PO and ibuprofen) represents the control extruded sample that is characterised with a single glass transition temperature at 9.6±0.2°C, implying a one phase system. However, the addition of sucrose at the FM1 composition led to separation of ibuprofen, as demonstrated from the melting endotherm observed in these films (Figure 6.1). This endothermic peak was observed in both

reversing and total heat flow signals, confirming that it is related to ibuprofen melting rather than water loss. Nevertheless, the extent of separation is not complete, as the melting peak of the ibuprofen is depressed ( $T_{m \text{ (onset)}}$  at  $51.2 \pm 1.2^\circ\text{C}$ ) in comparison to the pure ibuprofen (Chapter 3,  $T_{m \text{ (onset)}}$   $75.7 \pm 0.2^\circ\text{C}$ ), indicating a possible involvement in a certain interaction or miscibility (Abdul-Fattah and Bhargava, 2002). This is supported by the recorded glass transition temperature of approximately  $35.6 \pm 0.3^\circ\text{C}$  ( $n=2$ ), which is lower than the reported  $T_g$  of Eudragit RS PO (Chapter 3,  $53.3 \pm 0.5^\circ\text{C}$ ), thereby representing the ibuprofen-Eudragit RS PO miscible phase as the sucrose is still crystalline due to extrusion temperature ( $100^\circ\text{C}$ ) far below its melting point (Chapter 3,  $T_{m \text{ (onset)}}$  at  $175.2 \pm 1.8^\circ\text{C}$ ), thus it is unlikely to be involved in this amorphous phase.



FM0

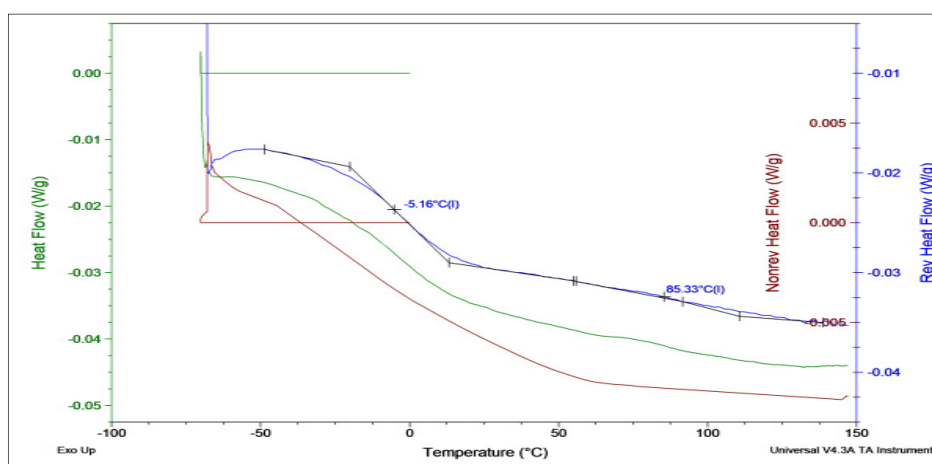


FM1

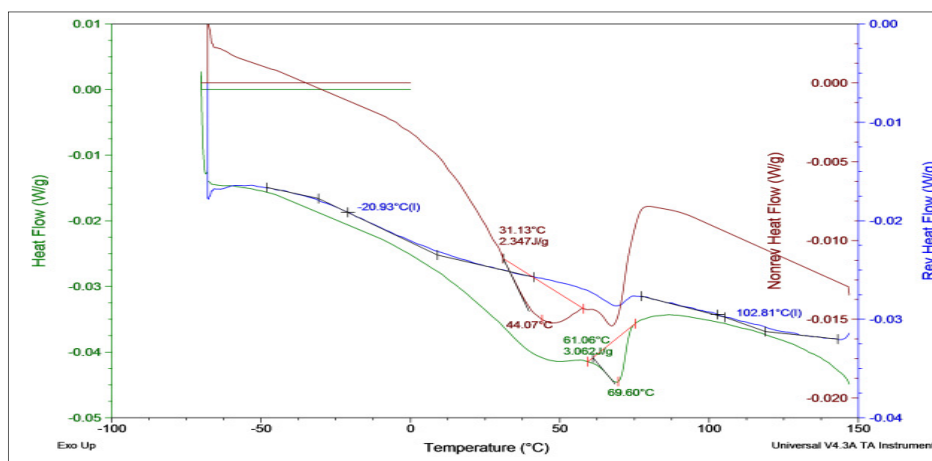
**Figure 6.1: MTDSC heating scans of different hot melt extruded films (see Table 6.3) in standard aluminium pans. Underlying scan rate of  $1^\circ\text{C min}^{-1}$  with a modulation amplitude of  $\pm 0.265^\circ\text{C}$  and a period of 100 seconds. The traces have been offset for clarity**



In Figure 6.2, the extruded system at FM3 composition (low level of methylcellulose) exhibited two amorphous phases. The first one was characterised with a low glass transition temperature (Mid-point  $T_g = -3.5 \pm 1.6^\circ\text{C}$ ), that is highly likely to result from a combination of the amorphous ibuprofen (Mid-point  $T_g = -43.4 \pm 0.2^\circ\text{C}$ , Chapter 3) and Eudragit RS PO (Chapter 3,  $53.3 \pm 0.5^\circ\text{C}$ ). The second glass transition temperature at  $87.0 \pm 1.7^\circ\text{C}$  (Mid-point  $T_g$ ) might indicate a methylcellulose rich phase as this value close to the glass transition temperature of this polymer (Mid-point  $T_g = 103.0 \pm 0.1^\circ\text{C}$ , Chapter 3), lowered due to plasticization effect of ibuprofen (Kidokoro et al. 2001). Increasing the level of methyl cellulose as the major polymeric constituent in FM4 films resulted in a three-phase system (Figure 6.2). In comparison to the FM3 films, the first amorphous phase was shifted to a lower glass transition temperature indicating amorphous drug rich-phase, while the second amorphous phase was shifted to a higher glass transition temperature almost equals aforementioned  $T_g$  value of the raw methylcellulose polymer. The third phase obtained was crystalline ibuprofen indicated by its melting endotherm.



FM3

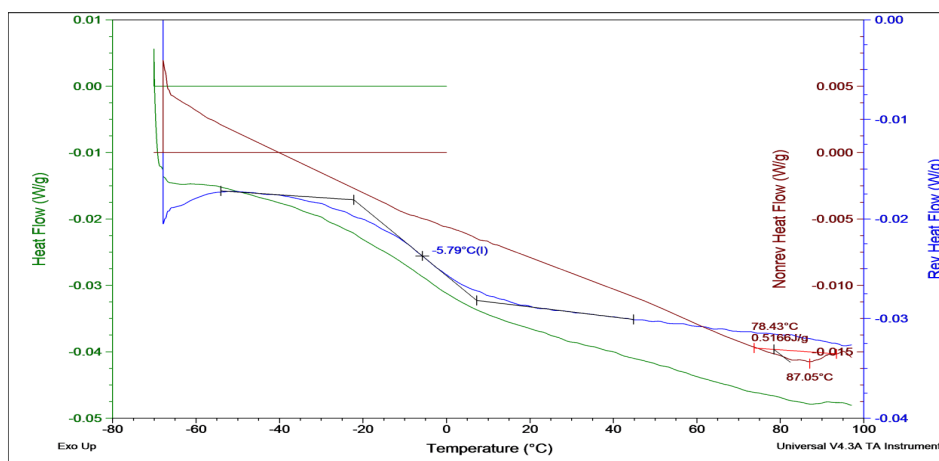


FM4

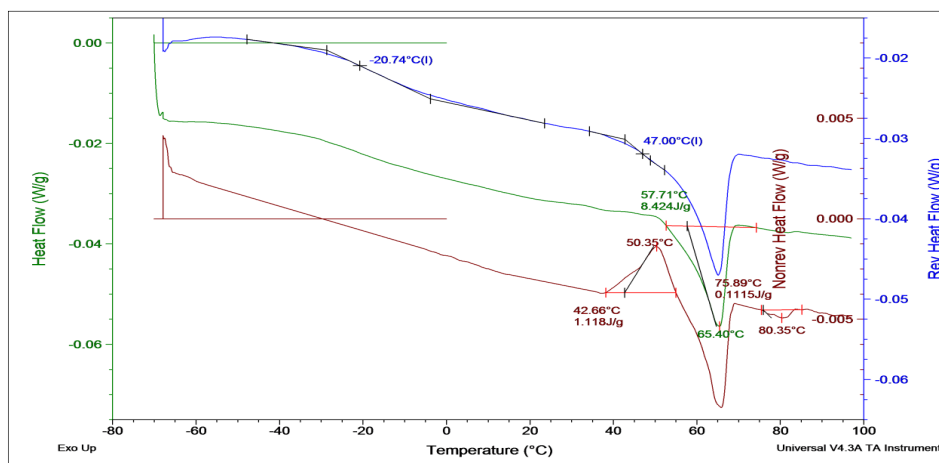
**Figure 6.2: MTDSC heating scans of different hot melt extruded films containing methylcellulose, Eudragit RS PO and ibuprofen (see Table 6.3) in standard aluminium pans. Underlying scan rate of  $1^{\circ}\text{C min}^{-1}$  with a modulation amplitude of  $\pm 0.265^{\circ}\text{C}$  and a period of 100 seconds. The traces have been offset for clarity**

Replacing methylcellulose by Xantural® 75 (xanthan gum) resulted in a one phase system at FM5 composition with a low glass transition temperature occurring around  $-6.7 \pm 0.9^{\circ}\text{C}$  (Mid-point Tg), as shown in Figure 6.3. However, at higher loaded amounts of xanthan gum found in FM6 films a three-phase system was manifested (Figure 6.3). At this composition, the ibuprofen was partially solubilised in the liquefied polymeric phase(s) and a melting peak was detected, though associated with a depressed onset in comparison to the pure ibuprofen, indicating partial miscibility. The remaining two phases were amorphous with glass transition temperatures at  $-20.4 \pm 0.3^{\circ}\text{C}$  and  $47.4 \pm 0.4^{\circ}\text{C}$ , possibly related to amorphous ibuprofen rich- phase and xanthan gum rich-phase, respectively. This was inferred based on

the proximity of values to the estimated glass transition temperature (Mid-point) of ibuprofen ( $-43.4 \pm 0.2^\circ\text{C}$ ) and xanthan gum ( $37.7 \pm 2.6^\circ\text{C}$ ) reported in Chapter 3. An exotherm was observed in the non-reversing heat flow signal of FM6 films with an extrapolated onset temperature at  $43.0 \pm 0.4^\circ\text{C}$  ( $n=2$ ). This event is highly related to recrystallization of ibuprofen because it was followed by the endothermic peak characteristic of the melting of the conventional crystalline phase of this drug.



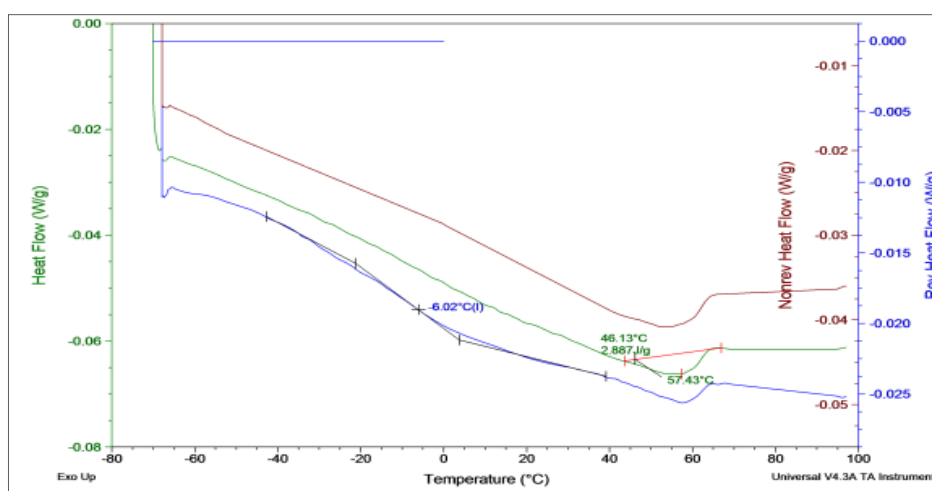
FM5



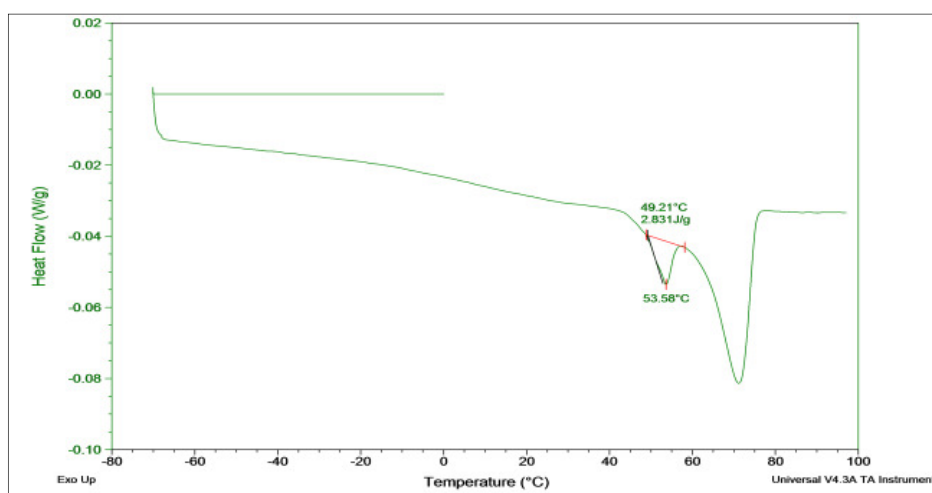
FM6

**Figure 6.3: MTDSC heating scans of different hot melt extruded films containing Xantural® 75, Eudragit RS PO and ibuprofen (see Table 6.3) in standard aluminium pans. Underlying scan rate of  $1^\circ\text{C min}^{-1}$  with a modulation amplitude of  $\pm 0.265^\circ\text{C}$  and a period of 100 seconds. The traces have been offset for clarity**

As illustrated in Figure 6.4, phase separation was evident in the FM7 solid composition of ibuprofen in the hydrophilic poloxamer polymer (Pluronic® F127) and Eudragit RS PO; however, it is believed that the Pluronic® F127 is separated not the drug. This polymer is known to have a good solubilising capacity (Escobar-Chávez et al., 2006) and this was demonstrated in the formation of amorphous phase system with a glass transition temperature at  $-5.4 \pm 1.5^\circ\text{C}$  which is expected to consist of amorphous fraction of this polymer (Mid-point  $T_g = -64.2 \pm 0.3^\circ\text{C}$ ) and the dissolved amorphous ibuprofen therein along Eudragit RS PO. A melting transition was also observed with an extrapolated onset temperature at  $47.4 \pm 2.9^\circ\text{C}$  and peak temperature at  $56.2 \pm 1.9^\circ\text{C}$  which correlated well with the values obtained from the melting of this semi-crystalline polymer (Pluronic® F127) in the physical mix of FM7 as seen in Figure 6.5 (extrapolated onset temperature at  $49.5 \pm 0.8^\circ\text{C}$  and peak temperature at  $53.5 \pm 0.1^\circ\text{C}$ ). The hypothesis presented herein of these phases is consistent with the observations of Smithey et al. (2007) who found that the amorphous drug will primarily reside in amorphous segments of the poloxamer i.e. PPO domains, wherein the glass transition temperature of this dispersion will be dependent on the amount of the amorphous drug and PPO regions. However, PEO segments of poloxamer will generally recrystallize. These segments or domains of poloxamer were described earlier in Chapter 2.

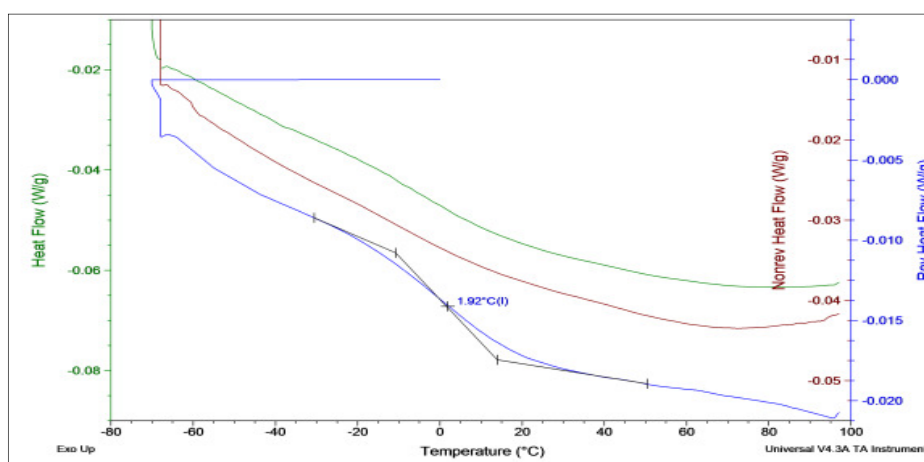


**Figure 6.4: MTDSC heating scan of FM7 hot melt extruded film containing Pluronic® F127 Eudragit RS PO ibuprofen ratio of (1:6:3) in standard aluminium pans. Underlying scan rate of  $1^\circ\text{C min}^{-1}$  with a modulation amplitude of  $\pm 0.265^\circ\text{C}$  and a period of 100 seconds. The traces have been offset for clarity**

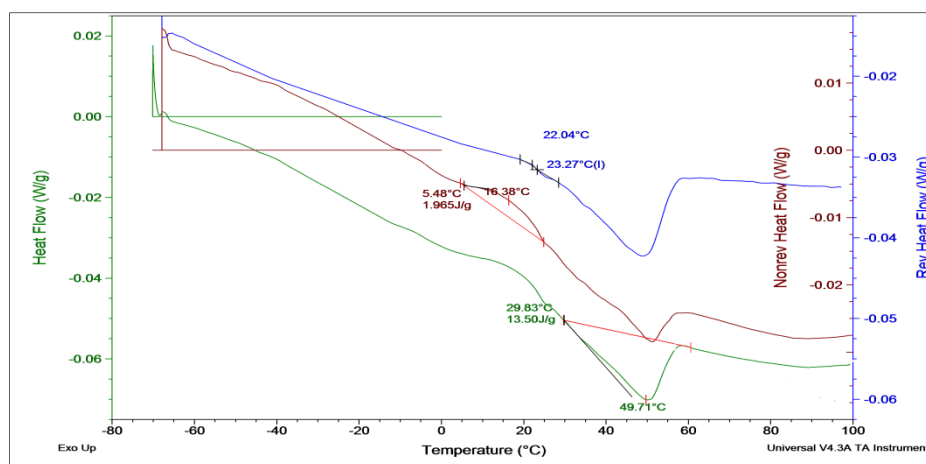


**Figure 6.5: MTDSC total heat flow signal of the FM7 physical mix Pluronic® F127 Eudragit RS PO ibuprofen ratio of (1:6:3) in standard aluminium pans. Underlying scan rate of  $1^{\circ}\text{C min}^{-1}$  with a modulation amplitude of  $\pm 0.265^{\circ}\text{C}$  and a period of 100 seconds**

The films formulated with Gelucire 44/14 showed two different MTDSC profiles according to the level of Gelucire incorporation as seen in Figure 6.6. At low level of this lipid as represented by FM9 films, the system showed one phase characterised by a single glass transition temperature at  $1.5 \pm 0.7^{\circ}\text{C}$  (Mid-point  $T_g$ ). This might suggest homogenous dissolution of the amorphous drug in the used carrier blend of Gelucire 44/14 and Eudragit RS PO. The effect of increasing the amount of Gelucire 44/14 was shown at FM10 composition and resulted in two-phase system formation. The first phase was amorphous characterised by a glass transition at  $21.8 \pm 0.4^{\circ}\text{C}$  (Mid-point  $T_g$ ) while the second phase was associated with an exotherm having an extrapolated onset temperature around  $5.4 \pm 1.1$  and peak temperature at  $17.6 \pm 0.2$ , followed by endothermic peak which starts at  $29.3 \pm 1.5^{\circ}\text{C}$  (extrapolated onset temperature). This peak might suggest melting of either crystalline ibuprofen or Gelucire 44/14. This might be more understood using PXRD technique to relate this transition.



FM9



FM10

**Figure 6.6:** MTDSC heating scans of different hot melt extruded films containing Gelucire 44/14, Eudragit RS PO and ibuprofen (see Table 6.3) in standard aluminium pans. Underlying scan rate of  $1^{\circ}\text{C min}^{-1}$  with a modulation amplitude of  $\pm 0.265^{\circ}\text{C}$  and a period of 100 seconds. The traces have been offset for clarity

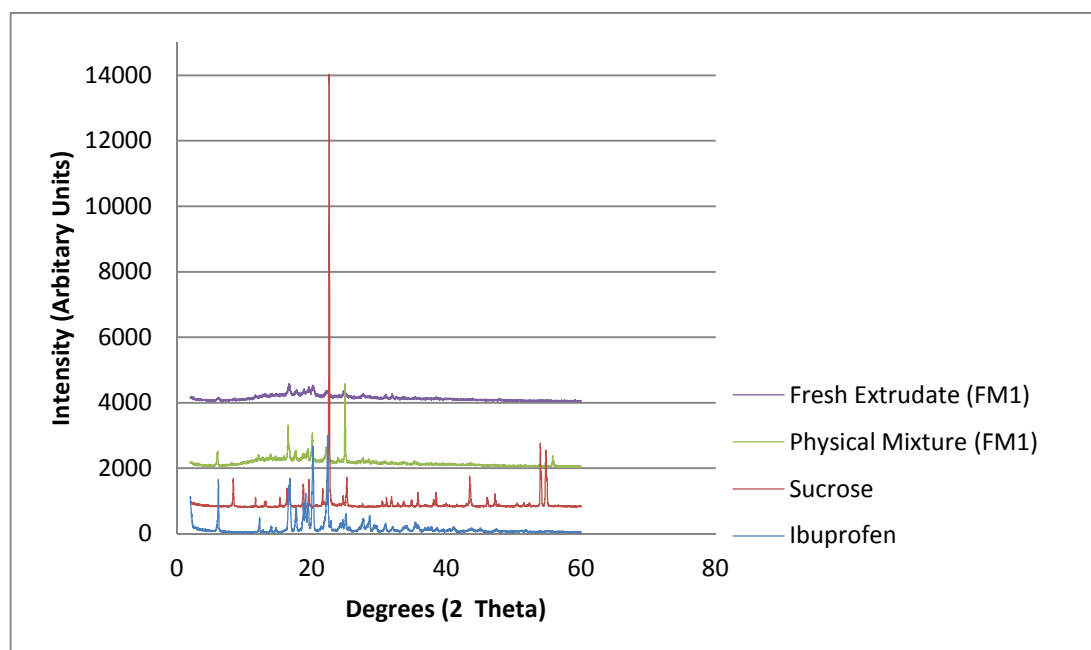
In summary, changes of the molecular distribution of the drug took place with different compositions. Control extruded films (FM0) were described as solid solutions of the amorphous ibuprofen dissolved at molecular level in Eudragit RS PO as detailed in Chapter 4. The addition of sucrose (FM1) resulted in a decrease of ibuprofen miscibility and therewith the drug recrystallized from the extruded matrix. However, in methylcellulose-Eudragit RS PO FM3 extruded films, two Tg's were observed, indicating fully amorphous 'glassy' solid dispersion system (see Chapter 1). One Tg is highly likely to result from a combination of the amorphous ibuprofen and Eudragit RS PO, whereas the other Tg was attributed to a methylcellulose-rich phase. Attempts to replace the Eudragit RS PO using high proportion of the methylcellulose in FM4 films resulted in a phase separation and ibuprofen crystallization. Xanthan gum (Xantural® 75) showed a similar behaviour when incorporated at high level (FM6), indicating that a relatively high concentration of Eudragit RS PO was necessary in both cases to maintain and/or enhance the ibuprofen miscibility, which was previously discussed in Chapter 4. However, at low level of Xnatural® 75 as in FM5 films, one phase system was formed similar to the control films but with lower Tg.

Films formulated with Pluronic® F127 (Poloxamer 407) in the FM7 composition showed interesting behaviour. It is believed that the amorphous drug was dissolved in the amorphous fraction of this polymer in addition to Eudragit RS PO, whereas the crystalline part of this poloxamer was shown to be highly likely to cause the observed melting endotherm. This behaviour is well documented for semi-crystalline polymers wherein some drugs are concentrated in the amorphous regions of these polymers (Delahaye et al., 1997).

Gelucire 44/14 has a lipidic nature while also containing polymeric constituents; the presence of the lower concentrations of this material appeared to facilitate solubilisation of the drug in the mixed films (FM9). These films were characterised by a single glass transition temperature at  $1.5 \pm 0.7^\circ\text{C}$  (Mid-point Tg) which is indicative of solid solution formation. However, the drug seems to be only partially miscible at higher levels of this lipid, as indicated by the detection of melting peaks which could correspond to the crystalline ibuprofen. However, given the crystalline nature of the Gelucire 44/14 it was not certain whether these endothermic events might be attributable to the carrier rather than the drug. In order to clarify this, and other anomalous results from the MTDSC studies, PXRD studies were employed to identify the nature of the crystalline material detected using the thermal approach. The X-ray powder diffraction profiles (diffractograms) are shown from Figure 6.7 through to Figure 6.11. Overlay of these diffractograms were obtained for the fresh extruded films and compared to their equivalent physical mixes and raw materials of

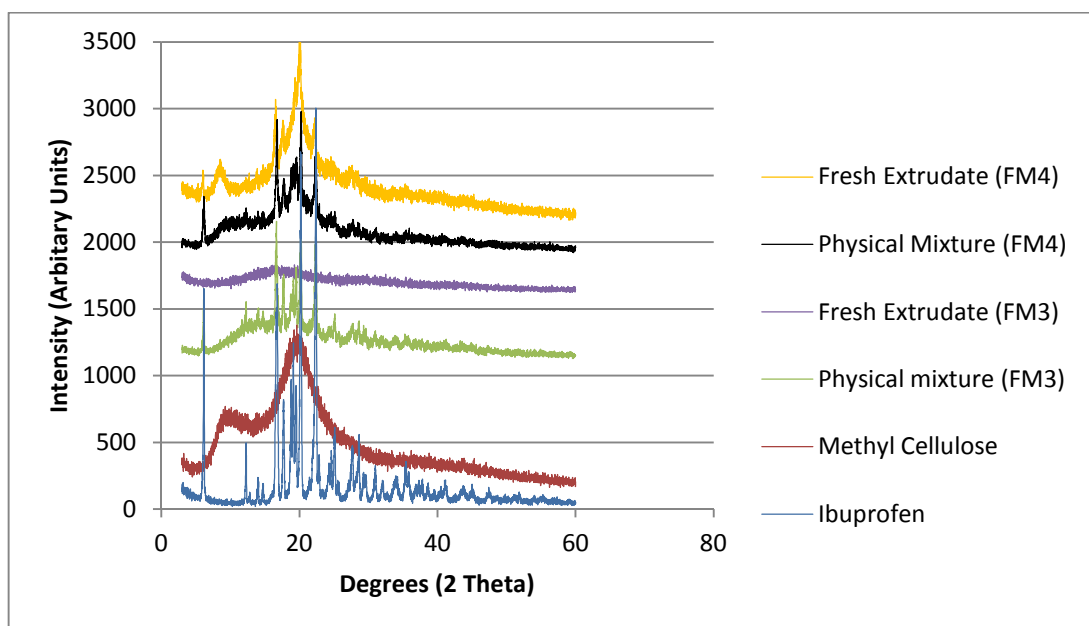
crystalline ibuprofen and newly introduced hydrophilic excipient. Eudragit RS PO is glassy (amorphous) polymer that exhibits halo PXRD pattern as described in Chapter 3.

As shown in Figure 6.7, PXRD pattern of fresh FM1 (Eudragit RS PO 60% (w/w) and sucrose 10% (w/w) as carriers) film gave characteristic peaks of both ibuprofen and sucrose indicating their recrystallization. The diffractograms of fresh FM3 (low level of methylcellulose) and FM4 (high level of methylcellulose) films are displayed in Figure 6.8. While FM3 films exhibited a fully amorphous halo pattern, FM4 films revealed diffraction peaks of the crystalline ibuprofen. Films containing xanthan gum at FM5 composition showed broad halos in their diffractograms, indicating amorphous systems (Figure 6.9). Alternatively, diffraction peaks of crystalline ibuprofen were detected in the films with higher level of xanthan gum (FM6) as seen in Figure 6.9, indicating phase separation in these films. All these data were consistent with the foregoing MTDSC results.

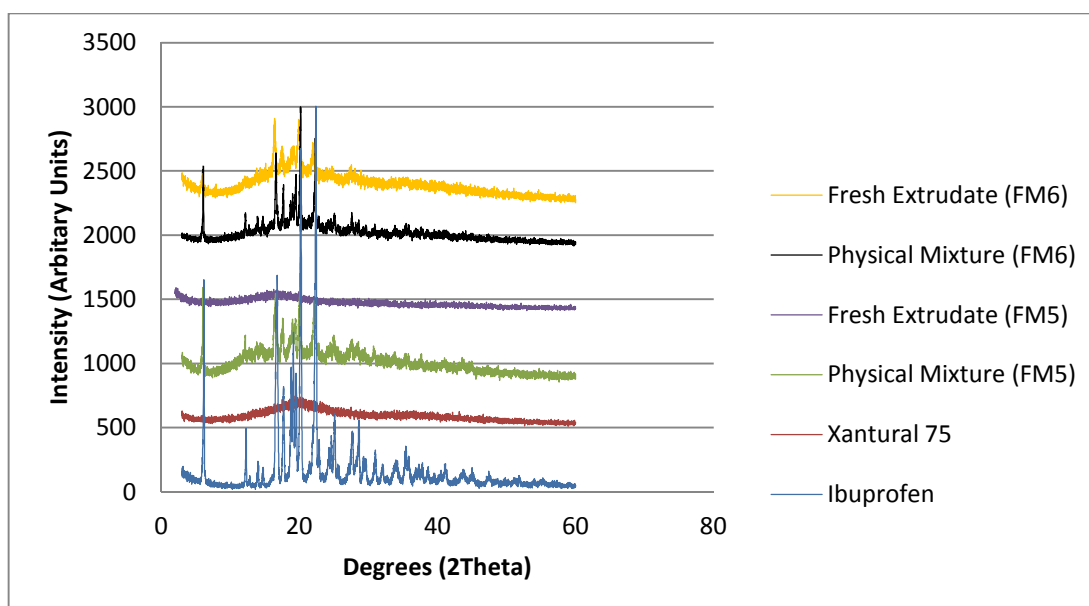


**Figure 6.7: X-ray powder diffraction profiles of raw materials, physical mixture (sucrose, Eudragit RS PO and ibuprofen) and the corresponding hot melt extruded films of FM1composition**



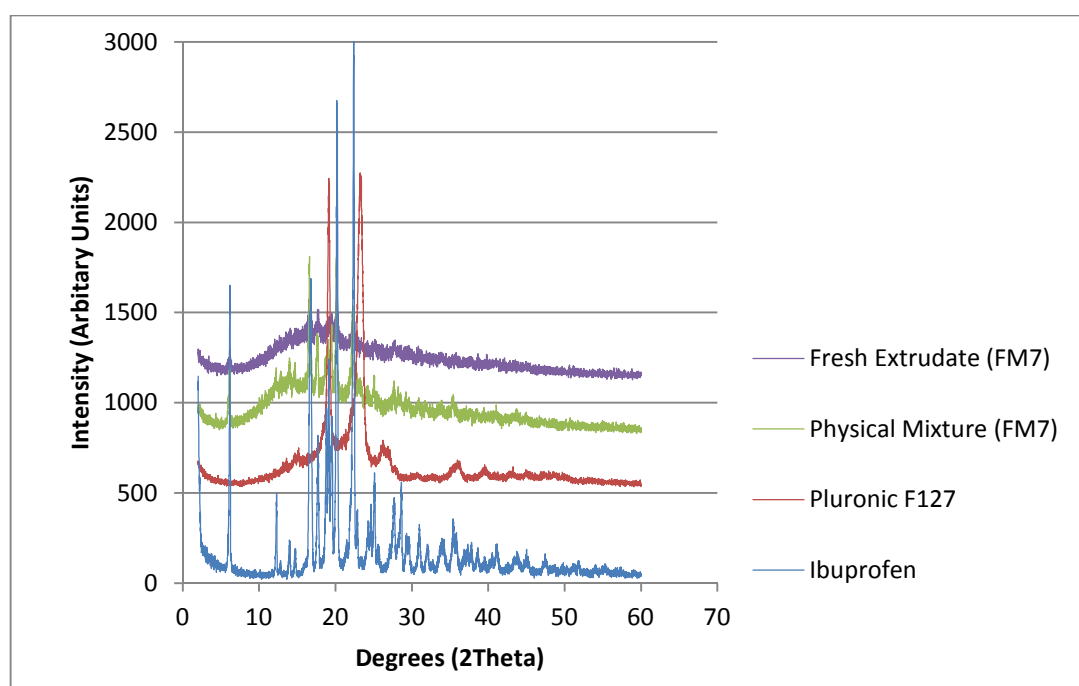


**Figure 6.8:** X-ray powder diffraction profiles of raw materials, physical mixtures (methylcellulose, Eudragit RS PO and ibuprofen) and the corresponding hot melt extruded films of FM3 (low level of methylcellulose) and FM4 (high level of methylcellulose) compositions



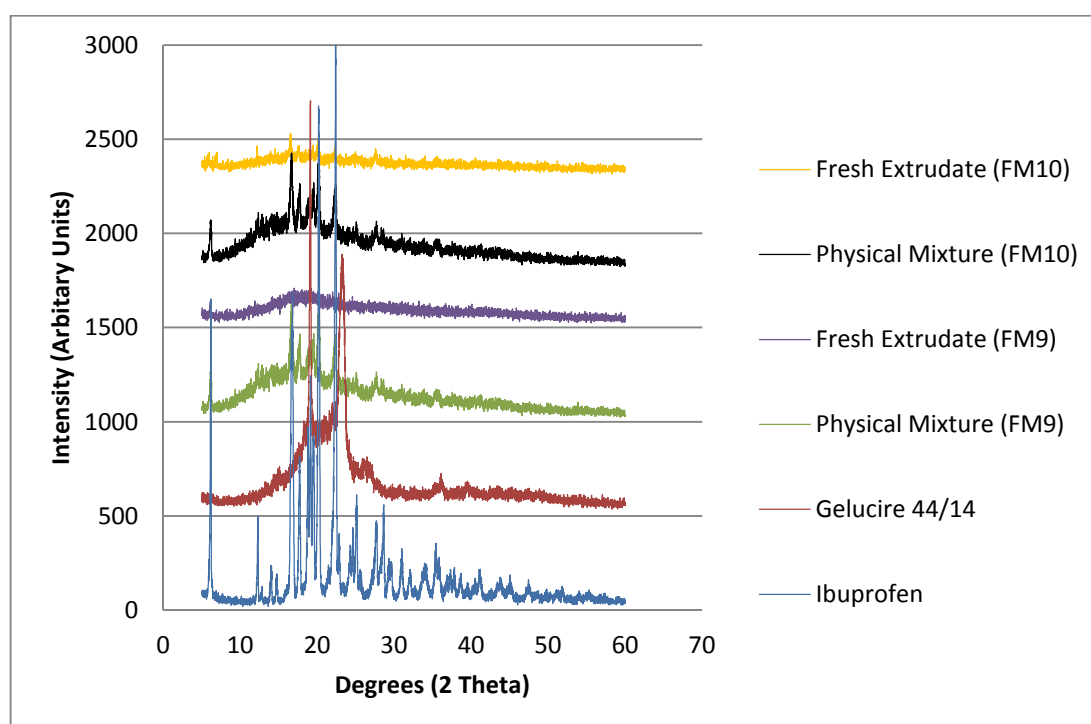
**Figure 6.9:** X-ray powder diffraction profiles of raw materials, physical mixtures (Xantural® 75, Eudragit RS PO and ibuprofen) and the corresponding hot melt extruded films of FM5 and FM6 compositions

The PXRD pattern of the FM7 extruded sample identified both Pluronic® F127 and ibuprofen crystals as shown in Figure 6.10. However, the melting endotherm detected by MTDSC experiment in this extruded system was very close to the melting endotherm of the Pluronic® F127 in the equivalent physical mix. It is therefore believed that low glass transition temperature of this FM7 extruded system ( $-5.4 \pm 1.5^\circ\text{C}$ , Mid-point  $T_g$ ) facilitated recrystallization of ibuprofen over the timescale of the PXRD scan (almost one hour), and thus the detection of ibuprofen crystals. This can be understood in the light of amorphous material stability. The metastable nature of the amorphous materials results in them having a great tendency to assume stable crystalline form. Enhanced molecular mobility of the amorphous system at and above its glass transition temperature often results in recrystallization. Thus, at room temperature ( $\sim 25^\circ\text{C}$ ), which is far above the  $T_g$  of this FM7 system, it is expected that the molecular mobility was enhanced to the degree of ibuprofen crystallization during PXRD examination.



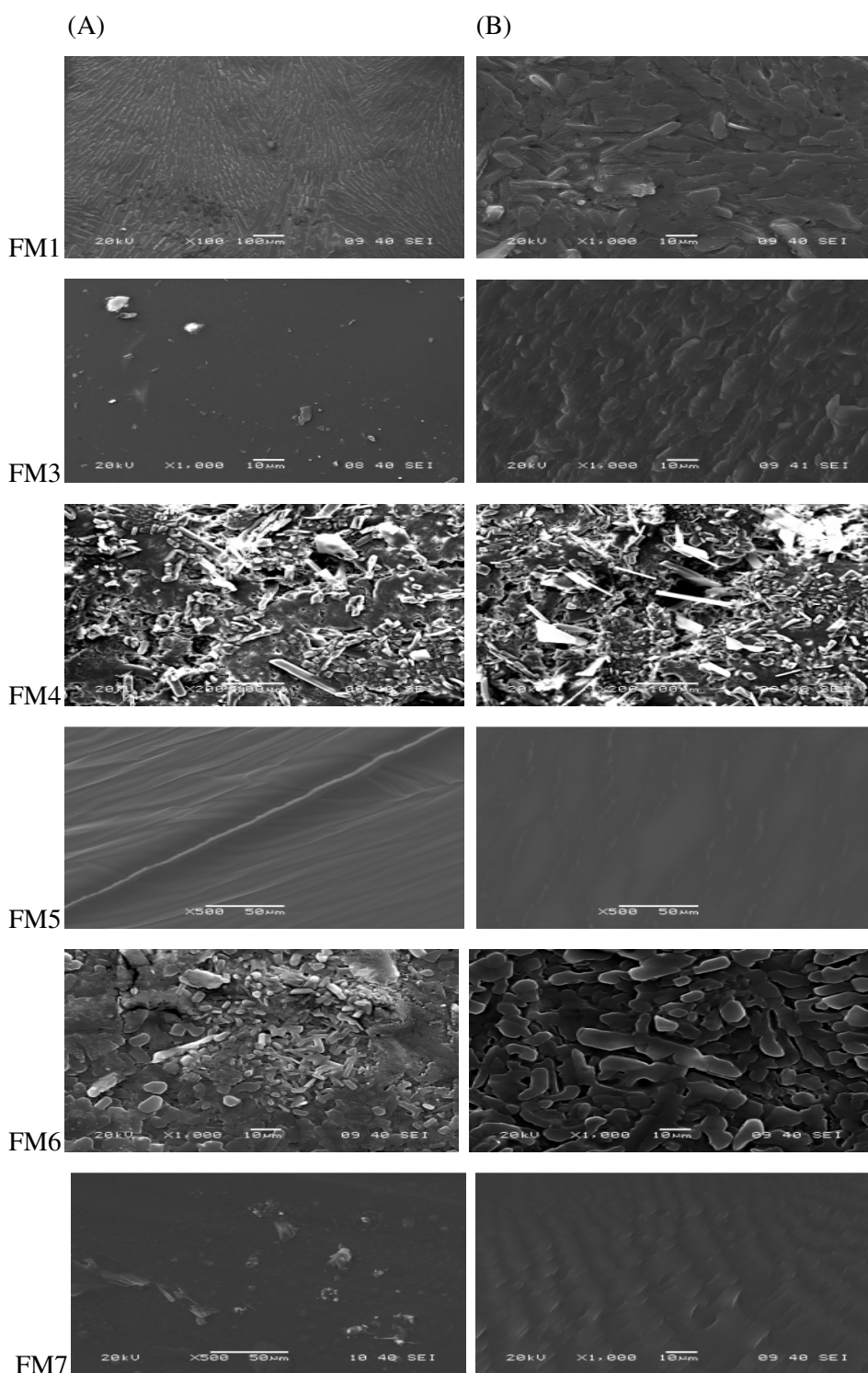
**Figure 6.10:** X-ray powder diffraction profiles of raw materials, physical mixture (Pluronic® F127, Eudragit RS PO and ibuprofen) and the corresponding hot melt extruded films of FM7 composition

Interestingly, the diffractogram of FM9 films containing low level of Gelucire 44/14 showed halo pattern typical for amorphous material though having relatively low  $T_g$  (Figure 6.11). This conforms with the MTDSC results and suggests enhanced stability in comparison to the FM5 or FM7 films containing Xantural® 75 and Pluronic® F-127, respectively. Alternatively, higher level of Gelucire 44/14 in FM10 extruded films showed principal peaks of ibuprofen crystals in their PXRD traces as shown in Figure 6.11. Thus, it could be inferred that the phase separation of the FM10 extruded films resulted in drug crystallization rather than the lipid itself with subsequent melting endotherm observed in its MTDSC profile (Figure 6.6).



**Figure 6.11: X-ray powder diffraction profiles of raw materials, physical mixtures (Gelucire 44/14, Eudragit RS PO and ibuprofen) and the corresponding hot melt extruded films of FM9 (low level of Gelucire 44/14) and FM10 (high level of Gelucire 44/14) compositions**

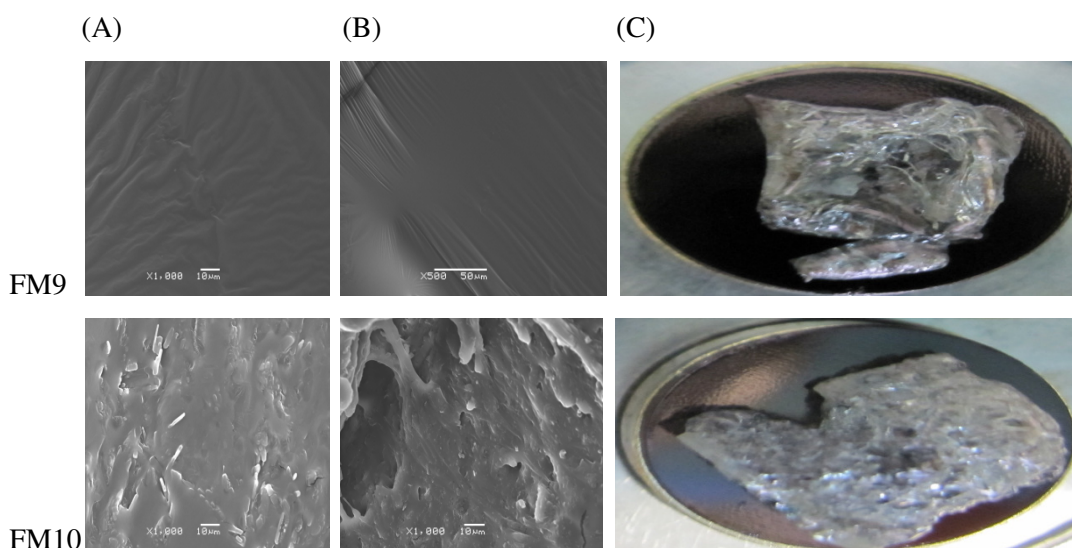
MTDSC and PXRD techniques were also supplemented with SEM of the extruded films as illustrated in Figure 6.12 and Figure 6.13. Analysis by scanning electron microscopy showed that phase separation was evident in all tested films except FM5 (low level of xanthan gum) and FM9 (low level of Gelucire 44/14) films, through indication of their morphological features. SEM images of the extruded film containing sucrose, Eudragit RS PO and ibuprofen (FM1) as depicted in Figure 6.12, showed lines of crystals coating the surface whereas the cross section was full of these crystals but in less organized manner. This conforms to MTDSC and PXRD results which stated the presence of crystalline materials of sucrose and ibuprofen, indicating phase separation. The formulation of FM3 films (low levels of methylcellulose) showed fine granules which might be related to ibuprofen crystals whereas the cross sections were free from crystals. However, drug recrystallization in these samples was undetected using MTDSC or PXRD, suggesting that the small amount of crystalline material present may be below detection limits of these methods. The lower limit of quantification of crystalline material in amorphous dispersion by these techniques has been reported to be approximately 5% (Shah et al., 2006). However, for films comprising higher levels of methylcellulose (FM4), the structure was less compact (see photo in Table 6.2) and the ibuprofen crystals were more developed protruding from the surfaces and cross sections of these extruded films. This indicates a high extent of phase separation in comparison to the FM3 films containing lower levels of methylcellulose.



**Figure 6.12: SEM morphological features of the surfaces (column A) and cross sections (column B) obtained for different fresh extruded films loaded with ibuprofen (see text or Table 6.3 for their compositions)**

The surface and cross section features of the FM5, FM6 and FM7 films are also shown in Figure 6.12. FM5 extruded films containing low level of xanthan gum did not show crystals on their surfaces or cross sections, complying with both MTDSC and PXRD results. At higher levels of xanthan gum, the resulting FM6 films showed agglomeration of ibuprofen crystals mainly on the surface, while the cross section exhibited a leaf-like texture. The FM7 (10% (w/w) Pluronic® F127) extruded films showed granular-shaped crystal formations only on their surfaces. These findings are consistent with previous MTDSC and PXRD results which indicated the presence of crystalline materials in these extruded films and hence phase separation.

For the films containing Gelucire 44/14, the surface morphology of the low lipid loaded films (FM9) did not indicate the presence of any crystallinity (Figure 6.13), while needle-shape crystals appeared for the higher lipid content (FM10) films. It was noted that the SEM imaging process itself did appear to cause damage to the lipid-loaded film surfaces, as evidenced by visible macroscopic changes; such effects are well known and are a result of the heating effects generated by the use of the electron beam (see Chapter 2). Therefore, SEM is not suitable to detect morphological features of these samples.



**Figure 6.13: SEM images of the surfaces (column A) and cross sections (column B) for fresh FM9 and FM10 extruded films. Column C: photographs illustrating the deformations of the tested films post SEM scanning**

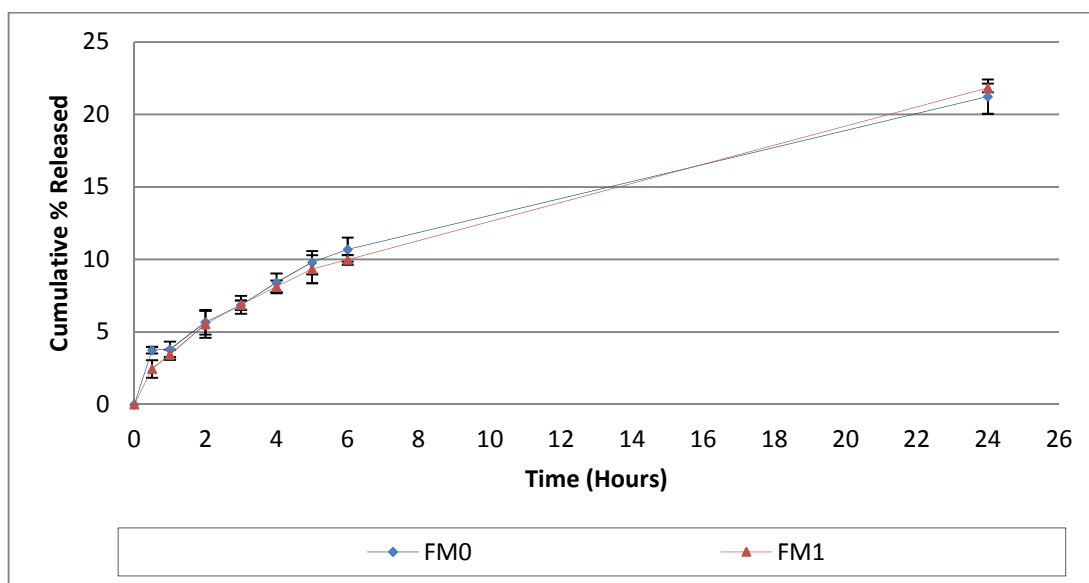
In summary, the results obtained from MTDSC, PXRD and SEM methods were relatively comparable and complementary to each other. Overall, these techniques showed that multi-component extruded systems of ibuprofen, Eudragit RS PO and the newly introduced hydrophilic excipients were not forming complete solid solutions except at FM5 (low level of xanthan gum) and FM9 (low level of Gelucire 44/14) compositions. Separation of the drug phase as crystallites can be observed in all other formulations, which seems to be extensive in FM1 (with sucrose), FM4 (high level of methylcellulose) and FM6 (high level of xanthan gum) films.

#### 6.2.2.2 *In vitro* release of ibuprofen from the viable hot melt extruded formulations

As discussed in the previous section, the decision regarding which of the formulations to select initially focussed on the attributes to the manufacturing variables. The extrudable or processable samples were then investigated for their solid state characteristics, knowledge of which is essential for understanding the subsequent release performance. Given the basic hypothesis that the addition of these hydrophilic modifiers can enhance fluid access into the films and this might enhance drug release, this section of the study examines the efficiency of the drug release from the 'extrudable' carrier systems in comparison to the control films of ibuprofen and Eudragit RS PO (FM0). This was performed using *in vitro* drug release testing (dissolution test) in phosphate buffer (pH 7.2) at 37°C over 24 hours and the resultant release profiles for these formulations are shown from Figure 6.14 through to Figure 6.17 in addition to Figure 6.19 and Figure 6.20.

The release profile of ibuprofen from FM1 system (10% (w/w) sucrose and 60% (w/w) Eudragit RS PO as carriers) is shown in Figure 6.14. The inclusion of sucrose in this extruded formulation had no significant effect on decreasing the retardation influence of Eudragit RS PO on the drug release. This was indicated from similar release profile to the control films (FM0) containing Eudragit RS PO alone as a carrier. Thus the expected increased wettability or water influx due to sucrose polarity was not achieved in these matrices (Saharan et al., 2009).

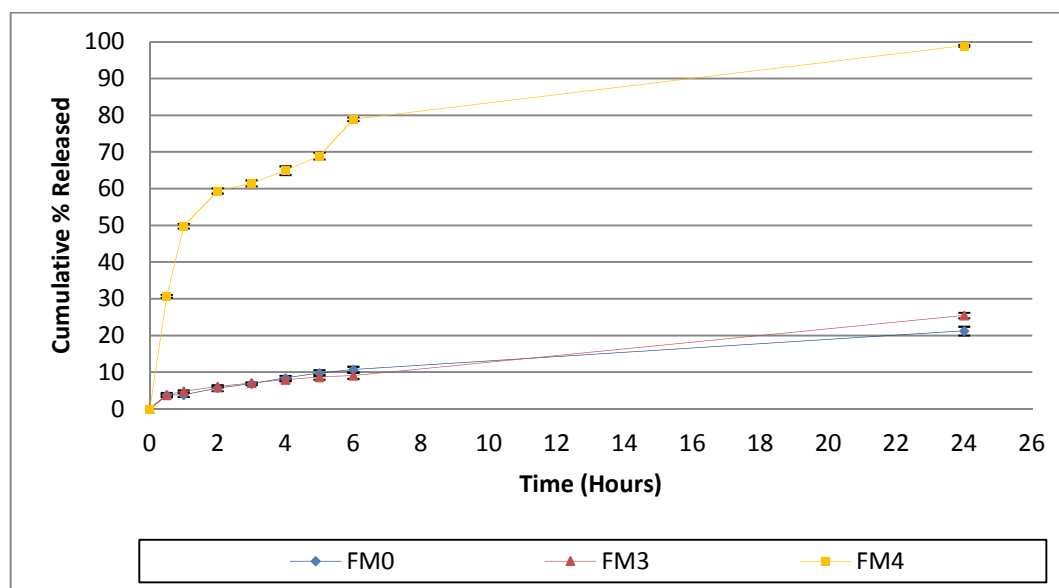




**Figure 6.14: Ibuprofen release profiles from hot melt extruded films of FM0 (Eudragit RS PO as a carrier) and FM1 (Eudragit RS PO and sucrose as carriers) formulations in phosphate buffer solution (pH=7.2) at  $37.0 \pm 0.1^\circ\text{C}$ . Each data point represents the mean  $\pm$  S.D. of three measurements**

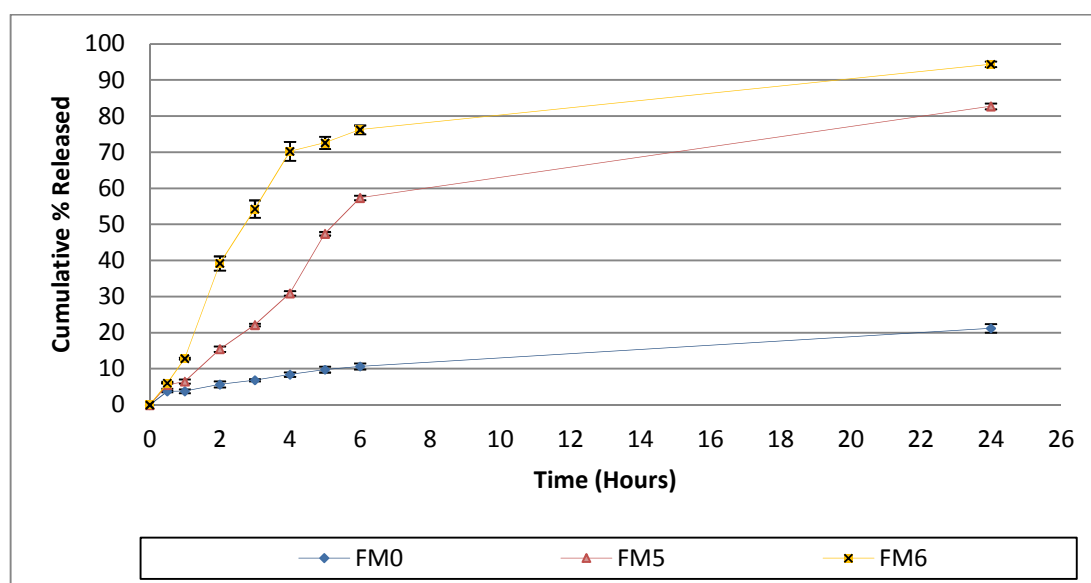
The 10% w/w methylcellulose system (FM3) also released ibuprofen to the same extent as the control films as seen in Figure 6.15. However, in this figure the increased level of methyl cellulose in FM4 extruded films resulted in a fast complete overall release of the drug after 24 hours. These extruded films were less compact or less consolidated that the ibuprofen crystals were observed easily; macroscopically (Table 6.2) and using SEM (Figure 6.12). Thus it is believed that the crystalline ibuprofen was readily exposed to the dissolution medium which resulted in a complete release over a relatively short time.



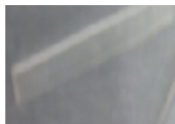



**Figure 6.15: Ibuprofen release profiles from hot melt extruded films of FM0 (Eudragit RS PO as a carrier), FM3 (10% (w/w) methylcellulose and 60% (w/w) Eudragit RS PO as carriers) and FM4 (60% (w/w) methylcellulose and 10% (w/w) Eudragit RS PO as carriers) formulations in phosphate buffer solution (pH=7.2) at  $37.0 \pm 0.1^\circ\text{C}$ . Each data point represents the mean  $\pm$  S.D. of three measurements**

Similarly, films formulated with xanthan gum (FM5-FM6) were evaluated for the alteration of ibuprofen release profiles as illustrated in Figure 6.16. These extruded films demonstrated enhanced release profile, especially at higher level of xanthan gum (Xantural® 75). Ibuprofen release from FM6 films (60%(w/w) xanthan gum and 10%(w/w) Eudragit RS PO as carriers) was rapid with almost complete release after 24 hours while the drug release from FM5 films (10%(w/w) xanthan gum and 60%(w/w) Eudragit RS PO as carriers) was slower with approximate 83% drug release after the same period. This suggests that a little change in the concentration of this hydrophilic polymer could result in a desired release profile with reasonable amount and extent (sustained release). Therefore, extruded films formulated with the compositions listed in Table 6.4 and using the same processing parameters of FM5 and FM6 were tested to assess this point.

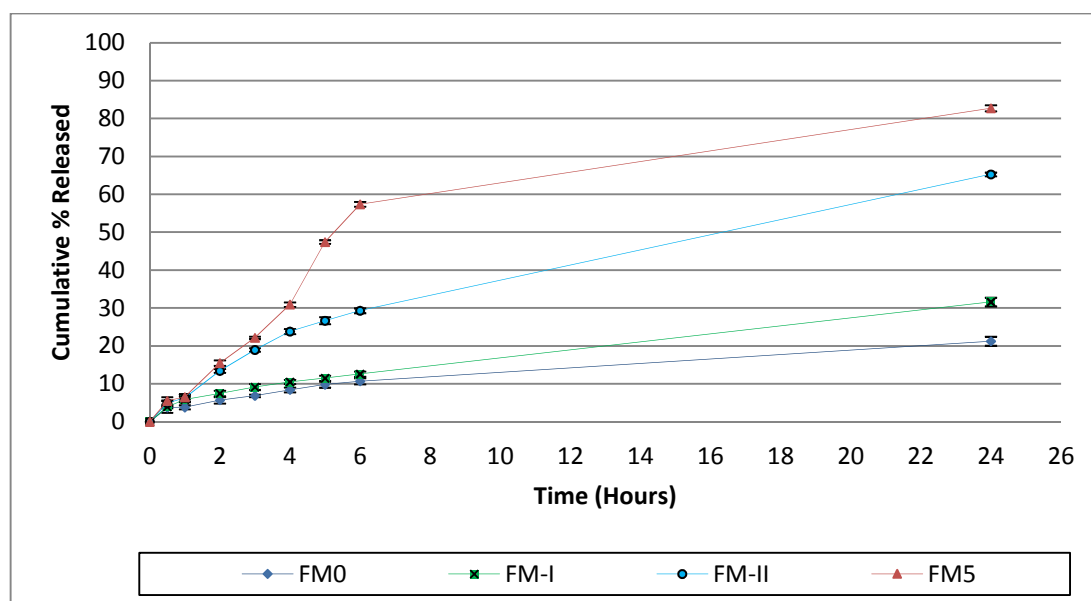


**Figure 6.16: Ibuprofen release profiles from hot melt extruded films of FM0 (Eudragit RS PO as a carrier), FM5 (10% (w/w) xanthan gum and 60% (w/w) Eudragit RS PO as carriers) and FM6 (60% (w/w) xanthan gum and 10% (w/w) Eudragit RS PO as carriers) formulations in phosphate buffer solution (pH=7.2) at 37.0±0.1°C. Each data point represents the mean±S.D. of three measurements**

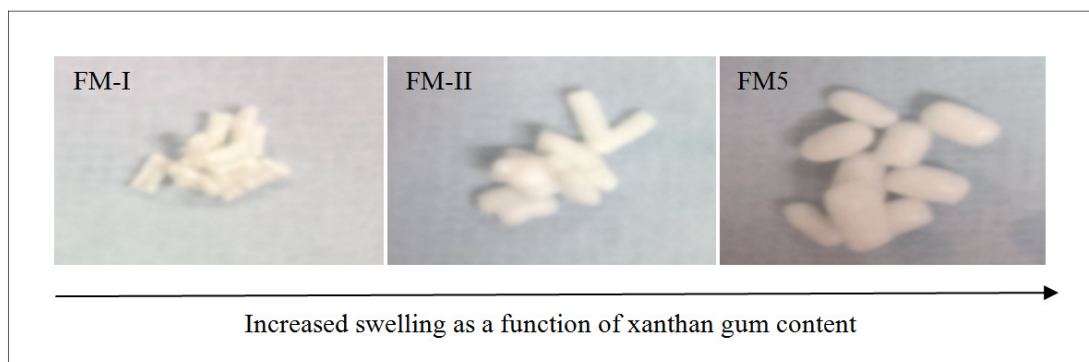
Carrier system(s) with drug loading of 30% w/w	Carrier blend(s) (%w/w)	Photos	Formula code	Appearance	Thickness (±0.02mm)
Eudragit RS PO/ Xantural® 75 ratios	67.5:2.5		FM-I	Smooth, no cracks, low stickiness.	1
	65:5		FM-II	Smooth, no cracks, medium stickiness.	1

**Table 6.4: Description of Eudragit RS PO-based hot melt extruded films loaded with ibuprofen and different amounts of Xantural® 75 polymer**

As can be seen in Figure 6.17, the decrease of the amount of added xanthan gum in the FM-II films (5%(w/w) xanthan gum and 65%(w/w) Eudragit RS PO) modulate the drug release to be slow yet higher than control films (FM0). On the other hand the lowest concentration of xanthan gum in FM-I films resulted in a non-remarkable increase in the ibuprofen release as compared with FM0 films (Eudragit RS PO as a carrier). It was therefore concluded that extrudates with FM-II composition might provide a suitable vehicle to deliver ibuprofen from these films at a reasonable amount and extent. These variations can be related to the swelling properties as a function of the level of incorporation of the hydrophilic polymer xanthan gum (Figure 6.18). Verhoeven et al. (2006) and Mundargi et al. (2007) suggested that this polymer will swell upon exposure to the aqueous medium; thereby the structure of the matrices will be disrupted, resulting in pore formation. Therefore, it is believed that these pore channels in the extruded carrier matrices (Eudragit RS PO and xanthan gum) facilitated drug release into the dissolution medium. Moreover, these findings indicate that the release from these extruded formulations is directed by xanthan gum concentration, thus adjusting the used ratio of this polymer can result in the desired release profile.

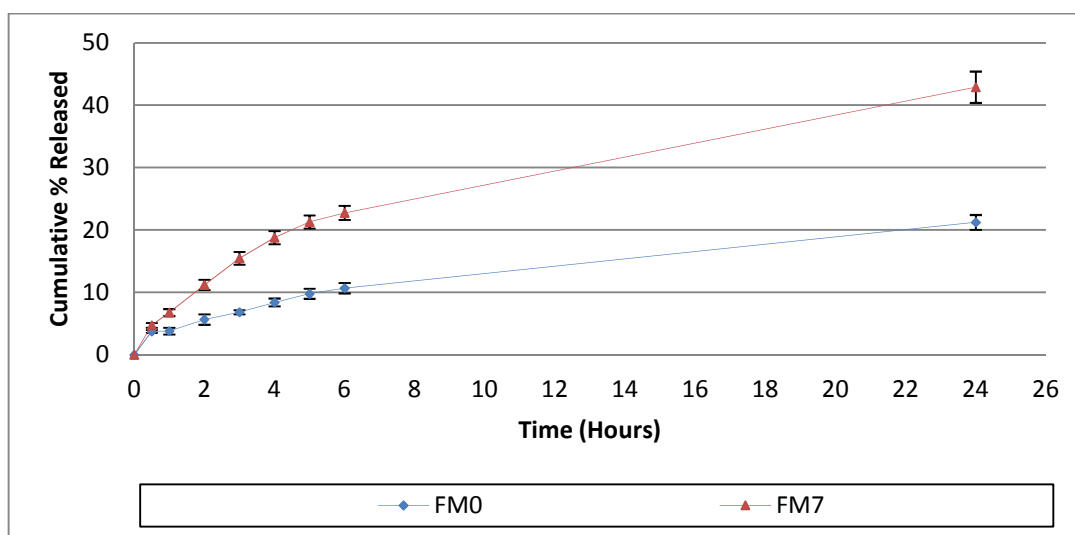


**Figure 6.17: Ibuprofen release profiles from hot melt extruded films of FM0 (Eudragit RS PO as a carrier), FM-I (2.5% (w/w) xanthan gum and 67.5% (w/w) Eudragit RS PO), FM-II (5% (w/w) xanthan gum and 65% (w/w) Eudragit RS PO) and FM5 (10% (w/w) xanthan gum and 60% (w/w) Eudragit RS PO) formulations in phosphate buffer solution (pH=7.2) at 37.0±0.1°C. Each data point represents the mean±S.D. of three measurements**



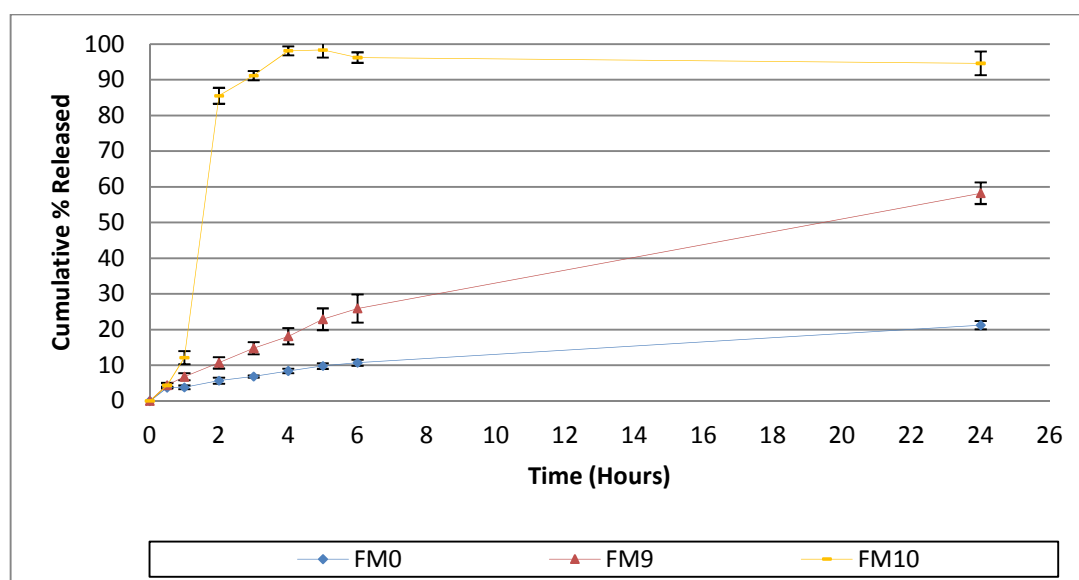
**Figure 6.18: Photographs of hot melt extruded films of ibuprofen with Eudragit RS PO and different proportions of xanthan gum after 24 hours of dissolution in phosphate buffer solution (pH=7.2) at  $37\pm0.1^{\circ}\text{C}$**

Being a non-ionic surfactant and with the hydrophilic polyoxyethylene chains, Pluronic® F127 or poloxamer 407 in FM7 extruded films achieved an increase of the drug release as indicated in Figure 6.19. More than 40% of the ibuprofen was released from these films in comparison to approximately 20% release of ibuprofen from the parent control extrudates (FM0); both after 24 hours.



**Figure 6.19: Ibuprofen release profiles from hot melt extruded films of FM0 (Eudragit RS PO as a carrier) and FM7 (Eudragit RS PO and Pluronic® F127 as carriers) formulations in phosphate buffer solution (pH=7.2) at  $37.0\pm0.1^{\circ}\text{C}$ . Each data point represents the mean $\pm$ S.D. of three measurements**

On the other hand, the most rapid and complete drug release was obtained from films containing Gelucire 44/14 in FM10 films, while the lower level of this lipid gave an intermediate release profile from FM9 extruded films (Figure 6.20). Gelucire 44/14 can act as a surfactant and self-emulsifying agent (Chambin et al., 2004; Kale and Patravale, 2008; Kallakunta et al., 2013; Rowe et al., 2009), providing a significant increase in the total amount of the released ibuprofen. As depicted in Figure 6.20, FM9 produced not less than 60% of ibuprofen release after 24 hours, whereas FM10 resulted in a complete release of the ibuprofen after 4 hours of the test. One of the interesting changes observed for the FM10 films was almost complete disappearance of these films after the test, transforming the dissolution medium into milk-like liquid. This suggests possible emulsification which might be responsible on the fast-dissolving immediate release observed amongst other tested formulations.



**Figure 6.20: Ibuprofen release profiles from hot melt extruded films of FM0 (Eudragit RS PO as a carrier), FM9 (10% (w/w) Gelucire 44/14 and 60% (w/w) Eudragit RS PO as carriers) and FM10 (20% (w/w) Gelucire 44/14 and 50% (w/w) Eudragit RS PO as carriers) formulations in phosphate buffer solution (pH=7.2) at 37.0±0.1°C. Each data point represents the mean±S.D. of three measurements**

In an attempt to consider the relative strengths and weakness of each tested formulation up to this stage of development, Table 6.5 was constructed. The extruded system(s) that can satisfy most of the favourable criteria, namely which, exhibit enhanced drug release and achieved homogenous drug distribution without phase separation might be considered as a good candidate for the transdermal delivery. The latter would be further verified using *in vitro* permeation studies in the following section. As seen in Table 6.5, phase separation extent was defined by the number of the phases formed as indicated previously in the MTDSC findings. The presence of crystalline drug at the stage of fabrication of the fresh films might indicate significant tendency of more recrystallization during equilibrium which could alter drug release properties from these extruded formulations. Thus, utilization of matrix wherein the active substance inclusion is contained in the dissolved non-crystalline form is preferable.

Formulation Code	Number of observed phases	Physical Appearance		Detected crystalline ibuprofen	Ibuprofen release at 24 hours (w/w %)
		Translucency	Elasticity		
FM1	Three	x	x	√	21.84±0.29
FM3	Two	√	√	√	25.46±0.07
FM4	Three	x	x	√	98.97±0.22
FM5	One	√	√	x	82.73±0.08
FM6	Three	x	x	√	94.40±0.74
FM7	Two	√	√	√	42.89±2.51
FM9	One	√	√	x	58.21±3.02
FM10	Two	√	√	√	At 4 hours: 98.11±1.24

**Table 6.5: Ibuprofen extruded formulations, extent of phase separation (number of observed phases) and physical appearance along with drug crystalline state and *in vitro* release (see text or Table 6.3 for their compositions)**

As is evident from Table 6.5, formulations of FM1 (10% (w/w) sucrose and 60 % (w/w) Eudragit RS PO as carriers), FM3 (10% (w/w) methylcellulose and 60 % (w/w) Eudragit RS PO as carriers) and FM6 (60% (w/w) xanthan gum and 10 % (w/w) Eudragit RS PO as carriers) lack homogenous drug distribution with a high extent of phase separation and crystalline drug, indicating poor compatibility and miscibility. Moreover, these films lack appealing transparency with poor flexibility and, as described in Table 6.3, they have low stickiness. Therefore, their physical appearance is not appealing, not suitable for handling due to hardness of FM1 (sucrose) films and brittleness of FM3 (methylcellulose) and FM6 (xanthan gum) films; in addition to their low stickiness means that they can impart limited adherence to the site of action i.e. the skin. Thus, it was decided not to progress these films to the next stages of development as drug delivery systems for ibuprofen.

In accordance with the requirements mentioned previously, FM5 films (10% (w/w) xanthan gum and 60% (w/w) Eudragit RS PO as carriers) and FM9 films (10% (w/w) Gelucire 44/14 and 60% (w/w) Eudragit RS PO as carriers) appear to be the most encouraging formulations. However, FM7 films with 10% (w/w) Pluronic® F127 and FM10 films with 20% (w/w) Gelucire 44/14 present a potential for ibuprofen delivery. In spite of the fact that these formulations contain crystalline ibuprofen as predicted from PXRD results, there are still opportunities to investigate their permeation properties. This is partially due to their acceptable physical appearance and enhanced drug release *in vitro*. Furthermore, a key observation was that relatively fast release of ibuprofen from FM10 formulation. This result demonstrates that various indications can be obtained from these formulations. While slow controlled release of ibuprofen is desired to relieve pain in cases such as osteoarthritis and rheumatoid arthritis, a fast ibuprofen release can be advantageous for indications required rapid onset of analgesic effect that is maintained for a reasonable extent.

In summary, *in vitro* drug release (dissolution testing) undertaken for different ibuprofen extruded formulations revealed the effect of assortment of the hydrophilic release promoters. It is believed that retardation influence of Eudragit RS PO was decreased after the addition of xanthan gum (FM5), Pluronic® F127 (FM7) and Gelucire 44/14 (FM9-FM10) due to possible increase of fluid access into the extruded films as a result of hydrophilic properties of these promoters. Other speculated mechanisms for increase drug release are reported ability of xanthan gum to swell with subsequent pore formation for drug release, and possible emulsifying effect after inclusion of Gelucire 44/14. A comparative study between the extruded compositions here based on their solid state characteristics, appealing physical appearance and enhanced *in vitro* release properties showed that extruded formulations of FM5, FM7, FM9 and FM10 can be further explored in terms of their *in vitro* permeation properties.

#### 6.2.2.3 *In vitro* permeation studies of the selected formulations

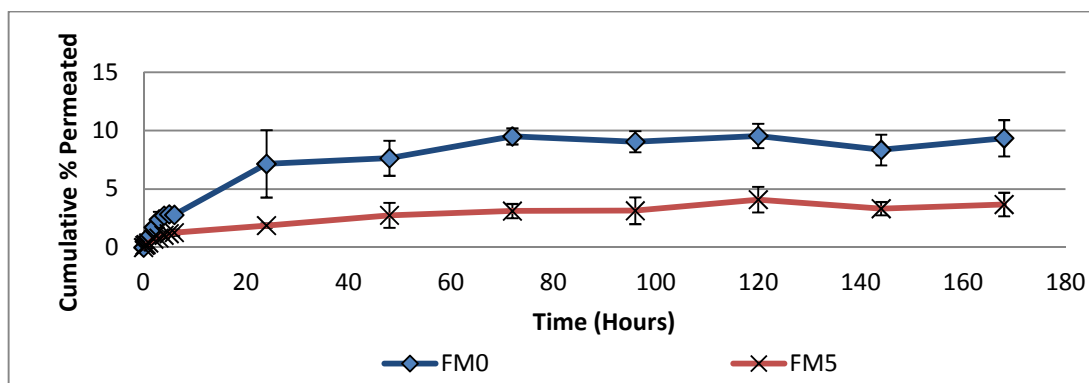
The transdermal patch development in this work continues with the analysis of the interplay between the selected extruded films and their enhancing effect on the permeation of ibuprofen. Therefore, these formulations were evaluated using an *in vitro* model of Franz diffusion cells fitted with silicone membranes. Ibuprofen permeation was shown in the diffusion profiles in Figure 6.21 and Figure 6.22 from these selected films.

As previously addressed in Chapter 5 the films based only on Eudragit RS PO matrices showed poor ibuprofen permeability through the silicone membranes due to the very low release from the extruded films themselves. Therefore, it is expected that formulations which have shown improved drug release in the previous section to affect the permeation of the ibuprofen positively. However, in contrast to the observed enhanced release behaviour, the ibuprofen permeation profile from the FM5 extruded films (10% (w/w) xanthan gum and 60 % (w/w) Eudragit RS PO as carriers) was even lower than control films containing Eudragit RS PO alone (FM0) as illustrated in Figure 6.21 (A). This can be explained by swelling characteristics of the xanthan gum polymer included in these films. It is believed that this hydrophilic polymer requires enough amount of water to swell and enhance drug release. However, the only available water to be absorbed herein is the evaporated water from the receptor medium in the Franz cells, which seems to be not enough for this swelling to take place. Therefore, it is expected that if we decrease the amount of this polymer, the diffusion profiles can be enhanced. This approach has been examined as shown in Figure 6.21 (B) and revealed that the highest overall permeation was achieved using the lowest level of xanthan

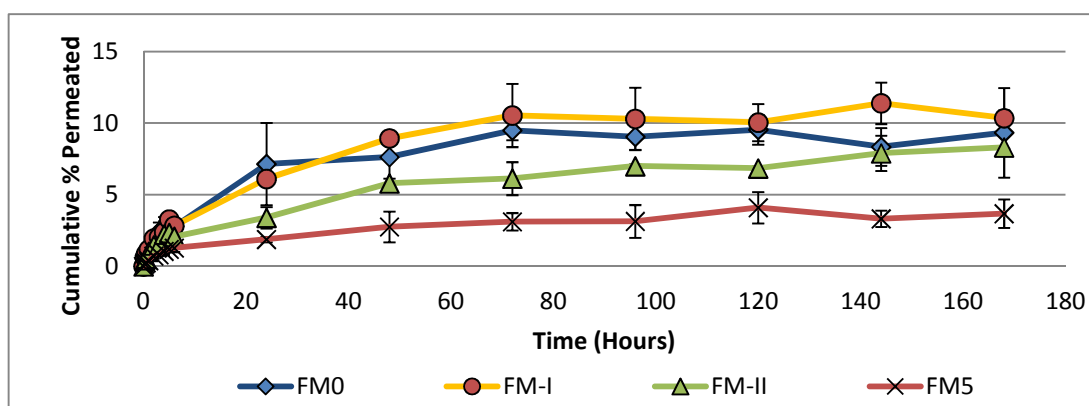


gum at FM-I composition; however, the permeation profile was poor as that of the control films (Eudragit RS PO as a carrier). This can be related to the limited ability of these films to provide sufficient drug release in the first place (Figure 6.17).

(A)



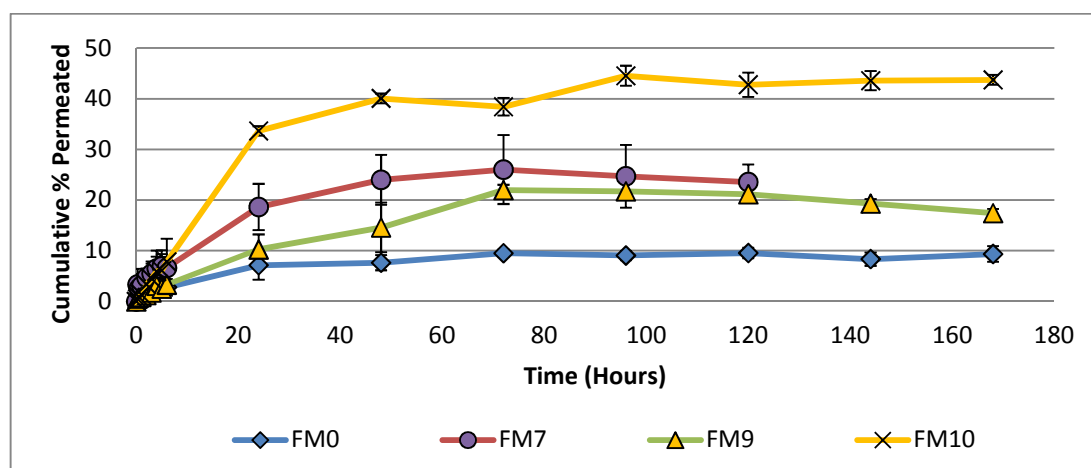
(B)



**Figure 6.21: Comparative diffusion profiles of ibuprofen from (A) FM0 (Eudragit RS PO as a carrier) and FM5 (10% (w/w) xanthan gum and 60% (w/w) Eudragit RS PO as carriers) extruded films and (B) from FM-I (2.5% xanthan gum), FM-II (5% xanthan gum) and FM5 films, tested approximately at 32°C and permeated across silicone membrane into phosphate buffer solution (pH=7.2) at 37°C. Each data point represents the mean  $\pm$  S.D. of no less than three measurements**

For Pluronic® F127 loaded films (FM7), the permeation profile was enhanced with circa 26% drug permeation after three days in comparison with a total of about 9% drug permeated after the same period from the control films (FM0) as seen in Figure 6.22. The inclusion of Gelucire 44/14 in Eudragit RS PO films showed a maximum of circa 22% of the total drug permeated after three days from FM9 films which contained the lower lipid content (10% w/w). However, a remarkable increase in the permeation was detected using FM10 formulation (higher lipid content) as compared to other formulations tested here. More specifically, these films showed a permeation of nearly 45% of the loaded ibuprofen after four days (Figure 6.22).

However, the drug permeation was not completed over the course of the experiment i.e. five to seven days. This can be a major spur to investigate other factors that can control active substance permeation from these films. Among these factors or measures, as cited in Chapter 1 (Grawe et al., 2005), crystallinity of the active substance, as well as the interaction of the active substance and polymer with the water adsorbed from the skin can affect the permeation of the active constituent across the skin from transdermal patches. The first factor will be explored in this section, whereas the second one will be discussed in the following section since it is more related to the performance properties at the level of the site of action rather than vehicle formulation effects.



**Figure 6.22: Ibuprofen diffusion profiles from hot melt extruded films of FM0, FM7, FM9 and FM10 formulations tested approximately at 32°C and permeated across silicone membranes into phosphate buffer solution (pH=7.2) at 37°C. Each data point represents the mean±S.D. of no less than three measurements**

The percentage crystallinity was calculated from MTDSC total heat flow signals of the samples and based on the following equation:

$$\text{Crystallinity (\%)} = \left( \frac{\Delta H_m \text{ of the Extruded sample}}{\Delta H_m \text{ Ibuprofen} \times W} \right) \times 100 \quad (\text{Eq.6.1})$$

Where, ‘ $\Delta H_m$  of the Extruded sample’ represents the melting enthalpy of the ibuprofen in the extruded system (J/g). For this term, difficulty arose with the films containing crystalline ibuprofen and crystalline or semi-crystalline constituents as Gelucire 44/14 and Pluronic®F-127. The integration range used to measure the area of their melting endotherms was associated with some uncertainty, due to broadness of these peaks as illustrated from Figure 6.24 through to Figure 6.26. However, for the same kind of samples the same ranges were used.

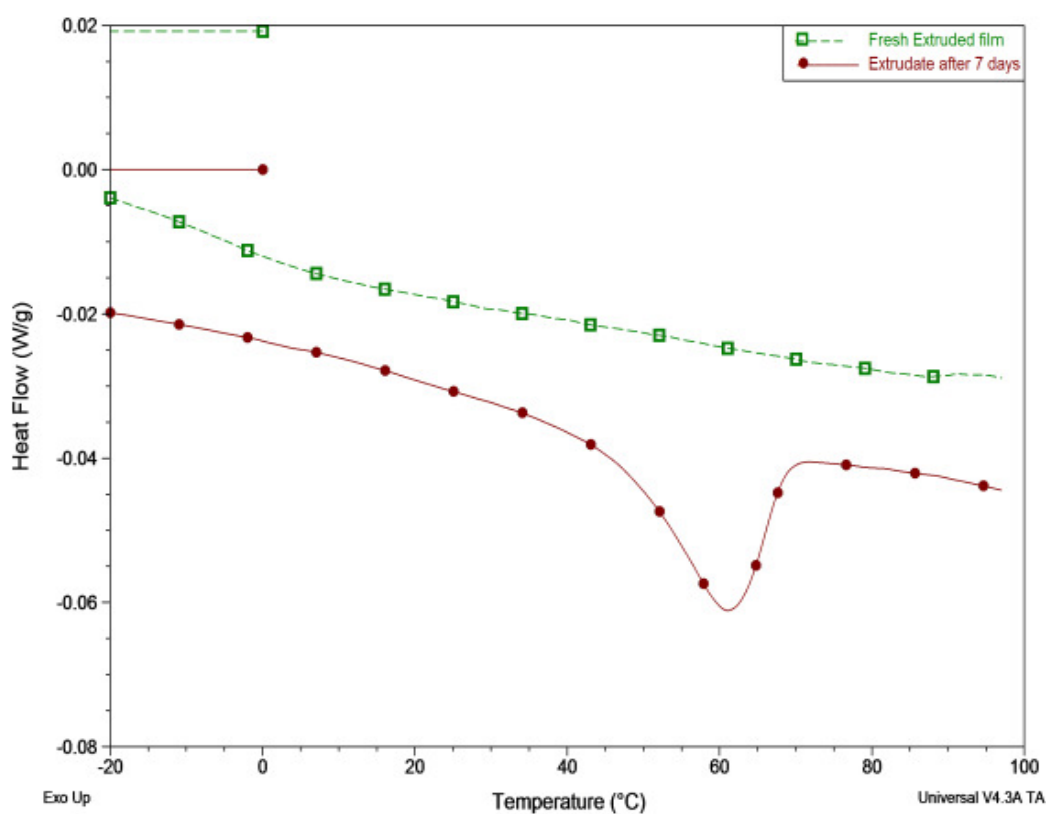
Moreover, the observed melting peak of the FM10 films was mainly ascribed to ibuprofen, as per PXRD findings, but this does not preclude the existence of crystalline Gelucire 44/14. This suggestion is consistent with the location of the broad peak in the extrudate as compared to its respective physical mixture as seen in Figure 6.26. The melting range of the peak in the extruded film seems to embrace both constituents (ibuprofen and Gelucire 44/14) which were otherwise observed individually in the equivalent physical mix. Therefore, the estimated values of the percent crystallinity in this work are understood to be indicative rather than quantitative. Furthermore, it is recommended that the melting peak magnitude approach to be used for intra-comparison purposes for the same material constituents or formulations rather than inter-comparison between different formulations.

Other terms in Equation 6.1 are ‘W’ and ‘ $\Delta H_m$  Ibuprofen’. The first one is defined as the weight fraction of ibuprofen in the extruded sample. It should be pointed out that this weight fraction of ibuprofen will be less after the permeation experiment due to diffusion of ibuprofen into the receptor medium and its retention in the used silicone membrane. On that basis the calculations were performed. Therefore the amounts of the drug recovered in the silicone membranes and permeated into the receptor medium were subtracted from the original assayed amount (before the permeation study). The resultant weight was used in this equation to represent ibuprofen amount in the films examined *via* MTDSC after the permeation experiment. The results were recorded as ‘relative’ percent crystallinity to allow for better comparative results (Table 6.6). The ‘ $\Delta H_m$  Ibuprofen’ is the melting enthalpy of the ibuprofen standard, which is assumed to represent full crystallinity (100%).

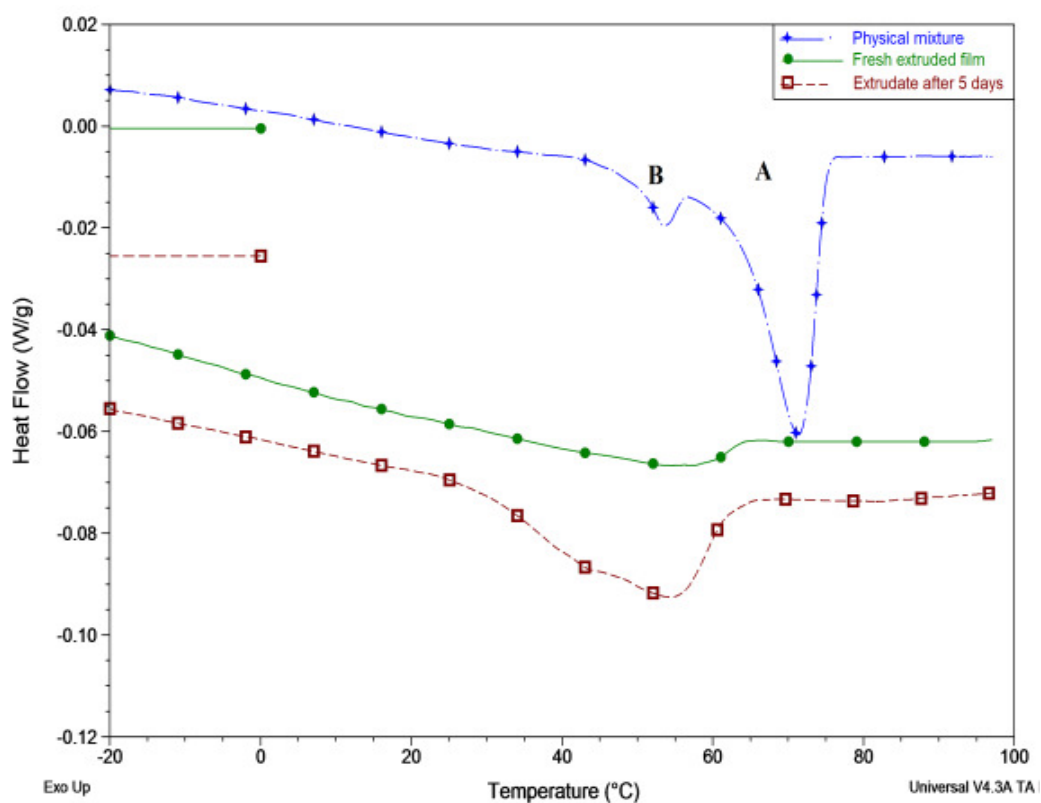
The extruded films removed after the end of the diffusion experiments and assessed for any signs of ibuprofen recrystallization using MTDSC measurements are displayed from Figure 6.23 through to Figure 6.27. It was noted that the ibuprofen recrystallized within these matrices after the permeation study, thus melting endotherms were detected in FM5 (10% (w/w) xanthan gum) and FM9 films (10% (w/w) Gelucire 44/14) as shown in Figure 6.23 and Figure 6.24, respectively, or increased in size (melt  $\Delta H$ ) as in FM7 films (10% (w/w) Pluronic® F127) shown in Figure 6.25, and in the case of FM10 films (20% (w/w) Gelucire 44/14), two melting peaks were observed (Figure 6.26). One of these two peaks has a similar melting range to the one detected in the fresh samples and is preceded with a second peak that is similar to the melting range of the secondary melting endotherm of the Gelucire 44/14 (see Chapter 3). This can explain the contradiction of the relative percent crystallinity observed for these films as seen in Table 6.6. In other words, the fresh films were estimated to have about 10% crystalline ibuprofen, whereas the films after the experiment had almost half this value. This might indicate that melting endotherm used in the calculation of this percentage in the fresh samples was in fact a function of both Gelucire 44/14 and ibuprofen crystals rather than only ibuprofen. This suggests the possibility of obtaining a lower relative percent crystallinity of ibuprofen in these fresh samples, if we take into account contribution of the crystalline Gelucire 44/14. The broad melting endotherm observed for FM9 (10% (w/w) Gelucire 44/14) extruded films after the permeation experiment might also follow the same behaviour. As depicted in Figure 6.25, the range of this melting peak occurs within the range of the melting events of both Gelucire 44/14 and ibuprofen as compared to their equivalent physical mix. Thus the calculated drug percent crystallinity in this case might be overestimated.

Formula code	Relative Percent Crystallinity	
	Fresh extruded film (before the test)	Extruded films after the test
FM0	Not applicable	2.95±0.62
FM5	Not applicable	13.65±0.35
FM7	1.82±0.28	22.18±0.89
FM9	Not applicable	12.66±0.92
FM10	10.08±0.66	5.74±0.88

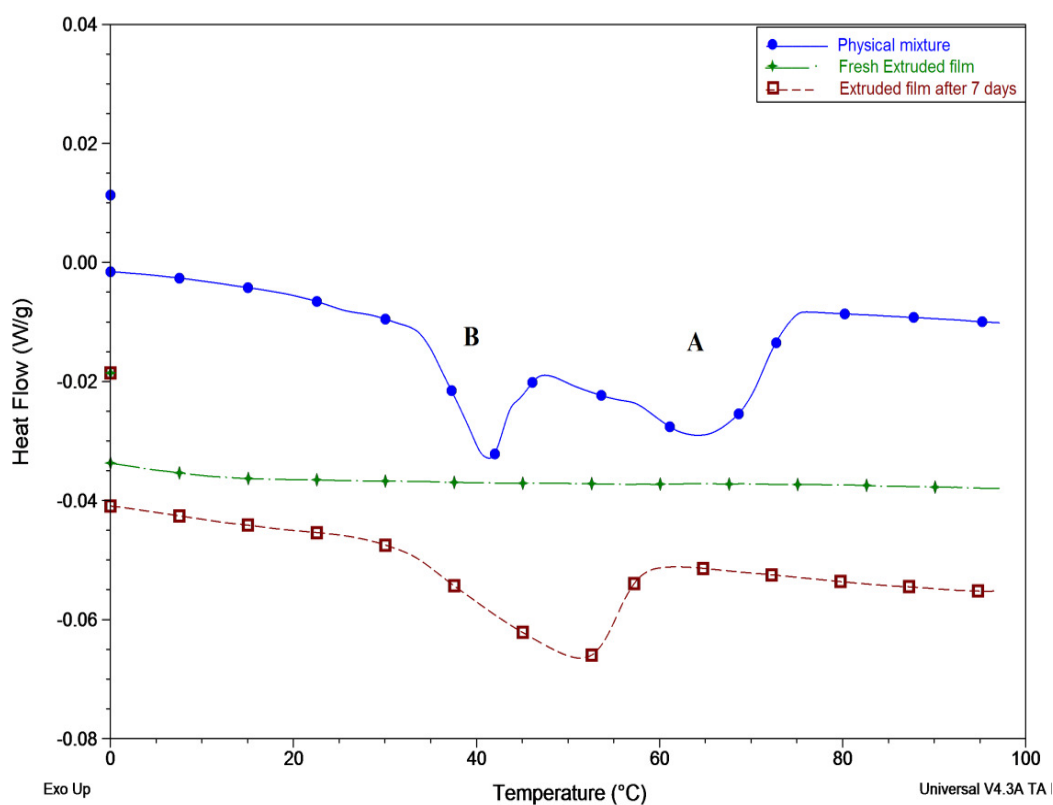
**Table 6.6: Estimated relative percentage crystallinity of ibuprofen from different hot melt extruded formulations before and after the end of the permeation experiments (see text or Table 6.3 for their compositions)**



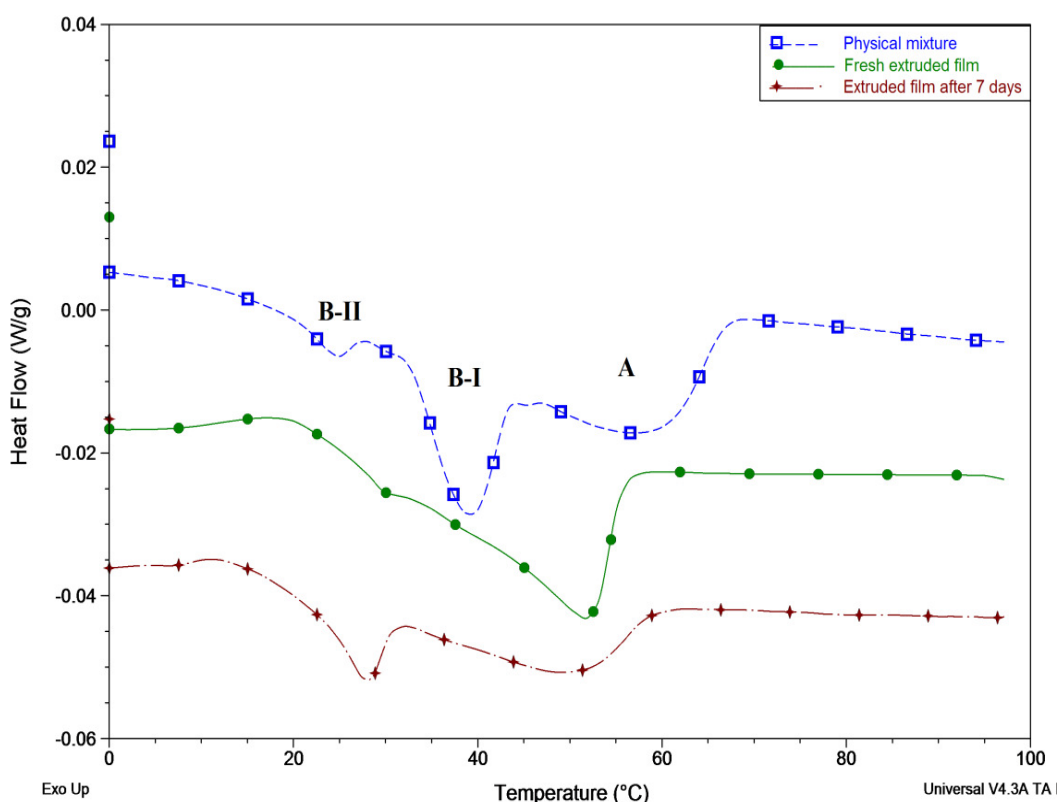
**Figure 6.23: Observed melting endotherm in the MTDSC total heat flow signals of FM5 (10% (w/w) xanthan gum and 60% (w/w) Eudragit RS PO as carriers) extruded film examined before (fresh) and after the permeation experiment. Underlying scan rate of 1°C min<sup>-1</sup> with a modulation amplitude of ±0.265°C and a period of 100 seconds**



**Figure 6.24:** Observed melting endotherms in the MTDSC total heat flow signals of FM7 (10% (w/w) Pluronic® F127 and 60% (w/w) Eudragit RS PO as carriers) extruded film before (fresh) and after the permeation experiment in comparison to its equivalent physical mixture. ‘A’ and ‘B’ symbols denoted for peaks related to ibuprofen and Pluronic® F127, respectively. Underlying scan rate of  $1^{\circ}\text{C min}^{-1}$  with a modulation amplitude of  $\pm 0.265^{\circ}\text{C}$  and a period of 100 seconds



**Figure 6.25:** Observed melting endotherms in the MTDSC total heat flow signals of FM9 (10% (w/w) Gelucire 44/14 and 60 % (w/w) Eudragit RS PO as carriers) extruded film examined before (fresh) and after the permeation experiment in comparison to its equivalent physical mixture. ‘A’ and ‘B’ symbols denoted for peaks related to ibuprofen and Gelucire 44/14, respectively. Underlying scan rate of  $1^{\circ}\text{C min}^{-1}$  with a modulation amplitude of  $\pm 0.265^{\circ}\text{C}$  and a period of 100 seconds

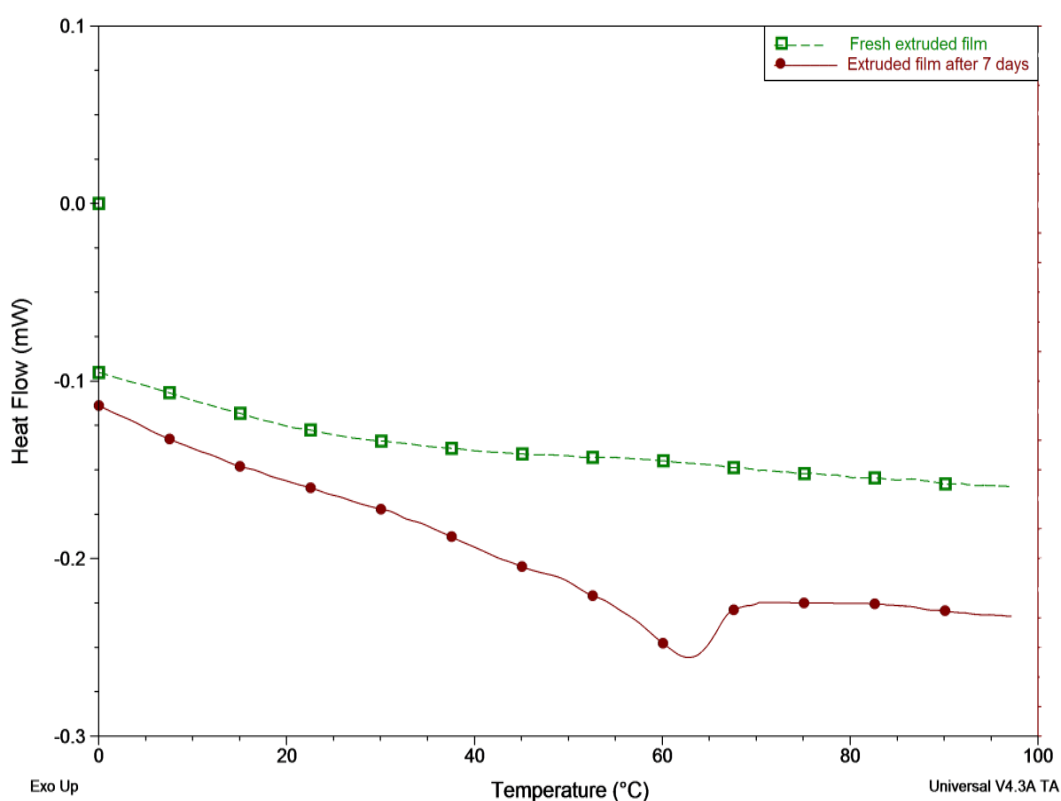


**Figure 6.26:** Observed melting endotherms in the MTDSC total heat flow signals of FM10 (20% (w/w) Gelucire 44/14 and 50% (w/w) Eudragit RS PO as carriers) extruded film before (fresh) and after the permeation experiment in comparison to its equivalent physical mixture. ‘A’ symbol denoted for peak related to ibuprofen whereas ‘B-I’ and ‘B-II’ symbols denoted for peaks related to Gelucire 44/14. Underlying scan rate of  $1^{\circ}\text{C min}^{-1}$  with a modulation amplitude of  $\pm 0.265^{\circ}\text{C}$  and a period of 100 seconds

Although the aforementioned limitations could affect the estimated relative percent crystallinity, the approach represents a simple means of assessing the occurrence of drug recrystallization as well as giving some indication of its extent. In the control films (FM0), containing 30% (w/w) ibuprofen in 70% (w/w) Eudragit RS PO, recrystallization took place as shown in Figure 6.27. This can be understood with reference to the equilibrium saturation solubility study after incubation at 60%RH/25°C (Chapter 4). This earlier study, in brief, stated that water adsorbed under these conditions for one month dropped down the solubility of the ibuprofen in Eudragit RS PO matrices to almost 10% (w/w). A certain relative humidity can be generated inside Franz cells because they were occluded using parafilm to prevent water loss. The crystallization in the permeation studies took place within a shorter time in comparison to the films incubated under 60%RH/25°C. Therefore, it could be



inferred that a higher relative humidity conditions exist in this experiment (inside Franz cells) and/or the effect of high temperature employed ( $\sim 32^{\circ}\text{C}$  compared to  $25^{\circ}\text{C}$ ) which in either case, drove a faster crystallization. As known, storage at temperatures higher than the glass transition of the amorphous material, along with possible water plasticization, can enhance mobility of the amorphous compound and speed up its conversion to the stable crystalline state. Accordingly, it could be speculated that in response to these conditions, the recrystallization took place or increased in other tested formulations during the permeation studies. It was with hindsight performing water content measurements of the samples after permeation study that would have indicated if the water amount in these samples differed to the samples stored under 60%RH/ $25^{\circ}\text{C}$ .



**Figure 6.27: Observed melting endotherm in the MTDSC total heat flow signals of the control extruded FM0 film (Eudragit RS PO as a carrier) examined before (fresh) and after the permeation experiment. Underlying scan rate of  $1^{\circ}\text{C min}^{-1}$  with a modulation amplitude of  $\pm 0.265^{\circ}\text{C}$  and a period of 100 seconds**

Overall, as shown in Table 6.6, the estimated fraction of the drug that has been recrystallized after the permeation experiment is minimal; which alone might not be enough to account for the observed poor diffusion from the studied systems. Nevertheless, it can be argued that the observed recrystallization within the tested films could decrease the drug release and the permeation thereof would be low.

In summary, ibuprofen permeation was limited from the FM5 (10% (w/w) xanthan gum), FM7 (10% (w/w) Pluronic® F127), FM9 (10% (w/w) Gelucire 44/14) and FM10 (20% (w/w) Gelucire 44/14) formulations. Possible factors contributing to the poor diffusion profiles were lack of sufficient hydration, which was clearly demonstrated in the films formulated with the xanthan gum (FM5), in addition to the recrystallization of ibuprofen. It was therefore decided to investigate other approaches for enhancement of the ibuprofen permeation from the selected films. This will be discussed in the following section and concerns the influence of hydration as a possible means of permeation enhancement. This technique corresponds to one of the most common design modifications that are applied at the level of the application site rather than optimisation of the drug-vehicle formulation (Benson, 2005). For that purpose, two categories of films were selected from the optimized formulations. Firstly, films whereby the ibuprofen is not crystalline in the fresh samples were selected (FM5 (10% (w/w) xanthan gum) and FM9 (10% (w/w) Gelucire 44/14)). The second type of film chosen is the one that achieved the maximum permeation of the drug, namely, the FM10 (20% (w/w) Gelucire 44/14) films.

### 6.3 Effects of hydration

In the previous section we have defined some elements important for designing feasible formulations for extrusion with improved release profiles. However, poor permeation profiles of these selected systems steer the discussion on the possible reasons behind that, including drug recrystallization and lack of proper hydration. Therefore, the main objective of this section is to explore how hydration may influence permeation from selected films. The study will examine the issue of the relationship between drug permeation and hydration level inside the Franz cells, as measured by the relative humidity level established in these cells. The relationship between ibuprofen permeability from the optimized selected matrices and the approximate hydration level that can be produced by skin occlusion will also be addressed.

### 6.3.1 Methodology

A Franz Cell diffusion system composed of six diffusion cells with identical characteristics were used to measure the release of ibuprofen from FM5 (10% (w/w) xanthan gum), FM9 (10% (w/w) Gelucire 44/14) and FM10 (20% (w/w) Gelucire 44/14) films through silicone membranes in a similar procedure to Chapter 5. However, to probe the influence of hydration on the enhancement of ibuprofen release from the tested films thereafter its penetration across the silicone membranes, two conditions were applied, namely, Test 1 and Test 2.

In Test 1, the extruded films in the donor phase were immersed with 0.3 ml (maximum capacity of the donor chamber) of the phosphate buffer medium (pH=7.2), which is also used in the receptor phase. The second condition (Test 2) was exposing fresh films to a controlled relative humidity of 95% at 25°C using DVS machine (see Chapter 2) and the films were held at this humidity level for 3 hours to achieve near equilibrium at this condition prior application to the Franz Cell diffusion system. TGA was used to measure the water content as documented in Chapter 4. The level of the relative humidity that could be established inside the Franz cells was monitored through setting up the diffusion experiments as described in Chapter 5, but without any tested films. Humidity indicator cards were assembled with the donor chambers of the Franz cells in order to give an approximation on that humidity level as depicted in Figure 6.28. Gelucire 44/14 containing films, coded as FM9 (10% (w/w) Gelucire 44/14) and FM10 (20% (w/w) Gelucire 44/14) were also probed for their permeation behaviour in a similar procedure with the Test 1, but using 0.14 ml volume of the PBS (pH=7.2) in attempt to mimic hydration established after skin occlusion. MTDSC experiments, as described in Chapter 3, were carried out to study the changes in film integrity after the drug permeation following hydration.



**Figure 6.28:** PermeGear Franz Cell diffusion system includes six jacketed Franz cells; securely located to a stirrer. The receptor chambers were filled with phosphate buffer solution (pH=7.2) maintained at 37°C and covered with silicone membranes. Humidity indicator cards were mounted on the top of each donor chamber and all openings were sealed with double layers of Parafilm®

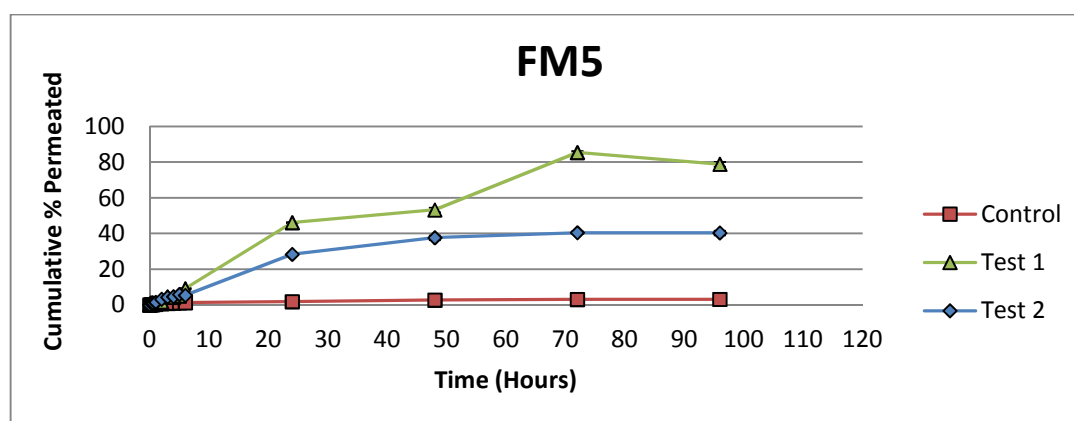
### 6.3.2 Results and discussion

#### 6.3.2.1 Hydration dependence of the *in vitro* permeation of ibuprofen from hot melt extruded films

Due to the enhanced *in vitro* release (dissolution test) behaviour of the FM5 (10% (w/w) xanthan gum), FM9 (10% (w/w) Gelucire 44/14) and FM10 (20% (w/w) Gelucire 44/14) films compared to the films with no hydrophilic additives, understanding the influence of hydration is necessary in order to understand the *in vitro* permeation properties. Figure 6.29 shows to what extent the permeation profiles of the ibuprofen depends on these films' hydration. The permeation profiles of these samples were firstly compared to the samples hydrated using 0.3 ml of the phosphate buffer (pH=7.2) in 'Test 1'. This level of hydration is the maximum volume can be added in the donor chamber of each cell of the Franz diffusion system. It is clearly seen that this hydration provoked a significant enhancement in the permeation profiles as compared with the control samples of the same compositions but without hydration. The maximum drug permeation was 85.44% after 72 hours from FM5 films (xanthan gum), 98.91% after 96 hours from FM9 films (low level of Gelucire 44/14) and around 94.26% after 5 hours from FM10 films (higher level of Gelucire 44/14).

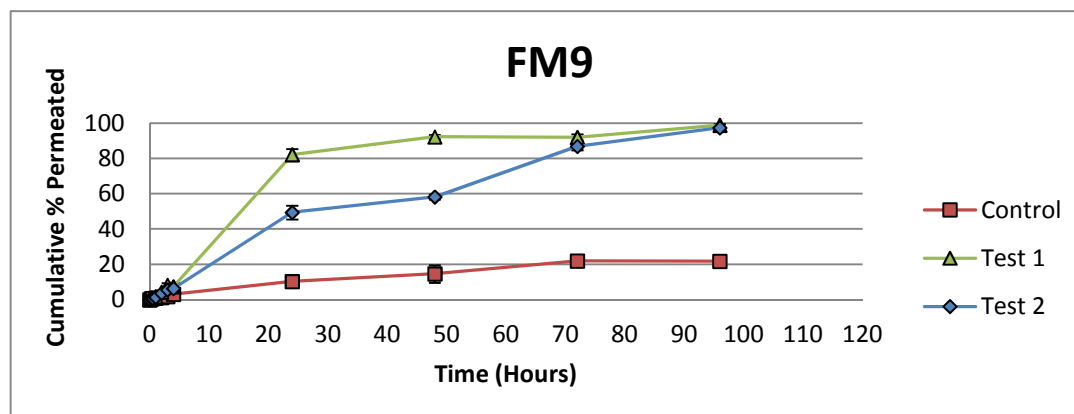
Additionally the samples were conditioned at a controlled level of humidity using the DVS at 95%RH/25°C for three hours and examined for their *in vitro* permeation behaviour (Figure 6.29, Test 2). The water content of these samples was measured using TGA and compared to the non-hydrated samples as shown in Figure 6.30. This increase in the water content resulted in a profound change of the drug permeation in comparison with non-hydrated samples (control) as depicted in Figure 6.29. An increase in the percent of the drug permeated was noticed but in a slower rate than samples exposed to the hydration level in 'Test 1'. This was illustrated in Figure 6.31 using the time parameter which is required to attain 80 percent or higher of the cumulative drug permeation.

(A)

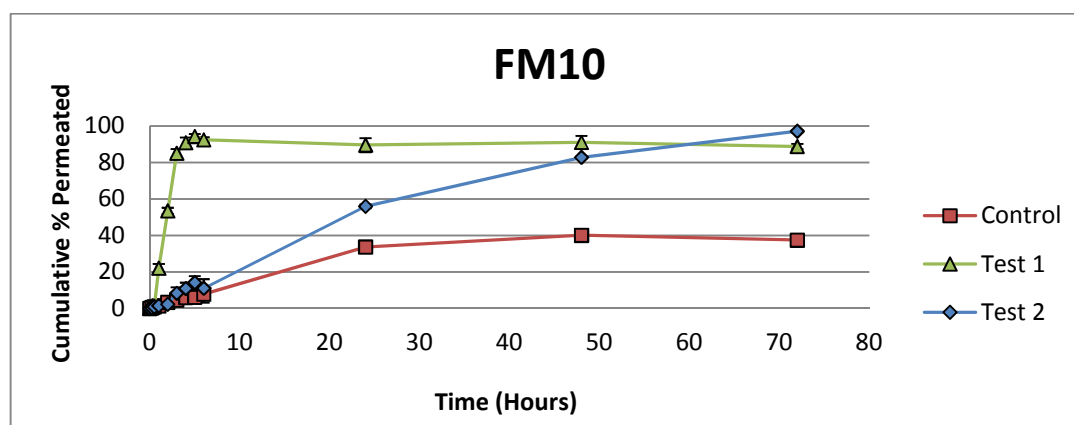


**Figure 6.29: Ibuprofen diffusion profiles from hot melt extruded films of (A) FM5 (60% (w/w) Eudragit RS PO and 10% (w/w) xanthan gum as carriers) tested approximately at 32°C and permeated across silicone membrane into phosphate buffer solution (pH=7.2) at 37°C. Control: samples without hydration. Test 1: each sample was placed in 0.3 ml of PBS (pH=7.2) in the donor chamber of the Franz cells. Test 2: samples were moistened at 95%RH/25°C for three hours prior testing in the Franz cells. Each data point represents the mean±S.D. of no less than three measurements**

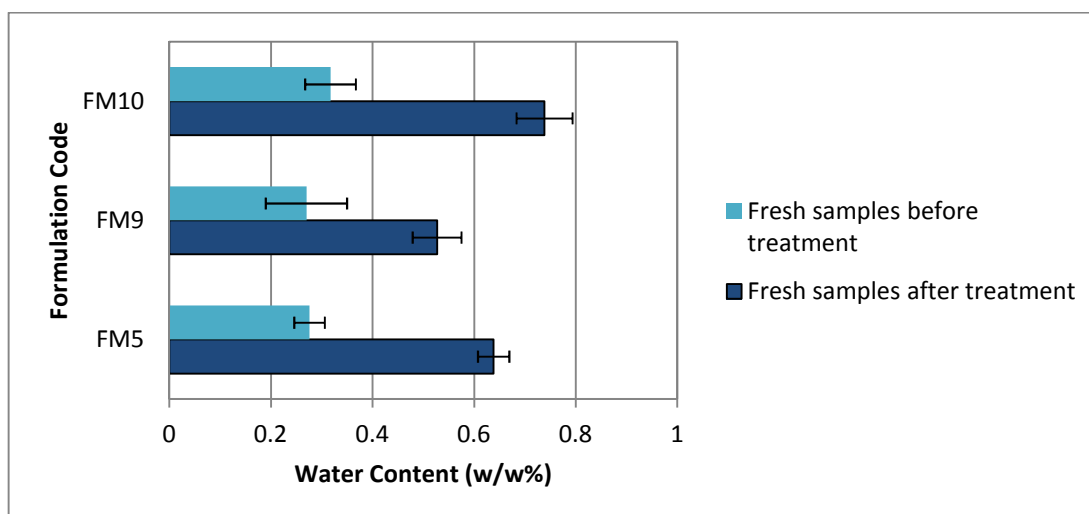
(B)



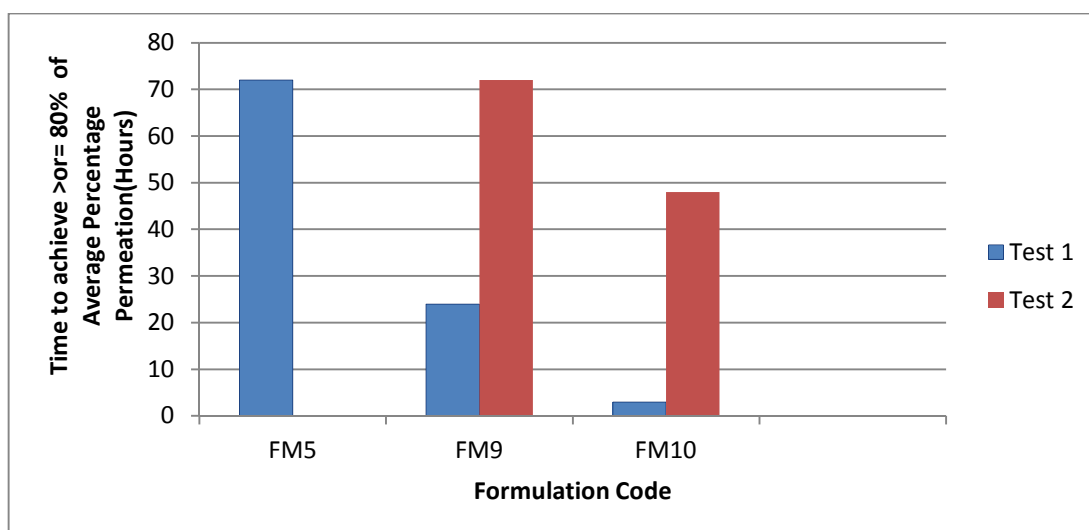
(C)



**Figure 6.29 (Contd.):** Ibuprofen diffusion profiles from hot melt extruded films of (B) FM9 (60% (w/w) Eudragit RS PO and 10% (w/w) Gelucire 44/14 as carriers) and (C) FM10 (50% (w/w) Eudragit RS PO and 20% (w/w) Gelucire 44/14 as carriers) tested approximately at 32°C and permeated across silicone membrane into phosphate buffer solution (pH=7.2) at 37°C. Control: samples without hydration. Test 1: each sample was placed in 0.3 ml of PBS (pH=7.2) in the donor chamber of the Franz cells. Test 2: samples were moistened at 95%RH/25°C for three hours prior testing in the Franz cells. Each data point represents the mean±S.D. of no less than three measurements



**Figure 6.30:** Summary of the measured percentage water contents of different hot melt extruded films (see text for their compositions) determined by TGA on freshly basis immediately after extrusion (before treatment) and after incubation at 95%RH/25°C for three hours in the DVS (after treatment)



**Figure 6.31:** The time corresponding to 80% or higher of the cumulative percentage permeation of the ibuprofen from hot melt extruded films of Eudragit RS PO-based films containing Xantural® 75 (FM5 composition), Gelucire 44/14 (FM9 and FM10 compositions) tested approximately at 32°C and permeated across silicone membrane into phosphate buffer solution (pH=7.2) at 37°C. Test 1: each sample was placed in 0.3 ml of PBS (pH=7.2) in the donor chamber of the Franz cells. Test 2: samples were moistened at 95%RH/25°C for three hours prior testing in the Franz cells

Furthermore, the permeation kinetics of the *in vitro* drug permeation from these films was explored with and without hydration under different conditions. Zero order, first order and Higuchi equation models were used to study the effect of hydration on the permeation kinetics from these films as shown in Table 6.7, whereas the power model was used to explain the possible release mechanism as seen in Table 6.8. As detailed in Chapter 5, the correlation coefficient,  $R^2$ , was used to assess the fit of a model equation. The model with the highest  $R^2$  will be considered to be the best fit to describe the kinetics of the permeation. FM5 (10% (w/w) xanthan gum), FM9 (10% (w/w) Gelucire 44/14) and FM10 (20% (w/w) Gelucire 44/14) films, studied at different hydration conditions and compared to the non-hydrated samples exhibited non-linear ibuprofen permeation with time wherein the first order release kinetics was the best model to describe these profiles (Table 6.7). This indicates that hydration level did not alter these profiles kinetically and that the permeation rate will decrease with time. Consequently, these systems can act as matrices that control the permeation profile of the drug. This control can be advantageous for enhanced reproducibility of the transdermal drug delivery because inter- and intra-subject variations can be minimized (Hillery et al., 2001).



Used Kinetic model	First order model	Zero order model	Higuchi square-root of time model
Tested sample	$R^2$	$R^2$	$R^2$
(A) FM5 Films			
Control	0.9655	0.8895	0.9491
Test 1	0.9756	0.9238	0.9557
Test 2	0.9902	0.8701	0.9523
(B) FM9 Films			
Control	0.9823	0.9553	0.9787
Test 1	0.9741	0.8156	0.9108
Test 2	0.9845	0.9587	0.9811
(C) FM10 Films			
Control	0.9831	0.8419	0.9384
Test 1	0.9742	0.2198	0.4133
Test 2	0.9916	0.9543	0.9741

**Table 6.7: Fit correlation coefficients ( $R^2$ ) of different applied kinetics models for the permeation profiles of the FM5 (10% (w/w) xanthan gum), FM9 (10% (w/w) Gelucire 44/14) and FM10 (20% (w/w) Gelucire 44/14) films tested under different hydration conditions. Control: samples without hydration. Test 1: each sample was placed in 0.3 ml of PBS (pH=7.2) in the donor chamber of the Franz cells. Test 2: samples were moistened at 95%RH/25°C for three hours prior testing in the Franz cells**

In Table 6.8 the power model was used to predict the involved release with subsequent permeation mechanism(s) from these films. As mentioned in Chapter 5, the measured release exponent can be used to describe these mechanisms. The permeation profiles from FM5 films (10% (w/w) xanthan gum) showed anomalous transport in all the tested samples regardless of the applied hydration condition. This means that diffusion and swelling were the main mechanisms involved in the ibuprofen release from these films and permeation through the silicone membranes. However, it could be argued that hydrated samples can also follow case-II transport, because their release exponents are almost approaching 1. In this case it would be assumed that drug release is mainly controlled by swelling of these matrices. On either way, it is believed that swelling is a feasible prediction of the release mechanism herein, because it is characteristic of the xanthan gum contained in these films to allow drug release and permeation. These films were swelled after being hydrated in Test 1 and in Test 2 assuming the shape of the diffusion area (circular) of the Franz cells.

Kinetic model		Korsmeyer-Peppas model (Power law)	
	$R^2$	Release exponent (n)	Expected release mechanism
(A) FM5 Films			
Control	0.9480	0.45	Anomalous transport
Test 1	0.9676	0.97	Anomalous transport
Test 2	0.9776	0.95	Anomalous transport
(B) FM9 Films			
Control	0.9820	0.67	Anomalous transport
Test 1	0.9253	1.00	Case-II transport
Test 2	0.9833	0.93	Anomalous transport
(C) FM10 Films			
Control	0.9779	0.79	Anomalous transport
Test 1	0.9538	2.52	Super case-II transport
Test 2	0.9698	1.18	Super case-II transport

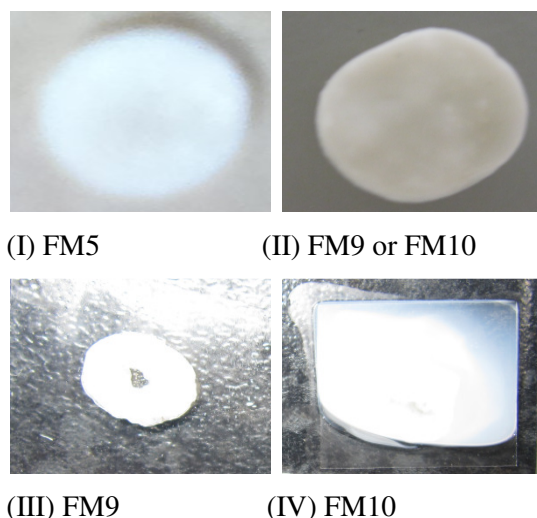
**Table 6.8: Interpretation of the measured release exponents from the power law model and their correlation coefficients ( $R^2$ ) for the permeation profiles of the FM5 (10% (w/w) xanthan gum), FM9 (10% (w/w) Gelucire 44/14) and FM10 (20% (w/w) Gelucire 44/14) films tested under different hydration conditions. Control: samples without hydration. Test 1: each sample was placed in 0.3 ml of PBS (pH=7.2) in the donor chamber of the Franz cells. Test 2: samples were moistened at 95%RH/25°C for three hours prior testing in the Franz cells**

The release exponent determined in the FM9 films (10% (w/w) Gelucire 44/14) revealed that matrix swelling is expected to control the faster permeation of these films achieved by hydration in Test 1. Conversely, the slower permeation obtained after being hydrated at low levels in Test 2 is believed to be controlled by combination of matrix swelling and diffusion, resembling the mechanism of control samples (non-hydrated). The films hydrated in Test 2 had a release exponent close to 1, so we could also assume that swelling would be the main mechanism of drug release from these films (case-II transport).

The swelling in the FM9 films could take place as a function of the swelling of Gelucire 44/14 in these systems as expected after contact with aqueous medium as other Gelucires (Sutananta et al., 1995). This was further supported by the appearance of these films. In like

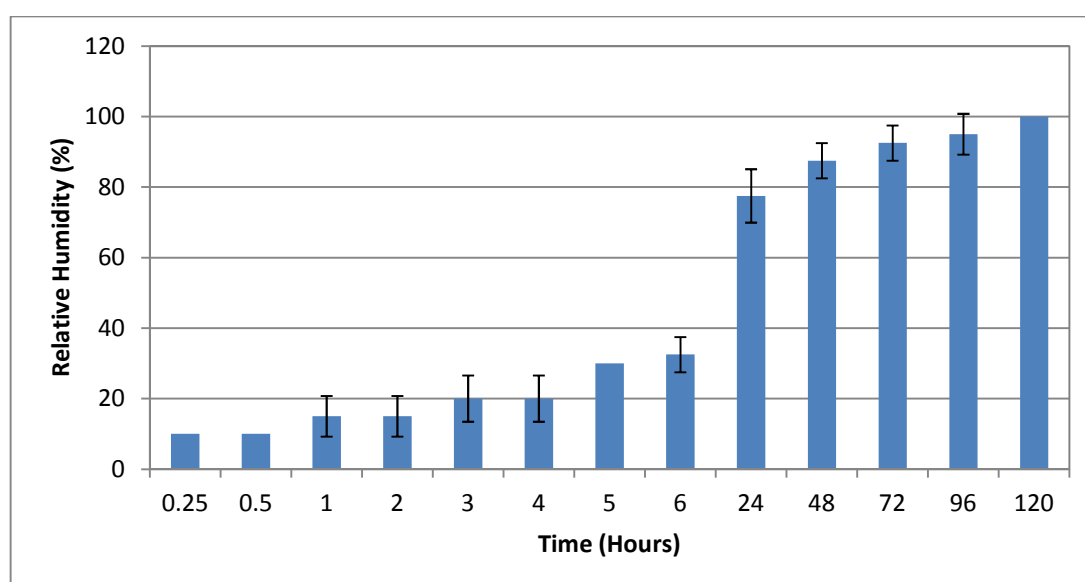
manner to the FM5 films, the films exposed to hydration in Test 1 and 2 were swelled and jellified adapting the shape of the diffusion area (circular) of the Franz cells.

Incorporation of higher level of Gelucire 44/14 in the FM10 films demonstrates an alteration of the predicted mechanism after being hydrated in both Test 1 and Test 2. The control systems (non-hydrated) changed from anomalous transport controlled by swelling and diffusion into super case-II transport that is controlled by swelling and relaxation mechanisms. However, films tested under Test 2 have a release exponent close to 1, so it could also be speculated that drug release is controlled mainly by swelling (case-II transport). The control samples herein retained their normal rectangular shape after the permeation study whereas the films hydrated in Test 2 swelled and jellified as FM9 films. Surprisingly samples in Test 1 transferred into homogenous liquid-like emulsion. Figure 6.32 is set forth to exemplify the shape deformation of different films after permeation experiment or otherwise after being hydrated externally under glass slides to illustrate mainly the liquid-like formation of FM10 films similar to Test 1 condition.



**Figure 6.32: Representative photographs of shape and consistency changes of hot melt extruded films removed from Franz cells post testing (top row) and exposed to 0.3 ml PBS (pH=7.2) at 32°C to imitate Test 1 condition over three hours and under glass slides (bottom row). (I) FM5 films (10% (w/w) xanthan gum) after Test 1 and Test 2. (II) FM9 films after Test 1 and Test 2 or FM10 after Test 2. (III) FM9 films (10% (w/w) Gelucire 44/14). (IV) liquid-like emulsion of hydrated FM10 films (20% (w/w) Gelucire 44/14). Images of these films before the tests were captured in Table 6.2**

From earlier discussion it is evident that hydration left appreciable impact on the observed permeation profiles of ibuprofen from the studied films. Therefore, humidity level was further evaluated inside Franz cells, which is assumed to closely mimic *in vivo* skin conditions. It is believed that these measurements would be useful to get insight into the suggested relation between the onset of maximum permeation from the studied systems and applied humidity condition. Using the same conditions employed in the used permeation studies the humidity levels were estimated. Figure 6.33 shows the experimentally determined relative humidity values over five days. It is noted that the relative humidity levels increased over time. However, the water accumulated in these cells does not meet the threshold to enhance the drug liberation from the studied films as reflected by poor permeation profiles, but rather it is expected to facilitate drug recrystallization as suggested in section 6.2.

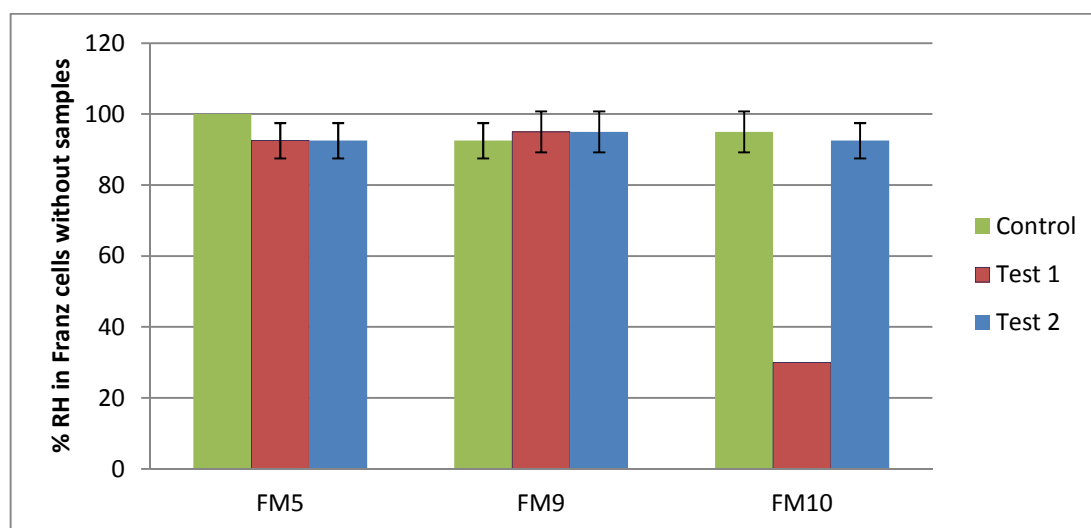


**Figure 6.33: Variation of the percent relative humidity (%RH) over 120 hours inside the donor chambers of Franz Cell diffusion system encompasses receptor chambers covered with silicone membranes and filled with phosphate buffer solution (pH=7.2) maintained at 37°C. Each measurement recorded from humidity indicator card represents the mean±S.D. of six measurements**

Notably, the maximum percentages of the drug permeated from the FM5 (xanthan gum), FM9 (low level of Gelucire 44/14) under control conditions (without hydration) and used hydration levels of Test 1 and Test 2 were achieved at the times which correspond to the humidity levels higher than 80%RH inside Franz cells as seen in Figure 6.34. This reinforces

the role of the water taken from the surrounding environment (Franz cells) in achieving maximum permeation from the studied films. This also conforms to the observed permeation behaviour of FM10 films under control conditions and at Test 2 conditions (humidification at 95%RH/25°C for 3 hours prior test).

However, using higher hydration condition in Test 1, the maximum permeation achieved in FM10 films was not correlated with the high humidity level inside Franz cells. This may likely be attributable to some observed aspects of this formulation. At this hydration level, profound changes of the solid state consistency took place wherein a liquid-like emulsion formed. This may suggest possible emulsion formation with subsequent enhanced solubilisation and permeation of ibuprofen. This would be expected by knowing the good solubilisation (Karatas et al., 2005; Kawakami et al., 2004), permeation enhancement (Li et al., 2008) and self-emulsifying (Chambin et al., 2004; Kale and Patravale, 2008; Kallakunta et al., 2013; Rowe et al., 2009) properties of Gelucire 44/14. Another possibility is formation of supersaturated systems after immersion in the buffer solution. These systems are known to have high chemical potential that can drive significant increase of the active substance permeation as evident here from the significant increase of the percent ibuprofen permeated.



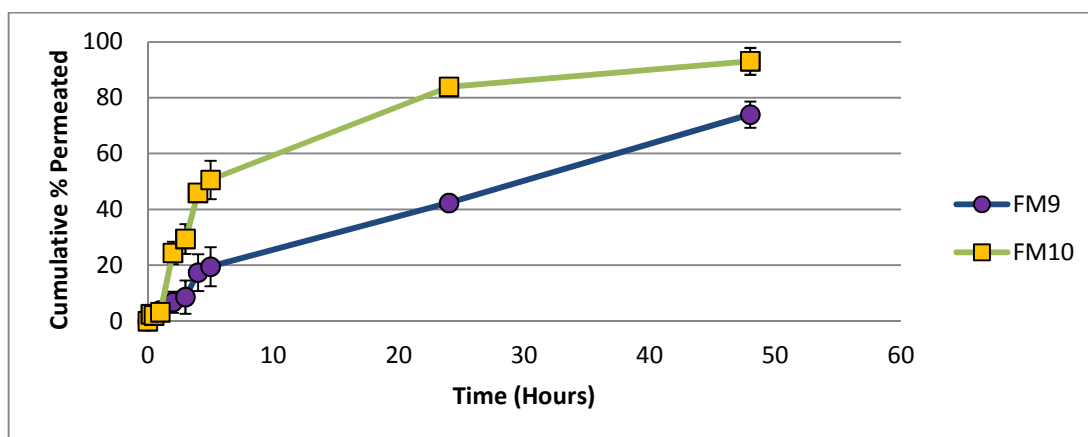
**Figure 6.34: Relative humidity values as recorded from Franz cells (from Figure 6.33) at the time point corresponding to the maximum total permeation from formulations of FM5 (10% (w/w) xanthan gum), FM9 (10% (w/w) Gelucire 44/14) and FM10 (20% (w/w) Gelucire 44/14), tested at different hydration levels**

Overall, the hydration was essential to achieve improved drug permeation from the studied systems. Thus, the application of these films looks as innovative approach to deliver the ibuprofen transdermally due to simple matrix design and the safety of employing water to activate drug permeation (Hadgraft, 1999). Moreover, different permeation programs in the same type of the system were created depending on the applied hydration level.

Therefore, variation of either the vehicle used or the applied hydration level will result in a different permeation program. As the permeation profiles from vehicles containing Gelucire 44/14 were notably conditioned and improved even at low levels of hydration in comparison to the FM5 formula containing xanthan gum, it was decided to continue with these formulations, coded as FM9 and FM10. However, the need of high hydration of FM5 films to release the ibuprofen can be solved if we use this system, for example, for wound dressings when inflammation is present and where an excess of fluid is coming from exuding wounds. Thereafter, the exudate will be removed or absorbed by this system and simultaneously the anti-inflammatory agent i.e. ibuprofen will be released.

For FM9 (10% (w/w) Gelucire44/14) and FM10 (20% (w/w) Gelucire44/14) films, it is believed that the hydration produced by skin occlusion might be enough to activate them. Skin occlusion is a common therapy approach that is usually utilized to improve permeation of the drugs into the skin (Warner et al., 1999; Williams and Barry, 2004). This approach relies mainly on the profound hydration it can produce, wherein water can act as “absorption accelerator” through the proposed mechanisms detailed in Chapter 1. However, in our case the hydration will not only be useful to modulate the skin barrier function *per se* and facilitate drug permeation, but also to improve drug release from the used formulations.

To get insight into the performance of these formulations under skin occlusion, the Franz cells were used and a volume of 0.14 ml of the PBS (pH=7.2) was used to hydrate the samples. This volume is expected to approximate the water volume that might accumulate after 48 hours of the human skin occlusion over the used diffusional cell area (0.785 cm<sup>2</sup>) based on the transepidermal water loss rate measurements performed by Roskos and Guy (1989) after skin occlusion with polypropylene chambers. Figure 6.35 set forth aspects of the permeation behaviour of ibuprofen from the FM9 and FM10 films on the assumption that they were hydrated under occlusion conditions.



**Figure 6.35: Ibuprofen diffusion profiles from hot melt extruded Eudragit RS PO-based films which contain 10% (w/w) and 20% (w/w) Gelucire 44/14 in FM9 and FM10 systems, respectively, tested at approximately 32°C and permeated across silicone membrane into phosphate buffer solution (pH=7.2) at 37°C. Each sample was hydrated with 0.14 ml of PBS (pH=7.2) in the donor chamber of the Franz cells. Each data point represents the mean±S.D. of no less than three measurements**

In similar manner to the previous experiments performed under hydration conditions, Figure 6.35 showed that the permeation of the drug was enhanced in both FM9 and FM10 films as compared to their permeation profiles without hydration (see Figure 6.22) and the rate of ibuprofen permeation was faster in the FM10 films which contain higher level of Gelucire 44/14. In link with Figure 6.29, the maximum percent of ibuprofen permeated was obtained at slower rate than the samples examined in Test 1 but faster than Test 2, supporting the suggestion of permeation dependence on the applied level of hydration. On the other hand the proposed kinetics and mechanism(s) of drug release and permeation from FM10 films showed same behaviour at different hydration levels (Table 6.8 and Table 6.9).

However, FM9 films, as seen in Table 6.9, demonstrated for the first time fitness to zero-order model after being hydrated with 0.14 ml of the buffer solution. Alternatively, this opens another door for the usefulness of using this system, wherein concentration independent release may be attained with steady-state release. The proposed mechanism of the release from these systems was ‘anomalous transport’, based on the power model. This indicates possible role of swelling and diffusion to control the release from these matrices.

(A)

Used Kinetic model	First order model	Zero order model	Higuchi square-root of time model
Tested sample	$R^2$	$R^2$	$R^2$
FM9 Films	0.9691	0.9769	0.9685
FM10 Films	0.9850	0.7374	0.9048

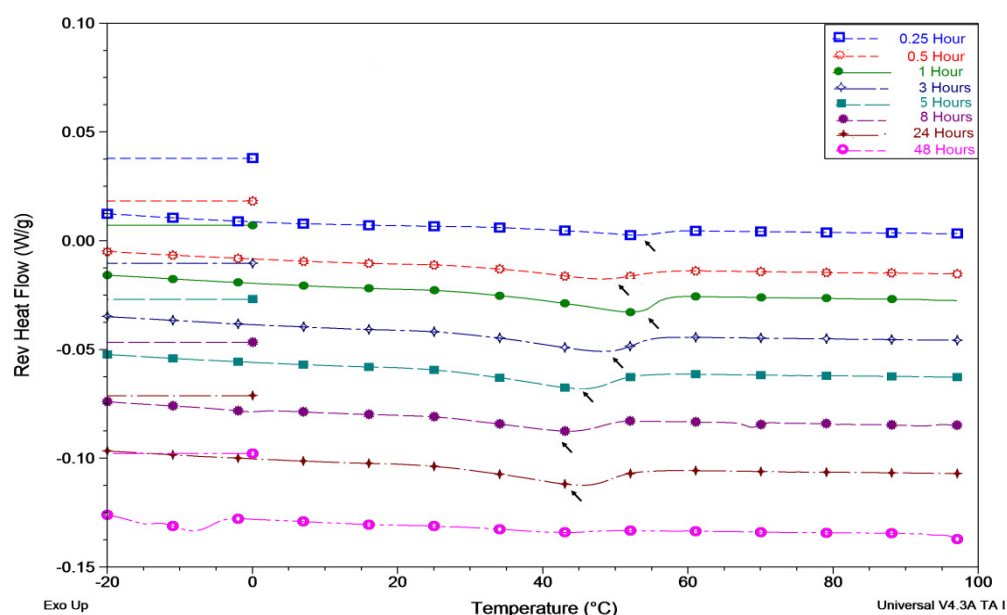
(B)

Kinetic model		Korsmeyer-Peppas model (Power law)	
	$R^2$	Release exponent (n)	Expected release mechanism
FM9 Films	0.9704	0.76	Anomalous transport
FM10 Films	0.8876	1.21	Super case-II transport

**Table 6.9: (A) Fit correlation coefficients ( $R^2$ ) of different applied kinetics models and (B) possible interpretation of the measured release exponents from the power law model and their correlation coefficients ( $R^2$ ), both for the permeation profiles of the FM9 and FM10 films under the condition of hydration with 0.14 ml of PBS (pH=7.2) in the donor chambers of the Franz cells**

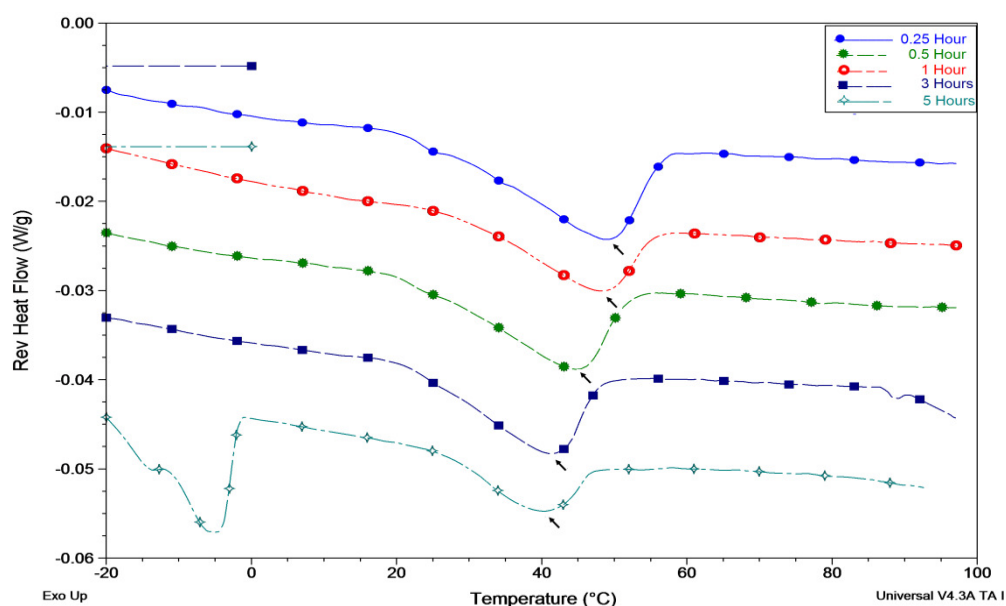
In Figure 6.36 and Figure 6.37, the MTDSC was used to get further insight into possible changes on these films while being tested in Franz cells under the applied hydration level (0.14 ml of PBS, pH=7.2). Though these samples were blotted onto filter papers to dry them prior the MTDSC experiment, these samples kept some water. Therefore, the changes were observed from the reversing heat flow signals rather than the total heat flow signals, as the latter were distorted with overlapped broad dehydration peaks. Thus and due to quantitative limitations associated with using reversing heat flow signal (see Chapter 2), the relative trend of changes in the ‘apparent’ melting peaks will be discussed herein. For the FM9 films (Figure 6.36), an endothermic peak started to appear with a peak temperature around 51.8°C ( $n=2$ ) after 15 minutes of the permeation experiment, this peak sharpened (higher melt  $\Delta H$ ) after one hour, indicating possible recrystallization due to possible perturbation of moisture and temperature found inside Franz cells. Afterwards, this peak was shifted to lower temperatures, indicating possible solubilisation. This peak almost disappeared after the end of the experiment (48 hours) with a very broad and subtle endotherm detected around 41.1°C ( $T_{m(\text{peak})}$ ,  $n=1$ ).





**Figure 6.36:** MTDSC reversing heat flow signals for fresh hot melt extruded FM9 (10% (w/w) Gelucire 44/14) removed at different times from the permeation experiment in the Franz-type diffusion cells. The tested samples were hydrated with 0.14 ml of PBS (pH=7.2) in the donor chambers of the Franz cells at approximately 32°C. Underlying scan rate of 1°C min<sup>-1</sup> with a modulation amplitude of ±0.265°C and a period of 100 seconds

By the same token, FM10 films (Figure 6.37) showed a shifting of its melting endotherm towards a lower temperature with a relative decrease in the observed  $\Delta H$  of the melt transition, which again indicates possible solubilisation or even involvement in a certain interaction (Abdul-Fattah and Bhargava, 2002). However, the monitoring of these samples was extended up to 5 hours after which the samples were transformed into liquid-like emulsion. These observations corroborate the addressed improvement of the performance of these films under the used hydration level, which is believed to approximate the level initiated after skin occlusion. Therefore, what is decisive for the possible usefulness of these films as promising drug delivery systems is depending on the presence of the safest and efficient penetration enhancer i.e. water (Aulton, 2007; Escobar-Chávez, 2010; Hadgraft, 1999) that can be accumulated under occlusive conditions.



**Figure 6.37:** MTDSC reversing heat flow signals for fresh hot melt extruded FM10 (20% (w/w) Gelucire 44/14) films removed at different times from the permeation experiment in the Franz-type diffusion cells. The tested samples were hydrated with 0.14 ml of PBS (pH=7.2) in the donor chambers of the Franz cells at approximately 32°C. Underlying scan rate of 1°C min<sup>-1</sup> with a modulation amplitude of ±0.265°C and a period of 100 seconds

## 6.4 Conclusions

The objectives of the work described in this chapter were to highlight the significance of formulation composition (polymer type and ratio used) for fabrication of hot melt extruded films with enhanced release properties and to determine the influence of hydration on further improvement of ibuprofen release and permeation from the studied hot melt extruded matrices. The aim of this work is to investigate feasibility of Eudragit RS PO-based films to deliver ibuprofen using various modification techniques of increasing ibuprofen release and permeability *in vitro*.

Section 6.2 detailed the compositions and ratios of hydrophilic additives in the drug-loaded carriers that demonstrated acceptable processing features i.e. whether they produced extrudable formulations. MTDSC, PXRD and SEM were used as solid state characterisation tools to investigate the compatibility and miscibility of the extrudable matrices loaded with ibuprofen. Changes of the molecular distribution of the drug took place with different compositions. Although Eudragit RS PO and ibuprofen were found to be completely miscible in the solid-state (Chapter 4), addition of small amounts (10% (w/w)) of sucrose or Pluronic® F127 or methylcellulose to this system led to phase separation. This separation was also observed using large amounts (60% (w/w)) of methylcellulose or xanthan gum (Xantural® 75) or higher level of 'extrudable' Gelucire 44/14 (20% (w/w)). However, multiple component systems made up of Eudragit RS PO, ibuprofen and small amounts (10% (w/w)) of xanthan gum (FM5) or Gelucire 44/14 (FM9) maintained the miscibility.

The results obtained from MTDSC, PXRD and SEM methods were relatively comparable and complementary to each other, suggesting a multi-disciplinary approach for investigating the solid state characteristics of these extruded films. Both PXRD and MTDSC were found to be less sensitive for tracing low crystallinity as compared to visually determined crystallites using SEM. PXRD aided in identification of crystalline species in the mixtures containing more than one crystalline type.

*In vitro* release studies (dissolution testing) revealed the effect of inclusion of the hydrophilic release promoters. It is believed that retardation influence of Eudragit RS PO was decreased after the addition of xanthan gum (FM5), Pluronic® F127 (FM7) and Gelucire 44/14 (FM9-FM10) due to possible increase of fluid access into the extruded films as a result of hydrophilic properties of these promoters. It was also concluded that formulations with the xanthan gum (Xantural® 75) were correlated with polymer concentration and proper adjustment of the ratio used of this polymer can result in the desired release profile. Information derived from solid state characterisation, physical appearance and *in vitro* release properties were used to decide the encouraging formulations for further exploration of their *in vitro* permeation properties. Formulations which completely dissolve the drug as FM5 (10% (w/w) xanthan gum) and FM9 (10% (w/w) Gelucire 44/14) together with formulations showed superior release profile with acceptable physical features were selected i.e. FM7 (10% (w/w) Pluronic® F127) and FM10 (20% (w/w) Gelucire 44/14) films. Diffusion or permeation profiles improvement was limited from these selected films. Drug recrystallization as indicated by MTDSC measurements and

lack of proper hydration, as clearly evident in formulations with the xanthan gum (FM5), appeared as possible factors that contributed to the poor diffusion (permeation) profiles.

Section 6.3 detailed the use of two major types of films from the optimized formulations to investigate the influence of hydration as a possible enhancement technique. The first type encompassed the samples wherein the ibuprofen is not crystalline in the fresh samples until they are tested in the Franz cells and involved FM5 (10% (w/w) xanthan gum) and FM9 (10% (w/w) Gelucire 44/14) extruded films. The second type was the one achieved the maximum permeation of the drug amongst other tested formulations and this complies with the FM10 films (20% (w/w) Gelucire 44/14). Drug overall permeation profiles from the studied matrices were described mainly with first order kinetics and hydration influence was manifested on changing the drug release mechanism for the most systems. It was also concluded that variation of either the vehicle used or the applied hydration level will result in a different permeation program. Hydration, especially in films containing Gelucire 44/14 was notably influential and appeared as efficient technique to enhance ibuprofen permeation profiles, in terms of the amount permeated and extent. It is therefore preferable to use these films under occlusive conditions.

A simulative study of the hydration under occlusion conditions augments the usefulness of films containing Gelucire 44/14 in formulations coded as FM9 (10% (w/w) Gelucire 44/14) and FM10 (20% (w/w) Gelucire 44/14). MTDSC experiment of these hydrated films indicated possible solubilisation during the permeation experiment. Swelling and swelling with polymer relaxation were found to be the most relevant mechanisms of drug release from these hydrated FM9 and FM10 films, respectively, as predicted from the used power model. FM10 film, which contains higher level of Gelucire 44/14 (20% (w/w)) showed interesting behaviour upon hydration and depending on the applied level, its consistency changed into liquid-like emulsion, which is believed to be the reason which led to the maximum permeation enhancement through either emulsification or oversaturation. Overall, what was decisive for the possible usefulness of these films as promising drug delivery system (patches) was depending on the presence of water that can be accumulated under occlusive conditions. Thus, it is concluded that with such affordable smart drug delivery design activated by hydration, further studies can be carried out using the carrier blends of Eudragit RS PO and Gelucire 44/14 as promising vehicle to deliver drugs transdermally.

**Chapter 7: Investigation into Eudragit RS PO/Gelucire 44/14 hot melt extruded films as promising carrier systems for ibuprofen transdermal delivery**

## 7.1 Introduction

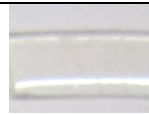
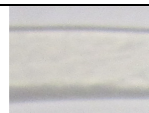
On the basis of improving the amount of the ibuprofen liberated from Eudragit RS PO based matrices, the optimisation of the choice of the vehicle or carrier was discussed in Chapter 6. Among these carriers, inclusion of Gelucire 44/14 resulted in enhancement of *in vitro* drug release and significant improvement of the *in vitro* ibuprofen permeation from these extruded matrices which changes with hydration level. To reap the potential of using these Gelucire 44/14 in Eudragit RS PO extruded carriers in transdermal delivery with concomitant extended implications for different applied medicines, this Chapter was introduced. These carrier systems were extruded using two concentrations of Gelucire 44/14 in Eudragit RS PO. A physicochemical characterisation of these systems was performed using various techniques, followed by exploration of possible interactions between Eudragit RS PO and Gelucire 44/14 using ATR-FTIR. As hydration played a major role in achieving the maximum drug enhancement from these vehicles, it was vital to assess its influence on these vehicles without the drug to understand the possible mechanism(s) involved in the release. Furthermore, the aged systems of these carriers were evaluated in the light of the influence of temperature and relative humidity. Bringing together what has been learnt from these aged carrier systems without the drug; a link to the ageing studies of the corresponding systems containing the drug was established. Franz-type diffusion cells in this chapter were not only useful to perform *in vitro* permeation studies of the ibuprofen from these carrier systems but were also used as a valuable *in vitro* model to provide a predictive simulation of the possible changes on the “non-medicated” Eudragit RS PO/Gelucire 44/14 carrier devices under hydration.

## 7.2 Characterisation of the Eudragit RS PO/Gelucire 44/14 hot melt extruded films

This section is devoted to the solid state characteristics of the carrier matrix system or the vehicle based on Eudragit RS PO at two levels of Gelucire 44/14; in particular we study drug-free films so as to allow comparison with the loaded systems. This was performed through bringing some useful common characterisation techniques, such as cDSC, MTDSC, PXRD and SEM.

### 7.2.1 Methodology

The films were prepared *via* hot melt extrusion as described in Chapter 4. The parameters of extrusion were selected to exert tolerable torque values. A speed of 100 rpm was set for five minutes, with a temperature of 120°C from feed to the die end. These parameters allowed for the extrusion of the formulations shown in Table 7.1. The hot melt extruded films were cut neatly into units with roughly equal dimensions and then sandwiched between two pieces of aluminium foil. The hot melt extruded films were evaluated using techniques of MTDSC, PXRD and SEM. These experiments were the same as detailed in Chapter 3. Physical mixtures equivalent to the studied extrudates in this section were prepared through mixing of Gelucire 44/14 and Eudragit RS PO with pestle and mortar, for five minutes and were also characterised using PXRD and MTDSC. Conventional DSC (cDSC) experiments were also performed for both physical mixes and freshly extruded films, similar to the experimental method developed in Chapter 3. A heating rate of 1°C min<sup>-1</sup> was also used in the conventional mode with the appropriate calibrations, at the same rate as was used for sample analysis. The purpose of using this heating rate was to compare results with those obtained by the MTDSC method at the same heating rate. The amounts of the pure Gelucire 44/14 used in the comparative cDSC and MTDSC studies on the physical mixtures, were equivalent to its amounts in these mixes. These physical mixtures were prepared inside DSC pans and shown to be comparable to those produced with pestle and mortar based on similarity of the results obtained by DSC measurements. All the reported values were measured as mean±S.D (n=3) unless otherwise mentioned in the relevant section.

Gelucire 44/14: Eudragit RS PO ratio	Extrusion temperature (°C)	Appearance	Formula code	Photos
1:6	120	Translucent, smooth, no cracks, low stickiness and rigid.	FM-A	
2:5	120	Translucent, smooth, no cracks, low stickiness and flexible.	FM-B	

**Table 7.1: Formulation and description of the placebo Eudragit RS PO/Gelucire 44/14 hot melt extruded films**

## 7.2.2 Results and discussion

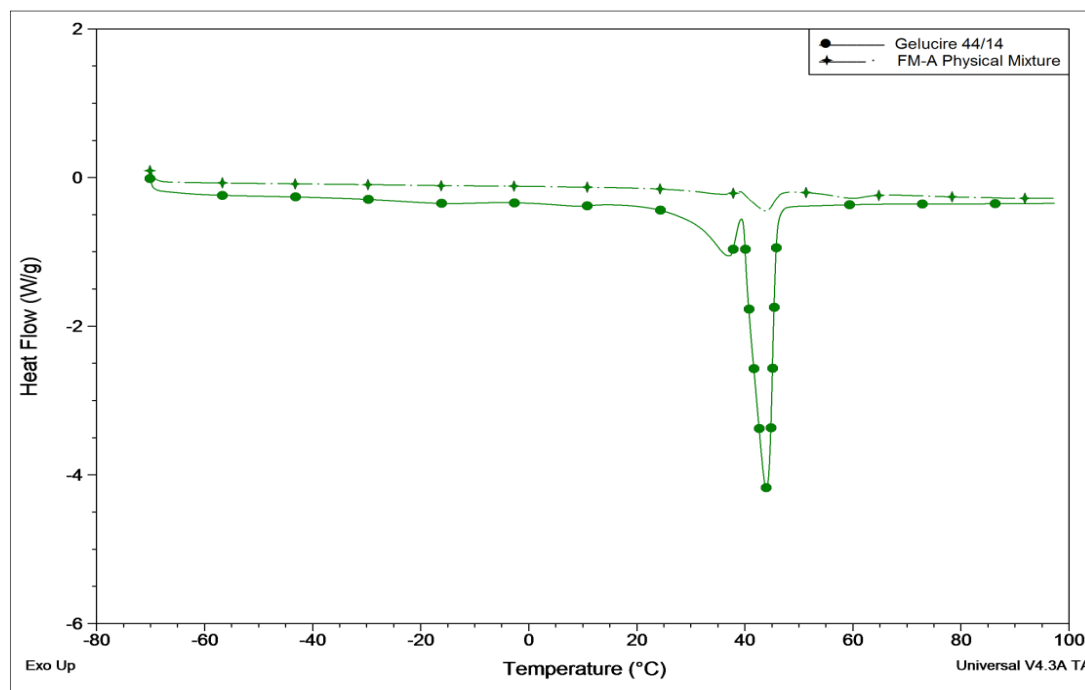
### 7.2.2.1 Investigation into thermal properties using conventional DSC (cDSC) and modulated temperature DSC (MTDSC)

#### 7.2.2.1.1 Analysis of the physical mixes

Analysis using conventional DSC (cDSC) with a heating rate of  $10^{\circ}\text{C min}^{-1}$ , revealed two dominant melting endotherms of Gelucire 44/14 at  $29.3 \pm 1.4^{\circ}\text{C}$  (secondary) and  $39.4 \pm 0.5^{\circ}\text{C}$  (primary), measured as the  $T_{m(\text{onset})}$ . Physical mixtures of Gelucire 44/14 and Eudragit RS PO were prepared inside DSC pans. In these mixes, when the Eudragit RS PO was incorporated in a ratio of 6:1 (Eudragit RS PO:Gelucire 44/14), identified as FM-A system, a marked reduction in the Gelucire 44/14 melt  $\Delta H$  of both melting peaks took place to what is expected to pure Gelucire 44/14 ( $15.4 \text{ Jg}^{-1}$ ). This was associated with a small variation in the  $T_{m(\text{onset})}$  of the observed primary or secondary endotherms which instead occurred at  $40.3 \pm 1.3$  and  $30.5 \pm 2.0^{\circ}\text{C}$ , respectively, as seen in Figure 7.1 and determined as the  $T_{m(\text{onset})}$ . This could imply miscibility and a possible interaction between the two components (Abdul-Fattah and Bhargava, 2002). At higher loading of Gelucire 44/14 in the ratio of 2:5 (Gelucire 44/14:Eudragit RS PO), the physical mixture coded as FM-B showed similar behaviour as illustrated in Figure 7.2. A significant reduction was detected in the melt  $\Delta H$  with respect to the pure Gelucire 44/14 ( $30.7 \text{ Jg}^{-1}$ ). The onset temperatures of the melting peaks of the

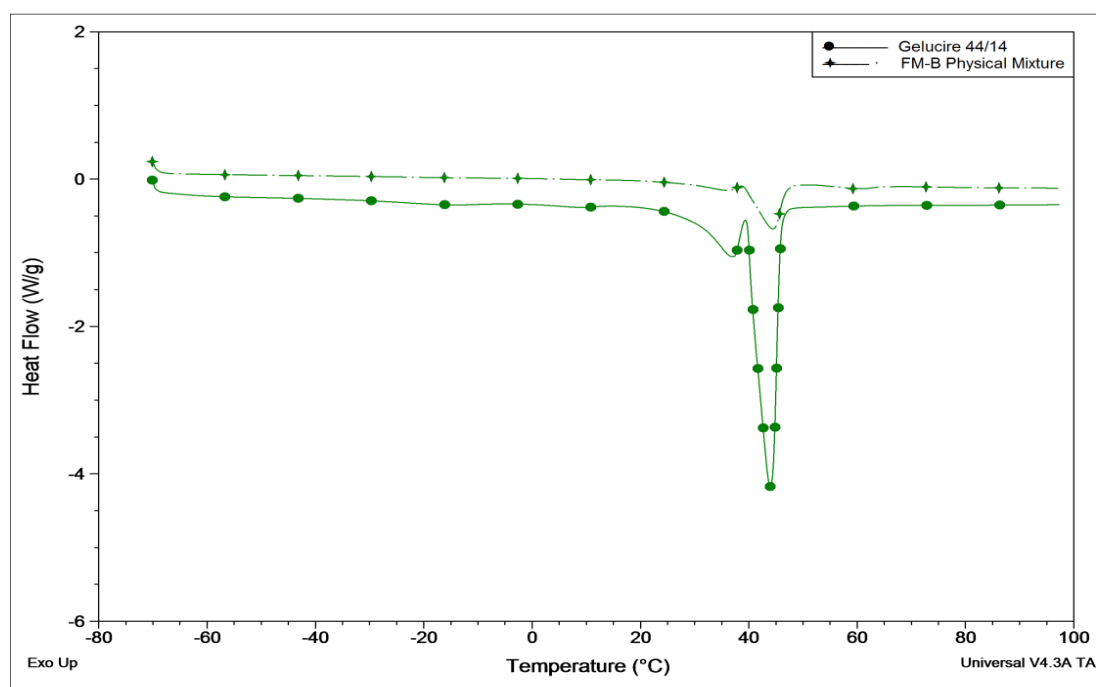


Gelucire 44/14 therein were observed at  $39.3 \pm 0.4^\circ\text{C}$  (primary peak) and at  $28.5 \pm 0.3^\circ\text{C}$  (secondary peak).

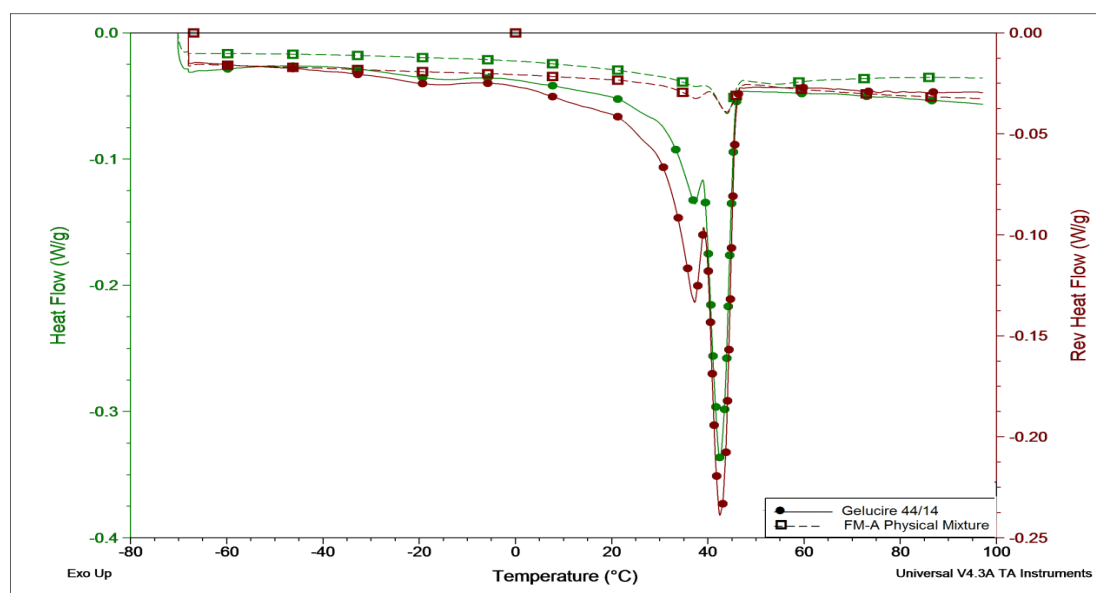


**Figure 7.1: Heat flow signal for Gelucire 44/14 and FM-A physical mixture heated at  $10^\circ\text{C min}^{-1}$  in standard aluminium pans. See Table 7.1 for composition**

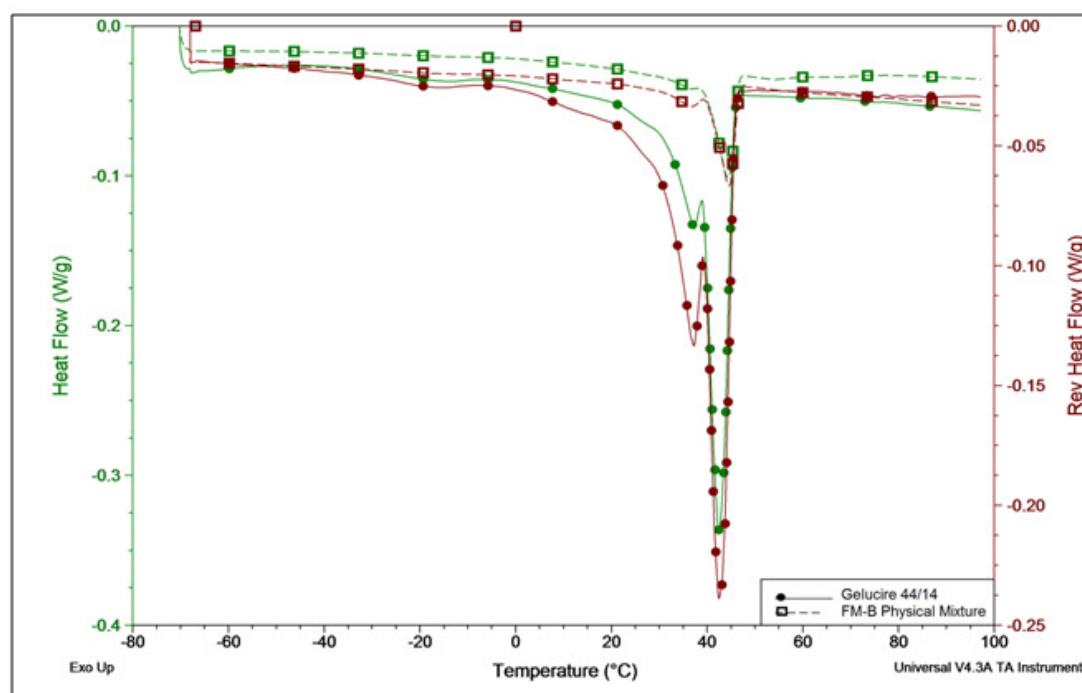
A further investigation was performed using MTDSC with an experimental method which was developed in Chapter 3. The samples were heated from  $-70^\circ\text{C}$  to  $100^\circ\text{C}$  with an underlying heating rate of  $1^\circ\text{C min}^{-1}$ , modulation amplitude of  $\pm 0.265^\circ\text{C}$  and a period of 100 seconds. The reversing and the total heat flow signals are displayed in Figure 7.3 and Figure 7.4 for FM-A and FM-B physical mixtures, respectively (see Table 7.1 for their compositions), in comparison to pure Gelucire 44/14. Table 7.2 summarises the MTDSC results of the FM-A and FM-B physical mixtures.



**Figure 7.2:** Heat flow signal for Gelucire 44/14 and FM-B physical mixture heated at  $10^{\circ}\text{C min}^{-1}$  in standard aluminium pans. See Table 7.1 for composition



**Figure 7.3:** MTDSC heating scans (total and reversing heat flow signals) of Gelucire 44/14 (closed circles) and FM-A physical mixture (open squares) in standard aluminium pans. Underlying scan rate of  $1^{\circ}\text{C min}^{-1}$  with a modulation amplitude of  $\pm 0.265^{\circ}\text{C}$  and a period of 100 seconds



**Figure 7.4:** MTDSC heating scans (total and reversing heat flow signals) of Gelucire 44/14 (closed circles) and FM-B physical mixture (open squares) in standard aluminium pans. Underlying scan rate of  $1^{\circ}\text{C min}^{-1}$  with a modulation amplitude of  $\pm 0.265^{\circ}\text{C}$  and a period of 100 seconds

Sample	T <sub>g</sub> (Mid-point)*	T <sub>m</sub> (onset) **	T <sub>m</sub> (onset)**
		Primary peak	Secondary peak
FM-A-Physical mix	53.3 $\pm$ 0.5 $^{\circ}\text{C}$	40.5 $\pm$ 0.4 $^{\circ}\text{C}$	33.8 $\pm$ 0.4 $^{\circ}\text{C}$
FM-B-Physical mix	53.1 $\pm$ 0.4 $^{\circ}\text{C}$	40.6 $\pm$ 0.6 $^{\circ}\text{C}$	31.5 $\pm$ 0.6 $^{\circ}\text{C}$

\*Measured from the reversing heat flow signal.

\*\*Measured from the total heat flow signal.

**Table 7.2:** Summary of the MTDSC experiment with the underlying heating rate  $1^{\circ}\text{C min}^{-1}$ , modulation amplitude of  $\pm 0.265^{\circ}\text{C}$  and period of 100 seconds. Values were measured as mean $\pm$ S.D (n=3). (See Table 7.1 for composition)

The results in Table 7.2 showed that detected glass transition temperatures of these mixes and related to Eudragit RS PO were either equal to or slightly less than the range of values observed for glass transition temperature of Eudragit RS PO alone, which was reported in Chapter 3 as  $53.3 \pm 0.5^\circ\text{C}$  (Mid-point  $T_g$ ). Therefore it could be concluded that there is no appreciable change in the  $T_g$ . In the same way as in previous conventional DSC results, the MTDSC total heat flow signals revealed slight variation of the onset melting peaks' values yet a significant decrease in the melt  $\Delta H$ , with respect to the pure Gelucire 44/14. Again, this decrease in the melt  $\Delta H$  might indicate miscibility and a possible interaction between Gelucire 44/14 and Eudragit RS PO (Abdul-Fattah and Bhargava, 2002).

For comparative purposes, the amount of crystalline Gelucire 44/14 (G44/14) detected in these physical mixtures was calculated after heating at the selected rate and methods, using the following equation:

$$\text{Crystallinity (\%)} = \left( \frac{\Delta H_m \text{ of the G44/14 in the Physical mix}}{\Delta H_m \text{ of the pure G 44/14} \times W} \right) \times 100 \quad (\text{Eq.7.1})$$

Where ' $\Delta H_m$  of the G44/14 in the Physical mix', is the total melting enthalpy of the Gelucire 44/14 in the physical mix (J/g) of the primary and secondary melting endotherms to obtain more reliable enthalpy value as the peaks overlap. 'W' is the weight fraction of Gelucire 44/14 in the physical mixture. ' $\Delta H_m$  of the pure G44/14' is the melting enthalpy of the Gelucire 44/14 standard, assumed to represent full crystallinity (100%). Hence all crystallinity levels reported in this work are relative to the original Gelucire 44/14 sample.

Sample	Crystallinity (%)	Method	Comments
Physical mix FM-A	$52.93 \pm 0.06$	$10^\circ\text{C min}^{-1}$ , cDSC	Fig.7.1
Physical mix FM-A	$72.87 \pm 0.61$	$1^\circ\text{C min}^{-1}$ , MTDSC	Total heat flow signal, Fig.7.3
Physical mix FM-B	$31.00 \pm 0.03$	$10^\circ\text{C min}^{-1}$ , cDSC	Fig.7.2
Physical mix FM-B	$46.53 \pm 0.46$	$1^\circ\text{C min}^{-1}$ , MTDSC	Total heat flow signal, Fig.7.4

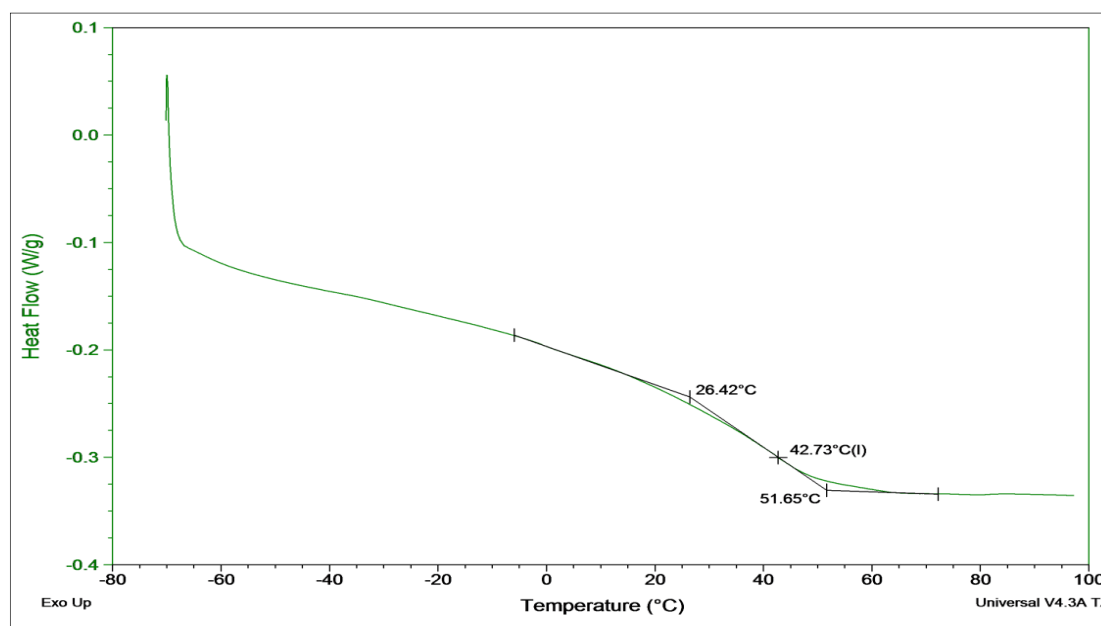
**Table 7.3: Summary of the calculated percent crystallinity of Gelucire 44/14 in the physical mixtures of FM-A (Gelucire 44/14 Eudragit RS PO ratio of 1:6) and FM-B (Gelucire 44/14 Eudragit RS PO ratio of 2:5) from cDSC and MTDSC experiments**

The results in Table 7.3 showed that there is a decrease in the percentage crystallinity of Gelucire 44/14 in the physical mixture with Eudragit RS O after heating *in situ* in the DSC pans. This suggests that simple contact between these components results in miscibility during heating. A further intriguing observation is the difference in the percent crystallinity measured using the MTDSC method with slower heating rate of  $1^{\circ}\text{C min}^{-1}$  in comparison to the cDSC method with a higher heating rate of  $10^{\circ}\text{C min}^{-1}$  for each studied physical mix. Though we cannot compare these two methods for this reason and due to the different principle of the techniques, but it is speculated that a use of a faster heating rate results in a greater difference in the measured heat input; therefore the investigated thermal event will be observed largely over the experiment time. This was contrary to our case, where the use of a slow heating rate of  $1^{\circ}\text{C min}^{-1}$  in the MTDSC led to sharper, larger, defined melting peaks of the Gelucire 44/14 and subsequent higher calculated percentage crystallinity. This can be related to the Gelucire 44/14 properties which is a multi-component heterogeneous system with complex crystallization behaviour (Sutananta et al., 1994). The longer time offered by the MTDSC experiment with an underlying slow heating rate of  $1^{\circ}\text{C min}^{-1}$  is believed to give enough time for Gelucire 44/14 to rearrange into a better packed crystalline structure to yield the melting profiles of its components. This behaviour is very common for broad-melting polymers. In these polymers, enough time provided during ‘characterisation’ experiment, for example, can lead to so-called secondary crystallization after the spherulitic space filling of primary crystallization is complete and thus there are larger melting enthalpies in the DSC curve (Hunt and James, 1993).

#### 7.2.2.1.2 Analysis of the extruded films

Upon DSC analysis of the extruded films of the 1:6 ratio of Gelucire 44/14: Eudragit RS PO (FM-A system), a single glass transition was detected with the absence of the Gelucire 44/14 melting endotherms. As shown in Figure 7.5, this single glass transition temperature was observed at  $43.1 \pm 1.1^{\circ}\text{C}$  (Mid-point,  $n=3$ ), using a cDSC experiment ( $10^{\circ}\text{C min}^{-1}$ ). This glass transition temperature is far less than the glass transition temperature of the Eudragit RS PO alone, which was detected in Chapter 3 around  $50.4^{\circ}\text{C}$ . This indicates that the Gelucire 44/14 has contributed to the reduction of this glass transition temperature and formed a one phase system with Eudragit RS PO. cDSC, at a heating rate of  $1^{\circ}\text{C min}^{-1}$  was also used to characterise these samples as shown in Figure 7.6. Based on the investigations in the previous section, MTDSC measurements resulted in a better distinction of the Gelucire 44/14 peaks. This was attributed to the use of a slow heating rate. Therefore, using this specific heating rate of  $1^{\circ}\text{C min}^{-1}$  in the conventional mode of DSC is for the purpose of

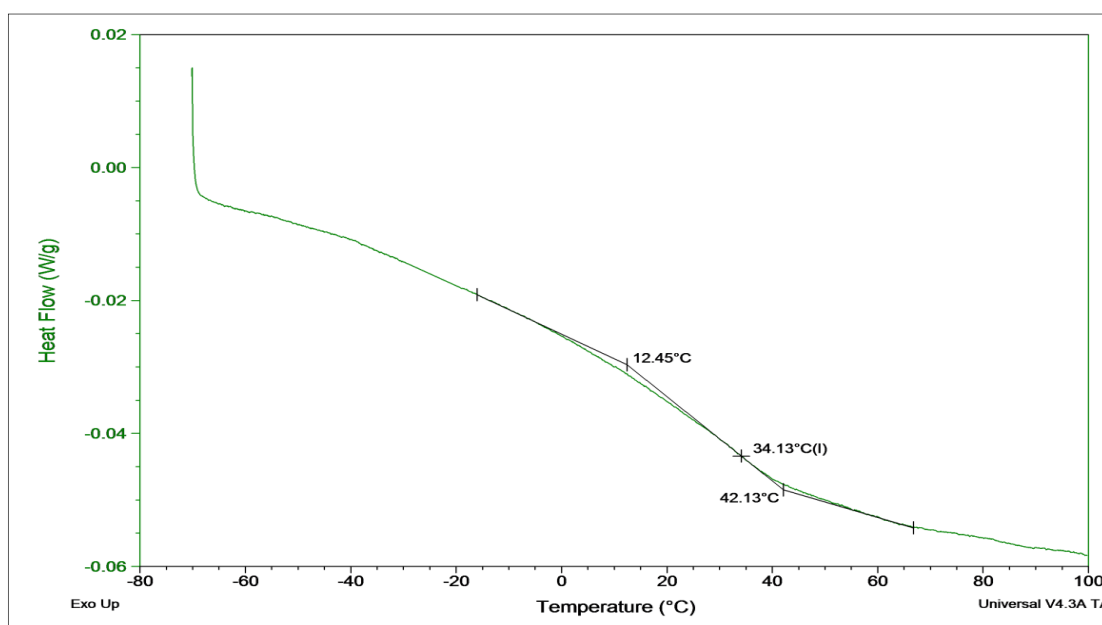
allowing better detection of the Gelucire 44/14 melting peaks, if any, regardless of the used technique. The heat flow signals using this technique in Figure 7.6 showed only a single (Mid-point) glass transition temperature at  $33.3 \pm 0.9^\circ\text{C}$  ( $n=3$ ), confirming the absence of any melting endotherm(s). To allow better detection of this glass transition event, the MTDSC technique was used.



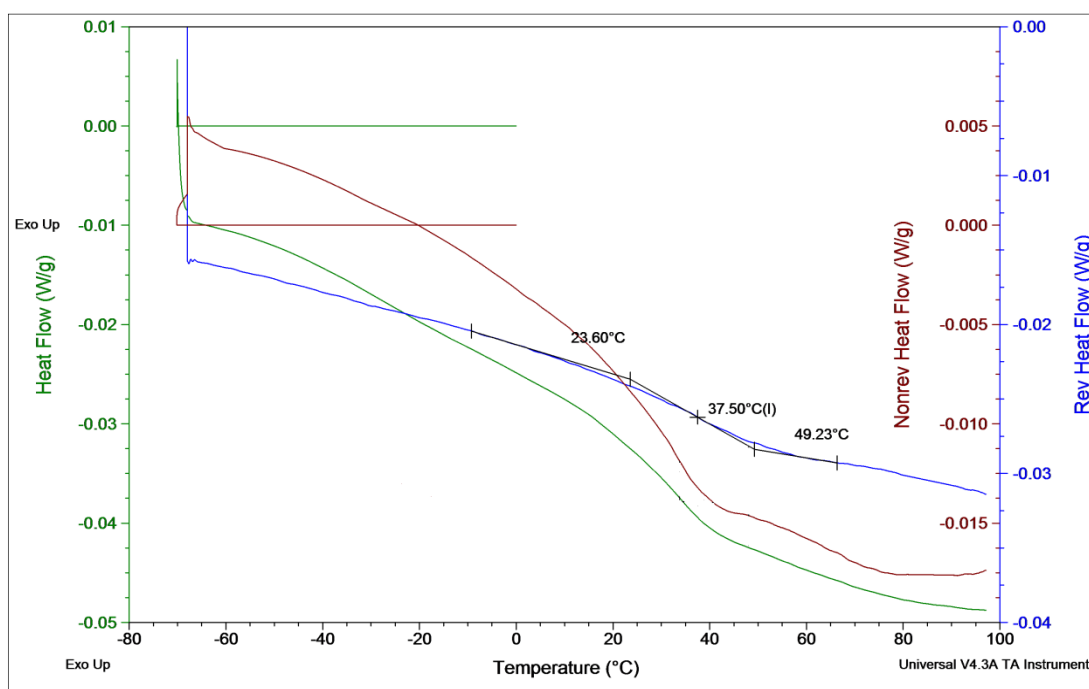
**Figure 7.5: Heat flow signal for FM-A hot melt extruded film (Gelucire 44/14 Eudragit RS PO ratio of 1:6) heated at  $10^\circ\text{C min}^{-1}$  in standard aluminium pans**

The MTDSC profile of these samples using an underlying heating rate of  $1^\circ\text{C min}^{-1}$  is shown in Figure 7.7. A broad endotherm in the non-reversing heat flow signals was detected with an extrapolated onset temperature around  $30.3 \pm 2.1^\circ\text{C}$ . This event could be ascribed to either water desorption or associated endothermic relaxation at this point of analysis. The reversing heat flow signal allowed measurements of the glass transition temperature of the FM-A extruded system without the effect of this accompanying endothermic event, which was detected around  $37.1 \pm 0.5^\circ\text{C}$  ( $n=3$ , Mid-point  $T_g$ ). All these findings indicated that FM-A extruded system exhibits a single glass transition over the entire composition range, and could be described as a miscible single phase. This demonstrates solid solution system formation.

It is noteworthy that the obtained  $T_g$  values were different according to which characterisation method was used, which is related to the  $T_g$  dependence on the heating rate (Höhne et al., 1996), its occurrence over broad temperature intervals and any overlapping with the endothermic peak as observed from the MTDSC experiment. Therefore, it is recommended to use one method for further comparison, which would be the MTDSC method, because of its great advantage in determining the glass transition from the reversing heat flow signal as detailed in Chapter 2.



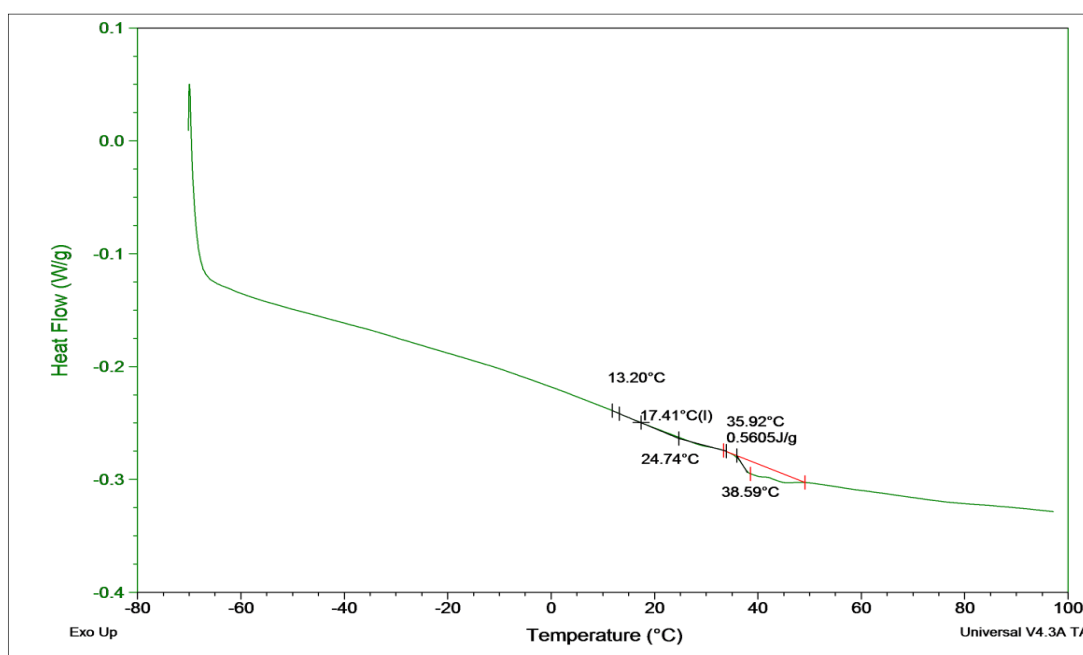
**Figure 7.6: Heat flow signal for FM-A hot melt extruded film (Gelucire 44/14 Eudragit RS PO ratio of 1:6) heated at  $1^{\circ}\text{C min}^{-1}$  in standard aluminium pan**



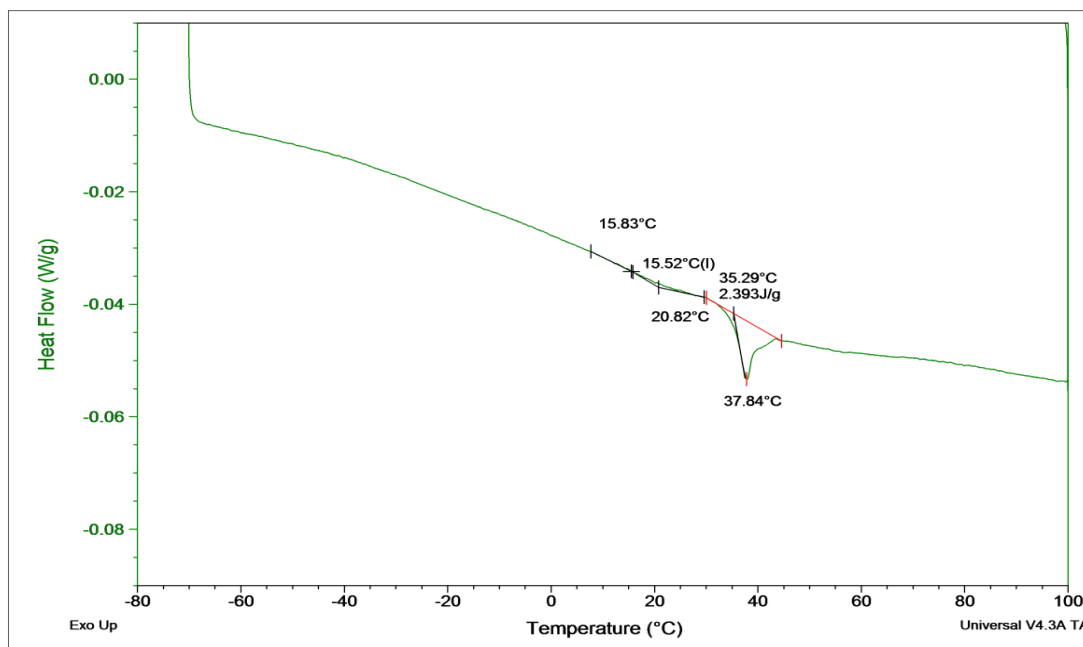
**Figure 7.7: MTDSC heating scans of FM-A hot melt extruded film (Gelucire 44/14 Eudragit RS PO ratio of 1:6) in standard aluminium pans. Underlying scan rate of  $1^{\circ}\text{C min}^{-1}$  with a modulation amplitude of  $\pm 0.265^{\circ}\text{C}$  and a period of 100 seconds**

The FM-B hot melt extruded films were characterised in a similar approach to the FM-A extruded films using either cDSC or MTDSC as shown in Figure 7.8 through to Figure 7.10. The FM-B system contains Gelucire 44/14 at a higher level than in the FM-A system (see Table 7.1). In the conventional DSC method at a heating rate of  $10^{\circ}\text{C min}^{-1}$ , a broad melting endotherm was detected with a  $T_{m(\text{onset})}$  of  $35.9^{\circ}\text{C}$  ( $n=3$ ) as illustrated in Figure 7.8. This melting peak is closely related to the primary melting fraction of the Gelucire 44/14, reported in section 7.2.2.1.1. In addition, a glass transition temperature was detected at  $17.4 \pm 0.2^{\circ}\text{C}$  ( $n=3$ , Mid-point  $T_g$ ). At a lower heating rate of  $1^{\circ}\text{C min}^{-1}$ , a sharper melting endotherm with a larger melt enthalpy was observed as displayed in Figure 7.9, consistent with our discussions in the previous section. This melting peak could be ascribed to the primary melting fraction of the Gelucire 44/14 with a  $T_{m(\text{onset})}$  value of  $35.4 \pm 0.1^{\circ}\text{C}$  ( $n=3$ ). A glass transition temperature was also detected (Mid-point) around  $15.9 \pm 1.7^{\circ}\text{C}$ . In the MTDSC scan as seen in Figure 7.10, this melting endotherm was assigned from the total heat flow signal with a  $T_{m(\text{onset})}$  of  $37.1 \pm 1.4^{\circ}\text{C}$  ( $n=3$ ) and a glass transition (Mid-point) was measured from the reversing heat flow signal at  $20.8 \pm 1.0^{\circ}\text{C}$  ( $n=3$ ).

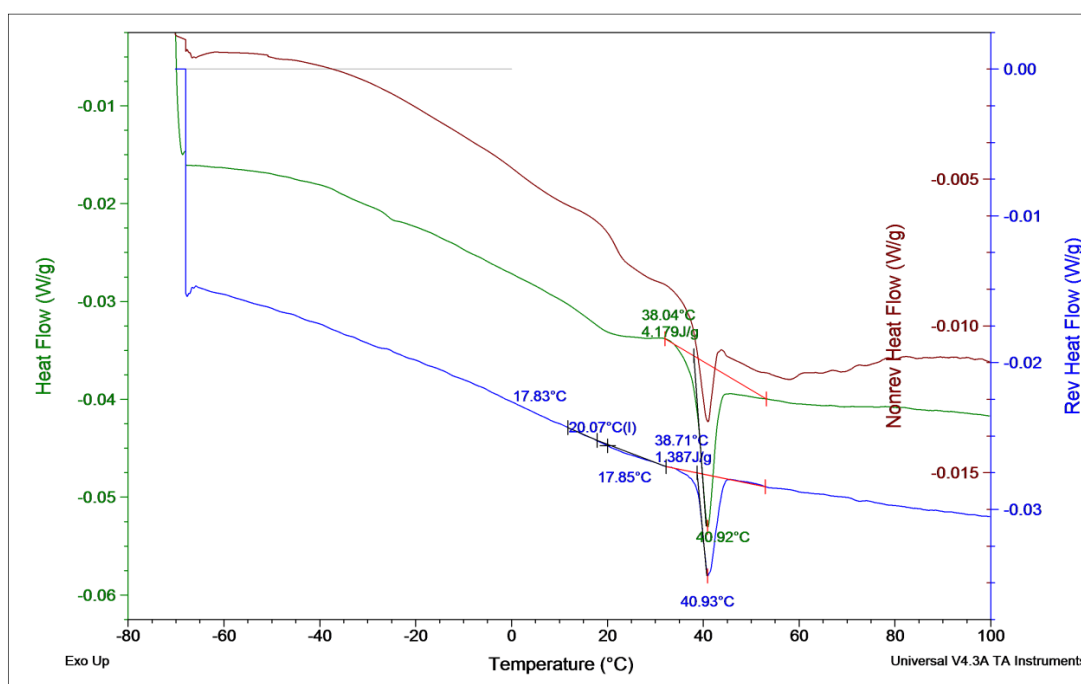




**Figure 7.8:** Heat flow signal for FM-B hot melt extruded film (Gelucire 44/14 Eudragit RS PO ratio of 2:5) heated at  $10^{\circ}\text{C min}^{-1}$  in standard aluminium pans



**Figure 7.9:** Heat flow signal for FM-B hot melt extruded film (Gelucire 44/14 Eudragit RS PO ratio of 2:5) heated at  $1^{\circ}\text{C min}^{-1}$  in standard aluminium pans

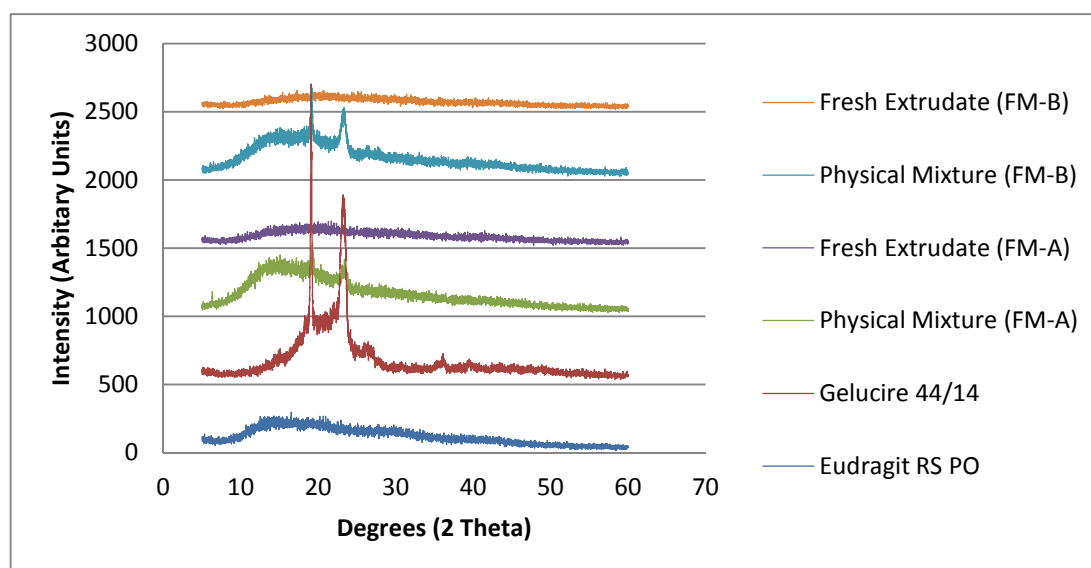


**Figure 7.10: MTDSC heating scans of FM-B hot melt extruded film (Gelucire 44/14 Eudragit RS PO ratio of 2:5) in standard aluminium pans. Underlying scan rate of  $1^{\circ}\text{C min}^{-1}$  with a modulation amplitude of  $\pm 0.265^{\circ}\text{C}$  and a period of 100 seconds**

In summary, a melting transition was detected in the FM-B extruded films (Gelucire 44/14 Eudragit RS PO ratio of 2:5) in all the methods used with more defined aspects using a slow heating rate of  $1^{\circ}\text{C min}^{-1}$ . The  $T_{m(\text{onset})}$  of the melting peak of Gelucire 44/14 in these extruded films occurred at a lower temperature i.e. depressed with marked reduction in the melt  $\Delta H$  compared to the pure Gelucire 44/14. This suggests a possible interaction and miscibility (Abdul-Fattah and Bhargava, 2002). This system also exhibits a glass transition temperature ( $\sim 21^{\circ}\text{C}$ ) that occurs at a lower temperature than the FM-A (Gelucire 44/14 Eudragit RS PO ratio of 1:6) extruded film single  $T_g$  ( $\sim 37^{\circ}\text{C}$ ) does. This would suggest that a higher amount of Gelucire 44/14 in the FM-B extruded system has led to greater reduction in the observed glass transition temperature with respect to the glass transition temperature of the Eudragit RS PO alone ( $\sim 53^{\circ}\text{C}$ ). Therefore, FM-B system is better described as a solid dispersion system which contains a crystalline Gelucire 44/14 phase and an amorphous Eudragit RS PO/Gelucire 44/14 phase.

## 7.2.2.2 Characterisation by X-ray powder diffraction (PXRD) and scanning electron microscopy (SEM)

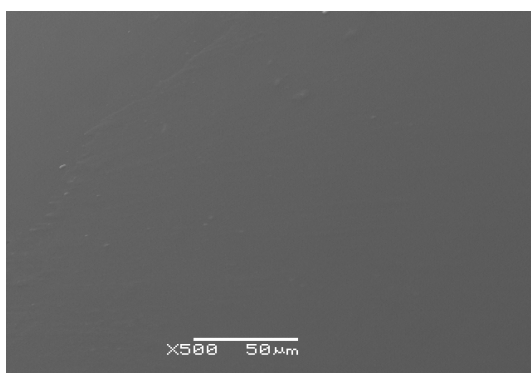
An overlay of the diffractograms obtained for the fresh hot melt extruded films of FM-A (Gelucire 44/14 Eudragit RS PO ratio of 1:6) and FM-B (Gelucire 44/14 Eudragit RS PO ratio of 2:5) is illustrated in Figure 7.11. In this figure, the studied extrudates showed halo-patterns in their diffractograms, typical for amorphous materials, in comparison to the crystalline peaks observed for their equivalent physical mixtures. This suggests the presence of a solid solution system for formulation of extruded FM-A and FM-B compositions, based on the absence of crystalline peaks related to the Gelucire 44/14. However, the combination of the previous cDSC, MTDSC findings from the previous section with the current PXRD results supports the formation of a solid solution system only for the FM-A extrudate (low Gelucire 44/14 level), characterised by a single Tg. For the FM-B extruded system (high Gelucire 44/14 level), the detected melting endotherm indicates the presence of Gelucire 44/14 crystallites and the system was described as a solid dispersion. Therefore, the lack of diffraction peaks in the PXRD profile of the extruded FM-B system is not ascribed to the absence of crystalline Gelucire 44/14, but rather can be related to the small crystalline traces found in this extruded system that fall below the detection limits of the PXRD experiment.



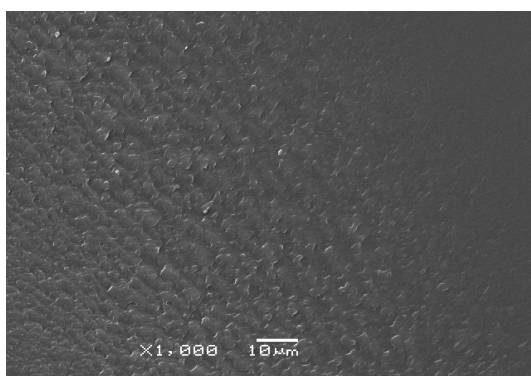
**Figure 7.11: X-ray powder diffraction profiles of the raw materials, physical mixtures and their corresponding hot melt extruded films of Gelucire 44/14 and Eudragit RS PO of FM-A (Gelucire 44/14 Eudragit RS PO ratio of 1:6) and FM-B (Gelucire 44/14 Eudragit RS PO ratio of 2:5) systems**

The SEM images of the surfaces of the studied fresh extrudates and their cross sections are shown in Figure 7.12 and Figure 7.13. The surface of the FM-A film with a ratio of 1:6 (Gelucire 44/14: Eudragit RS PO) was smooth with no visible crystals. Conversely, the FM-B film had a few granules scattered on its surface. These granules were approximately between 0.4-2.6 microns in diameter. There is therefore a visible indication of phase separation within the FM-B extruded system. These findings are in agreement with the MTDSC and cDSC results mentioned earlier. This suggests formation of an amorphous one phase solid solution between the Eudragit RS PO and Gelucire 44/14 in the FM-A extruded system (Gelucire 44/14 Eudragit RS PO ratio of 1:6) and formation of two phases solid dispersion between these components in the FM-B extrudate (Gelucire 44/14 Eudragit RS PO ratio of 2:5).

(A-I)

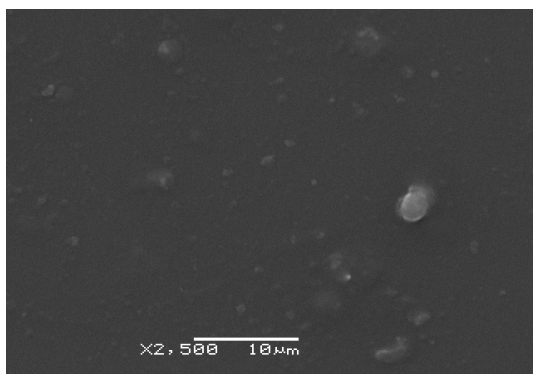


(A-II)

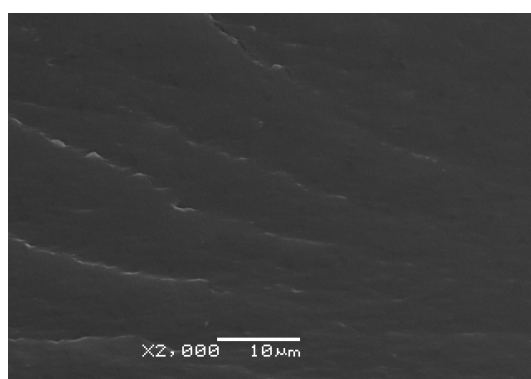


**Figure 7.12: Morphological features of the surface (A-I) and cross section (A-II) of the fresh extrudate of FM-A system (Gelucire 44/14 Eudragit RS PO ratio of 1:6)**

(B-I)



(B-II)



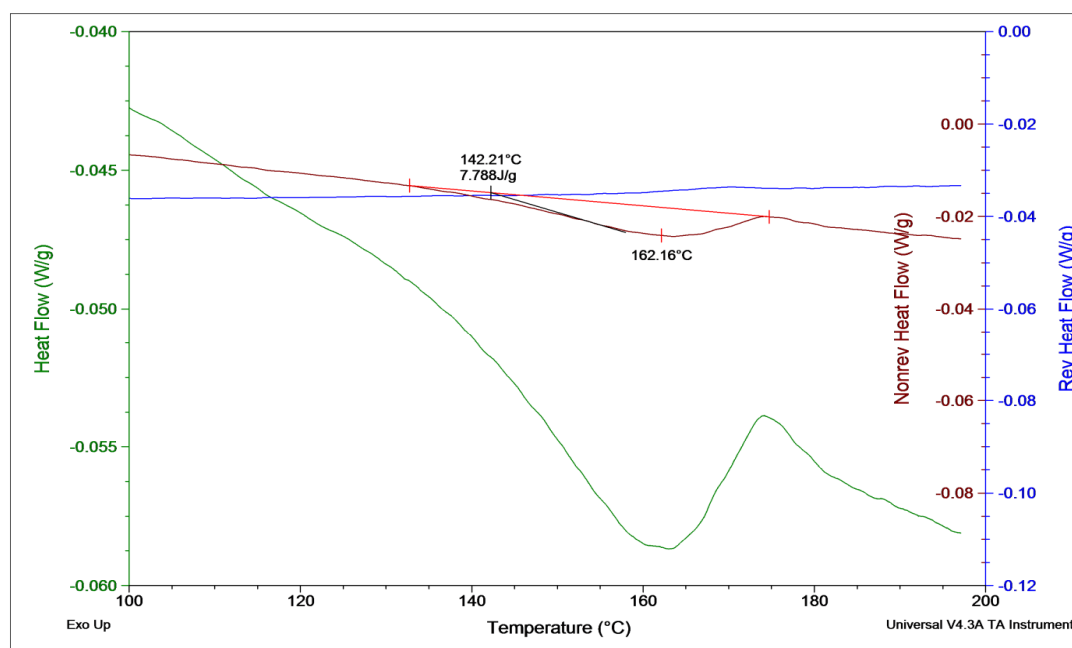
**Figure 7.13: Morphological features of the surface (B-I) and cross section (B-II) of the fresh extrudate of FM-B system (Gelucire 44/14 Eudragit RS PO ratio of 2:5)**

#### 7.2.2.3 A note on the decomposition of Gelucire 44/14 and Eudragit RS PO using the selected temperature of the extrusion

The temperature of the extrusion of the FM-A (Gelucire 44/14 Eudragit RS PO ratio of 1:6) and FM-B (Gelucire 44/14 Eudragit RS PO ratio of 2:5) systems was set to achieve adequate mixing of the materials used, through efficient transfer of these materials and tolerable torque values. In addition, this temperature was selected below the point of their thermal degradation. In this case a temperature of 120°C was chosen in an attempt to satisfy these requirements. This temperature is also higher than 15-60°C above the melting or the glass transition temperature of the used materials, which is the usual range for extrusion temperatures as reviewed by Crowley et al. (2007). A further experiment using the MTDSC method up to 200°C was used to analyse the onset of the decomposition of these materials more closely.

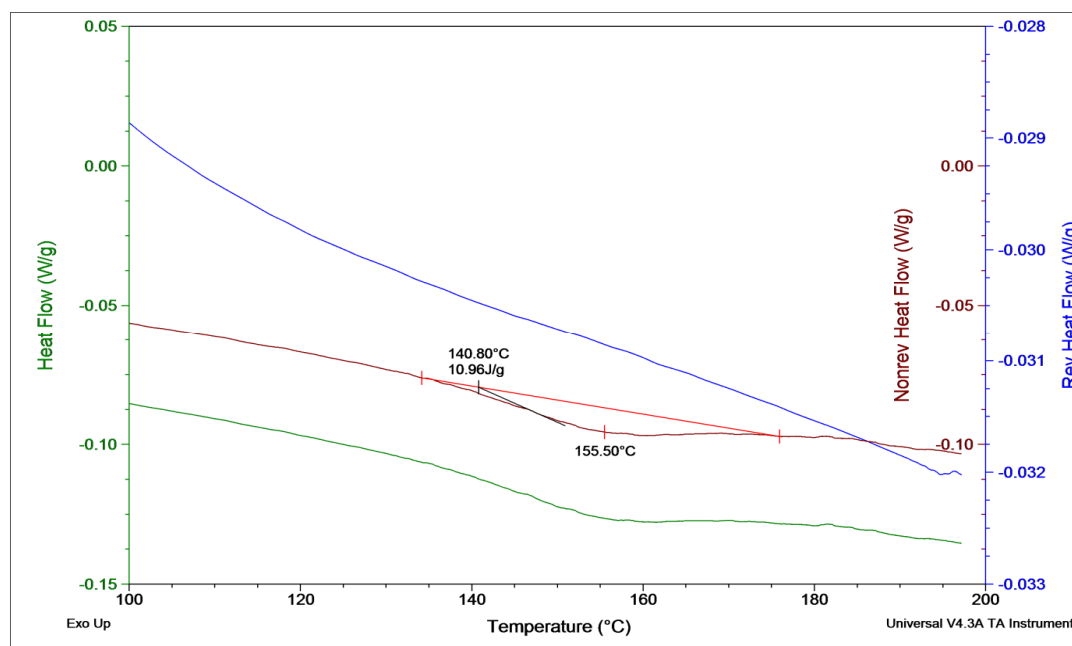
As shown in Figure 7.14 (A) and (B), possible degradation peaks appeared in the non-reversing heat flow signal with a  $T_{m(\text{onset})}$  of approximately  $142.2 \pm 0.1^\circ\text{C}$  ( $n=2$ ) and  $140.7 \pm 0.7^\circ\text{C}$  ( $n=2$ ), for Gelucire 44/14 and Eudragit RS PO, respectively. These results agree with the findings of their TGA decomposition profiles shown in Chapter 3, which demonstrate that  $120^\circ\text{C}$  is well below their thermal degradation onset temperatures.

(A)



**Figure 7.14: MTDSC heating scans of Gelucire 44/14 in standard aluminium pans (A).** Underlying scan rate of  $1^\circ\text{C min}^{-1}$  with a modulation amplitude of  $\pm 0.265^\circ\text{C}$  and a period of 100 seconds

(B)



**Figure 7.14 (Contd.): MTDSC heating scans of Eudragit RS PO in standard aluminium pans (A). Underlying scan rate of  $1^{\circ}\text{C min}^{-1}$  with a modulation amplitude of  $\pm 0.265^{\circ}\text{C}$  and a period of 100 seconds**

### 7.3 ATR-FTIR assessment of the Eudragit RS PO/Gelucire 44/14 hot melt extruded films

The study of the molecular state and presence of any specific interaction in the drug delivery systems can aid in the understanding of their mechanism of delivery and therefore their efficiency. ATR-FTIR was used to explore these aspects for FM-A (Gelucire 44/14 Eudragit RS PO ratio of 1:6) and FM-B (Gelucire 44/14 Eudragit RS PO ratio of 2:5) systems and provide more information about their stated miscibility and potential as novel drug delivery devices.

#### 7.3.1 Methodology

In this section we have used both physical mixes and the extrudates of FM-A and FM-B compositions as detailed in section 7.2.1, in addition to the pure components (Gelucire 44/14 and Eudragit RS PO). The evaluation using ATR-FTIR experiment was documented in Chapter 3. Using the same parameters, the ATR-FTIR spectra were also collected for heated samples, to mimic the temperature applied during the extrusion, utilising a Golden Gate

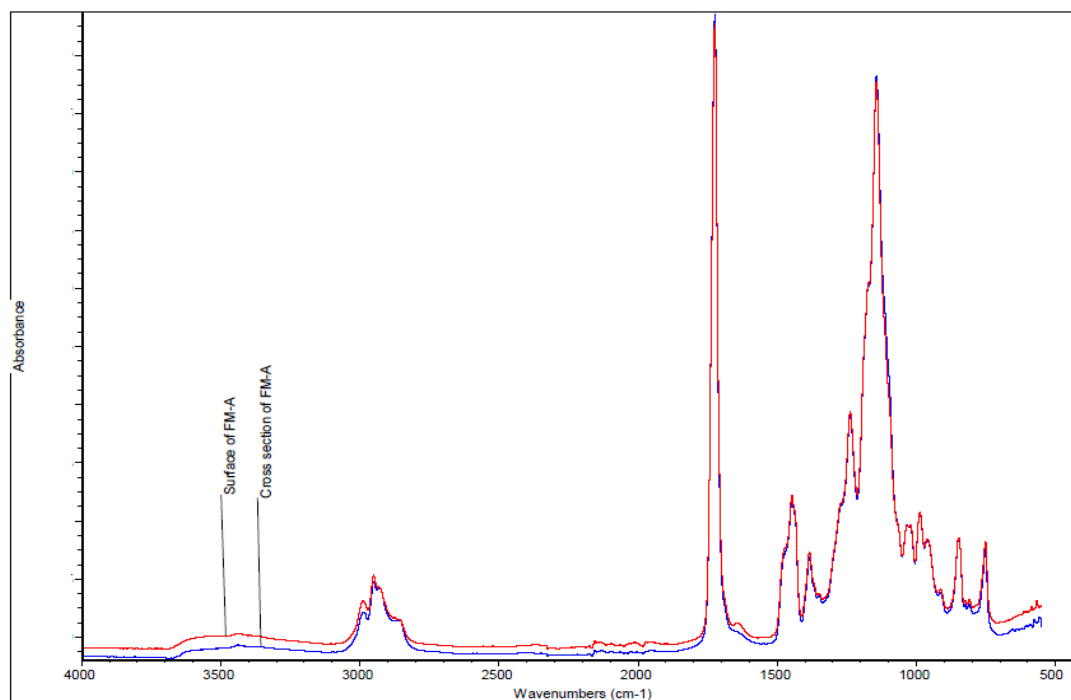
heated diamond attenuated reflection top-plate with a 3000 series high stability temperature controller with RS232 control (Specac Ltd., Kent, UK). Samples were placed on a preheated ATR diamond at the extrusion temperature of 120°C. Cooling of the samples was achieved at room temperature (~25°C) until they were solidified. ATR-FTIR was also used quantitatively to assess the relative concentration of the functional groups on the basis that the intensities of the absorbance bands are related to the concentrations of the functional groups producing them (Socrates, 2001). To determine if there is an appreciable change on the studied samples 'quantitatively', the values of the integrated areas under the ATR-FTIR spectra which fall outside the range of experimental error as determined by  $\text{mean} \pm \text{S.D}$  of the undertaken measurements will be considered a significant change. A further tracking of any distinct vibrational bands that can be correlated with crystallinity changes was addressed (Khanna and Khun, 1997). Omnic software (version 6.1a) was used to analyze the obtained results and to perform a comparison. As a supportive technique, hot stage microscopy (HSM) was used to visualize the effect of the thermal treatment on the studied physical mixtures as will be detailed in section 7.3.3.

### 7.3.2 Results and discussion

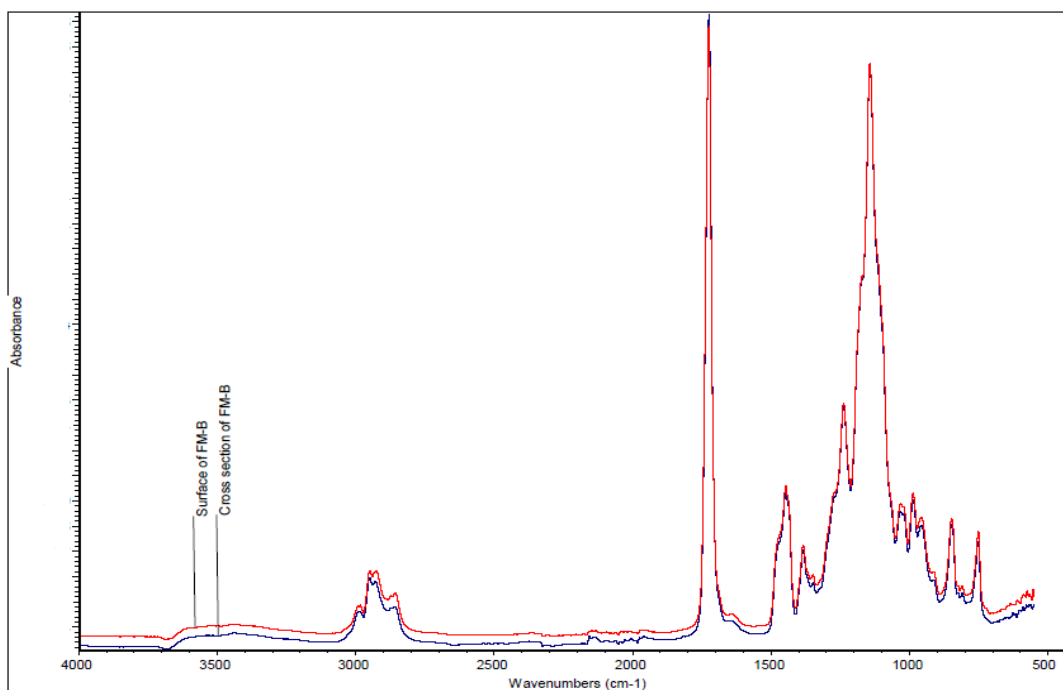
The ATR-FTIR spectra of the extruded systems were collected for FM-A (Gelucire 44/14 Eudragit RS PO ratio of 1:6) and FM-B (Gelucire 44/14 Eudragit RS PO ratio of 2:5) fresh films. An overlay of the ATR-FTIR spectra of the surface and cross section of the tested films were superimposable as shown in Figure 7.15. Therefore their surfaces' spectra were used for comparison and further analysis.



(A)



(B)



**Figure 7.15: Overlay of superimposable ATR-FTIR spectra of the surface and cross section of hot melt extruded films of system FM-A (A) and system FM-B (B). See text for their compositions**

The ATR-FTIR spectra related to the extruded films were then compared to their equivalent physical mixtures as shown in Figure 7.16. The absorbance bands which correspond to the vibrations of specific functional groups within the structure of Eudragit RS PO and Gelucire 44/14 were determined in Chapter 3. Therefore, each tested spectrum in Figure 7.16 can be divided generally into three regions as follows:

-Region I:  $3172\text{-}2702\text{cm}^{-1}$ : This region is indicative of the changes that could be related to the alkyl C-H groups of both components i.e. Gelucire 44/14 and Eudragit RS PO.

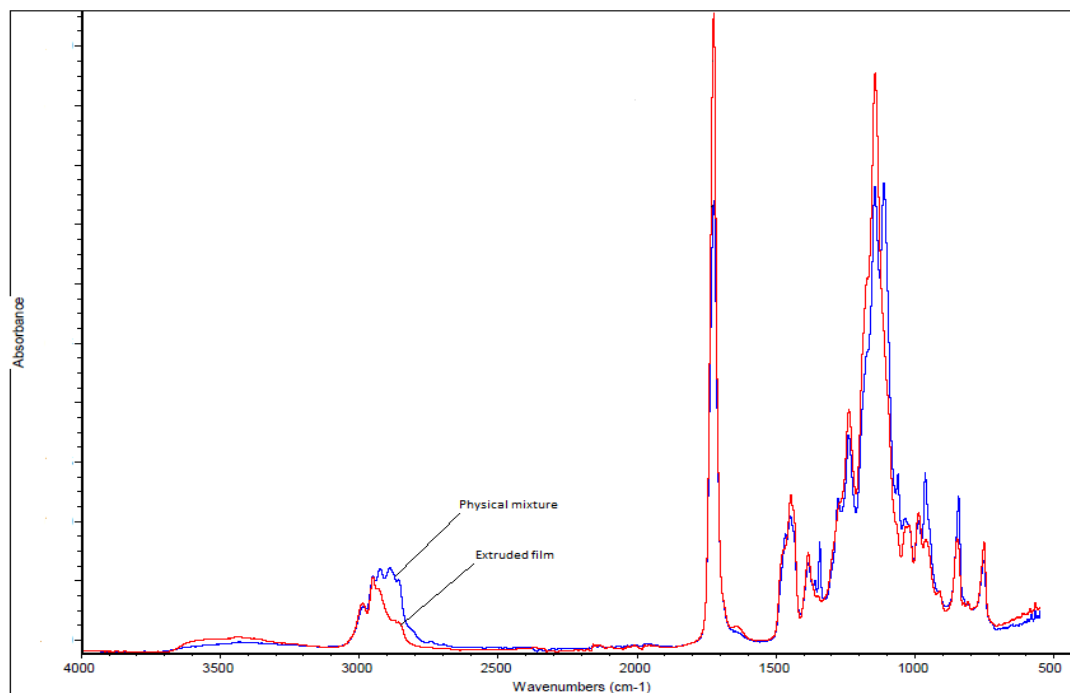
-Region II:  $1857\text{-}1605\text{ cm}^{-1}$ : This region presents changes in the C=O stretching of the ester groups in both Gelucire 44/14 and Eudragit RS PO.

-Region III:  $1547\text{-}885\text{ cm}^{-1}$ : This region is associated with the changes mainly in the C-O stretch of alcohols (primary or secondary) of Gelucire 44/14 and C-CO-C stretching in Eudragit RS PO.

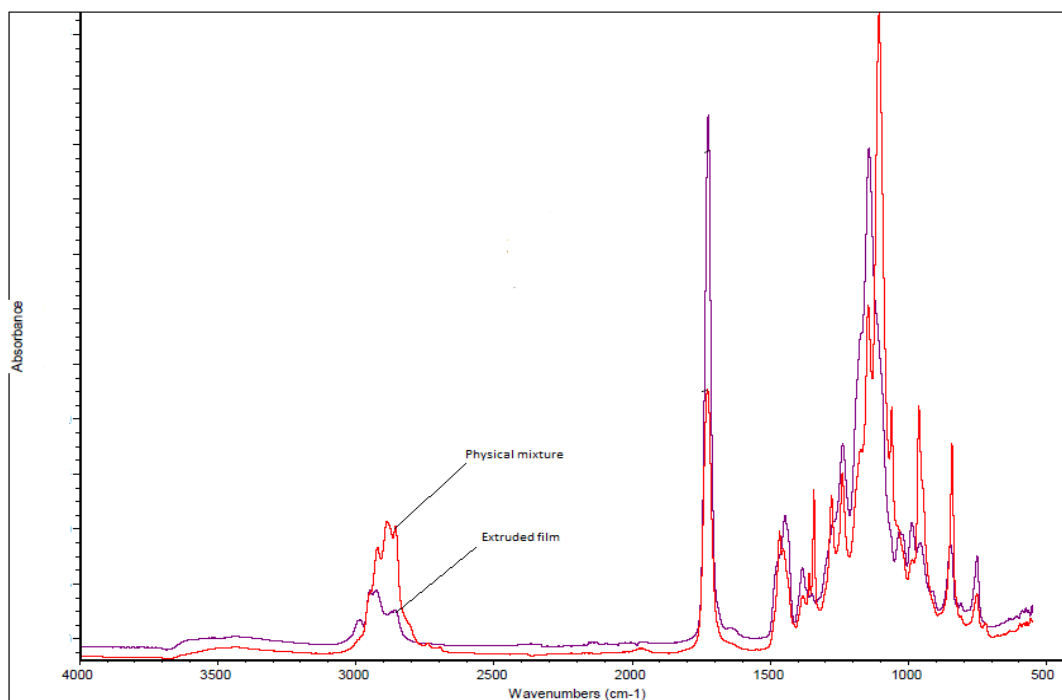
It is worth mentioning that band assignment to these regions was based on characteristic absorption bands of these materials while these regions in the acquired spectra contained bands from other vibrational modes. The relative areas integrated under these three regions were used to give an idea about the possible changes of the samples under investigation. For comparative purposes, relative percentage area region was calculated as the percentage of the normalized integrated area of the total region with respect to the total integrated area of the studied spectrum.

In this study, collection of the spectra was also performed for the pure components and studied physical mixtures after thermal treatment *in situ* at the extrusion temperature, using a built-in heating accessory in the ATR-FTIR, followed by cooling to room temperature. This allows the tracking of possible changes in these systems during heating and after thermal treatment and to observe the trend of intensity changes in comparison to the hot melt extruded films of these materials.

(A)



(B)

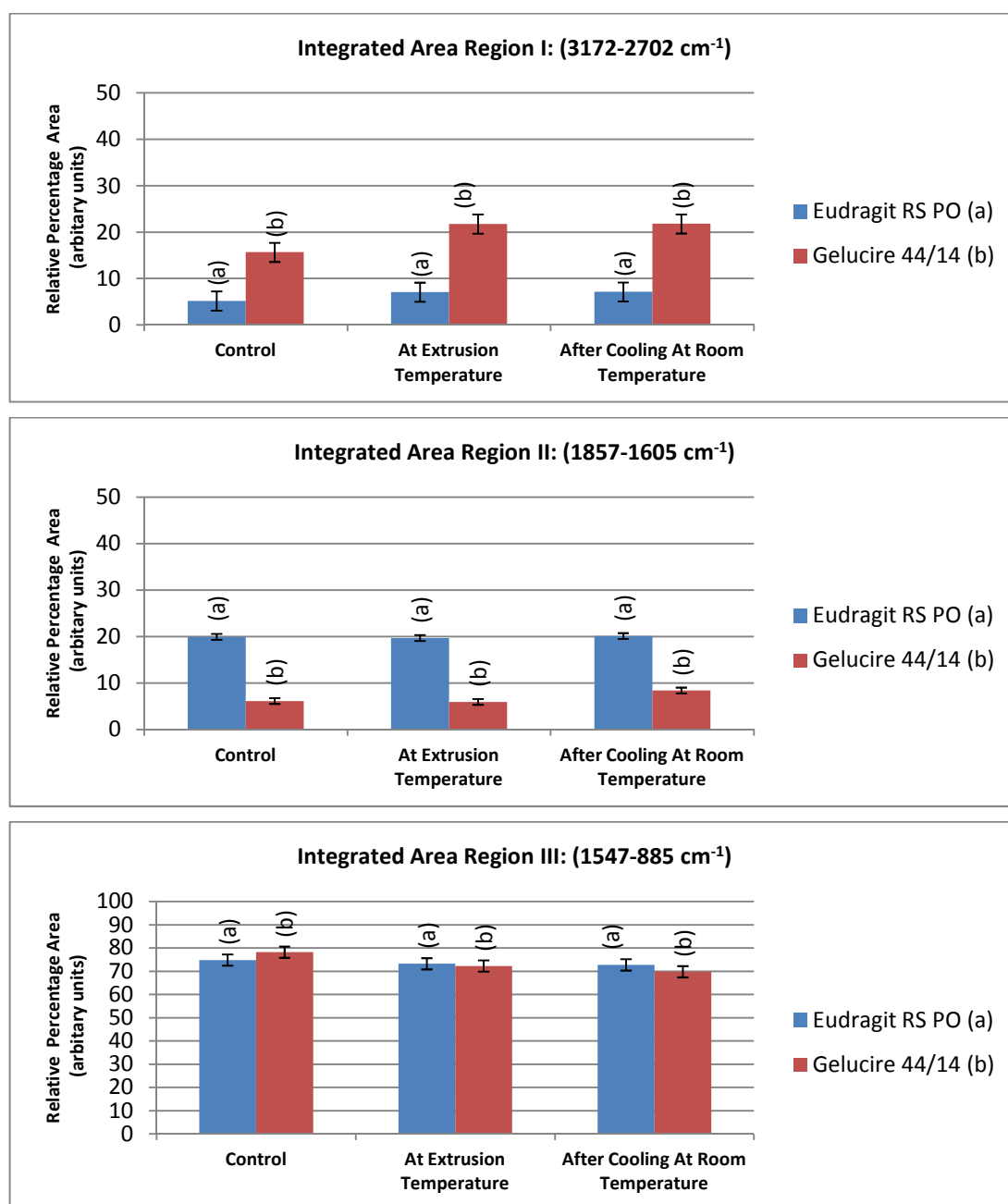


**Figure 7.16: Overlay of the ATR-FTIR spectra of the physical mixtures and corresponding hot melt extruded films of FM-A (Gelucire 44/14 Eudragit RS PO ratio of 1:6) system (A) and FM-B (Gelucire 44/14 Eudragit RS PO ratio of 2:5) system (B). See text for composition**

The quantitative data of the integrated areas of the ATR-FTIR spectra of the Gelucire 44/14 and Eudragit RS PO are presented in Figure 7.17. The changes in the relative percentage areas with respect to control samples were as follows:

1. The absorption in region I, between  $3172$  and  $2702\text{ cm}^{-1}$ , has essentially increased only in Gelucire 44/14 after thermal treatment.
2. The absorption in region II, between  $1857$  and  $1605\text{ cm}^{-1}$ , arises mainly from C=O stretching mode of the ester groups, which has increased after thermal treatment in both Gelucire 44/14 and Eudragit RS PO.
3. The absorption in region III, between  $1547$  and  $885\text{ cm}^{-1}$ , has decreased only in Gelucire 44/14 after thermal treatment.

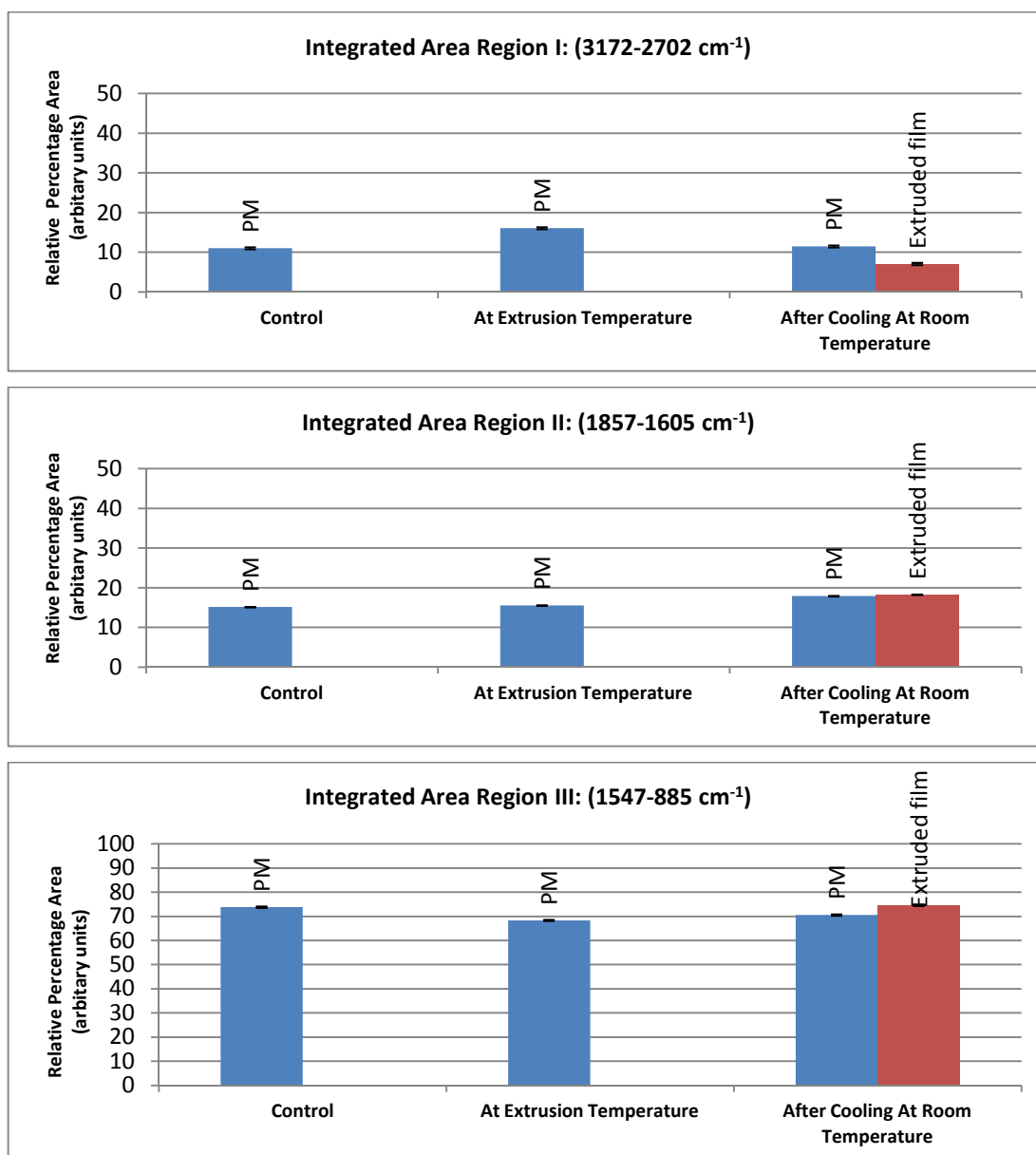
These observations were not appreciably significant except in region I of Gelucire 44/14. It is believed that thermal treatment of this lipid might be associated with a possibility of reorientations in the alkyl groups therein or changes in the transition dipole of these groups. As the infrared absorbance is due to interaction between the electric field vector and the molecular dipole transition moments due to molecular vibration, the orientations can be observed. Thus, differences in the molecules' alignment could result in changes in the band intensities. An alternative idea of change in transition dipole is the hypothesis that thermal treatment of these samples might change their optical properties. It is expected that as the material is heated, the sample will have better contact with the ATR crystal, thus enhancing contact with the evanescent wave (see Chapter 2). The resulting spectrum will therefore provide information within this range of more penetration depth.



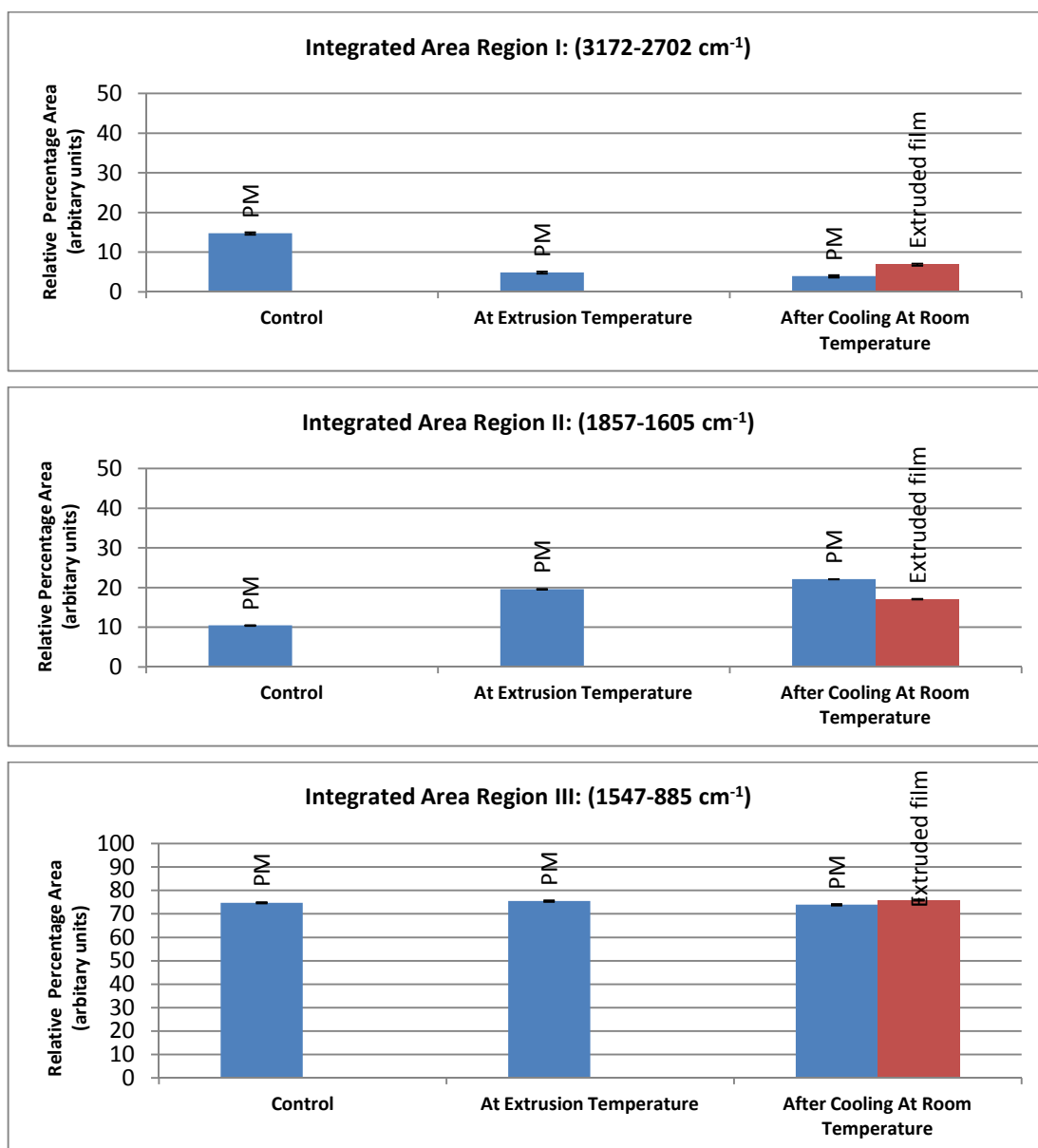
**Figure 7.17:** Histograms of the integrated relative percentage areas of Eudragit RS PO (a) and Gelucire 44/14 (b), of the alkyl C-H group stretching (3172-2702 cm<sup>-1</sup>), C=O stretching of the ester groups (1857-1605 cm<sup>-1</sup>) and C-O stretch of alcohols (primary or secondary) of Gelucire 44/14 and C-CO-C stretching in Eudragit RS PO (1547-885 cm<sup>-1</sup>). Samples were examined as the following sets: Control (no thermal treatment). At the temperature of extrusion (120°C). The cooled samples to the room temperature after thermal treatment (solidified samples). Average values of three spectra of each set were calculated and S.D. error bars were estimated accordingly

Similarly, the ATR-FTIR spectra of the thermally treated physical mixtures and their equivalent extrudates were analyzed as shown in Figure 7.18 and Figure 7.19. The analysis of these data revealed the following main changes with respect to the controls (untreated equivalent physical mixes) of these samples:

- In region I, the heat-cooled physical mixture of FM-B (higher content of Gelucire 44/14) showed a decrease in the absorption.
- In the same region, related to C-H alkyl group stretching, the extruded systems of FM-A (lower content of Gelucire 44/14) and FM-B (higher content of Gelucire 44/14) showed a decrease in the absorption. This complies with FM-B heat-cooled physical mixture behaviour.
- In region II, heat-cooled physical mixtures and the extruded films of both FM-A and FM-B systems showed the same trend of increased absorption in the region associated with the C=O stretching mode, especially for the FM-B systems which contained a higher level of Gelucire 44/14.



**Figure 7.18:** Histograms of the integrated relative percentage areas of FM-A system (1: 6 ratio of Gelucire 44/14: Eudragit RS PO), for both physical mixture (PM) and equivalent fresh extruded film. The alkyl C-H group stretching related to the region between 3172 and 2702 cm<sup>-1</sup>, C=O stretching of the ester groups (1857-1605 cm<sup>-1</sup>) and C-O stretch of alcohols (primary or secondary) of Gelucire 44/14 and C-CO-C stretching in Eudragit RS PO (1547-885 cm<sup>-1</sup>). Samples were examined as the following sets: Control (no thermal treatment). At the temperature of extrusion (120°C). The cooled samples after thermal treatment at the room temperature (solidified samples). Average values of three spectra of each set were calculated and S.D. error bars were estimated accordingly



**Figure 7.19:** Histograms of the integrated relative percentage areas of FM-B system (2: 5 ratio of Gelucire 44/14: Eudragit RS PO), for both physical mixture (PM) and equivalent fresh extruded film. The alkyl C-H group stretching related to the region between 3172- 2702  $\text{cm}^{-1}$ , C=O stretching of the ester groups (1857-1605  $\text{cm}^{-1}$ ) and C-O stretch of alcohols (primary or secondary) of Gelucire 44/14 and C-CO-C stretching in Eudragit RS PO (1547-885  $\text{cm}^{-1}$ ). Samples were examined as the following sets: Control (no thermal treatment). At the temperature of extrusion (120°C). The cooled samples after thermal treatment at the room temperature (solidified samples). Average values of three spectra of each set were calculated and S.D. error bars were estimated accordingly

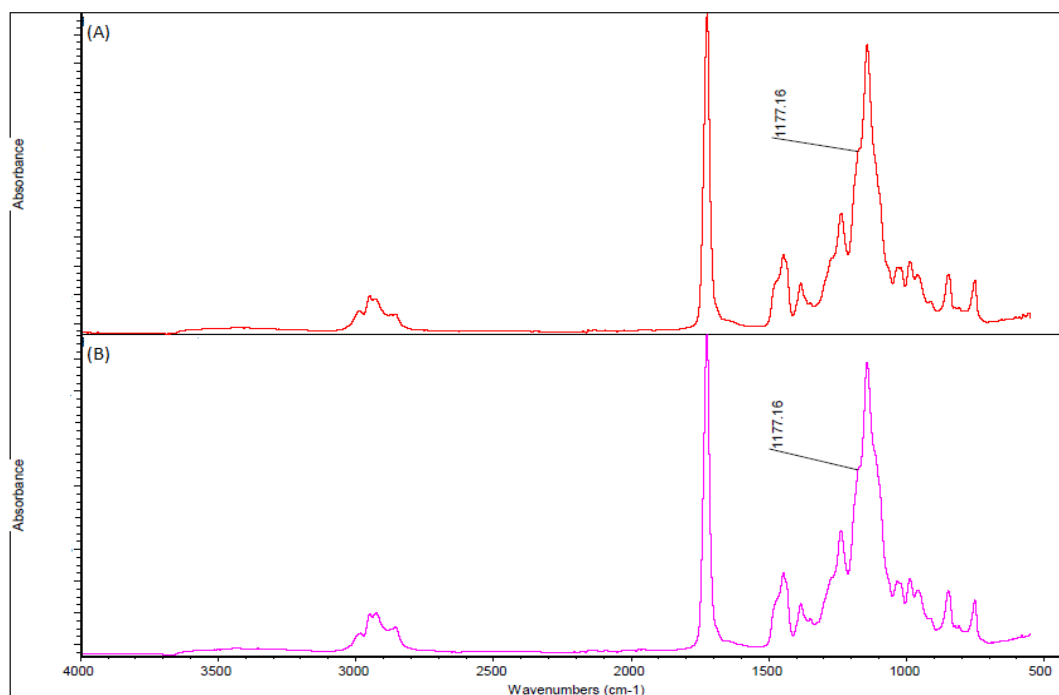


These observations (Figure 7.18 and 7.19) can be rationalized by the proposal that extrusion of Gelucire 44/14 in Eudragit RS PO in the ratio of 1:6 and 2:5 in FM-A and FM-B systems, respectively, in addition to the thermal treatment of the FM-B physical mix might result in migration of alkyl groups. Thus, absorption bands associated with the hydrophobic alkyl groups in region I were decreased, whereas an increase of the absorption was detected in the carbonyl group in region II.

Consequently, it is hypothesized that the interior of these samples is enriched with the C-H groups, in which hydrophobic side chains would be expected to be more involved in interactions (a decrease in the detected absorption), whereas the remaining hydrophilic functional groups will be “expelled” or readily available on the surface for these samples (an increase of their measured absorptions). The formation of such construct is consistent with the properties of Gelucire 4/14 as reported by Wehrung et al. (2012) and supported by the formation of a new shoulder, appearing around  $1177\text{ cm}^{-1}$  (C-O stretch) in both studied extrudates as shown in Figure 7.20. This trend of group rearrangements could be facilitated by intimate mixing provided during hot melt extrusion (HME) or the availability of more Gelucire 44/14 in the thermally treated physical mix (FM-B system).

However, it could be argued that if the interior of the extruded samples is enriched with C-H groups this will be mirrored as an increase of the measured absorption of these groups from the cross sections of these extrudates. This was not the case in these samples because the surfaces were superimposable to the cross sections. Nonetheless this hypothesis can hold true because the ATR-FTIR technique offers a limited depth of penetration into the sample, typically around the values from  $<0.2\text{ micron}$  to  $>1\text{ micron}$  (Tang et al., 2007). Therefore, it could be speculated that the alkyl groups are embedded deeply in these systems and that examination of the cross sections will not detect them.

In summary, the changes associated with the relative percentage areas of the acquired spectra from thermally treated or extruded samples can be explained by three possible hypotheses, namely, change in transition dipole, change in optical properties or migration of the alkyl groups. Further explanation as to these changes is beyond this thesis, because at present there is insufficient evidence to decide which effect is operating.

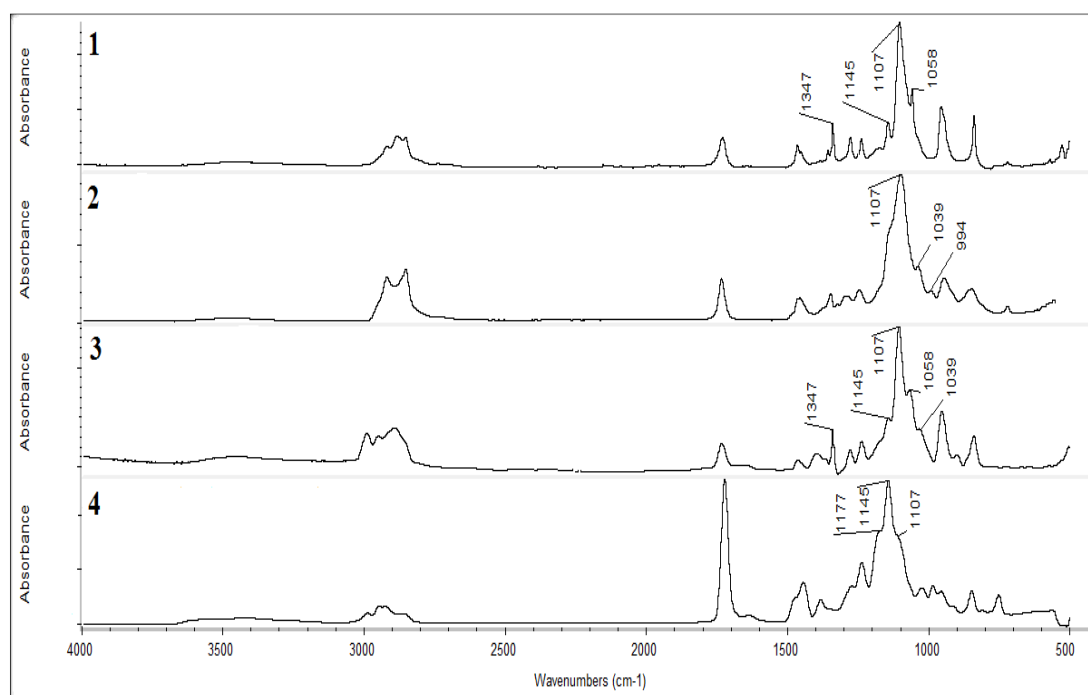


**Figure 7.20: ATR-FTIR spectra of hot melt extruded films of (A) FM-A (Gelucire 44/14 Eudragit RS PO ratio of 1:6) system and (B) FM-B (Gelucire 44/14 Eudragit RS PO ratio of 2:5) system (absorption intensities of these spectra vary)**

To probe the molecular state of Gelucire 44/14 inside the extruded systems of FM-A and FM-B using ATR-FTIR, the Eudragit RS PO spectra were subtracted from the spectra of the extruded systems (Gelucire 44/14 in Eudragit RS PO). The resultant subtraction spectra are shown in Figure 7.21 and Figure 7.22. These spectra were compared to the Gelucire 44/14 spectra that had also been extracted from the equivalent physical mixes without thermal treatment (control) through subtraction of Eudragit RS PO spectra. In addition, Gelucire 44/14 spectra collected during heating at the extrusion temperature (assuming that the molten Gelucire 44/14 is behaving like amorphous material) and after cooling at room temperature (solidified) were shown for further comparison.

In Figure 7.21, the Gelucire 44/14 spectrum stripped from the physical mixture was superimposable to the raw pure Gelucire 44/14 spectrum described in Chapter 3 (data not show here), indicating a good subtraction. Furthermore, the subtraction is justified because the Eudragit spectrum does not change with temperature and the subtraction does not result in any misshaped peaks which would occur if shifts in the Eudragit spectrum had occurred.

As illustrated in this figure (7.21), four characteristic peaks were assigned in this spectrum (Gelucire 44/14). These peaks will be named peak (A) at  $1347\text{ cm}^{-1}$  related to C-O stretching, peak (B) at  $1145\text{ cm}^{-1}$ , peak (C) at  $1107\text{ cm}^{-1}$  and peak (D) at  $1058\text{ cm}^{-1}$ . Peak (B), (C) and (D) are mainly due to the PEG 1500 C-O-C stretching vibration (Feng et al., 2011). As illustrated in this figure, these peaks were the most changed bands after thermal treatment of the Gelucire 44/14 at the extrusion temperature (molten Gelucire 44/14) and to a lesser extent the peak around  $1347\text{ cm}^{-1}$  (peak (A)).

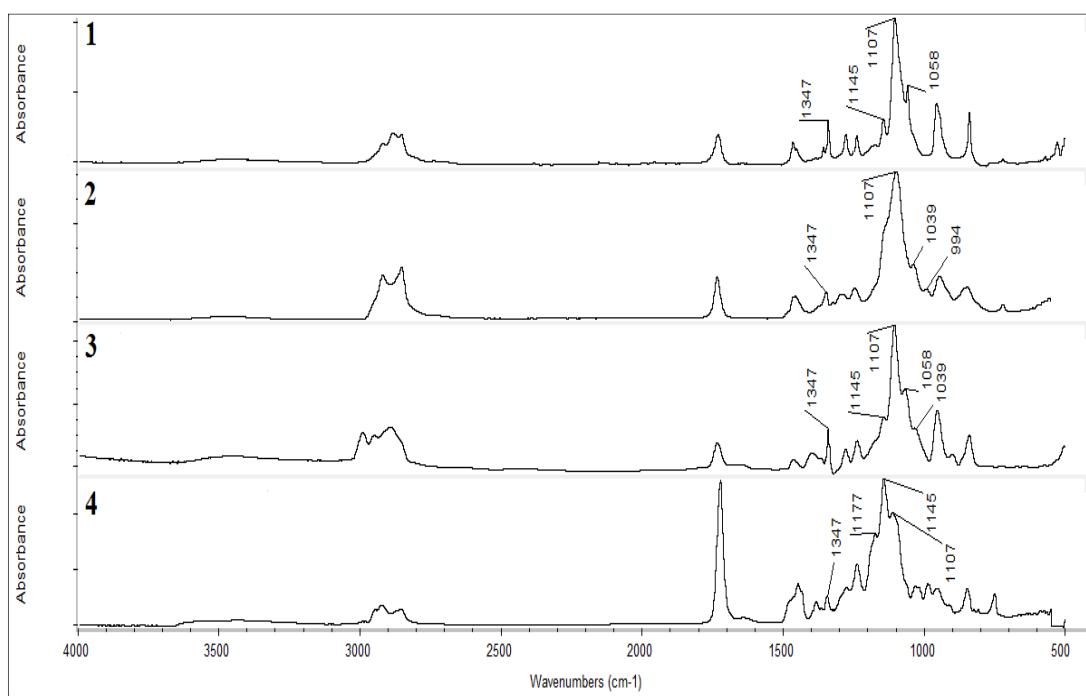


**Figure 7.21: ATR-FTIR spectra of (1) Eudragit RS PO-subtracted spectrum of physical mixture containing Eudragit RS PO Gelucire 44/14 in a ratio of 6:1, without thermal treatment (control), (2) molten Gelucire 44/14 at the extrusion temperature ( $120^{\circ}\text{C}$ ), (3) solidified Gelucire 44/14 after thermal treatment at extrusion temperature and (4) Eudragit RS PO-subtracted spectrum of extruded film containing Eudragit RS PO Gelucire 44/14 in a ratio of 6:1 (FM-A system)**

As illustrated in Figure 7.21, the previously mentioned peaks (B-D) were overlapped or merged into one peak with the apex of band (C) around  $1107\text{ cm}^{-1}$  at the extrusion temperature ( $120^{\circ}\text{C}$ ) in the molten Gelucire 44/14. In addition, new peaks appeared around  $1039$  and  $994\text{ cm}^{-1}$ . These new bands occur at similar locations of glycerol C-O stretching bands (Calvino-Casilda et al., 2011), suggesting a hydrolysis of the ester structure in the Gelucire 44/14. After cooling of Gelucire 44/14 to the room temperature (solidified samples), the characteristic peaks (B), (C) and (D) appeared again at their locations at  $1145$ ,  $1107$  and  $1058\text{ cm}^{-1}$ , respectively. However, a newly detected peak around  $1039\text{ cm}^{-1}$  remained, suggesting hydrolysis at a certain extent. Furthermore, the sharpness (intensity) of peak (A) at  $1347\text{ cm}^{-1}$  became similar to the control crystalline Gelucire 44/14. It is therefore concluded that solidified samples underwent recrystallization and this peak (at  $1347\text{ cm}^{-1}$ ) is sensitive to the crystallinity of Gelucire 44/14.

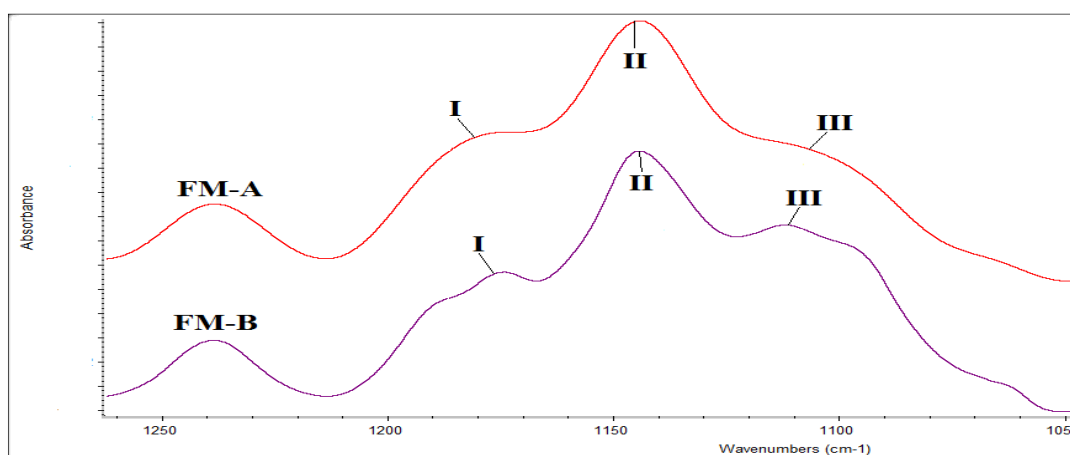
In the amorphous state (like molten Gelucire 44/14 herein), the less ordered molecules in comparison to the crystalline structure can result in a greater distribution of the molecular frequencies due to non-specific intermolecular bonding. This will be viewed as broader absorbance (less intense) bands in the ATR-FTIR spectrum, which in some cases can spread over a large extent and thus the absorbance peaks will be flattened, because it can be smeared with the baseline of the spectrum. Peak (A) around  $1347\text{ cm}^{-1}$ , for example, can be used as a marker to correlate with the crystallinity changes of Gelucire 44/14. This is because it has been broadened in the molten state (which is assumed to resemble the amorphous state) and then changed into a more defined shape peak in the solidified sample, similar to the crystalline Gelucire 44/14 in the control samples.

In Figure 7.21, this marker peak (A,  $1347\text{ cm}^{-1}$ ) was flattened in the Gelucire 44/14 spectrum extracted from the FM-A extrudate (after subtraction of Eudragit RS PO spectrum), whereas it has been elevated in the Gelucire 44/14 spectrum extracted from FM-B extrudate in Figure 7.22. In conjunction with the previous findings using MTDSC, cDSC and SEM, which indicated that Gelucire 44/14 recrystallization was inhibited only in the FM-A system (lower content of Gelucire 44/14) upon extrusion, it could be reasonably concluded that the distinction of this peak in the FM-B extrudate (higher content of Gelucire 44/14) is related to the presence of crystalline Gelucire 44/14.



**Figure 7.22: ATR-FTIR spectra of (1) Eudragit RS PO-subtracted spectrum of physical mixture containing Eudragit RS PO Gelucire 44/14 in a ratio of 5:2, without thermal treatment (control), (2) molten Gelucire 44/14 at the extrusion temperature (120°C), (3) solidified Gelucire 44/14 after thermal treatment at extrusion temperature and (4) Eudragit RS PO-subtracted spectrum of extruded film containing Eudragit RS PO Gelucire 44/14 in a ratio of 5:2 (FM-B system)**

Furthermore, an overlay of the Gelucire 44/14 spectra from FM-A (lower content Gelucire 44/14) and FM-B (higher content Gelucire 44/14) extrudates was obtained after subtraction of Eudragit RS PO spectra as displayed in Figure 7.23. This figure shows the spectral region of the most changing peaks of Gelucire 44/14 after thermal treatment. It can be seen that Gelucire 44/14 spectra (extracted from the extruded samples) retain the evolved new shoulder detected in these extrudate around  $1177\text{ cm}^{-1}$  (see Fig.7.20), and denoted here as (I). This shoulder appears as a more distinct peak in the Gelucire 44/14 spectrum extracted from FM-B extruded system (higher content of Gelucire 44/14). In this Figure (7.23), peak around  $1107\text{ cm}^{-1}$ , denoted here as (III) and related to C-O-C stretching, appeared as a shoulder in FM-A system and sharpened as a distinct peak in the FM-B system, indicating crystalline Gelucire 44/14 in the latter. To conclude, the bands related to the peak at  $1347\text{ cm}^{-1}$  and peak at  $1107\text{ cm}^{-1}$  can be used as bench marks for the amorphous Gelucire 44/14 inside the extruded systems of FM-A and FM-B compositions. Crystalline Gelucire 44/14 will exhibit sharper or more distinct peaks in these locations.

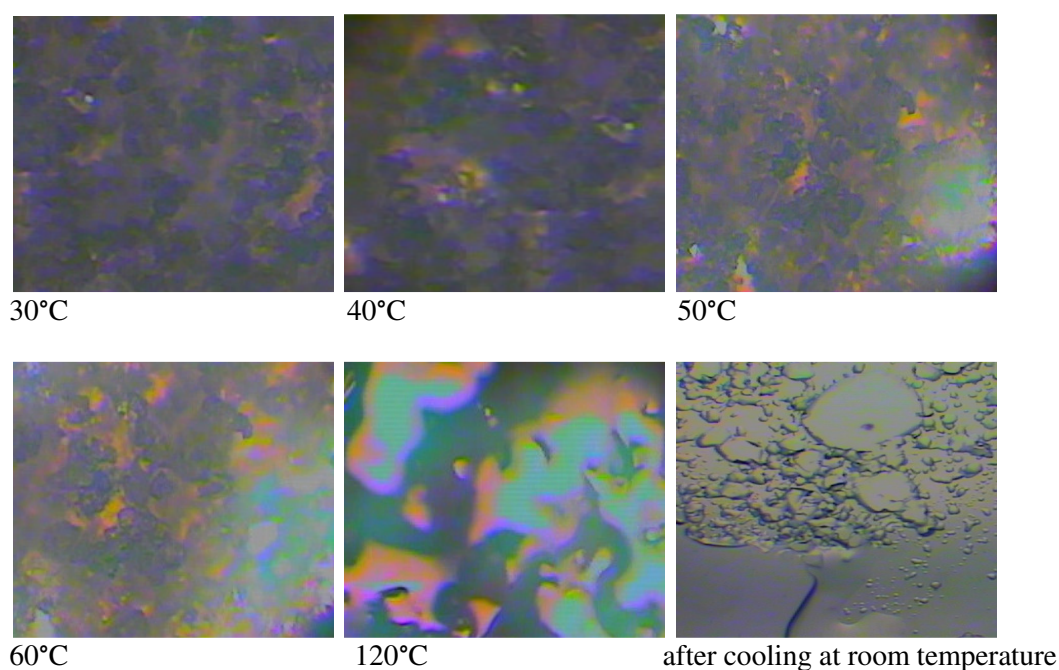


**Figure 7.23: ATR-FTIR Eudragit RS PO-subtracted spectra of extruded films containing Eudragit RS PO Gelucire 44/14 in the ratios of 6:1 (FM-A system) and 5:2 (FM-B system)**

### **7.3.3 A note on the observed behaviour of Eudragit RS PO/Gelucire 44/14 physical mixtures under thermal treatment by hot stage microscopy (HSM)**

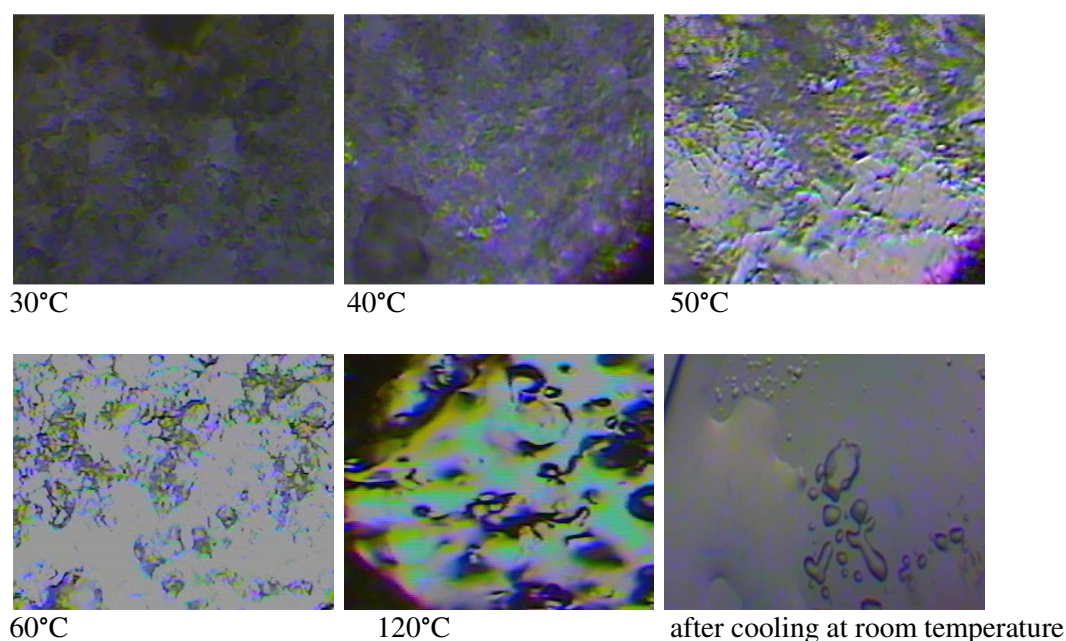
The HSM technique, described in Chapter 2, can be used in conjunction with the previous characterisation techniques to provide visual evidence of the affinity or miscibility between Gelucire 44/14 and Eudragit RS PO in the FM-A (Gelucire 44/14 Eudragit RS PO ratio of 1:6) and FM-B (Gelucire 44/14 Eudragit RS PO ratio of 2:5) systems, during heating of their physical mixes. The HSM experiment involved a video capture microscope while exposing the samples to a controlled temperature program heating from 30°C to 120°C at 5°C min<sup>-1</sup>. Photos of these blends were taken immediately after cooling to the room temperature (~25°C). The approximate cooling rate was 2°C/min.

Figure 7.24 and 7.25 showed a series of images captured during the heating of the physical mixtures of FM-A and FM-B systems, respectively. As can be seen from Figure 7.24 the melting of Gelucire 44/14 was apparent from 40°C and more visible for the higher content of Gelucire 44/14 in the FM-B system, as indicated in Figure 7.25. Above 60°C, which is higher than the glass transition of the Eudragit RS PO, we can find that more material is involved in the liquefied-molten zone as illustrated in both figures. Finally at the extrusion temperature (120°C), one phase system was observed for FM-A and FM-B composition with a clear appearance after cooling at room temperature, suggesting good miscibility. It is noteworthy that this one phase system was formed at approximately 118°C for FM-A and around 111°C for the higher ratio of Gelucire 44/14 at FM-B composition. Therefore, this technique is supplementary to the MTDSC, cDSC and ATR-FTIR techniques. All these techniques indicated that there is miscibility and possible interactions between Eudragit RS PO and Gelucire 44/14 at the studied compositions even after simple heating of their physical mixes.



**Figure 7.24:** Hot stage microscope images captured at specific temperatures for physical mixture of FM-A composition (Gelucire 44/14 Eudragit RS PO ratio of 1:6) while being heated at 5°C per minute





**Figure 7.25:** Hot stage microscope images captured at specific temperatures for physical mixture of FM-B composition (Gelucire 44/14 Eudragit RS PO ratio of 2:5) while being heated at 5°C per minute

#### **7.4 Hydration behaviour of Eudragit RS PO/Gelucire 44/14 hot melt extruded films**

In order to design an effective transdermal patch dosage form, it is recommended to recognize and investigate the main factors contributing to its success. Among these factors, hydration appears to be essential to achieve the desired drug release from these extruded films as detailed in Chapter 6. Therefore this section explores the water sorption features of these carrier systems followed by a deep investigation of the changes that may associate hydration of these films and contribute to their delivery mechanism.

##### **7.4.1 Investigation into water sorption properties of Eudragit RS PO/Gelucire 44/14 hot melt extruded systems**

In this section an attempt to elucidate some aspects of the sorption behaviour was carried out for the pure components of Gelucire 44/14 and Eudragit RS PO, their physical mixtures and equivalent extruded systems at FM-A (Gelucire 44/14 Eudragit RS PO ratio of 1:6) and FM-B (Gelucire 44/14 Eudragit RS PO ratio of 2:5) compositions.



#### 7.4.1.1 Methodology

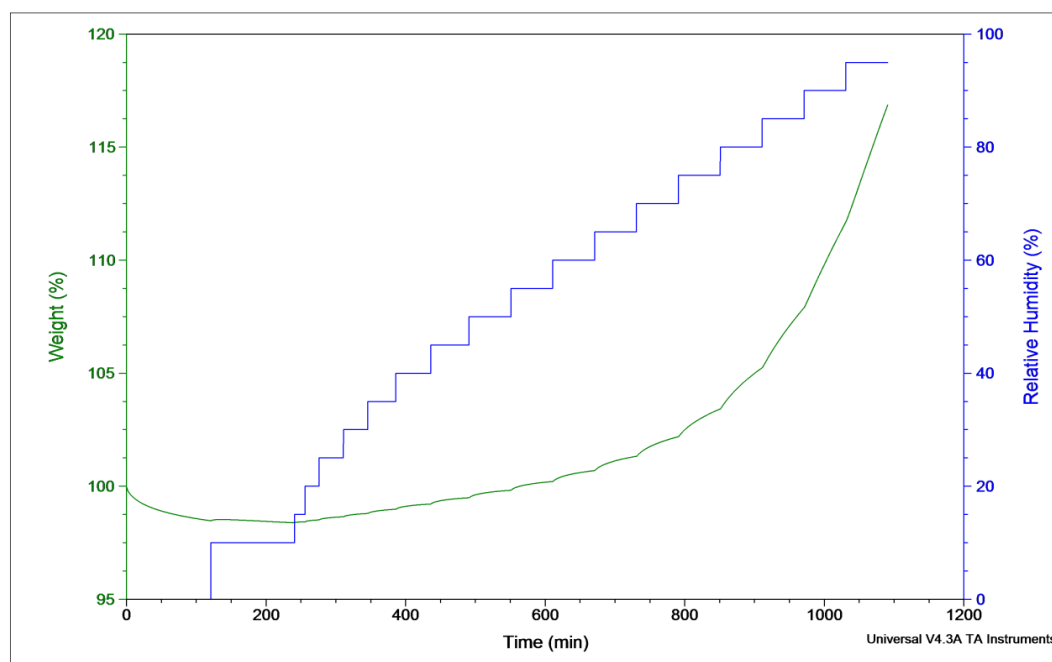
Samples of the basic ingredients of Gelucire 44/14 and Eudragit RS PO were examined for their moisture sorption behaviour using dynamic vapor sorption technique (DVS) documented in Chapter 2. In this part, two DVS experiments were carried out. The first experiment will be termed here 'method A'. In this method a general procedure of stepping the humidity (%RH) over a range of 0%RH-95%RH at 25°C was performed. In this method the humidity was raised in steps of 5%RH, where the sample is held in each step for one hour, to enable equilibrium prior the next humidity level. The second experiment will be termed 'method B'. This method involved exposure to a single high relative humidity of 95%RH at 25°C for 24 hours. In this experiment, the pure components, the physical mixtures of FM-A (Gelucire 44/14 Eudragit RS PO ratio of 1:6) and FM-B formulae (Gelucire 44/14 Eudragit RS PO ratio of 2:5), described in section 7.2.1, and their equivalent extruded systems were tested. The basic ingredients and the tested physical blends were further divided into two groups based on the thermal treatment. The first group involves the controls of untreated samples, whereas the second group consists of the heated samples at the extrusion temperature (120°C) followed by solidification at room temperature. In the first step of all the experiments, the samples were held for three hours at 0%RH at 25°C to allow drying. The program in method A and B was set to advance the humidity or the holding time, respectively, when weight percentage is less than 0.01 in five minutes. Samples were spread evenly to fill standard aluminium open pans (surface area of approximately 38.5 mm<sup>2</sup>) in an attempt to unify the exposed surface area of these samples to the moisture; thereby a direct comparison can be made between different tested samples.

#### 7.4.1.2 Results and discussion

The resulting sorption isotherms of Gelucire 44/14 and Eudragit RS PO from method A are shown in Figure 7.26 (A) and (B), respectively. The isotherm of Eudragit RS PO seems to level out at low relative humidity values, approaching a maximum (plateau). On the contrary, the moisture sorption isotherm of Gelucire 44/14 could not achieve that equilibrium at any studied humidity level. This suggests that the more hydrophobic nature of Eudragit RS PO allows for faster equilibrium moisture content in comparison to the amphiphilic nature of the Gelucire 44/14 (Svensson et al., 2004). This inferred that the time for the latter should be long enough to ensure moisture or humidity equilibrium. Furthermore in Figure 7.27, it can be seen that Eudragit RS PO begins to take up water earlier than Gelucire 44/14, though very small amount (less than 0.05 % (w/w)). However,

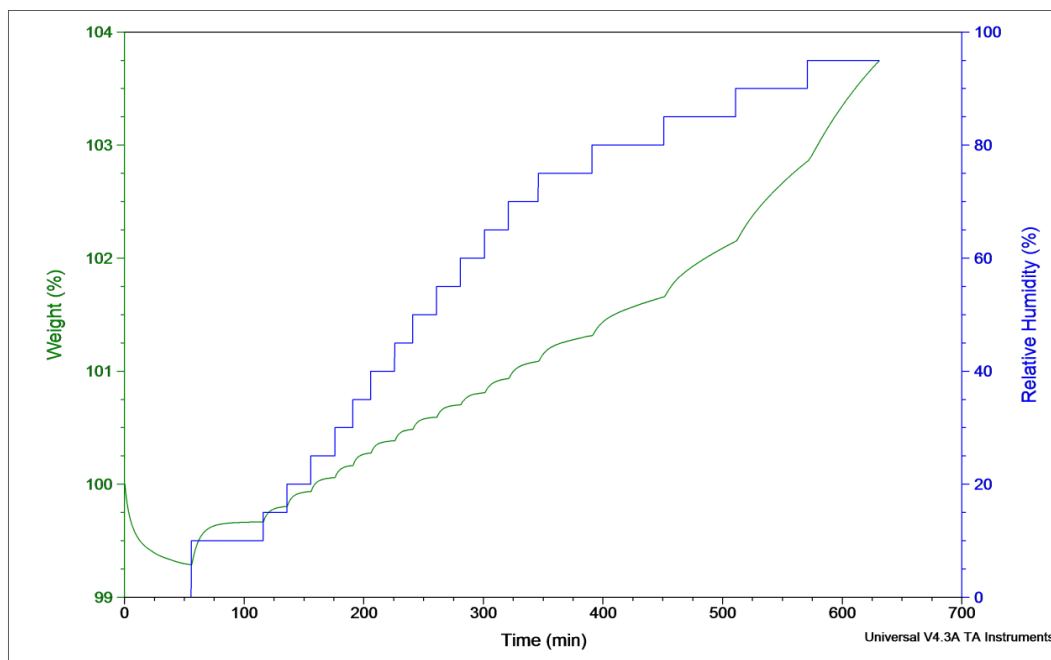
after 53%RH, Gelucire 44/14 began to hydrate with an abrupt increase in the moisture uptake curve after 75%RH at 25°C. This behaviour is consistent with the manufacturer's specifications of Gelucire 44/14, whereby little or no moisture absorption is detected below 80%RH at room temperature (Gattefossé, 2000). However, the water uptake by Gelucire 44/14 above approximately 70%RH/25°C is higher than Eudragit RS PO as illustrated in Figure 7.27. For example, at 95%RH/25°C, the total water content of Gelucire 44/14 exceeds 16% (w/w) in comparison to the Eudragit RS PO with around 3.72% (w/w) moisture content. Therefore this confirms that Gelucire 44/14 is the main component in absorbing water when combined with the Eudragit RS PO especially at high relative humidities ( $\sim \geq 70\%$  RH) at room temperature.

(A)

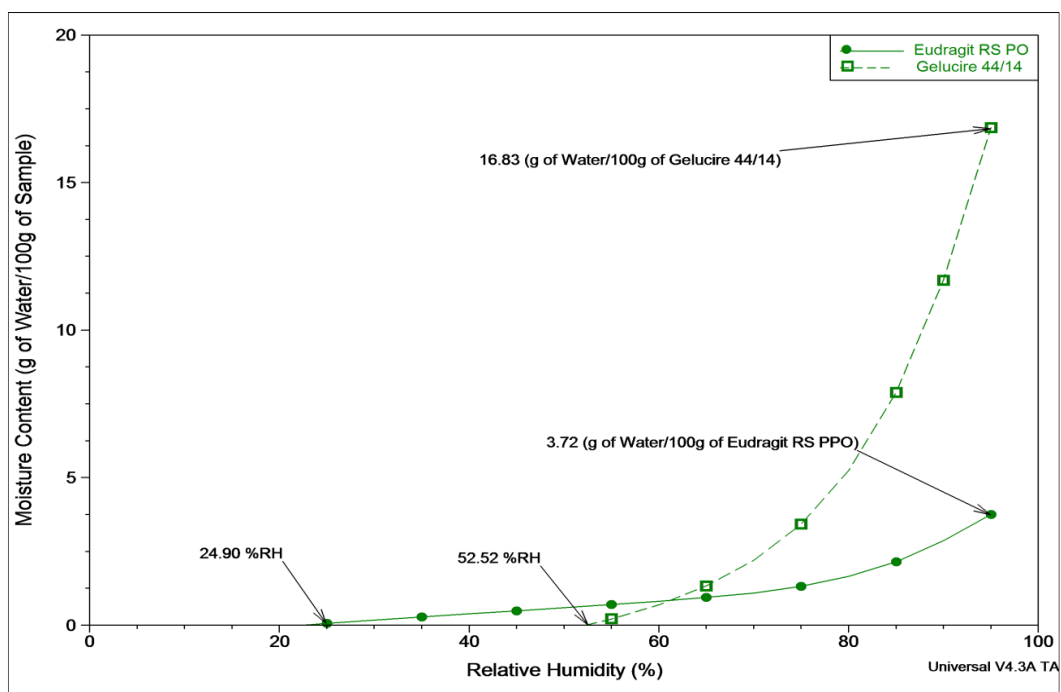


**Figure 7.26: Weight percent versus time signal for Gelucire 44/14 at 25°C with an RH ramp from 0 to 95% (A)**

(B)



**Figure 7.26 (Contd.): Weight percent versus time signal for Eudragit RS PO at 25°C with an RH ramp from 0 to 95% (B)**

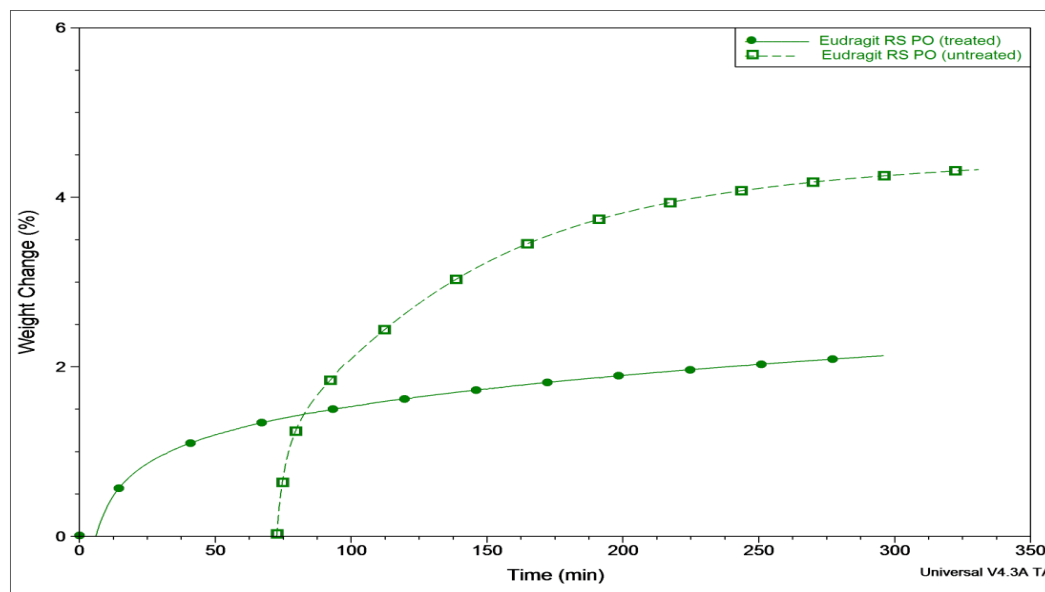


**Figure 7.27: Overlay of the moisture content of Gelucire 44/14 (open squares) and Eudragit RS PO (filled circles) according to the relative humidity at 25°C**

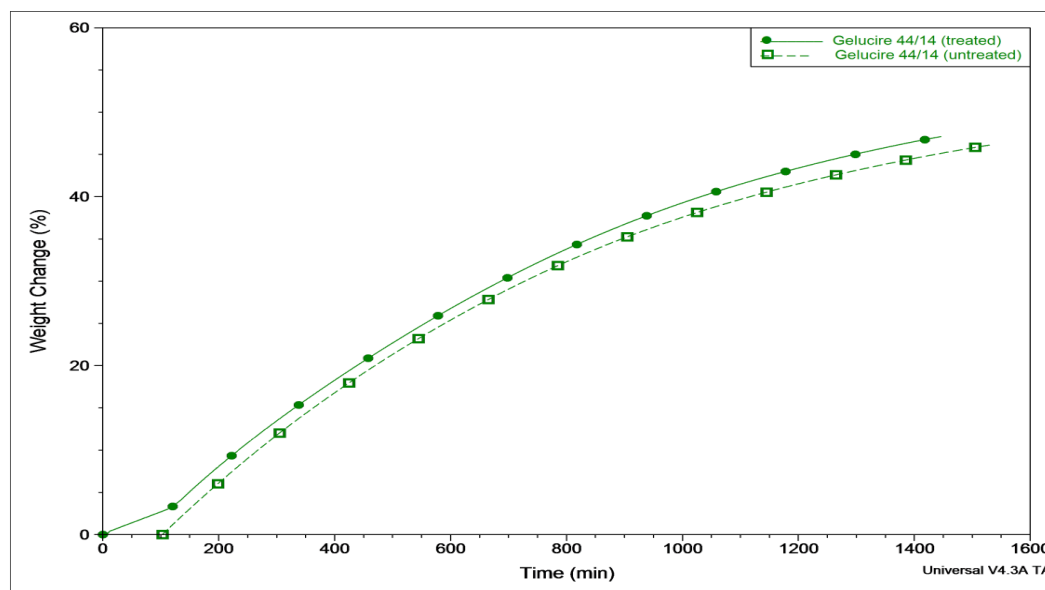
Based on the findings of method A, the parameters of the second experiment were set (method B). This method was performed using high relative humidity of 95% RH at 25°C, which corresponds to the highest water uptake of the studied ingredients (Gelucire 44/14 and Eudragit RS PO). Samples were held for one day at this condition to enable equilibrium of moisture content. As presented in Figure 7.28 (A) and (B), the water uptake ability for Eudragit RS PO was decreased by thermal treatment, while being increased for the Gelucire 44/14. When these components are combined in the ratio of 1:6 and 2:5 (Gelucire 44/14: Eudragit RS PO) in FM-A and FM-B systems, respectively, the resulting moisture isotherms are illustrated in Figure 7.29 (A) and (B). It can be seen from these figures that samples of the FM-A system (Fig. 7.29 A) absorbed less water in comparison to the FM-B system (Fig. 7.29 B) as a function of Gelucire 44/14 loading. Alternatively, the general trend of the moisture uptake by the physical mixtures after thermal treatment follows the Eudragit RS PO behaviour, because of its high proportion in both systems. Therefore, thermally treated samples of the physical mixes took up less water than untreated ones and approached a maximum earlier or achieved a faster humidity equilibration. Azarmi et al. (2005) and Hasanzadeh et al. (2009) found that thermal treatment of Eudragit RS PO above its glass transition temperature results in increase of the coalescence of matrices made from this polymer, rendering it less accessible to the aqueous medium. This is consistent with our findings, wherein thermal treatment of the systems composed mainly of Eudragit RS PO results in less water uptake in comparison to the equivalent untreated samples.

The extruded samples showed an increase in moisture uptake in comparison to the equivalent thermally treated physical mixes. This observation could support our previous FT-IR-ATR spectroscopic hypothesis of the migration of alkyl groups. In other words, it was speculated that the interior of the extrudate is enriched with hydrophobic alkyl groups whereas the hydrophilic side branches are more available on its surface, thereby allowing more moisture or water uptake. However, this increase was barely significant in the FM-A extruded systems but was more evident in the FM-B extruded system (higher content of Gelucire 44/14), as shown in Table 7.4. The moisture uptake of the FM-B extrudate was even higher than the equivalent untreated physical mix (control). This can be explained by the existence of free Gelucire 44/14 or solid dispersion at this composition as indicated in the previous sections, in addition to the assumption of concentrated hydrophilic regions on the surface of these samples. Table 7.4 summarizes the moisture content values obtained from method B that was represented in Figure 7.28 (A and B) and Figure 7.29 (A and B).

(A)

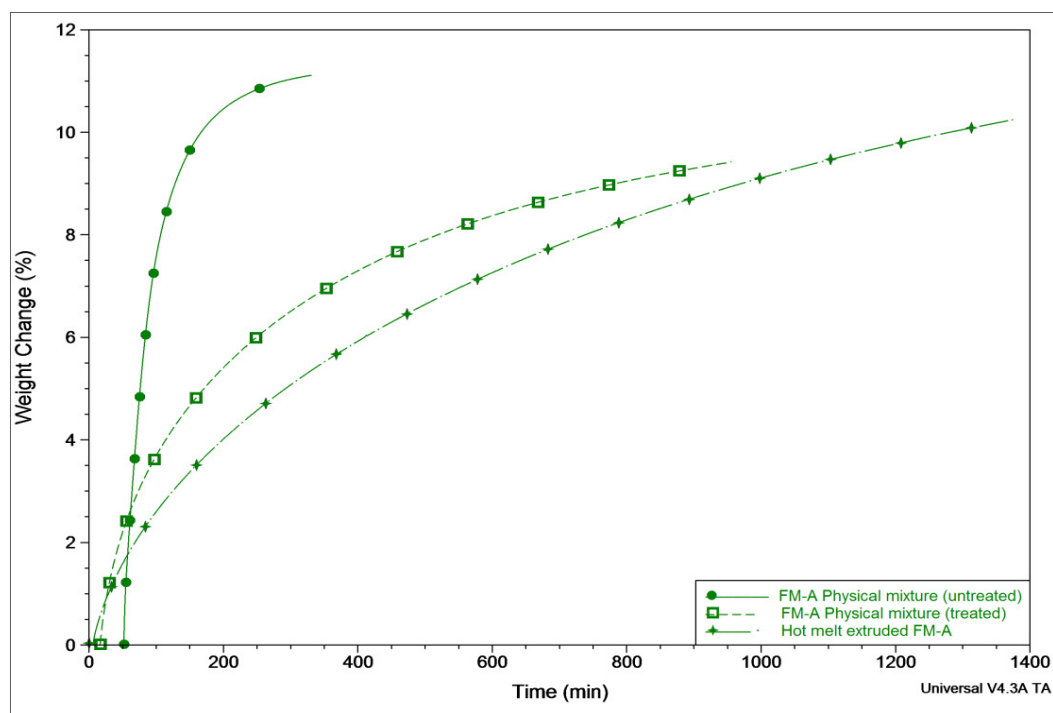


(B)

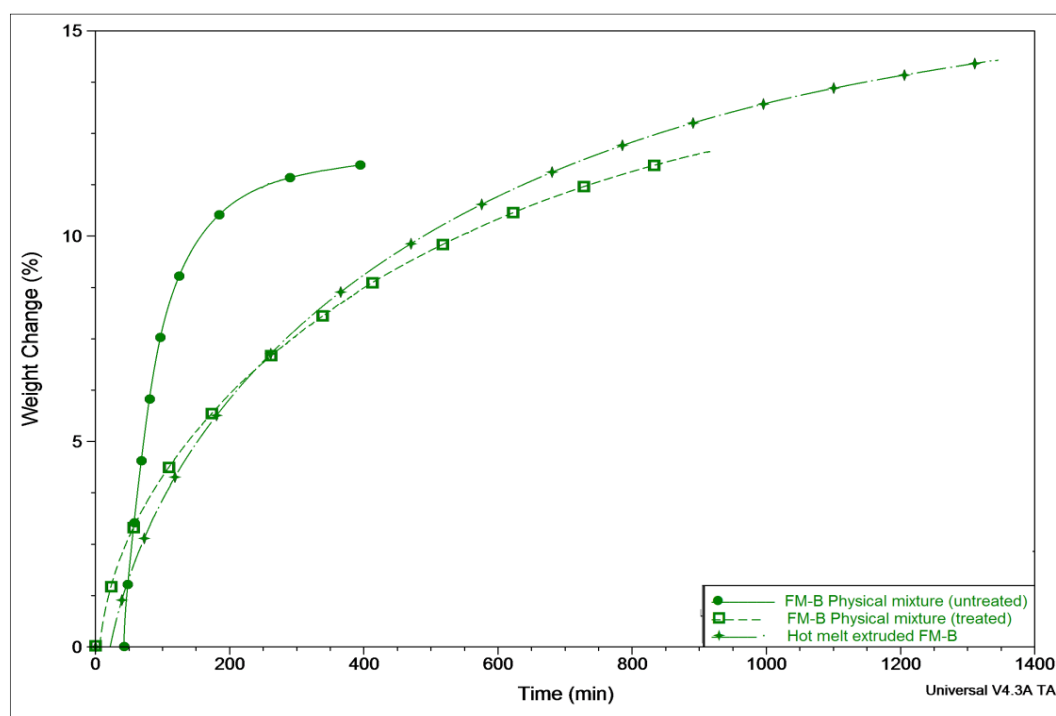


**Figure 7.28: Moisture uptake of Eudragit RS PO (A) and Gelucire 44/14 (B) expressed as percentage of weight change versus time, both tested at 95%RH/25°C. Samples were examined as the following sets: untreated (no thermal treatment), at the temperature of extrusion (120°C) followed by solidification at room temperature (treated)**

(A)



**Figure 7.29: Moisture uptake for the samples of FM-A (Gelucire 44/14 Eudragit RS PO ratio of 1:6) system (A) expressed as percentage of weight change versus time tested at 95% RH/25°C. Samples were examined as the following sets: untreated physical mixtures (filled circles), treated physical mixtures at the temperature of extrusion (120°C) followed by solidification at room temperature (open squares) and samples prepared *via* hot melt extrusion (filled stars)**



**Figure 7.29 (Contd.): Moisture uptake for the samples of FM-B system (Gelucire 44/14 Eudragit RS PO ratio of 2:5) system (B) expressed as percentage of weight change versus time tested at 95%RH/25°C. Samples were examined as the following sets: untreated physical mixtures (filled circles), treated physical mixtures at the temperature of extrusion (120°C) followed by solidification at room temperature (open squares) and samples prepared *via* hot melt extrusion (filled stars)**

Sample	Untreated	Treated	Hot melt extruded
Eudragit RS PO	4.70±0.45	2.11±0.32	-
Gelucire 44/14	46.01±0.18	47.04±0.27	-
FM-A physical mixture	11.02±0.23	9.432±0.35	10.08±0.31
FM-B physical mixture	12.06±0.37	11.97±0.31	14.11±0.36

**Table 7.4: Summary of the water content (w/w %) of different samples determined at the apparent moisture equilibrium level of 95%RH/25°C (method B) and measured by DVS (n=2, mean±SD)**

#### **7.4.2 Investigation into the influence of hydration on the properties of Eudragit RS PO/Gelucire 44/14 hot melt extruded systems**

This section aims to define the structural and microscopic appearance changes associated with the water uptake by the hot melt extruded FM-A (Gelucire 44/14 Eudragit RS PO ratio of 1:6) and FM-B (Gelucire 44/14 Eudragit RS PO ratio of 2:5) systems, using an *in vitro* model i.e. Franz cells under occlusive conditions, and dissolution bath. This is important for at least two reasons. First, to understand the changes of the matrix system without the drug. Second, to extrapolate the likely behaviour with a drug loaded system. Therefore, the basis of the process by which the drug was released can be established.

##### **7.4.2.1 Methodology**

In this section we have used the extruded films of FM-A (Gelucire 44/14 Eudragit RS PO ratio of 1:6) and FM-B (Gelucire 44/14 Eudragit RS PO ratio of 2:5) systems, described in section 7.2.1. These films were characterised for any change in their properties outlined in section 7.2, after being tested in two conditions. The first condition is testing in the dissolution bath in a similar way to the *in vitro* drug release studies described in Chapter 5. This test will be termed herein as dissolution testing or a dissolution study. The second condition is testing in the Franz-type diffusion cells. These cells were used to model *in vitro* behaviour of the tested films when applied to the skin under occlusive conditions. This modelling, utilized the same conditions detailed in Chapter 5, with the added parameter of occlusion. The latter was achieved through hydrating the films, each with a 0.07 ml volume of the used receptor medium of the PBS (pH=7.2). This value was chosen to approximate the films' behaviour under skin occlusion, in a similar assumption mentioned in Chapter 6 for the medicated films. However, in this case the experiment was conducted only for 24 hours, thus a volume of 0.07 ml rather than 0.14 ml was used to hydrate the samples.



The films were cut manually and their dimensions were measured using an electronic digital caliper (MS092Toolzone Vernier Caliper, UK). In the dissolution study, the films of system FM-A and FM-B were tested with similar dimensions and of a total weight of not less than 2500 mg. The applied samples in the dissolution test were evaluated after 24 hours. In the Franz cells, six films of size  $(24.12 \pm 1.31 \text{ mm}^3)$  were mounted for each studied system. In which the average weight of  $(24.94 \pm 1.17 \text{ mg})$  and  $(25.85 \pm 1.45 \text{ mg})$  corresponds to the used dimensions of FM-A and FM-B films, respectively. These films were removed after 0.25, 1, 2, 3, 4 and 24 hours and placed in sealed containers for further evaluation. The samples in the dissolution bath and Franz cells were weighed before and after testing at the scheduled intervals using a XS205, Dual range analytical balance (Mettler Toledo).

After removal of each sample from the test, the films were blotted gently by applying filter paper (Fischer brand, Fischer Scientific, Whatman No.1 70mm diameter) for 30 seconds. After blotting, the weight measurements were performed for the film to a constant weight. Then, the water absorption capacity measurements were calculated with respect to the initial weight of the films as follows:

$$\text{Water absorption capacity (w/w\%)} = \left[ \frac{(W(n)h - W_0)}{W_0} \right] \times 100\% \quad (\text{Eq.7.2})$$

Where  $W((n)h)$  is the weight of the films removed at  $(n)$  hour(s) and  $W_0$  is the initial weight of the films before the test. These measurements indicate the percentage increase in the weight of the film over its initial weight, after the testing time in hour(s).

Furthermore, the swelling ratio percentages were found for these films using the following equation:

$$\text{Swelling ratio (\%)} = \left[ \frac{(\text{Volume}((n)h) - \text{Volume}(t_0))}{\text{Volume}(t_0)} \right] \times 100\% \quad (\text{Eq.7.3})$$

Volume  $((n)h)$  and Volume  $(t_0)$  are the volumes of the films after  $(n)$  hour(s) and films before the test ( $t=0$  hour), respectively.

The films tested in the dissolution bath were stored under phosphorous pentoxide ( $P_2O_5$ ) at room temperature (0%RH/RT) for one week to achieve efficient drying after this test. The weight loss percentage was calculated using the following formula:

$$\text{Weight loss percentage} = \left[ \frac{(W_0 - W_d)}{W_0} \right] \times 100\% \quad (\text{Eq.7.4})$$

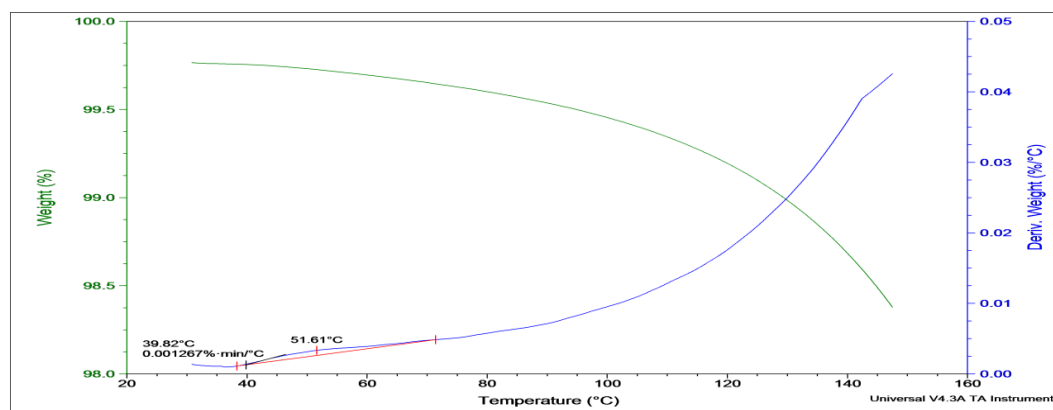
Where  $W_0$  is the initial weight of the films before immersion in the dissolution bath and  $W_d$  is the weight of the films after immersion for 24 hours and dried for one week (0%RH/RT).

The characterisation of these tested hot melt extruded films (FM-A and FM-B systems) was performed using MTDSC to assess thermal properties, SEM for morphological aspects and TGA to measure the water content as documented in Chapter 4. Other techniques include PXRD for the films studied in the dissolution bath, while further evaluation was performed for films studied in the Franz cells using ATR-FTIR and polarized light microscopy (PLM) techniques. A Leica DML S2 polarized microscope (Wetzlar GmbH, Germany) equipped with a video capture system was used to take the sample photos with a 10x (optical zoom) lens. This is the same microscope used in the HSM studies and described in Chapter 2, but without the heating accessory. The rest of the experimental techniques and the used methods were outlined in Chapter 3.

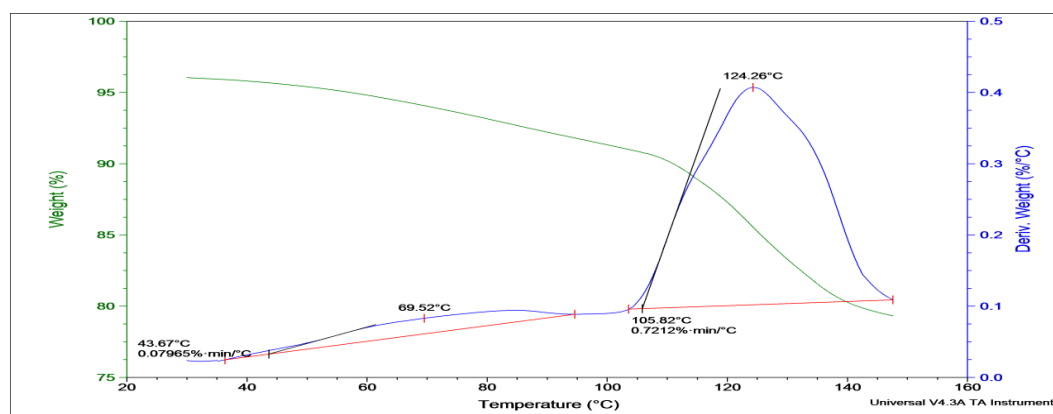
#### 7.4.2.2 Results and discussion

Thermogravimetric analysis (TGA) of the FM-A and FM-B extruded samples was used to determine the water content as water loss from the region between approximately 100°C and 120°C. This region is the common range of water loss. The hydrated samples tested using dissolution bath or inside Franz cells were associated with significant water loss in this region as indicated from the peaks of the percentage and temperature derivative weight loss in Figure 7.30 (B) and (C), respectively. This is not to be confused with the decomposition profiles obtained for Eudragit RS PO and Gelucire 44/14 using TGA in Chapter 3, wherein the onset temperatures of degradation were detected above 150°C. This weight loss was preceded with a much broader derivative weight change for all the samples and occurred with an onset at approximately  $38.7 \pm 0.8^\circ\text{C}$  for the control samples. This event could be the responsible for the observed endothermic peak in the non-reversing signal of the FM-A fresh extruded sample shown previously in section 7.2.2.1.2. Thus, it is more likely to be attributed to water desorption rather than endothermic relaxation event.

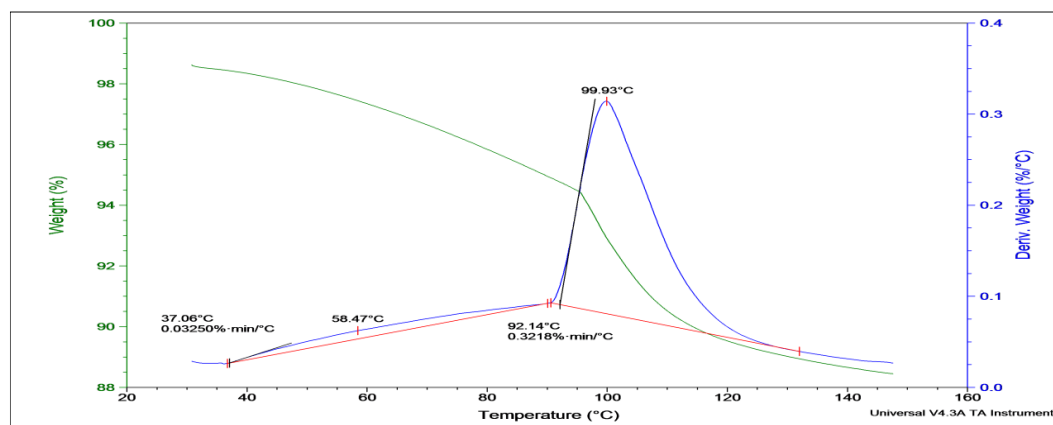
(A)



(B)



(C)



**Figure 7.30: Representative TGA weight loss profiles of (A) control extruded film while (B) for tested extruded films in dissolution bath and (C) for tested extruded films in Franz-type diffusion cells. All heated at  $10^{\circ}\text{C min}^{-1}$  to  $150^{\circ}\text{C}$**

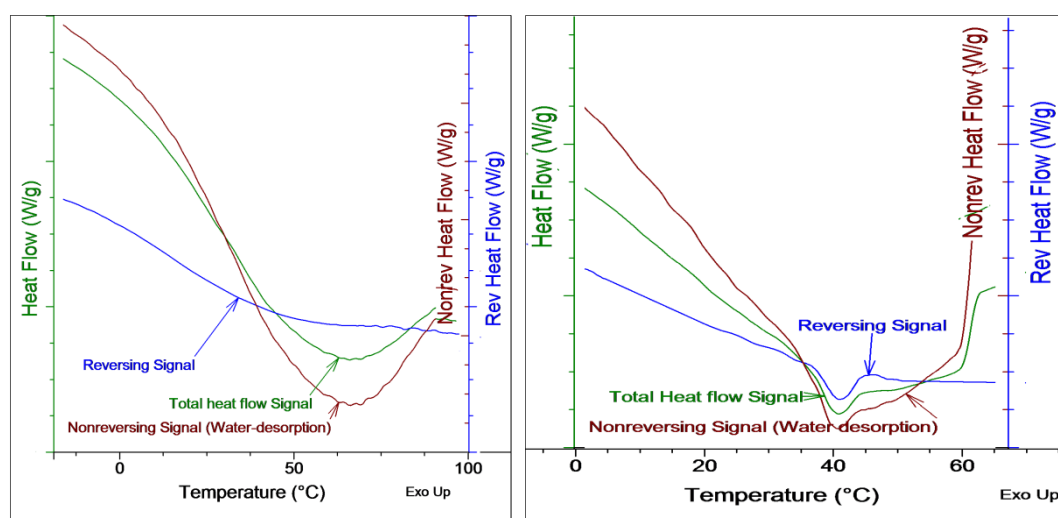
The measurements of the water absorption capacity, water content ( $W_c$ ), swelling ratio (%) and the percent weight loss of the films after dissolution testing are given in Table 7.5. These results demonstrate increased water absorption capacity and subsequent swelling as the amount of Gelucire 44/14 increased, thus higher values for FM-B (Gelucire 44/14 Eudragit RS PO ratio of 2:5) extruded films in comparison with FM-A (Gelucire 44/14 Eudragit RS PO ratio of 1:6) films. However, it is believed that swelling is a function of both components. While Gelucire 44/14 aid in the aqueous medium penetration and ease the Eudragit RS PO swelling, it may swell when in contact with aqueous media as is the case with other Gelucires (Sutananta et al., 1995), which is also one proposed mechanism for its self-emulsification ability (Chambin et al., 2004; Craig et al., 1995).

Extruded sample	Swelling ratio (%)	Water absorption capacity (w/w %)	$W_{c1}$ (w/w %)	$W_{c2}$ (w/w %)	Weight loss (w/w %)
FM-A System	45.92±0.79	54.51±0.43	16.36±0.13	0.27±0.03	3.17±0.5
FM-B System	109.45±0.52	76.16±0.80	17.26±0.08	0.27±0.02	5.47±0.2

**Table 7.5: The water uptake properties and weight loss measurements of the hot melt extruded films of FM-A (Gelucire 44/14 Eudragit RS PO ratio of 1:6) and FM-B (Gelucire 44/14 Eudragit RS PO ratio of 2:5) systems after dissolution testing in phosphate buffer solution (pH=7.2) at 37±0.1°C.  $W_c$  represents the water content measured *via* TGA immediately after the test ( $W_{c1}$ ) and after drying under 0% RH/RT for one week ( $W_{c2}$ ). Values represent mean ± S.D (n=2)**

Furthermore, the water content measurements did not show a large difference between FM-A and FM-B extruded systems. This feature could be related to removal of the residual water at the time of the testing and evaporation prior to thermal treatment, suggesting poor water holding capacity. Weight loss would be expected in these samples, mainly due to washing of the Gelucire 44/14 into the dissolution medium, because Eudragit RS PO as mentioned in Chapter 2 is not water soluble. According to the small values of the weight loss percentage, a strong association between Gelucire 44/14 and Eudragit RS PO is suggested.

These samples were tested by MTDSC as recommended in section 7.2.2.1. The changes were observed from the reversing heat flow signals and shown in Figure 7.32 without using the total heat flow signals to detect the melt observed in FM-B extruded system. This is due to overlapping with broad dehydration peaks as seen in Figure 7.31. Though these samples were blotted onto filter papers to dry them prior to the MTDSC experiment, these samples retained water. Therefore, the reversing heat flow signals were used, detecting the glass transition temperatures mainly and only to show the relative trend of changes in the melting peaks due to the limitations mentioned in Chapter 2.

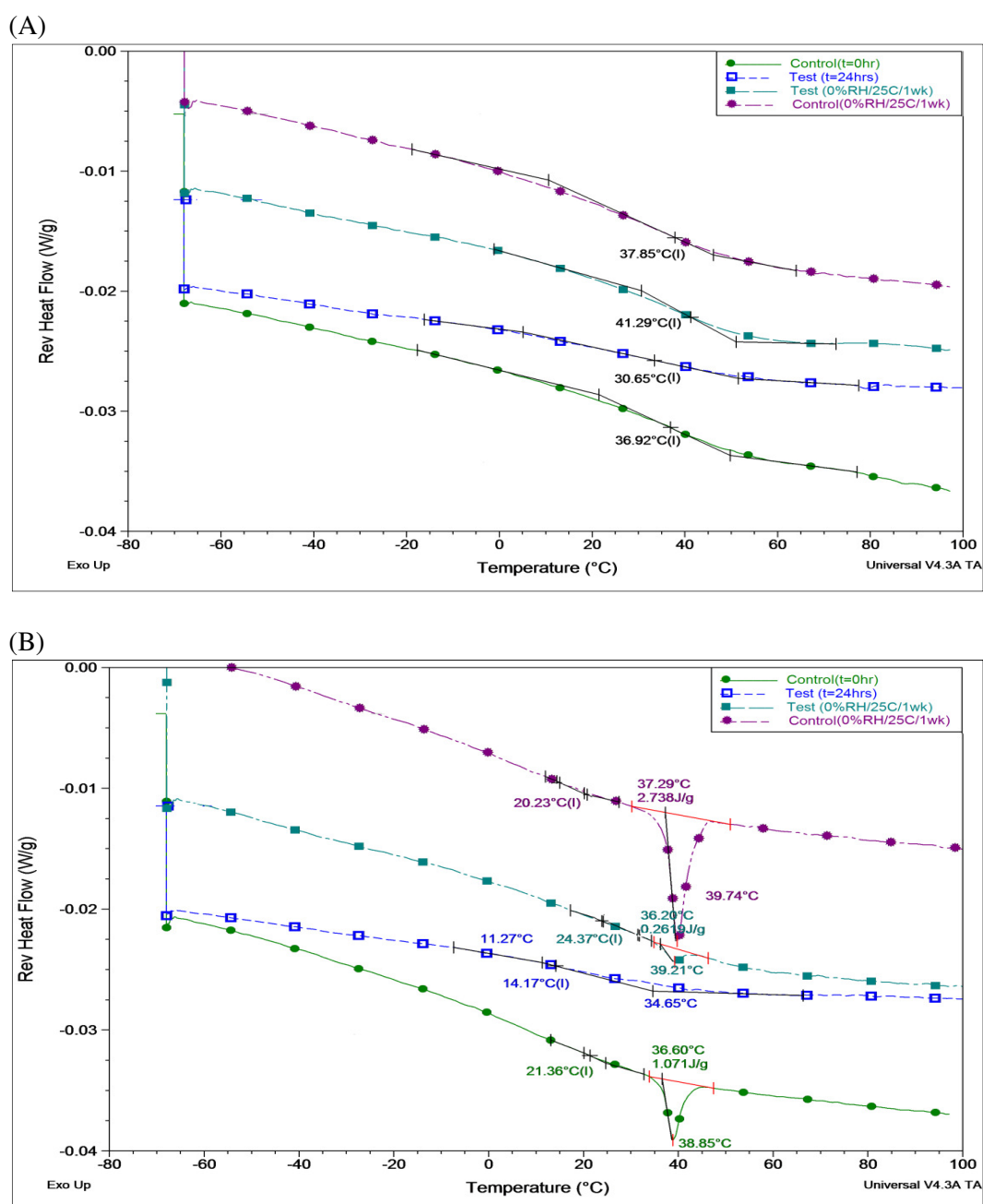


**Figure 7.31: Representative MTDSC profiles of tested FM-A (left) and FM-B (right) films in the dissolution experiment showing the dehydration (water-desorption) event in the non reversing and total heat flow signals. Underlying scan rate of  $1^{\circ}\text{C min}^{-1}$  with a modulation amplitude of  $\pm 0.265^{\circ}\text{C}$  and a period of 100 seconds**

Samples of the FM-A extruded system (solid solution, Gelucire 44/14 Eudragit RS PO ratio of 1:6) showed a decrease in the glass transition temperature after testing in the dissolution bath with a Mid-point  $T_g$  of  $32.4 \pm 1.8^{\circ}\text{C}$  ( $n=3$ ) as illustrated in Figure 7.32 A. This corresponds to an almost 13% reduction from the  $T_g$  of the control samples ( $37.1 \pm 0.5^{\circ}\text{C}$ ). Water can act as a plasticizing agent, resulting in a depression of the glass transition temperature and a more flexible film. After drying of these tested samples for one week, the glass transition temperature showed an approximately 9% increase in comparison to the fresh control samples with a Mid-point  $T_g$  of  $40.8 \pm 1.8$  ( $n=3$ ). However, in order to account for ageing effect, these samples were further compared to the untested samples (control) that were stored using the same conditions for one week. The Mid-point  $T_g$  of the aged control samples was  $39.0 \pm 1.2$  ( $n=3$ ). Therefore, the glass transition temperature of the efficiently

dried tested samples is not significantly higher than the  $T_g$  of the aged control samples. In summary, the glass transition temperature of the FM-A extruded films was depressed after the dissolution test as a result of being hydrated. The absence of water after drying resulted in an unplasticized glass transition.

The effect of immersion in the dissolution bath on the FM-B extruded system (solid dispersion, Gelucire 44/14 Eudragit RS PO ratio of 2:5) using MTDSC experiment (Fig. 7.32 B) was also addressed (Table 7.6). To begin with, the melting endotherm disappeared after the test. This infers removal of the excess Gelucire 44/14 into the dissolution medium, resulting in weight loss after the test. Additionally, the glass transition temperature depressed by approximately 33% from the original value detected for the control samples, giving softer films and demonstrates again, the profound effect of water as a plasticizing agent. After the storage of these samples under dry conditions for one week, the melting endotherm reappeared besides unplasticized  $T_g$ . However, the melt  $\Delta H$  of this peak is markedly less than the corresponding control as shown in Figure 7.32. This is more likely to be associated with formation of new crystals, rather than any remaining portion of the original crystals in the fresh sample. For the original crystals, they were mainly detected on the surface of these extrudates as revealed by SEM images previously. Therefore, it would be the first candidate to leave the films upon contact with the dissolution medium and if any melt will be detected later, is expected to result from new crystal formation that would increase as a function of storage time. This ageing effect was confirmed from the sharper fusion peak with higher melt  $\Delta H$  observed for the control films stored for one week in comparison to the fresh control films (Figure 7.32 B).



**Figure 7.32:** MTDSC reversing heat flow signals of fresh hot melt extruded (A) FM-A (Gelucire 44/14 Eudragit RS PO ratio of 1:6) and (B) FM-B (Gelucire 44/14 Eudragit RS PO ratio of 2:5) films examined after testing in the dissolution bath for 24 hours ( $t=24$  hrs), followed by drying at 0% relative humidity/25°C for one week (0%RH/25°C/1wk) and compared to the controls of: fresh films ( $t=0$  hr) and after ageing for one week at the same storage conditions (0%RH/25°C/1wk). Underlying scan rate of  $1^{\circ}\text{C min}^{-1}$  with a modulation amplitude of  $\pm 0.265^{\circ}\text{C}$  and a period of 100 seconds

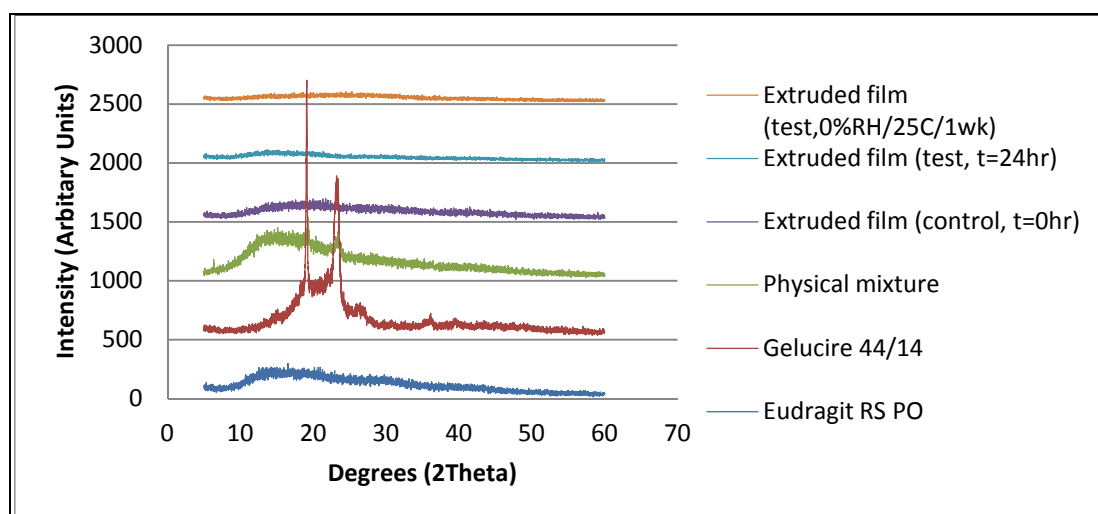
Sample	T <sub>g</sub> (Mid-point, °C)	T <sub>m(onset)</sub> (°C)
Control (t=0 hr)	20.8±1.0	37.0±1.2
Test (t=24 hrs)	13.9±0.3	-
Control (0%RH/25°C/1wk)	20.8±0.8	36.7±1.0
Test (0%RH/25°C/1wk)	23.5±0.9	36.0±0.4

**Table 7.6: Summary of the MTDSC results derived from the reversing heat flow signals of the hot melt extruded FM-B films examined as shown in Figure 7.32 (B). Values represent mean ± S.D (n=2)**

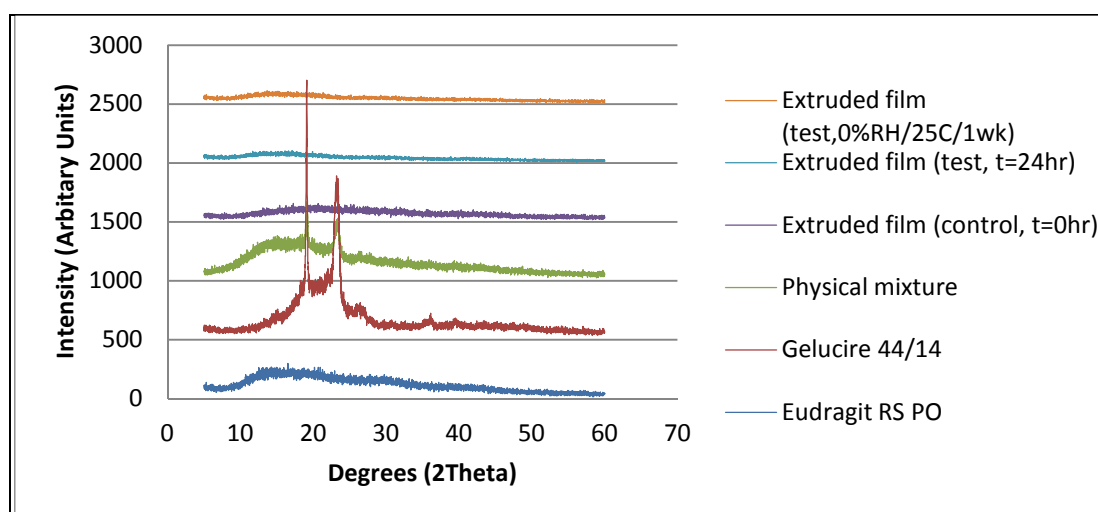
Figure 7.33 (A) and (B) illustrate PXRD profiles of the FM-A (lower content of Gelucire 44/14) and FM-B (higher content of Gelucire 44/14) extruded systems, respectively, after immersion in the dissolution bath and after drying of these tested samples. These profiles showed that samples of these films were completely amorphous after testing using the dissolution bath and after storage under dry conditions for one week. However, these data conflict with the conclusions drawn from the MTDSC results for the FM-B hot melt extruded system. A dried sample of FM-B extruded system showed a melting endotherm, indicating crystalline Gelucire 44/14. However, the small amount of the crystalline Gelucire 44/14 might fall below the detection limit of the PXRD technique.



(A)

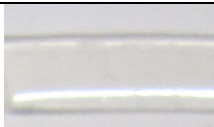

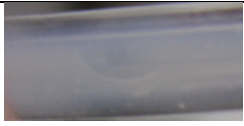
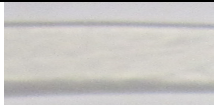
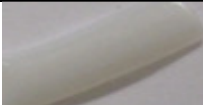



(B)

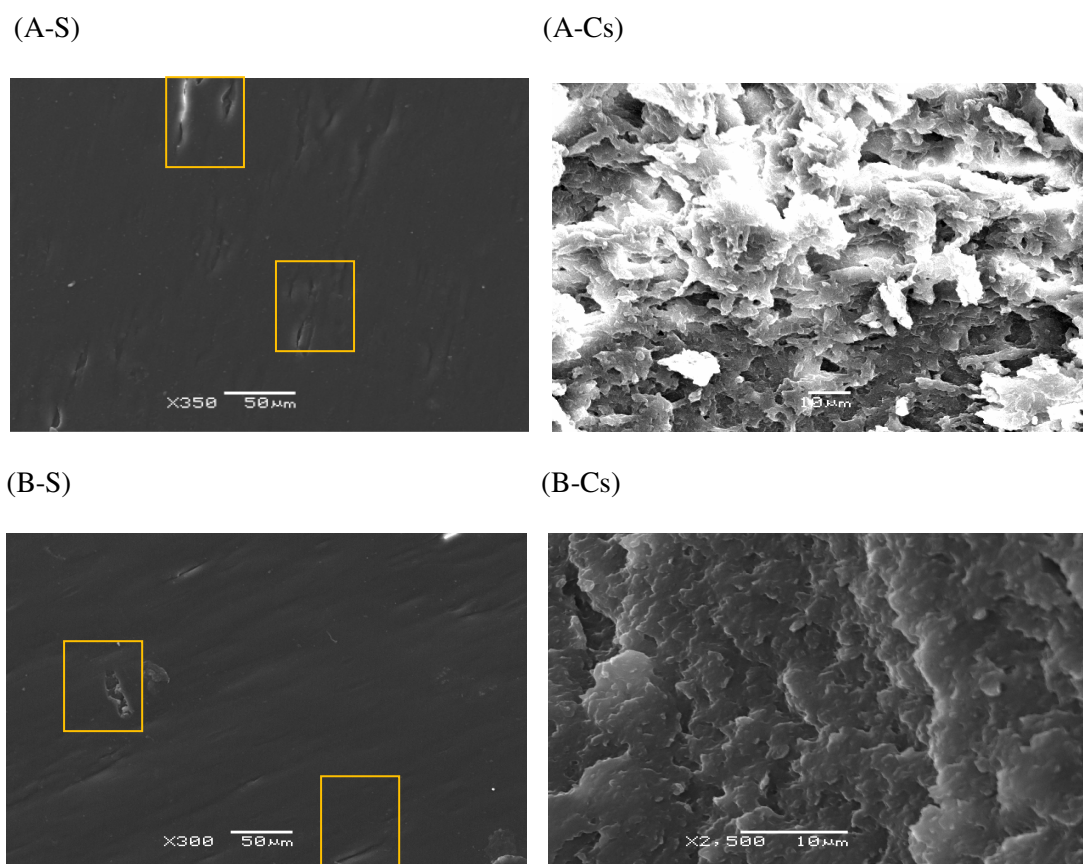


**Figure 7.33: X-ray powder diffraction profiles of the raw materials, physical mixtures and their corresponding hot melt extruded films of Gelucire 44/14 Eudragit RS PO 1:6 ratio (FM-A composition, A) and 2:5 ratio (FM-B composition, B). The films were examined after testing in the dissolution bath for 24 hours (t=24 hrs), followed by storage under dry conditions for one week at 0% relative humidity, 25°C to allow drying (0%RH/25°C/1wk) and compared to the controls of fresh extruded films (t=0 hr)**

To show the real morphology changes of these tested extrudates, SEM was used in association with the photographs taken for these samples, before and after the dissolution testing, to aid in detection of the corresponding discoloration of these films. As shown in a Table 7.7 the transparent appearance of the FM-A and FM-B extruded films changed into white dispersion after the dissolution, indicating Gelucire 44/14 hydration (Svensson et al., 2004). After drying for one week, the samples separated into white and transparent phases. The white zone could be related to the crystals of the Gelucire 44/14, because it is a white semi-solid waxy material as mentioned in Chapter 2. However, MTDSC and PXRD results did not support this suggestion for the FM-A system. Therefore, SEM can provide compelling evidence as to whether this white zone is actually crystalline Gelucire 44/14 or not. If not, it could be solubilised Gelucire 44/14. SEM images of the tested FM-A (Gelucire 44/14 Eudragit RS PO ratio of 1:6) and FM-B (Gelucire 44/14 Eudragit RS PO ratio of 2:5) extruded films from the dissolution bath are shown in Figures 7.34 and 7.35, respectively. These extrudates were characterised previously using SEM in section 7.2.2.2 and represent the control or untested films.

Gelucire 44/14: Eudragit RS PO ratio	Formula code	Control (t=0 hr)	Test (t=24 hrs)	Test (0%RH/25°C/1wk)
1:6	FM-A			
2:5	FM-B			

**Table 7.7: Photographs illustrating the colour changes of the hot melt extruded films of the FM-A and FM-B systems pre and post the dissolution experiment**



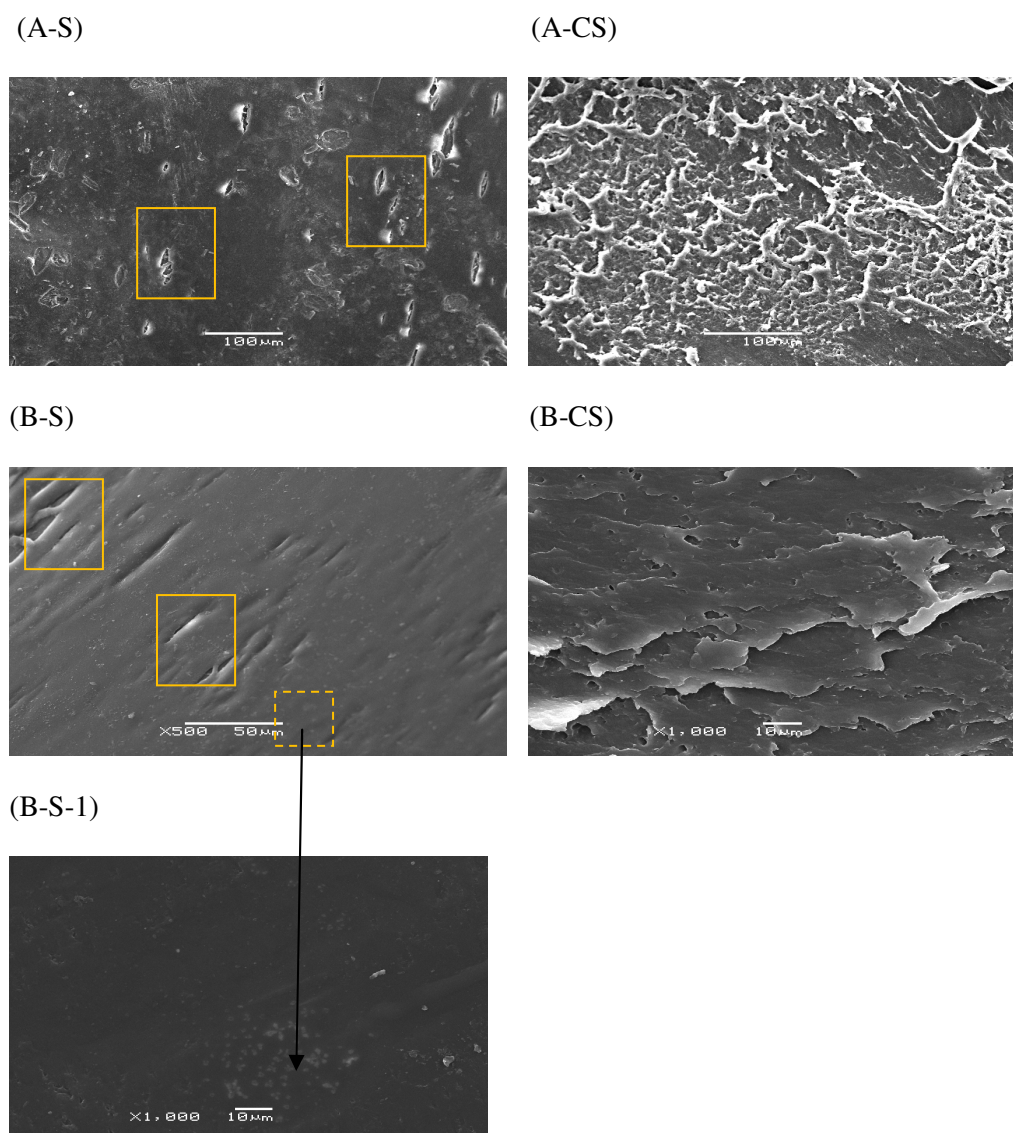
**Figure 7.34: SEM images of the surfaces (S) and cross sections (Cs) of FM-A extruded films after the dissolution testing ( $t=24$  hrs) represented by A series, followed by drying at 0% RH/25°C for one week and shown in B series. Examples on the micro-cracks are enclosed by orange rectangles. See text for composition**

After dissolution, the surfaces of the FM-A films developed micro-cracks, whereas the cross sections deformed with a fluffy appearance as illustrated in Figure 7.34. These changes remained after drying with disappearance of the white colour in the cross section. No visible crystals were detected on the surfaces or cross sections of these samples. This could infer that the white colour observed earlier (Table 7.6) is more likely related to the solubilised Gelucire 44/14. The surface imperfections or formation of these cracks on the surfaces of these samples could be rationalized with the removal of some Gelucire 44/14 into the dissolution bath during the test. Water was proven to be absorbed by these extruded samples (water absorption capacity measurements). As a result, the glass transition temperature was decreased (MTDSC experiment), offering a greater system mobility i.e. softening. Collectively this would impact the diffusion of the amphiphilic Gelucire 44/14 into the dissolution medium, which is believed to be washed out, thus a weight loss and increase of the glass transition temperature were observed after the test. The increase of the glass

transition could also contribute to possible matrix contraction that has been reported to initiate similar cracks (Khan and Craig, 2004).

Comparing the SEM images of the FM-B extruded films in Figure 7.35 with the control samples clearly demonstrates the effect of the dissolution experiment. The surface was associated with a rough appearance and micro-cracks and the cross section was characterised with layered white scales. In comparison to the FM-A system, these cracks occurred with greater propensity and the cross section of the FM-B system was more congealed. The first would be expected for a relatively higher amount of the Gelucire 44/14 leaving the structure, while the second can be related to a more plasticized system that would result in a smoother more uniform appearance of the swelled films. Following storage for one week under 0%RH/25°C to allow drying, the surface of these films showed small distribution of granules, while the cross section was still free from crystals similar to the control samples. This would indicate recrystallization after the removal of the water. In conjunction with the MTDSC findings, this observation could be explained with the following scenario:

- The glass transition temperature of the extruded system was less than the temperature of the dissolution test (37°C) by approximately 44%, which could be reflected on the enhanced Gelucire 44/14 mobility during the dissolution.
- The Gelucire 44/14 is believed to migrate towards the surface of the films to flow into the aqueous dissolution medium, owing to its amphiphilic properties.
- Immediately after the test, the water in the sample was enough to solubilise or dilute nuclei of the Gelucire 44/14 and the system was characterised by a single glass transition temperature of  $13.9 \pm 0.3^\circ\text{C}$ .
- After the water removal, the Gelucire 44/14 was able to rearrange into fine crystallites distributed sparsely on the surface and detected by MTDSC.



**Figure 7.35: SEM images of the surfaces (S) and cross sections (Cs) of FM-B extruded films after the dissolution testing ( $t=24$  hrs) represented by A series, followed by drying at 0%RH/25°C for one week and shown in B series. (B-S-1) is an insert showing magnification of granules (dashed orange square) detected on the surface of FM-B extruded films after drying. Examples on the micro-cracks are enclosed by orange rectangles. See text for composition**

To communicate the changes that can affect FM-A (low level of Gelucire 44/14) and FM-B (high level of Gelucire 44/14) extruded systems after the application to the skin, Franz-type diffusion cells (*in vitro* model) were used. The films were hydrated to mimic occlusive conditions. These changes were characterised in a similar manner to the dissolution studies and the techniques of TGA, MTDSC and SEM were used, in addition to polarized light microscopy and ATR-FTIR.

In Table 7.8 and 7.9, the water content, absorption capacity and swelling ratio values increased with testing time and as the level of Gelucire 44/14 was increased. This effect was addressed similarly in dissolution testing, but we can observe here that after four hours the values approached near a maximum, for both FM-A and FM-B extruded systems. This would indicate that incubation for a longer time under these conditions is less likely to enhance their ability to uptake the water from the surrounding environment.

Time (Hours)	Water content (w/w %)	Water absorption capacity (w/w %)	Swelling ratio (%)
0 (Control)	0.25		
0.25	1.32	3.60	10.60
1	1.77	10.20	21.20
2	2.20	23.30	33.00
3	2.43	27.00	34.30
4	4.64	34.70	35.70
24	4.99	43.10	39.90

**Table 7.8: Water uptake properties of the hot melt extruded films of FM-A system as analysed at each sampling time in Franz-type diffusion cells**

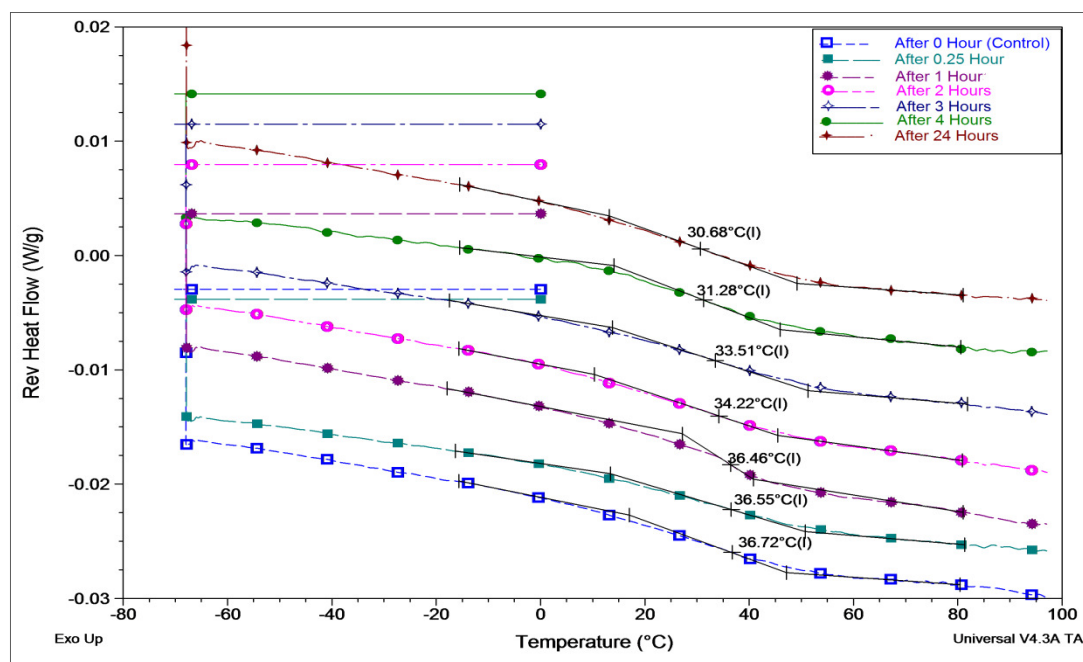
Time (Hours)	Water content (w/w %)	Water absorption capacity (w/w %)	Swelling ratio (%)
0 (Control)	0.28		
0.25	1.45	13.40	20.10
1	2.60	34.90	43.20
2	4.31	46.80	51.80
3	5.33	51.80	55.20
4	5.80	58.70	63.40
24	6.42	63.10	66.60

**Table 7.9: Water uptake properties of the hot melt extruded films of FM-B system as analysed at each sampling time in Franz-type diffusion cells**

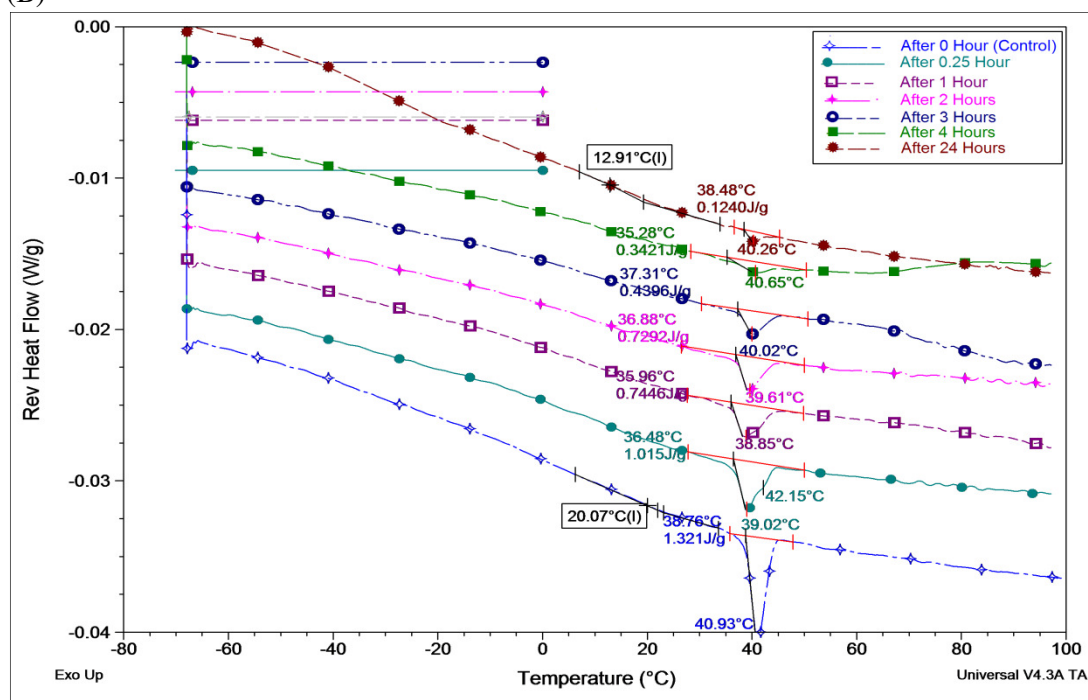


The reversing heat flow signals of the MTDSC experiment were used for the detection of both glass transition temperatures and melting endotherms to separate out other overlapping events such as observed dehydration peaks. For FM-A extruded system (Gelucire 44/14 Eudragit RS PO ratio of 1:6), the glass transition temperature as seen in Figure 7.36 (A) has been decreased as a function of water involvement which acted as a plasticizing agent. However, the water played a dual role in the studied FM-B extruded system (Gelucire 44/14 Eudragit RS PO ratio of 2:5) as illustrated in Figure 7.36 (B). On one hand it lowered the glass transition temperature (plasticization effect) and on the other hand it aided in solubilisation of Gelucire 44/14 crystals, thus the melting peaks were decreased over time as a function of water content. Interestingly, both FM-A and FM-B systems showed a glass transition value at the end of the diffusion test similar to the one reported after the dissolution experiment, despite the higher water content measured in the latter. This similarity would indicate that the extent of the glass transition temperature depression induced by water is limited.

(A)



(B)

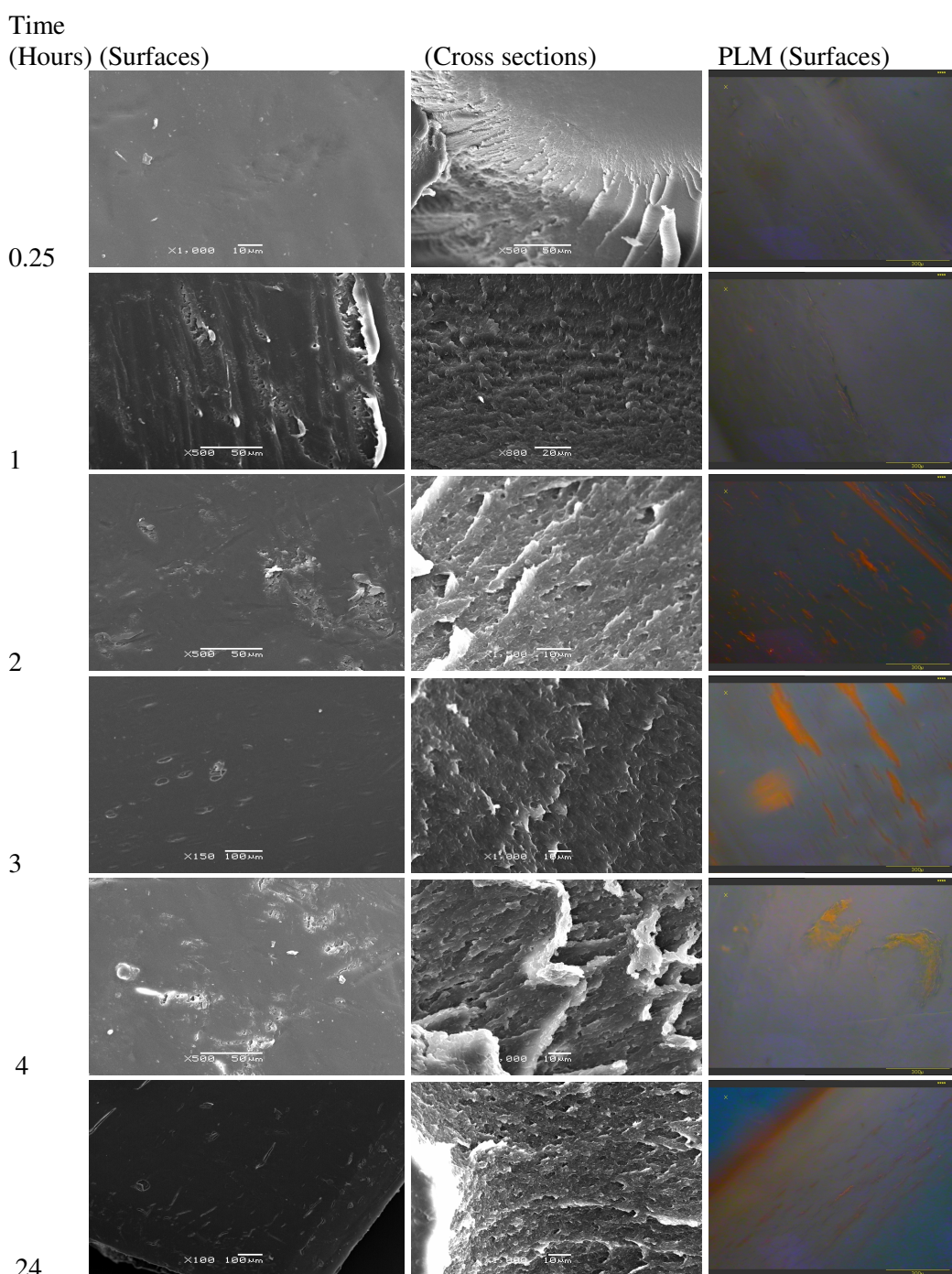


**Figure 7.36: MTDSC reversing heat flow signals of hot melt extruded FM-A (A) and FM-B (B) films after testing in the Franz-type diffusion cells at different times and compared to their respective controls (t=0 hour). Underlying scan rate of  $1^{\circ}\text{C min}^{-1}$  with a modulation amplitude of  $\pm 0.265^{\circ}\text{C}$  and a period of 100 seconds. See text for composition**



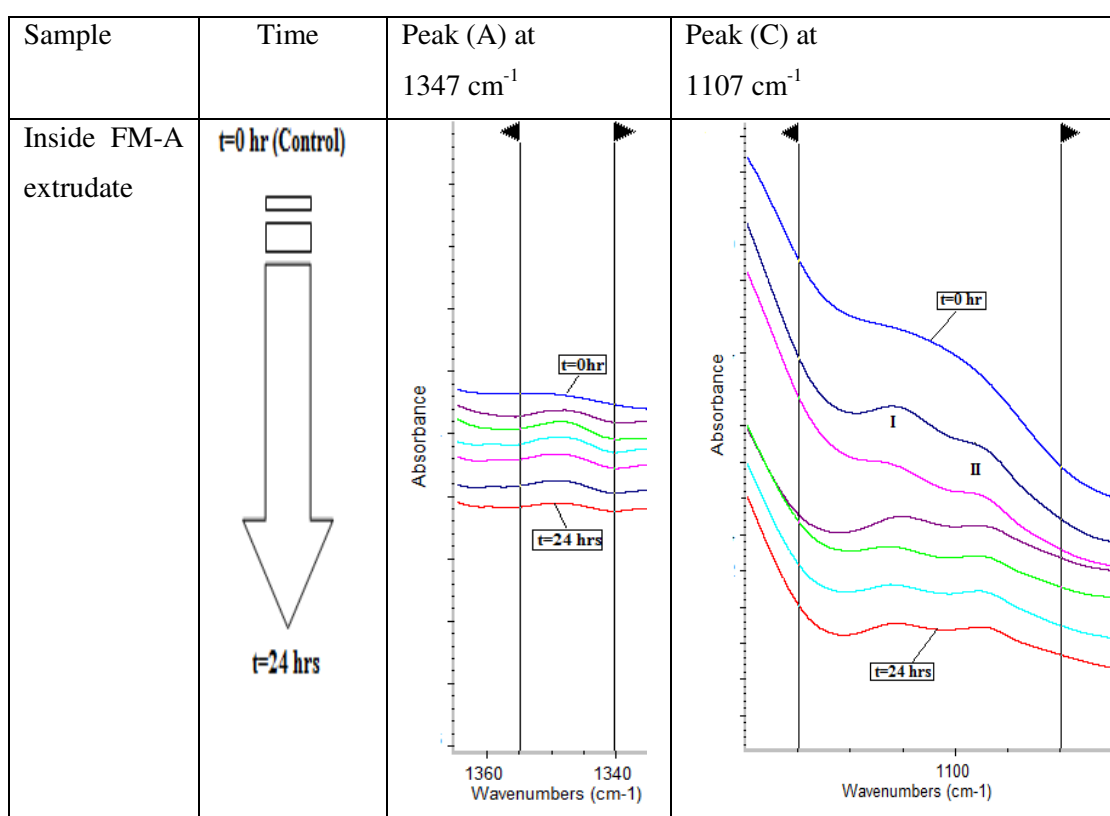
The next step in the characterisation is to identify the surface morphology of the samples and detect any change in their structures through examination of surfaces and cross sections of these extrudates. While these structures and surface artefacts can be observed efficiently using the SEM, due to the built in features of high resolution, magnification and greater depth of the applied field, the standard light microscope was used in its polarized mode (PLM) as a conjunction technique to confirm suspected crystals on the surfaces of the tested extrudates. Figure 7.37 shows the SEM photos of the FM-A extruded films tested at different times. Imperfections or micro-cracks were formed on the surfaces similar to the dissolution testing results. However, the swelling of the cross sections was less distinguishable compared to the samples tested in the dissolution bath. This is expected because of less aqueous medium available herein to cause swelling of these matrices. Polarized light images enhanced the contrast at the edges of the observed fissures (cracks) and revealed an orange colored material without birefringence. Therefore, formation of crystalline Gelucire 44/14 is precluded and this is also supported by previous MTDSC measurements.

In a previous study by Khan and Craig (2003) a similar material was observed for Gelucire 50/13 and was described as an ‘oil streak’. Gelucire 50/13 and Gelucire 44/14 have shared features such as they are both derived partially from hydrogenated palm kernel oil (Gattefosse s.a, St Priest, France). Therefore, it is highly expected that this material is an oily part of the Gelucire 44/14 transferred to the surface due to the enhanced mobility of the components after plasticization by water and solubilisation in the buffer solution.



**Figure 7.37: SEM images of the surfaces and cross sections of FM-A extruded films at different testing times using Franz-type diffusion cells. PLM images represent pattern of the tested surfaces with polarized light microscopy**

Previous investigations in section 7.3 have demonstrated that the ATR-FTIR technique can be used to differentiate crystalline Gelucire 44/14 in the extruded samples at two characteristic absorbance peaks ( $1347$  and  $1107\text{ cm}^{-1}$ ). Consequently, it has been used to further confirm the physical nature of this material observed in the PLM photos. In Table 7.10, we can see that over time the changes were mainly at the region of the peak denoted as (C) around  $1107\text{ cm}^{-1}$ . This peak was a little more distinct than a shoulder over time, but with definite broadening and a new adjacent broad peak was observed and designated as peak (II). This would suggest that it is less likely to have crystalline material yet the appearance of this new peak around  $1096\text{ cm}^{-1}$  could support the hypothesis that the observed orange material under PLM is an oil leakage into the surface, because palm oil (from which Gelucire 44/14 is derived) absorbs at this wavelength (Ajiwe et al., 2003) related to C-H deformation of alkyl groups.

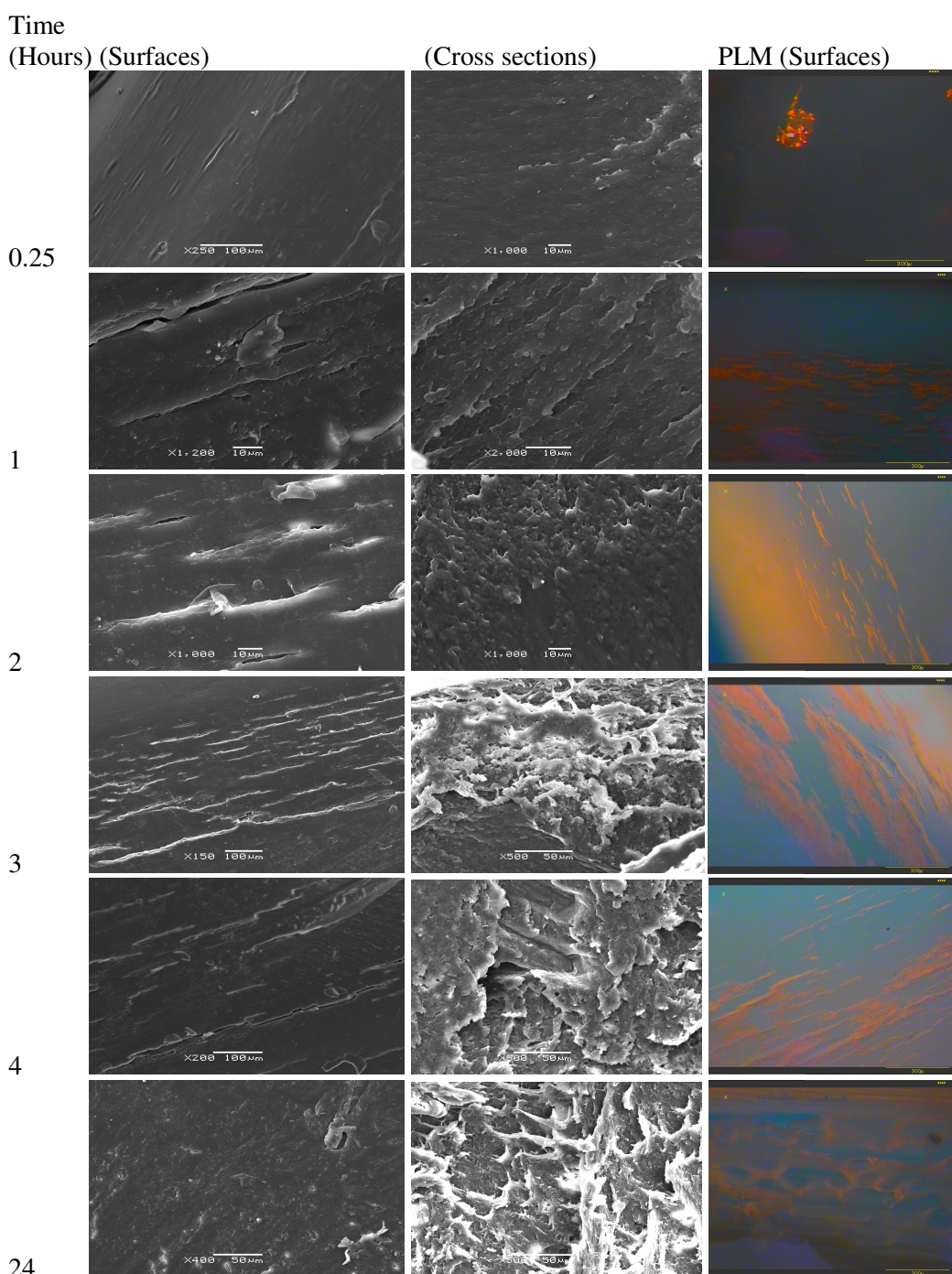


**Table 7.10: Summary of the assignments of the proposed crystalline peaks of Gelucire 44/14 from Eudragit RS PO-subtracted extruded films ATR-FTIR spectra of FM-A (Gelucire 44/14 Eudragit RS PO ratio of 1:6) system tested at different times using Franz-type diffusion cells**

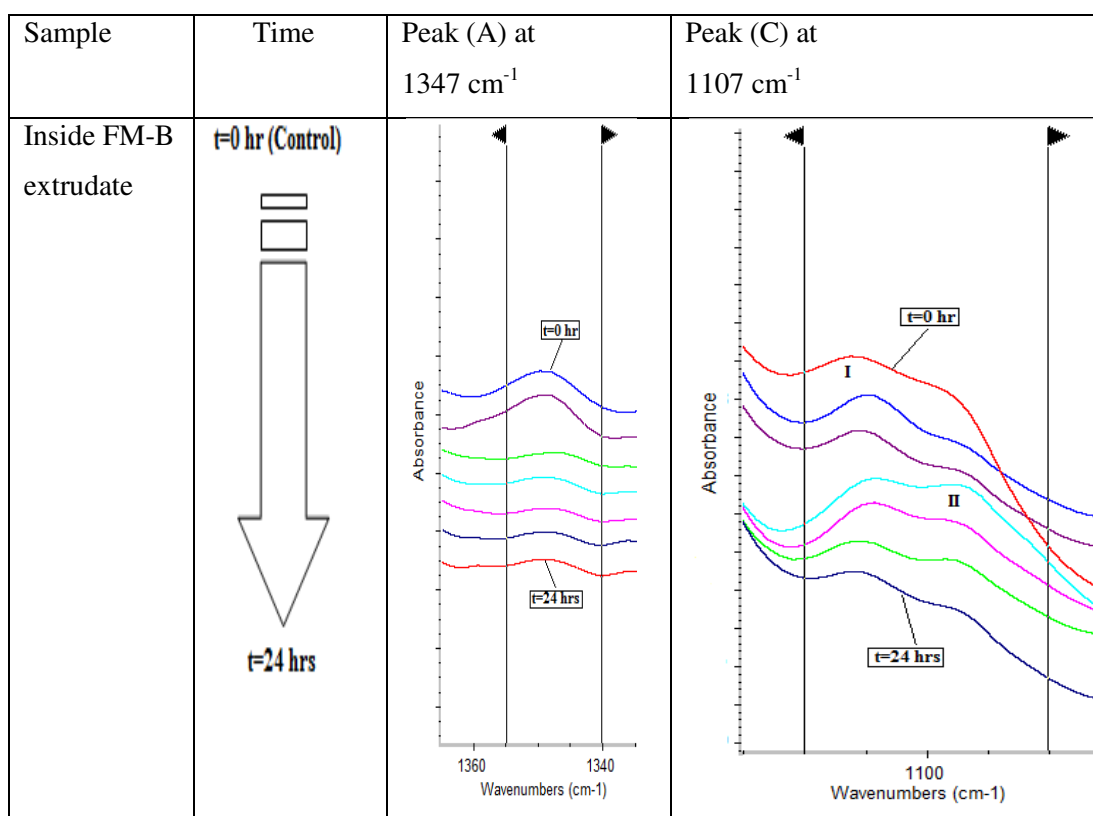
In Figure 7.38, the richness of this ‘orange’ material was more observed as would be envisaged from higher amount of Gelucire 44/14 in the FM-B extruded films. This is also associated with more extended micro-cracks as observed from the SEM images. After 15 minutes of testing, PLM could still detect small sparkling aggregates of the crystals on the surface of these samples, which soon disappeared from the film removed after one hour of testing and onwards. This implies that the solubilisation of Gelucire 44/14 crystals was occurring as previously demonstrated using MTDSC experiment. The cross sections showed notable swelling, due to increased access of the aqueous medium over time as indicated in Table 7.9.

In similar manner to the FM-A system, the extruded films of FM-B systems were monitored using ATR-FTIR as presented in Table 7.11. Crystalline Gelucire 44/14 was observed in peak (A) around  $1347\text{ cm}^{-1}$ , but disappeared after the first hour of testing. This is consistent with the PLM findings, where sparkling crystal aggregates were not visible after one hour of the test. It was noted; however, that peak (C) around  $1107\text{ cm}^{-1}$  seems to start to sharpen during the first two hours of the testing, but in fact it was separating from another peak marked as (II) and detected at  $1096\text{ cm}^{-1}$ . Giving rise to this peak, which is possibly ascribed to the palm oil, indicates that the process of solubilisation is taking place in a gradual manner. Therefore, part of the crystalline Gelucire 44/14 responsible on peak A dissolved completely, followed by other components responsible for peak (C) accompanied with the evolution of peak (II). This behaviour could be reasonably expected from Gelucire 44/14 owing to its many components, which can hydrate and dissolve depending on the temperature and amount of water available as addressed by Svensson et al. (2004).





**Figure 7.38: SEM images of the surfaces and cross sections of FM-B extruded films at different testing times using Franz-type diffusion cells. PLM images represent pattern of the tested surfaces with polarized light microscopy**



**Table 7.11: Summary of the assignments of the proposed crystalline peaks of Gelucire 44/14 from Eudragit RS PO-subtracted extruded films ATR-FTIR spectra of FM-B (Gelucire 44/14 Eudragit RS PO ratio of 2:5) system tested at different times using Franz-type diffusion cells**

In summary, the changes associated with these unloaded extruded films of Gelucire 44/14 in Eudragit RS PO examined in a dissolution bath or under occlusive conditions in Franz-type diffusion cells are mainly surface imperfections, possible leakage of the Gelucire 44/14 into these surfaces and softening of the films accompanied with appreciable swelling of the matrices. While the mechanisms of the enhanced drug release from these matrices were defined kinetically in Chapter 6, this set of observations is also important to the fundamental understanding of the underpinning mechanism(s) of the drug release process from these matrices. Two scenarios are possible as indicated in a review by Craig (2002) to describe such mechanisms. The principle of the first one could be interrelated with the possible Gelucire 44/14 transfer into the surface and enrichment of the dissolving layer. The drug particles will be dissolved into this layer first and then introduced to the receptor medium as molecular dispersion and thus referred to as ‘carrier-controlled dissolution’.

The second scenario is dependent on the drug properties such as the degree of crystallinity, size, etc. The release in this case is 'drug-controlled'. The drug is assumed to transfer as intact particles into the receptor medium and in our case this can be facilitated by the cracks created on the surface of the extrudates upon hydration. It is also useful to know that if the first scenario will dominate, the physical form of the drug will have no effects on the release rate (in the most cases) as argued by Lloyd et al. (1999). It is then proposed that a further inspection on the ageing influence on the drug solid state structure and subsequent release properties might provide valuable information about the mechanism of the drug release in these systems as will be introduced in the following section.

## **7.5 The behaviour of aged Eudragit RS PO/Gelucire 44/14 hot melt extruded films with and without ibuprofen**

This section explores the changes in the unloaded and ibuprofen-loaded Eudragit RS PO-Gelucire 44/14 carrier systems on storage. The aged films with the drug will be further evaluated for their permeation properties.

### **7.5.1 Methodology**

Hot melt extruded films of FM-A (Gelucire 44/14 Eudragit RS PO ratio of 1:6) and FM-B (Gelucire 44/14 Eudragit RS PO ratio of 2:5) systems, as described in section 7.2.1, were characterised after ageing under three conditions for one month. The first two conditions were performed at room temperature (25°C) with varied relative humidity of 0%RH under phosphorous pentoxide ( $P_2O_5$ ), creating dry conditions and supersaturated solution of sodium chloride (NaCl) in distilled water to control humidity to a level of 75%RH, for high humidity. The third condition utilized the same salt to create 75%RH at 40°C as recommended in the literature (O'Brien, 1948); this last condition was used to assess the combined effect of relatively high temperature with high humidity. Airtight jars were used as storage chambers, whereby the temperature was controlled in a vacuum oven and the humidity level was checked using both hygrometer and humidity strips.

Characterisation involved MTDSC, PXRD, SEM, and ATR-FTIR as explained in Chapter 3. In addition, TGA was used for water content determination as documented in Chapter 4. DVS was used to detect the hydration behaviour of the samples that have been stored for one month at dry conditions as a function of temperature variation over the range from 22 to 48°C in 5°C steps, in which the samples were held for one hour at each temperature. The samples were equilibrated before the experiment for one hour at 0%RH/22°C.

The loaded films of ibuprofen were prepared as described in Chapter 6, these hot melt extruded FM9 and FM10 films were stored at the same aforementioned conditions for one month with subsequent characterisation using the same methods of MTDSC, PXRD, and water content determination using TGA. Ibuprofen: Gelucire 44/14: Eudragit RS PO ratios of 3:1:6 and 3:2:5 were used in FM9 and FM10 systems, respectively.

HSM studies were performed to visualise thermal events associated with the aged films and involved a video capture microscope while exposing the samples to a controlled temperature program heating from 25°C to 100°C at 1°C min<sup>-1</sup>. Photos of the blends were taken to show the events and were correlated with the ones obtained *via* MTDSC measurements which used the same underlying rate of heating of 1°C min<sup>-1</sup>. The permeation studies were also carried out for the aged films following the same procedure in Chapter 5 under hydration conditions. Each film was hydrated using a 0.3 ml of the used receptor medium (PBS, pH=7.2) applied to these samples in the donor chambers of Franz-type diffusion cells. It is noteworthy that ratios of Gelucire 44/14:Eudragit RS PO of (1:6) and (2:5) in FM-A and FM-B systems, respectively are equivalent to the used ratios in the loaded films of FM9 and FM10 systems, respectively, wherein the drug 'ibuprofen' loading is 30%(w/w). All the reported values were measured as mean±S.D. (n=3) unless otherwise mentioned in the relevant section.



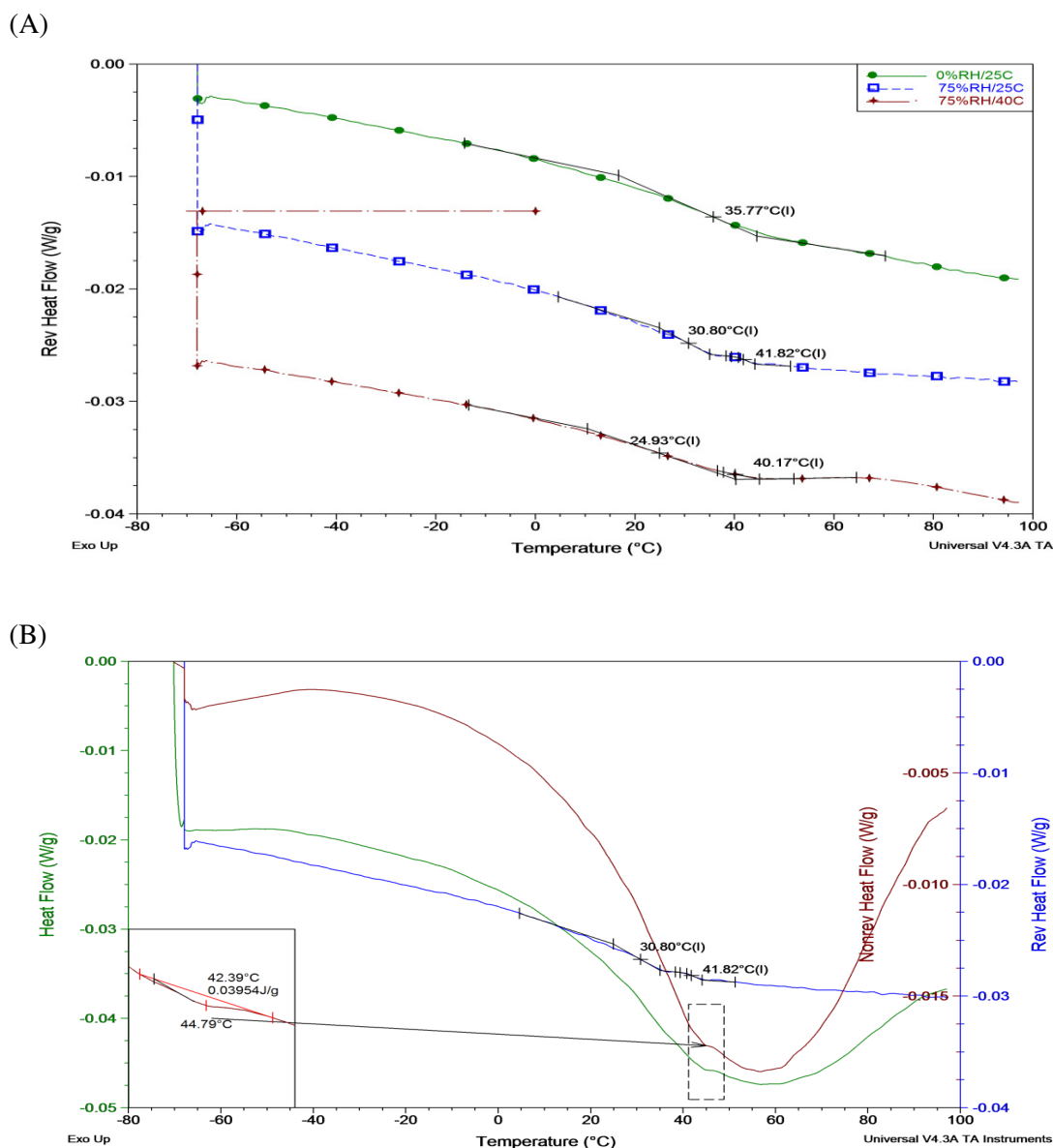
## 7.5.2 Results and discussion

### 7.5.2.1 Characterisation of the aged carrier systems of Eudragit RS PO/Gelucire 44/14 hot melt extruded films

Further to the importance of water in the effectiveness of these carrier systems for drug delivery, the storage study at relative high humidity of 75%RH can aid in understanding of how water can affect their physical stability. To achieve that, samples were divided into three groups dealing with each selected storage condition for one month, where the samples were kept under dry conditions (0%RH/25°C) represent the control of the samples tested at (75%RH/25°C) and highlighting the impact of water at room temperature. While samples stored at 75%RH/25°C can be considered as a control to those tested at 75%RH/40°C and would indicate the role of temperature increase. However, the universal control will be the fresh samples representing zero ageing time, thus giving an insight into the ageing influence at different storage conditions.

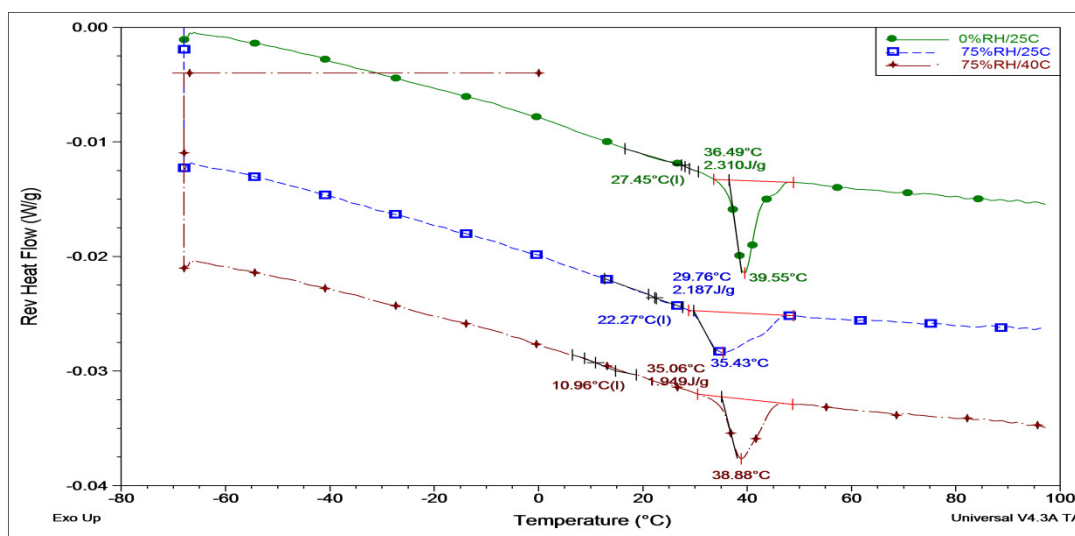
As illustrated in Figure 7.39 (A), the reversing heat flow signals of the MTDSC scans for the FM-A extruded samples (Gelucire 44/14 Eudragit RS PO ratio of 1:6) indicated a single glass transition temperature ( $37.6 \pm 1.8^\circ\text{C}$ ) slightly above the glass transition temperature of the fresh samples reported in section 7.2.2.1.2 i.e.  $37.1 \pm 0.5^\circ\text{C}$ , after ageing under dry conditions. This would be expected as the water content was measured to be  $0.09 \pm 0.54$  (w/w%) that is also slightly less than amount found in the fresh samples (i.e.  $0.25 \pm 0.46$  w/w%). During the storage at 75%RH/25°C, an indication of phase separation was manifested as two glass transition temperatures of  $30.8 \pm 1.2^\circ\text{C}$  and  $41.8 \pm 0.7^\circ\text{C}$  were detected. The first T<sub>g</sub> might indicate an amorphous system of both Gelucire 44/14 and Eudragit RS PO that has a lower glass transition temperature in comparison to the fresh samples due to water presence, whereby the measured water content was  $0.91 \pm 0.04$  (w/w%). The second T<sub>g</sub> ( $41.8 \pm 0.7^\circ\text{C}$ ) indicates more likely a polymer-rich phase of Eudragit RS PO, as the value approaching its glass transition temperature ( $53.3 \pm 0.5^\circ\text{C}$ ); however, it is still plasticized due to water inclusion in the structure. At a higher temperature of 40°C with 75%RH, the aged system under these conditions exhibited also two glass transition temperatures. The first T<sub>g</sub> was approximately 33% less than the recorded T<sub>g</sub> of the fresh samples and the second T<sub>g</sub> indicated Eudragit separation but with a reduced T<sub>g</sub>. This could be explained by the role of water as a plasticizer, whereby the measured water content was  $1.20 \pm 0.19$  (w/w%). Samples at all storage conditions showed relaxation endotherms in their

non-reversing heat flow signal as exemplified in Figure 7.39 (B). Alternatively, this relaxation can contribute to the phase separation of polymer-rich regions as can be seen in samples stored at 75%RH humidity level at 25°C or 40°C.



**Figure 7.39:** MTDSC reversing heat flow signals (A) for aged hot melt extruded FM-A films at different storage conditions for one month whereby (B) is showing representative MTDSC profile of samples stored at 75%RH/25°C with enlarged insert of the relaxation endotherm occurring simultaneously after the glass transition temperature and detected in the non-reversing heat flow signal. Underlying scan rate of  $1^{\circ}\text{C min}^{-1}$  with a modulation amplitude of  $\pm 0.265^{\circ}\text{C}$  and a period of 100 seconds

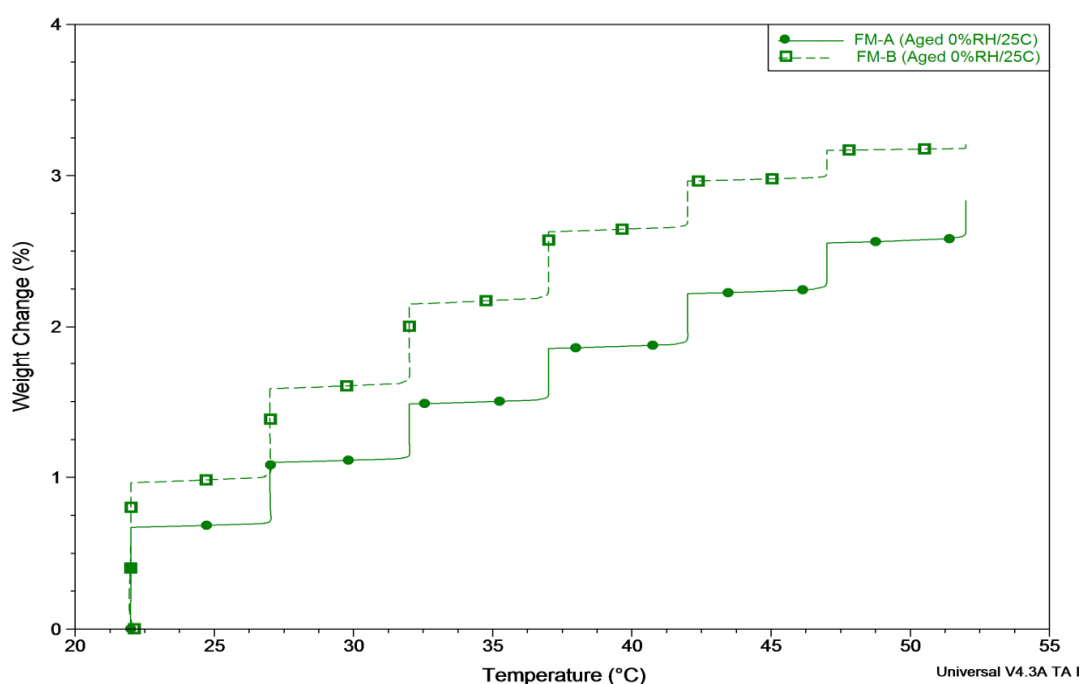
For FM-B extruded systems (Gelucire 44/14 Eudragit RS PO ratio of 2:5), the solid dispersion two-phase system was maintained over all storage conditions as can be seen in Figure 7.40. At dry conditions (0%RH/25°C), the observed changes from the reversing heat flow signals indicated a sharper melting endotherm with an increased melt  $\Delta H$  in comparison to the fresh samples examined in section 7.2.2.1.2, suggesting an increase in the crystalline fraction of the Gelucire 44/14 over time. In addition, an increase in the glass transition temperature was detected in comparison with the fresh samples, mainly due to efficient water loss, whereby the water content of these samples equals  $0.08 \pm 0.12$  (w/w%). After ageing at 75%RH; however, the melting endotherm was broadened and the melt  $\Delta H$  decreased due to possible solubilisation of the Gelucire 44/14 crystals and the observed glass transition temperatures were lowered, all as a function of water involvement at a level of  $0.93 \pm 0.29$  (w/w%). Samples stored at 40°C and 75%RH showed the effect of water presence more clearly (with a water content of  $1.29 \pm 0.9$  w/w%) as characterised with even a lower melt  $\Delta H$  melting endotherm and almost 50% reduction of the glass transition temperature in comparison to the fresh samples.



**Figure 7.40:** MTDSC reversing heat flow signals for aged hot melt extruded FM-B films at different storage conditions for one month. Underlying scan rate of  $1^{\circ}\text{C min}^{-1}$  with a modulation amplitude of  $\pm 0.265^{\circ}\text{C}$  and a period of 100 seconds

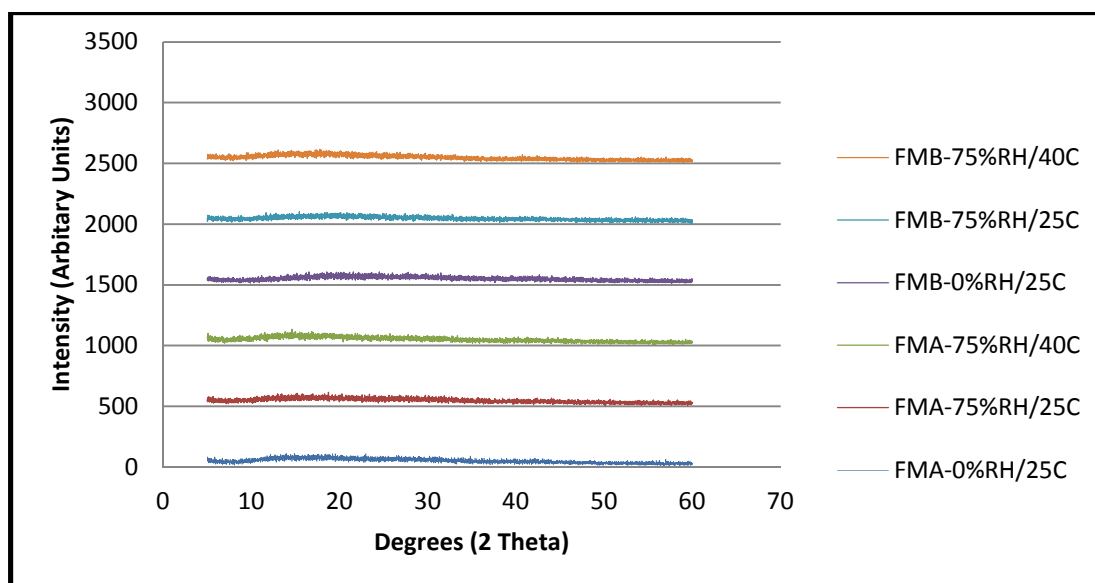
In summary of the MTDSC experiments, the glass transition temperatures of the FM-A and FM-B extruded systems were reduced the most as a function of both temperature and water, under storage conditions of 75%RH/40°C. These conditions also aid in more solubilisation of the crystalline Gelucire 44/14 inside FM-B extruded aged systems. An amorphous phase indicates polymer-rich areas in the tested films was detected after storage at 75%RH/25°C and 75%RH/40°C for FM-A system. The occurrence of this phase is more relevant to the polymer relaxation observed at 75%RH humidity level. Extruded system relaxation to relieve the mechanical stress associated with the HME process can result in phase separation (Qi et al., 2010) as shown in our systems. On that basis it is now obvious why the FM-A system aged at dry conditions is more difficult to exhibit this phase separation, owing to its higher T<sub>g</sub> than the used storage temperature (25°C).

It is also expected that water and increased temperature can work collaboratively to enhance the mobility inside these systems. While temperature above the T<sub>g</sub> can increase system fluidity and improves the moisture ingress, the moisture (or the water) itself will reduce the glass transition temperature making the effect of temperature more influential on these systems. This is further supported by the observed water uptake increase as a function of stepping up the temperature at a fixed relative humidity of 75%RH, for films aged at 0%RH/25°C for FM-A (low level of Gelucire 44/14) and FM-B (high level of Gelucire 44/14) systems in Figure 7.41. In this figure we can also observe increased water uptake as a function of increasing the amount of the Gelucire 44/14 in these films as addressed in previous discussions.



**Figure 7.41: Weight change percent profiles at 75%RH humidity level versus temperature for the aged FM-A (Gelucire 44/14 Eudragit RS PO ratio of 1:6) and FM-B (Gelucire 44/14 Eudragit RS PO ratio of 2:5) systems under 0%RH/25°C for one month**

Throughout previous characterisation of the fresh FM-A and FM-B systems using PXRD, no crystalline peaks were detected even though MTDSC results indicated crystalline Gelucire 44/14 in FM-B films (see section 7.2.2.1.2). As with these samples, no diffraction pattern of the crystalline Gelucire 44/14 was obtained for FM-A and FM-B systems after storage at different conditions as shown in Figure 7.42. Instead a broad hump in the XRD pattern, characteristic of amorphicity, was seen in all the samples. While this finding supports the presence of amorphous material as such, detected using MTDSC in FM-A films, it did not show the second population of the newly existed amorphous material, suggesting lower extent of phase separation. On the other hand, PXRD could not reveal diffraction peaks of crystalline Gelucire 44/14 detected by MTDSC measurements in the FM-B system, indicating less amount of the crystalline material that can be detected using this technique in comparison to the diffraction pattern detected for its equivalent physical mixture.

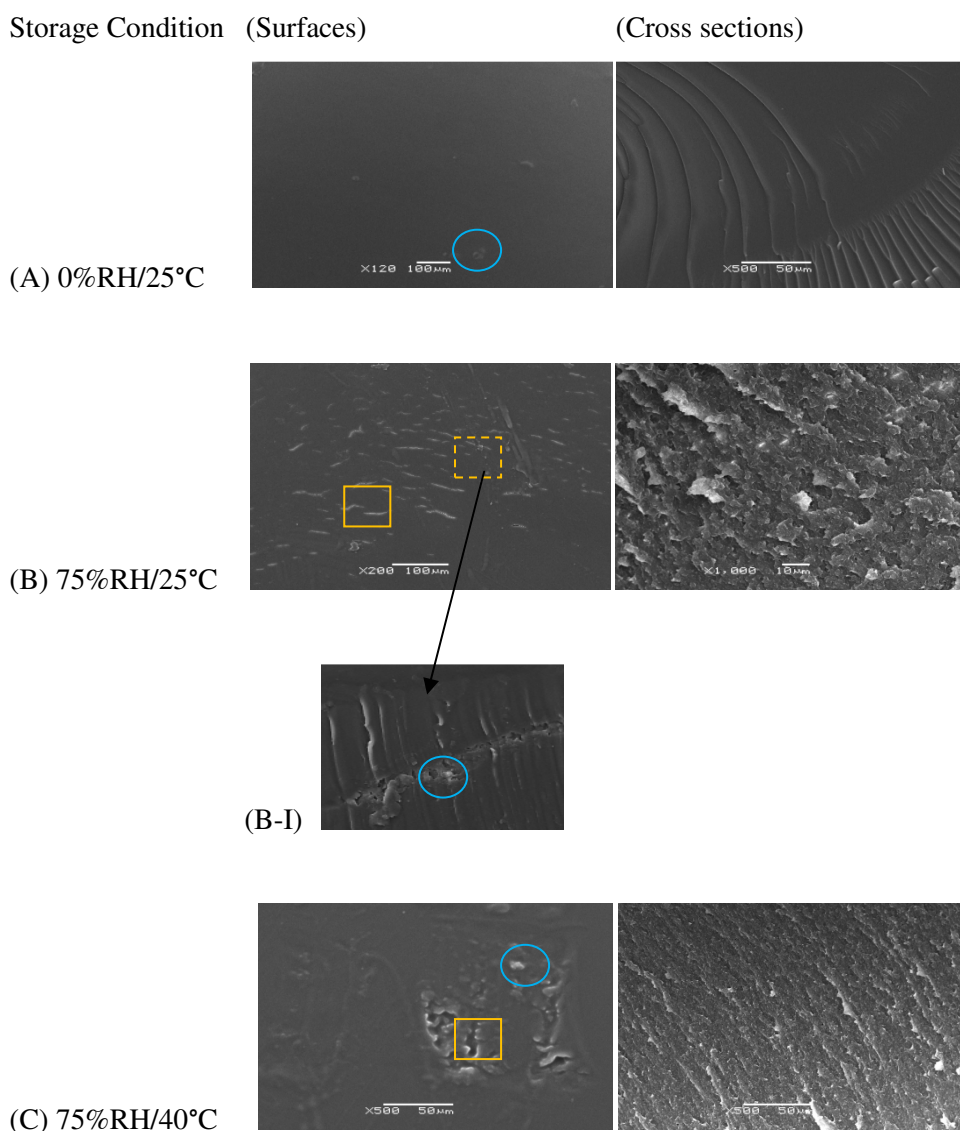


**Figure 7.42: Overlay of X-ray powder diffraction profiles of FM-A and FM-B extruded system aged for one month at 0%RH/25°C, 75%RH/25°C and 75%RH/40°C**

The impact of the storage conditions on the morphology aspects of these aged samples was traced using SEM as seen from Figure 7.43 through to Figure 7.44. The surface of the FM-A films after storage at dry conditions revealed few micro-granules as indicated in the blue circle in Figure 7.43, whereas the cross section was free from any crystals. For the samples stored at the same temperature but higher relative humidity of 75%RH, micro-cracks were seen on the surface associated with more developed micro-granules protruding from these fissures. The cross section deformed in a similar way to the films tested after hydration in section 7.4.2.2, indicating swelling. In this case, we can ascribe the swelling to both polymer chains' relaxation as observed in the MTDSC experiment and water uptake. For the samples stored at 75%RH and 40°C, the micro-cracks were tempered owing to enhanced flow of the material above its detected glass transition temperature, which seems to play a role in sealing these cracks. However, this 'sealing' was not efficient, because the matrix showed signs of swelling as appeared in the cross section. Micro-granules were also detected on the surface of these samples. Therefore, it can be concluded that ageing after one month resulted in Gelucire 44/14 crystallization under all the used storage conditions.

Samples of this system (FM-A) stored under 75%RH/25°C developed micro-cracks on their surfaces, which are more likely ascribed to the association of the hydrophilic chains on the surface with the adsorbed water (see section 7.4.2.2). Gelucire 44/14 also seems to leach into these edges and crystallise as micro-granules to lower the surface energy. At higher

temperature of 40°C and 75%RH, the same scenario took place owing to the same humidity level, but the material fluidity is expected to increase, therefore leached Gelucire 44/14 seems to fill these cracks because smoother surfaces were observed.

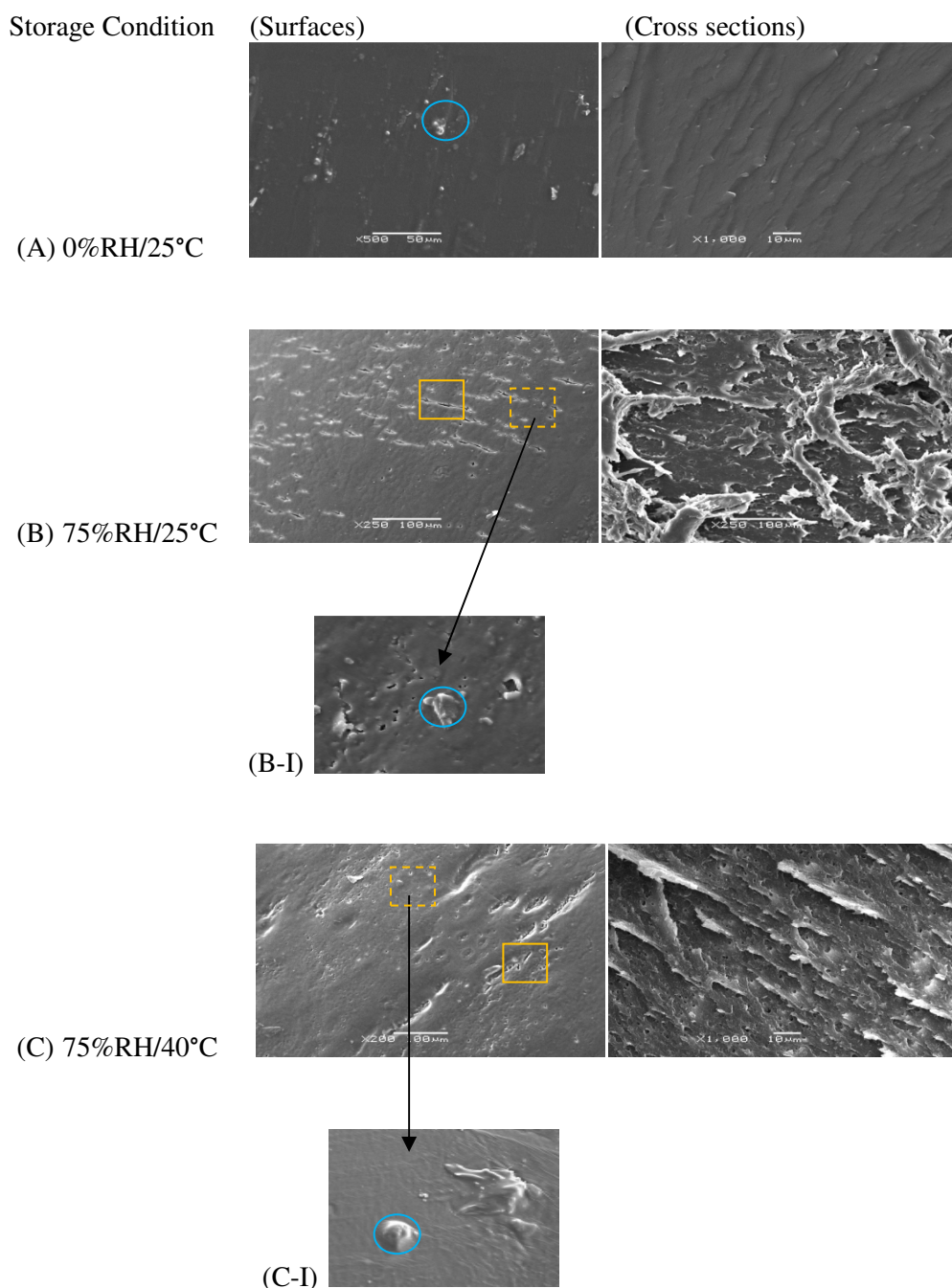


**Figure 7.43: SEM images of the surfaces and cross sections of FM-A extruded films at different storage conditions for one month. (B-I) is an insert showing magnification of granules (dashed orange square) detected on the surface of FM-A extruded films aged under 75%RH/25°C. Examples on the observed micro-cracks and granules (crystals) are enclosed by orange squares and blue circles, respectively**

The changes in the morphological features of the aged films of FM-B system as displayed in Figure 7.44 are similar to the ones observed for the aged FM-A extruded systems with few variations. Firstly, the propensity of crystalline regions after ageing at 0%RH/25°C is higher than FM-A system which is expected from this solid dispersion system that had these granules originally on its surface. This finding was supported in MTDSC results as sharper melting peak with increased melt  $\Delta H$  were observed. Furthermore, the average diameter of these micro-granules increased to about 2.5-7 microns in comparison to their average diameter of about 0.4-2.6 microns in fresh samples, indicating crystal growth. The crystal development into large crystals in lipids such as Gelucire 44/14 is known as ‘blooming’ and it is usually associated with more softened lipids (Khan and Craig, 2004). Therefore, it would be expected to have even larger granules in the systems stored at 75%RH/25°C and 75%RH/40°C as their glass transition temperatures were reduced far beyond the used storage temperatures which would enhance Gelucire 44/14 mobility and diffusivity into the surface with high propensity to build up into larger crystals. This conforms to the observed largest granules on the surfaces of the FM-B aged films where more plasticized systems (lower  $T_g$ ) such as the ones stored at 75%RH/40°C showed the largest granule with approximate diameter of 25 microns in comparison to the granules observed after storage at 75%RH/25°C, with a maximum approximate diameter of only 5.3 microns.

Secondly, the swelling of the cross sections was more pronounced especially at the storage conditions of 75%RH/25°C, implying more water involvement as a function of Gelucire 44/14 high level in FM-B films in comparison to the FM-A films.

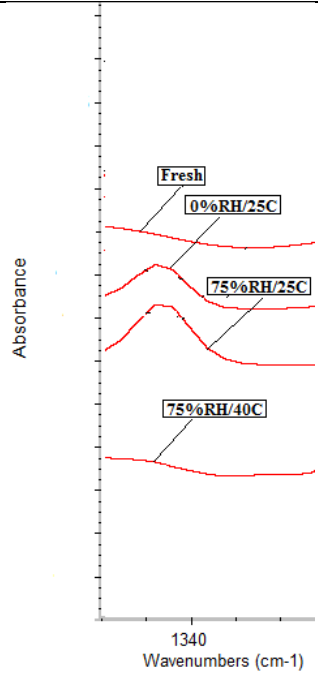
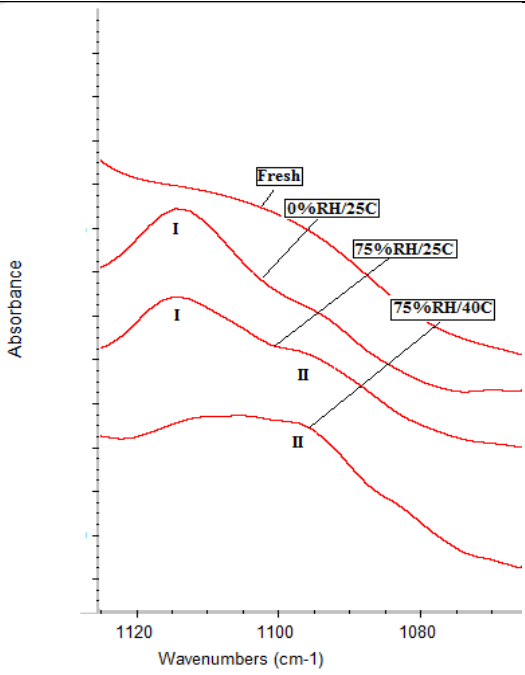




**Figure 7.44:** SEM images of the surfaces and cross sections of FM-B extruded films at different storage conditions for one month. (B-I) and (C-I) are inserts showing magnifications of granules (dashed orange square) detected on the surface of FM-B extruded films aged under 75%RH/25°C and 75%RH/40°C, respectively. Examples on the observed micro-cracks and granules (crystals) are enclosed by orange squares and blue circles, respectively

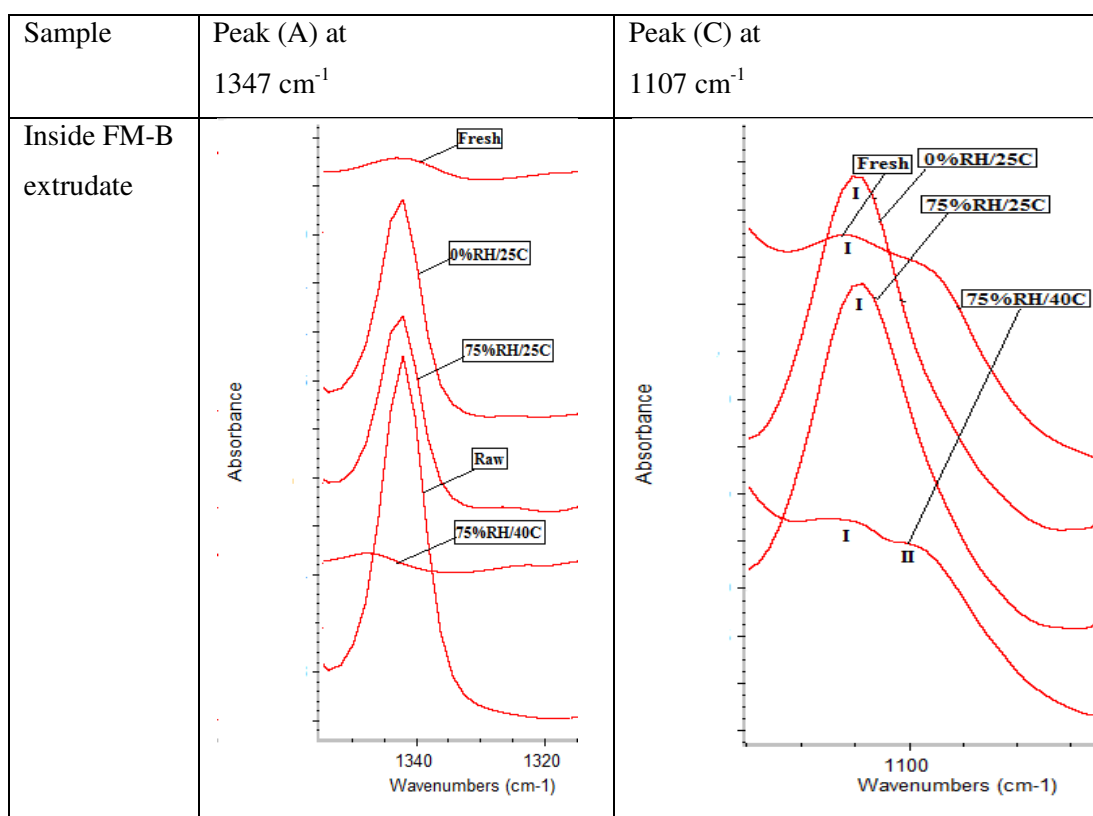
As opposed to the MTDSC and PXRD results, SEM indicated the presence of Gelucire 44/14 crystallites on the surfaces of the aged FM-A films at all storage conditions. SEM might carry some limitations in the identification of the crystals, such as misinterpretation of the topological features of the samples with the granule formation or otherwise electron beam interaction with the tested surface, whereby hump-like structures can form. Therefore ATR-FTIR was used to further investigate the presence of Gelucire 44/14 crystals in the aged samples of either FM-A or FM-B films. Using characteristic absorption bands of crystalline Gelucire 44/14 as detailed in section 7.3.2, Table 7.12 to Table 7.13 were constructed and revealed interesting observations. For the aged FM-A systems, the presence of crystalline Gelucire 44/14 was consistent with the SEM findings for samples stored at 0%RH/25°C and 75%RH/25°C. In these samples, the characteristic peaks for crystalline Gelucire 44/14 denoted as A ( $1347\text{ cm}^{-1}$ ) and C ( $1107\text{ cm}^{-1}$ ) retained sharper appearance in comparison to the fresh samples; however, peak C was boarder after storage at 75%RH/25°C compared to the samples stored under dry conditions, indicating solubilisation of this lipid. This resembles hydrated films' behaviour with the differentiation into another peak (denoted as II,  $1096\text{ cm}^{-1}$ ) that was assumed in section 7.4.2.2 to result from the solubilisation of the Gelucire 44/14 with subsequent oil leakage into the surface.

For the samples stored at 75%RH/40°C, the solubilisation was increased as a function of both water and high temperature and peak A was not detected whereas peak C ( $1107\text{ cm}^{-1}$ ) showed only the new peak (II) around  $1096\text{ cm}^{-1}$ , which is another indication of solubilisation of Gelucire 44/14. At 75%RH/40°C there are few small crystallites as indicated by SEM but the process of their solubilisation was dominant as indicated by ATR-FTIR results, thus could not stand as a distinct crystalline peak in the spectrum. Therefore, we can conclude that the aged films of FM-A composition exhibited crystallites at all storage conditions with varying extent.

Sample	Peak (A) at 1347 $\text{cm}^{-1}$	Peak (C) at 1107 $\text{cm}^{-1}$
Inside FM-A extrudate		

**Table 7.12: Summary of the assignments of the proposed crystalline peaks of Gelucire 44/14 from Eudragit RS PO-subtracted extruded films ATR-FTIR spectra of FM-A (Gelucire 44/14 Eudragit RS PO ratio of 1:6) system examined after storage for one month at different conditions**

For FM-B aged films, the crystals detected using ATR-FTIR were mainly at storage conditions of 0%RH/25°C and 75%RH/25°C. As shown in Table 7.13, these samples exhibited distinct sharp peaks at the location of previously identified peak A (1347  $\text{cm}^{-1}$ ) similar to the raw crystalline Gelucire 44/14. This sharpness in comparison to the Gelucire 44/14 crystals in the fresh extruded samples would be assumed to correspond to more developed crystallites coincided with the detected ‘blooming’ effect on the surfaces of these films using SEM. For the films stored at 75%RH/40°C, the peak A resembles the fresh samples with even more diffused character, due to possible solubilisation of the Gelucire 44/14 crystals facilitated by the presence of water and temperature. This was supported by MTDSC findings of very broad melting endotherm and low melt  $\Delta H$  in comparison to other aged extrudates. This is also manifested at the peak C (1107  $\text{cm}^{-1}$ ), wherein the solubilised fraction of the expected oily part from Gelucire 44/14 is indicated in the observed peak around 1096  $\text{cm}^{-1}$  (II) shown in Table 7.13.



**Table 7.13: Summary of the assignments of the proposed crystalline peaks of Gelucire 44/14 from Eudragit RS PO-subtracted extruded films ATR-FTIR spectra of FM-B (Gelucire 44/14 Eudragit RS PO ratio of 2:5) system examined after storage for one month at different conditions. The spectrum of the raw Gelucire 44/14 extracted from the equivalent physical mixture spectrum (no thermal treatment) was displayed along other spectra at peak (A) region to show similarity**

In summary, the aged films of FM-A and FM-B extruded films at the selected storage conditions for one month developed crystalline Gelucire 44/14 to varying extent. A moisture level of 75%RH and a temperature of 40°C were able to make efficient solubilisation of the Gelucire 44/14 crystals without a marked swelling as the one detected at 75%RH/25°C. This could be attributed to more tempered cracks facilitated by enhanced material flow at higher temperatures on the surface of the extruded film which might impede further diffusion of the water into the matrices, thus a lesser extent of swelling would be expected.

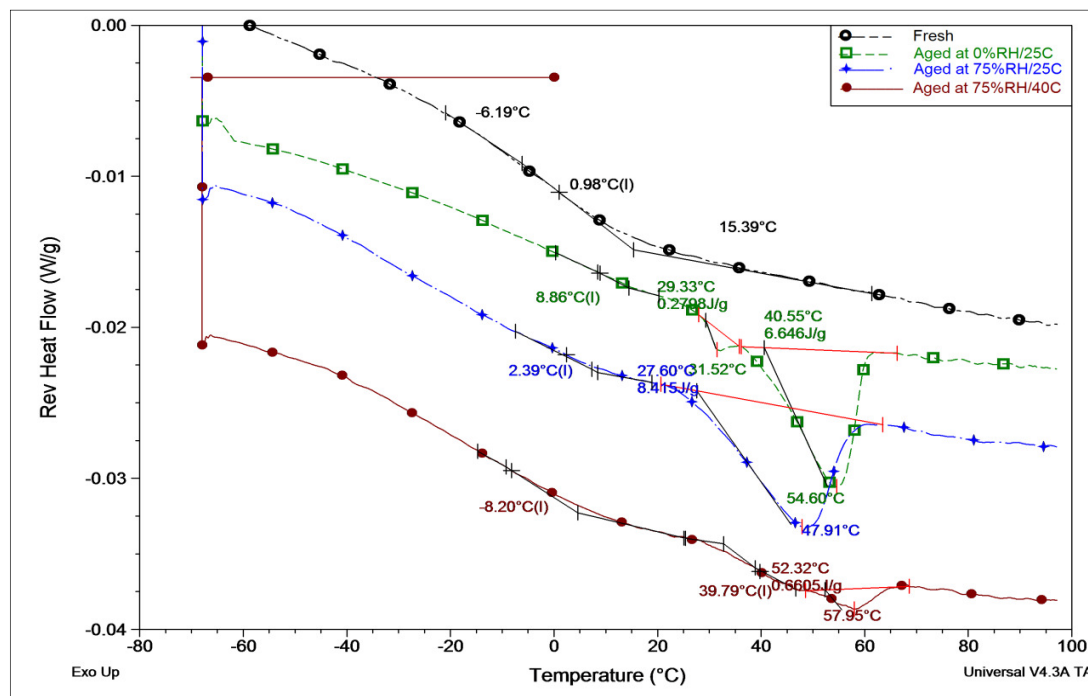
#### 7.5.2.2 Characterisation of the aged hot melt extruded films of Eudragit RS PO/Gelucire 44/14 loaded with ibuprofen

Gelucire 44/14:Eudragit RS PO ratios of (1:6) and (2:5) in FM-A and FM-B systems, respectively, are equivalent to the ratios used in the loaded films of FM9 and FM10 systems, respectively, wherein the drug (ibuprofen) was loaded at 30%(w/w) level, as developed in Chapter 6. These medicated samples (FM9 and FM10 systems) were stored for one month using the same previous conditions of the carrier systems (without the drug). These samples were characterised accordingly using MTDSC, PXRD, HSM and TGA.

In an attempt to relate the behaviour of the aged carrier system (Gelucire 44/14 in Eudragit RS PO) to the complex aged medicated system, MTDSC has been used in a similar convention to the previous section. Thus the reversing signals were used to observe the melting and glass transition events wherein the trend of changes will be addressed with expected reliable deconvolution from other mixed events such as dehydration peaks or relaxation endotherms, which would appear in total and non-reversing heat flow signals.

As can be seen from Figure 7.45, FM9 extruded films containing a lower level of Gelucire 44/14 than FM10 films showed two melting peaks after storage at dry conditions of 0%RH/25°C, indicating recrystallisation. The glass transition temperature was increased in comparison to the fresh samples with a  $T_g$  (Mid-point) of  $8.8 \pm 0.6^\circ\text{C}$ , as both ibuprofen and Gelucire 44/14 may contribute to the reduction of the resultant glass transition temperature of the extruded film and the recrystallization of one or both might affect their efficiency as plasticizers. A greater proportion of the crystalline material was detected in the second broad peak (higher melt  $\Delta H$ ) with a  $T_{m(\text{onset})}$  of  $40.6 \pm 0.3^\circ\text{C}$  preceded by the smaller melting endotherm (lower melt  $\Delta H$ ) with a  $T_{m(\text{onset})}$  of  $30.6 \pm 1.2^\circ\text{C}$ . In comparison to these samples, storage at 75%RH/25°C resulted in one broader melting peak with a  $T_{m(\text{onset})}$  of  $27.6 \pm 0.2$  shifted to a lower temperature and accompanied with a depressed glass transition temperature of  $2.3 \pm 1.0^\circ\text{C}$ . Consequently, the water involved in these films played two roles. Possible solubilisation of the crystalline material as indicated from the shifting of the melting endotherm and as plasticizing agent with a profound impact on the reduction of the glass transition temperature though a moisture content of only  $0.58 \pm 0.05$  (w/w%) was measured. At 75%RH/40°C storage conditions, the resulting composition was characterised by the absence of the melting endotherms starting approximately in the range of 27.6-30.6°C and appearance of a very broad melting peak with a  $T_{m(\text{onset})}$  of  $52.4 \pm 1.1^\circ\text{C}$ . Though this

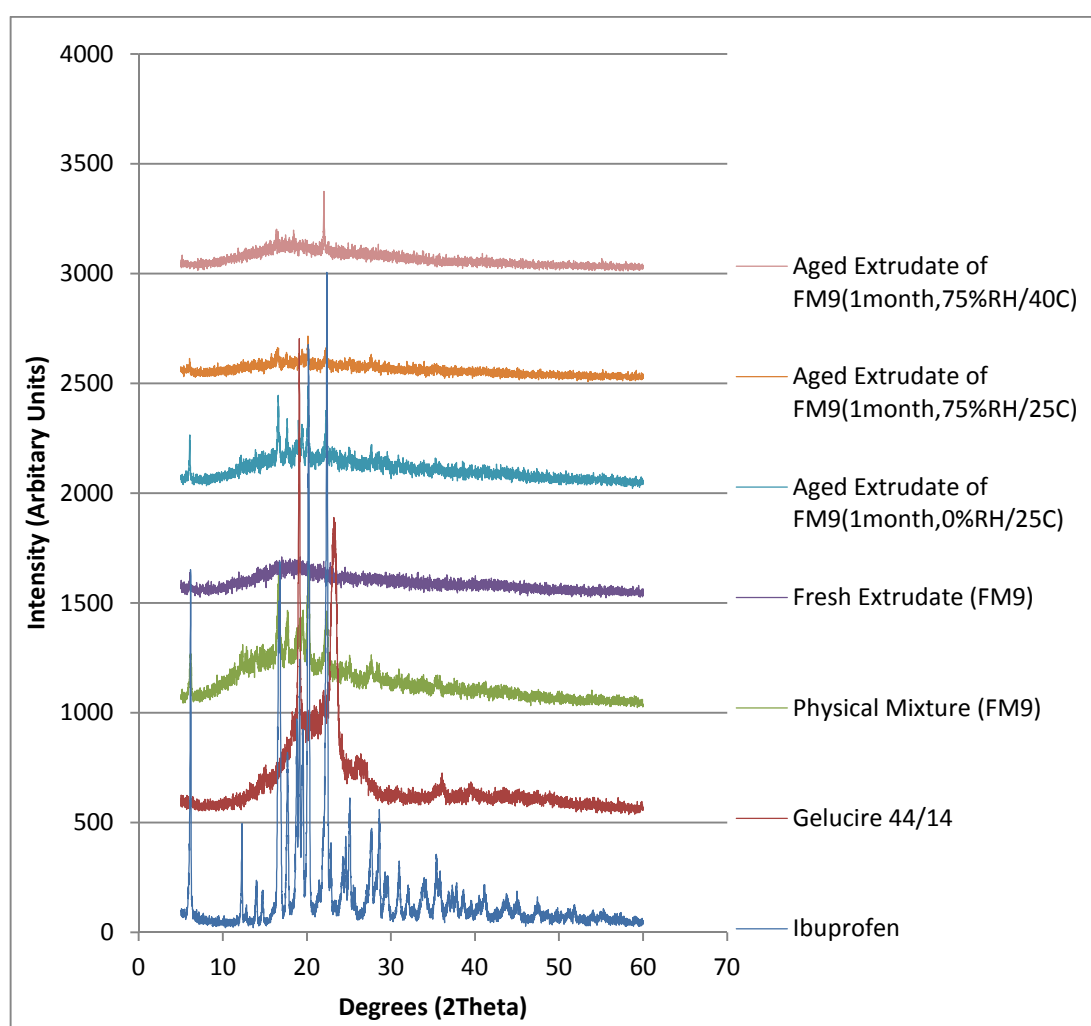
peak was shifted to a higher temperature it was associated with the lowest melt  $\Delta H$  in comparison to the samples stored at all other storage conditions.



**Figure 7.45: MTDSC reversing heat flow signals of aged hot melt extruded FM9 films (Gelucire 44/14: Eudragit RS PO: ibuprofen ratio of 1:6:3) at different storage conditions for one month in comparison to the fresh tested film**

As addressed earlier (section 7.5.2.1), temperature and water (75%RH/40°C) can lead to greater solubilisation for Gelucire 44/14 crystals in the aged films of the carrier systems (FM-A and FM-B). Therefore, it could be inferred that disappearance of these peak herein is associated with the crystalline material solubilisation under these conditions while the remaining peak represents the slight excess of unsolubilised crystalline material. Furthermore, two glass transition temperatures were visible in the reversing heat flow signal. While a glass transition temperature (Mid-point) was observed at  $-8.6 \pm 0.4^\circ\text{C}$  which reflects the water's influence as a plasticizing agent with a measured water content of  $0.65 \pm 0.08$  (w/w%), another glass transition temperature was detected at  $39.6 \pm 0.3^\circ\text{C}$  (Mid-point Tg) similar to the Tg of the FM-A carrier system (without the drug) stored at the same conditions (Figure 7.45). This might indicate a possible Eudragit RS PO-rich phase as inferred from the FM-A system (carrier system without the drug). Therefore, it could be concluded that storage at  $40^\circ\text{C}$  will yield a complex response in terms of phase separation, which may be described as extensive in comparison to other storage conditions.

As per this discussion, it would be expected that Gelucire 44/14 in the aged FM9 films is contributing to the observed melting peaks as these endotherms shifted to a lower temperature or decrease as a function of exposure to water in comparison to the ones stored at dry condition, because Gelucire 44/14 crystals are miscible with water. In addition, the studied aged carrier system (FM-A) of these films (unloaded), showed crystalline Gelucire 44/14 in all storage conditions whereby storing at 75%RH/40°C led to almost disappearance of these crystals. However, PXRD profiles of the aged FM9 films (loaded) as illustrated in Figure 7.46 demonstrated only ibuprofen crystals at all storage conditions. This could indicate a low amount of crystalline Gelucire 44/14 in these aged films.

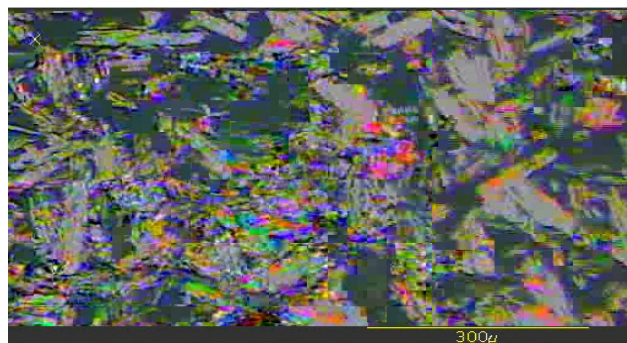


**Figure 7.46: Overlay of X-ray powder diffraction profiles of FM9 extruded systems aged for one month at 0%RH/25°C, 75%RH/25°C and 75%RH/40°C in comparison to their corresponding fresh sample, physical mixture and pure crystalline components i.e. ibuprofen and Gelucire 44/14**

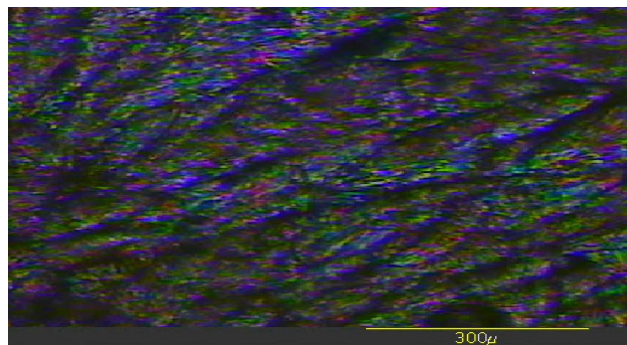


Collectively, all aforementioned observations are expected to be a result of the drug dissolution over a wide range of the molten carrier (Gelucire 44/14 in Eudragit RS PO) as reported by Lloyd et al. (1997). Consistent with these findings, a hot stage microscopy (HSM) experiment showed that the melt process occurred over a wide range, wherein the Gelucire 44/14 crystals melted first followed by gradual melting of the ibuprofen crystals. As we can see in Figure 7.47, ibuprofen crystals exhibit rod-shape whereas Gelucire 44/14 crystals exhibit a spherulitic structure. A series of images were captured accordingly for the aged FM9 samples stored at different conditions and heated at  $1^{\circ}\text{C min}^{-1}$ . These images correspond to the softening of the sample, the melt onset and complete disappearance of the crystals as illustrated in Figure 7.48. For example, the samples stored at 0%RH/25°C started to soften and expand in the approximate range of 32.1–42.1°C and the melt onset observed around 50°C, then mixed crystals were detected around 55.5° of both Gelucire 44/14 and ibuprofen. The disappearance of the spherulites related to the Gelucire 44/14 was almost completed by 61.2°C followed by melting of the remaining observed rod-shape crystals due to ibuprofen which finished around 70.3°C.

(A)



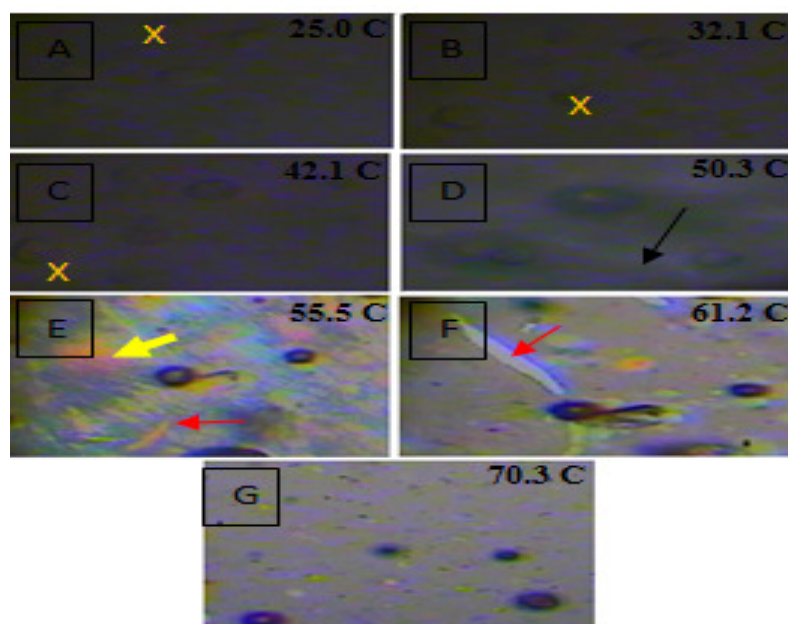
(B)



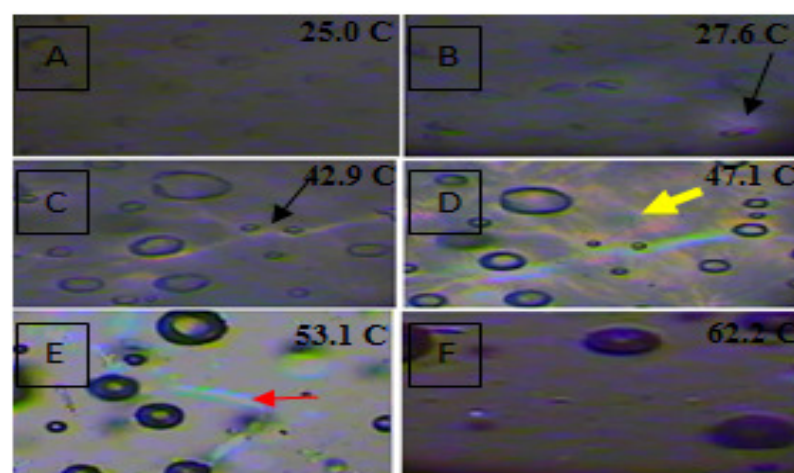
**Figure 7.47: Polarized light images of the (A) ibuprofen crystals and (B) Gelucire 44/14**



(I)

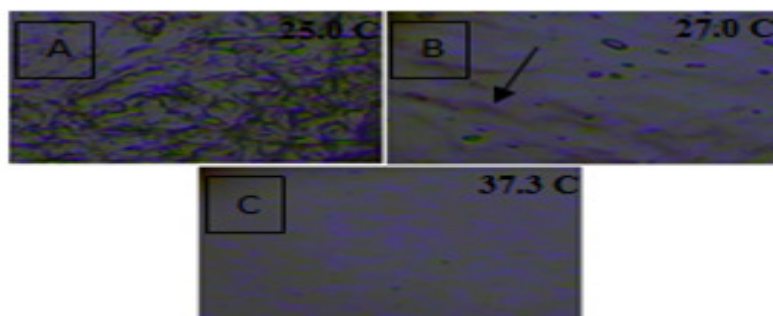


(II)



**Figure 7.48: Hot stage microscope images capturing the melting of the crystals after ageing for one month of the FM9 samples (I) under 0%RH/25°C and (II) under 75%RH/25°C. Samples were heated at 1°C min<sup>-1</sup>. Arrows indicate the area associated with the onset of melting (in black), the Gelucire 44/14 spherulites (in thick yellow) and ibuprofen crystals (in red). Orange cross marks the movement of the sample as a result of its expansion. Circular bubbles are due to nitrogen gas entrapped during manufacturing of these loaded samples**

(III)



**Figure 7.48 (Contd.): Hot stage microscope images of the FM9 samples stored at 75%RH/40°C for month. These samples showed only signs of liquefaction or glass disappearance as displayed in (III) set. Samples were heated at 1°C min<sup>-1</sup>. Arrows indicate the area associated with the onset of softening (in black)**

MTDSC data (Fig.7.45) showed a reasonable agreement with the observed melting in this HSM study (Fig.7.48). In particular the broadest peak (last peak) in the case of the samples stored at 0%RH/25°C and the peak observed for samples stored at 75%RH/25°C. The temperature at the peak of the melting endotherm (MTDSC profile) fairly corresponds to the temperature associated with the visual disappearance of the spherulites. The temperature at which this melting endotherm returns to the baseline in the MTDSC thermogram is in a good agreement with the complete melt of the ibuprofen crystals, Table 7.14. However, small shoulders or peaks (lower melt  $\Delta H$ ) for the samples stored at 0%RH/25°C and at 75%RH/40°C and observed in Figure 7.45 were difficult to detect using HSM as they were subtle (an enthalpy in the approximate range of 0.28-0.66 J/g). Furthermore, samples stored at 75%RH/40°C showed signs of softening followed by complete disappearance of a wrinkled texture into smoother one around 37.3°C that agreed well with the predicted glass transition temperature in the MTDSC reversing heat flow signal characteristic for this system (around 39.8°C).

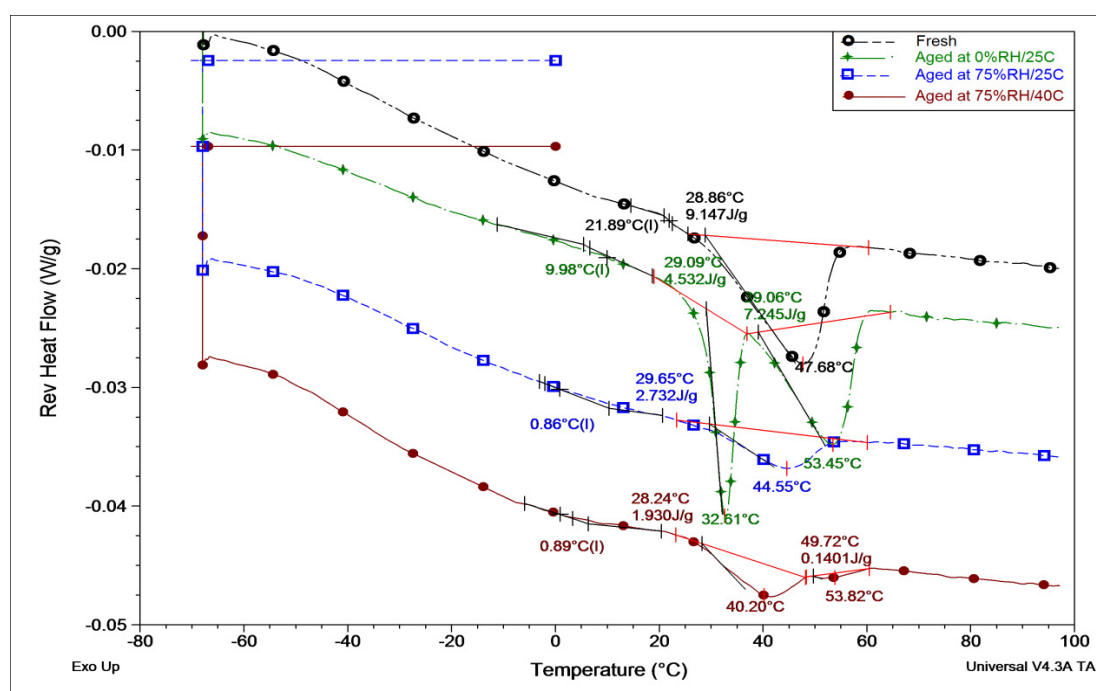
Reference	Figure 7.48 (I)	Figure 7.45 Aged at 0%RH/25°C	Figure 7.48 (II)	Figure 7.45 Aged at 75%RH/25°C
Image symbol	Temp.(°C)		Temp.(°C)	
E			53.1(*)	47.9 T <sub>m(p)</sub>
F	61.2(*)	54.6 T <sub>m(p)</sub>	62.2(**)	63.6 T <sub>m(b)</sub>
G	70.3(**)	66.0 T <sub>m(b)</sub>		

**Table 7.14: A summary of the correlation between the temperatures associated with disappearance of the spherulites (\*) and rod-shape crystals (\*\*) as obtained from hot stage microscopy and the melting temperature at the peak (T<sub>m(p)</sub>) and at the baseline (T<sub>m(b)</sub>) of the last peak recorded from MTDSC reversing heat flow signals (aged FM9 films)**

It should also be noted that variation of the data resulting from comparison between HSM and DSC is expected and this could be ascribed to the differences in the measuring techniques. For example, samples tested using DSC were enclosed in aluminium pans under nitrogen gas whereas samples in HSM were exposed to open environment and under atmospheric conditions, this would result in a different heat flux experienced by the samples. Moreover, DSC technique averages the behaviour of all crystals that melt at similar temperature while HSM measurements indicate that for individual crystals (Sutananta et al., 1994).

In a similar way to the approach used to characterise aged FM9 films, the aged FM10 films (higher level of Gelucire 44/14) were tested as seen from Figure 7.49 through to Figure 7.51. Previously, the melting endotherm observed for the fresh FM10 film had been assumed to be ascribed only to the crystalline ibuprofen based on the PXRD data (Chapter 6). However, the carrier system (without the drug) which corresponds to this formula i.e. FM-B films showed crystalline Gelucire 44/14 supported by MTDSC and ATR-FTIR measurements in the previous sections. Therefore it is more logical to consider that the detected broad peak of the fresh films resulted from both crystalline ibuprofen and Gelucire 44/14. The reversing heat flow signals of the MTDSC experiment are presented for the fresh sample compared to the aged ones in Figure 7.49.

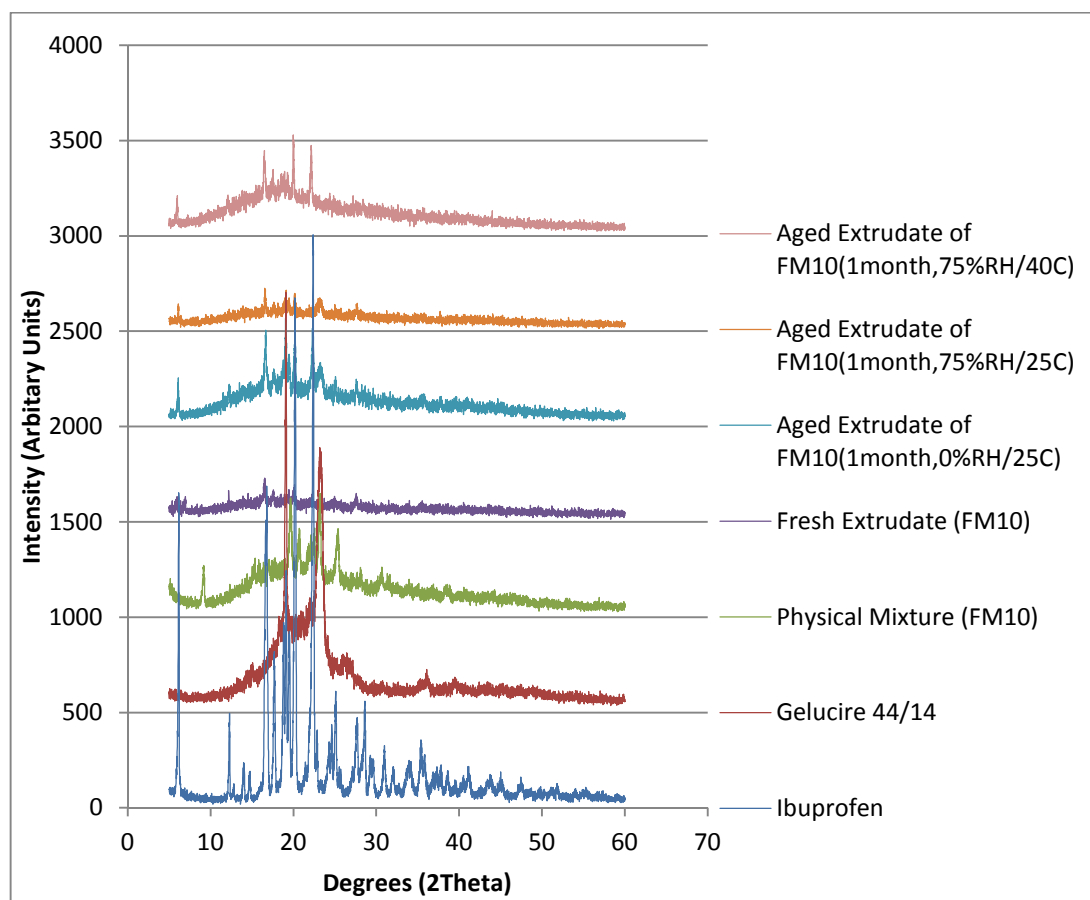
As shown in Figure 7.49, ageing of these samples under dry conditions (0%RH/25°C) for one month was associated with differentiation of the melting peak of the fresh samples ( $T_{m(\text{onset})} = 29.3 \pm 1.5^\circ\text{C}$ ) into a broad one with a melting onset temperature ( $T_{m(\text{onset})}$ ) at  $39.3 \pm 1.5^\circ\text{C}$  preceded by a sharper melting peak with a  $T_{m(\text{onset})}$  of  $29.3 \pm 1.5^\circ\text{C}$ . The glass transition temperature detected for these aged samples was at  $10.2 \pm 0.6^\circ\text{C}$  ( $T_g\text{-Midpoint}$ ), which is less than the one recorded for the fresh samples ( $21.8 \pm 0.4^\circ\text{C}$ ). As addressed before, ibuprofen can act as a plasticizer and Gelucire 44/14 also aids in the reduction of the glass transition temperature of the mixture. Thereof the amorphous phase detected in this system and characterised with this depressed glass transition temperature is expected to be enriched with amorphous state of one of these components or both.



**Figure 7.49:** MTDSC reversing heat flow signals for aged hot melt extruded FM10 films (Gelucire 44/14: Eudragit RS PO: ibuprofen ratio of 2:5:3) at different storage conditions for one month in comparison with the fresh tested film

For the samples stored at the same temperature but at higher level of humidity (75%RH/25°C), as shown in Figure 7.49, the glass transition temperature was significantly reduced into  $0.9 \pm 0.1^\circ\text{C}$  due to the presence of water which can act as a powerful plasticizer, and the measured water content of these samples was only  $0.68 \pm 0.44$  (w/w%). Furthermore the water influence on these samples was manifested in one broad peak ( $T_{m(\text{onset})} = 29.7 \pm 0.2^\circ\text{C}$ ) associated with low melting enthalpy and shifting to a lower temperature as observed from the melting temperature at the apex, which could be attributed to possible solubilisation of the Gelucire 44/14. The latter impact was even more obvious in the samples stored at higher temperature of  $40^\circ\text{C}$  in presence of water at humidity level of 75%RH, because, as mentioned earlier, Gelucire 44/14 water uptake enhanced as a function of temperature with subsequent possible solubilisation. The shifting of the broad peak was observed mainly from the decrease of the temperature of the melting endotherm apex to a lower value and appearance of a shoulder-like melting peak with a  $T_{m(\text{onset})}$  of  $49.7 \pm 0.3^\circ\text{C}$  (Figure 7.49). The glass transition temperature of the system did not show a significant change in comparison to the systems stored at 75%RH/25°C and a  $T_g$  value of  $0.9 \pm 0.4^\circ\text{C}$  (Mid-point  $T_g$ ) was observed with a measured water content of these samples of about  $0.76 \pm 0.12$  (w/w%).

PXRD measurements as depicted in Figure 7.50 supported the presence of crystalline Gelucire 44/14 and ibuprofen crystals in all aged samples as linked with the diffraction peaks observed in their diffractograms. This coincided with the broad peaks obtained by MTDSC results. Since the fresh samples, though having these broad peaks which are most likely to be a function of both crystalline ibuprofen and Gelucire 44/14, did not show the diffraction peaks of Gelucire 44/14, this may be related to the low level of this material in its crystalline state in the fresh samples compared to the aged ones. However, it can be argued that solubilised Gelucire 44/14 after storage at high relative humidity of 75%RH should result in a low level of crystalline Gelucire 44/14 during testing that is hard to be detected using PXRD. Despite this, it is believed that these samples undergo rapid recrystallization, probably due to water evaporation, which was observed visually especially for the samples stored under 75%RH/40°C, as they transformed within almost 15 minutes into opaque films, indicating recrystallization. Thus the time needed to handle the samples and to test them using PXRD (approximately one hour for each sample) is expected to be enough to render recrystallization of the solubilised Gelucire 44/14 in enough amount to be detectable using PXRD technique in these aged samples.

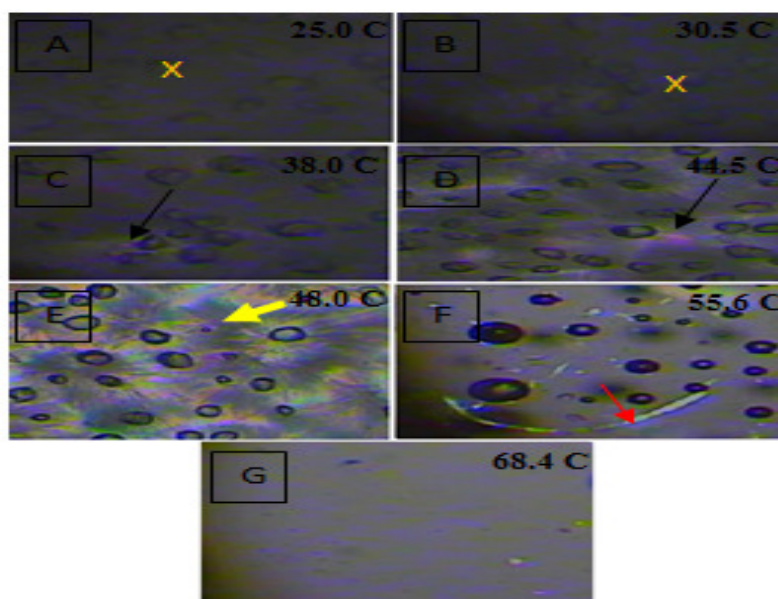


**Figure 7.50: Overlay of X-ray powder diffraction profiles of FM10 extruded systems aged for one month at 0%RH/25°C, 75%RH/25°C and 75%RH/40°C in comparison to their corresponding fresh sample, physical mixture and pure crystalline components i.e. ibuprofen and Gelucire 44/14**

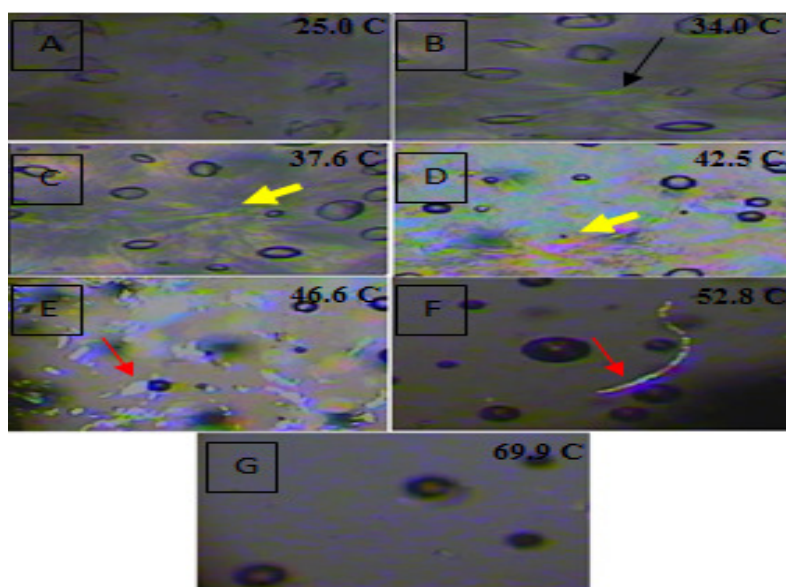
Additionally, the appearance and melting of these aged films were examined using HSM as illustrated in Figure 7.51. In both samples stored at 0%RH/25°C and 75%RH/25°C, the crystalline ibuprofen with rod-shape appearance and spherulites related to Gelucire 44/14 were observed. For the samples stored at 75%RH/40°C, the ibuprofen crystals were visible and their complex mixture with Gelucire 44/14, Eudragit RS PO and water was manifested as a wrinkled-like texture that soon liquefies and clear around 29.4°C, implying that the phase is amorphous or more likely a mixed phase of amorphous material and solubilised Gelucire 44/14 crystals as supported by MTDSC findings in which the  $T_{m(\text{onset})}$  of the first melting endotherm was about  $28.7 \pm 0.5^\circ\text{C}$ . This correlates well with the temperature associated with the smoothness of the ‘wrinkled’ texture as observed in HSM (29.4°C) that is believed to be facilitated by high mobility of the amorphous phase with very low glass transition temperature predicted around  $0.9 \pm 0.4^\circ\text{C}$  (Mid-point  $T_g$ ).



(I)

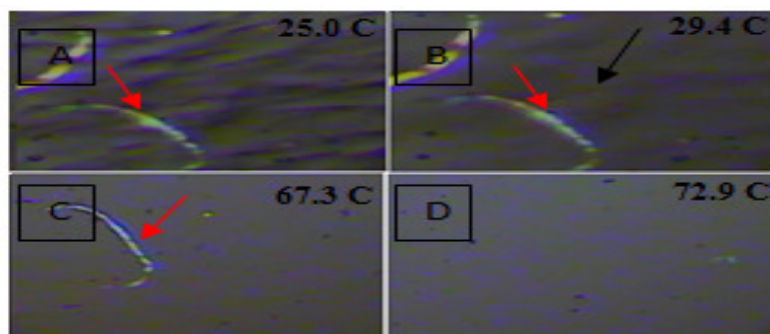


(II)



**Figure 7.51:** Hot stage microscope images capturing the melting of the crystals after ageing for one month of the FM10 samples (I) under 0%RH/25°C and (II) under 75%RH/25°C. Samples were heated at 1°C min<sup>-1</sup>. Arrows indicate the area associated with the onset of melting (in black), the Gelucire 44/14 spherulites (in thick yellow) and ibuprofen crystals (in red). Orange cross marks the movement of the sample as a result of its expansion. Circular bubbles are due to nitrogen gas entrapped during manufacturing of these loaded samples

(III)



**Figure 7.51 (Contd.): Hot stage microscope images capturing the melting of the crystals after ageing for one month of the FM10 samples stored at 75%RH/40°C which showed mainly signs of liquefaction or glass disappearance as displayed in (III) set. Samples were heated at 1°C min<sup>-1</sup>. Arrows indicate the area associated with the onset of melting or softening (in black) and ibuprofen crystals (in red)**

Though limitations associated with the direct comparison between DSC and HSM data, mentioned in the earlier discussion, Table 7.15 demonstrates that they were closely related to each other. Mainly the visual disappearance of the spherulites was linked to the melting peak temperature ( $T_{m(p)}$ ) and the observed melting of the ibuprofen rod-shaped crystals with the melting temperature at the baseline ( $T_{m(b)}$ ), both of the last melting endothermic peaks in the reversing heat flow thermograms (Figure 7.49).



Reference	Figure 7.51 (I)	Figure 7.49 Aged at 0%RH/25°C	Figure 7.51 (II)	Figure 7.49 Aged at 75%RH/25°C
Image symbol	Temp.(°C)		Temp.(°C)	
F	55.6(*)	53.5 $T_{m(p)}$	52.8(*)	44.6 $T_{m(p)}$
G	68.4(**)	64.6 $T_{m(b)}$	69.9(**)	60.1 $T_{m(b)}$

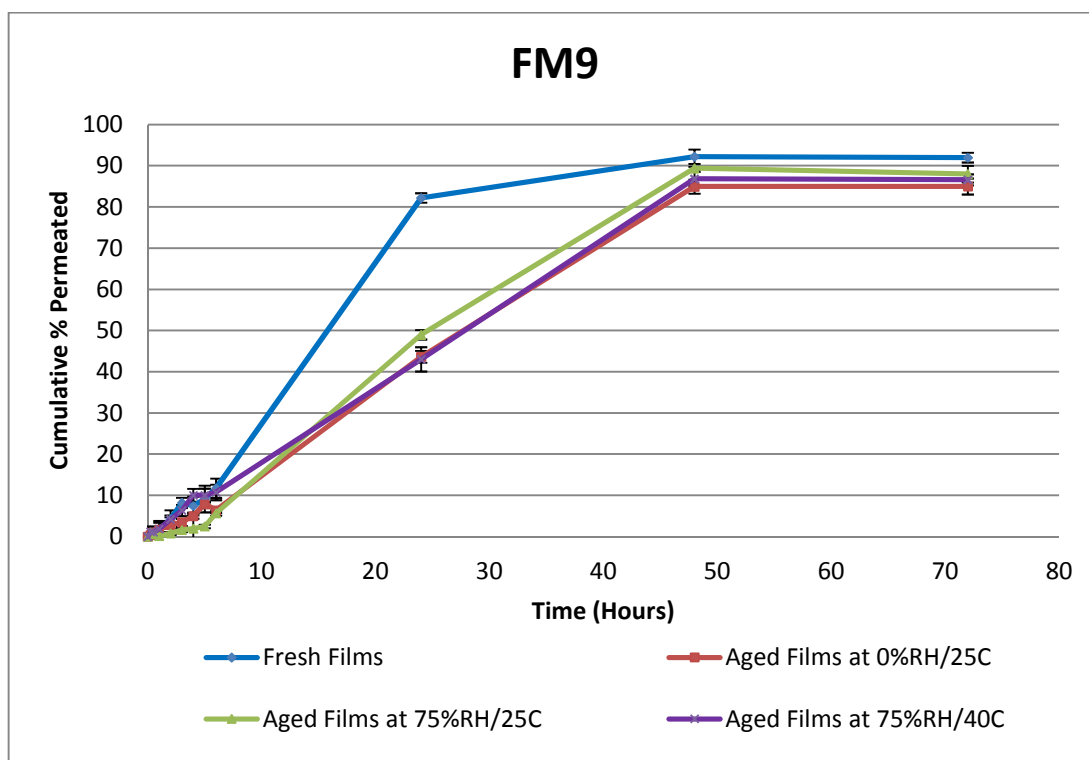
**Table 7.15: A summary of the correlation between the temperatures associated with disappearance of the spherulites (\*) and rod-shape crystals (\*\*) as obtained from hot stage microscopy and the melting temperature at the peak ( $T_{m(p)}$ ) and at the baseline ( $T_{m(b)}$ ) of the last peak recorded from MTDSC reversing heat flow signals (aged FM10 films)**

In summary, ageing under all conditions enhanced recrystallization of both ibuprofen and Gelucire 44/14 in the loaded films of the FM9 and FM10 compositions as indicated by MTDSC and HSM findings. A humidity level of 75%RH is sufficient to solubilise Gelucire 44/14 crystals and this effect was enhanced at a higher temperature of 40°C. This moisture level was also sufficient to reduce the glass transition temperatures associated with the tested samples. PXRD data were useful for qualitative assessment of the degree of crystallinity of Gelucire in the tested samples. For example, fresh samples of FM10 are now considered to have both crystalline Gelucire 44/14 and ibuprofen as related to the carrier FM-B system and supported by MTDSC broad peaks, though PXRD revealed only ibuprofen crystals. After ageing, the X-ray diffractograms of the FM10 samples indicated recrystallization of both ibuprofen and Gelucire 44/14, possibly due to increase of the amount of recrystallized Gelucire 44/14, which become easier to be detected. The increase of extent of recrystallization was observed clearly in the reversing heat flow signals for samples stored under dry conditions, where the effect of Gelucire 44/14 solubilisation is precluded. Thus, it could be inferred that fresh samples of FM10 contained approximately less than 5% of crystalline Gelucire 44/14 and upon ageing this percent level increased and made crystalline Gelucire 44/14 detectable, whereby 5% value represents the common detection level of the crystalline material by the PXRD technique (Shah et al., 2006). Also it could be concluded that ibuprofen is the main constituent to cause phase separation and to recrystallize, in addition to ageing impact which will be manifested as an increase in the extent of phase separation where Gelucire 44/14 crystals are fully developed and detectable.

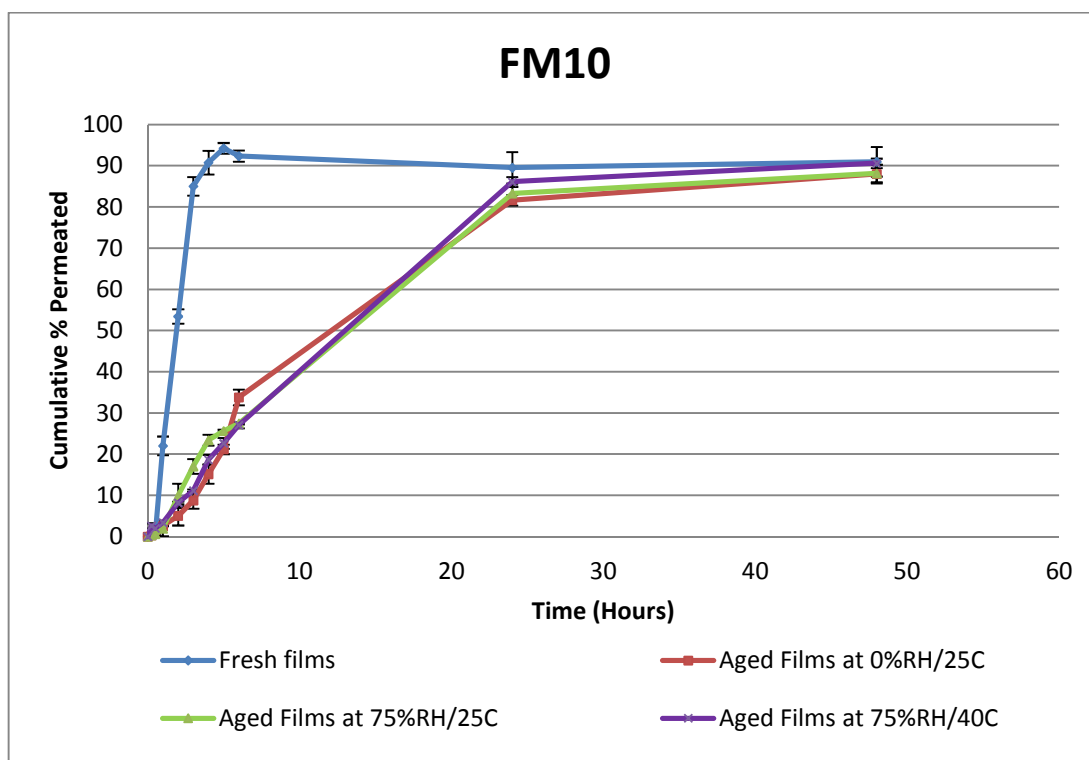
However, the question remains how that will be reflected on the permeation profiles. This knowledge will be useful not only to evaluate the efficiency of these systems as function of their stability, but also to determine the mechanism of the drug release in these devices as described in section 7.4.2.2. Therefore, the release profiles of the FM9 and FM10 will be discussed in the following section wherein the combined effect of ageing and hydration are assessed using Franz-type diffusion studies.

#### 7.5.2.3 *In vitro* permeation studies of ibuprofen from Eudragit RS PO/Gelucire 44/14-based extruded films: Effect of ageing

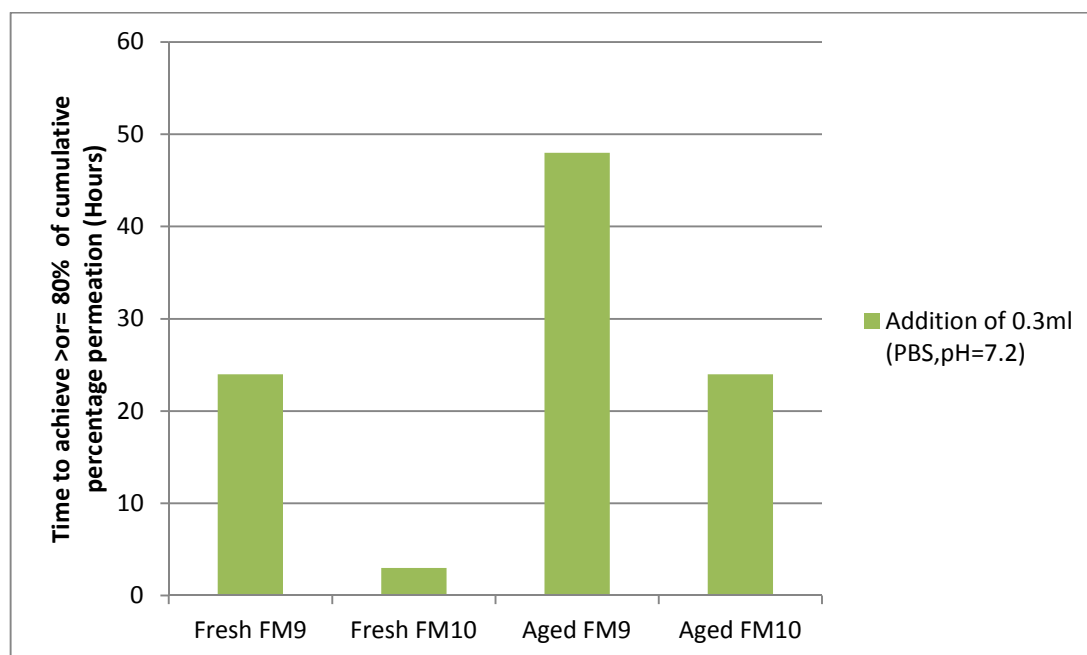
In Chapter 6, the permeation-enhanced profiles of the ibuprofen from FM9 and FM10 films were achieved by hydration. Thus the hydration level associated with highest permeation of the ibuprofen was used here to assess the permeation behaviour of the aged films in comparison with the fresh samples. As demonstrated in Figure 7.52 and Figure 7.53, the aged films of each tested formula showed similar permeation behaviour to each other regardless of their storage conditions. For example, samples of FM9 system stored under dry condition (0%RH/25°C) exhibited a similar release profile compared to the samples stored under 75%RH/25°C. Moreover, the aged films of the FM9 formula manifested a slower permeation profile in comparison to the fresh samples. This retardation was even more dramatic for the aged films of the FM10 compared to their respective fresh films. Figure 7.54 addresses the observed retardation using the time needed to achieve 80% or higher of the percent cumulative permeation *in vitro*. One day was needed to achieve this cumulative percentage of permeation for fresh FM9 formulation and two days for the aged ones. For those containing higher level of Gelucire 44/14 i.e. FM10 films, the aged formulations needed one day whereas the fresh films only three hours.



**Figure 7.52: Ibuprofen diffusion (permeation) profiles from hot melt extruded films of aged FM9 system (1:6:3 ratio of Gelucire 44/14:Eudragit RS PO:ibuprofen) for one month at different conditions and compared to the fresh samples, tested approximately at 32°C and permeated across silicone membrane into phosphate buffer solution (pH=7.2) at 37±0.1°C. Aliquot 0.3 ml of this solution was applied into each film to achieve hydration. Each data point represents the mean±S.D. of no less than three measurements**



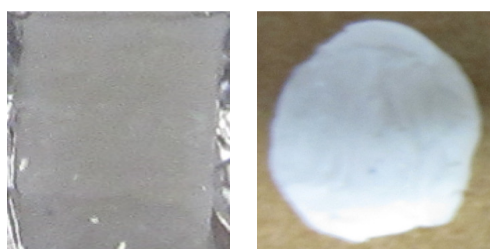
**Figure 7.53: Ibuprofen diffusion (permeation) profiles from hot melt extruded films of aged FM10 system (2:5:3 ratio of Gelucire 44/14:Eudragit RS PO:ibuprofen) for one month at different conditions and compared to the fresh samples, tested approximately at 32°C and permeated across silicone membrane into phosphate buffer solution (pH=7.2) at 37±0.1°C. Aliquot 0.3 ml of this solution was applied into each film to achieve hydration. Each data point represents the mean±S.D. of no less than three measurements**



**Figure 7.54:** The time corresponding to 80% or higher of the cumulative percentage permeation of ibuprofen from the hot melt extruded films of aged FM9 (lower content of Gelucire 44/14) and FM10 (higher content of Gelucire 44/14) systems for one month at different conditions and compared to their respective fresh samples, tested approximately at 32°C and permeated across silicone membrane into phosphate buffer solution (pH=7.2) at 37±0.1°C. Aliquot 0.3 ml of this solution was applied into each film to achieve hydration

These observations suggest common feature(s) which led to the similarity of the permeation profiles of these aged films on one hand. On the other hand they implied that a different environment caused the permeation delay with respect to the fresh films. As shown in the previous section (7.5.2.2), aged films of FM9 and FM10 systems contain both crystalline ibuprofen and Gelucire 44/14. Therefore, it would be difficult to ascribe the cause for this slow permeation to one of these materials. However, we know now that fresh films of FM10 contain these materials in crystalline form and still achieve very fast release after being hydrated with 0.3 ml level. It is also believed that these films upon ageing will contain higher fraction of crystalline Gelucire 44/14 of 5% or higher as assumed from PXRD evaluation. This suggests that crystalline Gelucire 44/14 might play a major role for slowing down the permeation or ‘controlling’ the release regardless of the physical state of the ibuprofen. Furthermore, the dramatic change of the cumulative amount permeated in the aged films of FM10 system in relation to the fresh films was also associated with different appearance of the samples after the test.

In other words, the fresh films hydrated with 0.3 ml or 0.14 ml as shown in Chapter 6 and tested for their permeation were seen to be homogenised with the applied solution for hydration to form liquid-like emulsion. Whereas the aged films (rectangular shape) swell and jellified, adapting the shape of the diffusion area (circular shape) in a like manner to the hydrated fresh or aged FM9 films without being transformed into a liquid-like emulsion (Figure 7.55). Therefore, the suggested dispersion of the drug is less likely to be as efficient as in the liquid state, which might affect the release rate. Consequently, it could be speculated that the presence of more fraction of Gelucire 44/14 crystals may adversely affect the speed of the release and subsequent permeation, which means that the drug release mechanism is highly expected to be carrier-controlled.



(A) Before the test (B) After the test

**Figure 7.55: Representative photographs of the aged FM10 films demonstrating shape change appearance seen before (A) and after (B) the permeation study using Franz-type diffusion cells with applied hydration volume of 0.3 ml PBS (pH=7.2)**

Additionally, the release mechanism of the studied films can be described using model fitting as detailed in Chapter 5. As seen in Table 7.16, the permeation profiles were fitted to different kinetic models, where the correlation coefficient,  $R^2$ , was used to assess the fit of a model equation, so the ‘best’ model would be the one with the highest  $R^2$  value. Of these models, the first order kinetic model seems to prevail in the permeation profiles of all the tested hydrated films, whether they are fresh or aged samples.

Used Kinetic model	First order model	Zero order model	Higuchi square-root of time model
Tested sample (Hydrated with 0.3 ml PBS, pH=7.2)	$R^2$	$R^2$	$R^2$
(A) FM9 Films			
Fresh films	0.9741	0.8156	0.9108
Aged films at 0%RH/25°C	0.9653	0.9435	0.9414
Aged films at 75%RH/25°C	0.9607	0.9309	0.9262
Aged films at 75%RH/40°C	0.9696	0.9450	0.9533
(B) FM10 Films			
Fresh films	0.9742	0.2198	0.4133
Aged films at 0%RH/25°C	0.9795	0.8636	0.9381
Aged films at 75%RH/25°C	0.9890	0.8563	0.9521
Aged films at 75%RH/40°C	0.9801	0.8721	0.9416

**Table 7.16: Fit correlation coefficients ( $R^2$ ) of different applied kinetic models for the permeation profiles of the FM9 and FM10 films tested after ageing at different conditions for one month and compared to the fresh films**

The power model was used to give further insight into the involved release mechanism(s) using the measured release exponent as shown in Table 7.17. For all the aged films of FM9 system, the release was described as ‘anomalous’, wherein both swelling and diffusion mechanisms are expected to control the release while their fresh films are controlled mainly by swelling as known by case-II transport. The proximity of the release exponent values; however, suggest that ageing did not cause appreciable change of the release mechanism as compared to the fresh samples and overall, swelling is believed to contribute to the drug release from these matrices (fresh or aged).

Characterisation of the aged films of the FM10 films, where a higher amount of Gelucire 44/14 is incorporated, showed a tendency to release ibuprofen by swelling and relaxation i.e. super case-II transport mechanisms, similar to the fresh samples except for the samples aged under 75%RH /40°C. Alternatively, the release from these samples was predicted in this model to be governed by swelling and diffusion i.e. anomalous. This is possibly associated with their storage conditions, as a high temperature of 40°C might be sufficient for these

systems to cause the relaxation of the polymeric chains and lipid material for one month, and after testing with the a set temperature in the donor chamber of the diffusion cells (approximately 32°C) the samples would be expected to show minimal relaxation to control the release which occurs otherwise significantly for other aged samples that has been stored at 25°C.

Kinetic model		Korsmeyer-Peppas model (Power law)	
Tested sample (Hydrated with 0.3 ml PBS, pH=7.2)	$R^2$	Release exponent (n)	Expected release mechanism
(A) FM9 Films			
Fresh films	0.9253	1.00	Case-II transport
Aged films at 0%RH/25°C	0.9648	0.95	Anomalous transport
Aged films at 75%RH/25°C	0.9533	0.94	Anomalous transport
Aged films at 75%RH/40°C	0.9664	0.86	Anomalous transport
(B) FM10 Films			
Fresh films	0.9538	2.52	Super case-II transport
Aged films at 0%RH/25°C	0.9753	1.31	Super case-II transport
Aged films at 75%RH/25°C	0.9780	1.51	Super case-II transport
Aged films at 75%RH/40°C	0.9133	0.85	Anomalous transport

**Table 7.17: Interpretation of the measured release exponents from the power law model and their correlation coefficients ( $R^2$ ) for the permeation profiles of the FM9 and FM10 films tested after ageing at different conditions for one month and compared to the fresh films**

If we have a closer look at the *in vitro* permeation profiles of the aged films of both FM9 and FM10 systems, there appear to be an interesting implication in the associated delayed release compared to the fresh films. If we link figures from Figure 7.52 through to Figure 7.54, we can see that the majority of the drug released (80% or higher) from the fresh and aged films is associated with steady state release phase demonstrating ‘zero order’ release. The fitness coefficients of zero order model for this part was shown to be satisfactory as illustrated in Table 7.18. This phase is followed by plateau or gradual release during the rest time, thereby the whole release phase could be characterised preferably by simultaneous mechanisms of



release i.e. zero order followed by first order kinetic. As the aged samples exhibited a longer period of this nearly zero order release, the subsequent absorption from these samples would be expected to be concentration independent, providing, in theory, predictable uniform drug release for a longer time than fresh samples.

Kinetic model	Zero order model	
Tested sample (Hydrated with 0.3 ml PBS, pH=7.2)	$R^2$	Phase interval (Hours)
(A) FM9 Films		
Fresh films	0.9817	0-24
Aged films at 0%RH/25°C	0.9971	0-48
Aged films at 75%RH/25°C	0.9887	0-48
Aged films at 75%RH/40°C	0.9990	0-48
(B) FM10 Films		
Fresh films	0.9839	0-3
Aged films at 0%RH/25°C	0.9682	0-24
Aged films at 75%RH/25°C	0.9710	0-24
Aged films at 75%RH/40°C	0.9925	0-24

**Table 7.18: Fit correlation coefficients ( $R^2$ ) of the zero order model describing the first phase of the permeation profiles of the FM9 and FM10 films tested after ageing at different conditions for one month and compared to the fresh films**

Overall, ageing of either FM9 or FM10 extruded films for one month at varying conditions, between low (dry) to high relative humidity with different temperatures, resulted in similar permeation profiles which are notably lower than their corresponding fresh films. The data relating to the FM10 films is believed to shed the light on the possible role of recrystallized Gelucire 44/14 as a matrix which can act to control the release of the ibuprofen from the studied films. It can also be observed that the aged films carry promising behaviour in the release in terms of kinetics, through achieving a steady-state release of the drug for a longer time than the equivalent fresh samples.

## 7.6 Conclusions

The aim of the work described in this chapter was to continue studying the extruded films based on Eudragit RS PO with Gelucire 44/14 but without ibuprofen to specifically address their role as promising carrier systems for potential transdermal drug delivery activated by hydration. Thus with the objective to further understanding their properties, the characterisation of solid state structure was carried out in section 7.2. cDSC and MTDSC allowed prediction of miscibility between Eudragit RS PO and Gelucire 44/14 on the basis that Eudragit RS PO lowered the melting enthalpy of Gelucire 44/14 during heating of their physical mixes at the used concentrations. MTDSC, PXRD and SEM results confirmed solid solution formation of the extruded films containing lower level of Gelucire 44/14 i.e. FM-A system, whereas at higher level of this lipid i.e. FM-B system, a molecular dispersion of Gelucire 44/14 in the Eudragit RS PO as a solid dispersion was formed as detected by MTDSC and supported by SEM investigations.

In the light of these results ATR-FTIR was used in section 7.3 to reveal the nature of molecular interaction that could exist between these components. Characteristic bands of the Gelucire 44/14 in Eudragit RS PO have shown different intensities as indicated from changes in the calculated relative percentage areas under their spectra after thermal treatment and extrusion. These changes were explained by three possible hypotheses, namely, change in transition dipole, change in optical properties and migration of the alkyl groups and no evidence of significant interactions was revealed. ATR-FTIR could differentiate between the crystalline and amorphous nature of Gelucire 44/14 based on the lack of structural uniformity associated with the amorphous material.

A further preliminary visual observation of the physical mixtures of Gelucire 44/14 in Eudragit RS PO treated thermally was undertaken using HSM. Affinity between these components at the compositions of the FM-A and FM-B formulae were indicated, through formation of clear miscible blends simulating to a limited degree the extrusion process. Section 7.4 allows us to reveal the sorption behaviour of these ‘unloaded’ films using DVS. An increase of water uptake as a function of increasing the level of the Gelucire 44/14 was observed. A specific emphasis was placed on the changes associated with the hydration of these carrier systems using *in vitro* model (Franz cells) under occlusive conditions and using dissolution test. TGA, MTDSC, PXRD, SEM, PLM and ATR-FTIR were used to track these changes. The unloaded extruded films showed surface imperfections, possible leakage of the Gelucire 44/14 into their surfaces and softening of the films accompanied with appreciable

swelling of the matrices after being hydrated. It could therefore be inferred that this enhanced mobility of the materials, indicated by lowering of the glass transition temperature of the studied systems (softening), and the soluble parts of the Gelucire 44/14 caught out into the surfaces of these films (leakage) and formation of the cracks as consequences of hydration, could lead to creating paths for the release of the active ingredient and its solubilisation when loaded in these vehicles. The combined techniques strategy used here to probe these changes showed that MTDSC and ATR-FTIR can be better techniques to reveal the crystalline Gelucire 44/14 in comparison to the PXRD method.

A fundamental issue regarding the development of these carrier systems for extended applications for other medications is the physical stability which was detailed in section 7.5. Short term storage at different humidity levels and temperatures showed molecular arrangement changes of these systems. While FM-A systems showed a limited degree of Gelucire 44/14 crystallization and formation of a solid dispersion as supported by SEM and ATR-FTIR results, an extended phase separation was observed for the originally solid dispersed FM-B systems supported by MTDSC, SEM and ATR-FTIR findings. High humidity of 75%RH at room temperature is believed to aid in solubilisation of crystalline Gelucire 44/14 and reduction in the observed glass transition temperature with subsequent softening. The combination of this humidity level with higher temperature of 40°C further aided in the solubilisation of the Gelucire 44/14. This phenomenon is well suited with the trend of enhanced water uptake of these films as a function of increased temperature as found by DVS investigations.

If one considers the variations which impacted the stability of these formulations, it would form a good basis for understanding their behaviour when loaded with the drug and aged under the same conditions. Thus aged systems containing ibuprofen were characterised using MTDSC, PXRD, TGA and HSM techniques and compared to their aged carrier systems (unloaded films). HSM was used to get insight into the nature of the broad melting peaks detected from MTDSC profiles of the aged loaded films, and it was demonstrated that the drug could be molten over a broad range of temperatures with concomitant melting of Gelucire 4/14 crystals. In light of these findings and in relation to the aged carrier systems, it was concluded that aged loaded FM9 and FM10 formulations which contain 30%w/w ibuprofen and used FM-A and FM-B carrier systems, respectively, had crystalline materials of ibuprofen and Gelucire 44/14.

PXRD indicated the presence of crystals of this lipid in the aged FM10 films (ibuprofen Gelucire 44/14 Eudragit RS PO ratio of 3:2:5) but not in the aged FM9 films (ibuprofen Gelucire 44/14 Eudragit RS PO ratio of 3:1:6), despite being identified using other techniques. The poor sensitivity of the PXRD is precluded, providing that Gelucire 44/14 crystalline peaks were detected in the corresponding physical mixes of these formulations (FM9 and FM10). It was therefore concluded that the quantity of crystallites in the FM9 is less than in the FM10 extruded systems after ageing, falling below the detection limit of this technique (~5%). These aged extruded films were further assessed for their *in vitro* permeation behaviour using diffusion cells. The hydration level which was associated with the maximum permeation profiles from the fresh films (Chapter 6) was used to clearly indicate changes in the performance as a result of the ageing of these loaded films. It is believed that drug recrystallization did not influence the effective utilisation of the films for rapid release formulations under the used hydration level. Instead, it is more likely that recrystallized Gelucire 44/14 has a retardation effect on the release and permeation rate of the ibuprofen from these matrices after ageing. Alternatively, this influence, as described kinetically, was not assumed to be negative. This is because slow permeation profiles of the ibuprofen from these aged films were associated with prolonged steady state zero order release.

Kinetic models were also used side by side to propose possible mechanism(s) of drug release from the tested matrices. It was found that permeation profiles of these aged loaded films were best fitted to the first order release kinetics for the whole permeation profiles and more accurately as profiles composed of simultaneous zero order release followed by first order release pattern. The Power model indicated the role of swelling and relaxation in controlling the drug release. Overall, the mechanism of drug release from these devices under the influence of hydration is believed to be more related to the carrier rather than the drug. This provides promise in using these carrier systems for potential transdermal drug delivery where more control can be achieved using these carrier regardless of the physical state of the drug. Additionally, the approach used herein to release the drug rivals conventional methods for transdermal drug delivery through simple, yet effective, activation using hydration that could be created using skin occlusion.

**Chapter 8: Influence of occlusion-induced hydration on the properties of Eudragit RS PO/Gelucire 44/14 hot melt extruded systems: *in vivo* behaviour**

## 8.1 Introduction

Hydration of the stratum corneum may result from skin occlusion. The occlusion process enhances the accumulation of water diffusing from underlying tissues of the skin or resulted from secretions of eccrine sweat glands (Hurkmans et al., 1985; Taylor and Machado-Moreira, 2013). This occlusion-induced hydration often produces marked increase of skin permeation as detailed in Chapter 1. In this work, hydration is also essential to promote drug release from Gelucire 44/14-containing extruded systems as described in Chapter 6. The previous chapter discussed the physicochemical properties of Eudragit RS PO/Gelucire 44/14 extruded films and structural changes associated with the hydration of these matrices without the drug. Because these studies were conducted using an *in vitro* model, the hydration created after application to the occluded skin has not been elucidated yet. Therefore, this chapter aims to continue the study of these films to gain insight into their *in vivo* behaviour. This is essential to understand the structural changes of these matrices, which could impart in the drug release mechanism, when applied to the human skin. More specifically, the hydration resulting from occlusion may serve the dual purposes of altering skin permeability and altering the structure of the Eudragit RS PO/Gelucire 44/14 films, potentially acting as a trigger mechanism for release. It is therefore necessary to understand the manner in which occlusion, as opposed to *in vitro* hydration, may influence film structure. For this purpose, drug-free films were used, although clearly if these studies were to prove promising then a drug absorption study would be highly desirable.

## 8.2 Methodology

The hot melt extruded films were prepared from mixtures of Eudragit RS PO loaded with different levels of Gelucire 44/14 as described in Chapter 7 (section 7.2.1). FM-A extruded system containing approximately 15% w/w Gelucire 44/14, while FM-B system contains approximately 30% w/w Gelucire 44/14. These extruded films were cut manually and the dimensions were measured with an electronic digital caliper (MS092Toolzone Vernier Caliper, UK). Films of size ( $24.12 \pm 1.31 \text{ mm}^3$ ) were prepared for each system. An average film weight of ( $24.94 \pm 1.17 \text{ mg}$ ) and ( $25.85 \pm 1.45 \text{ mg}$ ) were used for FM-A and FM-B films, respectively. These films were attached to 3M Blendederm® occlusive, hypoallergenic adhesive tape measuring 5 cm by 2 cm to prepare strips. These strips were applied on dry, clean inner forearms of four healthy-skin volunteers; two males and two females (age range 28-35, mean age  $32.5 \pm 3.1$  year old). The study was divided into two parts, the first part for assessment of FM-A extruded films and the second part for FM-B extruded films. In each part four strips of these films were attached randomly on the left or right forearm of each volunteer and arranged for removal after 3, 5, 8 and 24 hours of application to the skin and occlusion by the used adhesive tape.

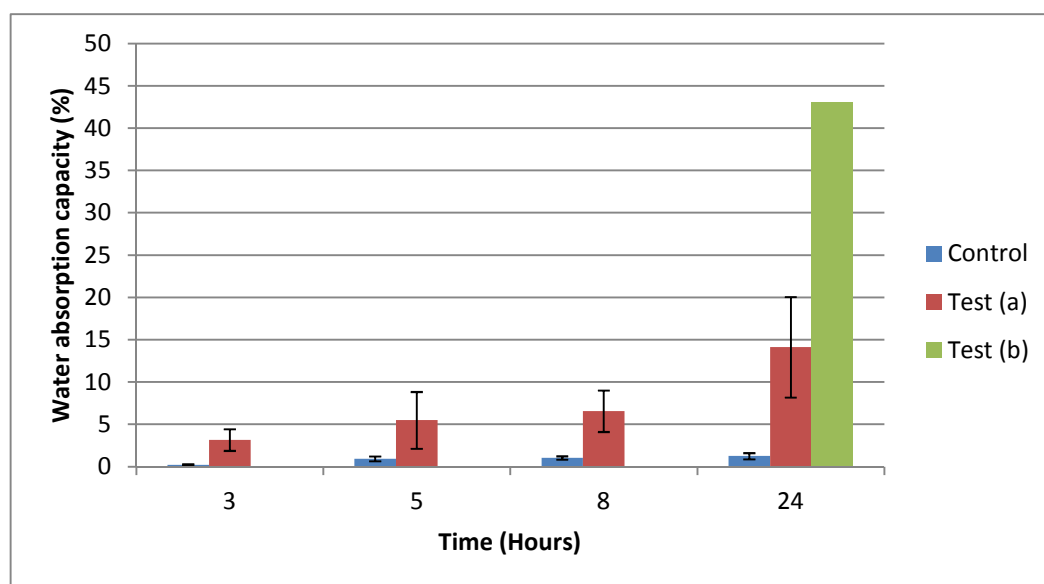
In addition, strips of these films were kept under controlled humidity condition of 75%RH at room temperature, representing control samples. Supersaturated solution of sodium chloride in distilled water was used to control humidity to a level of 75%RH at room temperature and an airtight jar was used as a storage chamber. The humidity level was checked using a hygrometer. Water absorption capacity, swelling ratio measurements and characterisation performed using MTDSC, PLM, SEM, ATR-FTIR were conducted as detailed in Chapter 7 section 7.4.2.1 for the films hydrated *in vitro* using Franz-type diffusion cells. TA-XT2 Texture Analyzer (Stable Micro system, UK) was used to assess the hardness of the investigated films. The measuring principles as well as the parameters employed were described in details in Chapter 2 (section 2.2.2.6). The faculty research ethics committee of university of East Anglia at Norwich had approved the study (enclosed in the Appendix).

### 8.3 Results and discussion

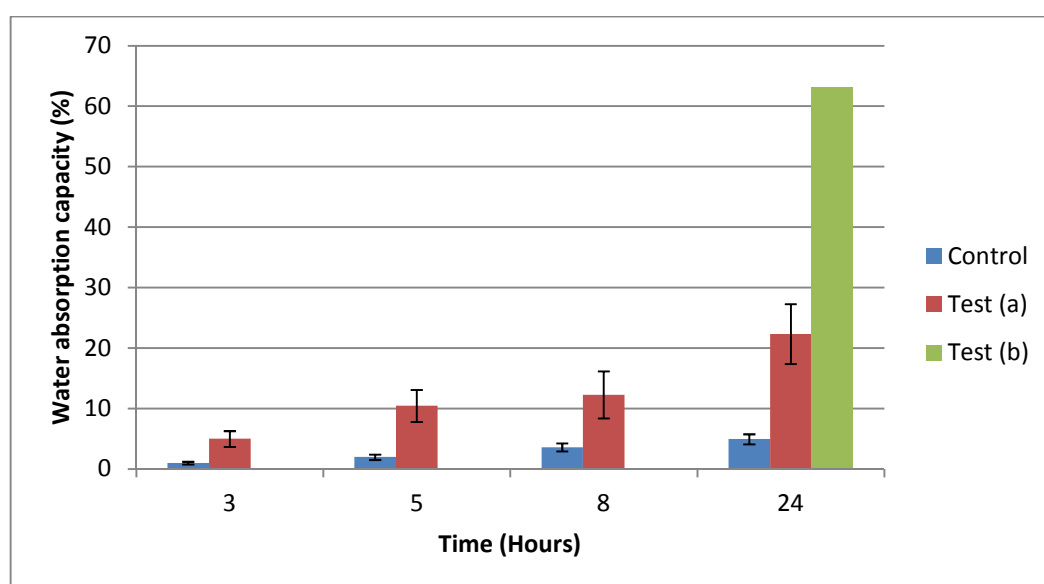
The first objective in this study was to confirm whether or not the Eudragit RS PO/Gelucire 44/14 hot melt extruded systems will be hydrated after application to the skin under occlusion. Therefore, water absorption capacities were determined for these extruded films of FM-A and FM-B systems containing approximately 15% and 30% (w/w) Gelucire 44/14, respectively. As shown in Figure 8.1 and Figure 8.2, the films of both systems absorbed water after being hydrated under the influence of skin occlusion and the percent of water absorption capacity with subsequent swelling ratio increased with increasing occlusion time and Gelucire 44/14 concentration. In comparison to the *in vitro* model (Franz cells) detailed in Chapter 7, these values were markedly less, indicating possible overhydration conditions used in Franz-type diffusion cells. On the other hand, the young age of the volunteers might produce less hydration than elderly after stratum corneum perturbation by occlusion as suggested by Roskos and Guy (1989). However, the water absorption percent and swelling ratio were higher than control samples incubated at 75%RH and room temperature, which might indicate higher relative humidity levels under skin occlusion in this study and/or warm wet conditions which enhanced water uptake properties of these films.



(A)

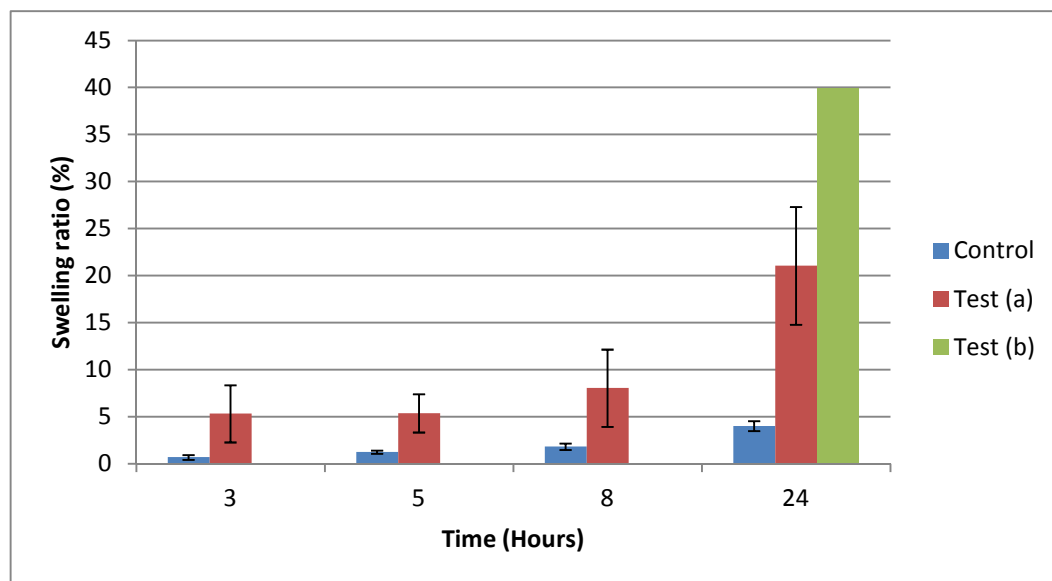


(B)

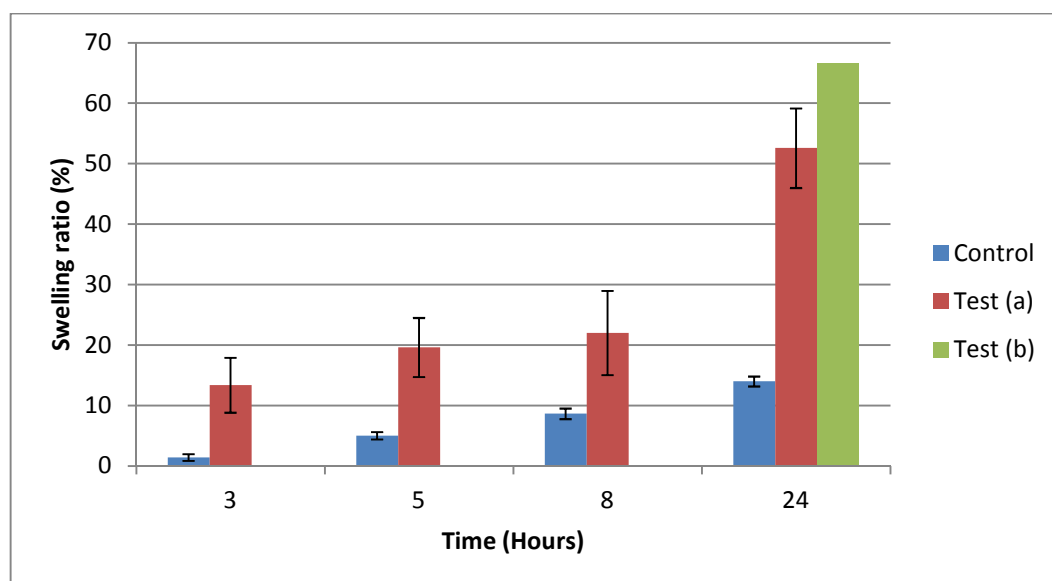


**Figure 8.1:** The percent water absorption capacity of the hot melt extruded films of (A) FM-A and (B) FM-B systems at different time intervals of hydration. Control samples: samples incubated under 75%RH/25°C. Test (a) samples: samples applied to the skin under occlusion. Test (b) samples: samples removed from Franz diffusion cells after being hydrated using PBS solution (detailed in Chapter 7). Error bars represent  $\pm$ S.D. of not less than three measurements

(A)



(B)

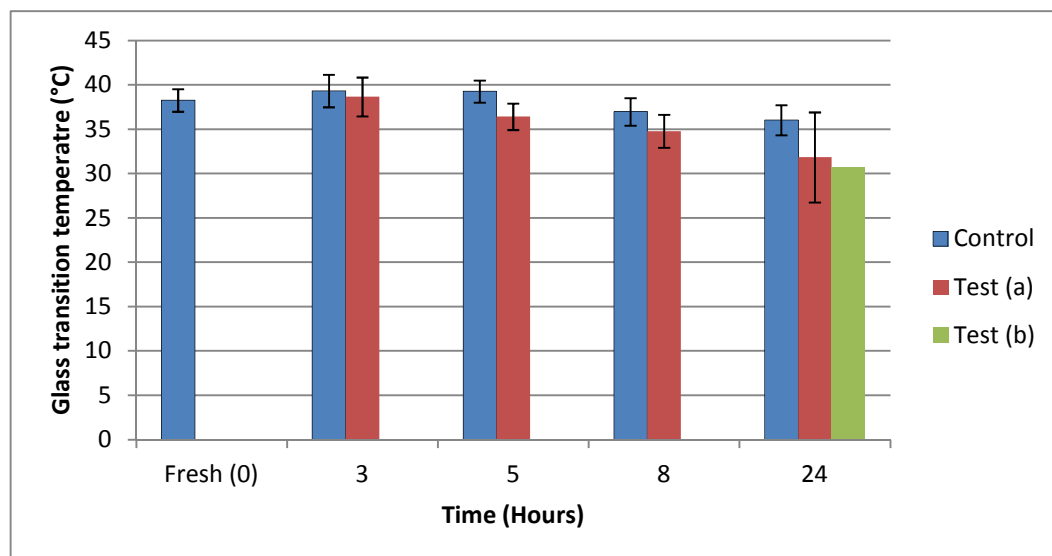


**Figure 8.2:** The percent swelling ratio of the hot melt extruded films of (A) FM-A and (B) FM-B systems at different time intervals of hydration. Control samples: samples incubated under 75% RH/25°C. Test (a) samples: samples applied to the skin under occlusion. Test (b) samples: samples removed from Franz diffusion cells after being hydrated using PBS solution (detailed in Chapter 7). Error bars represent  $\pm$ S.D. of not less than three measurements

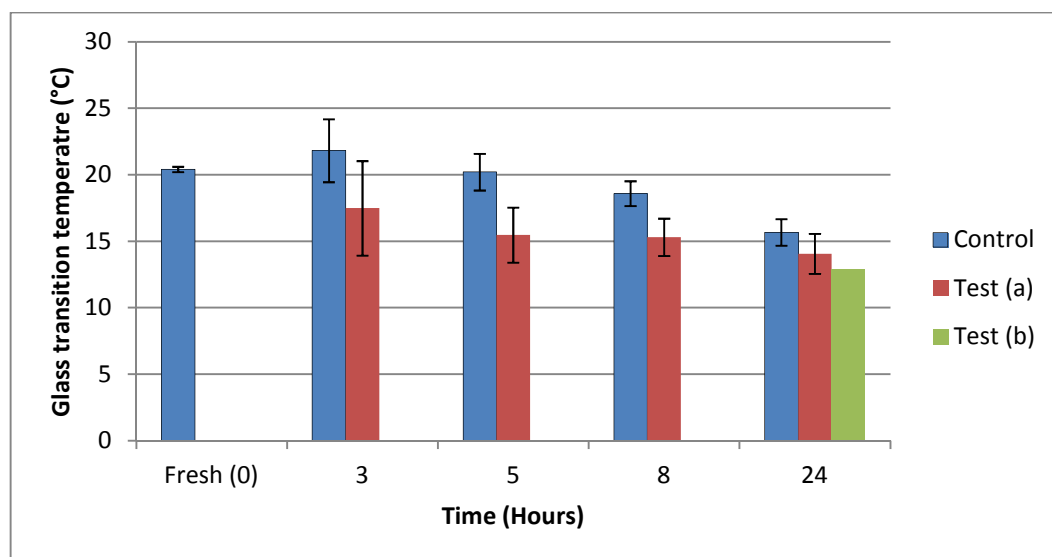
The reversing heat flow signals of the MTDSC experiment were used for the detection of glass transition temperatures (Mid-point T<sub>gs</sub>) as reported in Figure 8.3. It is clear from this figure that there is a reduction in the glass transition temperatures for both FM-A and FM-B systems over hydration time under skin occlusion. This could be explained by the water plasticization effect. However, lowering of the glass transition temperature appears to be comparable to that observed for samples tested in Franz diffusion cells (*in vitro* model), though the samples hydrated more in the latter. This observation is consistent with the one aforementioned in Chapter 7. The hydration induced glass transition temperature depression was concluded to be limited. In that discussion the values of the glass transition temperatures at the end of hydration using Franz cells and after soaking in the dissolution bath were similar. This was observed in spite of higher level of hydration after the dissolution test as indicated by water absorption capacity and swellability of the tested samples.

The total heat flow signals of the MTDSC scan were used to probe changes on the melting peaks of Gelucire 44/14, originally detected in the fresh samples of FM-B extruded system. In Figure 8.4, the melting enthalpy of the hydrated samples under occlusion was decreased over time, indicating solubilisation of water soluble Gelucire 44/14 crystals. This reduction was observed as a function of hydration level, thus the samples well-hydrated in Franz cells showed the lowest melting enthalpy value. Interestingly, control samples showed an increase of melting enthalpy. This increase of melting fraction indicates an increase of the Gelucire 44/14 recrystallization over time under storage conditions of 75%RH/25°C. This emphasizes that hydration and high temperature potentiate the solubilisation of Gelucire 44/14 as detailed in Chapter 7 and detected for samples applied to the skin under occlusion.

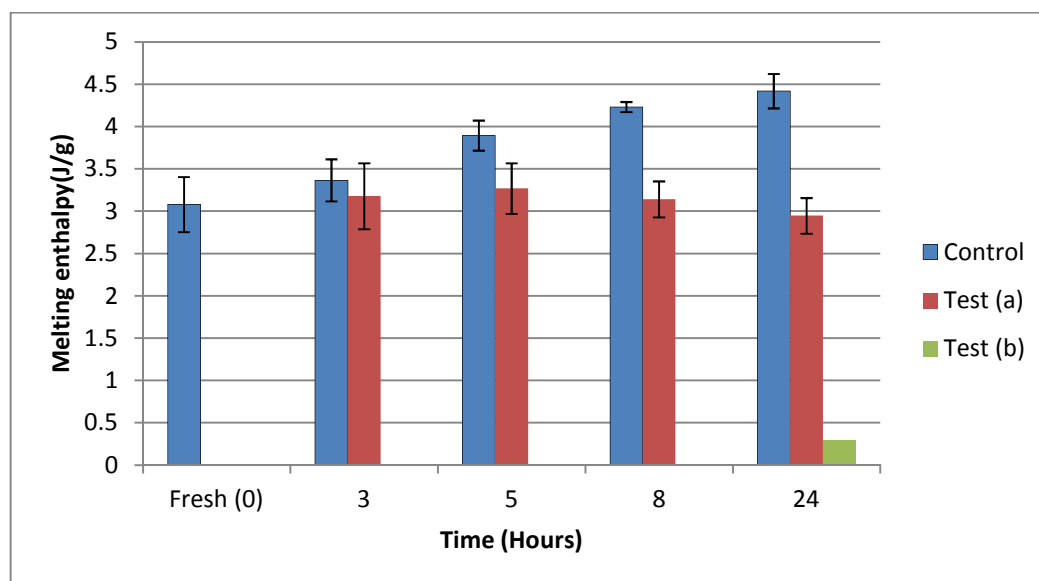
(A)



(B)

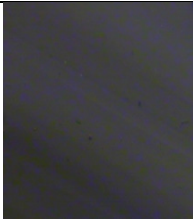
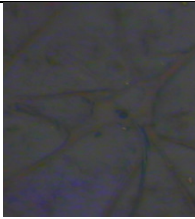
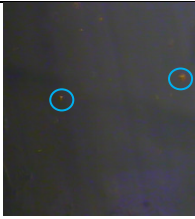
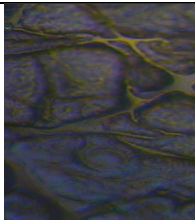

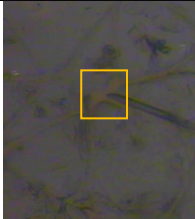
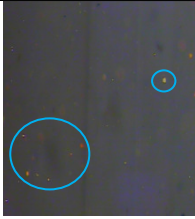
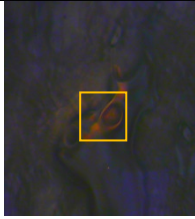

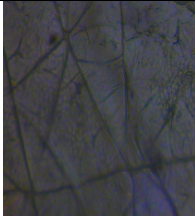

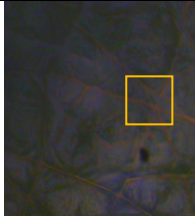

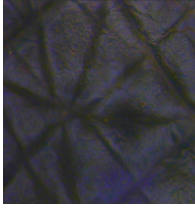
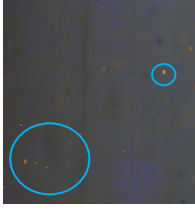
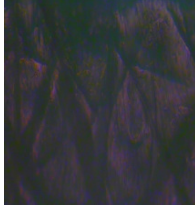


**Figure 8.3:** Glass transition temperatures detected from MTDSC reversing heat flow signals scans of (A) FM-A and (B) FM-B system at different time intervals of hydration. Underlying scan rate of  $1^{\circ}\text{C min}^{-1}$  with a modulation amplitude of  $\pm 0.265^{\circ}\text{C}$  and a period of 100 seconds. Control samples: encompass fresh sample ( $t=0$  hours) and samples incubated under 75% RH/ $25^{\circ}\text{C}$ , tested at different times. Test (a) samples: samples applied to the skin under occlusion. Test (b) samples: samples removed from Franz diffusion cells after being hydrated using PBS solution (detailed in Chapter 7). Error bars represent  $\pm$ S.D. of not less than three measurements



**Figure 8.4: Melting enthalpies detected from MTDSC total heat flow signals scans of FM-B system at different time intervals of hydration. Underlying scan rate of  $1^{\circ}\text{C min}^{-1}$  with a modulation amplitude of  $\pm 0.265^{\circ}\text{C}$  and a period of 100 seconds. Control samples: encompass fresh sample ( $t=0$  hours) and samples incubated under 75% RH/ $25^{\circ}\text{C}$ , tested at different times. Test (a) samples: samples applied to the skin under occlusion. Test (b) samples: samples removed from Franz diffusion cells after being hydrated using PBS solution (detailed in Chapter 7). Error bars represent  $\pm$ S.D. of not less than three measurements**

Occluded samples of FM-A and FM-B films were further examined using scanning electron microscopy (SEM) and polarized light microscopy (PLM) as depicted from Table 8.1 through to Table 8.3. Images photographed with PLM in Table 8.1 revealed that samples at different levels of Gelucire 44/14 concentrations captured a print of the skin. This indicates flexibility of these films after being hydrated as supported by the MTDSC findings, where the glass transition temperature reduced as a function of hydration time under occlusion. The plasticization of these films and this behaviour (flexibility) is not only important aesthetically to adapt skin irregularities upon application, but also can increase the effective contact area necessary for efficient drug delivery. In common to the samples hydrated *in vitro* (Chapter 7), the oil-like streaks were also detected on the surface of these samples and will be, similarly, further investigated using ATR-FTIR. The density of the sparkling fine-crystallite regions detected on the surface of the control sample containing higher level Gelucire 44/14 (FM-B) increased as a function of hydration time supporting MTDSC results.

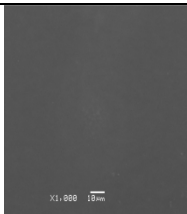
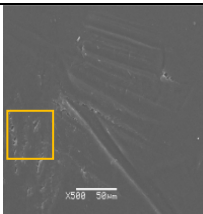
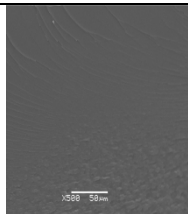
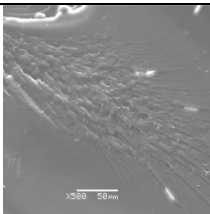
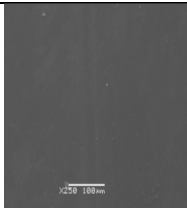
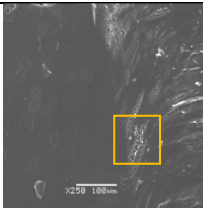
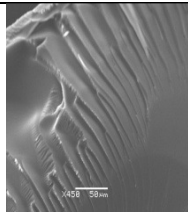
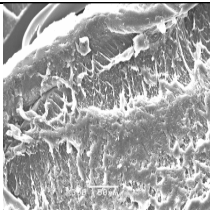
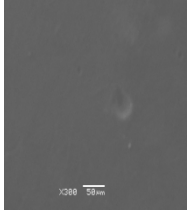
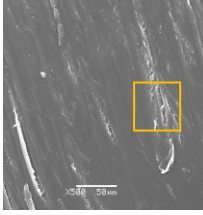
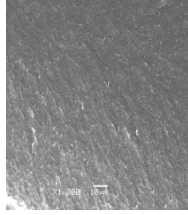
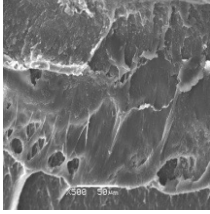
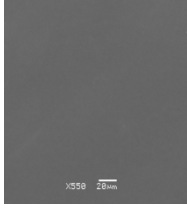
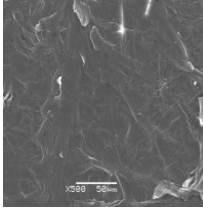
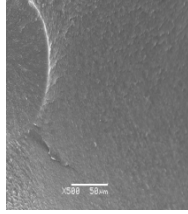
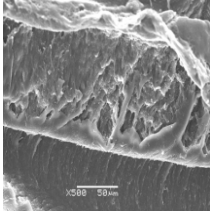
	FM-A extruded films		FM-B extruded films	
Time (Hours)	Control	Test	Control	Test
3				
5				
8				
24				

**Table 8.1: Representative polarized light microscope images capturing the surface appearance of the FM-A and FM-B extruded films, occluded on the skin at various time points in comparison to their corresponding control samples incubated at 75%RH/25°C. Examples on the observed oil-like streaks are enclosed by orange squares, and fine crystallites by blue circles. ( — ) Represents a scale bar that corresponds to 300  $\mu$ m**

Scanning electron microscopy of samples of FM-A and FM-B extruded films containing approximately 15% (w/w) and 30% (w/w) Gelucire 44/14 in Eudragit RS PO, respectively, revealed that the hydrated films printed the shape of the skin cells similar to the PLM findings, supporting their elasticity. More importantly, these films developed micro-cracks on their surfaces and swelled as observed from their corresponding cross sections as shown in Table 8.2 and Table 8.3. This is consistent with previous chapter observations *in vitro*. In brief, it was speculated that hydration of these films with subsequent softening, aids Gelucire

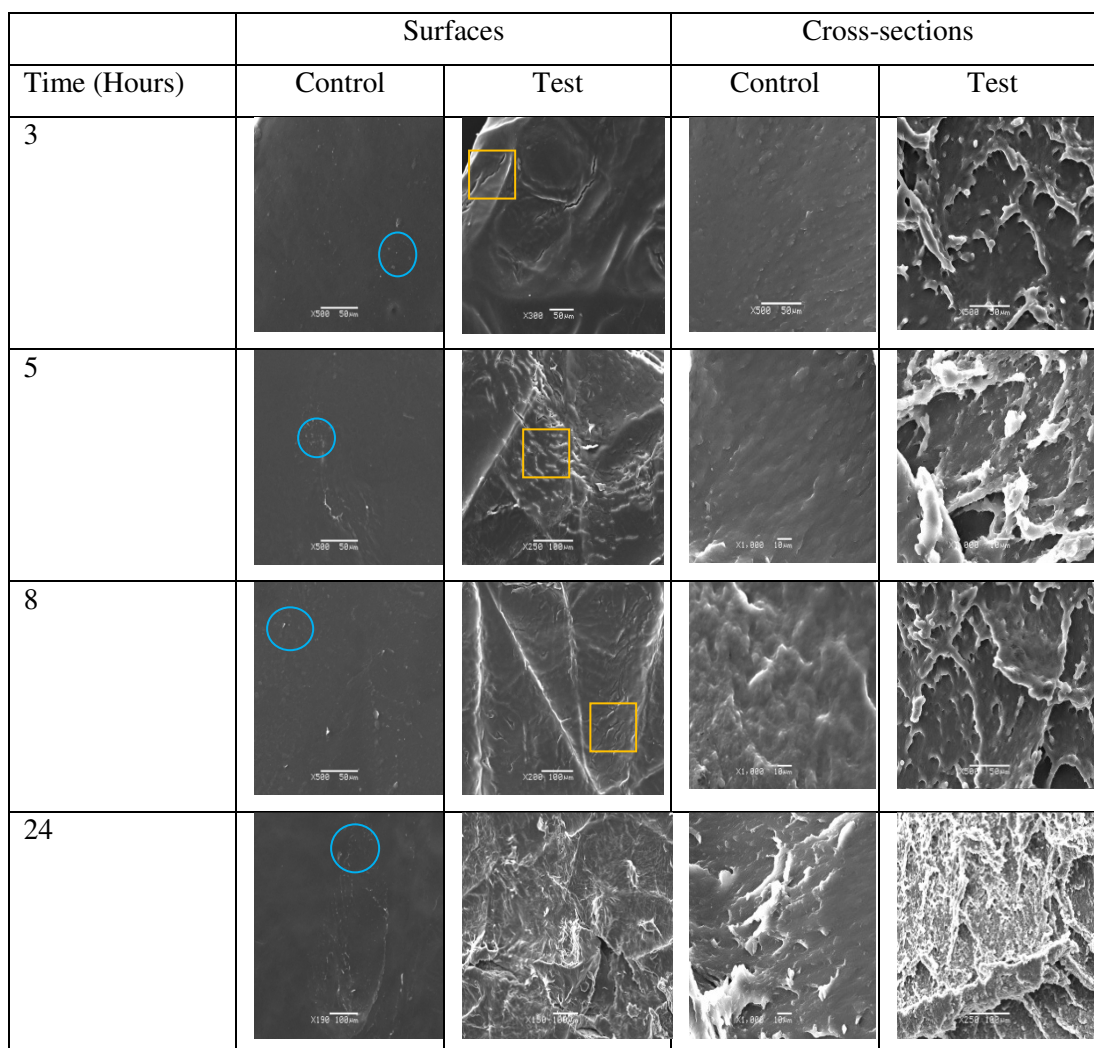
44/14 mobility and leakage into the surface, wherein solubilised material leaving the films might contribute to the formation of the surface imperfections or micro-cracks.

It is noteworthy that the control samples of FM-B films showed swelling signs in their cross sections after 8 hours of occlusion, indicating high affinity of water absorption as a function of increasing the level of this lipid compared to the control samples of FM-A films. Sparse crystallites on the surfaces of these samples were also detected, similar to the PLM findings and supported by MTDSC results.

	Surfaces		Cross-sections	
Time (Hours)	Control	Test	Control	Test
3				
5				
8				
24				

**Table 8.2: Representative SEM images showing surfaces and cross-sections of the FM-A extruded films (circa 15 % w/w Gelucire 44/14), occluded on the skin at various time points and compared to the control samples incubated at 75%RH/25°C. Examples on the observed micro-cracks are enclosed by orange squares**

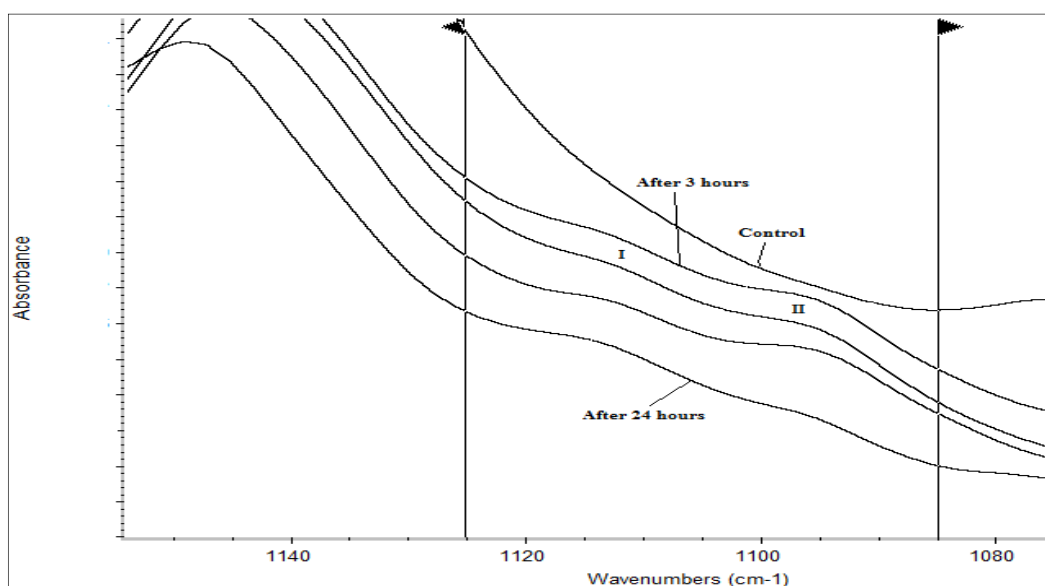




**Table 8.3: Representative SEM images showing surfaces and cross-sections of the FM-B extruded films (circa 30% w/w Gelucire 44/14), occluded on the skin at various time points and compared to the control samples incubated at 75%RH/25°C. Examples on the observed micro-cracks and small crystallites are enclosed by orange squares and blue circles, respectively**

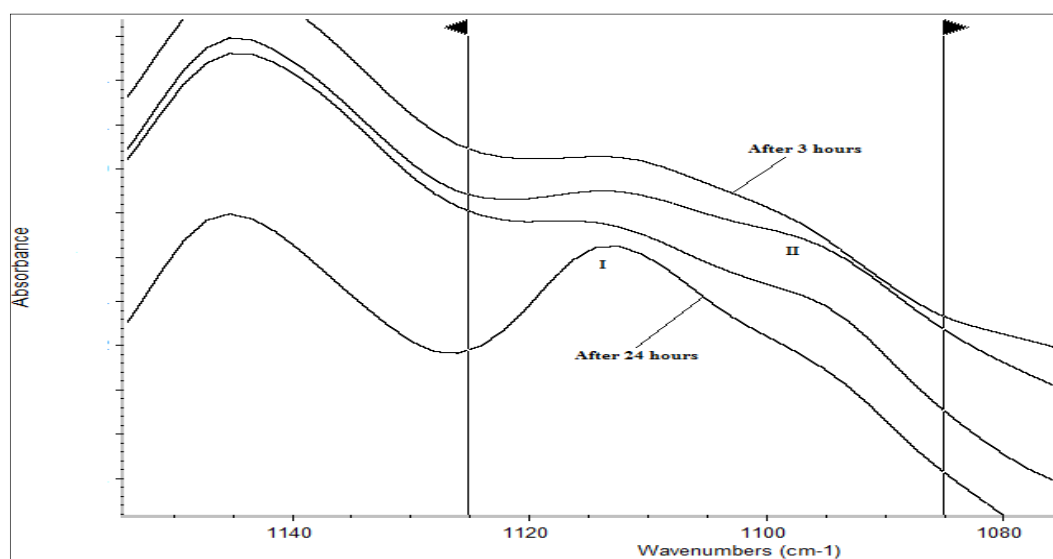


Previous investigation in Chapter 7 has demonstrated the utility of the ATR-FTIR to distinguish crystalline Gelucire 44/14 in the extruded samples at two characteristic absorbance peaks around  $1107\text{ cm}^{-1}$  and  $1347\text{ cm}^{-1}$ . Thus the occluded samples of FM-A films and FM-B films were examined accordingly and compared to their corresponding control samples stored at high humidity of 75%RH at room temperature. The Gelucire 44/14 within extruded films with FM-A composition (circa 15% w/w G44/14) showed no signs of crystallinity, as indicated from flattened and broadened peaks at the aforementioned locations in the ATR-FTIR spectra (data not shown here). This complies with previous MTDSC, PLM and SEM findings. However, around  $1107\text{ cm}^{-1}$  peak there was a small change for the samples applied to the skin as shown in Figure 8.5. In this figure, it was noticed that while control samples exhibit almost smeared smooth line in this region at different times, the occluded samples start to show shoulders around this region which differentiate into two parts over hydration time. The first shoulder at  $1107\text{ cm}^{-1}$  is very diffused and broadened, precluding possible crystallinity. The second shoulder is more differentiated over time, occurred around  $1096\text{ cm}^{-1}$  and denoted as (II) in the ATR-FTIR spectra. This region dissipated after 24 hours of occlusion and it was assigned in previous chapter to the absorbance band related to palm oil, from which Gelucire is derived. This could explain the oil-like streaks observed on the surface of these samples.

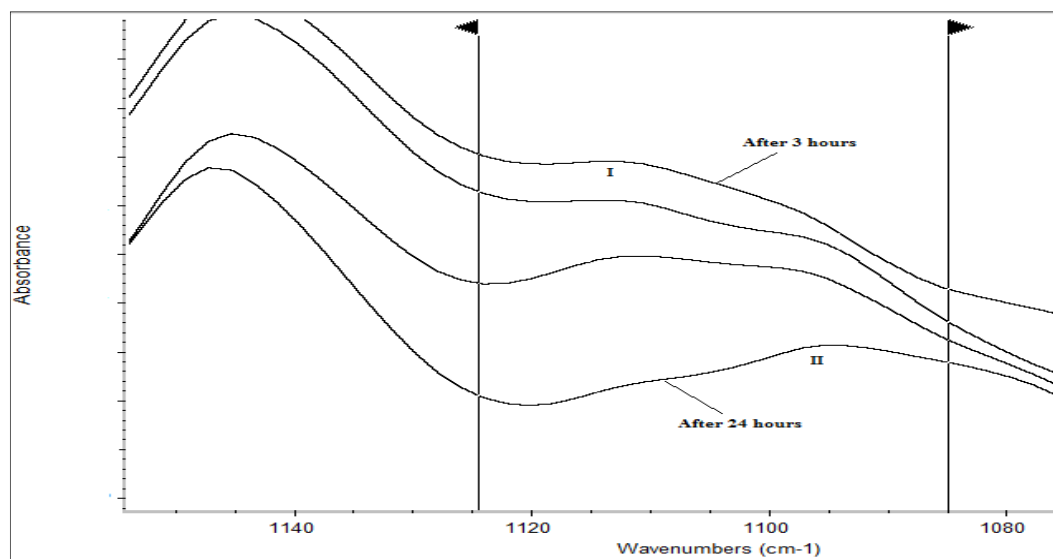


**Figure 8.5:** Overlay plot of representative ATR-FTIR spectra of Gelucire 44/14 inside FM-A extruded films (Gelucire 44/14 Eudragit RS PO ratio of 1:6) at different occlusion times arranged in ascending order (3-24 hours) and compared to the Gelucire 44/14 spectrum in the equivalent control extruded film incubated at 75%RH/25°C. (I) and (II) represent shoulders around 1107 cm<sup>-1</sup> and 1096 cm<sup>-1</sup>, respectively. These spectra were obtained through subtraction of Eudragit RS PO spectra

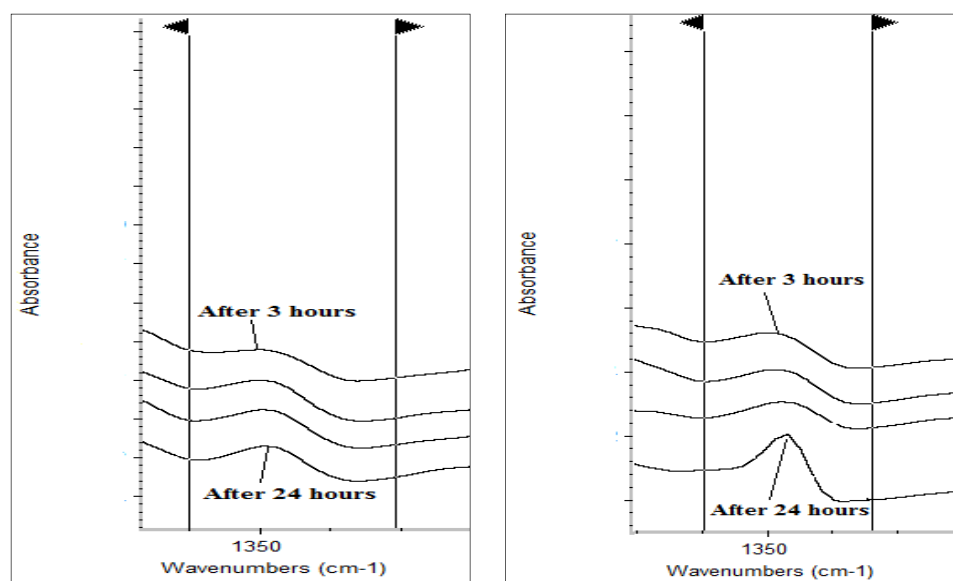
Gelucire 44/14 in FM-B extruded films (circa 30% w/w G44/14) showed an increase of the crystallinity over time of incubation at 75%RH/25°C as shown in Figure 8.6 and Figure 8.8. In these figures, the aforementioned sensitive absorbance bands for Gelucire 44/14 crystallization become more distinct, indicating an increase in the structural uniformity associated with crystalline material. This conforms to previous MTDSC, PLM and SEM findings. In contrast, occluded films applied to the skin showed a decrease of the crystallinity over time, as illustrated in Figure 8.7. In this figure, the peak around 1107 cm<sup>-1</sup> denoted as (I) almost flattened to the baseline after 24 hours of occlusion, indicating solubilisation of the Gelucire 44/14 crystals. This was concomitant with an increase of the oil-related peak around 1096 cm<sup>-1</sup> and observed on the surface of these films using PLM. However, these samples retained some crystalline regions, as indicated by well-defined absorbance peaks around 1347 cm<sup>-1</sup> presented in Figure 8.8. This could be attributed to lower level of hydration achieved after skin occlusion that was not sufficient to solubilise these crystals over the time of the experiment i.e. 24 hours.



**Figure 8.6:** Overlay plot of representative ATR-FTIR spectra of Gelucire 44/14 inside control extruded samples of FM-B composition (Gelucire 44/14 Eudragit RS PO ratio of 2:5) at different times of storage at 75% RH/25°C arranged in ascending order (3-24 hours). (I) and (II) represent shoulders around 1107 cm<sup>-1</sup> and 1096 cm<sup>-1</sup>, respectively. These spectra were obtained through subtraction of Eudragit RS PO spectra



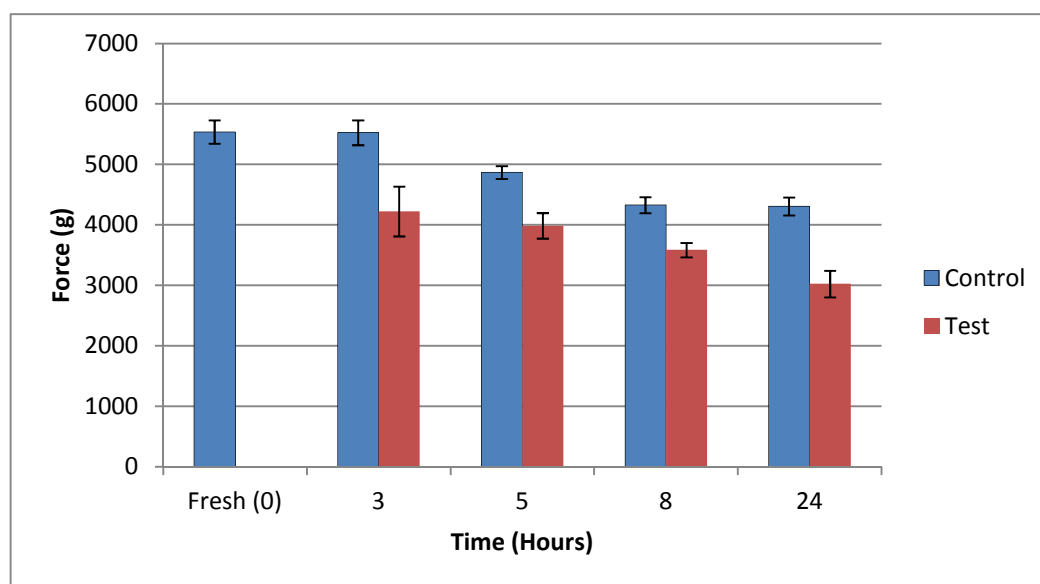
**Figure 8.7:** Overlay plot of representative ATR-FTIR spectra of Gelucire 44/14 inside FM-B extruded films (Gelucire 44/14 Eudragit RS PO ratio of 2:5) at different occlusion times arranged in ascending order (3-24 hours). (I) and (II) represent shoulders around 1107 cm<sup>-1</sup> and 1096 cm<sup>-1</sup>, respectively. These spectra were obtained through subtraction of Eudragit RS PO spectra



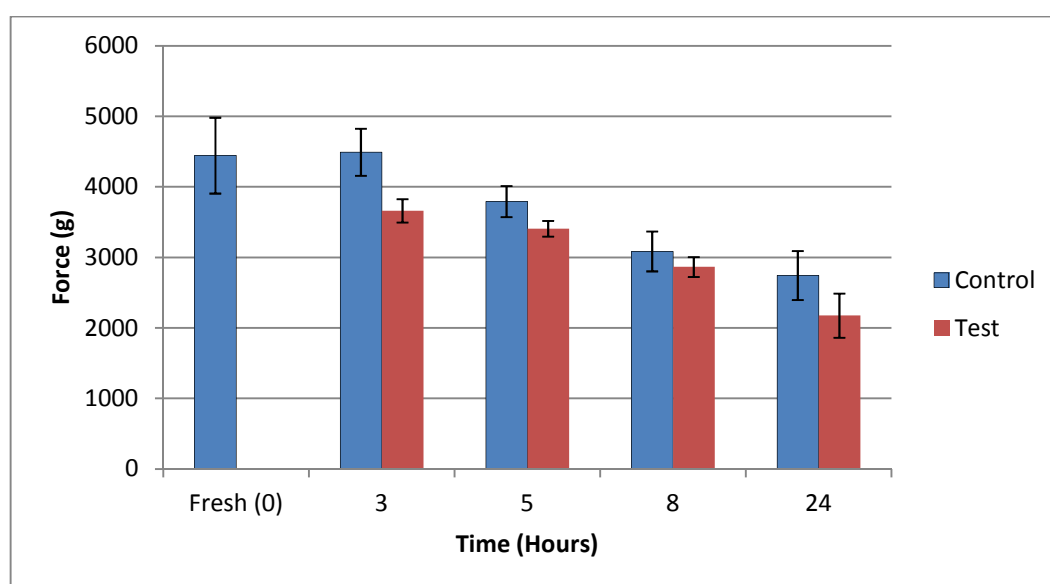
**Figure 8.8:** Representative plots of ATR-FTIR spectra of Gelucire 44/14 around 1347  $\text{cm}^{-1}$  peak, inside FM-B extruded films at different occlusion times (left side plot) and compared to the Gelucire 44/14 spectra in the equivalent control extruded film incubated at 75%RH/25°C (right side plot), overlaid in ascending order of sampling times (3-24 hours). These spectra were obtained through subtraction of Eudragit RS PO spectra

The flexibility of these extruded films, with occlusion (test) and without occlusion (control), was investigated using hardness measurements. The parameter measured was the peak hardness force (PHF) needed to penetrate these films according to the experiment methodology detailed in Chapter 2 (section 2.2.2.6). As shown in Figure 8.9, there was a decrease in the PHF for the films occluded on the skin over time. Moreover, the PHF of the occluded samples was lower than those without occlusion (fresh and stored under 75%RH/25°C) at different testing times. This correlates well with the MTDSC findings. The control samples (without occlusion) showed higher glass transition temperatures than those with occlusion, indicating lower flexibility. Thus higher force will be required to compress the harder, less flexible films. Therefore, plasticization by water was manifested by a decrease in both the glass transition temperature and hardness (PHF) of the samples hydrated by occlusion.

(A)

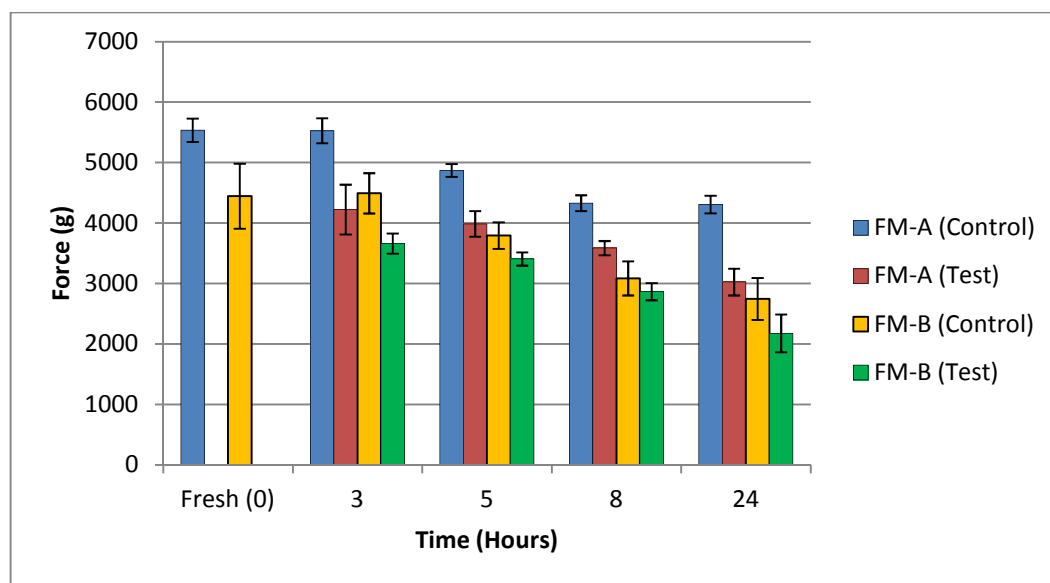


(B)



**Figure 8.9:** Effect of hydration time on the measured peak hardness forces of the extruded films of (A) FM-A and (B) FM-B compositions applied to the skin under occlusion, referred as test samples and compared to their corresponding control extruded samples stored at 75%RH/25°C. Error bars represent  $\pm$ S.D. of no less than three measurements

A summary of the obtained peak hardness forces for the extruded films of approximately 15%(w/w) and 30%(w/w) Gelucire 44/14 concentrations in FM-A and FM-B systems, respectively, is shown in Figure 8.10. This summary demonstrates that for each set of data, fresh, control and occluded samples, the films containing higher level of Gelucire 44/14 (FM-B composition) are more flexible as indicated by lower measured PHF values.



**Figure 8.10: Effect of the Gelucire 44/14 concentration on the measured peak hardness forces of the extruded films of (A) FM-A and (B) FM-B compositions applied to the skin under occlusion, referred as test samples and compared to their corresponding control extruded samples. Controls encompass fresh sample (t=0hours) and samples incubated under 75%RH/25°C, tested at different times. Error bars represent  $\pm$ S.D. of no less than three measurements**

## 8.4 Conclusions

The hydration of the extruded films of FM-A and FM-B formulation was possible when applied to the skin under occlusion, as indicated by water absorption capacity and swelling ratio measurements. The *in vivo* behaviour of these films showed that both formulations underwent similar pattern of changes after hydration. These changes were mainly surface imperfections and softening of the films accompanied with swelling of their matrices. These changes were more evident over time due to increased hydration of these occluded films. In addition, a gradual decrease of crystalline Gelucire 44/14 in FM-B samples was observed as a function of occlusion time, indicating solubilisation. Further, these samples with higher level of Gelucire 44/14 i.e. FM-B films, exhibited a distinctly higher water absorption capacity and swelling with subsequent extended structural changes and more flexibility as indicated by lower measured PHF values. All these structural changes are believed to be contributing to an enhanced drug delivery from these extruded Eudragit RS PO/Gelucire 44/14 matrices upon hydration.

Flexibility of the extruded films of FM-A and FM-B systems was indicated by reduction in both glass transition temperatures and hardness values. This elasticity resulted from plasticization effect of water. These occluded films captured a print of the skin due to this flexibility, and therefore, represent a promise for application to the skin regardless of its surface irregularities, thereby achieving higher contact area.

Since the observed patterns of structural changes using *in vivo* model in this study were similar to the ones probed using *in vitro* model using Franz cells, we could use this *in vitro* model as a predictive approach for the behaviour of these samples when loaded with the drug *in vivo*, as performed in Chapter 6 and 7. However, no statement can be made on the quantity of the drug released using *in vitro* model, because *in vivo* experiment revealed that it is associated with overhydration. It is therefore believed that the employed *in vitro* model using Franz cells to mimic skin occlusion could be only supportive for further clinical settings, and incorporation of the drug in these matrices for *in vivo* assessment is necessary to confirm their therapeutic efficiency. Nevertheless, it could be concluded at this stage of drug delivery development that FM-A and FM-B extruded films under the influence of human skin occlusion hold a promise for potential transdermal drug delivery in a relevant way to the ongoing interesting approach of improved drug release by hydration.

## **Chapter 9: Conclusions and Future work**



## 9.1 Conclusions

The design of a delivery system involves not only the selection of the correct material composite, but also needs the proper equipment for its production. HME is a solvent-free technology and was utilized in this project as the main method of manufacture. This technique has moved from plastics industry to being well-recognized, viable technology in pharmaceutical industry for preparation of various dosage forms, ranging from oral to transdermal. This project attempted to craft a novel strategy for transdermal drug delivery. Thus the work herein was focused on the variation of design parameters and developing various formulations using HME technology that would ultimately synergize the concept of simplicity and enhanced release program in one system for transdermal application. These investigations were assisted by multiple analytical techniques which were exploited to evaluate the usefulness of the developed hot melt extruded films and their optimization as potential transdermal patches.

Chapter 3 set out a general assessment of physicochemical properties of ibuprofen as a model drug throughout this work and the carrier excipients used to embed this drug by means of hot melt extrusion (HME). Screening tools as TGA, DSC, MTDSC, SEM, ATR-FTIR and PXRD were used to characterise these properties. The information derived formed the basis for interpreting subsequent data from multi-component systems. All these materials exhibited a range of thermal stability of not less than 140°C, thus providing an estimate for the temperature range in which HME can be used.

Chapter 4 took the principle of physicochemical characterisation further by studying composite mixtures of ibuprofen and Eudragit RS PO and their hot melt extruded formulations. The key findings obtained can be summarized by:

- TGA results demonstrated minimal weight losses after thermal treatment of their physical mixes at the selected extrusion temperature (100°C) for the intended mixing time (four minutes), indicating low degradation and thermal stability at these conditions.
- Extrudability was enhanced by the presence of a plasticizer i.e. ibuprofen.
- Hot melt extrusion technology was utilized successfully for the development of solid solutions of ibuprofen at high loading (up to 35% w/w) incorporated in Eudragit RS PO.

- The theoretical approaches of miscibility estimation using solubility parameters and melting point depression provided relatively good prediction of the practical solubility found for the studied extruded systems.
- Ibuprofen and Eudragit RS PO did not exhibit significant interactions but appeared to form compatible blends, supported by the one phase system existence of these systems i.e. solid solutions.
- The extent of solid state miscibility or equilibrium saturation solubility was approximated for the resulted extruded solid solutions under two relative humidity levels for one month. It was noted that the equilibrium solubility composition of the extruded mixture without phase separation or drug recrystallization slightly dropped under dry conditions (0%RH/25°C) to 30% (w/w) drug loading. Indicating good physical stability in dry conditions. However, a significant decrease in miscibility was noted on storage at 60% RH/25°C to about 10% (w/w) drug loading, despite the water uptake being relatively low. This indicates extra molecular mobility resulting from the strong plasticizing effect of water, wherein the drug is also poorly soluble.
- Supplementary information has been provided with regard to the fragility of the extruded ibuprofen-Eudragit RS PO solid solution systems. The results predicted strong glassy systems, and thus storage below their glass transition temperatures might not affect their stability in terms of drug recrystallization.

Chapter 5 demonstrated *in vitro* drug release and permeation profiles from hot melt extruded Eudragit RS PO films. Basing evaluation off their *in vitro* performance, a number of main points were highlighted as follows:

- The drug release was dependent on the drug load.
- A key feature of these hot melt extruded films was a significant retardation of drug release. This finding is consistent with those of Azmari et al. (2005) and Hasanzadeh et al. (2009), who found that thermal treatment of Eudragit RS PO matrices could control the drug release.
- With respect to the *in vitro* permeation behaviour, the retarding role of the Eudragit matrices on the drug permeation was evident in comparison to the diffusion of the ibuprofen from its saturated solution across the used silicone membranes.
- Films maintained stability after ageing at wet conditions (60%RH/25°C) studied in previous chapter at 10% (w/w) drug loading extrudate liberated drug more than their corresponding aged dry extrudate. Thus water inclusion in these films might facilitate drug release. Therefore, adjustments of these formulations to achieve

desired release may involve judicious choice of hydrophilic components, enabling fluid access into these extruded films.

- The glassy solid solution films at 30% w/w drug loading were chosen as a prototype to introduce further adjuvants to optimise and establish usefulness of these formulations. Good physical stability of these films addressed in previous chapter after one month of ageing under dry conditions was demonstrated here as comparable *in vitro* release and *in vitro* permeation profiles between aged samples and fresh samples.
- Both *in vitro* release/dissolution and *in vitro* permeation studies aided in better understanding of the release of the ibuprofen from the tested films and directed the need of a modification.

Chapter 6 attempted to address the issue of what modification can be introduced to improve ibuprofen release and permeation from hot melt extruded formulations. The key points were found to be:

- Formulation-based parameter, which involved modulation of formulation composition (carrier excipient type and the ratio used), resulted in changes of the molecular distribution of the drug in the extrudable matrices.
- Only extruded films made up of Eudragit RS PO, ibuprofen and small amounts of xanthan gum (FM5) or Gelucire 44/14 (FM9), among other prepared multiple component systems, maintained their miscibility without detected phase separation.
- *In vitro* drug release studies identified the hydrophilic components that decreased the release retardation effect of the Eudragit RS PO. The most plausible general explanation of release enhancement was the improving of water ingress into the extruded films or exposure of the ibuprofen into the dissolution medium.
- Information derived from solid state characterisation, physical appearance and *in vitro* release properties were used to decide the encouraging formulations for further exploration of their *in vitro* permeation properties. Formulations which completely dissolved the drug as FM5 (xanthan gum) and FM9 (~10% (w/w) Gelucire 44/14) together with formulations showed superior release profile with acceptable physical features were selected, and included FM7 (Pluronic® F127) and FM10 (~20% (w/w) Gelucire 44/14) films.
- Problems led to limited *in vitro* permeation properties from the selected formulations were addressed. Recrystallization of the drug and lack of proper hydration appeared to define, or at least contribute to these problems.

- Attention was drawn towards the role of hydration as an enhancement technique for *in vitro* permeation of ibuprofen from two major types of selected optimized extruded formulations. This embraced formulations of FM5 (xanthan gum) and FM9 (~10% (w/w) Gelucire 44/14) wherein the drug is completely miscible, and FM10 (~20% (w/w) Gelucire 44/14) wherein higher overall permeation achieved in the dry state amongst other formulations.
- The variations of the vehicle used or the applied hydration level in the same composition resulted in a different permeation program, which included immediate and sustained release schemes. In addition, the proposed mechanism of drug release using power model was changed for most systems as a result of the hydration.
- Hydration, especially in films containing Gelucire 44/14 was notably influential and appeared as a key parameter which allowed for improved ibuprofen permeation profiles, in terms of the amount permeated and extent. It is therefore preferable to use these films under occlusive conditions.
- An *in vitro* simulative study of the hydration under skin occlusion supported the usefulness of extruded films containing Gelucire 44/14 to enhance ibuprofen permeation.
- Hydration of these extruded films represents a strategy towards simple yet effective approach to release the drug and modulate its permeation program in the same system; therefore it rivals conventional methods for transdermal drug delivery.
- Intriguing consistency changes driven by hydration to activate drug release from Eudragit RS PO/Gelucire 44/14 carrier systems presents a promising possibility as smart transdermal drug delivery systems.

Chapter 7 focused on the characterisation of the key features of Eudragit RS PO/Gelucire 44/14 extruded films based on their relevance for potential applications as transdermal delivery activated by hydration. The ageing effect was outlined for these extruded systems formulated with and without the drug. Dealing with these issue, the data suggested that:

- Gelucire 44/14 was found to be in solid solution within the extruded formulation containing Gelucire 44/14:Eudragit RS PO in the ratio of 1:6 (FMA), whereas the ratio of 2:5 (FMB) demonstrated a solid dispersion.
- ATR-FTIR investigations suggested a possibility of certain rearrangements between these components wherein the interiors of these extruded systems are enriched with the C-H groups, in which hydrophobic side chains would be expected to be more involved in interactions; thereby the remaining functional groups will be “expelled”

or become readily available on the surfaces of these extrudates. However, no evidence of significant interaction was detected.

- HSM further supplemented the hypothesis of a certain affinity between Gelucire 44/14 and Eudragit RS PO, and DVS complement ATR-FTIR results about the possibility of specific arrangement between these extruded materials of concentrated hydrophilic regions on the surface, in addition to the increase of water uptake as the level of the lipid i.e. Gelucire 44/14 increased.
- Changes associated with the hydration of these extruded carrier systems without the drug were probed *in vitro* and endeavoured to further understanding of their possible mechanism of drug delivery. Hydration consequences involved: surface imperfections, possible leakage of the Gelucire 44/14 into these surfaces and softening of the films accompanied with appreciable swelling of the matrices. These changes could impart in creating paths of active ingredients release and its solubilisation when loaded in these vehicles.
- Changes of molecular arrangements of the studied extruded systems were detected at different used humidity and temperatures in the conducted basic storage studies. While FM-A extruded systems showed limited degree of Gelucire 44/14 crystallization and formation of solid dispersion as supported by SEM and ATR-FTIR results, an extended phase separation was observed for the originally solid dispersed FM-B systems supported by MTDSC, SEM and ATR-FTIR findings. A combination of high humidity 75%RH and high temperature 40°C is believed to aid in the solubilisation of Gelucire 44/14 formed crystallites, as a function of increased water uptake tendency as indicated by DVS investigations.
- By using the same storage conditions, it was possible to relate the physical stability of corresponding extruded systems conjugated with the drug. On that basis alongside MTDSC and HSM studies, it was concluded that Gelucire 44/14 and ibuprofen recrystallized in these systems containing 30%(w/w) ibuprofen and Gelucire 44/14: Eudragit RS PO ratios of 1:6 or 2:5.
- *In vitro* permeation studies conducted for these aged extruded films with the ibuprofen under hydration. Considering rapid release from corresponding fresh extruded formulations containing crystalline drug in the previous chapter, it was inferred that observed retardation of release from these aged films is primarily a function of Gelucire 44/14 recrystallization. Alternatively, this impact, as described kinetically was not assumed to be negative because a delayed release of these tested aged films was associated with prolonged 'steady state' zero order release. Overall, the mechanism of drug release from these devices under the influence of hydration is believed to be more related to the carrier rather than the drug. This provides a

promise of using these carrier systems for drugs intended for skin application wherein a more control can be achieved using these carrier regardless of the physical state of the drug.

- Kinetic models were also used side by side to propose the possible mechanism of the drug release from the tested matrices. Fitting to first order release kinetic was suggested for the whole profile and more accurately as a profile composed of simultaneous zero order release followed by first order release pattern. Power model indicated the possible role of swelling and relaxation in controlling the drug release.

During development of the Eudragit RS PO/Gelucire 44/14 extruded systems by establishing them as drug carriers for transdermal delivery, interests sparked by improved *in vitro* ibuprofen permeation and consistency changes (Chapter 6), in addition to the observed structural changes of these carriers without the drug (Chapter 7), all after hydration. These impacts of hydration gave an intuitive reason for proceeding with investigations of these carrier systems when applied to the skin under occlusion in Chapter 8. Two main points were embedded in this chapter. The hydration of the extruded films of Gelucire 44/14: Eudragit RS PO in ratios of 1:6 and 2:5 was possible when applied to the human skin under occlusion. The structural changes observed *in vitro* for these films in Chapter 7 after occlusion simulation in Franz diffusion cells were consistent with those observed in this *in vivo* study, giving confidence in the use of these carrier systems as platforms for potential transdermal drug delivery in a relevant way to the ongoing interesting approach of improved drug release by hydration. This also provides a natural guide towards future research as will be suggested in the following section.

Overall, this thesis presented that extruded one layer ibuprofen-Eudragit RS PO based transdermal patch could be developed using HME technology, which enabled fabrication with consistent and high process yield without solvent concerns. Various analytical techniques were used to understand how well the extruded system meets the desired physicochemical properties and drug release, and therefore accompanied the project framework to provide thorough characterisations, from the point of the production through to performance channels evaluated by *in vitro* drug release and permeation studies. Eudragit RS PO carrier matrices offered a stable embedding system for the drug but showed retarding impact on the ibuprofen release. Because desired drug release is one of the most critical aspects determining performance success, these matrices were modified for improving drug release by addition of other auxiliary components. Considerable emphasis was directed towards achieving reasonable effective release from these extrudable systems. It was found that the matrix-type transdermal patches of ibuprofen exhibited better permeation with the

Eudragir RS PO/Gelucire 44/14 matrices upon hydration. This satisfies or at least enables to proceed with the advancement of the desired aim of the project of introducing a novel strategy for transdermal drug delivery. The structural elements of this delivery strategy were tied into two things, simple Eudragit RS PO/Gelucire 44/14 extrudate and hydration as a safe enhancement technique. To allow active delivery, the films should be hydrated upon the application to the skin. As a delivery mechanism, hydration can be achieved by skin occlusion. These carrier systems were able to hydrate after application to the human skin *in vivo* under occlusion.

## 9.2 Future work

An integrated multi-disciplinary approach is usually required for a development process. Pharmaceutically, this approach involves communication between proper physicochemical properties of the drug and the delivery system used to achieve desired bioavailability. Understanding stability requirements, investigating factors that drive patient compliance and scale-up feasibility for commercialization purposes are also important to be identified during this process to find the applications of the final pharmaceutical product.

In this work, the fundamental feasibility of designing transdermal patches using hot melt extrusion was established. The analytical techniques used and approaches offered a comprehensive understanding of the investigations and streamlined the development process, and thus would be of benefits to characterise other pharmaceutically relevant extruded materials. The design of hydration-responsive compositions of lipid-contained extruded matrices is to be considered a promising drug delivery approach that can realize concentration enhancement when applied to the skin under occlusion. Research on that domain approached the basic level of maturity and presented possible future areas of this research. In order to progress the development of this study, interventions structured horizontally and vertically are proposed.

Saturated drug concentration within the formulation with appropriate stability is important to maximize the flux into the skin. Therefore, a delicate balance is preferred to be found between saturation concentration of the drug inside the carrier system enough to load amounts required for sufficient therapeutic dose for the intended time, and the stability of the drug. Thus as a first step in the vertical line modifications, we will reduce the total amount of incorporated drug in the studied extruded systems from 30% to about 10% (w/w) as a crystallization inhibition approach. If the drug recrystallization is avoided, then *in vivo* study of the ibuprofen loaded extruded matrices shall be conducted and the films shall be applied



to the skin under occlusive conditions. The estimation of hydration level of the occluded human skin will also be considered using for example trans-epidermal weight loss measurements, thus a quantitative relationship can be established between this level and the drug bioavailability. A change to horizontal line can be implemented at this stage. Interesting permeation enhancement and structural changes induced by hydration can also be elucidated for other drugs, expanding the utility of these carrier systems, and further our understanding if the ibuprofen was the only answer for these extruded systems activated by hydration with accompanying intriguing consistency changes and possibility of emulsion formation.

At this point of research, the work said that all the inputs are directed towards a plausible conclusion of a carrier-controlled ibuprofen release from Eudragit RS PO/Gelucire 44/14 matrices. Therefore, particle size or the physical forms of the drug are of minimal importance. However, the presence of the drug in a solid solution system is favourable to enhance its escaping tendency to the surrounding environment. This is ascribed to the tendency of glassy solid solution to reach high initial supersaturation (Albers et al., 2009) associated with high thermodynamic activity. Therefore, its stabilization would be important to empower the leaving tendency of the drug once applied to the skin with subsequent concentration and flux enhancement. The horizontal line of development is continued at this stage. Limiting the amount of the drug incorporated in the used matrices can be avoided by changing the Eudragit RS PO. The ideal candidate would be a crystallization inhibitor polymer, miscible with the Gelucire 44/14, does not affect the drug release negatively and preferably plasticized under the influence of applied hydration to ease liberation of the drug by the proposed strategy in this work.

Polymeric constituents of other Eudragits have been utilized during the work, which was selected to have more hydrophilic character than RS PO grade with a potential for crystallization inhibition such as Eudragit RL (Kotiyani and Vavia, 2001) and Eudragit L100 (Warren et al., 2010). However, these polymers showed drug recrystallization at 30% (w/w) ibuprofen loading without even incorporation of the third constituent (Gelucire 44/14). Therefore, the next stage will be investigation of other groups of polymers, known of their crystallization inhibition properties and application in transdermal dosage forms like highly dispersed silicon, macromolecules such as cyclodextrins, polyvinylpyrrolidones, and polyvinyl alcohol (Lipp et al., 1997). Polyvinyl alcohol was also tried and found unextrudable at the selected extrusion temperature with the ibuprofen. Miscibility estimations, extrudability, storage at different temperature and humidity and monitoring of the performance *in vitro* would accompany all these investigations to facilitate further



developments of these systems. In these multi-component extruded systems of the drug, Gelucire 44/14 and the new polymer, it would be recommended to carry out investigation in a step-wise manner as described throughout this work. While the main emphasis would be directed on the performance and the ability of the newly-introduced material to form stable solid solution with the drug, it would also be beneficial to investigate the stabilization of the bulk carrier matrix itself. At this stage of design it might be proper to determine the required scheme of the drug release, through elucidation of the drug release mechanism. For example, if it is maintained as carrier-controlled release process and prolonged release is desired, it may be adequate to have crystalline Gelucire 44/14 to control the drug release. This approach, for instance, is derived from the insights gained during the assessment of the aged films with ibuprofen, Eudragit RS PO and Gelucire 44/14, which represents another avenue for future research.

## References

- Abdul Rasool, B.K., Aziz, U., Sarheed, O., Abdul Rasool, A.A. (2011). Design and evaluation of a bioadhesive film for transdermal delivery of propranolol hydrochloride. *Acta Pharmaceut.* **61**: 271–282.
- Abdul-Fattah, A.M., Bhargava, H.N. (2002). Preparation and *in vitro* evaluation of solid dispersions of halofantrine. *Int J Pharm.* **235**(1-2): 17-33.
- Adibkia, K., Javadzadeh, Y., Dastmalchi, S., Mohammadi, G., Niri, FK. Alaei-Beirami, M. (2011). Naproxen-eudragit® RS100 nanoparticles: preparation and physicochemical characterization. *Colloids Surf B Biointerfaces.* **83**(1): 155-159.
- Ahmad, A., Barry, B.W., Williams, A.C., Davis, A.F. (2004). Penciclovir solubility in Eudragit films: a comparison of X-ray, thermal, microscopic and release rate techniques. *J Pharm Biomed Anal.* **34**(5): 945-956.
- Ahuja, N., Katare, O.P, Singh, B. (2007). Studies on dissolution enhancement and mathematical modelling of drug release of a poorly water-soluble drug using water-soluble carriers. *Eur J Pharm Biopharm.* **65**: 26-38.
- Aitken-Nichol, C., Zhang, F., McGinity, J.W. (1996). Hot melt extrusion of acrylic film. *Pharm Res.* **13**: 804-808.
- Ajiwe, V.I.E., Ajibola, V.O., Martins, C.M.A.O. (2003). Biodiesel fuels from palm oil methylester and ester-diesel blends. *Bull.Chem.Soc.Ethiop.* **17**(1): 19-26.
- Albers, J., Alles, R., Matthee, K., Knop, K., Nahrup, J.S., Kleinebudde, P. (2009). Mechanism of drug release from polymethacrylate-based extrudates and milled strands prepared by hot-melt extrusion. *Eur J Pharm Biopharm.* **71**: 387-394.
- Al-Saidan, S. M. (2004). Transdermal self-permeation enhancement of ibuprofen. *J Control Release* .**100**(2): 199-209.
- Andrews, G. P., Jones, D.S. (2010). Formulation and characterization of hot melt extruded dosage forms: challenges and opportunities. *Cheminform.* **41**(43).
- Andrews, G.P., Jones, D.S., AbuDiak, O., Margeston, D.N., McAllister, M.S. (2009). Hot-melt extrusion: an emerging drug delivery technology. *Pharm Tech Europe.* **21**(1): 18-23.

- Antunes, A.B., Geest, B.G. Vervaet, C., Remon, J.P. (2013). Gelucire 44/14 based immediate release formulations for poorly water-soluble drugs. *Drug Dev In Pharm.* **39**(5): 791-798.
- Argin-Soysal, S., Kofinas, P., Lo, Y.M. (2009). Effect of complexation conditions on xanthan-chitosan polyelectrolyte complex gel. *Food Hydrocolloids.* **23**: 202-209.
- Aulton, M.E.ed. (2007). *Aulton's pharmaceuticals: the design and manufacture of medicines.* 3<sup>rd</sup> Edition. Edinburgh: Churchill Livingstone Elsevier.
- Azarmi, S., Ghaffari, F., Löbenberg, R., Nokhodchi, A. (2005). Mechanistic evaluation of the effect of thermal-treating on Eudragit RS matrices. *II Farmaco.* **60**: 925-930.
- Babu, V.R., Sairam, M., Hosamani, K.M., Aminabhavi, T.M. (2007). Preparation of sodium alginate-methylcellulose blend microspheres for controlled release of nifedipine. *Carbohydr Polym.* **69**: 241-250.
- Barichello, J.M., Handa, H., Kisyuku, M., Shibata, T., Ishida, T., Kiwada, H. (2006). Inducing effect of liposomalization on the transdermal delivery of hydrocortisone: creation of a drug supersaturated state. *J Control Release.* **115**: 94-102.
- Barker, S., A., Yap, S., Yuen, K., McCoy, C., Murphy, J., Craig, D.Q.M. (2003). An investigation into the structure and bioavailability of  $\alpha$ -tocopherol dispersions in Gelucire® 44/14. *J Control Release.* **91**: 477-488.
- Barry, B.W. (2001). Is transdermal drug delivery research still important today?. *Drug Discov Today.* **6**(19): 967-971.
- Benson, H.A.E. (2005). Transdermal Drug Delivery: Penetration Enhancement Techniques. *Curr Drug Deliv.* **2**: 23-33.
- Bettinetti, G., Mura, P., Sorrenti, M., Faucci, M.T., Negri, A. (1999). Physical Characterization of Picotamide Monohydrate and Anhydrous Picotamide. *J Pharm Sci.* **88**(11): 1133-1139.
- Bhende, S., Jadhav, N. (2012). Moringa Coagulant as a Stabilizer for Amorphous Solids: Part I. *AAPS PharmSciTech.* **13**(2): 400-410.

Borde, B., Bizot, H., Vigier, G., Buleon, A. (2002). Calorimetric analysis of the structural relaxation in partially hydrated amorphous polysaccharides. I. Glass transition and fragility. *Carbohydr Polym.* **48**(1): 83-96.

BP-2010, In: Ibuprofen; The department of health. *British Pharmacopoeia* Commission Office, Market Towers, The stationery office, London, **2009**, Vol. 1, pp. 1089-1091. Cited In: Mansouri, M., Pouretedal, H.R., Vosoughi, V. (2011). Preparation and Characterisation of Ibuprofen Nanoparticles by using Solvent/Antisolvent Precipitation. *The Open Conference Proceedings Journal.* **2**: 88-94.

Breitenbach, A., Drews, R., Messe, C., Wolff, H-M. (2009). Transdermal delivery of (R)-3, 3-Diphenyl-propylamin-monoestern. US Patent 2009/0274761A1.

Breitenbach, J. (2002). Melt extrusion: from process to drug delivery technology. *Eur J Pharm Biopharm.* **54**(2): 107-117.

British Pharmacopoeia Commission. (2011). *British pharmacopoeia*. London, England: Stationary office.

Brizuela, A.B., Bichara, L.C., Romano, E., Yurquina, A., Locatelli, S., Brandan, S.A. (2012). A complete characterization of the vibrational spectra of sucrose. *Carbohydr Res.* **361**: 212-218.

Bruce, L. D., Shah, N. H., Malick, A.W., Infled, M.H., McGinity, J.W. (2005). Properties of hot-melt extruded tablet formulations for the colonic delivery of 5-aminosalicylic acid. *Eur J Pharm Biopharm.* **59** (1): 85-97.

Buskirk, G.A.V., Gonzalez, M.A., Shah, V.P., Barnhardt, S., Barrett, C., Berge, S., Cleary, G., Chan, K., Flynn, G., Foster, T., Gale, R., Garrison, R., Gochnour, S., Gotto, A., Govil, S., Gray, V.A, Hammar, J., Harder, S., Hoiberg, C., Hussain, A., Karp, C., Llanos, H., Mant, J., Noonan, P., Swanson, D., Zerbe, H. (1997). Scale-up of adhesive transdermal drug delivery systems. *Eur J Pharm Biopharm.* **44**: 327-331.

Buslov, D.K., Sushko, N.I., Tretinnikov, O.N. (2008). Study of thermal gelatine of methylcellulose in water using FTIR-ATR spectroscopy. *J Appl Spectrosc.* **75**(4): 514-518.

Byrne, G.A., Aylott, R.I. (1981). Controlled release suppositories. US Patent 4265875.

- Calvino-Casilda, V., Mul, G., Fernández, J.F., Rubio-Marcos, F., Bañare, M.A. (2011). Monitoring the catalytic synthesis of glycerol carbonate by real-time attenuated total reflection FTIR spectroscopy. *Appl Catal A: Gen.* **409-410**: 106-112.
- Cano, H., Gabas, N., Canselier, J.P. (2001). Experimental study on the ibuprofen crystal growth morphology in solution. *Journal Cryst Growth.* **244**: 335-341.
- Cassel, R.B. Physical Aging and Fragility of Amorphous Polyethylene Terephthalate. (2002). TA299: 1-7.TA Instruments, USA.
- Castelli, F., Messina, C., Sarpietro, M.G., Pignatello, R., Puglisi, G. (2003). Eudragit as controlled release system for anti-inflammatory drugs: A comparison between DSC and dialysis experiments. *Thermochim Acta.* **400**: 227-234.
- Cevec, G., Vierl, U. (2010). Nanotechnology and the transdermal route: A state of the art review and critical appraisal. *J Control Release.* **141**: 277-299.
- Chambin, O., Jannin, V., Champion, D., Chevalier, C., Rochat-Gonthier, M., Pourcelot, Y. (2004). Influence of cryogenic grinding on properties of a self-emulsifying formulation. *Int J Pharm.* **278**: 79-89.
- Chi, S-C., Tan, H-K, Chun, H-W. (1996). Anti-inflammatory and analgesic transdermal gel. US patent 5527832.
- Chokshi, R., Zia, H. (2004). Hot –Melt Extrusion Technique: A review. *Ir J Pharm Res.* **3**:3-16.
- Chokshi, R.J., Zia, H., Sandhu, H.K., Shah, N.H., Malick, W.A. (2007). Improving the dissolution rate of poorly water soluble drug by solid dispersion and solid solution: pros and cons. *Drug Deliv.* **14**(1): 33-45.
- Chokshi, R.J., Sandhu, H. K., Iyer, R.M., Shah, N., H., Malick, A.W., Zia, H. (2005). Characterisation of Physico-Mechanical Properties of Indomethacin and Polymers to Assess their Suitability for Hot-Melt Extrusion Process as a Means to Manufacture Solid Dispersion/Solution. *J Pharm Sci.* **94**(11): 2463-2474.

- Cilurzo, F., Minghetti, P., Pagani, S., Casiraghi, A., Montanari, L. (2008). Design and Characterization of an Adhesive Matrix Based on a Poly (Ethyl Acrylate, Methyl Methacrylate). *AAPS PharmSciTech*. **9**(3): 748-754.
- Cilurzo, F., Tosi, L. (2006). Transdermal Patches Having A Silicone Adhesive Matrix Stabilized With Methacrylic Copolymers. US Patent 2006/0015077 A1.
- Clas, S.D., Dalton, C.R., Hancock, B.C. (1999). Differential scanning calorimetry. *Pharm Sci Tech Today*. **2**(8):311-320.
- Coleman, N. J., Craig, D. Q. M. (1996). Modulated temperature differential scanning calorimetry: A novel approach to pharmaceutical thermal analysis. *Int J Pharm*. **135**(1-2): 13-29.
- Colorcon. (2009). Methocel<sup>TM</sup>. Premium Cellulose Ethers. *Product Information*.
- Coppens, K.A., Hall, M.J., Mitchell, S.A., Read, M.D. (2005). Hypermellose, Ethyl cellulose, and Polyethylene Oxide Use in Hot Melt extrusion. *Pharm Tech*. 1-6.
- Costa, P., Lobo, J.M.S. (2001). Modeling and comparison of dissolution profiles. *Eur J Pharm Sci*. **13**: 123-133.
- CPKelco. (2003). Xantural® 75 xanthan gum. *Product Datasheet*.
- Craig, D.Q.M. (2002). The mechanisms of drug release from solid dispersions in water-soluble polymers. *Int J Pharm*. **231**: 131-144.
- Craig, D.Q.M., Barker, S.A., Banning, D., Booth, S.W. (1995). An investigation into the mechanisms of self-emulsification using particle size analysis and low frequency dielectric spectroscopy. *Int J Pharm*. **114**: 103-110.
- Craig, D.Q.M., Reading, M. ed. (2007). *Thermal Analysis of Pharmaceuticals*. New York: CRC Press.
- Crowley, M.M., Zhang, F., Koleng, J.J., McGinity, J.W. (2002). Stability of polyethylene oxide in matrix tablets prepared by hot-melt extrusion. *Biomaterials*. **23**(21): 4241-4248.

Crowley, M.M., Justin, M.K., Koleng, J.J., Zhang, F. (2009). Process for the preparation of a hot-melt extruded laminate. EP2010366 A2.

Crowley, M.M., Fredersdorf, A., Schroeder, B., Kucera, S., Prodduturi, S., Repka, M.A., McGinity, J.W. (2004). The influence of guaifenesin and ketoprofen on the properties of hot-melt extruded polyethylene oxide films. *Eur J Pharm Sci.* **22**(5): 409-418.

Crowley, M.M., Zhang, F., Repka, M.A., Thumma, S., Upadhye, S.B., Battu, S.K., McGinity, J.W., Martin, C. (2007). Pharmaceutical Applications of Hot-Melt Extrusion: Part I. *Drug Dev In Pharm.* **33**: 909-926.

Cullity, D.B. (1978). *Elements of X-ray diffraction*. 2<sup>nd</sup> Edition. Reading Mass.; London: Addison-Wesley.

Cunha-Filho, M.S.S., Alvarez-Lorenzo, C., Martinez-Pacheco, R., Landin, M. (2012). Temperature-Sensitive Gels for Intratumoral Delivery of  $\beta$ -Lapachone: Effect of Cyclodextrins and Ethanol. *The Scientific World Journal*. 1-8.

Curatolo, W. (1987). The Lipoidal Permeability Barriers of the Skin and Alimentary Tract. *Pharm Res.* **4**(4): 271-277.

Das, A., Nayak, A.K., Mohanty, B., Panda, S. (2011). Solubility and Dissolution Enhancement of Etoricoxib by Solid Dispersion Technique Using Sugar Carriers. *International Scholarly Research Network Pharmaceutics*. 1-8.

Dash, A.K., Tyle, P. (1996). Solid-State Characterization of AG337 (Thymitaq), a Novel Antitumor Drug. *J Pharm Sci.* **85**(10):1123-1127.

Davis, NM. (1998). Clinical pharmacokinetics of ibuprofen. The first 30 years. *Clin Pharmacokinet.* **34**(2):101-154.

De Brabandera, C., Vervaeta, C., Fiermansb, L., Remona, J.P. (2000). Matrix mini-tablets based on starch/microcrystalline wax mixtures. *Int J Pharm.* **199** (2): 195-203.

Delahaye, N., Duclos, R., Saiter, J.M., Varnier, S. (1997). Characterization of Solid Dispersion Phase Transitions Using a New Optical Thermal Analyzer. *Drug Dev In Pharm.* **23**(3): 293-303.



- Delgado-Charro, M.B., Guy, R.H. (2001). Transdermal Drug Delivery, in *Drug Delivery and Targeting for Pharmacists and Pharmaceutical Scientists* (ed Hillery, A.M., Lloyd, A.W., Swarbrick, J). London and New York: Taylor & Francis. Ch8: 208-236.
- Dezfuli, A.R., Aravindram, A.S., Manjunath, M., Ganesh, N.S., Shailesh, T. (2012). Development and evaluation of transdermal films loaded with antihypertensive drug. *Int J Pharma Biol Sci.* **3**(3): 559-569.
- Dhamecha, D., Rathi, A.A., Saifee, M., Lahoti, S.R., Dehghan, M.H.G. (2009). Drug vehicle based approaches of penetration enhancement. *Int J Pharm Pharm Sci.* **1**(1): 24-46
- Djuris, J., Nikolakakis, I., Ibric, S., Djuric, Z., Kachrimanis, K. (2013). Preparation of carbamazepine-Soluplus® solid dispersions by hot-melt extrusion, and prediction of drug-polymer miscibility by thermodynamic model fitting. *Eur J Pharm Biopharm.* [In press: Online]. Available from: <http://dx.doi.org/10.1016/j.ejpb.2012.12.018>.
- Dudognon, E., Dane`de, F., Descamps, M., Correia, NT. (2008). Evidence for a new crystalline phase of racemic ibuprofen. *Pharm Res.* **25**: 2853-2858.
- Edwards, D.A. (1998). Hydrogels or lipogels with enhanced mass transfer for transdermal drug delivery. US Patent 5833647.
- Elias, P. M. (1991). Epidermal barrier function: intercellular lamellar lipid structures, origin, composition and metabolism. *J Control Release.* **15**(3): 199-208.
- Elias, P.M. (1983). Epidermal lipids, barrier function and desquamation. *The Journal of Investigative Dermatology.* **80**: 44-49. Cited In: Kulkarni, V.S.ed. (2010). *Handbook of Non-Invasive Drug Delivery Systems*. USA: Elsevier Inc.
- Elias, P.M., Tsai, J., Menon, G.K., Holleran, W.M., Feingold, K.R. (2002). The potential of metabolic interventions to enhance transdermal drug delivery. *JID Symp.Proceedings.* **7**: 79-85.
- Escobar-Chávez, J.J. ed. (2010). *Current Technologies to Increase the Transdermal Delivery of Drugs*. Bentham Science Publishers.

Escobar-Chávez, J.J., López-Cervantes, M., Naik, A., Kalia, Y.N., Quintanar-Guerrero, D., Ganem-Quintanar, A. (2006). Applications of thermo-reversible pluronic F-127 gels in pharmaceutical formulations. *J Pharm Sci.* **9**(3): 339-358.

European Pharmacopoeia 5.0. *European Pharmacopoeia*. Council of Europe. **2005**, Vol. 1, pp.231-233.

Evonik. (n. d.).Eudragit®RS PO. Available at: <http://eudragit.evonik.com/product/eudragit/en/products-services/eudragit-products/sustained-release-formulation/rs-po/pages/default.aspx>. [Accessed: October 2011].

Feng, L., Zhao, W., Zheng, J., Frisco, S., Song, P., Li, X. (2011).The shape-stabilized phase change materials composed of polyethylene glycol and various mesoporous matrices (AC, SBA-15 and MCM-41). *Solar Energy Materials & Solar Cells.* **95**: 3550-3556.

Feuge, R.O., Zeringue, H.J., Weiss, T.J. (1973). Process for the production of sucrose esters of fatty acids. US Patent 3,714,144.

Fini, A., Fazio, G., Feroci, G. (1995). Solubility and solubilisation properties of non-steroidal ant-inflammatory drugs. *Int J Pharm.* **126**: 95-102.

Flynn, G.L., Stewart, B. (1988). Percutaneous Drug Penetration: Choosing Candidates for Transdermal Development. *Drug Dev Res.* **13**: 169-185.

Forster, A., Hempenstall, J., Tucker, I., Rades, T. (2001). Selection of excipients for melt extrusion with two poorly water-soluble drugs by solubility parameter calculation and thermal analysis. *Int J Pharm.* **226**: 147-161.

Fujimori, J., Yoshihashi, Y., Yonemochi, E., Terada, K. (2005). Application of Eudragit RS to thermo-sensitive drug delivery systems .II. Effect of temperature on drug permeability through membrane consisting of Eudragit RS/PEG 400 blend polymers. *J Control Release.* **102**: 49-57.

Fukuda, M., Peppas, N.A., McGinity, J.W. (2006). Properties of sustained release hot-melt extruded tablets containing chitosan and xanthan gum. *Int J Pharm.* **310**: 90-100.

- Fukuoka, E., Makita, M., Yamamura, S. (1989). Glassy state of pharmaceuticals. III. Thermal properties and stability of glassy pharmaceuticals and their binary glass systems. *Chem.Pharm.Bull.* **37**(4): 1047-1050.
- Gao, Z. (2011). Mathematical Modeling of Variables Involved in Dissolution Testing. *J Pharm Sci.* **100**: 4934-4942.
- Gattefossé. (2000). Gelucire 44/14: Immediate Release and Enhanced Bioavailability. *Product Information*.
- Gavali, P., Gaikwad, A., Radhika, P.R., Sivakumar, T. (2010). Design and development of hydroxypropyl methylcellulose (HPMC) based polymeric film of enalapril maleate. *Int J Pharm Tech Res.* **2**(1): 274-282.
- Ghebremeskel, A. N., Vemavarapu, C., Lodaya, M. (2007). Use of surfactants as plasticizers in preparing solid dispersions of poorly soluble API: Selection of polymer-surfactant combinations using solubility parameters and testing the processability. *Int J Pharm.* **328**(2): 119-129.
- Ghebre-Selassie, I., Martin, C. ed. (2003). *Pharmaceutical Extrusion Technology*. New York: Marcel Dekker, Inc.
- Ghosh, T.K., Jasti, B.R. ed. (2005). *Theory and practice of contemporary pharmaceuticals*. Florida: CRC Press.
- Gohel, M.C., Nagori, S.A. (2009). Fabrication of Modified Transport Fluconazole Transdermal Spray Containing Ethyl Cellulose and Eudragit RS 100 as Film Formers. *AAPS PharmSciTech.* **10**(2): 684-691.
- Gordon, S., Taylor, J.S. (1952). Ideal copolymers and the second-order transitions of synthetic rubbers. I. Non-crystalline copolymers. *J Appl Chem.* **2**: 493-500.
- Gosau, M.I., Müller, B.W. (2010). Release of gentamicin sulphate from biodegradable PLGA-implants produced by hot melt extrusion. *Die Pharmazie-An International Journal of Pharmaceutical Sciences.* **65**(7): 487-492.

- Gowthamarajan, K., Singh, S.K. (2010). Dissolution Testing for Poorly Soluble Drugs: A Continuing Perspective. *Dissolution Technol.* 24-32.
- Grassi, M., Grassi, G. (2005). Mathematical Modelling and Controlled Drug Delivery: Matrix Systems. *Curr Drug Deliv.* **2**(1): 97-116.
- Grawe, D., Hoesel, P., Fischer, W. (2005). Laminates containing an active substance transdermal system. US Patent 6902741B1.
- Green, B.G., Lederman, S.J., Stevens, J.C. (1979). The effect of skin temperature on the perception of roughness. *Sensory Processes.* **3**: 327-333.
- Greenhalgh, D.J., Williams, A.C., Timmins, P., York, P. (1999). Solubility parameters as predictors of miscibility in solid dispersions. *J Pharm Sci.* **88**(11): 1182-1190.
- Grisedale, L.C., Belton, P.S., Jamieson, M.J., Barker, S.A., Craig, D.Q.M. (2012). An investigation into water interactions with amorphous and milled salbutamol sulphate: The development of predictive models for uptake and recrystallization. *Int J Pharm.* **422**: 220-228.
- Grundy, J.S., Anderson, K.E., Rogers, J.A., Foster, R.T. (1997). Studies on dissolution testing of the nifedipine gastrointestinal therapeutic system .I. Description of a two-phase *in vitro* dissolution test. *J Control Release.* **48**:1-8.
- Gryczke, A., Schminke, S., Maniruzzaman, M., Beck, J., Douroumis, D. (2011). Development and evaluation of orally disintegrating tablets (ODTs) containing ibuprofen granules prepared by hot melt extrusion. *Colloids Surf B Biointerfaces.* **86**(2): 275-284.
- Gutierrez-Rocca, J.C., McGinity, J.W. (1993). Influence of aging on the physical-mechanical properties of acrylic resin films cast from aqueous dispersions and organic solutions. *Drug Dev In Pharm.* **19**: 315-332.
- Hadgraft, J. (1999). Passive enhancement strategies in topical and transdermal drug delivery. *Int J Pharm.* **184**: 1-6.
- Hadgraft, J., Plessis, J., Goosen, C. (2000). The selection of non-steroidal anti-inflammatory agents for dermal delivery. *Int J Pharm.* **207**: 31-37.

Hall, M., Read, M. (2012). Hot-Melt Extrusion of Ethylcellulose, Hypromellose and Polyethylene Oxide, in *Hot-Melt Extrusion: Pharmaceutical Applications* (ed Douroumis, D.). Chichester, UK: John Wiley & Sons, Ltd. Ch7: 145-175.

Hansen, C.M. (1967). The three dimensional solubility parameter and solvent diffusion coefficient: Their importance in surface coating formulation. Copenhagen: Danish Technical press. pp: 14-15.

Hasanzadeh, D., Ghaffari, S., Monajjemzadeh, F., Al-Hallak, M., Soltani, G., Azarmi, S. (2009). Thermal treating of Acrylic Matrices as a tool for Controlling Drug Release. *Chem.Pharm.Bull.* **57**(12): 1356-1362.

Hatakeyama, H., Hatakeyama, T. (1998). Interaction between water and hydrophilic polymers. *Thermochim Acta.* **308**: 3-22.

Hatefi, A., Amsden, B. (2002). Biodegradable injectable in situ forming drug delivery systems. *J Control Release.* **80**: 9-28.

Healy, K.E., Dorfman, G.S. (1997). Biodegradable stent. US Patent 5670161.

Heinamaki, J.T., Lehtola, V.M., Nikupaavo, P., Yliruusi, J.K. (1994). Mechanical and moisture permeability properties of aqueous-based hydroxypropyl methylcellulose coating systems plasticized with polyethylene glycol. *Int J Pharm.* **112** (2): 191-196.

Higgins, J.D., Gilmore, T.P., Martellucci, S.A., Bruce, R.D. (2001). In: Brittain HG, editor. Analytical profiles of drug substances and excipients, Vol. 27: San Diego, London: Academic Press, pp 265-330. Cited In: Potthast, H., Dressman, J.B., Junginger, H.E., Midha, K.K., Oeser, H., Shah, V.P., Vogelpoel, H., Barends, D.M. (2005). Biowaiver monographs for immediate release solid oral dosage forms: Ibuprofen. *J Pharm Sci.* **94**(10): 2121-2131.

Hill, V. L., Craig, D. Q. M., Feely, L.C. (1998). Characterisation of spray-dried lactose using modulated differential scanning calorimetry. *Int J Pharm.* **161**(1): 95-107.

Hillery, A.M., Lloyd, A.W., Swarbrick, J. ed. (2001). *Drug Delivery and Targeting for Pharmacists and Pharmaceutical Scientists*. London and New York: Taylor & Francis.

- Ho, N.T., Kinget, R. (1996). Design and evaluation of two-phase partition-dissolution method and its use in evaluating artemisinin tablets. *J Pharm Sci.* **85** (10): 1060-1063.
- Hodge, I.M. (1994). *J Non-Cryst Solids*. **169**: 211. Cited In: Robertson, C.G., Santangelo, P.G., Roland, C.M. (2000). Comparison of glass formation kinetics and segmental relaxation in polymers. *J Non-Cryst Solids*. **275**: 153-159.
- Höhne, G.W.H., Hemminger, W., Flammershiem, H.-J. (1996). *Differential Scanning Calorimetry: An Introduction for Practitioners*. Germany: Springer-Verlag Berlin Hiedelberg.
- Horstmann, M.N., Kursawe, M.A., Dzekan, H.K. (1998). Transdermal Therapeutic System Comprising The Active Substance 17- $\beta$ -Estradiol (Anhydrous). US Patent 5827245.
- Hudson, R. (1995). *Development in the European Extrusion Industry-Machinery, Manufacturers and Markets*. UK: Rapra Technology Limited Publishing.
- Hunt, B.J., James, M.I ed. (1993). *Polymer Characterization*. UK: Blackie Academic & Professional, an imprint of Chapman & Hall.
- Hurkmans, J.F., Boddé, H.E., Van Driel, L.M., Van Doorne, H., Junginger, H.E. (1985). Skin irritation caused by transdermal drug delivery systems during long-term (5 days) application. *Br J Dermatol*. **112**(4): 461-467.
- Inoue, K., Ogawa, K., Okada, J., Sugibayashi, K. (2005). Enhancement of skin permeation of ketotifen by supersaturation generated by amorphous form of the drug. *J Control Release*. **108**: 306-318.
- Itoh, T., Xia, J., Magavi, R., Nishihata, T., Rytting, J.H. (1990). Use of Shed Snake Skin as a Model Membrane for *in Vitro* Percutaneous Penetration Studies: Comparison with Human Skin. *Pharm Res*. **7**(10): 1042-1047.
- Jain, R., Railkar, A.S., Mallick, A.W., Rhodes, C.T., Shah, N.H. (1998). Stability of a hydrophobic drug in presence of hydrous and anhydrous lactose. *Eur J Pharm Biopharm*. **46**: 177-182.

- Josephine, L.J., Mehul, R.T., Wilson, B., Shanaz, B., Bincy, R. (2011). Formulation and *in-vitro* evaluation of floating microspheres of Anti-Retro viral drug as a gastro-retentive dosage form. *Int J Res Pharm Chem.* **1**(3): 519-527.
- Joshi, H.N., Wilson, T.D. (1995). Calorimetric evaluation of hydration of cholestyramine. *J Pharm Pharmacol.* **47**: 188-192.
- Kale, A.A., Patravale, V.B. (2008). Design and Evaluation of Self-Emulsifying Drug Delivery Systems (SEDDS) of Nimodipine. *AAPS PharmSciTech.* **9**(1): 191-196.
- Kallakunta, V.R., Eedara, B.B., Jukant, R., Ajmeera, R.K., Bandari, S. (2013). A Gelucire 44/14 and labrasol based solid self emulsifying drug delivery system: formulation and evaluation. *J Pharm Invest.* 1-12.
- Karatas, A., Yuksel, N., Baykara, T. (2005). Improved solubility and dissolution rate of piroxicam using Gelucire® 44/14 and labrasol. *II Farmaco.* **60**: 777-782.
- Karl, M., Djuric, D., Kolter, K. (2011). Pharmaceutical excipients for Hot-Melt Extrusion. *Pharm Tech.* **35**(5): 74-82.
- Kaur, K., Kim, K. (2009). Studies of chitosan/organic acid/Eudragit® RS/RL-coated system for colonic delivery. *Int J Pharm.* **366**(1-2): 140-148.
- Kawakami, K., Miyoshi, K., Ida, Y. (2004). Solubilization behaviour of poorly soluble drugs with combined use of Gelucire® 44/14 and cosolvent. *J Pharm Sci.* **93**: 1471-1479.
- Khan, N., Craig, D.Q.M. (2003). The influence of drug incorporation on the structure and release properties of solid dispersions in lipid matrices. *J Control Release.* **93**: 355-368.
- Khan, N., Craig, D.Q.M. (2004). Role of Blooming in Determining the storage Stability of Lipid-Based Dosage Forms. *J Pharm Sci.* **93**(12): 2962-2971.
- Khan, S., Ali, A., Singhavi, D., Yeole, P. (2008). Controlled Ocular Delivery of Acyclovir through rate Controlling Ocular Insert of Eudragit: A Technical Note. *AAPS PharmSciTech.* **9**(1): 169-173.

- Khanna, Y.P., Khun, W.P. (1997). Measurement of Crystalline Index in Nylons by DSC: Complexities and Recommendations. *Journal of Polymer Science: Part B: Polymer Physics*. **35**: 2219-2231.
- Kidokoro, M., Shah, N., Malick, A.W., Infeld, M.H., McGinity, J.W. (2001). Properties of Tablets Containing Granulations of Ibuprofen and an Acrylic Copolymer Prepared by Thermal Processes. *Pharm Dev Tech*. **6**(20): 263-275.
- Kim, B.K., Hwang, S.J., Park, J.B., Park, H.J. (2002). Preparation and characterization of drug-loaded polymethylacrylate microspheres by an emulsion solvent evaporation method. *J Microencapsul*. **19**(6): 811-822.
- Knutson, R.A., Merbitz, L.A., Creekmore, M.A., Snipes, H.G. (1981). Use of sugar and povidone-iodine to enhance wound healing: Five years' experience. *Southern Medical Journal*. **74**(11): 1329-1335.
- Kobayasho, K., Huang, C-i., Lodge, T.P. (1999). Thermoreversible Gelatin of Aqueous Methylcellulose Solutions. *Macromolecules*. **32**: 7070-7077.
- Kocherbitov, V., Ulvenlund, S., Briggner, L-E., Kober, M., Arnebrant, T. (2010). Hydration of a natural polyelectrolyte xanthan gum: comparison with non-ionic carbohydrate. *Carbohydr Polym*. **82**: 284-290.
- Kolter, K., Karl, M., Gryczke, A. (2010). *Hot-Melt Extrusion with BASF Pharma Polymers. Extrusion Compendium*. 2<sup>nd</sup> Edition. Germany ISBN 978-3-00-039415-7.
- Korsmeyer, R.W., Gurny, R., Doelker, E., Buri, P., Peppas, N.A. (1983). Mechanisms of solute release from porous hydrophilic polymers. *Int J Pharm*. **15**(1): 25-35.
- Kotiyani, P.N., Vavia, P.R. (2001). Eudragits: Role as crystallization inhibitors in drug-in-adhesive transdermal systems of estradiol. *Eur J Pharm Biopharm*. **52**(2):173-180.
- Kulkarni, V.S. ed. (2010). *Handbook of Non-Invasive Drug Delivery Systems*. USA: Elsevier Inc.



- Kusum, D.V., Saisivam, S., Maria, G.R., Deepti, P.U. (2003). Design and evaluation of matrix diffusion controlled transdermal patches of verapamil hydrochloride. *Drug Dev In Pharm.* **29**(5): 495-503.
- Li, S., Jones, D.S., Andrews, G.P. (2013). Hot Melt Extrusion: A Process Overview and Use in Manufacturing Solid Dispersions of Poorly Water-Soluble Drugs, in *Drug Delivery Strategies for Poorly Water-Soluble Drugs* (ed Douroumis, D., Fahr, A.). Chichester, UK: John Wiley & Sons, Ltd. Ch11: 325-358.
- Li, X., Nie, S., Kong, J., Li, N., Ju, C., Pan, W. (2008). A controlled-release ocular delivery system for ibuprofen based on nanostructured lipid carriers. *Int J Pharm.* **363**: 177-182.
- Lii, C-Y., Liaw, S-C., Tomasik, P. (2003). Xanthan gum-ovalbumin complexes from electrosynthesis and coaceravation. *Polish Journal of Food and Nutrition Sciences.* **12/35**(3): 25-29.
- Lin, S-Y., Yu, H-L. (2000). Microscopic Fourier Transform Infrared/Differential Scanning Calorimetry System Used to Study the Different Thermal Behaviors of Polymethacrylate Copolymers of Eudragits RS, RL, E 30D, or E. *J Appl Polym Sci.* **78**:829-835.
- Lipp, R., Riedl, J., Tack, J. (1997). Transdermal therapeutic systems with crystallization inhibitors. US Patent 5676968.
- Lloyd, G. R., Craig, D. Q. M., Smith, A. (1997). An investigation into the melting behavior of binary mixes and solid dispersions of paracetamol and PEG 4000. *J Pharm Sci.* **86**(9): 991-996.
- Lopedota, A., Trapani, A., Cutrignelli, A., Chiarantini, L., Curci, R., Manuali, E., Trapani, G. (2009). The use of Eudragit® RS 100/cyclodextrin nanoparticles for the transmucosal administration of glutathione. *Eur J Pharm Biopharm.* **72**(3): 509-520.
- Lyons, J.G., Blackie, P., Higginbotham, C.L. (2008). The significance of variation in extrusion speeds and temperatures on a PEO/PCL blend based matrix for oral drug delivery. *Int J Pharm.* **351**(1-2): 201-208.

- Macêdo, R.O., do Nascimento, T.G. (2002). Quality control of thiabendazole pre-formulation and tablets by TG and DSC coupled to the photovisual system. *Thermochim Acta*. **392-393**: 85-92.
- Madana, S., Madanb, S. (2012). Hot melt extrusion and its pharmaceutical applications. *Asian Journal of Pharmaceutical Sciences*. **7**(2): 123-133.
- Mäkelä, A-L., Lempiäinen, M., Ylijoki, H. (1981). Ibuprofen Levels in Serum and Synovial Fluid. *Scandinavian Journal of Rheumatology*. **39**:15-17.
- Mandawgade, S., Patravale, V. (2008). Development of SLNs from natural lipids: Application to topical delivery of tretinon. *Int J Pharm*. **363**: 132-138.
- Maniruzzaman, M., Boateng, J.S., Snowden, M.J., Douroumis, D. (2012). A Review of Hot-Melt Extrusion: Process Technology to Pharmaceutical Products. *International Scholarly Research Network*. 1-9.
- Marsac, P.J., Li, T., Taylor, L.S. (2009). Estimation of Drug-Polymer Miscibility and Solubility in Amorphous Solid Dispersions Using Experimentally Determined Interaction Parameters. *Pharm Res*. **26**(1): 139-151.
- Marsac, P.J., Shamblin, S.L., Taylor, L.S. (2006). Theoretical and Practical Approaches of Drug-Polymer Miscibility and Solubility. *Pharm Res*. **23**(10): 2417-2426.
- Marthi, K., Ács, M., Pokol, G., Tomor, K., Eröss-Kiss, K. (1992). DSC studies on the polymorphism and pseudopolymorphism of pharmaceutical substances. *J Therm Anal Calorim*. **38**(4): 1017-1025.
- Masiz, J.J. (1998). Molecular Transdermal Transport System. US Patent 5853751.
- Megrab, N.A., Williams, A.C., Barry, B.W. (1995a). Oestradiol permeation through human skin and silastic membrane: effects of propylene glycol and supersaturation. *J Control Release*. **36**: 277-294.
- Megrab, N.A., Williams, A.C., Barry, B.W. (1995b). Oestradiol permeation across human skin, silastic and snake skin membranes: the effects of ethanol water cosolvent systems. *Int J Pharm*. **116**: 101-112.

- Mehuys, E., Vervaet, C., Remon, J.P. (2004). Hot-melt extruded ethylcellulose cylinders containing a HPMC–Gelucire® core for sustained drug delivery. *J Control Release*. **94** (2-3): 273-280.
- Menon, G. K. (2002). New insights into skin structure: scratching the surface. *Advanced Drug Delivery Reviews*. **54**, Supplement (1): S3-S17.
- Mididoddi, P.K., Prodduturi, S., Repka, M.A. (2006). Influence of tartaric acid on the bioadhesion and mechanical properties of hot-melt extruded hydroxypropyl cellulose films for the human nail. *Drug Dev In Pharm*. **32**(9): 1059-1066.
- Mitu, M., Lupuliasa, D., Dinu-Pirvu, E., Radulescu, F.S., Miron, D.S., Vlaia, L. (2011). Ketoconazole in topical pharmaceutical formulations. The influence of the receptor media on the *in vitro* diffusion kinetics. *FARMACIA*. **59**(3): 358-366.
- Mohammad, M.A., Alhalaweh, A., Velaga, S.P. (2011). Hansen solubility parameter as a tool to predict cocrystal formation. *Int J Pharm*. **407**: 63-71.
- Moore, T., Croy, S., Mallapragada, S., Pandit, N. (2000). Experimental investigation and mathematical modelling of Pluronic® F127 gel dissolution: drug release in stirred systems. *J Control Release*. **67**: 191-202.
- Morris, C., Sieve, B., Bullen, H. Department of Chemistry, Northern Kentucky University. Introduction to X-ray Diffraction (XRD). [www.asdlib.org/onlineArticles](http://www.asdlib.org/onlineArticles) [Accessed: March 2011].
- Morrow, D.I.J., McCarron, P.A., Woolfson, A.D., Donnelly, R.F. (2007). Innovative Strategies for Enhancing Topical and Transdermal Drug Delivery. *The Open Drug Delivery Journal*. **1**: 36-59.
- Moser, K., Kriwet, K., Naik, A., Kalia, Y.N., Guy, R.H. (2001). Passive skin penetration enhancement and its quantification *in vitro*. *Eur J Pharm Biopharm*. **52**: 103-112.
- Moustafine, R.I., Zaharov, I.M., Kemenova, V.A. (2006). Physicochemical characterisation and drug release properties of Eudragit E PO/Eudragit L 100-55 interpolyelectrolyte complexes. *Eur J Pharm Biopharm*. **63**: 26-36.

- Mundargi, R.C., Patil, S.A. (2007). Evaluation and Controlled Release Characteristics of Modified Xanthan Films for Transdermal Delivery of Atenolol. *Drug Dev In Pharm.* **33**: 79-90.
- Mundargi, R.C., Patil, S.A., Agnihortis, S., Aminabhavi, T. (2007). Evaluation of acrylamide-grafted-xanthan gum copolymer matrix tablets for oral controlled delivery of antihypertensive drugs. *Carbohydr Polym.* **69**(1): 130-141.
- Munday, D.L., Cox, P.J. (2000). Compressed xanthan and karaya gum matrices: hydration, erosion and drug release mechanisms. *Int J Pharm.* **203**:179-192.
- Munjal, M., Stodghill, S.P., Elsohly, M.A., Repka, M.A. (2006). Polymeric systems for amorphous Delta 9-tetrahydrocannabinol produced by a hot-melt method. Part I: chemical and thermal stability during processing. *J Pharm Sci.* **95**(8): 1841-1853.
- Mura, P., Faucci, M.T., Manderioli, A., Bramanti, G., Ceccarelli, L. (1998). Compatibility study between ibuprofen and pharmaceutical excipients using differential scanning calorimetry, hot-stage microscopy and scanning electron microscopy. *J Pharm Biomed Anal.* **18**: 151-163.
- Mura, P., Manderioli, A., Bramanti, G., Furlanetto, S., Pinzauti, S. (1995). Utilization of differential scanning calorimetry as a screening technique to determine the compatibility of ketoprofen with excipients. *Int J Pharm.* **119**: 71-79.
- Nicholas, S.J., John, T.M. (2003). Topical pharmaceutical formulations and methods of treatment. US Patent 20030138503 A1.
- O'Brien, F.E.M. (1948). The control of Humidity by Saturated Salt Solutions. *Journal of Scientific Instrument.* **25** (3):73-76.
- Oliary, J., Tod, M., Nicolas, P., Petitjean, O., Caille, G. (1992). Pharmacokinetics of ibuprofen enantiomers after single and repeated doses in man. *Biopharm Drug Dispos.* **13**: 377-344.
- Oth, M.P., Moës, A.J. (1989). Sustained release solid dispersions of indomethacin with Eudragit RS and RL. *Int J Pharm.* **55**(2-3): 157-164.

- Palem, C.R., Kumar B.S., Maddineni, S., Gannu, R., Repka, M.A., Yamsani, M.R. (2013). Oral transmucosal delivery of domperidone from immediate release films produced via hot-melt extrusion technology. *Pharm Dev Tech.* **18**(1): 186-195.
- Papageorgiou, G.Z., Bikiaris, D.N., Panayiotou, C.G. (2011). Novel miscible poly (ethylene sebacate)/poly (4-vinyl phenol) blends: Miscibility, melting behavior and crystallization study. *Polymer.* **52**(20): 4553–4561.
- Patidari, K., Kshirsagar, M.D., Saini, V., Joshi, P.B., Soni, M. (2011). Solid dispersion technology: A boon for water soluble drugs. *Indian Journal of Novel Drug delivery.* **3**(2): 83-90.
- Pellet, M.A., Roberts, M.S., Hadgraft, J. (1997a). Supersaturated solutions evaluated with an *in vitro* stratum corneum tape stripping technique. *Int J Pharm.* **151**: 91-98.
- Pellet, M.A., Castellano, S., Hadgraft, J., Davis, A.F. (1997b). The penetration of supersaturated solutions of piroxicam across silicone membranes and human skin *in vitro*. *J Control Release.* **46**(3): 205-214.
- Perrie, Y., Rades, T. (2010). *FASTtrack: Pharmaceuticals-Drug Delivery and Targeting*. London.Chicago: Pharmaceutical Press.
- Pershing, L.K., Lambert, L.D., Knutson, K. (1990). Mechanism of Ethanol-Enhanced Estradiol Permeation Across Human Skin *in Vivo*. *Pharm Res.* **7**(2): 170-175.
- Perumal, A., Dangor, C.M., Alcock, R.S., Hurbans, N., Mooppanar, K.R. (1999). Effect of formulation variables on *in vitro* drug release and micromeritic properties of modified release ibuprofen microspheres. *J Microencapsul.* **4**(16): 475-487.
- Perumal, D. (2001). Microencapsulation of ibuprofen and Eudragit® RS 100 by the emulsion solvent diffusion technique. *Int J Pharm.* **218**(1-2): 1-11.
- Pignatello, R., Spadaro, D., Vandelli, M.A., Forni, F., Puglisi, G. (2004). Characterization of the Mechanism of Interaction in Ibuprofen-Eudragit RL 100 Coevaporates. *Drug Dev In Pharm.* **30**(3): 277-288.

- Polat, T., Linhardt, R.J. (2001). Syntheses and Applications of sucrose-based esters. *Journal of Surfactant and Detergents*. **4**(4): 415-421.
- Potthast, H., Dressman, J.B., Junginger, H.E., Midha, K.K., Oeser, H., Shah, V.P., Vogelpoel, H., Barends, D.M. (2005). Biowaiver monographs for immediate release solid oral dosage forms: Ibuprofen. *J Pharm Sci*. **94**(10): 2121-2131.
- Prodduturi, S., Umran, K.L., Otaigbe, J.U., Repka, M.A. (2007). Stabilization of Hot-Melt Extrusion Formulations Containing Solid Solutions Using Polymer Blends. *AAPS PharmSciTech*. **8**(2):1-10.
- Qi, S., Belton, P., Nollenberger, K., Claydon, N., Reading, M., Craig, D. Q. M. (2010). Characterisation and prediction of phase separation in hot-melt extruded solid dispersions: A thermal, microscopic and NMR relaxometry study. *Pharm Res*. **27**: 1869-1883.
- Qi, S., Avalle, P., Saklatvala, R., Craig, D.Q.M. (2008b). An investigation into the effects of thermal history on the crystallization behavior of amorphous paracetamol. *Eur J Pharm Biopharm*. **69**: 364-371.
- Qi, S., Belton, P., Nollenberger, K., Gryczke, A., Craig DQ. (2011). Compositional analysis of low quantities of phase separation in hot-melt-extruded solid dispersions: a combined atomic force microscopy, photothermal Fourier-transform infrared microspectroscopy, and localised thermal analysis approach. *Pharm Res*. **28**(9): 2311-2326.
- Qi, S., Gryczke, A., Belton, P., Craig, D.Q.M. (2008a). Characterisation of solid dispersions of paracetamol and EUDRAGIT®E prepared by hot-melt extrusion using thermal, microthermal and spectroscopic analysis. *Int J Pharm*. **354**: 158-167.
- Qian, F., Huang, J., Hussain, M.A. (2010). Drug-polymer solubility and miscibility: Stability consideration and practical challenges in amorphous solid dispersion development. *J Pharm Sci*. **99**(7): 2941-2947.
- Raghavan, S.L., Trividic, A., Davis, A.F., Hadgraft, J. (2000). Effect of cellulose polymers on supersaturation and *in vitro* membrane transport of hydrocortisone acetate. *Int J Pharm*. **193**: 231-237.

- Rambali, B., Verreck, G., Baert, L., Massart, D.L. (2003). Itraconazole Formulation Studies of the Melt-Extrusion Process with Mixture Design. *Drug Dev In Pharm.* **29**(6): 641-652.
- Rapolu, K., Dharani, S., Yamsani, M.R. (2012). Preparation and evaluation of multiple-unit gastro retentive floating drug delivery system for ondansetron hydrochloride based on gas formation technique. *Int J Pharm.* **2**(1): 46-54.
- Rasenack, N., Müller, B.W. (2002). Ibuprofen crystals with optimized properties. *Int J Pharm.* **245**: 9-24.
- Repka, M.A., McGinity, J.W. (2001). Bioadhesive properties of hydroxylpropylcellulose topical films produced by hot-melt extrusion. *J Control Release.* **70**: 341-351.
- Repka, M.A., Prodduturi, S., Stodghill, S.P. (2003). Production and Characterization of Hot-Melt Extruded Films Containing Clotrimazole. *Drug Dev In Pharm.* **29** (7): 757-765.
- Repka, M.A., Repka, S.L., McGinity, J.W. (2002). Bioadhesive Hot-melt extruded film for topical and mucosal adhesion applications and drug delivery and process for preparation thereof. US Patent 6375963 B1.
- Repka, M.A., Gerding, T.G., Repka, S.L., McGinity, J.W. (1999). Influence of plasticizers and drugs on the physical-mechanical properties of hydroxypropylcellulose films prepared by hot melt extrusion. *Drug Dev In Pharm.* **25**: 625-633.
- Reza, M.S., Abdul Quadir, M., Haider, S.S. (2003). Comparative evaluation of plastic, hydrophobic and hydrophilic polymers as matrices for controlled-release drug delivery. *J of Pharm Pharm Sci.* **6**(2): 282-291.
- Rinaki, E., Valsami, G., Macheras, P. (2003). The power law can describe the 'entire' drug release curve from HPMC-based matrix tablets: a hypothesis. *Int J Pharm.* **255**(1-2): 199-207.
- Ritger, P. L. and N. A. Peppas. (1987). A simple equation for description of solute release I. Fickian and non-fickian release from non-swellable devices in the form of slabs, spheres, cylinders or discs. *J Control Release.* **5**(1): 23-36.

- Robertson, C.G., Santangelo, P.G., Roland, C.M. (2000). Comparison of glass formation kinetics and segmental relaxation in polymers. *J Non-Cryst Solids*. **275**: 153-159.
- Rohrs, B. (2001). Dissolution Method Development of Poorly Soluble Compounds. *Dissolution Technol*. **8**(3): 1-5.
- Roskos, K.V., Guy, R.H. (1989). Assessment of Skin Barrier Function Using Transepidermal Water Loss: Effect of Age. *Pharm Res*. **6**(11): 949-953.
- Rowe, R., Sheskey, P.J., Quinn, M.E.ed. (2009). *Handbook of Pharmaceutical Excipients*. 6<sup>th</sup> Edition. London. Chicago: Pharmaceutical Press.
- Saharan, V.A., Kukkar, V., Kataria, M., Gera, M., Choudhury, P.K. (2009). Dissolution Enhancement of Drugs Part II: Effect of Carriers. *International Journal of Health Research*. **2**(2): 207-223.
- Sarkar, N., Gandhi, I.S., Ghosh, M.N., Basu, S., Bhaumik, B., Dattagupta, A. (1988). A double-blind comparative study of conventional and sustained-release ibuprofen in Indian patients with osteoarthritis. *Current Therapeutic Research*. **44**: 11-21.
- Savova, M., Kolusheva, T., Stourza, A., Seikova, I. (2007). The use of group contribution method for predicting the solubility of seed polyphenols of *VITIS VINIFERA L*. Within a wide polarity range in solvent mixtures. *Journal of the University of Chemical Technology and Metallurgy*. **42**(3): 295-300.
- Schaefer, H., Zesch, A., Stuttgen, G. (1982). Skin Permeability. New York: Springer. Cited In: Tojo, K. (1988). Concentration profile in plasma after transdermal drug delivery. *Int J Pharm*. **43**: 201-205.
- Scheindlin, S. (2004). Transdermal Drug Delivery: Past, Present, Future. *Mol Interventions*. **4**(6): 308-312.



- Sears, J.K., Touchette, N.W. (1982). *Plasticizers*. In: Mark H F, Othmer D F, Overberger C G, Seaborg G T, editors. *Kirk-Othmer Encyclopaedia of Chemical Technology*, Vol. 18. New York: Wiley. pp: 111-182. Cited In: Kidokoro, M., Shah, N., Malick, A.W., Infeld, M. H., McGinity, J.W. (2001). Properties of Tablets Containing Granulations of Ibuprofen and an Acrylic Copolymer Prepared by Thermal Processes. *Pharm Dev Tech.* **6**(20): 263-275.
- Shah, B., Kakumanu, V.K., Bansal, A. (2006). Analytical Techniques for Quantification of Amorphous/Crystalline Phases in Pharmaceutical Solids. *J Pharm Sci.* **95**(8): 1641-1665.
- Shen, T.Y. (1972). Perspectives in Nonsteroidal Anti-inflammatory Agents. *Angewandte Chemie International Edition in English.* **11**(6): 460-472.
- Sheth, U.K., Kusum, G., Teresa, P., Pispati, P.K. (1980). Measurement of Antipyretic Activity of Ibuprofen and Paracetamol in Children. *J Clin Pharmacol.* **20**(11): 672-675.
- Siepmann, F., Le Brun, V., Siepmann, J. (2006). Drugs acting as plasticizers in polymeric systems: A quantitative treatment. *J Control Release.* **115**: 298-306.
- Siewert, M., Dressman, J., Brown, C., Shah, V. (2003). FIP/AAPS Guidelines for Dissolution/*In Vitro* Release Testing of Novel/Special Dosage Forms. *Dissolution Technol.* 6-15.
- Simha, R., Boyer, R.F. (1962). On a general relation involving the glass transition temperature and coefficients of expansion of polymers. *J Chem Phys.* **37**(5): 1003-1007.
- Singhal, S., Lohar, V. K., Arora, V. (2011). Hot Melt Extrusion Technique. *WebmedCentral Pharmaceutical Sciences.* **2**(1): WMC001459.1-20.
- Siripuram, P.K., Bandari, S., Jukanti, R., Veerareddy, P.R. (2010). Formulation and characterisation of floating Gelucire matrices of Metoprolol succinate. *Dissolution Technol.* 34-39.
- Six, K., Murphy, J., Weuts, I., Craig, D.Q., Verreck, G., Peeters, J., Brewster, M., Van den Mooter, G. (2003). Identification of phase separation in solid dispersions of itraconazole and Eudragit E100 using microthermal analysis. *Pharm Res.* **20**(1): 135-8.

- Smithy, D.T., Friesen, D.T., Miller, W.K., Babcock, W.C. (2007). Solid compositions of low-solubility drugs and poloxamers. US Patent 2007/0141143 A1.
- Socrates, G. (2001). *Infrared and Raman Characteristic Group Frequencies: Tables and Charts*. 3<sup>rd</sup> Edition. West Sussex. England: John Wiley & Sons Ltd.
- Steendam, R., Frijlink, H.W., Lerk, C.F. (2001). Plasticization of amylopectin by moisture. Consequences for compaction behaviour and tablet properties. *Eur J Pharm Sci.* **14**: 245-254.
- Stefanis, E., Panayiotou, C. (2008). Prediction of Hansen solubility parameters with a new group-contribution method. *Int J Thermophys.* **29**: 568-585.
- Stricker, H.S. (1983). Transdermal Release System for Pharmaceutical Preparation. US Patent 4409206.
- Sugibayashi, K., Morimoto, Y. (1994). polymers for transdermal drug delivery systems. *J Control Release.* **29**: 177-185.
- Sun, C.C. (2004). A novel method for deriving true density of pharmaceutical solids including hydrates and water-containing powders. *J Pharm Sci.* **93**(3): 646-653.
- Sutananta, W., Craig, D. Q. M., Newton, J. M. (1995). An evaluation of the mechanisms of drug release from glyceride bases. *J Pharm Pharmacol.* **47**: 182-187.
- Sutananta, W., Craig, D. Q. M., Newton, J.M. (1994). An investigation into the effect of preparation conditions on the structure and mechanical properties of pharmaceutical glyceride bases. *Int J Pharm.* **110**(1): 75-91.
- Svensson, A., Neves, C., Cabane, B. (2004). Hydration of an amphiphilic excipient, Gelucire®44/14. *Int J Pharm.* **281**: 107-118.
- Szczesniak, A.S. (1963). Classification of textural characteristics. *J Food Sci.* **28**(4): 385-389.

- Tang, C.Y., Kwon, Y. -N., Leckie, O. (2007). Probing the nano- and micro-scales of reverse osmosis membranes-A comprehensive characterization of physiochemical properties of uncoated and coated membranes by XPS, TEM, ATR-FTIR, and streaming potential measurements. *Journal of Membrane Science*. **287**(1): 146-156.
- Taylor, N.A.S., Machado-Moreira, C.A. (2013). Regional variations in transepidermal water loss, eccrine sweat gland density, sweat secretion rates and electrolyte composition in resting and exercising humans. *Extreme Physiology & Medicine*. **2**(4): 1-29.
- Thomas, L.C. (2005). Modulated DSC® Basics; Calculation and Calibration of MDSC® Signals. TA Instruments Technical Paper TP 007.
- Thumma, S., ElSohly, M.A., Zhang, S.Q., Gul, W., Repka, M.A. (2008). Influence of plasticizers on the stability and release of a prodrug of [Delta]9-tetrahydrocannabinol incorporated in poly (ethylene oxide) matrices. *Eur J Pharm Biopharm*. **70**(2): 605-614.
- Tojo, K. (1988). Concentration profile in plasma after transdermal drug delivery. *Int J Pharm*. **43**: 201-205.
- Tool, A.Q. (1953). *Journal of the American Ceramic Society*. **29**:240. Cited In: Yue, Y., Von der ohe, R., Jensen, S.L. (2004). Fictive temperature, cooling rate, and viscosity of glasses. (2004). *J chem phys*. **120**(17): 8053-8059.
- Trey, S.M., Wicks, D.A., Mididoddi, P.K., Repka, M.A. (2007). Delivery of itraconazole from extruded HPC films. *Drug Dev In Pharm*. **33**(7): 727:735.
- USP-31<sup>st</sup> Edition, NF-26<sup>nd</sup> Edition, In: chapter 724: Drug release; United State Pharmacopeial convention.**2008**, pp. 275-278. Cited In: Anand, O., Yu, L.X., Conner, D.P., Davit, B.M. (2011). Dissolution Testing for Generic Drugs: An FDA Perspective. *AAPS Journal*. **13**(3): 328-335.
- Valle-Jones, J.C., Smith, J., Rowley-Jones, D. (1984). A comparison in general practice of once and twice daily sustained-release ibuprofen and standard ibuprofen in the treatment of non-articular rheumatism. *Br J Clin Pract*. **38**: 353-358.
- Van Krevelen, D.W, Hoftyzer, P.J. (1976). *Properties of polymers*. 2<sup>nd</sup> Edition. Amesterdam: Elsevier Scientific Publishing Company. pp: 152-155.

Verhoeven, E., Vervaet, C., Remon, J.P. (2006). Xanthan gum to tailor drug release of sustained-release ethylcellulose mini-matrices prepared via hot-melt extrusion: *in vitro* and *in vivo* evaluation. *Eur J Pharm Biopharm.* **63**(3): 320-330.

Verhoeven, E., De Beer, T.R., Van den Mooter, G., Remon, J.P., Vervaet, C. (2008). Influence of formulation and process parameters on the release characteristics of ethylcellulose sustained-release mini-matrices produced by hot-melt extrusion. *Eur J Pharm Biopharm.* **69**(1): 312-319.

Verreck, G. (2012). The Influence of Plasticizers in Hot-melt Extrusion, in *Hot-Melt Extrusion: Pharmaceutical Applications* (ed Douroumis, D.). Chichester, UK: John Wiley & Sons, Ltd. Ch5: 93-112.

Verreck, G., Decorte, A., Heymans, K., Adriaensen, J., Liu, D., Tomasko, D., Arien, A., Peeters, J., Van den Mooter, G., Brewster, ME. (2006a). Hot stage extrusion of p-amino salicylic acid with EC using CO<sub>2</sub> as a temporary plasticizer. *Int J Pharm.* **327**(1-2): 45-50.

Verreck, G., Decorte, A., Li, H., Tomasko, D., Arien, A., Peeters, J., Rombaut, P., Van den Mooter, G., Brewster, M.E. (2006b). The effect of pressurized carbon dioxide as a plasticizer and foaming agent on the hot melt extrusion process and extrudate properties of pharmaceutical polymers. *The Journal of Supercritical Fluids.* **38**(3): 383-391.

Vitez, I.M., Newman, A.W., Davidovich, M., Kiesnowski, C. (1998). The evolution of hot-stage microscopy to aid solid-state characterizations of pharmaceutical solids. *Thermochim Acta.* **324**: 187-196.

Wang, X., Michoel, A., Van den Mooter, G. (2005). Solid state characteristics of ternary solid dispersions composed of PVP VA64, Myrj 52 and itraconazole. *Int J Pharm.* **303**(1-2): 54-61.

Warner, R.R., Biossy, Y.L., Lilly, N.A., Spears, M.J., McKillop, K., Marshall, J.L., Stone, K.J. (1999). Water Disrupts Stratum Corneum Lipid Lamellae: Damage is Similar to Surfactants. *Dermatol.* **113**(6): 960-966.

Warren, D.B., Benameur, H., Porter, C.H., Pouton, C.W. (2010). Using polymeric precipitation inhibitors to improve the absorption of poorly water-soluble drugs: A mechanistic basis for utility. *J Drug Target.* **18**(10): 704-731.

Washington, N., Washington, C., Wilson, C.G. (2003). *Physiological Pharmaceutics: Barriers to Drug Absorption*. 2<sup>nd</sup> Edition. New York: Taylor & Francis Inc.

Watkinson, A.C. (2013). A commentary on transdermal drug delivery systems in clinical trials. *J Pharm Sci*. 1-7

Watson, D.G. (2005). *Pharmaceutical Analysis: A textbook for Pharmacy Students and Pharmaceutical Chemists*. 2<sup>nd</sup> Edition. United Kingdom: Churchill Livingstone Elsevier.

Website: [eudragit.evonik.com](http://eudragit.evonik.com). [Accessed: November 2010].

Website: [www.cdc.gov](http://www.cdc.gov). [Accessed: May 2012].

Website: [www.ebdgroup.com/partneringnews/2012/03/sst-breaks-transdermal-charged-molecule-delivery-barrier/](http://www.ebdgroup.com/partneringnews/2012/03/sst-breaks-transdermal-charged-molecule-delivery-barrier/). [Accessed: April 2013].

Website: [www.iscrewbarrel.com](http://www.iscrewbarrel.com). [Accessed: May 2012].

Website: [www.omnimedicalsearch.com](http://www.omnimedicalsearch.com). [Accessed: May 2012].

Website: [www.polymerprocessing.com](http://www.polymerprocessing.com). [Accessed: June 2010].

Website: [www.thermo.com](http://www.thermo.com). [Accessed: May 2011].

Wehrung, D., Geldenhuys, J.W., Oyewumi, M.O. (2012). Effects of gelucire content on stability, macrophage interaction and blood circulation of nanoparticles engineered from nanoemulsions. *Colloids Surf B Biointerfaces*. **94**(0): 259-265.

Wilkes, C.E., Summers, J.W., Daniels, C.A. ed. (2005). *PVC Handbook*. Munich: Carl Hanser Verlag (HANSER).

Williams, A. C., Barry, B. W. (2004). Penetration enhancers. *Advanced Drug Delivery Reviews*. **56**(5): 603-618.

Williams, M., Tian, Y., Jones, D.S., Andrews, G.P. (2010). Hot-Melt extrusion technology: optimizing drug delivery. *Eur J Pharm*. **7**: 7-10.

- Wokovich, A.M., Prodduturi, S., Doub, W.H., Hussain, A.S., Buhse, L.F. (2006). Transdermal drug delivery system (TDDS) adhesion as a critical safety, efficacy and quality attribute. *Eur J Pharms Biopharm.* **64**: 1-8.
- Wolff, H.M. (2000). Optimal process design for the manufacture of transdermal drug delivery systems. *Pharm Sci Tech Today.* **3**(5): 173-181.
- Wu, C., McGinity, J.W. (1999). Non-traditional plasticization of polymeric films. *Int J Pharm.* **177**(1): 15-27.
- Wu, C., McGinity, J.W. (2003). Influence of methylparaben as a solid-state plasticizer on the physicochemical properties of Eudragit® RS PO hot-melt extrudates. *Eur J Pharm Biopharm.* **56**(1): 95-100.
- Yang, M., Wang, P., Gogos, C. (2013). Prediction of acetaminophen's solubility in poly (ethylene oxide) at room temperature using the Flory-Huggins theory. *Drug Dev In Pharm.* **39**(1): 102-108.
- Yener, G., Üner, M., Gönüllü, Ü., Yildirim, S., Kilic, P., Aslan, S.S., Barla, A. (2010). Design of Meloxicam and Lornoxicam Transdermal Patches: Preparation, Physical Characterization, *ex Vivo* and *in Vivo* Studies. *Chem Pharm Bull.* **58**(11): 1466-1473.
- Yin, S.X., Franchini, M., Chen, J., Hsieh, A., Jen, S., Lee, T., Hussain, M., Smith, R. (2005). Bioavailability enhancement of a COX-2 inhibitor, BMS-347070, from a nanocryatlline dispersion prepared by spray-drying. *J Pharm Sci.* **94**(7): 1598-607.
- Young, C.R., Koleng, J.J., McGinity, J.W. (2003). Properties of drug-containing spherical pellets produced by a hot-melt extrusion and spheronization process. *J Microencapsul.* **20**(5): 613-625.
- Yue, Y., Von der ohe, R., Jensen, S.L. (2004). Fictive temperature, cooling rate, and viscosity of glasses. (2004). *J chem phys.* **120**(17): 8053-8059.
- Yüksel, N., Karataş, A., Ozkan, Y., Savaşer, A., Ozkan, S.A., Baykara T. (2003). Enhanced bioavailability of piroxicam using Gelucire 44/14 and Labrasol: *in vitro* and *in vivo* evaluation. *Eur J Pharm Biopharm.* **56**: 453-459.

Zhang, F., McGinity, J.W. (1999). Properties of Sustained-Release Tablets Prepared by Hot-Melt Extrusion. *Pharm Dev Tech.* **4**(2): 241-250.

Zhang, Y., Lam, Y.M. (2005). Poly (ethylene oxide)-*b*-poly (propylene oxide)-*b*- poly (ethylene oxide)-*g*-poly (vinyl pyrrolidone): Synthesis and characterization. *J Colloid Interface Sci.* **285**: 80-85.

Zheng, W., Cerea, M., Sauer, D., McGinity, J.W. (2004). Properties of theophylline tablets powder-coated with methacrylate ester copolymer. *J Drug Deliv Sci Technol.* **14**(4): 319-325.

Zhu, Y., Shah, N.H., Malick, A.W., Infeld, M.H., McGinity, J.W. (2004). Influence of a lipophilic thermal lubricant on the processing conditions and drug release properties of chlorpheniramine maleate. *J Drug Deliv Sci Technol.* **14**(4): 313-318.

Zografi, G., Hancock, B.C. (1997). Characteristics and Significance of the Amorphous State in Pharmaceutical Systems. *J Pharm Sci.* **86**(1): 1-12.

Zohuriaan, M.J., Shokrolahi, F. (2004). Thermal studies on natural and modified gums. *Polymer Testing.* **23**: 575-579.

## **Appendix**



Faculty of Medicine and Health Sciences Research Ethics Committee



Duncan Craig  
School of Pharmacy  
University of East Anglia  
NR4 7TJ

Research & Enterprise Services  
West Office (Science Building)  
University of East Anglia  
Norwich Research Park  
Norwich, NR4 7TJ

Telephone: +44 (0) 1603 591566  
Email: [fmh.ethics@uea.ac.uk](mailto:fmh.ethics@uea.ac.uk)

Web: [www.uea.ac.uk/researchandenterprise](http://www.uea.ac.uk/researchandenterprise)

16<sup>th</sup> January 2013

Dear Duncan,

**Project title: An Investigation into the Use of Lipid Matrices for Application to the Skin: Changes in Lipid Consistency Induced by Water Sorption from the Stratum Corneum.**  
**Reference: 2012/2013 – 34**

The submission of your above proposal has been considered by the Chair of the Faculty Research Ethics Committee and we can confirm that your proposal has been approved.

Please could you ensure that any further amendments to either the protocol or documents submitted are notified to us in advance and also that any adverse events which occur during your project are reported to the Committee. Please could you also arrange to send us a report once your project is completed.

The Committee would like to wish you good luck with your project

Yours sincerely

A handwritten signature in blue ink, appearing to read 'Y. Kirkham', is written over a faint, larger blue signature.

Yvonne Kirkham  
Project Officer